Cranfield University

Taeweon Gim

Modelling and Evaluation of Time-varying Thermal Errors in Machine Tool Elements

School of Industrial & Manufacturing Science

PhD Thesis

Cranfield University
School of Industrial and Manufacturing Science

PhD Thesis
Academic Year 1994-6

Taeweon Gim*

Modelling and Evaluation of Time-varying Thermal Errors in Machine Tool Elements

Supervisors: Prof. J. Corbett and Dr. A.E. Gee

April 1997

This thesis is submitted in partial fulfilment of the requirements for the Degree of Doctor of Philosophy

---

* On leave from Machine Tool R&D Centre, Daewoo Heavy Industries Ltd., Nam-san-dong, Chang-won, Kyung-nam, 641-714, S. Korea

Abstract

This thesis addresses a comprehensive approach to understanding the time-varying thermal errors in machine tools. Errors in machine tools are generally classified as being time or spatial dependent. Thermal errors are strongly dependent on the continuously changing operating conditions of a machine and its surrounding environment. Uniform temperature rises or stable temperature gradients, which produce time-invariant thermal errors, are considered to be rare in ordinary shop floor environments. Difficulties in analysing time-varying thermal errors are that, first of all, the temperature distribution within the components of a machine should be evaluated, and secondly, the distribution is continuously changing with time. These difficulties can be overcome by introducing a point-wise description method with three thermal parameters. From the theoretical analysis of simple machine elements such as bars, beams and cylinders, and extensive finite-element simulation data for a straightedge subject to room temperature variations, three thermal parameters, i.e. time-delay, time-constant and gain, were identified to obtain a precise description of the thermal deformation of a point of a machine body.

Time-delay is dependent largely on thermal diffusivity, and the heat transfer mechanism. The time-constant is governed by heat capacity, heat transfer mechanism and body size. Gain, on the other hand, is determined by the thermal expansion coefficient, heat transfer mechanism and mechanical constraint. The three thermal parameters, in turn, imply that thermal deformation of a point in a body can be described by a simple first-order differential equation. Regarding their dependence on the heat transfer mechanism, a more refined description requires a time-varying linear first-order differential equation. Such an equation can be applied to each point of interest of a machine body. The final form of modelling, using the parameters, is a state-space equation gathering the governing equations for the points of interest. By adopting the point-wise discrete modelling method, we can overcome the difficulty of the spatial distribution of the temperature. Indeed, the calibration of a machine tool is usually performed at discrete points.

The completion of this approach was made by presenting the methods by which the three thermal parameters can be evaluated. The first method employs analytical tools based on simplifying assumptions about the shape and boundary conditions of machine components. The second method was to apply numerical techniques to complex machine components. Because there are many drawbacks in theoretical approaches, experimental techniques are essential to complement them. The three thermal parameters can be easily identified using popular parameter identification techniques which can be applied to time-varying cases by their recursive forms. The techniques described were applied to modelling the thermal errors in a single-point diamond turning research machine. It was found that the dominant error component was spindle axial growth. The predictive model for the time-constant was shown to be in agreement with both the machine and with the scaled physical model rig.

Acknowledgements

My great thanks are due to my supervisors, Prof. Corbett and Dr. Gee, without whose help and knowledge, this work would never have been completed.

They demolished a cultural iron-curtain bounding the way of my thinking, so I could taste a bit of the philosophy underlining precision engineering.

Also, I wish to acknowledge a lot of assistance of the staff of SIMS in the experimental part of this work.

A special appreciation goes to Daewoo Heavy Industries, Ltd., S. Korea, for providing me with the academic environment for several years.

Finally, I would like to thank my family for their support and endurance.

Contents

List of Figures

List of Tables

Notation

A	Rotation matrix
A	Area
Bi	Biot number
C	Thermal conductance
c_{th}	Thermal compliance
c_p	Constant-pressure specific heat
c_v	Constant-volume specific heat
d	Displacement
E	Error matrix
E	Energy
E_{sys}	Systematic error
e	Error vector
e	Error
e^t	Thermal error
e_x, e_y, e_z	Linear displacement errors
$e_{\theta x}$, $e_{\theta y}$, $e_{\theta z}$	Angular displacement errors
F	Load vector
F	Force
F	(also) Radiation shape factor
F_{th}	Thermal loading
Fo	Fourier number
Gr	Grashof number
$G(s)$	Transfer function
g	Gravitational acceleration
g	Vector of gravitational acceleration
H	Homogeneous transformation matrix
$H(t)$	Heaviside unit step function
h	Heat transfer coefficient
h_0	Mean radial bearing clearance
I	Area moment of inertia
I_e	Electric Current
i, **j**, **k**	Unit vectors along x, y, z axes
K	Stiffness matrix
K	(also) Conductivity matrix
K	Temperature gradient
K	(also) Gain
k	Thermal conductivity
L	length
M	Mass matrix
M	(also) Thermal mass matrix
M	Moment
m	Mass

Nu	Nusselt number
n	Outward-normal coordinate
O	Origin
P	Net resultant axial force
Pr	Prandtl number
p	Axial load intensity
q	Vector of heat transfer rate
q	Heat transfer rate
q	(also) Transverse load intensity
R, **r**	Position vectors
Ra	Rayleigh number
Re	Reynolds number
R_e	Electric resistance
$\mathbf{r}_u$	Undeformed local position vector
$\mathbf{r}_f$	Deformation vector
r	Cylindrical coordinate
s	Curvilinear coordinate axis
T	Temperature vector
T	Temperature
T_∞	Environmental temperature
T'	Temperature difference (Excess temperature)
t	Time
t_D	Dead time
U	Deformation vector
U	Uncertainty
u, v, w	Displacements in x, y, z directions (or in r, θ, z directions)
V	Volume
V	(also) Shear force
v	State vector
v	Speed
w_0	Centroidal axial displacement
x	Input vector
x	Cartesian coordinate
x_{error}, y_{error}, z_{error}	Components of position error vector **e**
y	Output vector
y	Cartesian coordinate
y	(also) System output
z	Cartesian coordinate
z	(also) Cylindrical coordinate

Greek Letters

α	Thermal expansion coefficient
α_V	Volumetric thermal expansion coefficient
β	Thermal diffusivity
$\Delta\mathbf{r}$	Displacement vector

δ	Penetration depth
δ	(also) Uncertainty of nominal coefficient of expansion
δ_{th}	Thermal deformation
ε	Strain
$\Phi(t)$	State-transition matrix
ϕ	Phase lag
ϕ	(also) Slope angle
ϕ_τ	Torsional angle
ϕ_I	Inclinational angle
γ	Strain
η	Efficiency
κ	Boltzmann constant
λ	Forgetting factor
μ	Mean
μ	(also) Viscosity
ν	Poisson's ratio
ν	(also) Kinematic viscosity
Π	Dimensionless variable
θ	Cylindrical coordinate
θ_x, θ_y, θ_z	Rotations about x, y, z axes
ρ	Density
ρ	(also) Curvature
σ	Standard deviation
σ	(also) Stefan-Boltzmann constant
σ	(also) Normal stress
τ	Time constant
τ	(also) Shear stress
τ_f	Frictional torque
ω	Angular speed
ω	(also) Angular frequency
ω_n	Natural angular frequency
ζ	Damping factor

Chapter 1 Introduction

1.1 Machine Tool and Thermal Error

Machine tools, as essential elements of many manufacturing systems, play vital roles in manufacturing industries and make highly sophisticated machining operations possible in conventional shop floor environments. Increasingly, changes in the business requirements of manufacturing industries are driving machining systems to be more accurate and more productive. Many solutions of automated machining operations are available for higher productivity and machine tools are evolving to higher accuracy. A marriage of machine tools and metrology has been an outstanding technical breakthrough in achieving higher dimensional accuracy of machined parts. Machine tool metrology is concerned with assessment of the accuracy capability of machine tools, and errors of machine motion mechanisms can be evaluated and presented in a standardised metrological manner. Figure 1.1 shows trends in limiting values of tolerances in discrete-parts manufacturing industries, which produce individual products (Swyt, 1992).

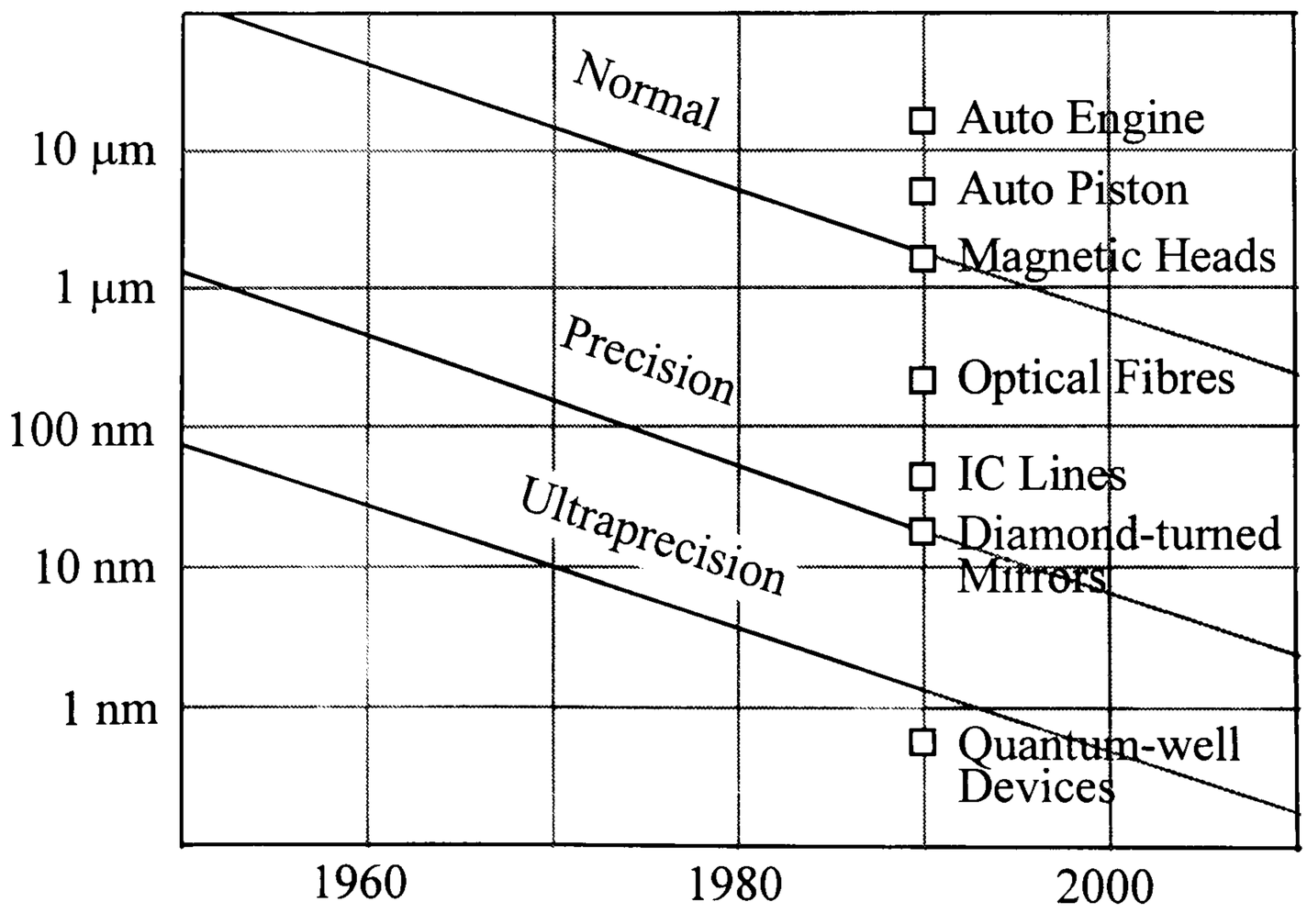

Figure 1.1 Trends in limiting values of tolerances

The overall trend to tighter manufacturing tolerances affects each of these three regimes, normal, precision and ultraprecision, as shown in the figure. According to Swyt (1992), the three regimes are defined such that:

- *Normal machining*, as done by conventional machine tools, verified by coordinate measuring machines, and used to manufacture products such as aircraft and automobiles.
- *Precision machining*, as done by diamond turning machines, measured by special laser interferometer systems, and used to manufacture products such as optical discs and X-ray mirrors.
- *Ultraprecision machining*, as done by various types of atom, ion, electron, optical-photon, and X-ray systems, measured by electron and tunnelling microscopy, and used to produce structures such as micro- and nano-electronic devices.

The general trend corresponds to roughly factor-of-three decreases in the size of tolerances every ten years. It can be considered that errors of machine tools have been reduced according to those trends and will continue to. Of those, errors caused by thermal deformations of machine structures account for as much as 70 % of workpiece inaccuracy (Bryan, 1990) and are the most difficult hurdle in achieving higher accuracy nowadays. Others are errors due to geometric inaccuracy of machine components, errors due to low static and dynamic stiffness of machine structures, tool wear, etc. All of them are well known to industry people as well as academic people, and can be controlled in an intended way in design stages. Various kinds of errors of machine tools will be dealt with in the next chapter.

Any dimensional change of machine structures due to thermal disturbances causes machined parts to deviate from intended dimensions. Moreover such thermal deformations often turn out to exhibit complex mechanical behaviours that are exhibited in unpredictable ways. The complex, unpredictable thermal deformations arise from a) continuously changing machine operating conditions, b) various kinds of heat sources around a machine, and c) complicated machine structure.

1.2 Literature Review of Thermal Error Research

In the early stage of thermal error research most of the work devoted to problems in dimensional metrology used a defined temperature point 20°C as a standard for measurements. A simple view of thermal errors would be to consider results from linear expansion or contraction of machine members, which involve a certain uniform temperature increase or decrease within the body of a machine member, the thermal expansion coefficients of materials used and the length of the member.

Bryan (1990) published a dedicated status report on thermal error research and classified that problem as the effects of uniform temperatures other than 20°C. In the first part of the report, he pointed out that the situation in industry, in connection with thermal problems, had changed very little since his first survey in 1967. He also gave a comprehensive diagram showing thermal effects on machine tools and coordinate

measuring machines, as shown in Figure 1.2. According to Bryan's survey, identification of the effects of uniform temperatures other than 20°C dated back to 1920; Peters and Boyd (1920) identified that it was necessary to consider thermal expansion of gauges together with the uncertainty of thermal expansion coefficients of the material for high accuracy measurement. Weck *et al*. (1995) also made a survey particularly on reduction and compensation of thermal errors in machine tools.

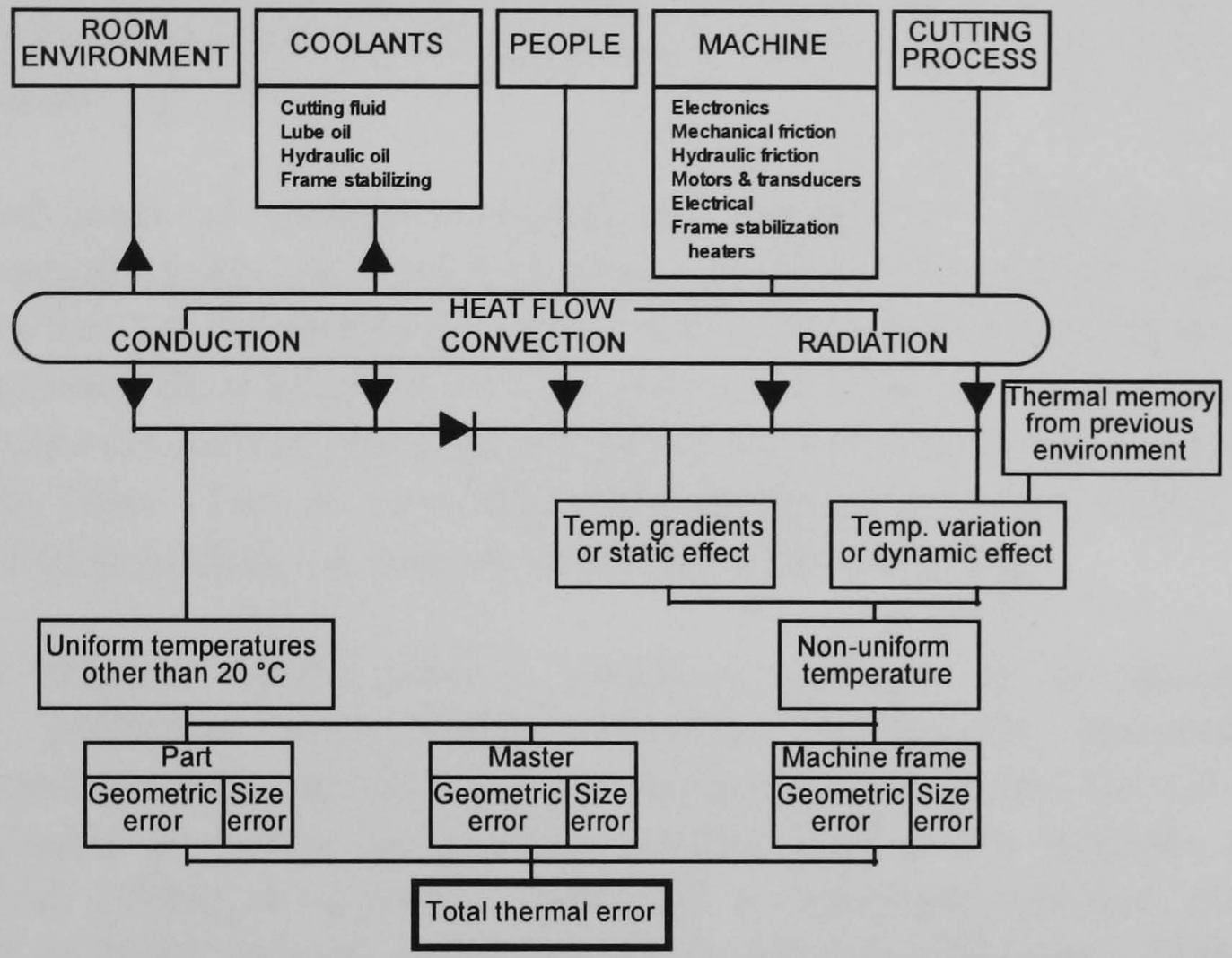

Figure 1.2 Thermal effects diagram

ANSI Standard B-89.6.2 (1973) was published to express measures of the effects of deviation from the standard temperature and nominal expansion coefficients as a consequence of the research efforts. In the meantime commercial applications of such research results have appeared. The idea of the commercial applications was based on the fact that that thermal errors due to uniform temperatures other than 20°C could be analysed and compensated by accurate measurements of temperature distribution in machine tools and coordinate measuring machines or reduced by temperature-controlled fluid showers or temperature-controlled enclosures. For example, many modern coordinate measuring machines are equipped with software error correction functions for differential expansion between parts and masters (Chou and DeBra, 1990; Breyer and Pressel, 1991). As a passive alternative, low expansion materials are widely used in machine structures nowadays (Youden, 1990).

Owing to these effective means we can deal with thermal errors due to uniform deviations from 20°C effectively. However the uncertainties of thermal expansion coefficients are still difficult to overcome. These degrade the quality of compensation action directly because we often do not know the exact values of thermal expansion coefficients. In relation to the determination of thermal expansion coefficients, Berthold and Jacobs (1976) presented a sophisticated optical system for ultraprecise measurement

of very low thermal expansion and an optical fibre interferometer was devised to measure thermal deformation by Kimura *et al.* (1991).

With an accumulation of the knowledge of the effects of uniform temperatures other than 20°C, researchers tried to work out those of non-uniform temperatures, which were further classified into static effects due to temperature gradients and dynamic effects due to temperature variations according to Bryan (1990). Steady-state temperature gradients are usual phenomena occurring in a typical industrial building. Vertical temperature gradients within the air may be 1°C per metre or greater, due to the tendency of air to stratify (Wasson *et al.*, 1993a).

Owing to advances of numerical techniques, research into thermal errors due to temperature gradients has made good progress. Weck and Zangs (1975) mentioned that calculation of thermal deformations would make an important contribution to increasing the work accuracy of a machine tool if more experience was gained in considering cumbersome factors such as geometric simplification, thermal and mechanical boundary conditions in finite element modelling. Venugopal and Barash (1986) verified the usefulness of finite element techniques in thermal error modelling.

Trapet and Waldele (1989) made a major contribution to an understanding of temperature gradients. They showed excellent agreements between analytical calculations and measured actual errors by employing a special box around a measuring machine in order to induce temperature gradients within the machine deliberately. Balsamo *et al.* (1990) developed a model for a measuring machine, which used a combination of finite element and black box empirical techniques. Under relatively large temperature gradients for experimental purposes, the results showed that 80 to 85 % of the deformations could be explained by the model. They also implemented automatic corrections to compensate for thermal errors.

Breyer and Pressel (1991) reported a radical development in coordinate measuring machine structures. They devised ceramic-coated aluminium beams for slideways. The high conductivity of aluminium minimises the temperature gradient between the top and bottom of the beam, which in turn minimises bending deformation. Wasson *et al.* (1993a) studied analytically the straightness errors of rectangular beams under ambient air temperature gradients and found layers of insulating materials that isolated beams from the surrounding air could be used to substantially reduce the thermal deflections.

The problem of temperature variations (or dynamic effects) is much more complicated than those of uniform temperatures other than 20°C and static temperature gradients, because they have time as well as spatial dependency. In a real situation, it is often necessary to deal with time-varying (or dynamic) temperature effects due to rapidly changing machine operating conditions and usually uncontrolled shop floor environments. According to Bryan (1990), there are no obvious means to determine the sensitivity of a machine to temperature variations before it has been built and tested.

Grand (1952, 1955) identified the frequency of temperature variations affecting dimensional measurements. As many dynamic systems have certain frequency response

characteristics, thermal systems also reveal a distinctive response to a particular frequency at which temperature varies. An analytical method on thermal growth of aerostatic spindles was developed by Baker and Hornung (1970) for steady-state conditions. They predicted the maximum growth of an aerostatic spindle over a range of spindle speeds due to the friction in aerostatic bearings that increases with spindle speeds.

Spur and De Haas (1973) applied the concept of the time-constant to spindle thermal growth problems. They introduced cooling systems as an effective means to diminish the inertia temperature of components of a machine governed by the time constant. Thermal behaviour around fixed joints is a difficult-to-analyse subject but Attia and Kops (1978, 1979a, 1979b) presented several papers on thermal deformations around them. Fixed joints in machine tools were considered to introduce a closed-loop interaction between the contact pressure distribution along the joint, the thermal field in both structural elements in contact and the deformation of these elements.

Teeuwsen *et al.* (1989) explored empirical thermal model approaches, as a more effective means to numerical and analytical techniques. Measured errors were fitted numerically to piecewise polynomials and error correction using the fitted polynomials proved to be effective. Bryan (1990) reported some poor results from finite element calculations applied to prediction of thermal deformations of a sphere as an indication of some drawbacks of theoretical approaches. Moriwaki *et al.* (1990) carried out numerical and experimental investigations into the effects of cutting heat in ultraprecision diamond turning. They estimated the temperature rise of a tool and workpiece employing a finite element technique based on measured cutting forces. The temperature rise of workpieces was relatively low (less than 1°C) as compared with that of tools (more than 10°C). The machining error due to the temperature rise reached the order of a few micrometers.

The influence of fluctuating ambient temperature to machine tool structures was investigated analytically and experimentally by Tanabe and Takada (1991, 1994). Under conditions of fluctuating ambient temperature, the thermal deformation of a concrete bed was about half of that of a cast iron bed. Due to the small thermal conductivity of concrete (1.2 W/m·K), the concrete bed experienced ambient temperature variations only at the surface layer. Moriwaki *et al.* (1991) also studied the effects of environmental temperature changes on the thermal deformation of a machining centre. The surface temperature of a machining centre followed the ambient air temperature with a time delay of 2 to 3 hours, but the amplitude of temperature change was slightly smaller than that of the ambient air. Stein and Tu (1991) proposed a semi-empirical state-space model for the heat generation of a machine tool spindle. The model estimated the dynamic as well as static thermally induced bearing preload, which is usually several thousand Newtons, of different spindle bearing systems for a wide speed range over 10,000 rpm.

Mishima *et al.* (1993) developed a thermo-hydrodynamic analysis method for aerostatic bearings and used it for evaluating thermal deformations of an aerostatic spindle. They could present time history of thermal growth under various spindle rotational speeds. A

model for heat generation due to mechanical friction was studied by Schulz and Schmitt (1994), which could give a basis for prediction of the amount of heat generated during machining. Weck and Schroeder (1994) worked out the problem of thermal expansion of a tool and workpiece and proposed an active tool-cooling system using Peltier elements attached to a tool. A thermal modelling method for diamond cutting was presented by Balkrishna *et al.* (1995) who tried to establish a method of determination of temperature distribution in the micro-domain.

Machine manufacturers tried to reduce thermal errors by incorporating temperature control or cooling systems into their machines. Though temperature control of machine structures seems to be an obvious, easy choice, the high cost prohibits them from applying that method. With needs of unconventional, high precision and sophisticated fabricating machines, some machines are now equipped with precise temperature controllers using oil showers or oil cooling techniques for the stabilisation of machine frames (Bryan, 1979a).

Many compensation techniques have been explored to reduce thermal errors in a direct or indirect way. Direct compensation techniques, simple yet efficient methods, make use of directly measured data of displacements between a tool and a workpiece. Process-intermittent probing units for relocating the origin of a machine are readily available to minimise thermal drifts of machine tools cost-effectively. However the measurements of thermal drifts are not always possible during machining using the units. Most research efforts have been directed towards indirect methods that employ a deformation model, which is often based on temperature distribution measurements and on models correlating temperature distribution to deformation.

Calibration methods of thermal errors were summarised by Tlusty and Mutch (1973). Moriwaki (1988) developed a hydrostatic spindle incorporating real-time thermal growth compensation using an analytical model of the spindle and temperature measurements. The correction was made by a tool post equipped with a micro-positioning mechanism using a piezoelectric actuator and the method proved to be effective in controlling spindle-tool relative displacements within less than 1 μm. Marshall and Hardwick (1989) regarded a machine tool as being composed of zones, which expand (or contract) with temperature. By using linear regression analysis, they tried to find the distortion algorithm, based on the measurement data, which represents the thermal deformation of critical zones that contribute significantly to the total thermal error. The work had indicated that potential improvements in workpiece accuracy of up to five times can be realised. Balsamo *et al.* (1990), using a semi-empirical model incorporating basic finite element codes on a coordinate measuring machine, corrected up to 65 % of thermal deformations and argued that compensation techniques must not be considered as an alternative to design improvements and thermal stabilisation of a machining system by the circulation of fluids or air-conditioning.

Chen *et al.* (1993) used an empirical model approach in order to compensate thermal errors in real time on a machining centre. They used 32 geometric and thermal error components to model the spatial- and time-variant volumetric errors of a machining centre. Of those, 11 thermal error components were estimated in real time using the

measured temperatures of a machine. The estimation was based on pre-established empirical models obtained from a multiple regression method using polynomials. This scheme was implemented on a horizontal machining centre and was shown to improve the machine accuracy by an order of magnitude.

A finite element model approach was applied to real-time compensation of thermal deformation of a planar step motor by Ish-Shalom and Wasfy (1994). An improvement of a factor of five was achieved in the positioning accuracy by compensating the thermal deformation based on the model. Hatamura *et al.* (1993) applied active compensation of thermal distortion to development of an intelligent machining centre. By controlling heaters and coolers on the column of the machine, they could compensate the distortion of the spindle within approximately 10 μm.

Mou and Liu (1993) presented an adaptive methodology for evaluating thermal errors using a state-space approach. Constructing multivariable state observers to track thermal effects in real time, they demonstrated a method of how to update thermal error models in real-time with least possible measurements during machine running conditions. A fuzzy-logic based neural network was successfully applied for the learning control of thermal errors (Srinivasa and Ziegert, 1993). Chen (1995) developed an online compensation scheme for dynamic thermal errors by using an artificial neural network model. The compensation scheme had been proven to improve the machine accuracy by an order of magnitude with the offline calibration of stationary geometric errors. Srinivasa *et al.* (1996) applied a laser ball bar to evaluation of spindle thermal drifts. The developed method required only a single experimental set-up for obtaining the thermally induced error map of a machine tool in contrast with conventional measurement methods measuring each error component one at a time. Allen *et al.* (1996) made a distinction between the temperature model and deformation model of a thermally affecting machine, and used a thermal imaging camera in order to identify problematic parts in a machine easily and establish the temperature models quickly. Recently a comprehensive survey paper on compensation techniques was given by Sartori and Zhang (1995).

As a design technique, Sata *et al.* (1973) developed a general computer program for the design and analysis of machine tool structures that could analyse and optimise thermal deformations. Also, a method of identifying the intensity of heat sources from temperature measurement was developed by modifying heat conduction equations based on finite element methods. They controlled either additional heat sources or spindle speed to reduce the change of temperature and deformation of machine tools. Spur *et al.* (1988) used non-metallic engineering materials, such as ceramics and fibre-reinforced plastics, to build experimental spindle units. They found that fibre-reinforced plastics deform much less than ceramics.

Yurin (1990) developed a computerised method of the earliest design stage of machine tool components with thermal analysis based on many years of experience. He suggested a knowledge-based expert system in dealing with thermal errors for designers. Jedrzejewski and Modrzycki (1992) presented a method of evaluating thermal deformations using operational conditions of a machine tool based on a finite element

technique. The method incorporated the automatic determination of power losses as a function of operating conditions and automatic division of heat flow in machine joints. Thermal performance evaluation was carried out for a water hydrostatic bearing using computational-fluid-dynamics codes by Wasson *et al.* (1993b). They showed that the use of materials with low thermal conductivities and low thermal expansion coefficients appeared to minimise the overall thermal growth errors in hydrostatic bearings.

This review reveals complexities inherent in thermal error problems, i.e. thermal errors are dependent on so many variables that are also related to each other intimately. Numerical techniques and error measurements in real machines seem to be the most effective tools to the problems in a case-by-case basis. It is obvious that a lot of confusion is present in expressing and interpreting thermal errors in industry and academic areas, partly from the lack of the knowledge that must be simple, unified and understandable and, in turn, partly from the absence of documentary standards for the evaluation of all kinds of thermal errors. In order to boost achievement of higher accuracy, it is necessary to devise a simply understandable, unified approach incorporating the basics of machine tool metrology.

1.3 Objectives of This Work

An underlying fundamental philosophy of this work is to describe engineering knowledge in a simple and easily understandable way so that every participant to a problem, having various levels of knowledge, can all actively talk to each other using a common language and conception of that problem, resulting in a cohesive solution. In that sense, this work encompasses the following disciplines:

- *Modelling*: In most cases, thermal errors of machine tools are not direct effects from simple elongation or contraction of thermally affected machine components. It is more likely that the overall thermal behaviour of a machine is complicated by the interactions of many components having different time-dependent characteristics, resulting in time-varying (or dynamic) thermal errors. It is believed that several parameters act upon thermal responses of a machine. Such parameters can serve as a measure of how things will occur and model of time-varying thermal errors. In order to obtain a detailed picture of the thermo-mechanical behaviour of machine components, it is necessary to detect such parameters and present them in a simple yet systematic manner.

- *Evaluation*: Having found these parameters, it is intended next to investigate evaluation methods of the parameters. Some would be envisaged during the course of prior background work. This study intends to demonstrate how to evaluate the governing parameters of thermal errors both analytically and empirically. If both of the analytic and empirical evaluation methods prove to be effective in identifying thermal characteristics of a machine tool, parameters detected will have a compatibility throughout theoretical and experimental studies, providing a unified background. That is, purely experimental or purely theoretical parameters are avoided in this study.

- *Design Methods*: A thorough understanding usually brings forth prediction ability. It is possible to predict thermal behaviour of a machine in an early design stage by assessing system parameters of the machine, which govern the thermal responses under given temperature conditions, so that a more forgiving machine in response to thermal disturbances can be realised. Due to the limited mechanical adaptability of machine components towards an ideal performance, the methods are likely to have limited, though, valuable application. It is, however, a firm belief in precision engineering that precision should be attained by a mechanical assembly as a whole rather than by other means, for example, by error detection and control actions. However, the knowledge obtained can be applied to a compensation stage for the further improvement of machine accuracy.

The literature review identified that the effects of temperature variations were difficult to understand and that only a few studies had been made in the field of design methods to reduce the thermal sensitivity of machines. In order to envisage thermal responses of machine components clearly in engineers' minds, a simple yet unified modelling method is required. The investigations will assist the designer to minimise the effects of temperature variations, resulting in machines of reduced thermal sensitivity. In-depth investigations of the interactions of time-dependent thermal responses of different machine components were shown to be a key subject of this study.

Chapter 2
Machine Tool Metrology and Errors

2.1 Accuracy of Machine Tools

Machine tools produce three dimensional machined objects that are subject to many dimensional requirements, such as dimensional tolerances, geometrical tolerances and specified surface finishes. In turn, the dimensional integrity of these objects is verified by instruments, such as micrometers, CMMs, surface roughness testers, etc., as shown in Figure 2.1. Machine tools themselves are calibrated by laser interferometers, electronic levels, precision squares, ball bars, etc., as covered by the national or international standards. Therefore, the fundamentals of machine tool accuracy can be found in the field of dimensional metrology. Dimensional measurements are considered to be the determination of the size of an object while displacement measurements imply measuring the movement of a point from one position to another. The accuracy of a machine tool is dependent on its displacement-measuring ability, and on the builders' ability to assess dimensional and displacement measurements. Strictly, accuracy is the deviation of a measured value from a true value, which is not determinable, but in metrological terms, is often defined as the estimate of the degree to which measurements are free from systematic error.

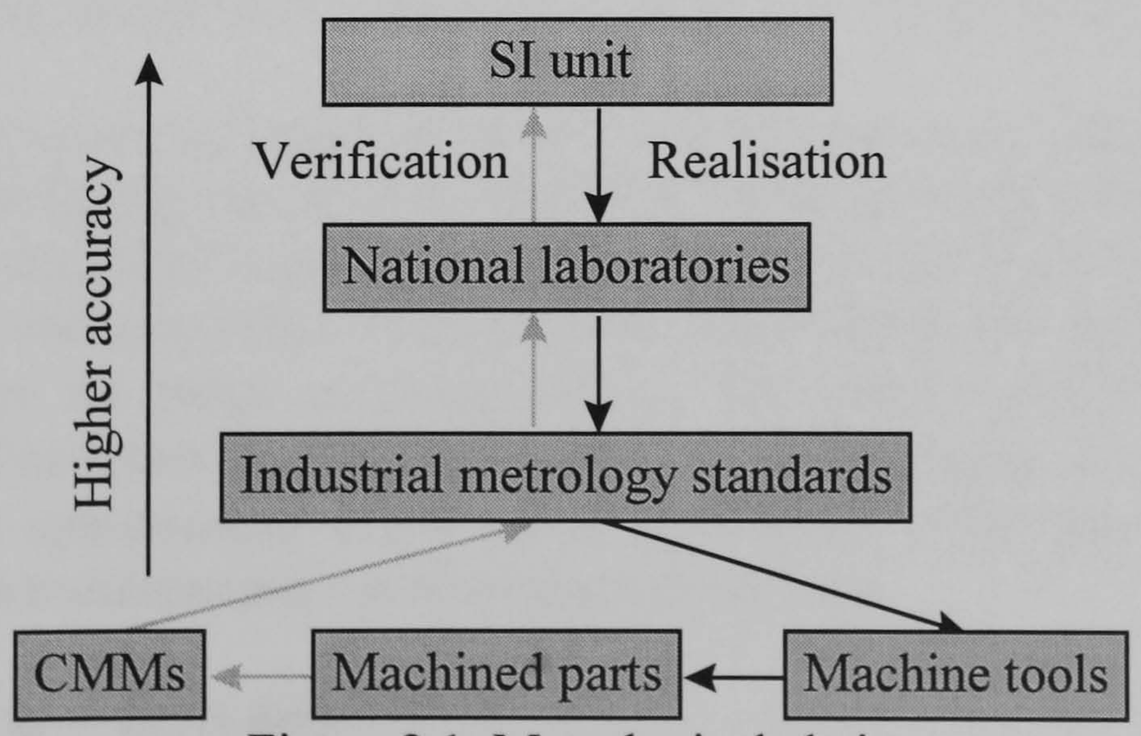

Figure 2.1 Metrological chain

Accuracy is often represented by the term systematic error (Swyt, 1991). A systematic error is drawn from a sample of tests by applying a Gaussian statistical distribution. Systematic errors have a repeatable value and sign at a given position and under given conditions. Precision or repeatability denotes a measure of the scatter of results obtained if an attempt is made to exactly repeat a given operation. Precision is conventionally represented numerically in terms of a standard deviation (Swyt, 1991). The metrological term for a combined measure of precision and accuracy is uncertainty, which means the amount by which a measured value disagrees with the true value (ISO, 1993). The term error is considered to be the difference between the estimated true value and value found by a measurement while the collection of all possible measurement errors is described by the measurement uncertainty (Phillips, 1995).

In many situations, we may not have a known value with which to compare instrument readings or machine positions, and yet we may feel fairly confident that the instrument or machine is within a plus or minus range of the true value. In such cases, we say that the plus or minus range expresses the uncertainty of the instrument readings or machine positions. Machine tool accuracy is sometimes represented by the maximum translational or rotational error between any two points in a machine's work volume as a peak-to-valley value. In this case, the accuracy is considered to represent approximately twice the positioning uncertainty.

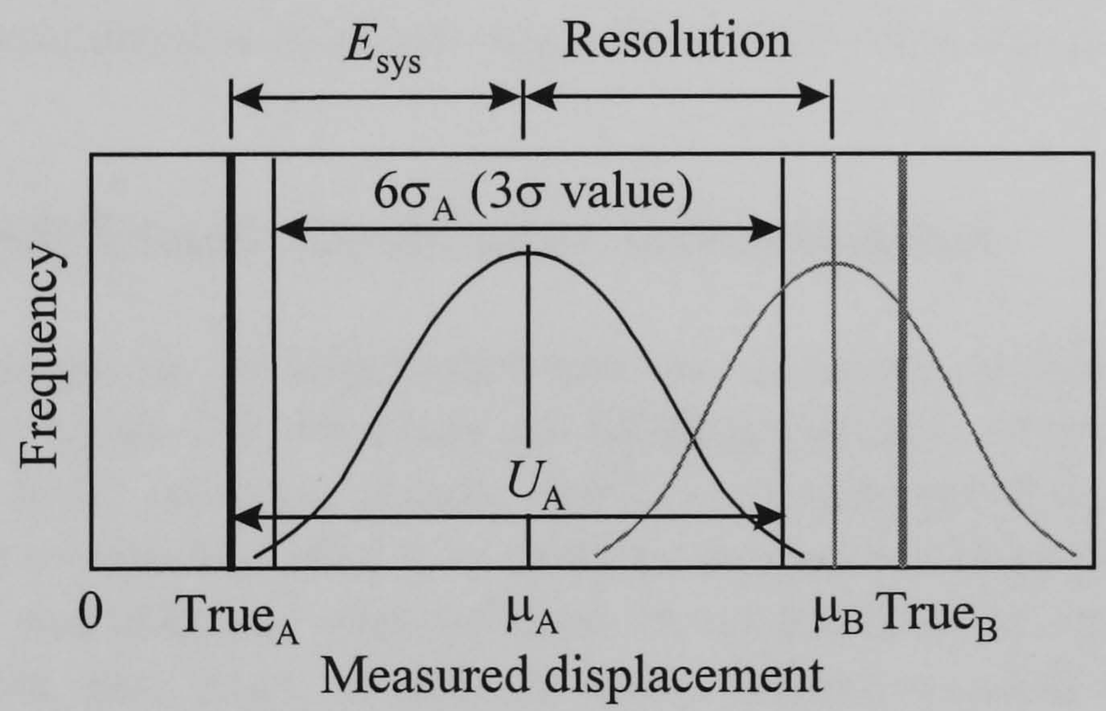

Figure 2.2 Frequency of occurrences of measurement data A and B
(E_{sys} = Systematic error, σ = Standard deviation, U = Uncertainty, μ = Mean)

In Figure 2.2, two sets of measurement data, obtained by moving a target with respect to a displacement measuring sensor and collected at the same position for each of the sets, are depicted in a statistical manner by counting the frequency of occurrences of a value in a large pool of measured data. The resolution of an instrument is the least detectable difference between the mean values μ_A and μ_B. The same is true for machine tools. Three-times or four-times standard deviation is usually taken for the precision or repeatability of a measurement and is called a 3σ or 4σ value respectively. Then the uncertainty U of a measurement can be expressed such that

$$U = E_{sys} + 3\sigma \text{ (or } U = E_{sys} + 4\sigma) \tag{2.1}$$

where E_{sys} is a systematic error; σ is a standard deviation. Each measured displacement $d_{measured}$ has the following relationship with the true displacement d_{true}:

$$d_{measured} = d_{true} \pm U \tag{2.2}$$

The positioning accuracy (in this case, uncertainty) of one axis of a machine tool often takes the following form (NMTBA, 1972; CIRP STC <<Me>> Working Party on 3DU, 1978):

$$U = A + B \times d$$

where A is a basis value for the accuracy for a specified distance; B is an additional allowance per additional unit length. The reason for using the above format is that the control system will generally function equally well at any point and that the accuracy of the machine's master measure is generally a direct function of length. In order to take account of thermal effects, the evaluation of the accuracy should be carried out for several different thermal states of a machine.

A high precision machine has very small uncertainties in positioning and that is the machine builder's prime objective. Ultraprecision machine tools have extremely small uncertainties in their positioning function so that collaborative efforts between builders and measurement accreditation standards organisations are often required.

2.2 Machine Tool Errors: Descriptive Interpretation

Machine tool structures can be subdivided into two elements: members and joints, as pictorially shown in Figure 2.3. Members are building elements of machine tools, such as carriage bodies, beds, columns, spindle shafts, etc. Joints provide two functions: a) for holding together component parts of a structure that are too large or too complex for the cost effective manufacture, manipulation or installation in one piece, and b) connecting two parts that must be able to move relative to each other due to the operational requirements of a machine.

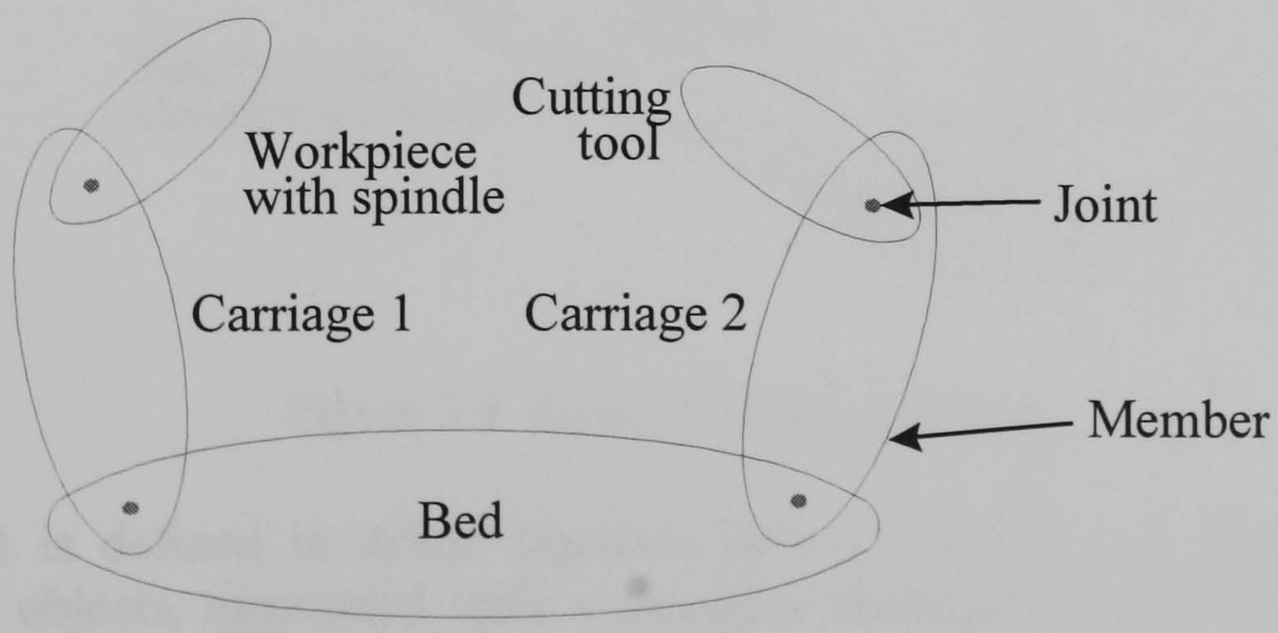

Figure 2.3 Conceptual structure of machine tool

The former is referred to as fixed joints that are usually held together under pressure by force exerted by bolts, studs, etc. Fixed joints are related with errors caused by stresses generated internally to a machine during assembly. The latter are regarded as sliding joints that are connected by anti-friction bearings, fluid films between sliding faces, etc. A sliding joint is often constrained in only one direction and motions in other directions generate errors. Depending on the machine structure, sliding joints are often the most compliant part of structures and thus lumping machine errors at sliding joint interfaces is likely to be an easy method to analyse the accuracy of machine tools.

Figure 2.4 shows errors occurring in a linear carriage, as an example. The coordinate system suffix 0 is a stationary global reference frame usually referenced to the bed of a machine for the analysis of machine error motions. The coordinate system suffix 1 is a moving reference frame attached to the carriage, where origin is often assigned to an important functional point. All error motions are measured with respect to the global reference frame. The function of the linear carriage is strict linear translation in the x direction, but due to the various kinds of parasitic motion in other directions and thermal drift, errors will occur under internal and external disturbances. Error motions are usually identified as (Hocken, 1980, pp. 8-37):

- Linear displacement error in the x direction, e_x, called positioning error
- Linear displacement error in the y direction, e_y, called vertical straightness error
- Linear displacement error in the z direction, e_z, called horizontal straightness error
- Angular displacement error about the x axis, $e_{\theta x}$, called roll
- Angular displacement error about the y axis, $e_{\theta y}$, called yaw
- Angular displacement error about the z axis, $e_{\theta z}$, called pitch

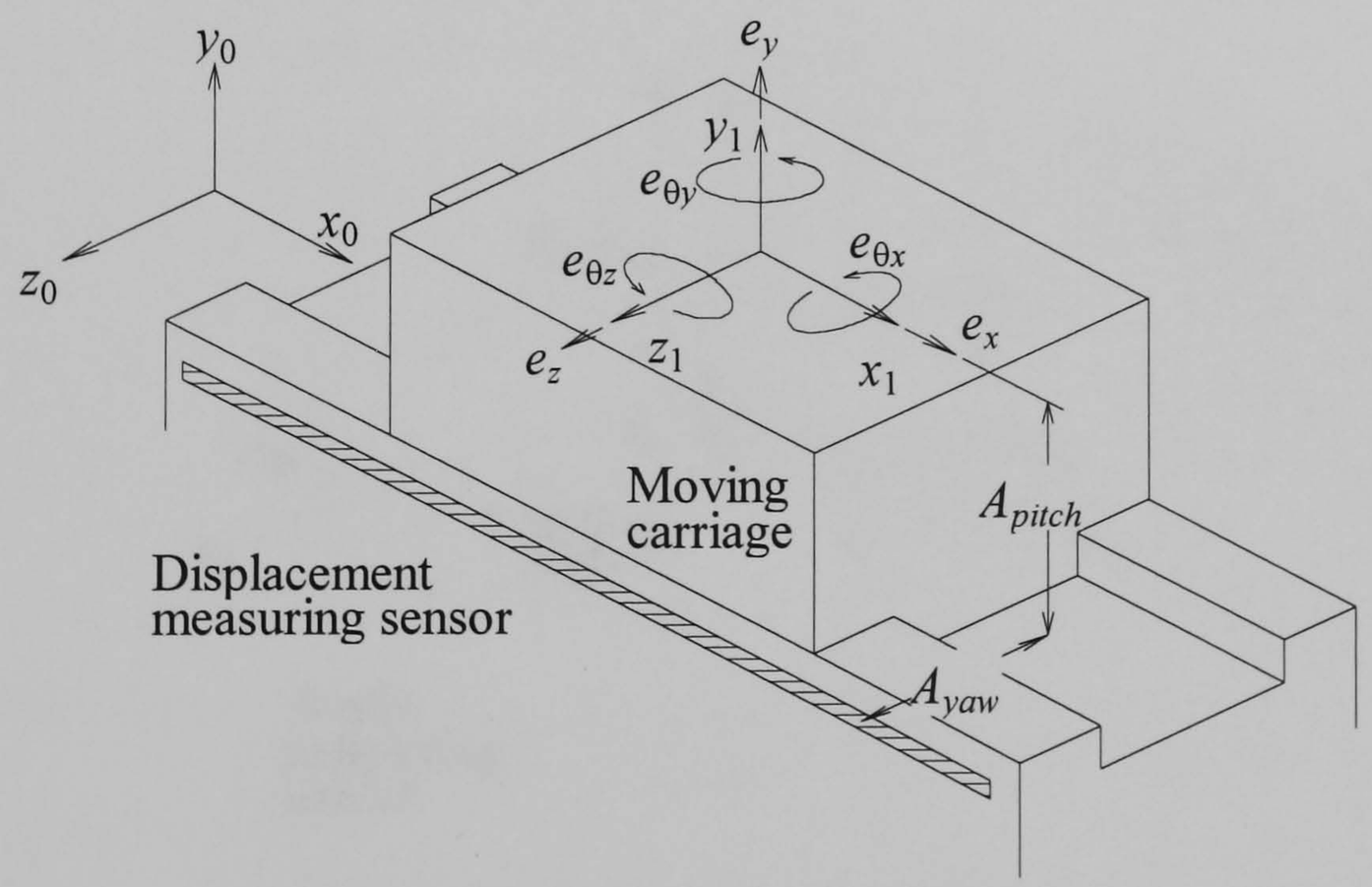

Figure 2.4 Errors in linear carriage

Thermal drift is defined in ANSI Standard B89.6.2 (1973) as a changing distance between two objects, associated with a changing temperature distribution within the structural loop due to internal and external heat sources.

The most important effect of angular displacement errors is the Abbé errors. The Abbé principle was proposed in generalised form by Bryan (1979b) as follows:

"The displacement measuring system should be in line with the functional point whose displacement is to be measured. If this is not possible, either the slideways that transfer the displacement must be free of angular motion or angular motion data must be used to calculate the consequences of the offset."

Hence, departures from the Abbé principle bring forth linear displacement errors due to the presence of angular displacement errors of a carriage. They are called the Abbé errors, which are a function of both angular displacement errors and a distance between the line of action of the functional point of a carriage and the line of the action of a measuring sensor. The latter dimension is referred to as the Abbé offset, i.e. A_{pitch} and A_{yaw} in Figure 2.4. The Abbé errors due to pitch and yaw generate errors in the x direction while the pitch and yaw also produce errors in the y and z direction respectively, but they are not the Abbé errors, and might be neglected in approximate prediction of the accuracy of a machine tool as they are of second order (Wills-Moren, 1993). Errors due to roll occur in a plane normal to the direction of motion, i.e. y direction and z direction in Figure 2.4. In such cases offset distances are in no way related to the Abbé offset, and they are referred to as roll arms.

In the case of a rotating body, as shown in Figure 2.5, an axis of rotation z_1 revolves around an axis of the stationary global reference coordinate system 0 with radial errors e_x and e_y, an axial error e_z, and tilt errors $e_{\theta x}$ and $e_{\theta y}$. The axis of rotation is a line about which the rotation occurs. If the rotating body is a rotary table, the angular error $e_{\theta z}$ due to a servomechanism should be considered, but for a spindle it is not necessary.

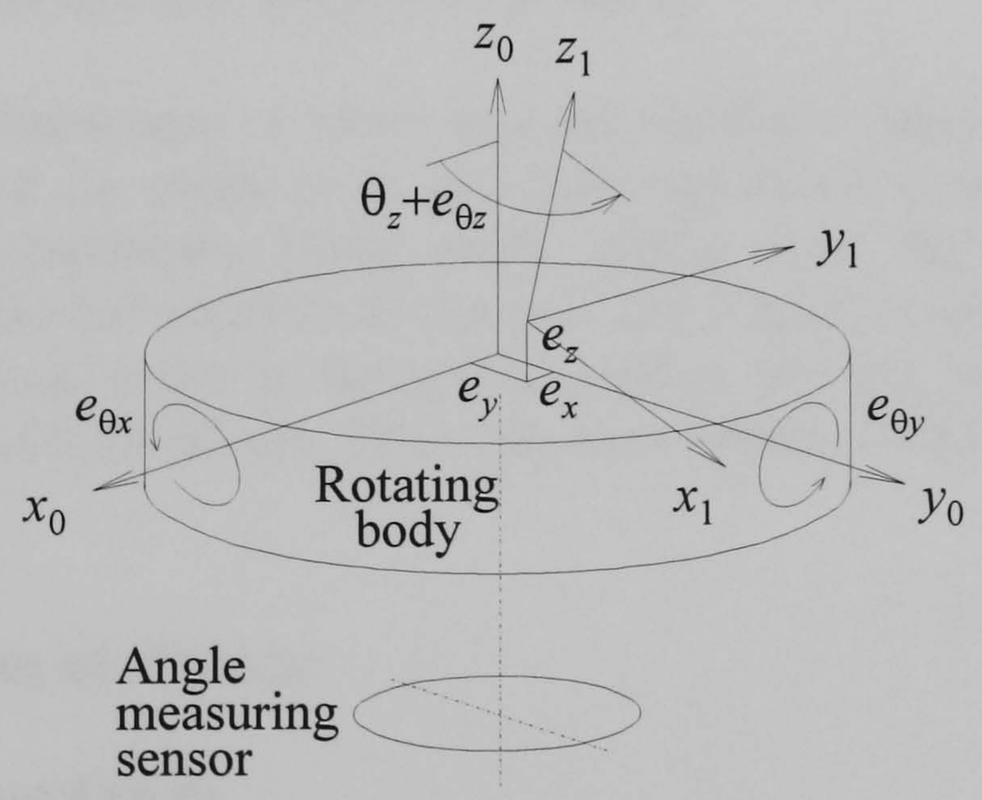

Figure 2.5 Errors occurring in a rotating body

The vector sum of e_x and e_y could be used for the error motion in a particular direction. The normally measured face motion would be the sum of three components: e_z, x roll arm multiplied by $e_{\theta y}$ and y roll arm multiplied by $e_{\theta x}$. A similar intuitive understanding can be obtained for rotary tables as done for linear carriages. Radial errors result in

errors in the x and y directions, and an axial error in the z direction with respect to the global reference frame. Errors due to tilt and associated roll-arms affect errors in the x and y directions. Errors due to the measuring sensors and servomechanisms generate errors in the x and y directions.

The axis of rotation errors of a spindle are of prime importance in machine tools. ANSI standard B89.3.4M (1985) provides a good guide to the description and measurement on the axis of rotation errors. The term error motion is defined as changes in position, relative to the reference coordinate axes, of the surface of a perfect workpiece with its centre line coincident with the axis of rotation. A perfect workpiece is a rigid body having a perfect surface of revolution about a centre line. The standard defines the following specific types of error motion; Radial motion is error motion in the direction normal to the z reference axis (z_0 axis in Figure 2.5) and at a specified axial location, axial motion is error motion co-linear with the z reference axis, face motion is error motion parallel to the z reference axis at a specified radial location, and tilt motion is error motion in an angular direction relative to the z reference axis.

The axis of rotation errors can be thought of as motions, through space, of the instantaneous axis of rotation about the average axis of rotation. In contrast, spindle thermal drifts can be thought of as a motion through space of the average, or nominal, axis of rotation caused by thermally induced deformations of spindle components and support structure (Srinivasa *et al.*, 1996). These thermal drifts have also five degree-of-freedom of motion, but they are not associated with the rotation of a spindle. Thermal drifts are motions of the average axis of rotation over time. Small cyclic thermal disturbances are dampened out during developing their temperature fields in machine structures due to attenuating effects caused by the large thermal mass. In the case of ultraprecision machines, however, that small cyclic variations of thermal drift could affect severely the dimensional integrity of products.

When two or more linear axes or rotary axes are combined, other geometric parameters should be considered, i.e. errors in an axis trajectory that are caused by misaligned or improperly sized components. These errors, arising from the combination of axes, include: orthogonality and parallelism of axes with respect to their ideal locations and each other; translational errors in the spatial position of axes; incorrect dimensions of the axis components (Wills-Moren, 1993; Shen and Duffie, 1993).

2.3 Classification of Errors

2.3.1 Time-invariant Errors

Errors arising in machine tools will, in general, be dependent on the position of moving components and time. Some errors can be considered a function of the position of axes only:

$$e = f(\text{position})$$

This type of error will be referred to as time-invariant; examples of time-invariant errors are:

- *Geometric errors*. Geometric errors are considered rigid body motions caused by inaccurate machine components and imperfect alignment of machine axes. Factors affecting geometric errors are dimensional accuracy, surface straightness, surface roughness, geometrical imperfections, assembly methods and design principles employed. Figure 2.6 shows an example of a kinematically designed slideway that reveals high repeatability. The linear carriage is supported by three balls that constrain its five degrees of freedom, of which directions are all directly related with error motions.

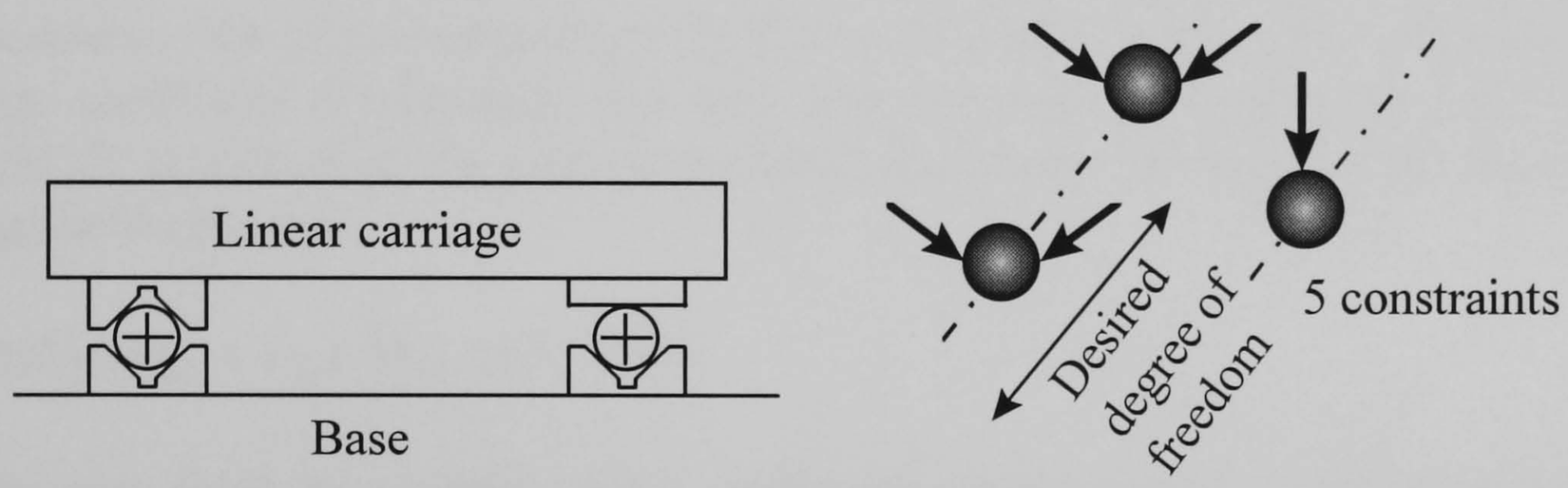

Figure 2.6 Kinematically designed slideway

- *Errors due to finite static stiffness of machine structures.* Finite static stiffness of machine structures often causes angular error motions due to bending of machine components. Heavy machine components and workpieces, large cutting forces, and fast accelerations of a carriage are responsible for the errors. In addition, during machine assembly errors can be induced from: Forced geometric congruence between moving parts; the effect of an assembly process on the stiffness of a structure itself; the deformation of a machine when force is applied to preload bearings and bolts. Furthermore, errors may also be caused by clamping or locking mechanisms. Installation methods also affect accuracy of a machine tool (Slocum, 1992, pp. 80-84).

- *Errors due to uniform deviations from 20 ℃ and steady-state temperature gradients.* Uniform temperature deviations from 20 °C cause machine components to expand or contract to a certain amount in a linear or angular direction depending on their mechanical constraints. Steady-state temperature gradients force machine members to bend. The results are errors in machine motions due to deformations of machine structures. Thermal errors are particularly bothersome because they often cause angular error motions that lead to the Abbé errors. Very smooth ultraprecision motions can be obtained using flexural bearings as depicted in Figure 2.7, which are employed in many instruments and semiconductor processing equipment. However, due to the large exposed surface area of flexures, the motion accuracy of carriages using flexural bearings is vulnerable to temperature changes. Also only relatively low displacements are possible.

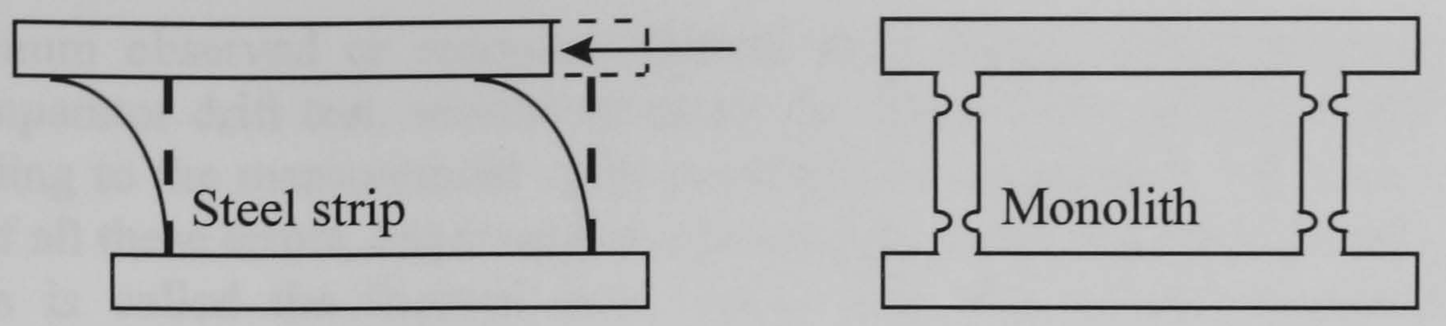

Figure 2.7 Two forms of flexural bearings

The thermal error index defined in ANSI Standard B89.6.2 (1973) gives a measure of the overall vulnerability of a part and master to temperature changes to other than 20°C. It has the desirable feature of taking account of differential response and uncertainties in the coefficient of thermal expansion. While the true coefficient of expansion α at a temperature of a body is the rate of change of length of the body with respect to temperature at the given temperature divided by the length at the given temperature, the average coefficient of expansion of a body over the range of temperature from 20°C to T, $\alpha(20,T)$, is defined as the ratio of the fractional change of length of the body to the change in temperature:

$$\alpha(20,T) = (L_T - L_{20}) / \left[L_{20} \times (T - 20)\right]$$

On the other hand, the estimate of the coefficient of expansion of a body shall be called the nominal coefficient of expansion α_{nom}. Then the maximum possible percentage difference between the true coefficient of expansion α and the nominal coefficient of expansion is called uncertainty of nominal coefficient of expansion δ:

$$\delta = 100\left(\alpha - \alpha_{nom}\right) / \alpha \ \%$$

This value, like that of α_{nom} itself, must be an estimate. The nominal differential expansion NDE, which is the difference between the nominal expansion of the part and of the master, is

$$\mathrm{NDE} = \mathrm{NE}_{part} - \mathrm{NE}_{master}$$

where the nominal expansion NE, which is the estimate of the expansion of an object from 20°C to its time-mean temperature, is $\alpha_{nom} \times L \times (T - 20)$. Uncertainty of nominal differential expansion UNDE, which is the sum of uncertainties of nominal expansion of the part and master, is

$$\mathrm{UNDE} = \mathrm{UNE}_{part} + \mathrm{UNE}_{master}$$

where the uncertainty of nominal expansion UNE, which is the maximum difference between the true thermal expansion and the nominal expansion, is

$$\mathrm{UNE} = \alpha_{nom} \times L \times (T - 20) \times (\delta / 100) \ \%$$

The maximum observed or recorded thermal drift during either part/comparator or master/comparator drift test, whichever gives the larger value, during a period of time corresponding to the measurement cycle is called the temperature variation error TVE. The sum of all these errors, expressed as a percentage of the total permissible error from all sources is called the thermal error index TEI. For length measurement if no correction for differential expansion is attempted, then

$$\text{TEI} = \frac{\text{NDE} + \text{UNDE} + \text{TVE}}{\text{Total permissible error}} \times 100\ \%$$

In addition to such the time-invariant errors, materials, sensors and control systems can degrade accuracy of a machine tool: materials often exhibit long-term distortion due to their stress state and alloying structure; sensors are very sensitive to external disturbances, such as environmental changes, loadings, etc., and their installation process might have faults; control systems usually filter out mechanical errors but careless determination of control parameters can cause appreciable errors.

2.3.2 Time-varying Errors

Much attention is now paid to time-varying errors due to advancements of machine structures that have made possible machines having small time-invariant errors. It is a fact that machine operating conditions as well as environmental conditions are changing with time. That time-varying nature triggers time-varying errors of machine tools in the end. Time-varying errors are a function of the position of moving components and time:

$$e = f(\text{position}, \text{time})$$

The frequency characteristics of time-varying errors are interesting. It is easy to correct errors occurring at a frequency much lower than the bandwidth of the axes of a machine, usually around 10 Hz (Donmez *et al.*, 1988), and they cause principally dimensional inaccuracy in machined products; high-frequency errors tend to affect surface quality of products, which are due to spindle dynamic error motions, low dynamic stiffness of structures vulnerable to internal or external vibration sources, etc. Examples of time-varying errors are:

- *Errors due to finite dynamic stiffness of machine structures*. Finite dynamic stiffness of structures cause a machine, subject to dynamic forces, to vibrate with an appreciable amplitude that produces an undesirable surface quality on products. Often it also degrades servocontrol functions so that large following errors can occur. Such structural vibrations can be either forced or self-excited. The sources are cutting processes, rotating machine components, ground vibrations, control limit cycling, fluid turbulence, aerostatic instability, sound pressure, friction, etc.

- *Errors due to dynamic temperature variations*. A normal industrial building experiences cyclic temperature variations on a daily basis. Longer term, it is also subject to yearly variations of the median of temperature changes according to

changes of the seasons. Furthermore, a machine usually operates under many kinds of machining conditions that change through the working time. These all generate time-varying temperature states of machine structures. In the end, dynamic temperature variations bring forth time-varying thermal errors, which are very difficult to characterise.

- *Kinematic errors.* Kinematic errors are defined as the relative deviations in movement of several moving machine elements whose movements should be characterised by a rigorous functional dependence (Hocken, 1980, pp. 38-52). A circular motion test now becomes the machine builders' critical inspection process to assess kinematic errors of a machining centre.

2.4 Modelling of Machine Motions having Errors

Most mechanical systems can be effectively modelled as systems of interconnected flexible and rigid components (or bodies), i.e. multi-body systems, such as shown in Figure 2.3. If a multi-body system is composed entirely of connected rigid bodies without closed loops, then it is sometimes called an open-chain or open-tree system. Machine tools and CMMs will generally constitute systems of flexible bodies with relative motions between bodies and with open-chains of bodies in the system. Because the members have finite stiffness and the joints often exhibit the most compliant behaviour, it is a good approximation to incorporate the flexibility effects into the joints as previously described. That is, we model the flexible system by rigid members with joints containing springs and dampers. This is a popular lumping technique dealing with distributed elastic behaviours of machine tools. In general, however, we should describe motions of machine tools in terms of their absolute rigid bodies and their elastic degrees of freedom. The study of rigid body error motions was carried out by the author (Gim, 1994; Gim and Gee, 1995).

2.4.1 Kinematics of Deformable Bodies

Two types of coordinate systems are required in the analysis of multi-body systems as briefly stated in Section 2.2. The first is a global frame of reference that is fixed in time. The second is a body reference frame assigned to each component in a system. This body reference translates and rotates with the body; therefore, its location and orientation change with time with respect to a global frame. The movement of a particle through three-dimensional space can be expressed as the following position vector with respect to a proper frame of reference, as depicted in Figure 2.8:

$$\mathbf{r}(t) = x(t)\mathbf{i} + y(t)\mathbf{j} + z(t)\mathbf{k} \quad \text{or} \quad \mathbf{r}(t) = \begin{bmatrix} x(t) & y(t) & z(t) \end{bmatrix}^{\mathrm{T}} \tag{2.3}$$

with an initial position (a, b, c), where **i**, **j**, **k** are unit vectors along the x, y and z axes respectively. The displacement of a particle is defined as the relative movement of a particle from one position to another. When a particle has moved from position P to P'

in Figure 2-8, the displacement is characterised by the difference $\Delta\mathbf{r}$ in two position vectors directing point P and P' with respect to a frame of reference.

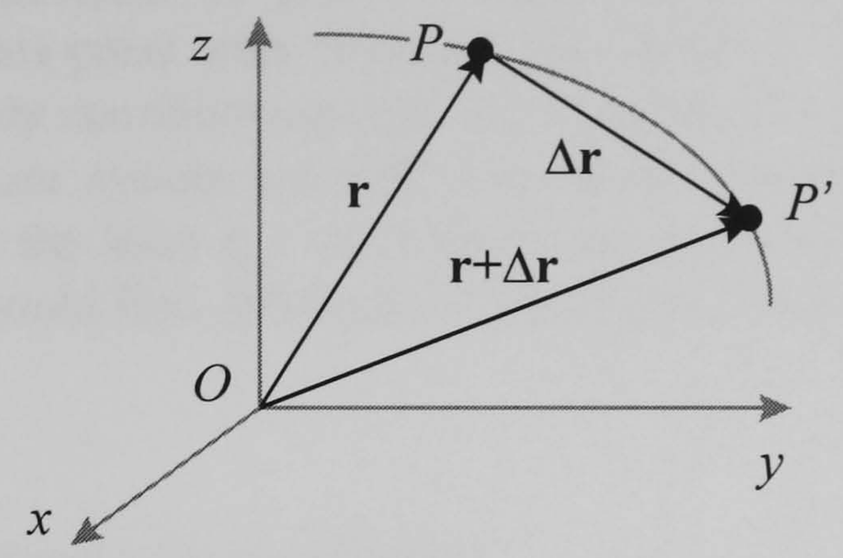

Figure 2.8 Position vector and displacement

In the case of a deformable body, two arbitrary points on it move relative to each other under the action of various kinds of loadings, and consequently the reference coordinates are no longer adequate to describe the kinematics of deformable bodies. In Figure 2.9, a body frame 1 is assigned in such a way that its origin is rigidly attached to a point O_1; that is, the origin of this body reference has the same translational displacements as point O_1 that occupy a new position after deformation of a body. This reference frame is referred to as a floating frame of reference (Shabana, 1989, pp. 8-27).

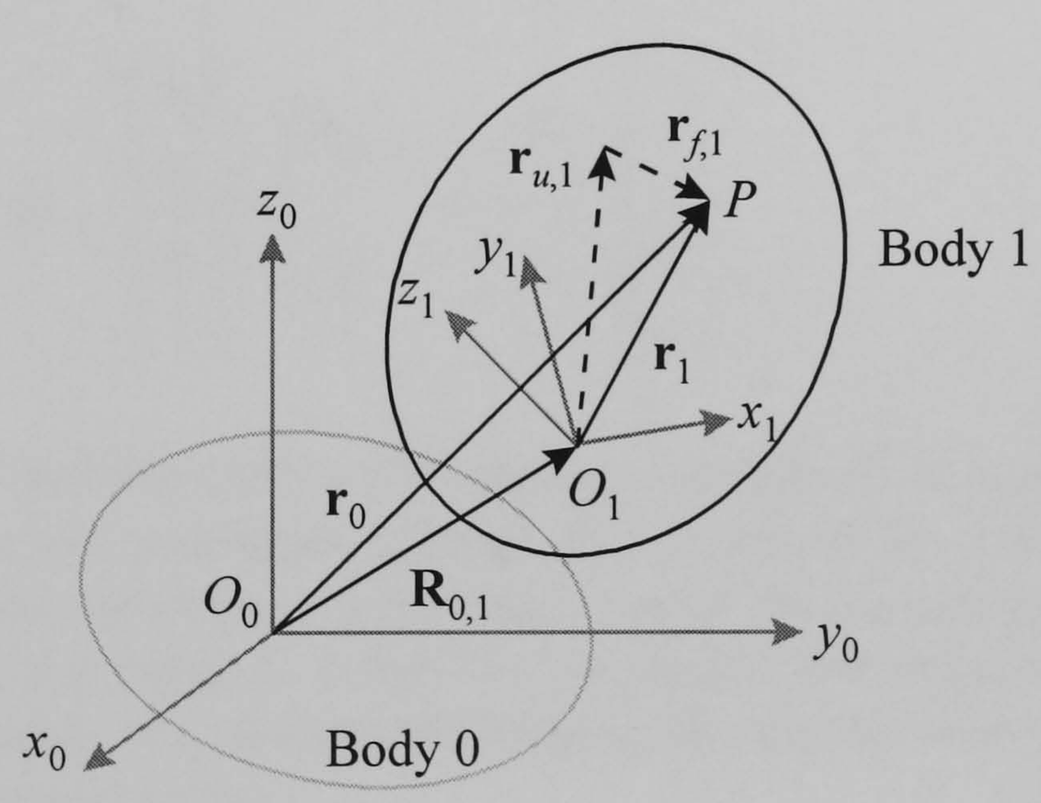

Figure 2.9 Global position of an arbitrary point on the deformable body

In order to determine changes in distance between points O_1 and P due to the body deformation, a rigid line element, represented by the vector $\mathbf{r}_{u,1}$, is drawn from point O_1. The vector has the same magnitude and direction as a vector between the two points O_1 and P in the undeformed state (reference configuration). Furthermore, we assume that this rigid line element $\mathbf{r}_{u,1}$ has no translational or rotational displacement with respect to the body coordinate system. Then we can write an expression for the position vector of point P as

$$\mathbf{r}_0 = \mathbf{R}_{0,1} + \mathbf{r}_{u,1} + \mathbf{r}_{f,1} \tag{2.5}$$

where $\mathbf{R}_{0,1}$ is the position vector of point O_1 with respect to the reference frame 0; $\mathbf{r}_{u,1}$ is the undeformed local position of point P with respect to the frame 1; $\mathbf{r}_{f,1}$ is the deformation vector at this point with respect to the frame 1. While the components of the vector $\mathbf{r}_{u,1}$ in the body coordinate system are constant, the components of the vector $\mathbf{r}_{f,1}$ in the body coordinate system are time- and space-dependent. In the case of rigid bodies, we do not need the term $\mathbf{r}_{f,1}$. In order to analyse errors due to mechanical and thermal loadings, we should find deformation vectors $\mathbf{r}_f$ for every interesting point of a body.

2.4.2 Homogeneous Transformation Matrix

General motion of a rigid body i in a multi-body system can be described by a rotation plus a translation. The position vector $\mathbf{r}_i$ of an arbitrary point on a rigid body i in a multi-body system has a constant component in the body-fixed coordinate system i. If a body translates in addition to the rotation the general motion can be described by the translation of a point and a rotation along the axis of rotation. The translation of the body can then be described by the position vector of the origin of the body reference. This position vector will be denoted as $\mathbf{R}_{0,i}$. Therefore, the global position vector of an arbitrary point on a rigid body can be expressed in terms of the translation and rotation of the body by the vector $\mathbf{r}_0$ given by (*ibid.*, pp. 35-47)

$$\mathbf{r}_0 = \mathbf{R}_{0,i} + \mathbf{A}_{0,i}\mathbf{r}_i \quad \text{or} \quad \begin{bmatrix} x_0 \\ y_0 \\ z_0 \\ 1 \end{bmatrix} = \begin{bmatrix} \mathbf{A}_{0,i} & \vdots & \mathbf{R}_{0,i} \\ \cdots & + & \cdots \\ \mathbf{0} & \vdots & 1 \end{bmatrix} \begin{bmatrix} x_i \\ y_i \\ z_i \\ 1 \end{bmatrix} \tag{2.6}$$

where $\mathbf{A}_{0,i}$ is a 3×3 rotation matrix representing transformation that defines the relative orientation between two coordinate systems; $\mathbf{0}$ is a null vector. The 4×4 transformation matrix of the second equation is sometimes called the homogeneous transform. The advantage of using this notation is that the translation and rotation of the body can be described by one matrix. For deformable bodies, the position vector $\mathbf{r}_i$ encompasses two components as described above:

$$\mathbf{r}_i = \mathbf{r}_{u,i} + \mathbf{r}_{f,i} \tag{2.7}$$

It should be noted that the product of transformation matrices resulting from two successive rotations about two different axes of rotation, in general, is not commutative. That is, the angular displacement vector is not commutative and the order of rotation is important. This is the summary of homogeneous transformation matrices encountered in the modelling of machine tool motions:

- Translations in the x, y, z directions respectively:

$$\begin{pmatrix} 1 & 0 & 0 & {}^{i-1}x \\ 0 & 1 & 0 & 0 \\ 0 & 0 & 1 & 0 \\ 0 & 0 & 0 & 1 \end{pmatrix}, \begin{pmatrix} 1 & 0 & 0 & 0 \\ 0 & 1 & 0 & {}^{i-1}y \\ 0 & 0 & 1 & 0 \\ 0 & 0 & 0 & 1 \end{pmatrix} \text{ and } \begin{pmatrix} 1 & 0 & 0 & 0 \\ 0 & 1 & 0 & 0 \\ 0 & 0 & 1 & {}^{i-1}z \\ 0 & 0 & 0 & 1 \end{pmatrix} \tag{2.8}$$

- Rotations in the x, y, z directions respectively:

$$\begin{pmatrix} 1 & 0 & 0 & 0 \\ 0 & \cos^{i-1}\theta_x & -\sin^{i-1}\theta_x & 0 \\ 0 & \sin^{i-1}\theta_x & \cos^{i-1}\theta_x & 0 \\ 0 & 0 & 0 & 1 \end{pmatrix}, \begin{pmatrix} \cos^{i-1}\theta_y & 0 & \sin^{i-1}\theta_y & 0 \\ 0 & 1 & 0 & 0 \\ -\sin^{i-1}\theta_y & 0 & \cos^{i-1}\theta_y & 0 \\ 0 & 0 & 0 & 1 \end{pmatrix} \text{ and}$$

$$\begin{pmatrix} \cos^{i-1}\theta_z & -\sin^{i-1}\theta_z & 0 & 0 \\ \sin^{i-1}\theta_z & \cos^{i-1}\theta_z & 0 & 0 \\ 0 & 0 & 1 & 0 \\ 0 & 0 & 0 & 1 \end{pmatrix} \tag{2.9}$$

where ${}^{i-1}x$, ${}^{i-1}y$, ${}^{i-1}z$ express linear displacements of body i with respect to body i-1 in the x, y, z directions respectively; ${}^{i-1}\theta_x$, ${}^{i-1}\theta_y$, ${}^{i-1}\theta_z$ denote angular displacements of body i with respect to body i-1 about the x, y, z axes respectively. It is noted that all the displacements are measured with respect to a coordinate system i-1.

2.4.3 Homogeneous Transformation Model

A method using homogeneous transformation matrices has been widely used for the description of machine tool metrology (Reshetov and Portman, 1988; Donmez *et al.*, 1988). Another approach to kinematic modelling employs a screw theory (Ziegert *et al.*, 1992). In the modelling process, machine structures are often decomposed into a series of transformation matrices describing the relative position of each axis and some intermediate coordinate frames. In a case of a linear carriage, the homogeneous transformation matrix expressing the contribution of errors can be derived as

$$\mathbf{E} = \begin{pmatrix} 1 & -e_{\theta z} & e_{\theta y} & e_x \\ e_{\theta z} & 1 & -e_{\theta x} & e_y \\ -e_{\theta y} & e_{\theta x} & 1 & e_z \\ 0 & 0 & 0 & 1 \end{pmatrix} \tag{2.10}$$

where $\mathbf{E}$ is a matrix representing generalised errors of a linear carriage. In the derivation a small angle approximation is employed to linearise sinusoidal functions. A similar formula can be obtained for a rotating body. The overall transformation matrices are obtained by the successive multiplication of relative transformation matrices between

connecting axes. If N rigid bodies are connected in series, the position of the coordinate system N or body N in terms of the reference coordinate system 0 will be:

$$ {}^{0}\mathbf{r} = \left({}^{0}\mathbf{H}_{1}\,{}^{1}\mathbf{H}_{2} \cdots {}^{N-1}\mathbf{H}_{N} \right) {}^{N}\mathbf{r} = \left(\prod_{i=1}^{N} {}^{i-1}\mathbf{H}_{i} \right) {}^{N}\mathbf{r} = {}^{0}\mathbf{H}_{N}\,{}^{N}\mathbf{r} \tag{2.11} $$

where **H** represents the homogeneous transformation matrix. However, machine tool chain structures can be divided into two subchains: workpiece-bed and bed-tool, and a bed is a popular choice for the reference coordinate system because it is a stationary member and no severe forces are acting upon it compared to other machine members. Thus a transformation matrix ${}^{\text{Bed}}\mathbf{H}_{\text{Tool}}$ is calculated by successive multiplication of transformation matrices representing a tool tip to the last axis, i.e. a convenient fixed reference frame that is often attached to a bed. Another matrix ${}^{\text{Bed}}\mathbf{H}_{\text{Work}}$ is obtained by the same procedure implemented from an ideal tool contact point on a workpiece to the same fixed reference frame. Then an error vector acting upon a workpiece is expressed as

$$ \mathbf{e} = {}^{\text{Bed}}\mathbf{H}_{\text{Work}}\,{}^{\text{Work}}\mathbf{r} - {}^{\text{Bed}}\mathbf{H}_{\text{Tool}}\,{}^{\text{Tool}}\mathbf{r} \tag{2.12} $$

Topography of machined surfaces can be predicted in the same way if a global frame is positioned on a workpiece and geometry of a tool is considered properly (Reshetov and Portman, 1988; Ehmann and Hong, 1994).

In the thermal error problems, the evaluation of the deformation vector $\mathbf{r}_f$ in Equation 2.7 is necessary to take account of non-rigid effects due to the thermal deformation of each machine component. The vector $\mathbf{r}_f$ encompasses all the possible modes of deformation such as the thermal drift of origins in each machine component, linear deformations and angular deformations. Many compensation techniques utilise a thermal deformation model based on polynomials such as (Donmez *et al.*, 1988; Teeuwsen *et al.*, 1989; Chen *et al.*, 1993)

$$ e^{t} = a_0 + a_1 T' + a_2 T'^{2} \cdots $$

or

$$ e^{t} = a_0 + \sum_{i=1}^{N} b_i T_i' + \sum_{i=1}^{N} \sum_{j=1}^{N} c_{ij} T_i' T_j' \cdots $$

where e^t is a component of thermal error; a_i, b_i, c_{ij} are the coefficients evaluated by regression methods using measurement data; T', T'_i, T'_j are temperature rises. The polynomial fitting procedure involves a great deal of calibration work. It takes a lot of time in obtaining the complete thermal model of a machine tool using such the model. Also, there are coupling effects between machine components undergoing elastic deformation due to mechanical loadings.

Chapter 3
Thermal Deformation of Simple Machine Elements

3.1 Analytical Approach to Thermal Deformations

There are many kinds of modelling methods to choose from in engineering sciences. They are based on analytical, numerical or empirical techniques. More than two kinds of techniques could be used for modelling a physical system. The result of modelling, a mathematical model having some parameters, should have the similar input-output characteristics to the real response of a physical system. The mathematical model of this study, whether it may be linear or nonlinear, is dynamic in nature to deal with time-varying thermal errors. The parameters can be lumped or should be treated as distributed, and may be time-invariant or time-varying. The result will show all of these.

The parameters required in this work should have a sound and easily understandable physical meaning so that they can be used from everyday engineering practices to sophisticated analyses. In this regard, the investigation of thermal deformation using analytical techniques applied to simple machine elements is considered to be the first step in detecting system parameters representing thermal responses of a machine tool, because the solutions of analytical analyses tend to show the details of a physical phenomenon at a glance.

Induced dynamic temperature fields due to time-varying heat sources affect the dimension and shape of every object in a different way. This effect is called dimensional response and the difference in response between any two objects is called differential response (Bryan, 1990). It is possible to evaluate the deformation vector of Equation 2.7 for temperature loadings to obtain these responses, i.e. the engineering problem of this work is based on the behaviour of thermoelastic solids that are subject to thermal loading conditions. A thermoelastic material is defined as one that possesses a stress-free state and in which stress is a single-valued function of strain and temperature (Allen and Haisler, 1985, pp. 84-85).

Changes of the amount of heat in a body generate strain and stress, and in turn, generally, strain also produces heat. A part of the mechanical energy due to strain is converted into heat. This coupling effect leads to the well-known phenomena of thermoelastic dissipation in elastic bodies. Coupling effects, however, are negligible in problems of thermal deformations which occur in machine structures undergoing small and slow distortions, and the theory of uncoupled thermoelasticity is a basis for this work. When uncoupling is introduced, the theory is referred to as uncoupled, quasi-static theory; it degenerates into heat transfer and thermoelasticity as two separate problems (Fung, 1965, pp. 389-390). It is also necessary to consider the nature of various kinds of heat sources.

3.2 Heat Sources

Heat sources around a machine can be divided into two groups: internal and external heat sources. Essentially, we assume that all the energy supplied to a machine is converted to heat, affecting machine structures, parts and metrology systems through three propagation modes, i.e. conduction, convection and radiation. If the heat input to a machine and the heat dissipation into the environment are balanced, a machine reaches a state of thermal equilibrium. Examples of internal heat sources are:

- *Heat released during cutting process*. The rate of cutting heat generation can be expressed as

$$q = \frac{\sum \eta_i F_i v_i t_i}{t_{tot}} \tag{3.1}$$

where η_i is an efficiency; F_i and v_i are a force and a cutting speed, respectively; t_i and $t_{tot} = \sum t_i$ are the time of utilisation of F_i and v_i, and a total time, respectively. We usually take unity for the efficiency η_i, i.e. all the cutting energy is converted to heat.

- *Mechanical losses*. Mechanical friction and fluid viscosity are responsible for mechanical losses. Heat generation rate due to mechanical losses can be formulated as:

$q = \eta F v$ for linear - motion elements

or (3.2)

$q = \eta \tau_f \omega$ for rotary - motion elements

where η is an efficiency; F is a frictional force; v is a sliding speed; τ_f is a frictional torque; ω is an angular speed. We also usually take unity for the efficiency, i.e. all the mechanical losses are converted to heat. Due to heavy moving components and large preloads, frictional losses contribute to reduce the total efficiency of a machine by several per cent.

- *Electrical losses*. Modern CNC machine tools utilise a lot of electric and electronic components so that basic mechanical assemblies become simpler and simpler nowadays. Consequently, electrical losses have to be taken into consideration. The typical efficiency of an electric-motor is approximately 80 %. In addition, the power loss of the control and amplifying systems is considered to be around 15 %. A spindle motor is normally the most hazardous heat source and its cooling is often recommended by electric-motor manufacturers.

Major external heat sources are:

- *Room environments*. An industrial building usually undergoes changes in temperature, humidity and atmospheric pressure according to the climatic conditions. The air state of a room can be either stratified or convected. Furthermore radiation from the sun and lighting equipment causes a machine to gain additional heat. These all act together upon a machine, resulting in complex deformation behaviours.

- *Personnel*. Direct contact between people and a machine change the thermal state of a machine. Moreover radiation from personnel often becomes an appreciable degrading-factor in ultraprecision machining or measuring operations.

- *Thermal memory from previous environments*. It takes a time to change the thermal state of a body into another state. That is generally called *soak-out* time. Often, workpieces are machined in separate rooms, which have different thermal environments, according to their process requirements, and can have an elevated thermal state from a prior machining-process. These kinds of thermal memory can be removed using an air shower, oil bath, or by *soak out*.

3.3 Transient Development of Temperature Fields

3.3.1 Governing Equations

Dynamic thermal errors are a consequence of transient temperature distributions in machine structures. Such transient temperature fields within a solid body are governed by the following heat conduction equation (Samarskii and Vabishchevich, 1995, pp. 16-21):

$$\frac{\partial^2 T}{\partial x^2}+\frac{\partial^2 T}{\partial y^2}+\frac{\partial^2 T}{\partial z^2}=\frac{1}{\beta}\frac{\partial T}{\partial t} \quad \text{for Cartesian coordinate systems}$$

or (3.3)

$$\frac{1}{r}\frac{\partial}{\partial r}\left(r\frac{\partial T}{\partial r}\right)+\frac{1}{r^2}\frac{\partial^2 T}{\partial \theta^2}+\frac{\partial^2 T}{\partial z^2}=\frac{1}{\beta}\frac{\partial T}{\partial t} \quad \text{for Cylindrical coordinate systems}$$

where $T = T(x, y, z, t)$ or $T(r, \theta, z, t)$ is a temperature field; β is a thermal diffusivity, i.e. $\beta = k/\rho c_v$; k is a thermal conductivity; ρ is a density; c_v is a constant-volume specific heat.

For solid materials, the constant-volume specific heat c_v is nearly equal to the constant-pressure specific heat c_p. The equation 3.3 neglects internal heat generation and variations in the thermal conductivity, density and constant volume specific heat within a solid body. That is true for most practical engineering problems.

Solutions of the heat conduction equation represent temperature distributions in a body under an initial condition and boundary conditions. Thermal memory of a body affects an initial condition, and boundary conditions are determined according to the nature of heat sources. Common boundary conditions are:

- ❑ Prescribed temperature: $T_b = T_0$
- ❑ Prescribed heat flux: $-k_b \left.\frac{\partial T}{\partial n}\right|_b = \frac{q_0}{A}$
- ❑ Convection boundary: $-k_b \left.\frac{\partial T}{\partial n}\right|_b = h(T_b - T_\infty)$
- ❑ Radiation boundary: $-k_b \left.\frac{\partial T}{\partial n}\right|_b = \sigma F_{b\infty}(T_b^4 - T_\infty^4)$
- ❑ Insulated boundary: $\left.\frac{\partial T}{\partial n}\right|_b = 0$

where subscript b denotes a boundary point; T_0 is a known temperature; n denotes the outward-normal coordinate from a boundary; q_0 is a known heat generation rate; A is a surface area; h is a convection heat transfer coefficient; T_∞ is a temperature of an environment; σ is the Stefan-Boltzmann constant; $F_{b\infty}$ is a known radiation shape factor.

When the temperature of a body is considered to be uniform, the following equation based on the first law of thermodynamics (Wylen and Sonntag, 1976, pp. 85-165) applied to a control volume can be used:

$$\dot{E}_{in} + \dot{E}_g - \dot{E}_{out} = \dot{E}_{st}\left(= \rho c_p V \frac{dT}{dt} \quad \text{for solids}\right) \tag{3.4}$$

where $\dot{E}_{in}$ and $\dot{E}_{out}$ is the rate at which thermal energy enter and leave, respectively, through the control surface; $\dot{E}_g$ is the rate of thermal energy generation within the control volume; $\dot{E}_{st}$ is the rate of change of energy stored within the control volume; V is a volume. It is noted that this equation describes lumped systems while Equation 3.3 does distributed ones.

The direct solutions of Equation 3.3 are likely to provide a valuable basis in detecting parameters wanted in this study. Most of them are, however, in the form of infinite series

as will be seen later and available for some simple bodies with restricted boundary conditions. Thus, in the following sections, a few simplified cases will be investigated with an emphasis on the approach methods available to solving the heat conduction equation.

3.3.2 Lumped-Parameter Method

The simplest case of transient temperature developments will be a uniform temperature distribution with which a body undergoes bulk deformations without any local distortion. In many real situations, thermal deformations start locally in the vicinity of heat sources, which do not usually surround a machine component uniformly. A ball screw, for instance, deforms largely due to friction losses occurring in its nut, and consequently, the temperature distribution will be non-uniform at the early stage of motion. As the nut moves along the screw axis repeatedly, the temperature distribution could become uniform in time. However this depends on the operating conditions of the machine. Therefore, realistically a ball screw can never attain a uniform temperature distribution.

The lumped-parameter method can be used when a temperature distribution is assumed to be uniform within a thermally affected body, i.e. the body temperature is dependent only on time: $T = T(t)$. This assumption implies that temperature gradients within a body are quite small. In cases when the controlling heat transfer mode is by convection, the Biot number expresses the ratio of internal conductive resistance to external convective resistance, that is

$$\mathrm{Bi} = \frac{hV/A}{k} \tag{3.5}$$

A lumped-parameter analysis can be conducted with a maximum analysis error of 0.5% if the Biot number is less than 0.1 (Welty *et al.*, 1984, pp. 297-300).

A good example of convection-controlling heat-transfer modes will be a conducting body immersed suddenly in a bath of fluid at a different temperature. The governing equation for this case can be derived from a simple energy balance based on Equation 3.4:

$$hA\left[T(t)_{\infty} - T(t)\right] = \rho c_p V \frac{dT}{dt}$$

When the fluid temperature and the heat transfer coefficient are constant, the solution is a form of exponential decay (White, 1988, pp. 194-198):

$$\frac{T(t) - T_{\infty}}{T_0 - T_{\infty}} = e^{-t/\tau}, \qquad \tau = \frac{\rho c_p V}{hA} \tag{3.6}$$

where τ is a characteristic decay time of lump temperature. The term $\rho c_p V$ is called a lumped capacitance. If the material properties ρ, c_p and heat transfer coefficient h are

supposed to be functions of temperature, then the thermal system has a time-varying characteristic decay time, i.e. $\tau = \tau(t)$.

When a body and a surrounding fluid are at the same temperature of zero initially, i.e. $T_0 = 0$, and the fluid temperature varies linearly with time, i.e.

$$T_\infty = at$$

where a is a constant (K/s), the solution becomes

$$T(t) = a\left[\tau\left(e^{-t/\tau} - 1\right) + t\right] \tag{3.7}$$

If the external fluid temperature changes with time such that

$$T_\infty = a + b\cos(\omega t)$$

where a is an average temperature; b is an oscillation amplitude; ω is an angular frequency, then the steady-state body temperature is expressed as

$$T(t) = a + \frac{b}{\sqrt{1+\omega^2\tau^2}}\cos(\omega t - \phi), \qquad \phi = \arctan(\omega\tau) \tag{3.8}$$

where ϕ is a phase lag.

We can also deal with problems of radiation-controlling heat transfer modes by means of a lumped-parameter method.

3.3.3 Integral Method

An integral method is a generalisation of a lumped-parameter method in which the temperature of a body is no longer idealised as constant, but is allowed to have some spatial distribution. Integral methods have been used to obtain approximate solutions to linear or nonlinear problems. Consider a semi-infinite wall subject to a varying heat flux $q(t)/A$ where A is the heat-affected surface area and having an initial uniform temperature T_0, as shown in Figure 3.1. The heat conduction equation for a half space is reduced to

$$\beta\frac{\partial^2 T'}{\partial x^2} = \frac{\partial T'}{\partial t}$$

where T' is excess temperature or temperature rise, i.e. $T' = T - T_0$.

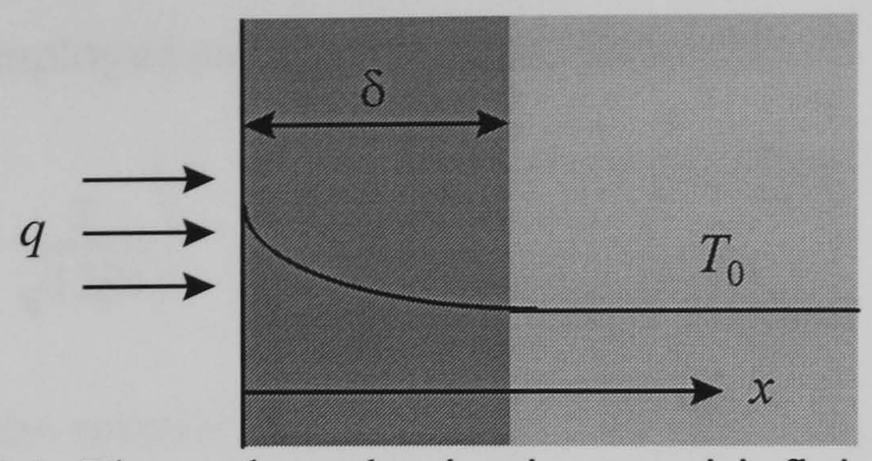

Figure 3.1 Thermal conduction in a semi-infinite wall

Corresponding initial and boundary conditions are

$$\text{at } t = 0 \qquad T' = 0$$

$$\text{at } x = 0 \qquad \frac{\partial T'}{\partial x} = -\frac{q / A}{k}$$

$$\text{at } x = \delta \qquad T'(\delta, t) = 0 \quad \text{and} \quad \frac{\partial T'}{\partial x} = 0$$

where δ is a penetration depth, which is the depth of a distinct skin layer that is thermally affected. As time goes, a penetration depth will grow all the way to the infinite region. Now assume the temperature T' to be a second-order polynomial that is usually taken to be the temperature profile. In the integral method (Goodman, 1964), it is found that this profile is an acceptable approximation to the full analytical solution:

$$T' = a(t) + b(t)x + c(t)x^2$$

Applying boundary conditions, we obtain the following solution:

$$T'(x,t) = \frac{(q / A)\delta}{2k}\left[1 - \frac{2x}{\delta} + \left(\frac{x}{\delta}\right)^2\right] \tag{3.9}$$

Integrating the heat conduction equation from 0 to δ and using the Leibnitz's rule (Hildebrand, 1976, pp. 364-367), a desired integral equation can be derived as

$$\frac{d}{dt}\int_0^{\delta} T'dx = -\beta\frac{\partial T'}{\partial x}(0,t)$$

The unknown function δ can be found from the above equation as the following:

$$\delta(t) = \sqrt{\frac{6\beta}{(q / A)}\int (q / A)dt} \tag{3.10}$$

If q is constant, then

$$\delta(t) = \sqrt{6\beta t}$$

When a cubic profile is employed and q is constant, then

$$T'(x,t) = \frac{q/A}{k}\sqrt{\frac{4}{3}\beta t}\left(1-\frac{x}{\sqrt{12\beta t}}\right)^3 \tag{3.11}$$

Similarly, we can obtain the solution for a constant boundary temperature T_b:

$$T'(x,t) = \left[1-\frac{x}{\sqrt{3}(2\sqrt{\beta t})}\right]^2 (T_b - T_0) \tag{3.12}$$

Consider another case depicted in Figure 3.2. An infinite slab of a thickness L is subject to a varying heat flux $q(t)/A$ on one side and a convection environment on the other side. Initially the temperature of a slab is the same with ambient air temperature. The heat conduction equation for an infinite slab is reduced to

$$\beta\frac{\partial^2 T'}{\partial x^2} = \frac{\partial T'}{\partial t}$$

where $T' = T - T_\infty$; T_∞ is an ambient air temperature.

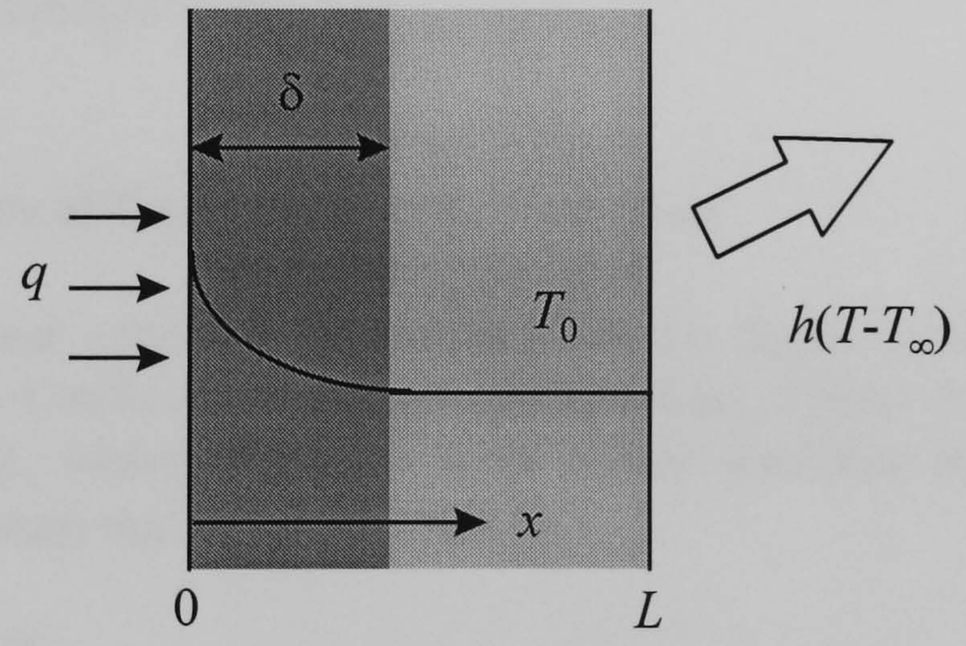

Figure 3.2 Thermal conduction in an infinite slab

Corresponding initial and boundary conditions are gathered:

at $t = 0$ $\quad T' = 0$

at $x = 0$ $\quad \dfrac{\partial T'}{\partial x} = -\dfrac{q/A}{k}$

at $x = \delta$ $\quad T'(\delta, t) = 0$

$$\frac{\partial T'}{\partial x} = 0$$

at $x = L$ $\quad \dfrac{\partial T'}{\partial x} = -\dfrac{h}{k}T'_L$

where $T_L' = T_L - T_\infty$; T_L is a temperature at $x = L$. Now assume the temperature T_L to be a second polynomial, i.e.

$$T' = a(t) + b(t)x + c(t)x^2$$

Initially, the effect of a boundary condition at $x = L$ is not felt, and a slab behaves as if it were semi-infinite. For this initial stage, therefore, the concept of penetration depth can be applied. When $\delta = L$, however, the initial stage is complete, and the time at which this occurs can be obtained by setting $\delta = L$ in the solution for a semi-infinite solid. In the second stage, the concept of penetration depth has no meaning. In this case integration extends from 0 to L. Thus an integral heat-balance equation is derived as

$$\beta\left[\frac{\partial T'}{\partial x}(L,t) - \frac{\partial T'}{\partial x}(0,t)\right] = \frac{d}{dt}\int_0^L T'dx$$

However, the solution of this equation was found to be unrealistic.

For problems involving polar symmetry such as the temperature distribution of cylinders, the volume into which heat propagates does not remain the same for equal increments of the radius as in the planar case, and consequently, a modification in the assumed-temperature profile is necessary. The suggested form of the profile (Goodman, 1964) is given by $T' = (\text{Polynomial in } r)\ln r$.

3.3.4 Direct Solutions of Heat Conduction Equation

Direct solutions of heat conduction equations can be found in many classic textbooks (e.g. Schneider, 1955; Carslaw and Jaeger, 1959; Arpaci, 1966). As an example, consider a slab of thickness $2L$, which is subject to an initial condition and uniform convection boundary conditions such that

$$\text{at } t = 0 \qquad T = T_0$$

$$\text{at } x = \pm L \qquad -k\frac{\partial T}{\partial x} = \pm h(T - T_\infty)$$

The exact solution is given as (Schneider, 1955)

$$\frac{T - T_\infty}{T_0 - T_\infty} = \sum_{i=1}^{\infty} C_i e^{-\psi_i^2 \beta t/L^2} \cos(\psi_i x / L) \tag{3.13}$$

where

$$C_i = \frac{4\sin\psi_i}{2\psi_i + \sin(2\psi_i)}$$

The constants ψ_i are the roots of the transcendental algebraic equation:

$$\psi_i \tan(\psi_i) = \mathrm{Bi} = hL / k$$

whose roots are tabulated in many textbooks on heat transfer (e.g. White, 1988, pp. 668-669).

In many situations, a lumped parameter method has advantages over a direct solution method. An exact solution is usually a form of an infinite series, as presented above, which is often difficult to manipulate. A lumped-method solution has a much simpler form, yet gives acceptable accuracy in many practical engineering problems. Moreover we cannot evaluate an infinite series with perfect accuracy.

3.3.5 Finite Difference Method

It is inevitable to introduce numerical techniques in solving the heat conduction equation. It is a difficult task to solve a partial differential equation such as Equation 3.3, directly. By employing discretisation techniques in the space domain, the approximate solutions can be obtained for complex problems. Among many discretisation techniques, finite difference methods are popular and easy in solving transfer problems (Adams and Rogers, 1973; Dusinberre, 1961; Smith, 1985).

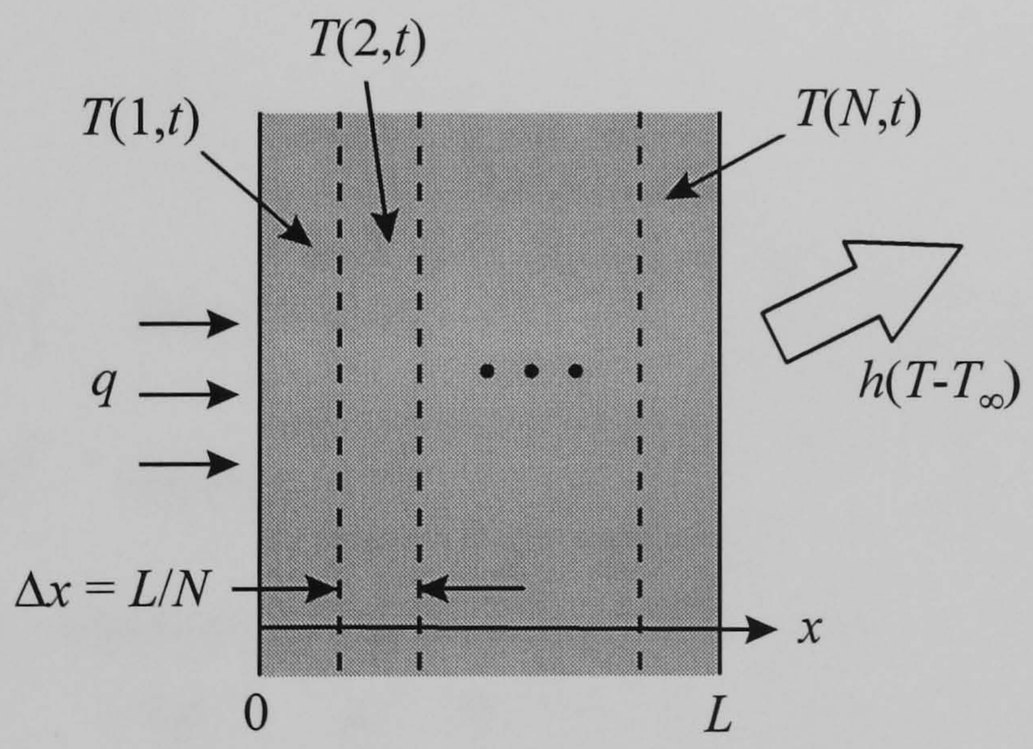

Figure 3.3 Finite difference mesh applied to problem of Figure 3.2

Consider the problem illustrated in Figure 3.2 again. Assuming that the plate is divided into N cells in the direction x as shown in Figure 3.3 and the temperature is uniform within each cell, the first and second order partial differential terms may be written in the approximate difference form as follows:

$$\frac{\partial T'(x,t)}{\partial t} \approx \frac{dT'(n\Delta x,t)}{dt}$$

$$\frac{\partial^2 T'}{\partial x^2} \approx \frac{T'\big((n+1)\Delta x,t\big) - 2T'\big(n\Delta x,t\big) + T'\big((n-1)\Delta x,t\big)}{(\Delta x)^2}$$

where Δx is the thickness of each cell, i.e. $\Delta x = L/N$; $x = n\Delta x$, $n = 1,2,\ldots,N$. The one-dimensional heat conduction equation becomes

$$\frac{dT'(n,t)}{dt} = \frac{\beta}{(\Delta x)^2}\left[T'(n-1,t) - 2T'(n,t) + T'(n+1,t)\right]$$

This equation applies to all the cells except two boundary cells:

$$\begin{aligned}
\dot{T}_2'(t) &= pT_1'(t) - 2pT_2'(t) + pT_3'(t) \\
\dot{T}_3'(t) &= pT_2'(t) - 2pT_3'(t) + pT_4'(t) \\
&\vdots \\
\dot{T}_{N-1}'(t) &= pT_{N-2}'(t) - 2pT_{N-1}'(t) + pT_N'(t)
\end{aligned}$$

where $p = \beta/(\Delta x)^2$. For the boundary cells, the following equations are applicable:

$$\rho c_p V_1 \frac{dT_1'(t)}{dt} = q - \frac{kA}{\Delta x}\left(T_1'(t) - T_2'(t)\right)$$

$$\rho c_p V_N \frac{dT_N'(t)}{dt} = \frac{kA}{\Delta x}\left(T_{N-1}'(t) - T_N'(t)\right) - hAT_N'$$

The governing equations of all the cells can be put into a state-space form such that:

$$\dot{\mathbf{v}} = \mathbf{A}(t)\mathbf{v} + \mathbf{B}(t)\mathbf{x} \tag{3.14}$$

where:

$$\mathbf{v} = \begin{bmatrix} T_1' & T_2' & \cdots & T_N' \end{bmatrix}^{\mathrm{T}} \quad \text{(state vector)}$$

$$\mathbf{x} = \begin{bmatrix} q/S & 0 & \cdots & 0 \end{bmatrix}^{\mathrm{T}} \quad \text{(input vector)}$$

$$\mathbf{A}(t) = \begin{bmatrix}
-kA/(S\Delta x) & kA/(S\Delta x) & 0 & \cdots & \cdots & \cdots & \cdots & 0 \\
p & -2p & p & 0 & \cdots & \cdots & \cdots & \vdots \\
0 & p & -2p & p & 0 & \cdots & \cdots & \vdots \\
\vdots & \vdots & \vdots & \vdots & \vdots & \vdots & \vdots & 0 \\
0 & \cdots & \cdots & \cdots & 0 & p & -2p & p \\
0 & \cdots & \cdots & \cdots & \cdots & 0 & kA/(S\Delta x) & -hA/S - kA/(S\Delta x)
\end{bmatrix}$$

$$\mathbf{B}(t) = \begin{bmatrix}
1 & 0 & \cdots & 0 \\
0 & 0 & \cdots & \vdots \\
\vdots & \vdots & \vdots & \vdots \\
0 & \cdots & \cdots & 0
\end{bmatrix}$$

$$S = \rho c_p V_1 = \rho c_p V_N$$

In this finite-difference equation, lumped-parameter techniques are applied to each cell. In order to obtain the solution, all the eigenvalues of the matrix **A** should be less than unity so that the model is convergent or stable. Once the matrices **A**, **B** are known, the temperature rise of each cell can be easily calculated using MATLAB from MathWorks* under an arbitrary input **x** at each time increment Δt. An example is shown in Figure 3.4. A steel plate of thickness 150 mm was considered (Material properties were taken from Slocum, 1992, pp. 334-336). The plate was divided into 10 cells. It can be seen that each cell stabilises its temperature due to the convection condition on the right side of the plate. But, there are temperature gradients all the time due to the heat source on the left side. This situation seems to be typical in machine tool structures.

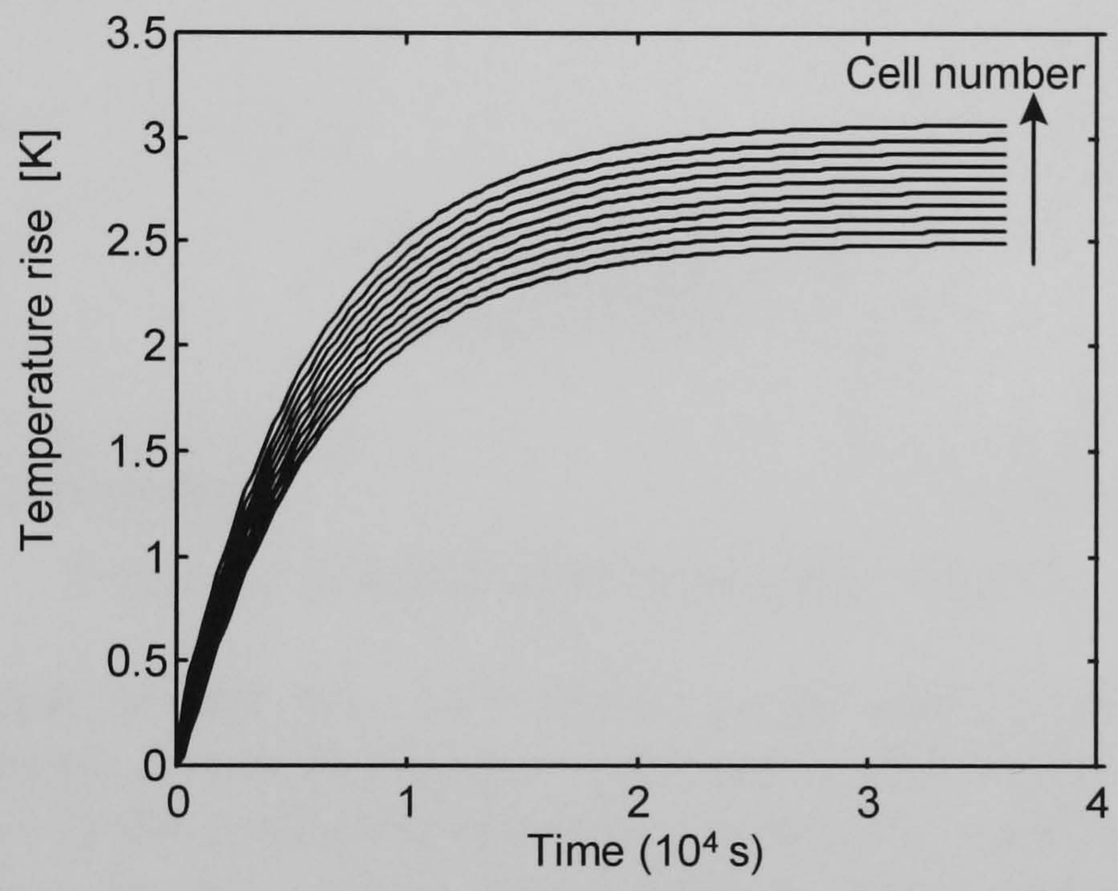

Figure 3.4 Temperature history of each cell**
(ρ=7900 kg/m^3, c_p=465 J/kg·K, k=60 W/m·K, β=16×10^{-6} m^2/s, N=10, L=0.15 m, A=0.12 m^2, h=100 W/m^2·K, q=30 W, Δt=300 sec)

---

* The MathWorks, Inc., Cochituate Place, 24 Prime Park Way, Natick, Massachusetts 01760, USA
** 10000 seconds = 2.8 hours

3.4 Thermal Deformation Models of Simple Machine Members

It is a common practice to analyse engineering-mechanics problems using simple engineering elements. Bar, beam and cylinder elements were considered here to describe thermal deformations of machine members and only temperature loadings were taken into consideration. The thermal deformations of the elements were expressed in terms of changes in temperature distribution. The temperature distribution of a simple machine component can be obtained using the methods explored in Section 3.3. Even if we cannot calculate changes in temperature distribution analytically, we can use the finite-difference method or directly measured temperature data for the prediction of dynamic thermal errors. The idea is that we approximate a continuously varying temperature profile to a stepwise-continuous counterpart as depicted in Figure 3.5. In each step, we consider the machine component to be in a thermal equilibrium condition.

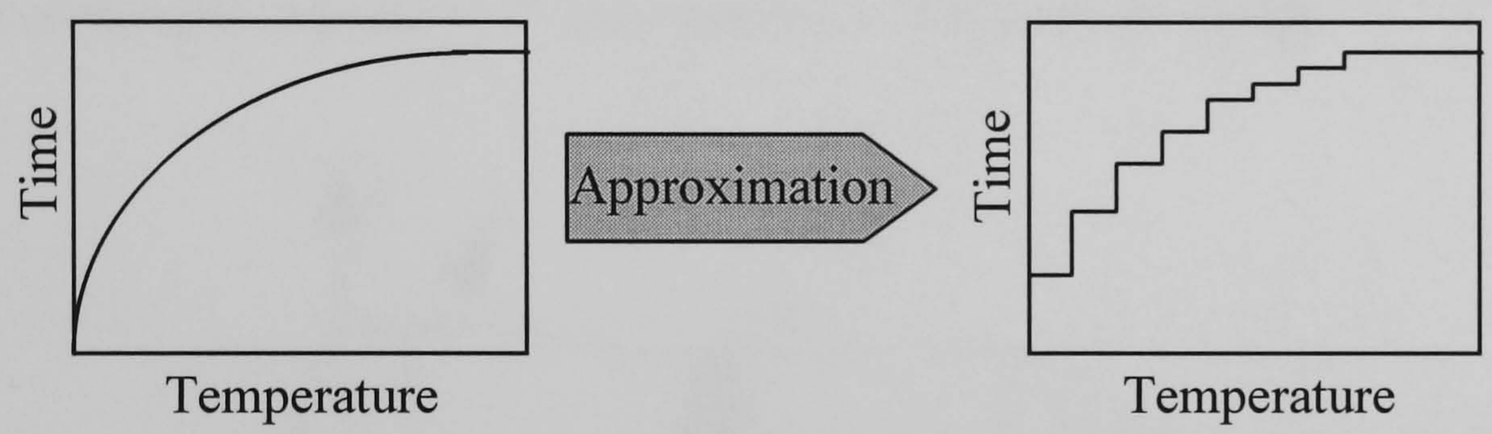

Figure 3.5 Stepwise-continuous approximation

A basic assumption is that the solid bodies to be studied are non-accelerating, homogeneous, isotropic, decoupled linear-thermoelastic and subject to small strains, and reveal no variations in the coefficient of thermal expansion. It was required to derive a complete expression for the thermal deformation of each element because thermal loadings are often ignored in engineering mechanics.

3.4.1 Uniaxial Bar

A uniaxial bar is a long slender member that is subject to mechanical and/or thermal loads acting concentrically in a direction parallel to the longest dimension of a body as depicted in Figure 3.6. Many components of a machine tool can be modelled as a uniaxial bar as long as the loading condition and the following assumptions are satisfied:

- A cross-sectional area $A(z)$ is a continuous function and slowly varying with the axial coordinate z.
- Equilibrium in the axial coordinate direction is satisfied only in an average sense.
- Equilibrium in the x, y coordinate directions is ignored.
- The transverse components of normal stress σ_x and σ_y are negligible compared to the axial stress σ_z.
- The axial displacement field $w(x,y,z)$ is a function of z only.

The equilibrium equation for a uniaxial bar is given as (Allen and Haisler, 1985, pp. 146-149)

$$\frac{dP}{dz} = -p(z)$$

where P is a net resultant axial-force; p is an externally applied axial load-intensity that is expressed as load per unit length of a body. Using the stress-strain-temperature relations and strain-displacement relations (Lardner, 1983, pp. 287-293) we obtain

$$\sigma_z = E\left[\frac{dw_0(z)}{dz} - \alpha T'\right] = \frac{P}{A}$$

where E is the Young's modulus; w_0 is a centroidal axial displacement; α is the coefficient of thermal expansion; T' is an amount of temperature change.

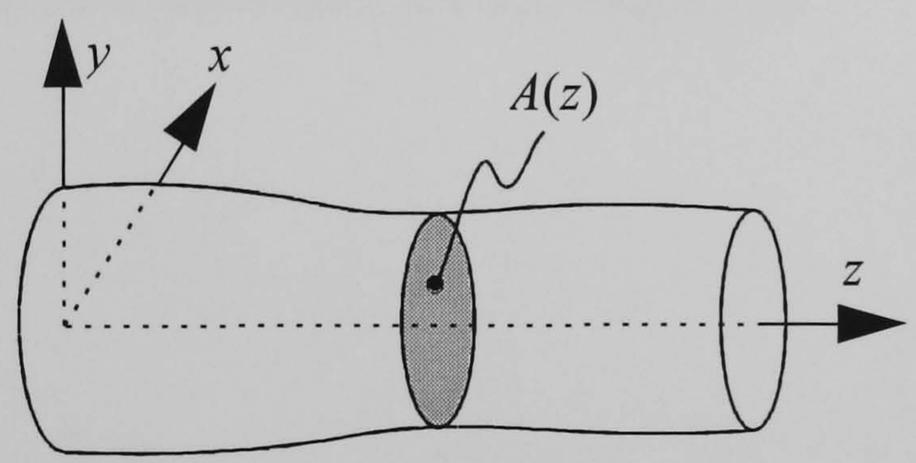

Figure 3.6 Uniaxial bar

Therefore, a centroidal axial displacement w_0 is related to an externally applied load intensity p and a temperature change T' by

$$\frac{d}{dz}\left[AE\left(\frac{dw_o}{dz} - \alpha T'\right)\right] = -p(z) \tag{3.15}$$

Integrating the above equation, and satisfying displacement and load boundary conditions on the ends, the axial displacement w_0 can be determined along the centroidal axis z. The following expression represents the thermal translational-error of uniaxial-bar components of a machine tool:

$$e_z^t = w_o = \alpha \int_0^z T'(z)dz \tag{3.16}$$

Thus the error in position **e** along the z-axis is

$$\mathbf{e} = \mathbf{r}' - \mathbf{r} = \mathbf{H}(e_z^t)\mathbf{r} - \mathbf{r}$$

or

$$\begin{bmatrix} x_{error} \\ y_{error} \\ z_{error} \\ 1 \end{bmatrix} = \begin{bmatrix} 1 & 0 & 0 & 0 \\ 0 & 1 & 0 & 0 \\ 0 & 0 & 1 & e_z^t \\ 0 & 0 & 0 & 1 \end{bmatrix} \begin{bmatrix} x \\ y \\ z \\ 1 \end{bmatrix} - \begin{bmatrix} x \\ y \\ z \\ 1 \end{bmatrix} = \begin{bmatrix} 0 \\ 0 \\ e_z^t \\ 1 \end{bmatrix}$$

where $\mathbf{r}'$ is a real position vector having errors; **H** is a homogeneous transformation matrix (Equation 2.8 and 2.9); x_{error}, y_{error} and z_{error} are the components of the position error vector **e**.

The governing equation for uniaxial bars, represented by Equation 3.15, can be rewritten such as

$$\frac{d}{dz}\left[EA\frac{dw_o}{dz} \right] = -p(z) + p_{th}(z)$$

where $p_{th}(z)$ is a thermal force-equivalent per unit length, i.e.

$$p_{th}(z) = \frac{d}{dz}(EA\alpha T')$$

3.4.2 Beam

A beam is a slender machine-member subjected to transverse mechanical or thermal loadings as shown in Figure 3.7. The Bernoulli-Euler beam theory (Donaldson, 1993, pp. 235-244) is adopted here to derive thermal deformation equations, i.e. beams are considered to be long enough to neglect effects of shear deformations. For Bernoulli-Euler beams the following requirements have to be satisfied:

- The cross section of a beam is symmetrical about the plane of transverse loadings and uniform along the length.
- In the plane of symmetry the plane cross sections remain plane after deformations, i.e. $\gamma_{yz} = \gamma_{xz} = 0$.
- Stresses σ_x, σ_y and τ_{xy} remain zero throughout the inside of a beam due to the slenderness of a beam.
- Shear forces do not contribute significantly to overall deformation.

Firstly, there is the extensional deformation due to transverse temperature gradients. It is noted that the extension is independent of the transverse bending. The extensional displacement w can be expressed as

$$w = w_o - y(dv/dz)$$

where w_o is the extension of the centroidal axis. Then, the normal stress σ_z can be written such as

$$\sigma_z = E\varepsilon_z - E\alpha T' = E\frac{dw}{dz} - E\alpha T' = E\left(\frac{dw_o}{dz} - y\frac{d^2v}{d^2z}\right) - E\alpha T'$$

It can be identified that there is the direct thermal stress $E\alpha T'$, which varies over the beam cross-section with temperature. Because the integral of y over the beam cross-section is zero, the stress-resultant in the z direction can be expressed as

$$P = \iint \sigma_z dA = EA\frac{dw_o}{dz} - P_{th}$$

where P is a beam axial force; P_{th} is a thermal force-equivalent, i.e.

$$P_{th} = E\alpha \iint T' dA$$

Therefore the governing equation for the extensional displacement is

$$\frac{dw_o}{dz} = \frac{P + P_{th}}{EA}$$

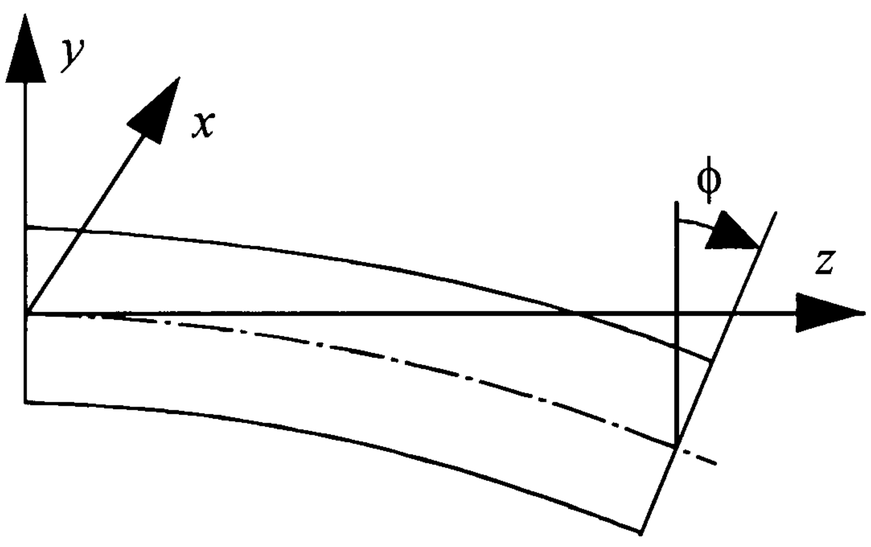

(a) Cantilever

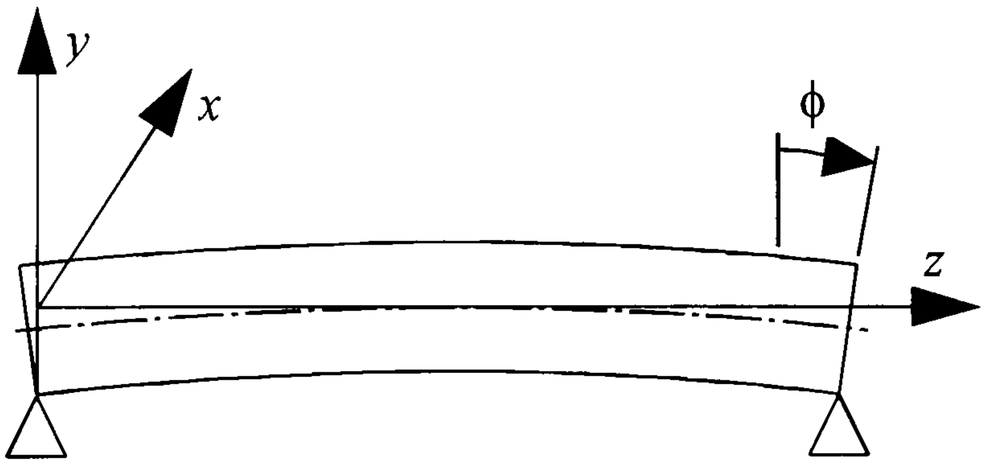

(b) Simply supported

Figure 3.7 Beams

For the transverse bending, the equilibrium equations for a beam can be formulated as (Lardner, 1983, pp. 158-164)

$$\frac{dV}{dz} + q(z) = 0$$

$$\frac{dM_b}{dz} + V = 0$$

where V is a shear force; q is a transverse load intensity per unit length; M_b is a bending moment. The curvature of a beam ρ can be found as

$$\frac{1}{\rho} = -\frac{d\phi}{ds} \approx \frac{d^2v}{dz^2}$$

where ϕ is a slope angle; s is the coordinate axis along a neutral axis; v is a transverse displacement. A longitudinal strain component is obtained as

$$\varepsilon_z = -\frac{y}{\rho} = \frac{d\phi}{ds} y = \frac{\sigma_z}{E} + \alpha T'$$

From the force equilibrium in the z direction, we can find the location of a neutral axis and the moment equilibrium about the x direction gives

$$\sum M_x = -\iint y\sigma_z dA = \frac{E}{\rho} I_{xx} + E\alpha \iint yT'dA = M_b$$

where I_{xx} is the second area moment about a neutral axis, i.e.

$$I_{xx} = \iint y^2 dA$$

Therefore, the transverse displacement v and slope angle ϕ are related to an externally applied load M_b and a temperature change T' by

$$\frac{d^2v}{dz^2} = -\frac{d\phi}{ds} = \frac{(M_b - E\alpha\overline{T})}{EI_{xx}} \tag{3.17}$$

where

$$\overline{T} = \iint yT'dA$$

Integrating the above equation and satisfying displacement and load boundary conditions on the ends, the transverse displacement v can be determined. From the governing equation for beams, represented by Equation 3.17, the thermal moment-equivalent $M_{b,th}$ can be expressed such that:

$$M_{b,th} = E\alpha\overline{T} = E\alpha \iint T'ydA$$

The following intermediate solutions are obtained for a cantilever (Figure 3.7(a)) subject to thermal loads only:

$$v = -\frac{\alpha \bar{T}}{2I_{xx}} z^2$$
$$\phi = \frac{\alpha \bar{T}}{I_{xx}} z \qquad (3.18a)$$

and for a simply supported beam (Figure 3.7(b)) subject to thermal loads only:

$$v = -\frac{\alpha \bar{T}}{2I_{xx}} z^2 + \frac{\alpha \bar{T} L}{2I_{xx}} z$$
$$\phi = \frac{\alpha \bar{T}}{I_{xx}} z - \frac{\alpha \bar{T} L}{2I_{xx}} \qquad (3.18b)$$

where L is the length of a beam. Now assume a beam has a rectangular cross-section of width b and height h, and a temperature profile has the following form:

$$T' = \frac{\Delta T}{h} y + C$$

where ΔT is a temperature difference between the upper and lower surface of a beam; C is an arbitrary constant. The corresponding solutions are for a cantilever

$$v = -\frac{\alpha K}{2} z^2$$
$$\phi = \alpha K z$$

and for a simply supported beam

$$v = -\frac{\alpha K}{2} z^2 + \frac{\alpha L K}{2} z$$
$$\phi = \alpha K z - \frac{\alpha L K}{2}$$

where K denotes the slope or gradient of a temperature profile, i.e.

$$K = \frac{dT'}{dx} = \frac{\Delta T}{h}$$

Transverse temperature gradients force a beam to deflect, i.e. they have the same effect as external bending moments. This type of thermal deflection generates a thermal rotational-error about the x-axis $e^t_{\theta x}$, such that

$$e_{\theta x}^{t} = \phi$$

and thus the error in position **e** along the *z*-axis will be

$$\mathbf{e} = \mathbf{r}' - \mathbf{r} = \mathbf{H}(e_z^t = w, e_{\theta x}^t = \phi)\mathbf{r} - \mathbf{r}$$

or

$$\begin{bmatrix} x_{error} \\ y_{error} \\ z_{error} \\ 1 \end{bmatrix} = \begin{bmatrix} 1 & 0 & 0 & 0 \\ 0 & \cos\phi & -\sin\phi & 0 \\ 0 & \sin\phi & \cos\phi & w \\ 0 & 0 & 0 & 1 \end{bmatrix} \begin{bmatrix} x \\ y \\ z \\ 1 \end{bmatrix} - \begin{bmatrix} x \\ y \\ z \\ 1 \end{bmatrix} = \begin{bmatrix} 0 \\ y\cos\phi - z\sin\phi - y \\ y\sin\phi + z\cos\phi + w - z \\ 1 \end{bmatrix}$$

where w is the extension due to temperature gradients.

In cases when the gradient K varies longitudinally, we can express the following relations for a cantilever

$$\begin{aligned} v &= -\alpha \int_0^z \int_0^z K(z)dzdz \\ \phi &= \alpha \int_0^z K(z)dz \end{aligned} \qquad (3.19)$$

and for a simply supported beam

$$\begin{aligned} v &= -\alpha \int_0^z \int_0^z K(z)dzdz + \frac{\alpha}{L} z \int_0^L \int_0^L K(z)dzdz \\ \phi &= \alpha \int_0^z K(z)dz - \frac{\alpha}{L} \int_0^L \int_0^L K(z)dzdz \end{aligned} \qquad (3.20)$$

It is noted that a displacement v and slope angle ϕ has the following relation

$$v = -\int \phi dz$$

The gradient K might vary in the transverse directions, and that causes a torsion. Figure 3.8 (a) depicts a torsion due to a y-direction gradient varying in the x direction, which can be expressed as

$$\frac{dK(x)}{dx} = \frac{\partial^2 T'}{\partial x \partial y}$$

From the following relations

$$\frac{\partial \phi}{\partial z} = \alpha K(x)$$

$$\phi_\tau = \frac{\partial v}{\partial x}$$

where ϕ_τ is a torsional angle, we can obtain a torsional angle for a cantilever

$$\phi_\tau = -\frac{1}{2}\alpha \frac{dK(x)}{dx} z^2 \tag{3.21}$$

and for a simply supported beam

$$\phi_\tau = -\frac{1}{2}\alpha \frac{dK(x)}{dx} z^2 + \frac{1}{2}\alpha L \frac{dK(x)}{dx} z \tag{3.22}$$

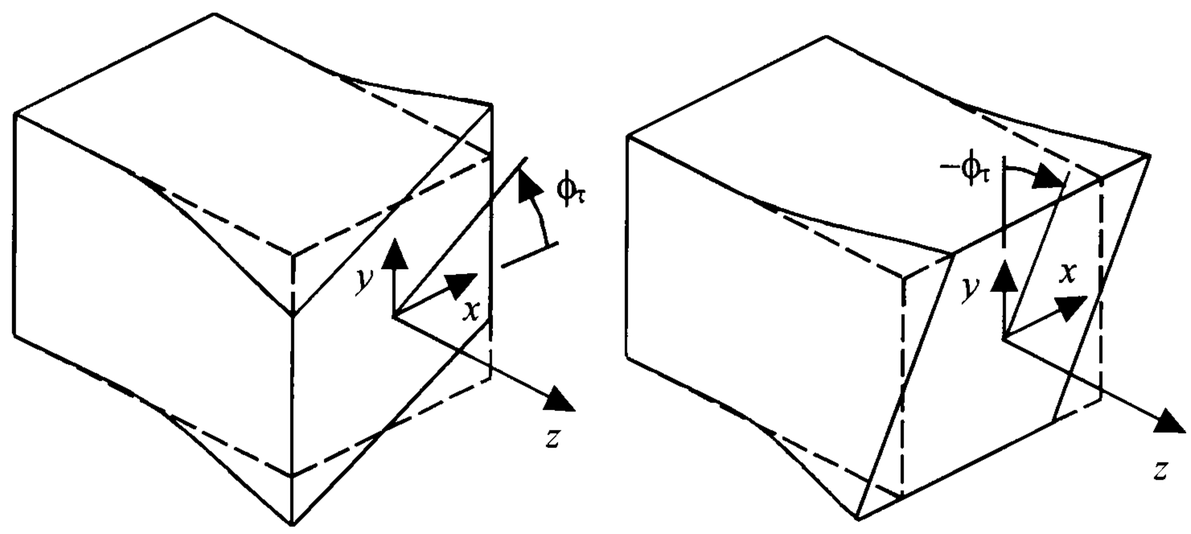

(a) (b)

Figure 3.8 Torsion due to non-uniform temperature gradient

On the other hand, there might be a x-direction gradient varying in the y direction as shown in Figure 3.8 (b), such that

$$T' = K(y)x + C$$

$$\frac{dK(y)}{dy} = \frac{\partial^2 T'}{\partial x \partial y}$$

Similarly, we can obtain a torsional angle for a cantilever

$$\phi_\tau = \frac{1}{2}\alpha \frac{dK(y)}{dy} z^2 \tag{3.23}$$

and for a simply supported beam

$$\phi_\tau = \frac{1}{2}\alpha\frac{dK(y)}{dy}z^2 - \frac{1}{2}\alpha L\frac{dK(y)}{dy}z \tag{3.24}$$

These thermal torsions cause rotational-errors about the z-axis $e^t_{\theta z}$, that is

$$e^t_{\theta z} = \phi_\tau$$

Thus the error in position **e** along the z-axis will be

$$\mathbf{e} = \mathbf{r}' - \mathbf{r} = \mathbf{H}(e^t_z = w, e^t_{\theta z} = \phi_\tau)\mathbf{r} - \mathbf{r}$$

or

$$\begin{bmatrix} x_{error} \\ y_{error} \\ z_{error} \\ 1 \end{bmatrix} = \begin{bmatrix} \cos\phi_\tau & -\sin\phi_\tau & 0 & 0 \\ \sin\phi_\tau & \cos\phi_\tau & 0 & 0 \\ 0 & 0 & 1 & w \\ 0 & 0 & 0 & 1 \end{bmatrix}\begin{bmatrix} x \\ y \\ z \\ 1 \end{bmatrix} - \begin{bmatrix} x \\ y \\ z \\ 1 \end{bmatrix} = \begin{bmatrix} x\cos\phi_\tau - y\sin\phi_\tau - x \\ x\sin\phi_\tau + y\cos\phi_\tau - y \\ w \\ 1 \end{bmatrix}$$

where w is the extension due to temperature gradients.

When heat is applied to elastic elements consisting of two layers made of materials of different thermal expansion coefficients and joined firmly, i.e. bimetal elements, greater thermal expansion occurs in the layer made of material with the higher coefficient of thermal expansion (hereinafter, element 2). In consequence the bimetal element bends towards the layer with the lower coefficient of thermal expansion (hereinafter, element 1). The radius of curvature of the deflection of bimetallic strips is given as (Eskin and Fritze, 1940; Trylinski, 1971, pp. 189-202)

$$\rho = \frac{t\left[3(1+m)^2 + (1+mn)(m^2 + {}^1\!/_{mn})\right]}{6(\alpha_2 - \alpha_1)T'(1+m)^2}$$

where t is the total thickness; m is the ratio of thickness of low- to high-expansion elements; n is the ratio of the moduli of elasticity of low- to high-expansion elements; α_1 is the coefficient of thermal expansion of element 1; α_2 is the coefficient of thermal expansion of element 2. When m and n are equal to unity, then

$$\rho = \frac{2}{3}\frac{t}{(\alpha_2 - \alpha_1)T'}$$

When bimetallic elements are mounted as a cantilever, the maximum deflection at the end v_{max} can be expressed as

$$v_{max} = \frac{L^2}{2\rho} = \frac{3}{4}\frac{(\alpha_2 - \alpha_1)T'L^2}{t}$$

When bimetallic elements are simply supported, the maximum defection at the centre v_{max} can be expressed as

$$v_{max} = \frac{L^2}{8\rho} = \frac{3}{16}\frac{(\alpha_2 - \alpha_1)T'L^2}{t}$$

3.4.3 Cylinder

We can find many cylindrical objects in a machine tool, and they are often used for a critical functional requirement, such as high-accuracy rotation of spindles and high-repeatability positioning of slideways. In a functional point of view, radial thermal deformations are as much important as longitudinal thermal deformations because cylindrical components are often mated with another hollow component with very tight tolerances.

An open-ended, thick-walled hollow cylinder depicted in Figure 3.9 has the following normal stress components (Timoshenko and Goodier, 1951, pp. 408-416):

$$\sigma_r = \frac{\alpha E}{1-\nu}\left[\frac{r^2 - R_i^2}{r^2(R_o^2 - R_i^2)}\int_{R_i}^{R_o} T'rdr - \frac{1}{r^2}\int_{R_i}^{r} T'rdr\right]$$

$$\sigma_\theta = \frac{\alpha E}{1-\nu}\left[\frac{r^2 + R_i^2}{r^2(R_o^2 - R_i^2)}\int_{R_i}^{R_o} T'rdr + \frac{1}{r^2}\int_{R_i}^{r} T'rdr - T'\right]$$

$$\sigma_z = \frac{\alpha E}{1-\nu}\left[\frac{2}{R_o^2 - R_i^2}\int_{R_i}^{R_o} T'rdr - T'\right]$$

where ν is the Poisson's ratio; R_i is the radius of a centre hole; R_o is the outer radius of a cylinder. The temperature T' is a function of r. Using the stress-strain-temperature relations and strain-displacement relations, the displacement u in the radial direction due to a temperature change is derived as

$$u(r) = \frac{\alpha r}{1-\nu}\left[\frac{(1-3\nu)r^2 + (1+\nu)R_i^2}{r^2(R_o^2 - R_i^2)}\int_{R_i}^{R_o} T'rdr + \frac{1+\nu}{r^2}\int_{R_i}^{r} T'rdr\right] \tag{3.25}$$

and the displacement at $r = R_o$ will be

$$u(R_o) = \frac{2\alpha R_o}{R_o^2 - R_i^2} \int_{R_i}^{R_o} T'r\,dr$$

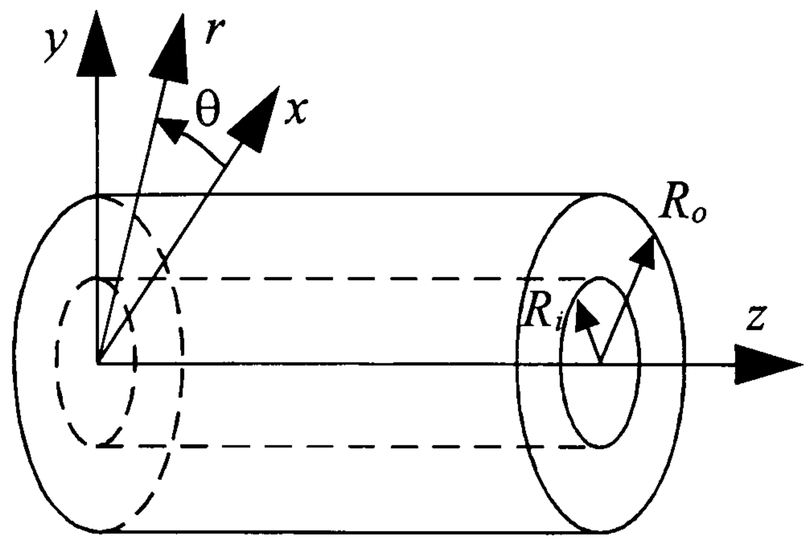

Figure 3.9 Thick-walled hollow cylinder

Similarly, the displacement w in the longitudinal direction can be derived as

$$w(z) = \frac{2\alpha z}{R_o^2 - R_i^2} \int_{R_i}^{R_o} T'r\,dr \tag{3.26}$$

and the displacement at $z = L$ (the length of a cylinder) is expressed as

$$w(L) = \frac{2\alpha L}{R_o^2 - R_i^2} \int_{R_i}^{R_o} T'r\,dr$$

Setting R_i to zero, we obtain the following solutions for a solid cylinder:

$$u(r) = \frac{\alpha r}{1-\nu}\left[\frac{1-3\nu}{R_o^2}\int_0^{R_o} T'r\,dr + \frac{1+\nu}{r^2}\int_0^{r} T'r\,dr\right]$$

$$u(R_o) = \frac{2\alpha}{R_o}\int_0^{R_o} T'r\,dr$$

$$w(z) = \frac{2\alpha z}{R_o^2}\int_0^{R_o} T'r\,dr$$

$$w(L) = \frac{2\alpha L}{R_o^2}\int_0^{R_o} T'r\,dr$$

These displacements correspond to thermal translational errors.

The following expression represents the thermal translational-error of a cylindrical machine component where radial thermal-deformations do not contribute to the total error in position:

$$e_z^t = w$$

Thus the error in position **e** will be

$$\mathbf{e} = \mathbf{r}' - \mathbf{r} = \mathbf{H}(e_z^t = w)\mathbf{r} - \mathbf{r}$$

or

$$\begin{bmatrix} x_{error} \\ y_{error} \\ z_{error} \\ 1 \end{bmatrix} = \begin{bmatrix} 1 & 0 & 0 & 0 \\ 0 & 1 & 0 & 0 \\ 0 & 0 & 1 & w \\ 0 & 0 & 0 & 1 \end{bmatrix} \begin{bmatrix} x \\ y \\ z \\ 1 \end{bmatrix} - \begin{bmatrix} x \\ y \\ z \\ 1 \end{bmatrix} = \begin{bmatrix} 0 \\ 0 \\ w \\ 1 \end{bmatrix}$$

In cases of slideways having cylindrical guide components, the radial deformations will give the thermal translational-error such that

$$e_y^t = u$$

and the error in position **e** will be

$$\mathbf{e} = \mathbf{r}' - \mathbf{r} = \mathbf{H}(e_z^t = u)\mathbf{r} - \mathbf{r}$$

or

$$\begin{bmatrix} x_{error} \\ y_{error} \\ z_{error} \\ 1 \end{bmatrix} = \begin{bmatrix} 1 & 0 & 0 & 0 \\ 0 & 1 & 0 & u \\ 0 & 0 & 1 & 0 \\ 0 & 0 & 0 & 1 \end{bmatrix} \begin{bmatrix} x \\ y \\ z \\ 1 \end{bmatrix} - \begin{bmatrix} x \\ y \\ z \\ 1 \end{bmatrix} = \begin{bmatrix} 0 \\ u \\ 0 \\ 1 \end{bmatrix}$$

Chapter 4
Method of Describing Thermal Errors

4.1 Consideration of Modelling Strategy

The investigations of Chapter 3 led to two modelling strategies by which dynamic thermal errors are described; their difference is in the choice of input variables. A simple choice will be to consider temperature as an input variable. That encompasses the need to know the distribution of a temperature field within a body in advance at any instant of time that may be interesting. Most studies conducted so far employ this method, i.e. describing thermal errors of a machine tool as a function of temperature at various points of the machine structure:

$$e^t = f(T_i = T_0, T_1, T_3, \cdots)$$

where T_i represents temperatures at points of interest in a machine structure. The exact relationship is obtained either analytically or empirically. Owing to the wide availability of temperature sensors, temperatures of most parts of a machine structure can be easily measured either in laboratory or shop floor environments. The author, however, would like to offer criticisms of this approach for the following reasons:

- It hardly yields an overall perspective of the design aspects although, more positively, it provides a basis for compensation actions.
- It is based on the results of heat transfer and not on the causes such as time-variations of internal heat sources due to continuously changing machine service conditions, environmental disturbances, etc.
- It cannot completely describe the dimensional response of a machine because the dimensional response is dependent on time-dependent thermophysical characteristics of machine components.

The preferred approach is to take a time-variable for the basis of input variables as the term dynamic thermal error indicates. The engineering-mechanics analysis of Chapter 3

showed that time-dependent behaviours came from heat-transfer. To achieve the objectives of this work, most effort should be made towards thermophysical nature of a machine structure. Ultimately we need to represent thermal errors in the following form:

$$e^t = f(t, t_i = t_0, t_1, t_2, \cdots) \tag{4.1}$$

where t is time and t_i represents an event of a service condition of a machine such as the start or stop of a spindle, the beginning or end of a coolant operation, etc. Using singularity functions, such events can be incorporated into a thermal error model. With this time-based approach, we can simulate machine thermal behaviour more precisely at design stages and the correction of an early design can be made more readily. Moreover available compensation procedures can be undertaken faster because at least a model structure for thermal errors is available. Various events of service conditions can be captured easily with the recent advancements of open-architecture CNC controllers.

4.2 Search for Governing Parameters

A mathematical representation of Equation 4.1 will be required in the form of an equation that reveals the internal behaviour of the thermophysical nature of a machine structure as well as input-output characteristics. Furthermore, it is required to reduce the complex thermophysical-nature to an interconnection of simple idealised elements that preserve the characteristics of a thermally affected machine structure. Having done that, we can readily identify details of thermal errors occurring in a machine tool and can achieve the key objective of this thesis. As a consequence, we have to work out the problem of how to reduce a thermophysical system undergoing linear thermal-deformation into simple elements which can be represented by one parameter for each element.

4.2.1 Close Examination of Governing Equations

A governing equation of a physical phenomenon represents all the details in a concise manner, that is we can deduce hidden truths from the equation. The heat conduction equation given by Equation 3.3 can be rewritten into the following, more general form:

$$\frac{\partial}{\partial x}\left(k\frac{\partial T}{\partial x}\right) + \frac{\partial}{\partial y}\left(k\frac{\partial T}{\partial y}\right) + \frac{\partial}{\partial z}\left(k\frac{\partial T}{\partial z}\right) = \rho c_v \frac{\partial T}{\partial t} \tag{4.2}$$

In this case, the thermal conductivity of a material is allowed to vary within a body. Although this study did not deal with such variable conductivity problems, the above equation is more appropriate for deducing physical meanings.

Referring to the Fourier law of heat conduction (White, 1988, pp. 7-10)

$$\mathbf{q} = q_x\mathbf{i} + q_y\mathbf{j} + q_z\mathbf{k} = -kA\left(\frac{\partial T}{\partial x}\mathbf{i} + \frac{\partial T}{\partial y}\mathbf{j} + \frac{\partial T}{\partial z}\mathbf{k}\right)$$

it is identified that each of the left-hand side terms of Equation 4.2 represents net heat transfer in the x, y, z directions respectively, i.e. the terms stand for the difference between the conduction heat flow that arrives at a given point and the conduction heat flow that leaves. Thermal conductivity determines the amount of heat that can be transported in a unit time. Consequently, higher conductivity materials, such as aluminium, give faster development of temperature fields in a machine structure, while a body made of low conductivity materials, such as granite, can easily develop temperature gradients as a result of small heat flow. Table 4.1 shows mechanical and thermal properties of some interesting materials (taken from Slocum, 1992, pp. 335).

	Aluminium (6061-T6)	Copper (Brass)	Granite	Invar	Iron (1018 steel)	Zerodur
Young's modulus (Pa)	68×10^9	110×10^9	↓19×10^9	150×10^9	↑200×10^9	91×10^9
Poisson's ratio	0.33	↑0.34	↓0.1	0.3	0.29	0.24
Density (kg/m^3)	2,700	↑8,530	2,600	8,000	7,900	↓2,530
specific heat (J/kg·K)	↑896	↓375	820	515	465	821
Heat storage capacity ($J/m^3\cdot K$)	$2,419\times10^3$	$3,199\times10^3$	$2,132\times10^3$	↑$4,120\times10^3$	$3,674\times10^3$	↓$2,077\times10^3$
Thermal conductivity (W/m·K)	↑167	120	↓1.6	11	60	1.64
Thermal diffusivity (m^2/s)	↑69×10^{-6}	38×10^{-6}	↓0.8×10^{-6}	2.7×10^{-6}	16×10^{-6}	0.8×10^{-6}
Expansion coefficient (1/K)	↑23.6×10^{-6}	19.9×10^{-6}	6×10^{-6}	0.8×10^{-6}	11.7×10^{-6}	↓0.05×10^{-6}

Table 4.1 Mechanical properties of engineering materials (↓: lowest, ↑:highest)

The thermal conductivity of metallic solids is attributed to the movement of conduction electrons and the effect of lattice vibrations, but the former plays the dominant role (Bejan, 1993, pp. 10-15). The movement of the conduction electrons is impeded by scattering, which is the result of the interactions between electrons and phonons (the energy quanta of lattice vibrations), as well as interactions between electrons and impurities and imperfections that may exist in the material. Thus there is a good correlation between the electrical and thermal conductivity of materials. Gases, with low density and few molecular collisions, have very low conductivity. For engineering

purposes we can measure and list apparent thermal conductivity that varies with temperature, density (or void fraction) and partial pressure of the air space.

The right-hand side of Equation 4.2 is called the *thermal inertia* term. Thermal inertia implies that a finite sample of a body must be the recipient of net heat transfer if its temperature is to rise. When the net heat transfer input is fixed, the temperature rises faster when the group ρc_v is smaller. Complementing the conductivity of a material is its heat storage capacity defined as ρc_p. Heat storage capacity represents the amount of energy absorbed per unit volume for each degree rise in temperature. Since almost all heat transfer applications involve free expansion of materials, the appropriate specific heat is the constant pressure value c_p*. According to Table 4.1, materials of high density generally have low specific heat so that most solids have comparable heat capacities.

Thermal diffusivity, $\beta = k/\rho c_p$, is a measure of the rate of change of temperature of a material, since conductivity expresses the rate of heat flow into a substance and thermal capacity denotes its ability to store this received energy. Substances with high conductivity and low capacity will react rapidly to transient external conditions.

Now, revisiting the governing equation of uniaxial-bar thermal deformation given by Equation 3.16, the thermal deformation is proportional to the thermal expansion coefficient, the amount of temperature change and the length of a bar. The equilibrium spacings between atoms are determined by a balance between their attractive and repulsive forces no matter which type of bond is involved, as shown in Figure 4.1. Changes in temperature and pressure will alter the spacing accordingly, so that thermal expansion or contraction occurs in a material. As the temperature of a material is increased from absolute zero on the Kelvin scale, the atoms begin vibrating about their equilibrium positions and the amplitude of vibration increases with temperature. This amplitude of vibration is not symmetric, however.

The repulsive forces increase as atoms are pushed together more drastically than do the attractive forces as atoms are pulled apart. In other words, it is easier to pull atoms apart than to push them together. Thus the amplitude of vibration is nonsymmetrical, resulting in a net atom positive displacement, the magnitude of which increases with increasing temperature. This phenomenon is well depicted in Figure 4.1 (modified from Barrett *et al.*, 1973, pp. 36) and is known as thermal expansion. There are a few exceptions to this behaviour. Uranium, for instance, has a negative temperature coefficient of expansion.

Thermal expansion is usually described by the macroscopic measure, the thermal expansion coefficient α. The average value over a range from 20 °C to another temperature is usually taken for the thermal expansion coefficient of materials as discussed in Section 2.3.1.

There is another type of thermal effect at the atomic level. The equipartition theorem states that a classical system in thermal equilibrium at temperature T has a mean energy

---

* For solid materials, constant-volume specific heat c_v is nearly equal to constant-pressure specific heat c_p as stated in Chapter 3.

of $\kappa T/2$ per degree of freedom, where κ is the Boltzmann constant, corresponding to each squared term in the expression for the energy of the system (Waldram, 1985, pp. 149-151). This phenomenon is referred to as thermal noise. In ordinary machine structures, the noise is too small to affect the functional quality of a machine, but in the nanotechnology realm, the thermal noise is significant.

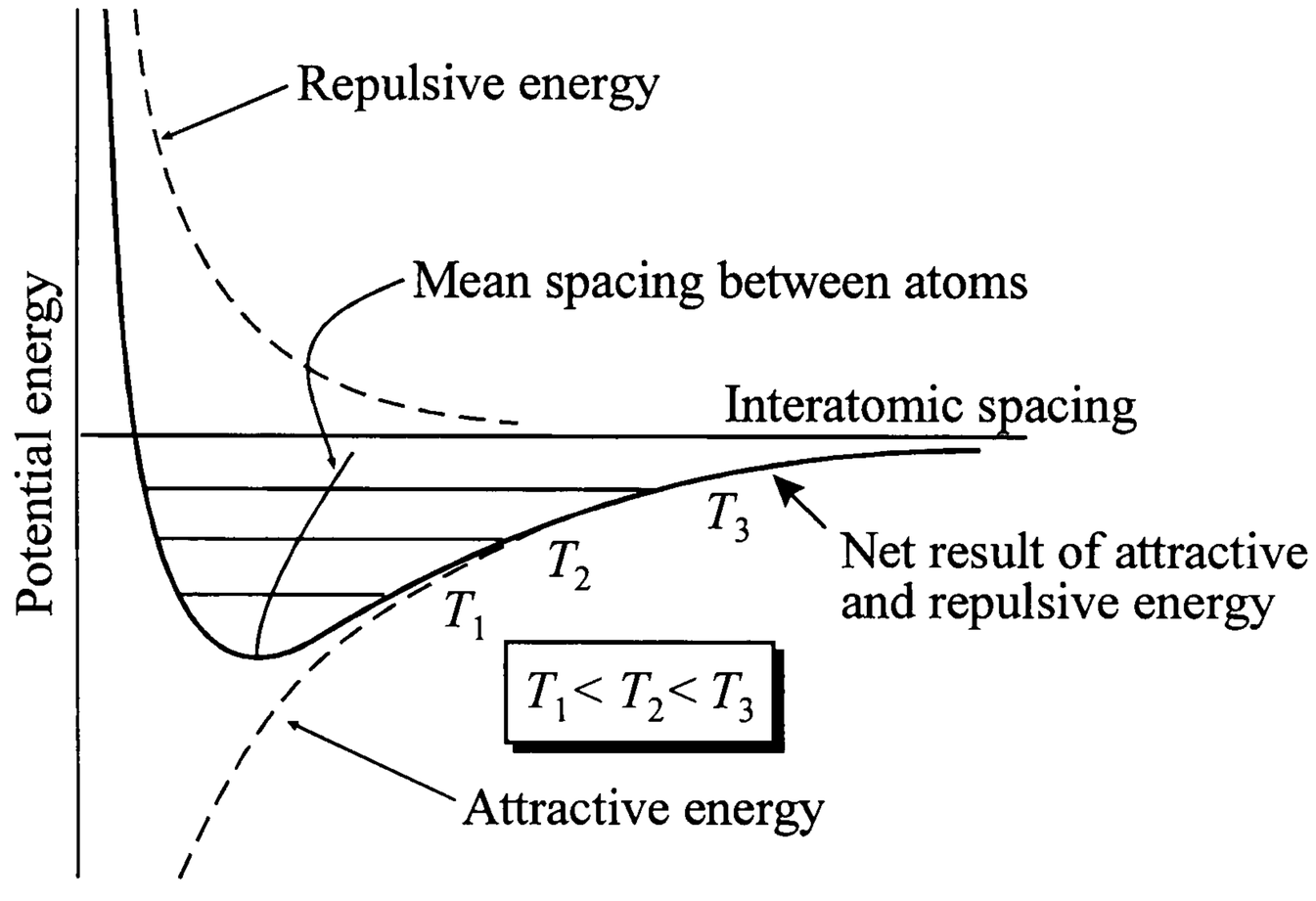

Figure 4.1 Increase in the nearest neighbour distance with increase in temperature

All the governing equations are derived in a differential element of a body, so that we cannot find more factors related to thermal deformations other than material properties. In fact, Cebon and Ashby (1994) chose the following combination to be a performance index for the selection of materials to resist thermal distortion:

$$k/\alpha$$

Thus for a given geometry and heat input, the distortion is minimised by selecting materials with large values of the performance index.

4.2.2 Close Examination of Solutions

The solutions of governing equations of thermal deformation yield a detailed picture of the thermophysical behaviour of a machine component. Consider the solutions for temperature development given by Equation 3.6 and 3.7: the former expresses the response of a lumped-capacitance thermophysical system in the case of step temperature-rises, so that it represents the step response of the system; the latter represents the ramp response. Figure 4.2 shows the responses of a lumped-capacitance system undergoing free thermal expansion according to temperature changes given by Equations 3.6 and 3.7.

Equation 3.6 indicates that the response is exponential, and also, the step response of Figure 4.2 shows that the step input causes the output to rise exponentially until a new, stable level is reached. In the case of spatially non-uniform temperature development of which an example is depicted in Figure 3.4 using the finite-difference method, this exponential rise also can be seen at each cell level.

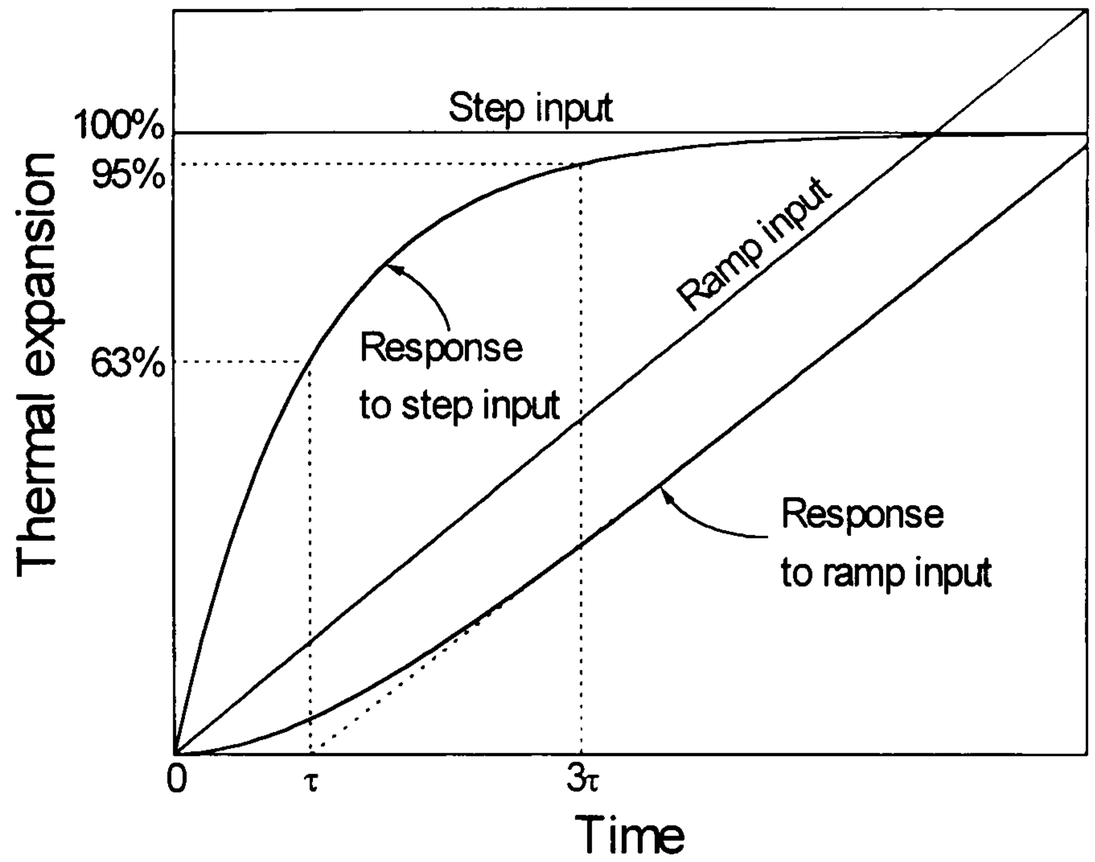

Figure 4.2 Responses of lumped-capacitance system

This class of self-regulating system is referred to as a first-order system in control theory. A measure of how rapidly that exponential behaviour changes is represented by the time constant. After the first time constant, the output is risen to 63.21% of its final value. At the end of 3τ, the output reaches 95.02% of the final value, and after 5τ the response is risen to 99.33% and is virtually complete.

During any one period of a time constant, the output will change by 63.21% of its maximum possible change. In this particular instance, the time constant τ is given by a combination, $\rho c_p V/(hA)$ in Equation 3.6. The ramp response of Figure 4.2 also suggests that the system is first-order. First-order systems are governed by two parameters, gain and time constant, and gain is the normalised output at the final stable state to the input, giving an overall measure of the system input-output characteristics.

Consider another case of Equation 3.8 applied to a freely expanding body, plotted in Figure 4.3. We can see an attenuating effect and a phase lag between the input and output. The frequency of the output response is equal to that of the input. This system is, therefore, conformed with the characteristics of first-order systems. According to Equation 3.8, the time-constant plays a vital role in these behaviours together with the frequency of input temperature variations.

Finally, the concept of penetration depth has an important physical meaning: there is a transportation lag in the heat-transfer process. It takes a finite time to transfer thermal energy from the vicinity of a heat source to other, far sides of a machine structure.

As a consequence of the foregoing points, we can describe thermal deformations of a body with a first-order system having three parameters, gain, time-constant and time-delay. However this conclusion has a limitation, i.e. it is only deduced from the behaviours of lumped systems. It is required to assess the goodness of the parameters by means of real data obtained by either numerical analyses or experiments.

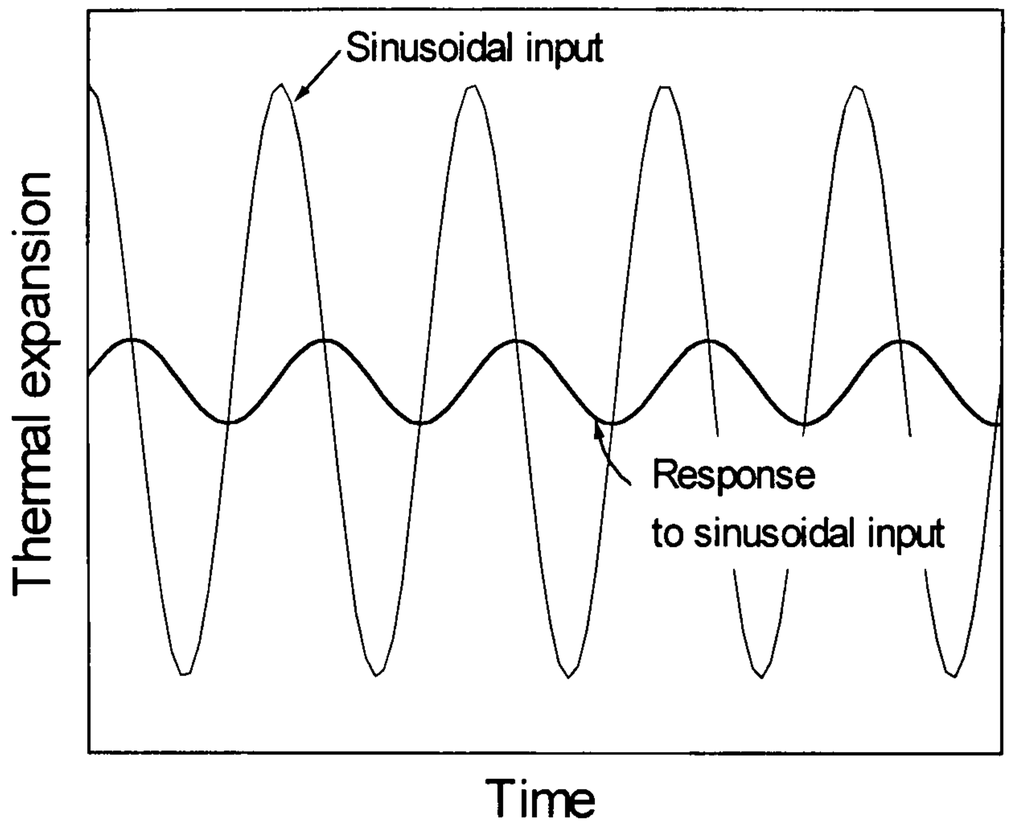

Figure 4.3 Response of lumped-capacitance system
subject to sinusoidal temperature variations

4.3 Numerical Simulation of Thermal Deformation

Although analytical methods provide means for elementary understanding of physical phenomena, they cannot deal with general distributed systems. Thermal behaviour of a machine can be identified with analytical means only if the structure is constructed with simple elements such as beams, rods or shells, which the theory of elasticity talks about. Lots of assumptions can also lead to deviations. However most structural components are complex in shape, and as seen in Section 3.3, unsteady heat transfer problems are difficult to deal with even in the simple cases. A machine bed, for example, cannot be readily analysed by the conventional analytical tools derived in Section 3.4.

When analytical techniques fail in engineering problems, one can take advantage of numerical methods. We can use the finite difference method that was employed in Section 3.3 for temperature calculations, finite element method (FEM), or boundary element method for identification of thermoelastic behaviour of a machine tool. Each of these methods has been proven to be acceptable as a powerful engineering tool, although the finite difference method is not suitable for the stress analysis of complex engineering components. The boundary element method has some advantages over the finite element method: it is more suitable for field problems such as temperature distribution calculations and consumes less computation resource.

Many FEM packages are now available to researchers interested in transient thermoelastic problems of 3-dimensional solid bodies. Of those, PAFEC* and ABAQUS** are distinguishable, but user-friendly; graphical-interfaced I-DEAS*** does not have a transient thermal conduction solver. For this study, the author used PAFEC Level 7.1. Using the FEM package it was intended to obtain the following:

- Response of a 3-dimensional thermoelastic body subject to a step change of an environmental thermal condition.
- Response of a 3-dimensional thermoelastic body undergoing cyclic thermal loadings. The results will explain the degree of the admittance of cyclic thermal inputs to a body.

4.3.1 FEM for Transient Thermoelastic Problems

Finite element techniques are based upon the solution of the governing integral equations of physical phenomena by means of piecewise discretisation (El-Zafrany, 1993, pp. 3). The domain integral equations are obtained by a variational principle or weighted-residual principle from governing differential equations. The problem domain is divided into a number of smaller and simpler subdomains, known as finite elements. If the equations of the elements are assembled together into a matrix form, the matrix equation is solved in terms of initial and boundary conditions. The finite element method is considered the most popular numerical technique used for engineering analysis, and it has a very wide range of applications. However FEM analysis of a real 3-dimensional problem may require considerable numbers of finite elements, leading to thousands of equations to be solved.

The usual procedure to carry out a temperature calculation leading to a thermal stress calculation is to run two separate jobs. For the temperature calculation, PAFEC solves the following matrix equation (PAFEC, 1984, pp. 2.113-2.122) with initial and boundary conditions:

$$\mathbf{M}\dot{\mathbf{T}} + \mathbf{K}\mathbf{T} = \mathbf{F}$$

where **M**, **K** are respectively a thermal mass matrix and square symmetric thermal conductivity matrix; **T** is a temperature vector of all nodes; **F** is a thermal loading vector whose elements are heat transfer rates entering at nodes; the dot over the temperature vector indicates a time-derivative. Once the temperature calculation is completed, the result is saved into a file.

---

* PAFEC Ltd., Strelley Hall, Strelley, Nottingham NG8 6PE
** Hibbitt, Karlsson & Sorensen (UK) Ltd.
The Genesis Centre, Science Park South, Birchwood, Warrington, Cheshire WA3 7BH
*** Structural Dynamics Research Corporation
2000 Eastman Drive, Milford, OH 45150, USA

Using the result of a temperature calculation and any other possible mechanical loading conditions, PAFEC solves the following matrix equation to obtain corresponding thermal stress and thermal strain:

$$\mathbf{KU} = \mathbf{F}$$

where **K** is a stiffness matrix; **U** is a displacement vector; **F** is a load vector.

4.3.2 Selection of Object

In order to extract useful information from numerical simulation, the selection of the object is important. Firstly, the object must be simple in shape, so that we can easily identify the distributed thermoelastic behaviour in terms of the least possible points on the object. We cannot deal with all the nodes of the finite element model of the object. Secondly, the distributed nature of the object should be preserved against the simplicity requirement, because we have to evaluate the effects of the distributed nature of system parameters which cannot be dealt by means of analytical methods. Thirdly, the object should have a certain standing on the field of precision engineering. In the end, a straightedge, measuring 0.1×0.1×0.5m, supported on the Airy points was selected to be the study object, as depicted in Figure 4.4.

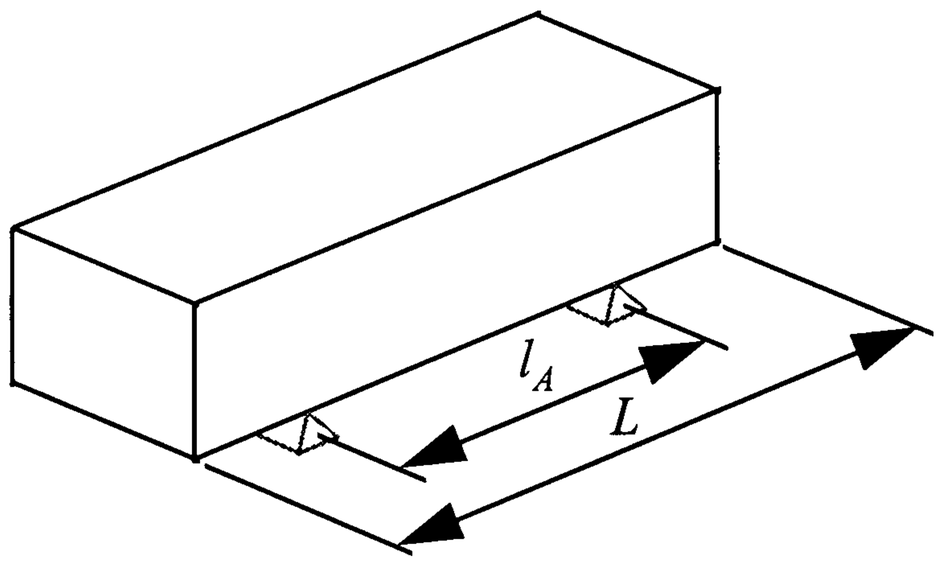

Figure 4.4 Straightedge supported on Airy points

Sir George Airy proved that bars could be supported, without significant loss of accuracy, on eight rollers mounted in a compensating frame as shown in Figure 4.5, which distributed the supporting reactions evenly. For a frame of N rollers, Airy's formula for the spacing of the rollers was (Rolt, 1929)

$$\frac{L}{\sqrt{N^2-1}}$$

where L is the length of a bar. The number of rollers could be reduced to two such as shown in Figure 4.4, where their separation l_A becomes $0.577L$. This is used to achieve parallelism of the end faces of a scale. Correspondingly, for minimum deviation from straightness, the supports should be spaced at $0.554L$ (Smith and Chetwynd, 1992, pp. 323). In this study, the latter case was employed.

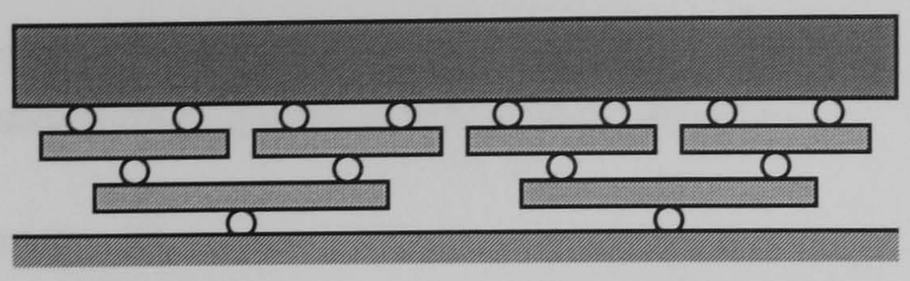

Figure 4.5 Bar supported on eight rollers

4.3.3 Analysis Conditions

The straightedge is considered to be placed in an environment having a uniform temperature distribution, i.e. without any spatial dependency of temperature. A temperature controlled bath will provide this type of thermal environment. The heat transfer mode involved is assumed to be natural convection only, shown in Figure 4.6, and the variation of surrounding air temperature is also assumed to be manifested on all the surfaces of the straightedge uniformly.

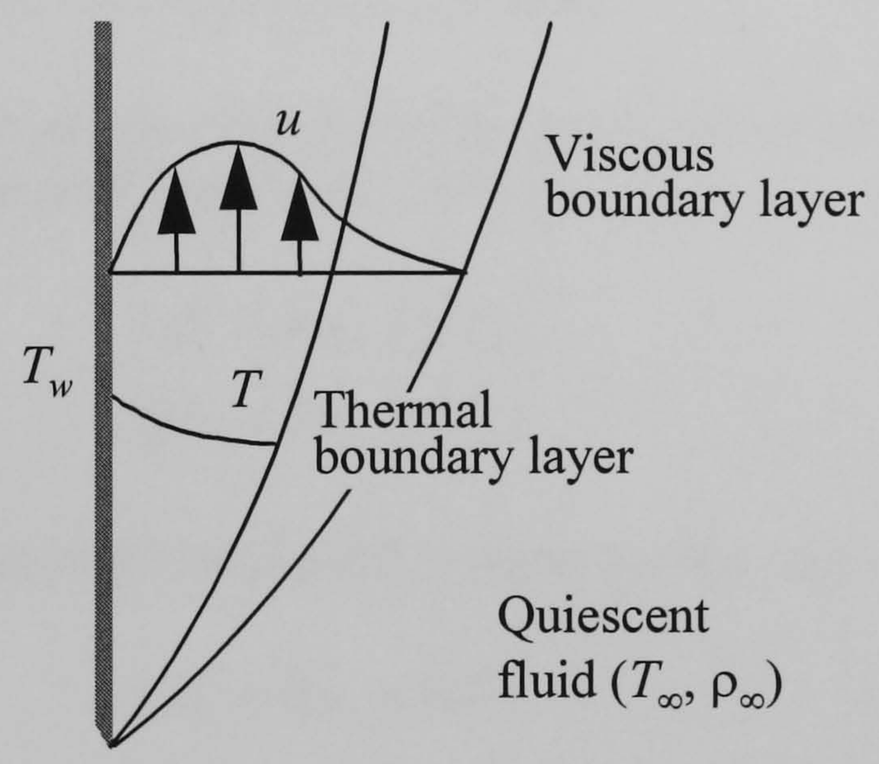

Figure 4.6 Natural convection

In natural convection, fluid flows naturally, driven by the effect of change in density. The layer adjacent to the warm vertical wall of Figure 4.6 becomes less dense than the rest of the fluid having a density ρ_∞. Its reduced density causes it to flow upward, to sweep the wall and to collect heat transferred from the wall. There are two boundary layers associated with natural convection; a viscous boundary layer and thermal boundary layer as shown in Figure 4.6. According to the properties of the fluid, a thermal boundary layer may include a viscous boundary layer. The heat transfer coefficient of natural convection changes with temperature difference between an environment and the surface of a body, but it is assumed to be constant. Furthermore the flow is assumed to be laminar. In this simulation work, the exactness of the calculation is a secondary problem. The primary objective is to extract an overall trend of the behaviour of a thermoelastic system under some input conditions.

For free convection from a vertical plate of constant wall temperature, an empirical correlation is recommended as (Churchill and Chu, 1975)

$$\overline{\mathrm{Nu}_L} = 0.68 + \frac{0.670\mathrm{Ra}_L^{1/4}}{\left[1+(0.492/\mathrm{Pr})^{9/16}\right]^{4/9}} \qquad (0 < \mathrm{Ra}_L < 10^9)$$

The notations used in the formula are:

- Average Nusselt number: $\overline{\mathrm{Nu}_L} = \frac{hL}{k_f}, \quad \bar{h} \equiv \frac{1}{A}\int h dA$

  where k_f is the thermal conductivity of a fluid; L is a characteristic length.

- Rayleigh number: $\mathrm{Ra} \equiv \mathrm{GrPr}, \quad \mathrm{Gr}_L \equiv \frac{g\alpha_V(T_s - T_\infty)L^3}{\nu^2}, \quad \mathrm{Pr} = \frac{\nu}{\beta}$

  where g is the gravitational acceleration; α_V is a volumetric thermal expansion coefficient (for a perfect gas, $1/T$); T_s is the temperature of a surface; T_∞ is the temperature of a fluid; ν is a kinematic viscosity.

The following formulae are correlated for the upper surface of a heated plate or lower surface of a cooled plate (Goldstein *et al.*, 1973):

$$\overline{\mathrm{Nu}_L} = 0.54\mathrm{Ra}_L^{1/4} \qquad (10^4 \le \mathrm{Ra}_L \le 10^7)$$

$$\overline{\mathrm{Nu}_L} = 0.15\mathrm{Ra}_L^{1/3} \qquad (10^7 \le \mathrm{Ra}_L \le 10^{11})$$

and for the lower surface of a heated plate or upper surface of a cooled plate (*ibid.*):

$$\overline{\mathrm{Nu}_L} = 0.27\mathrm{Ra}_L^{1/4} \qquad (10^5 \le \mathrm{Ra}_L \le 10^{10})$$

It is noted that the characteristic length L of horizontal surfaces should be chosen to be the ratio of the plate surface area to the perimeter.

The heat transfer coefficients of each side of the straightedge were evaluated using the above relations. Though the relations are valid for the constant wall-temperature objects, the values were calculated at the start of inputs, i.e. when t = 0, together with thermophysical properties of air in atmospheric pressure (Table 4.2, data taken from Welty *et al.*. 1984, pp. 756). For the sinusoidal input, the heat transfer coefficients are evaluated in an average sense.

T (K)	Density (kg/m^3)	Constant pressure specific heat (10^3J/kg·K)	Viscosity (10^{-5} Pa·s)	Kinematic viscosity (10^{-5} m^2/s)	Thermal conductivity (10^{-2}W/m·K)	Thermal diffusivity (10^{-5} m^2/s)	Prandtl number, Pr
260	1.3587	1.0054	1.6503	1.2146	2.3080	1.6896	0.719
280	1.2614	1.0057	1.7503	1.3876	2.4671	1.9448	0.713
300	1.1769	1.0063	1.8464	1.5689	2.6240	2.2156	0.708

Table 4.2 Thermophysical properties of air

For the identification of system parameters governing thermal deformations, two types of heat inputs were considered: sudden step temperature rise and sudden sinusoidal temperature variation. A step input has been used for the assessment of the transient behaviour of a system and sinusoidal excitation is widely used for the identification of frequency characteristics of a system. Three different step inputs, steps of 1, 2.5 and 5, were employed to investigate the linearity of a system undergoing thermal deformations. The amplitude of the sinusoidal input was chosen to be 2.5. Table 4.3 lists calculated heat transfer coefficients for each input case when $t = 0$.

	$\Delta T = 1$	$\Delta T = 2.5$	$\Delta T = 5$
Vertical plate			
Step input	2.57	3.18	3.75
Sinusoidal input	-	3.19	-
Cooled upper or heated lower			
Step input	1.56	1.97	2.34
Sinusoidal input	-	2.96	-
Cooled lower or heated upper			
Step input	3.13	3.93	4.67
Sinusoidal input	-	2.96	-

Table 4.3 Spreadsheet results of heat transfer coefficients used in simulation

Materials also play a vital role in thermal deformations as seen in Section 4.2.1. Aluminium, granite and steel were selected to simulate the effects of different materials; they are likely to behave distinctively.

The effects of mechanical constraints were also considered because they could minimise or magnify deformations due to temperature changes of a body. Two types of constraints were employed: simply-supported and fully-restrained. Simply-supported beams are likely to be a popular choice for a metrology system. When a metrology system is on a moving carriage, it is fully restrained in some cases.

The straightedge was divided into finite elements using an 8-noded brick element as shown in Figure 4.7 for the calculation of 3-dimensional transient temperature distribution and the following 3-dimensional thermal deformation.

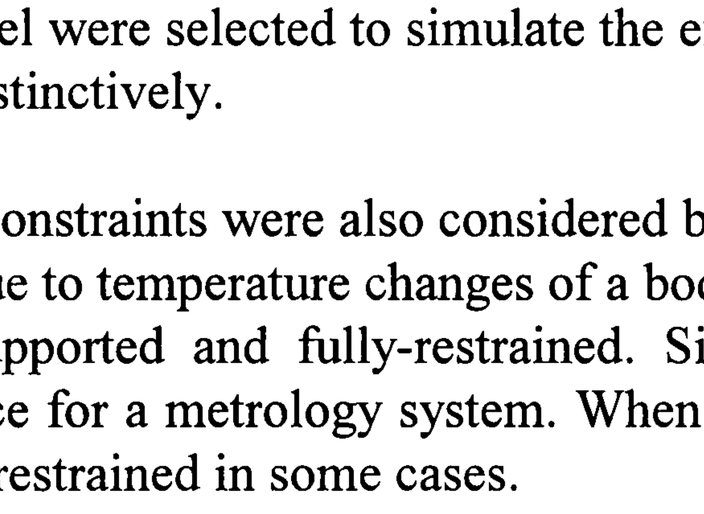

Figure 4.7 8-noded brick element

4.3.4 Results of Analysis

PAFEC gives the results of finite-element calculations basically in a tabulated list. PAFEC also provides a post-processor by which we can plot the results in a graphical format. Because we deal with a straightedge supported on the Airy points, the straightness is the most important factor we should look at. It is better to select several representative points on the straightedge, rather than deal with all the nodes. Connecting these points, the straightness will be reasonably obtainable. Figure 4.8 shows the selected points on the straightedge.

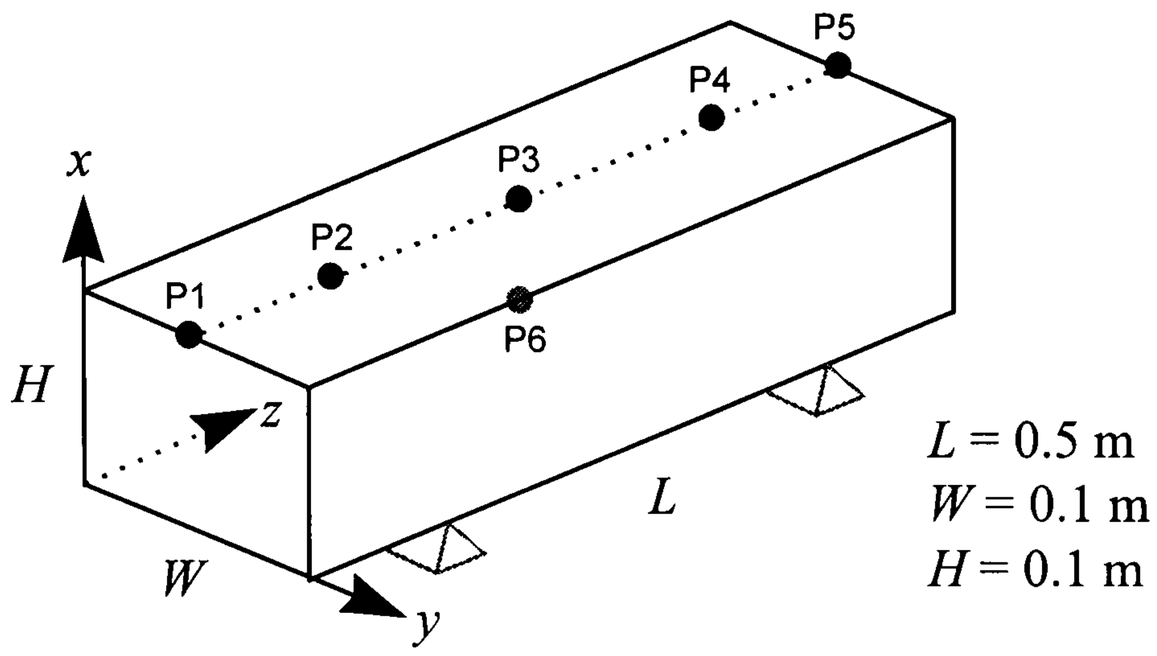

Figure 4.8 Selected representative points

Points P1 and P5 are located at either end of the straightedge. Point P3 represents the centre of the upper surface. It has the largest deflection components in the upper surface. The points P2 and P4 are chosen to be in line with the support position. Thus we can obtain straightness of the top surface by interpolating these points. Point P6 is located at the centre of the straightedge for the verification of a time-delay element. The coordinates of each point are tabulated in Table 4.4.

	P1	P2	P3	P4	P5	P6
x	0.1	0.1	0.1	0.1	0.1	0.05
y	0.05	0.05	0.05	0.05	0.05	0.05
z	0	0.1115	0.25	0.3885	0.5	0.25

Table 4.4 Coordinates of selected points in metres

All the calculation results on the selected points are plotted in Appendix A. Figures A.1 to A.37 are the results for step temperature-rise inputs. Figures A.1 to A.15 are the response of the temperature of the straightedge due to step temperature rise. We can calculate time-constants of the response using an interpolation technique. Examining the values of time constants, we can conclude that the time-constants of the different points of the straightedge are nearly equal except the points on the edges. The points on the edges will be strongly affected by the environmental temperature changes so that the values are smaller than those of other parts. This sort of edge effect is often neglected in engineering analysis. However, the response of the granite body reveals some difference between the time constant of the surface points and the centre point. This is due to smaller heat transfer rate attributed to low thermal conductivity and thermal diffusivity.

Thus, the spatial dependency of the time-constant can be assumed to be absent when the thermal conductivity or thermal diffusivity of the material is large.

We can also identify an interesting fact: the time-constant of the aluminium straightedge is similar to that of the granite straightedge. This is due to similar heat storage capacity between two materials (see Table 4.1). Steel has much larger heat capacity than aluminium and granite so that the time-constant is large. Thus, the investigations of thermal inertia in Section 4.2.1 are validated.

Figures A.16 to A.37 show the displacements of the selected points. Because the deformation response exactly follows that of the temperature of the body instantaneously, the characteristics of the time-constant are not dealt with further. First of all, we can see the straightness of the fully restrained straightedge is much worse than that of the simply supported straightedge because the restraints provide appreciable mechanical loadings in the straightedge. A simply-supported beam can be affected by the friction force between the supports and contact points with the supports, but the friction force can be neglected. The gain of a thermoelastic system undergoing thermal deflection is strongly dependent on the mechanical constraint conditions.

Figure A.25 explains the linearity of a thermoelastic system. We cannot find any nonlinearity inherent in the system for all the input cases: the displacement at point P3 increases linearly with the increase of the input temperature for all the simulation incidences. Thus a thermoelastic system can be assumed to be linear.

Figures A.38 to A.67 are the plots of the simulation results under sinusoidal input conditions. We can clearly see attenuating effects and phase lags. Furthermore, the exponential decay of the very first part of the response is observed. This is due to the time-constant of a system.

If we look at the responses of different points, we can observe slight phase differences among them. The response of the aluminium straightedge, depicted in Figure A.51, still has some differences. In fact, this behaviour is not that of phase differences: it is due to transportation lags between the points, because the phase lag is largely dependent on the time-constant and excitation frequency according to Equation 3.8. In the case of the aluminium, the time-constants of different points are nearly equal as can be seen in Figure A.4, A.9 and A.14. That is, time delay is present in a thermoelastic system undergoing thermal deformations and it is dependent on the spatial position of a point within a body.

4.4 Analysis Method of Dimensional Response

Machine tools and coordinate-measuring machines are built with many solid bodies that exhibit their own distinct dimensional responses under dynamic thermal loadings. Now we can propose a unified, simple analysis method of dimensional response due to dynamic thermal loadings using investigations done so far. A solid body considered in

this study was subject to thermal loadings only, but we can include mechanical loadings such as:

- Force due to gravitational acceleration **g**
- Constant or time varying forces $\mathbf{F}_i$ arising from other than gravity
- Reaction forces due to supports manifesting compliance, damping or rigidity

Figure 4.9 shows pictorially what we are dealing about.

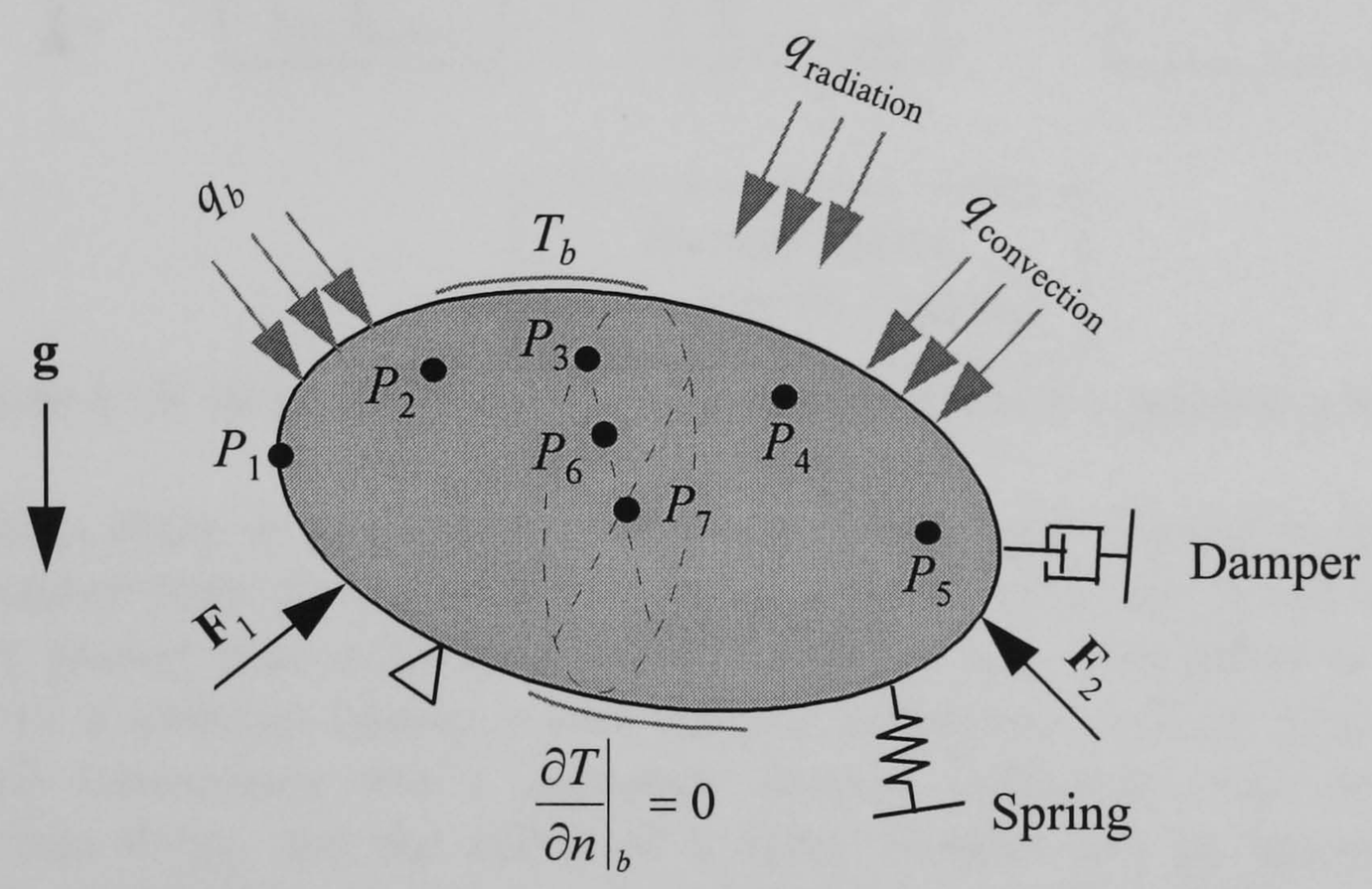

Figure 4.9 Body subject to external forces and thermal loadings

4.4.1 Descriptive Interpretation of Thermal Deformation

An accurate analysis of thermal deformation should accommodate the distributed nature of material properties, and afterwards a lumped one might be employed as an approximation. The distributed nature makes problems difficult in general because governing equations become too complex to be solved as seen in Chapter 3. From a metrological point of view, we often sample the behaviour of an object at discrete points that are considered to be interesting, so that the overall behaviour can be described reasonably with fewer efforts and resources. This will be true for the case of thermal error problems of machine tools and coordinate-measuring machines. Errors occurring in machine movement are often measured at discrete points along the path of the movements. On-the-fly measurements are applied only to some critical machine-units. A point-wise description of thermal errors is quite reasonable in a metrological sense and difficulties in analysing a distributed system will be overcome. Overall behaviour can be obtained by interpolation between points of interest.

In Figure 4.9, there are several points on the body, denoted by P_i, which are assumed to be interesting points for a particular body. Points P_1 to P_5 are located on the surface of a body, P_6 is between the surface and its centre, and P_7 is at its centre. Each point has its own response under thermal loadings. This response at a particular time can be

accurately described as a block diagram shown in Figure 4.10. A heat input will cause a movement of point P_i to another position, and it has three components in a Cartesian coordinate system. During the movement, four types of process-elements are acting, i.e. a delay element, first-order element, gain element and positive feedback element. This block diagram is the result of analyses done so far.

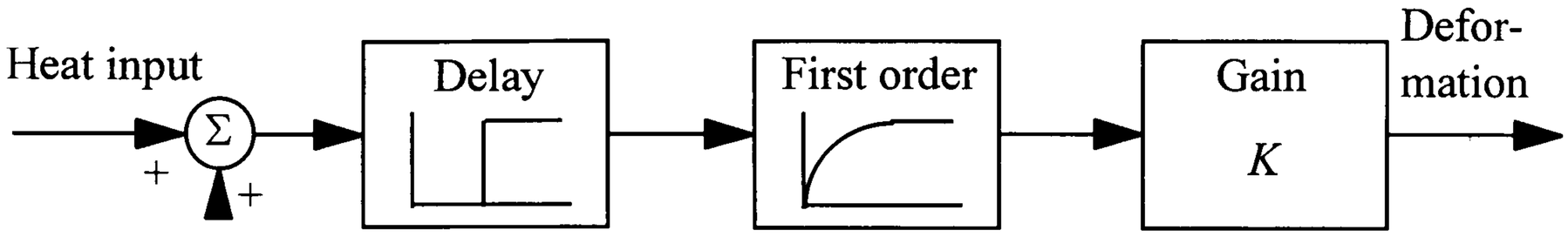

Figure 4.10 Block diagram of thermal deformation at a point in a body

By definition, a delay or dead-time element makes an output delayed in time. In heat-transfer processes there is a transportation delay of heat flux. Point P_6 at the centre will experience a greater time delay than points on the surface. This effect is particularly significant for a material having a low thermal diffusivity such as granite. A body having small dimensions and a moderate thermal diffusivity will not exhibit a significant time delay, and the effect of a delay element can be ignored. Thermal environments also affect the magnitude of time delay. Time delay, ranging from fractions of seconds to hours, depends on the location of a point of interest with respect to heat sources and material properties. Thermal environments generally vary with time, and thus time delay varies with time too.

A first-order element is well recognised in thermal deformations, and characterised by the time-constant. A particular characteristic of a thermal deformation process is that a first-order element has a very large time-constant in comparison with electrical or servo systems, i.e. on the order of hours to several days. Correspondingly, steady-state responses could not be of use for the problems of thermal deformations. It is understood that several factors are acting simultaneously to form the time-constant, i.e. the heat capacity of a body, the size of a body and the corresponding thermal environment. The thermal environment generally varies with time, and thus the time-constant varies with time too.

A gain element converts changes in temperature to the corresponding displacements. The coefficient of thermal expansion plays a main role in this process. A body of a high thermal expansion coefficient will generally exhibit a high gain in this process. Another important factor in this process is the constraint conditions of a body, and they affect the distribution of the gain of each point significantly. A freely-expanding body will have a uniform distribution of the gain throughout its surface and inside, whereas a constrained one will exhibit significant changes in the gain. Finally, thermal environments also affect gain. The thermal environment generally varies with time, and thus gain varies with time too.

As a final element, there is a positive feedback effect. It is related with two physical phenomena, i.e. inertial effects and thermoelastic coupling. Inertial effects are associated with the rate of change of strain rate. If an engineering component is stationary and external forces are applied gradually, then inertial effects are negligible. This is the case of machine tool components. Thermoelastic coupling is related to strain rate. A process involving high strain rate, such as tensile testing, produces heat even though there are no heat inputs, but machine tool components do not have such a high strain rate. In elastic bodies undergoing non-inertial loading, it is observed that strain rate is always small compared to the rate of change of temperature, and thus we can discard the positive feedback element for this problem. In conclusion, thermal deformation of a body can be understood accurately with a point-wise delay-plus-first-order process, and thus thermal errors can be described by several delay-plus-first-order processes of points of interest in a machine structure.

4.4.2 More Refinement of Point-wise Description Method

As a first step, a governing equation of thermal deformation of a point at a particular time will be obtained. Let $F_{th}(t)$ denote a time-varying thermal loading, then the output of a delay element will be

$$y_d = F_{th}(t - t_D)$$

where t_D is a dead time that can be estimated by using Equation 3.10. Its transfer function is obtained by applying a Laplace transform:

$$G_d(s) = \frac{\overline{y}_d(s)}{\overline{F}_{th}(s)} = e^{-t_D s}$$

where the overlaid bar expresses Laplace-transformed variables. A Taylor series expansion of the above transfer function is

$$G_d(s) = 1 - t_D s + \frac{1}{2!} t_D^2 s^2 + \cdots + \frac{1}{n!}(-t_D)^n s^n + \cdots$$

where n is an integer. The order of magnitude of dead time can be envisaged using the concept of penetration depth. If the dead time is very small, then we can neglect terms containing higher order of t_D:

$$G_d(s) \approx 1 - t_D s = \frac{(1 - t_D s)(1 + t_D s)}{1 + t_D s} \approx \frac{1}{1 + t_D s}$$

The transfer function of a first-order element is given as (Ogata, 1970, pp. 221)

$$G_f = \frac{1}{1 + \tau s}$$

where τ is the time-constant.

The transfer function of a gain element is simply a constant gain:

$$G_g = K$$

Gain K is a function of a thermal expansion coefficient, constraint conditions and thermal environments.

The total transfer function G is obtained by the product of G_d, G_f and G_g:

$$G = \frac{Ke^{-t_D s}}{1 + \tau s}$$

This transfer function is equivalent to the following first-order differential equation:

$$\tau \frac{du}{dt} + u = KF_{th}(t - t_D)H(t - t_D) \tag{4.3}$$

where u is the displacement of a point in a body caused by temperature rise; $H(t)$ is the Heaviside unit step function.

In the case of negligible dead time, we obtain the following total transfer function:

$$G = \frac{K}{1 + \tau s}$$

and the corresponding differential equation is

$$\tau \frac{du}{dt} + u = KF_{th}(t) \tag{4.4}$$

The above equation has an electrical analogy with an RL-circuit represented by the following equation:

$$L\frac{dI(t)}{dt} + RI(t) = E(t) \quad \text{or} \quad \tau_L \frac{dI(t)}{dt} + I(t) = \frac{1}{R}E(t)$$

where L is an inductance; $I(t)$ is a current; R is a resistance; $E(t)$ is an electromotive force; τ_L is inductive time constant, i.e. L/R.

In the case of small dead-time, the total transfer function is equivalent to a system built by cascading two first-order elements with different time constants:

$$G(s) = \frac{K}{1 + (\tau + t_D)s + \tau t_D s^2} = \frac{K\omega_n^2}{\omega_n^2 + 2\zeta\omega_n s + s^2}$$

where ω_n is a natural frequency equal to $1/\sqrt{\tau \cdot t_D}$; ζ is a damping factor equal to $(\tau + t_D)/(2\sqrt{\tau \cdot t_D})$. The time constant of a second-order system is defined by

$$\tau' = \frac{1}{\omega_n}$$

but if $t_D << \tau$, then ζ becomes large. This is true for the case of a small dead-time. The system is heavily damped, and it behaves like a first-order system with $\tau' = \tau$. The transfer function has a relation with the following differential equation:

$$\frac{d^2u}{dt^2} + 2\zeta\omega_n \frac{du}{dt} + \omega_n^2 u = K\omega_n^2 F_{th}(t) \qquad (4.5)$$

It is noted that all the governing differential equations are of constant coefficient, linear form.

4.4.3 State-space Representation: Final Form

The characteristics of the point-wise description approach explored in this study are:

- Time responses are thoroughly pursued.
- Distributed behaviours are analysed at the discrete points of a body.
- System parameters are allowed to be varied with time.

They constitute an analysis of a multiple-input, multiple-output, time-varying system. In a time-invariant system, the same input applied at different times will produce outputs that are identical in shape and size but shifted in time. This cannot be true in a time-varying system. Because system parameters are varying with time due to continuously changing thermal environments and some finite number of sampling points will be involved, the governing equations of the thermal deformation of a body will have the following form:

$$\begin{aligned}
&\text{Point } P_1: \quad \tau_1(t)\frac{du_1}{dt} + u_1 = K_1(t)F_{th_1}\left[t - t_{D_1}(t)\right]H\left[t - t_{D_1}(t)\right] \\
&\text{Point } P_2: \quad \tau_2(t)\frac{du_2}{dt} + u_2 = K_2(t)F_{th_2}\left[t - t_{D_2}(t)\right]H\left[t - t_{D_2}(t)\right] \\
&\qquad\qquad \vdots \\
&\text{Point } P_n: \quad \tau_n(t)\frac{du_n}{dt} + u_n = K_n(t)F_{th_n}\left[t - t_{D_n}(t)\right]H\left[t - t_{D_n}(t)\right]
\end{aligned} \qquad (4.6)$$

This set of equations can be effectively analysed by employing a state-space analysis method as introduced in Section 3.3.5. The state equation of the thermal deformation of a body can be expressed by

$$\dot{\mathbf{v}} = \mathbf{A}(t)\mathbf{v} + \mathbf{B}(t)\mathbf{x}$$

where:

$$\mathbf{v} = \begin{bmatrix} u_1 \\ u_2 \\ \vdots \\ u_n \end{bmatrix} \text{ (state vector)}$$

$$\mathbf{x} = \begin{bmatrix} F_{th_1}\left\{t - t_{D_1}(t)\right\} H\left\{t - t_{D_1}(t)\right\} \\ F_{th_2}\left\{t - t_{D_2}(t)\right\} H\left\{t - t_{D_2}(t)\right\} \\ \vdots \\ F_{th_n}\left\{t - t_{D_n}(t)\right\} H\left\{t - t_{D_n}(t)\right\} \end{bmatrix} \text{ (input vector)}$$

$$\mathbf{A}(t) = \begin{bmatrix} -1/\tau_1(t) & 0 & \cdots & 0 \\ 0 & -1/\tau_2(t) & \cdots & 0 \\ \vdots & \vdots & \vdots & \vdots \\ 0 & 0 & \cdots & -1/\tau_n(t) \end{bmatrix}$$

$$\mathbf{B}(t) = \begin{bmatrix} K_1(t)/\tau_1(t) & 0 & \cdots & 0 \\ 0 & K_2(t)/\tau_2(t) & \cdots & 0 \\ \vdots & \vdots & \vdots & \vdots \\ 0 & 0 & \cdots & K_n(t)/\tau_n(t) \end{bmatrix}$$

The output equation becomes

$$\mathbf{y} = \mathbf{C}(t)\mathbf{v} + \mathbf{D}(t)\mathbf{x}$$

where:

$$\mathbf{y} = \begin{bmatrix} y_1 \\ y_2 \\ \vdots \\ y_n \end{bmatrix} \text{ (output vector)}$$

$\mathbf{C}(t) = \mathbf{I}$ ($n \times n$ identity matrix)

$\mathbf{D}(t) = \mathbf{0}$ ($n \times n$ null matrix)

The solution of the state equation is given as (Ogata, 1970, pp. 694)

$$\mathbf{u}(t) = \Phi(t, t_0)\mathbf{v}(t_0) + \int_{t_0}^{t} \Phi(t, \xi)\mathbf{B}(\xi)\mathbf{x}(\xi)d\xi$$

where $\Phi(t, t_0)$ is a state-transition matrix that can be computed by the following series expansion:

$$\Phi(t, t_0) = \mathbf{I} + \int_{t_0}^{t} \mathbf{A}(\xi)d\xi + \int_{t_0}^{t} \mathbf{A}(\xi_1)\left[\int_{t_0}^{\xi_1} \mathbf{A}(\xi_2)d\xi_2\right]d\xi_1$$
$$+ \int_{t_0}^{t} \mathbf{A}(\xi_1)\left\{\int_{t_0}^{\xi_1} \mathbf{A}(\xi_2)\left[\int_{t_0}^{\xi_2} \mathbf{A}(\xi_3)d\xi_3\right]d\xi_2\right\}d\xi_1 + \cdots$$

In a linear time-invariant case, the state-transition matrix is an exponential of $\mathbf{A}t$, and the following equation will be solved as an example:

$$\tau\frac{du}{dt} + u = KF_{th}(t) \quad \text{or} \quad \frac{du}{dt} = -\frac{1}{\tau}u + \frac{K}{\tau}F_{th}(t)$$

When the initial condition is zero, the solution for a step input of magnitude T_a is obtained as

$$u = e^{-t/\tau}u(0) + \int_0^t e^{-(t-\xi)/\tau}\frac{K}{\tau}T_a d\xi = KT_a(1 - e^{-t/\tau}) \tag{4.7}$$

and the solution for a sinusoidal input $T_a \sin(\omega t - \phi)$ is derived as

$$u = e^{-t/\tau}u(0) + \int_0^t e^{-(t-\xi)/\tau}\frac{K}{\tau}T_a \sin(\omega\xi - \phi)d\xi = \frac{KT_a}{\sqrt{1+\omega^2\tau^2}}\left[\sin(\phi + \psi)e^{-t/\tau} + \sin(\omega t - \phi - \psi)\right]$$

where $\psi = \arctan(\omega\tau)$. The term $\sin(\phi + \psi)e^{-t/\tau}$ makes the median change exponentially.

One benefit of using Equation 4.6 is that it provides flexibility in choosing system input when analysing the thermal behaviour of a machine, because it describes the input-output characteristics. If a heat input to a machine component is chosen to be the spindle speed, then the gain has a unit of the form [(thermal deflection)(spindle speed)$^{-1}$].

Chapter 5
Test of Thermal Errors

5.1 Necessities

Three thermal parameters, time-delay, time-constant and gain, were proposed in Section 4.4 to model the thermal deformation of a machine tool. As complementary work, experimental investigations of physically real phenomena are required to re-enforce the theoretical approaches. At the same time we can learn the method of how to evaluate thermal parameters by testing a machine. On the other hand, many difficulties arise in the theoretical determination of thermal deformation of a machine tools. Most of them are related with modelling complex machine geometry and boundary conditions, but also there are fundamental matters regarding constants used in theoretical calculation, such as the thermal conductivity, heat transfer coefficient, thermal expansion coefficient, etc.

Table 5.1 shows the actual value range of the coefficient of thermal expansion for different scale materials (Kunzmann *et al.*, 1993), so we cannot know the exact value of the coefficient of thermal expansion for a given material unless specific measuring work has been done.

Material	Expansion coefficient (10^{-6} K^{-1})
Steel	10-12
Glass	6-10
Zerodur*	±0.01

Table 5.1 Range of thermal expansion coefficient

Thermophysical properties are not very well known. For example, the thermal conductivity of aluminium shows a ±20% uncertainty in measured data sets (Touloukian *et al.*, 1970-1977). The same is true for other solids, especially if impurities are present. Also, heat transfer experiments are difficult and uncertain. Typical measurement uncertainties are ±40% for emissivities, ±50% for convection coefficients (White, 1988, pp. 31-32). In free convection problems, the heat transfer coefficient is a sensitive

* Zerodur is a trademark of Schott Glass Technologies Inc., Mainz, Germany

function of temperature difference, leading to nonlinear heat transfer correlations. These problems impose the necessity of real tests. For the best possible accuracy, experimental evaluation is indispensable.

5.2 Test Object

A machine used in this study, developed by CPE*, is illustrated in Figure 5.1. The machine is of a horizontal work spindle configuration, and the spindle is fixed onto the bed while a tool traverses across the spindle on the linear carriage (X slide). The carriage is supported on the bed by an inverted V-shaped hydrodynamic guideway. This configuration lends itself to face turning of disc-shaped workpieces. The bed is made of synthetic granite while other components are mainly cast iron.

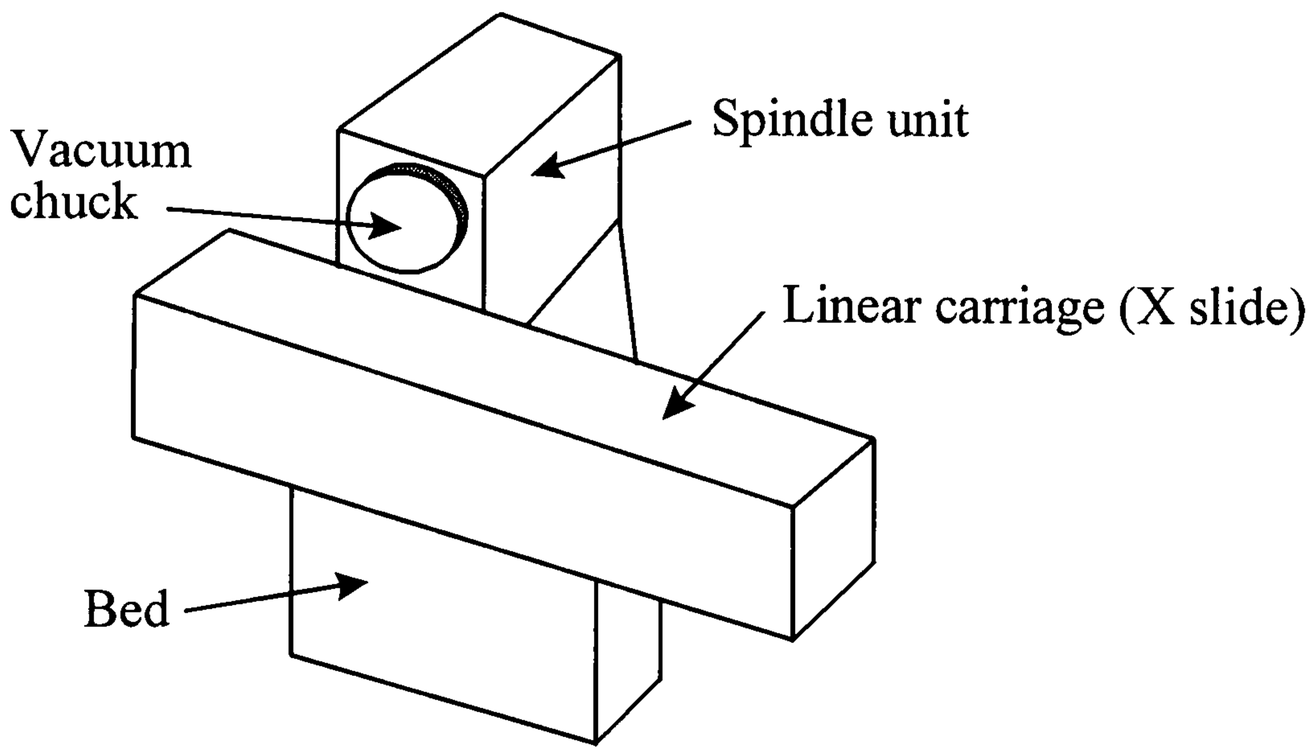

Figure 5.1 Precision facing lathe

The spindle has optically polished aerostatic thrust and radial bearings for precision machining, and is driven through a non-influencing coupling (pure-torque transmitter), as seen in Figure 5.2 that also gives the size of the spindle. Invar is used for the spindle shaft. A vacuum chuck, made of aluminium, is attached to the spindle nose for holding a workpiece by vacuum suction. The linear X-slide carriage is driven by a friction drive, but only the speed can be controlled because the machine is dedicated to the production of precision memory discs. This machine can routinely produce a plane of less than 10 nmRa roughness by diamond turning of aluminium workpieces.

Referring to the machine's machining operation, only motion along the spindle axis is the sensitive direction that is directly related with the accuracy of workpieces. Most thermal errors in that direction are likely to be from the spindle, which is believed to be the dominant heat source (Bryan, 1990). According to measurements, spindle thermal growth amounts to more than 6 μm in some cases (Mishima *et al.*, 1993) even in aerostatic spindles. Such an amount of deformation is not negligible in ultra-precision

---

* Cranfield Precision Engineering Ltd., Cranfield, Bedford

machining. In precision machine tools, indeed the ultimate attainable accuracy is limited by that of the spindle.

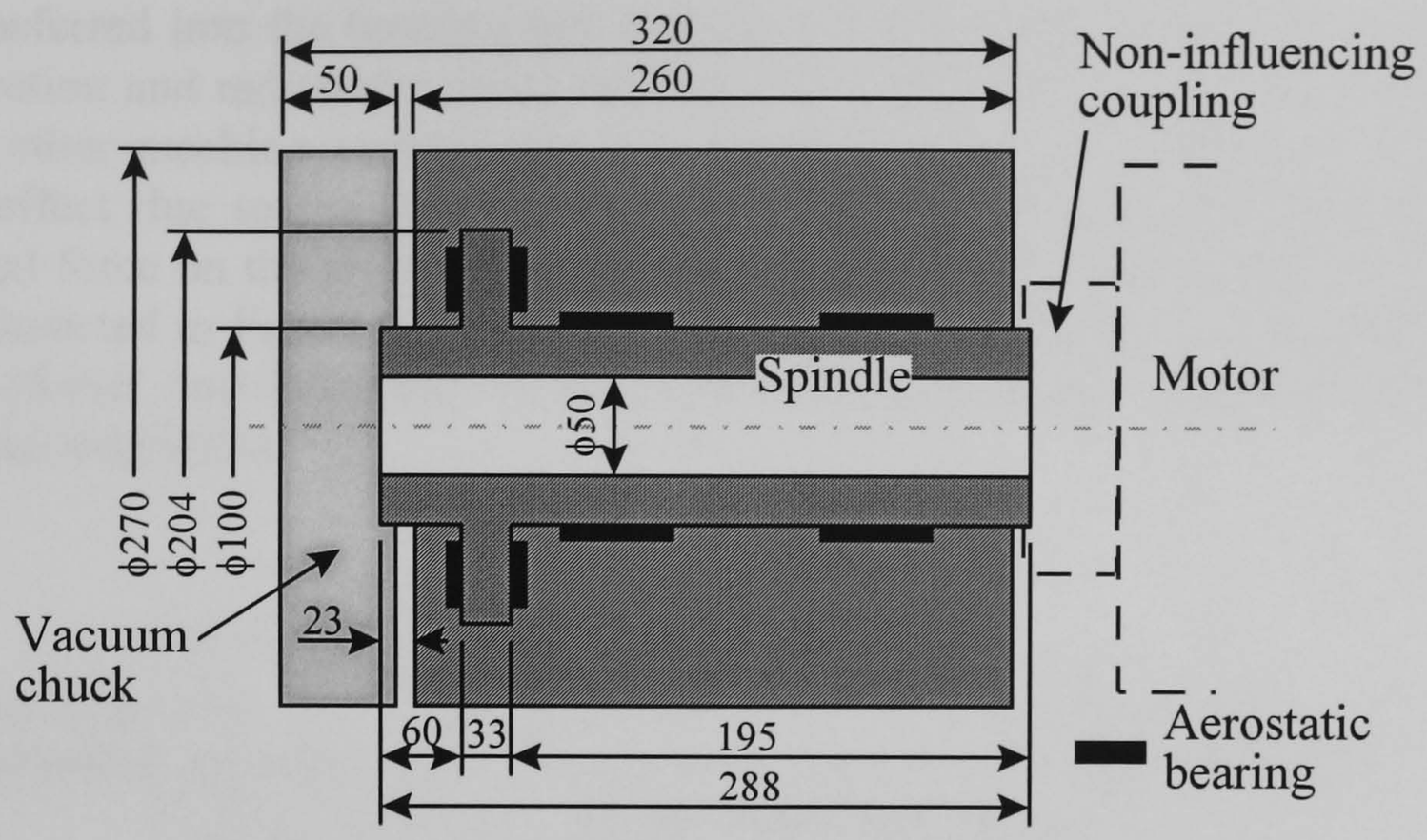

Figure 5.2 Dimension of spindle unit

Considering negligible cutting power is consumed in diamond turning (Sugano *et al.*, 1993) and other components, such as the bed, linear carriage and tool holder, are not directly subject to noticeable heat sources, only the spindle thermal drifts, discussed in Section 2.2, are the physical phenomena to be dealt with in this test work. For a facing lathe such as the machine of this study, important thermal drift errors are due to the axial growth and horizontal tilt of a spindle. Those due to radial movement and vertical tilt do not cause any considerable error to workpieces. Moreover the horizontal tilt is considered to be very small because of the symmetry of the spindle unit under consideration and is neglected.

5.3 Prior Considerations

5.3.1 Investigation of Heat Transfer in Spindle Unit

A rough estimate of heat generation rate, temperature rise and time-dependent characteristics is necessary to plan a test of thermal errors. Heat transfer occurring in the spindle unit is illustrated in Figure 5.3. Heat is generated in the bearing gap as a consequence of a frictional loss due to viscous flow and the spindle motor bearings. Some of the generated heat is conducted into the spindle shaft and housing, and the rest is carried away by the exhaust air with increased enthalpy.

According to Baker and Hornung (1970), most of the heat is dissipated through the shaft while very little is carried away with the air. Interestingly, there is a report that, in the case of water-hydrostatic bearings, leakage flow removes 80-90% of the heat generated under typical operating conditions (Wasson *et al.*, 1993b). This noticeable difference

between air and water bearings is likely to be due to the high heat capacity of water. There are also added effects from room temperature variations and radiation from surroundings.

Heat transferred into the housing and spindle is lastly dissipated into the surroundings by convection and radiation cooling mechanisms. Also, some of the heat can penetrate into the other machine components, e.g. the bed. It is noted that there is an added cooling effect due to the rotation of the spindle, i.e. windage. At high speeds, the centrifugal force on the air dragged around with the spindle shaft induces a circulatory flow as depicted in Figure 5.3. This can be a major heat dissipation mechanism for the housing (Baker and Hornung, 1970). Free convection losses from the sides of the housing are negligible.

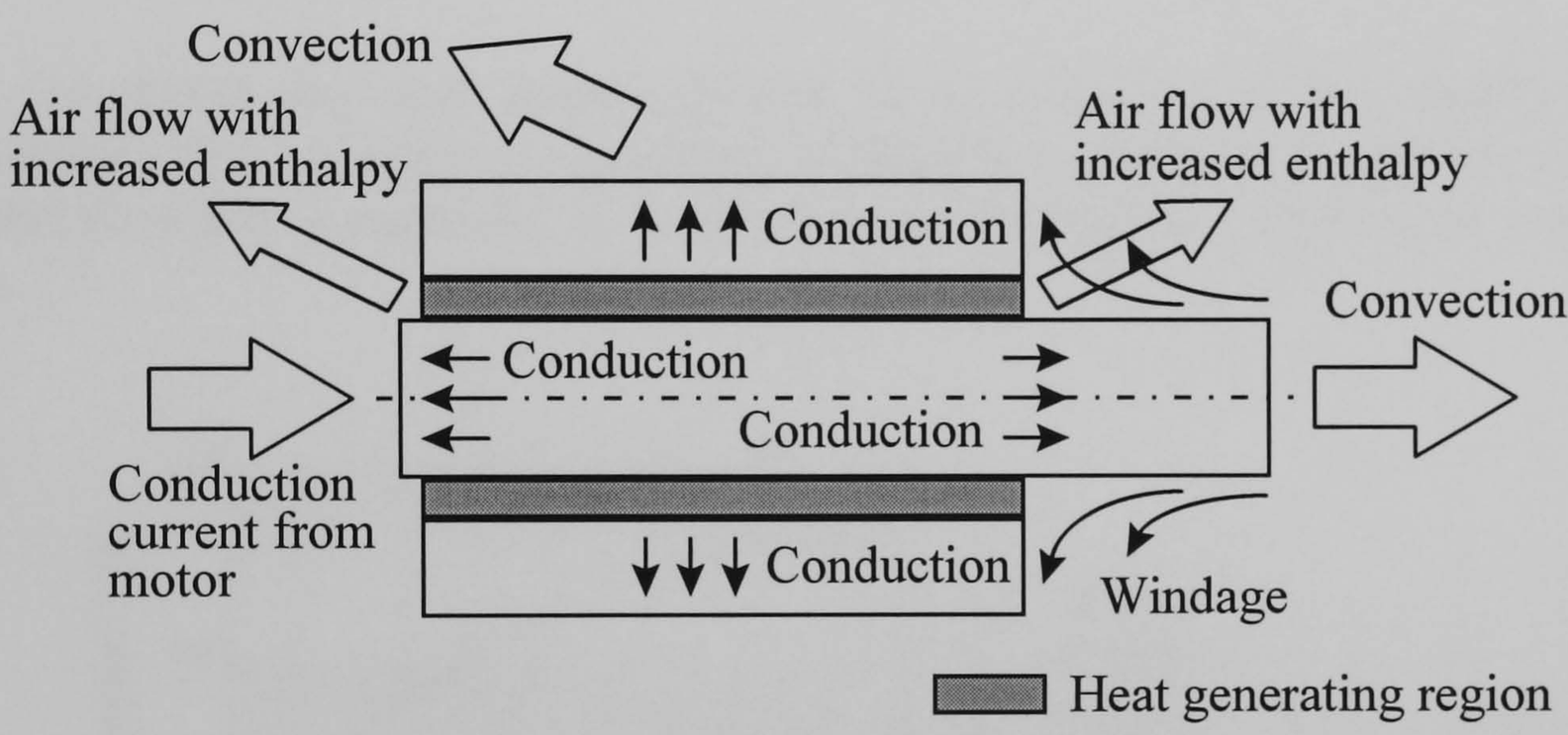

Figure 5.3 Heat transfer occurring on spindle

Neglecting the effects of room temperature variations and radiation from surroundings, the total heat generation rate of an aerostatic spindle q_S can be represented as:

$$q_S = q_B + q_M \tag{5.1}$$

where q_B is the heat generation rate of the bearings; q_M is that of the motor. Friction losses in aerostatic bearings arise from the viscosity of air ($\mu = 1.81\times10^{-5}$ Pa×s at 20 °C from Table 4.5) and can be evaluated using Equation 3.2. In this case the efficiency is assumed to be 1. There is a flow along the bearing axis but this is not related to any work of the system. Assuming laminar flow and constant viscosity throughout an isothermal bearing, we obtain a friction torque τ_f due to the viscosity for journals from the definition of viscosity (Welty *et al.*, 1984, pp. 96-98):

$$\tau_f = \mu \cdot \frac{R_B \omega}{h_0} \cdot \left(2\pi R_B L_B\right) \cdot R_B = \frac{2\pi\mu R_B^{\,3} L_B \omega}{h_0}$$

and a friction torque for thrusts

$$\tau_f = \int_{R_i}^{R_o} \mu \cdot \frac{r\omega}{h_0} \cdot r \cdot (2\pi r) dr = \frac{\pi\mu\omega\left(R_o^4 - R_i^4\right)}{2h_0}$$

where R_B is the radius of the bearing; L_B is the length of the bearing; ω is the angular speed; h_0 is the mean radial clearance; R_o is the outer radius of the thrust bearing; R_i is the inner radius of the thrust bearing. The friction power loss or heat generation due to bearing friction in watts will be

$$\begin{aligned} q_B = \tau_f \omega &= \frac{2\pi\mu R_B^{\,3} L_B \omega^2}{h_0} && \text{for journals} \\ &= \frac{\pi\mu\omega^2 (R_o^4 - R_i^4)}{2h_0} && \text{for thrusts} \end{aligned} \qquad (5.2)$$

Figure 5.4 shows the heat generation rate of the bearings of the machine under consideration. Tens of watts are generated in the usual operating conditions, but it is noted that the curve is parabolic, so the heat generation becomes much greater at higher speeds.

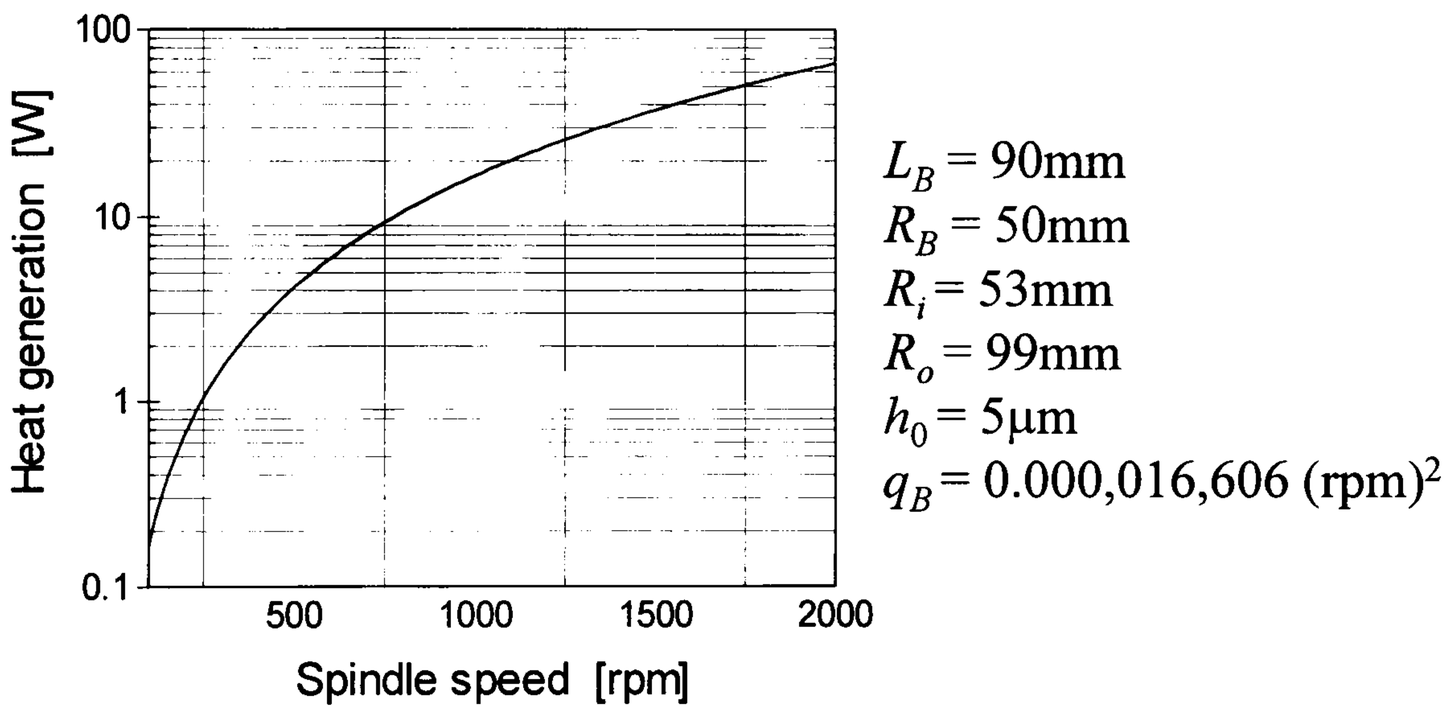

Figure 5.4 Heat generation rate of bearing due to friction loss (linear-log graph)

As stated in Chapter 3, the typical efficiency of an electric motor is approximately 80%. The sources of loss in a dc machine are resistance of windings and their associated resistive regulators (conduction loss), cyclic reversal of the magnetic flux in the armature body and teeth (core loss), windage, friction, and so on (Nasar, 1987, pp. 5-45 to 5-46). The dominant conduction loss can be expressed as

$$q_M = I_e^2 R_e$$

where I_e is the armature current; R_e is the resistance. The temperature rise of windings can be estimated approximately from a change of resistance from that at a known temperature such that (*ibid.* pp. 12-1 to 12-3):

$$T_h = \frac{R_{e,h}}{R_{e,c}}(T_c + a) - a$$

where T_h is the higher temperature of a winding in °C; $R_{e,h}$ is the winding resistance at T_h; T_c is the initial cold temperature in °C of a winding before starting; $R_{e,c}$ is the winding resistance at T_c; the constant a is 234.5 for copper and 225 for aluminium. Being separated from the spindle unit, the heat from the spindle motor, however, seems to have negligible contribution to total heat input to the spindle unit.

The generated heat is then dissipated into the shaft and housing, and some is taken away by the exhaust air:

$$q_S = q_N + q_H + q_A \tag{5.3}$$

where q_N is the rate of heat dissipation into the spindle shaft; q_H is that into the housing; q_A is that by the exhaust air.

Referring to Equation 3.4, an energy equation can be stated for the spindle shaft as follows:

$$m_N c_p \frac{dT_N}{dt} = q_N - q_{CN} \tag{5.4}$$

where m_N is the mass of the shaft, c_p is the specific heat, $T_N(t)$ is the temperature of the shaft and q_{CN} is the rate of heat dissipation from the spindle shaft by conduction and convection. Spatial distribution of temperature is neglected because the shaft is relatively thin in its structure. Similarly, for the housing, the energy equation yields

$$m_H c_p \frac{dT_H}{dt} = q_H - q_{CH} \tag{5.5}$$

or, if the temperature is dependent on the radial position r, then the energy equation yields

$$\int c_p \frac{\partial T_H(r,t)}{\partial t} dm = q_H - q_{CH}$$

When the temperature distribution, $T_H(r,t)$, is assumed to be linear along the radial direction, the result is

$$\frac{dT_{HB}}{dt} = \frac{q_H - q_{CH}}{\frac{1}{3}\pi L_B \rho c_p (R_H - R_B)(2R_B + R_H)} - \frac{dT_{HH}}{dt}$$

where L_B is the bearing width, ρ is the density, R_H is the outer radius of the housing, R_B is the radius of the bearing, T_{HB} is the temperature at the bearing surface and T_{HH} is the temperature at the housing surface.

The heat removed by the exhaust air is

$$q_A = \dot{m}_A c_p \left(T_{film} - T_\infty \right) \tag{5.6}$$

where $\dot{m}_A$ is the mass flow rate of the air, T_{film} is the air temperature at the bearing gap and T_∞ is the ambient air temperature.

Thus, the spindle thermal growth can be expressed as:

$$e_z^t = L_N \alpha (T_N - T_{N,0}) \tag{5.7}$$

where α is the coefficient of thermal expansion and L_N is the length of the spindle nose from the thrust plate that is taken as the origin.

Evaluating the thermal growth of the spindle from Equation 5.7 involves many steps as represented by Equations 5.1 to 5.6, and many of the variables are difficult to calculate exactly in an analytical manner. The order of magnitude is sufficient at this stage, so appropriate assumptions are made.

For the calculation of the temperature, the vacuum chuck made of aluminium is not considered because it has high thermal conductivity, low heat storage capacity in comparison with the invar steel shaft* and is considered to provide an extended surface for convection cooling of the spindle shaft. The frictional loss is taken to be the dominant source for the heat generation. Lastly, the fractional ratio at which the generated heat penetrates into the spindle shaft is determined by considering heat balance at the steady-state condition. At the steady-state condition, the right-hand terms of Equation 5.3 can be put into:

$$q_N = C_N (T_{film} - T_\infty)$$
$$q_H = C_H (T_{film} - T_\infty)$$
$$q_A = C_A (T_{film} - T_\infty)$$

where C_N, C_H, C_A are thermal conductances of the spindle shaft, housing and air film respectively. The thermal conductance of a hollow cylinder can be found in many textbooks (e.g. Welty *et al.*, 1984, pp. 256-259); thus we have for the hollow spindle and its housing

---

* The thermal conductivity of aluminium is over 15 times greater than that of invar. The heat storage capacity of invar is nearly 2 times greater than that of aluminium.

$$C_N = \frac{2\pi kL}{\ln\left(R_B/R_T\right)}$$

$$C_H = \frac{2\pi kL}{\ln\left(R_o/R_i\right)}$$

where L is the length and R_T is the radius of the through hole of the spindle shaft. From Equation 5.6, the thermal conductance of the air film can be expressed such that:

$$C_A = \dot{m}_A c_p$$

Now, we define the ratios of heat dissipation η_N, η_H, η_A such that:

$$q_N = \eta_N q_S, \qquad q_H = \eta_H q_S, \qquad q_A = \eta_A q_S$$

where $\eta_N+\eta_H+\eta_A = 1$. In turn, the ratios can be expressed by using the thermal conductance, i.e.

$$\eta_N = \frac{C_N}{C_N + C_H + C_A}, \qquad \eta_H = \frac{C_H}{C_N + C_H + C_A}, \qquad \eta_A = \frac{C_A}{C_N + C_H + C_A}$$

Table 5.2 shows the thermal conductance of the spindle unit under consideration with the ratios.

	Spindle shaft	Housing	Air film
Thermal conductance (W/K)	25900	98700	5.06E-07
Dissipation ratio	0.208	0.792	4.06E-12

Table 5.2 Thermal conductance and dissipation ratio of spindle unit

The thermal conductance of the air film is calculated using a mass flow equation governing choked flow through a pocketed orifice (Slocum, 1992, pp. 589-600) such that:

$$\dot{m}_o = 1.87 \times 10^{-4} C_d d_o^2 \frac{P_o}{P_a}$$

where C_d is a discharge coefficient (usually 0.8), d_o is the diameter of the orifice, P_o is the supply air pressure and P_a is the ambient air pressure. Although the choked condition is manifested in all the orifices of diameter 0.1mm in the air bearing (a total of 48 orifices, 16 for each journal bearing and 16 for the thrust) with $P_o/P_a = 7^*$, the thermal conductance of the air film is small enough to be neglected. The small thermal conductance of the spindle shaft is largely due to low thermal conductivity of invar.

---

* The supply pressure is typically 690 kPa in aerostatic bearings (Slocum, 1992, pp.580-581).

Thus Equation 5.4 can be written as

$$m_N c_p \frac{dT_N}{dt} = \eta_B q_B - hA(T_N - T_\infty) \tag{5.8}$$

where A is the area of the cooling surface. The solution is readily available by integration as

$$T_N = K_T\left(1 - e^{-t/\tau}\right) + T_\infty \tag{5.9}$$

where

$$K_T = \frac{\eta_B q_B}{hA}, \quad \tau = \frac{m_N c_p}{hA}$$

K_T denotes temperature rise at the steady state while τ represents time constant. Governed by a first-order differential equation, the growth time response is exponential.

The heat transfer coefficient associated with Equation 5.9 can be found referring to an assumption that the vacuum chuck is considered to act like an extended surface for convection cooling. Heat transfer by convection between a rotating cylinder and surrounding fluid is governed by a) peripheral-speed Reynolds number, which is defined as (Anderson and Saunders, 1953)

$$\mathrm{Re}_\omega = \frac{\omega \pi D^2}{\nu}$$

where D is the diameter and ν is the kinematic viscosity, and b) Grashof number defined in Section 4.3.3. Turbulence begins to appear at a critical peripheral-speed Reynolds number, 50. Below the critical number, simple free convection, characterised by the Grashof number, controls the rate of heat transfer. At speeds where $\mathrm{Re}_\omega > 8000$ in air, the peripheral speed Reynolds number becomes the controlling parameter. The combined effects of Reynolds, Prandtl and Grashof numbers on the average Nusselt number for a horizontal cylinder rotating in air above the critical velocity can be expressed by an empirical equation (Kays and Bjorklund, 1958)

$$\overline{\mathrm{Nu}_D} = \frac{\bar{h}D}{k} = 0.11\left[\left(0.5\,\mathrm{Re}_\omega{}^2 + \mathrm{Gr}_D\right)\mathrm{Pr}\right]^{0.35} \tag{5.10}$$

Heat transfer from a rotating disk in air is empirically given as (Wagner, 1948; Cobb and Saunders, 1956)

$$\overline{\mathrm{Nu}_D} = \frac{\bar{h}D}{k} = 0.35\left(\frac{\omega R^2}{\nu}\right)^{1/2} \tag{5.11}$$

for $Re_D < 500{,}000$, where R is the radius of a disk. The boundary layer on the disk is laminar and of uniform thickness at rotational Reynolds numbers $\omega D^2/\nu$ below about 10^6. At higher Reynolds numbers, the flow becomes turbulent and the boundary layer thickens with increasing radius.

For the circumferential surface of the vacuum chuck, Equation 5.10 can be applied and for the face, Equation 5.11. However only a part of the circumferential area, i.e. 30%, is likely to act as an extended surface because the chuck is made of two disks joining each other with a small area that can give high thermal resistance or insulation effects. Then, the axial growth of the spindle unit can be calculated as shown in Table 5.3. Due to the simplified calculation, Table 5.3 is subject to large uncertainties.

Spindle speed (rpm)	500	1000	1500	2000
Steady-state temperature rise K_T (K)	0.70	1.71	2.90	4.22
Time constant τ (hrs)	2.29	1.41	1.06	0.87
Steady-state axial growth e_z^t (μm)	0.05	0.13	0.22	0.31

Table 5.3 Axial thermal growth of spindle unit

5.3.2 Sensors

A thermometer and non-contacting displacement sensor are necessary for the test of spindle axial growth. A non-contacting displacement sensor is essential because the target, i.e. the spindle, rotates at high speeds while testing. Also time measurements are involved in the test. Unlike electrical systems, thermal systems are characterised by their large time constant, so that fast sensor response is not essential in the test.

Table 5.3 suggests that the temperature should be measured down to 0.1 K because, at lower spindle speeds, maximum temperature rise is likely to be less than 1 K. Also the measurement should be repeatable within 1 K to distinguish the characteristics of temperature rise at different speeds. One popular method of measuring temperature is using thermocouple instruments, which rely on the physical principle that, when any two different metals are connected together, an electromotive force, which is a function of the temperature, is generated at the junction between them. Such instruments can achieve an overall system accuracy of better than ±0.025 °C (e.g. manufacturer's specification of Labcal Plus from Labfacility*). Because thermocouples are sufficiently accurate as well as popular, they were adopted in the test.

Temperature was measured by a model 6600 microprocessor thermometer having 10 channel scanning capacity from Comark Electronics**, which seems to be satisfactory for the requirements of this test. The specification is shown in Table 5.4. The available sensors were type T (Cu/Cu-Ni) thermocouple probes with measurement range of -200 to 400 °C. The probes are in the form of thin rods, measuring ϕ3×250 mm, and they can be bent to enable fitting in awkward locations.

---

* Labfacility Ltd., 99 Waldegrave Road, Teddington, Middlesex TW11 8LR
** Comark Electronics Ltd., Rustington, Littlehampton, West Sussex BN16 3QZ

The overall system accuracy is a little better than ±0.1 °C according to the specification. In many cases, however, errors arising from installation may be considerably more than the error of the sensor itself. Temperature is not measurable without some disturbance of the heat paths of an object. Especially, large errors can arise in measuring the temperature of gases or poorly conducting solids (Polak, 1979, pp. 6-22). If we immerse a thermometer directly in the substance under test, there will be an interchange of energy until equilibrium is established, where heat flow into the sensor by convection, conduction and radiation equals the heat leakage outwards by conduction along the stem of the sensor and by radiation across the substance to distant surfaces.

Resolution	0.1 °C
Measurement accuracy	±0.05% of reading per input
Temperature coefficient	±35 ppm/°C
Thermocouple characterising error for type T	< ±0.05 °C within 0 to 400 °C
Cold junction compensation	No additional error from 20 to 25 °C. Temperature coefficient of less than ±0.05 °C per °C ambient outside this range
Response	1 sec to full accuracy

Table 5.4 Thermometer specification

The thermocouple wires also contribute to the total error budget. Moreover many primary sensors give very small signals that have to be fed to a bridge or other amplifying system. The small primary signal may be interfered with by external electromagnetic disturbances such as magnetic fields from electric motors. Temperature readings are likely to have negative error, i.e. low reading referring to the above discussion. Perfect insulation is needed around temperature sensors, but it is not possible.

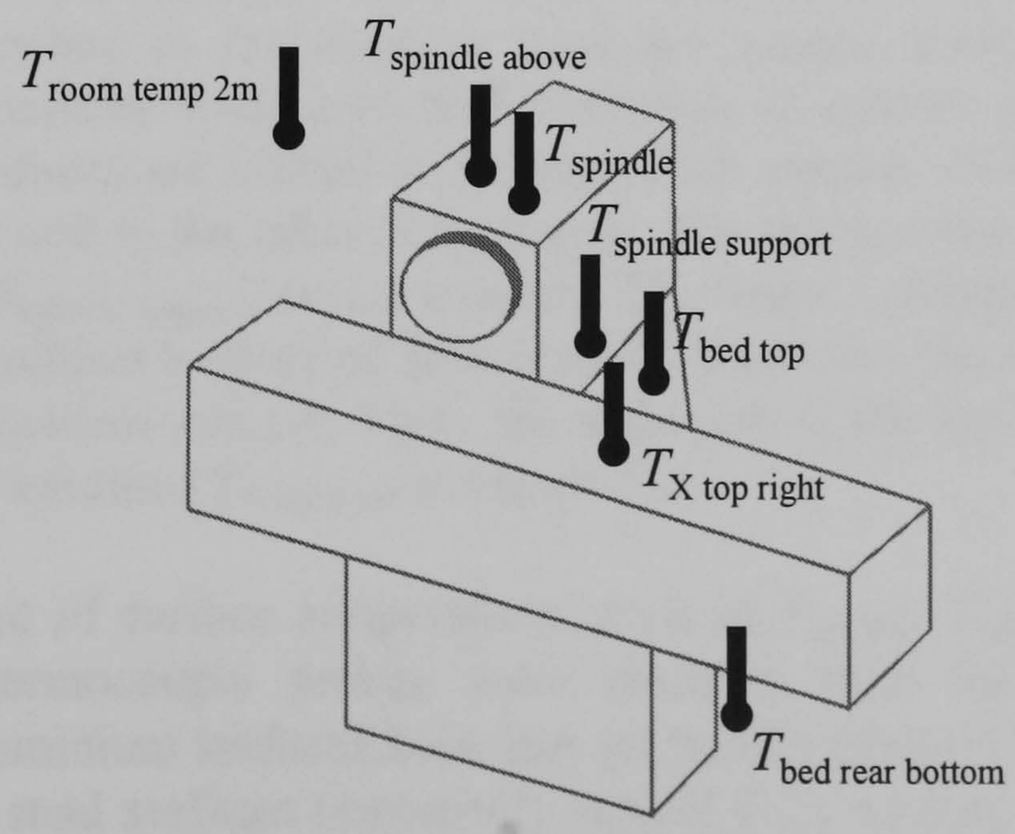

Figure 5.5 Location of temperature sensors

Knowledge of the temperature of the spindle unit and room air is fundamentally necessary for this test to characterise the axial thermal growth, and also some other locations of interest were chosen as follows:

- *Temperature of spindle unit*: The temperature of the spindle shaft is difficult to measure because the spindle will be running while testing the axial thermal growth. Although sensors can be attached to the rotating shaft and their signals can be fed to the outside, this would be expensive, involving modifications to the spindle shaft. Mainly due to the impossibility of modifications on a running machine, the test had to be conducted with temperature measurement of the upper outside surface of the spindle housing as depicted as T_{spindle} in Figure 5.5. It is assumed that not much temperature difference exists along the housing length. For the measurement of air film temperature, a sensor should be located at the bearing gap of the spindle. Still this needs some modifications, so the temperature of the air just above the spindle unit is measured in order to represent the temperature of the leakage air as shown as $T_{\text{spindle above}}$ in Figure 5.5.

- *Temperature of room air*: The temperature of the room air should be measured at locations that are just free from thermal environment actively interacting with the machine. Such an arrangement seems to give effective information regarding temperature variation effects on machine tools. Two locations along the vertical direction were selected in order to take account of temperature gradients of the room air. The first is the temperature of the air at a height of 2 m from the floor ($T_{\text{room temp 2m}}$ in Figure 5.5) near the machine. The second is attached to the rear bottom of the machine ($T_{\text{bed rear bottom}}$ in Figure 5.5). The bottom space was considered to be safe from the thermally elevated machine because it will be occupied by heavier cold air.

- *Temperature of machine frame*: Three more components are considered to be important in thermal response of the machine. The bed provides a stable grounding for all the other machine components, so that the temperature of the top surface ($T_{\text{bed top}}$ in Figure 5.5) was measured in the test. It is noted that the top surface is a steel plate tightly attached to the massive synthetic granite main body. The spindle support of the machine fixed onto that steel plate is another thick steel plate. The spindle unit and motor are located on the top of the support, so it provides heat paths from the spindle unit to the other components. The temperature of the upper surface of the support ($T_{\text{spindle support}}$) was measured. The linear carriage or X slide made of cast iron is also subject to thermal deformation. Moreover, the carriage was used for mounting displacement sensors. Thus, the right part of the top surface was selected as an measuring location ($T_{\text{X top right}}$ in Figure 5.5).

For the measurement of surface temperatures such as T_{spindle}, $T_{\text{spindle support}}$, etc., long, moderately thin thermocouple probes were attached onto the surfaces using an aluminium tape. Aluminium surfaces have low emissivity (around 0.1) and absorptivity in comparison with steel surfaces (emissivity around 0.2), so they provide an effective shield for radiation heat transfer between thermocouples and surroundings. Also the high conductivity of aluminium (167 W/m·K) helps develop temperature of the probes equal to the object under test.

The non-contacting displacement sensors were required to have high accuracy and repeatability within 0.1 μm according to Table 5.3. For the test, two types were selected to measure the axial growth of the spindle, i.e. fibre-optic back-scatter sensors and inductive ones that are accurate enough to detect displacements much less than 1 μm. Both sensors were used for comparative investigation of test results.

It is worth outlining the operating principle of fibre-optic sensors. Light can be transmitted through long thin glass fibres, even if they are bent. If the light ray enters a fibre rod at an angle to its axis less than some maximum angle, the ray will be totally reflected from the walls. Optical fibres can be arranged in bundles. One type of optical fibre sensors utilises intensity modulation as the mechanism by which the information to be measured is transmitted on to the light guided within fibres.

Figure 5.6(a) shows an optical-fibre sensor using a moving reflector target as an external intensity modulator (Gasvik, 1987, pp. 205-209). Two fibre bundles, illuminating and receiving, are mixed together in a bifurcated bundle in such a way that every second fibre in the cross section of a bifurcated bundle comes from, say, illuminating bundle. An illuminating bundle emits a conical light beam and a receiving bundle will receive light inside of a cone of the same magnitude as depicted in Figure 5.6(b).

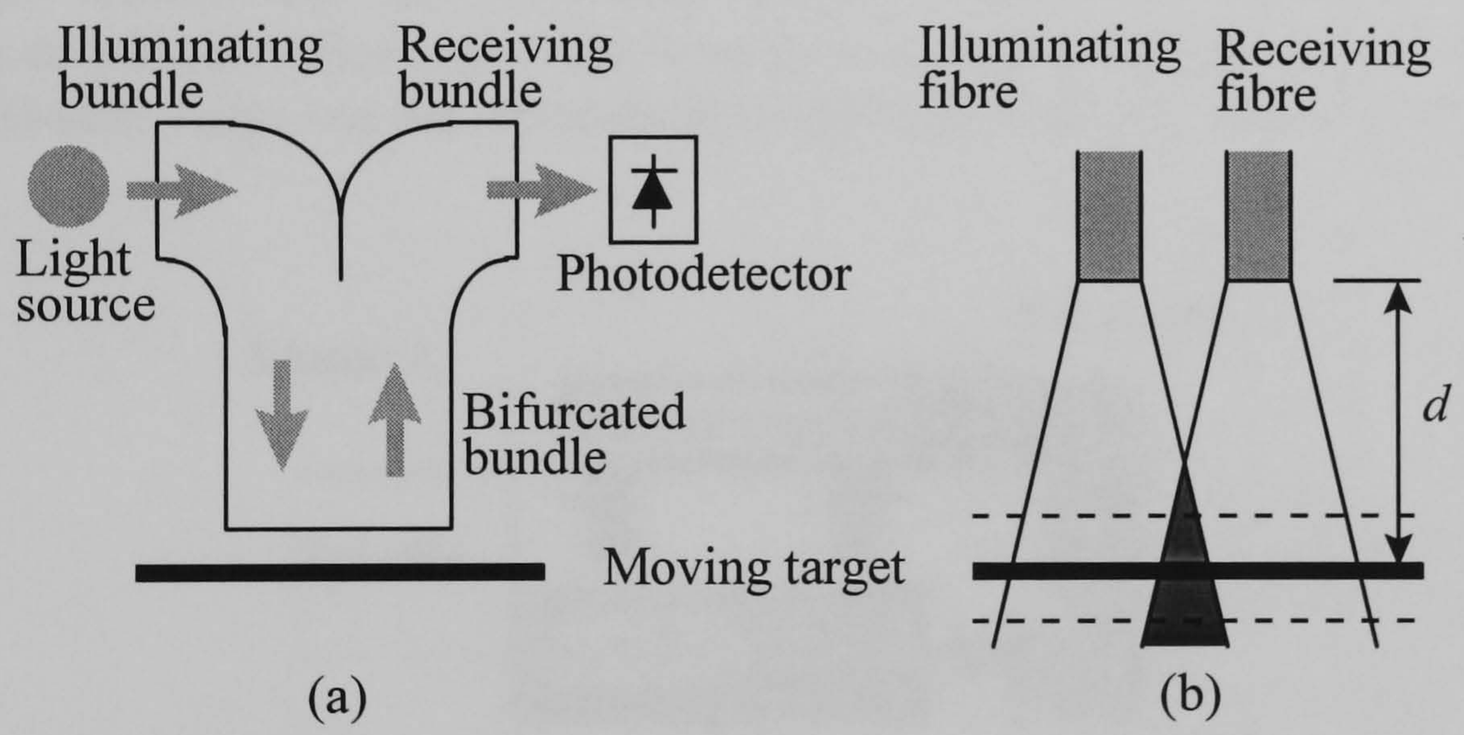

Figure 5.6 Operating principle of optical-fibre sensor

Placing a scattering plane surface a distance *d* in front of the fibre end, light will be scattered back and the amount of the light received by a receiving bundle will be proportional to the area of overlap between two cones as illustrated in the figure. If the whole cross section of a receiving bundle is covered with light, the intensity of the received light will have its maximum. A further increase in *d* will decrease the intensity. Thus, a curve describing the relation between the received light intensity versus the distance will have two flanks and the front flank is much steeper than rear. By placing the end of a bifurcated bundle close to a surface, a photodetector at the end of a receiving bundle will give a signal, which is proportional to the distance from the fibre end to the surface, as long as one is working within the linear portion of the front flank of the curve.

An Angstrom Resolver Series 201 from Opto Acoustic Sensors* operating on the principle above was used for one method to detect the thermal axial growth. It provides convenient LCD panel meter displaying the dc level of a measurand. Only a dc level is important in the measurement of the thermal axial growth, as stated in Section 2.2. That is, the rotation of the spindle gives ac components in the measurement signal while the axial growth correspond to the changes in the dc level of measurement signal. According to literature (Slocum, 1992, pp. 174-176), the repeatability of fibre-optic sensors can be order of 0.05% of full-scale range and the linearity can be as good as 0.1% of full-scale range, but they are sensitive to the effect of the environment of the surface of a moving target. Dirt on the surface of a target can degrade the performance of an optical-fibre sensor. For the test, a diamond-turned aluminium target, measuring $\phi 50 \times 14$ mm, was used because of its high reflectivity.

The other (inductive) sensor was from Kaman Instrumentation**. Its performance is dependent on the properties of target material. To achieve a high level of performance, the target should have uniform electrical properties, be a very good conductor and have low magnetic permeability (Slocum, 1992, pp. 133-135). The best target materials are aluminium, copper and brass. Ferrous targets degrade the performance of inductive sensors and ideally would have a thin piece of a good target material epoxied or plated on them. However, a stainless steel target, measuring $\phi 50 \times 14$ mm, was used in the test because the sensors had been calibrated against a stainless steel artefact for other purposes not relevant to this study. The linearity of inductive sensors is typically 0.1% at 25% of full-scale range and the repeatability is typically twice the resolution (*ibid.*).

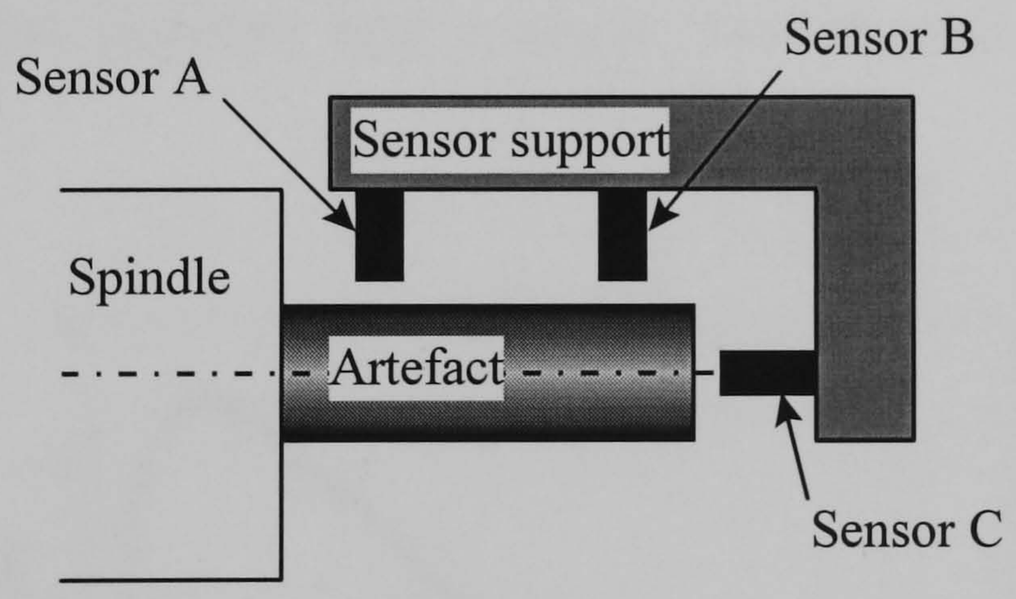

Figure 5.7 Measurement of spindle thermal drifts

A popular method of measuring spindle thermal drifts is depicted in Figure 5.7 (ANSI Standard B5.54, 1992). An artefact is mounted on the spindle nose and a sensor support is fixed on the machine frame. The difference in the readings of sensor A and B is used to calculate the tilt of a spindle while the average of sensor A and B readings provides the radial measurements (drift and/or run-out). Sensor C measures the axial motion of the spindle (including growth). In this test, we are interested in the axial thermal growth

---

* Opto Acoustic Sensors, Inc., 1706A Medfield Road, Raleigh, NC 27607, USA

** Kaman Instrumentation Corp., 1500 Garden of the Gods Road, Colorado Springs, Colorado 80933-7463, USA

only, so we need just one displacement sensor measuring the displacement of the centre position of the spindle unit. ANSI Standard B89.3.4M (1985) defines spindle axial motion as error motion co-linear with the fixed reference axis along the spindle, as discussed in Section 2.2. The mounting method for the sensors used in the test is illustrated in Figure 5.8.

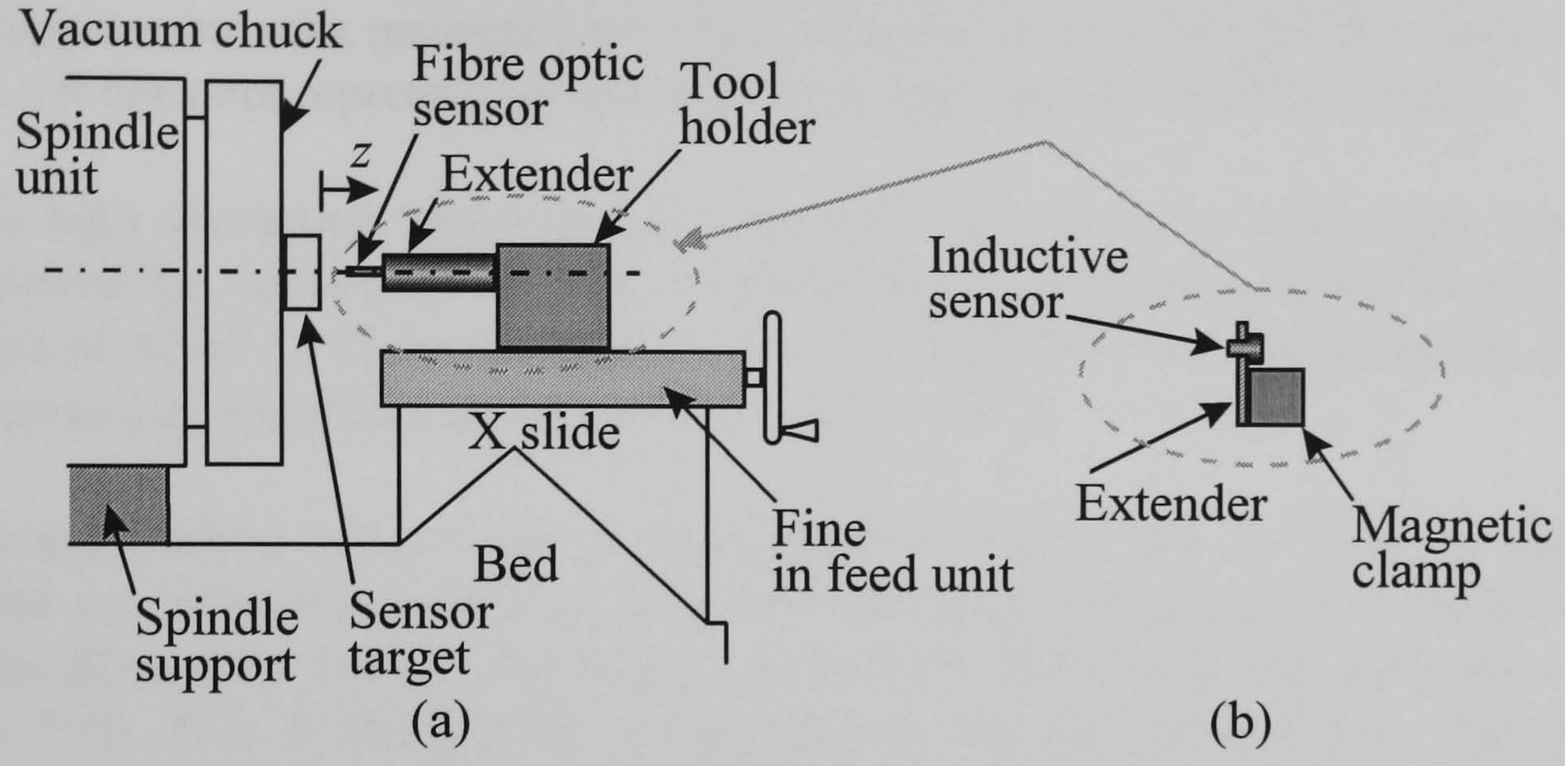

Figure 5.8 Sensor mounting method

The fibre-optic sensor was mounted at the end of an extender that was fixed horizontally to the tool holder of the machine in Figure 5.8(a). In turn the tool holder was placed on the fine in feed unit attached onto the X slide of the machine. The extender was used because of the difficulty in holding the small fibre-optic sensor only with the tool holder. The extender, however, had a slender structure that was vulnerable to temperature changes.

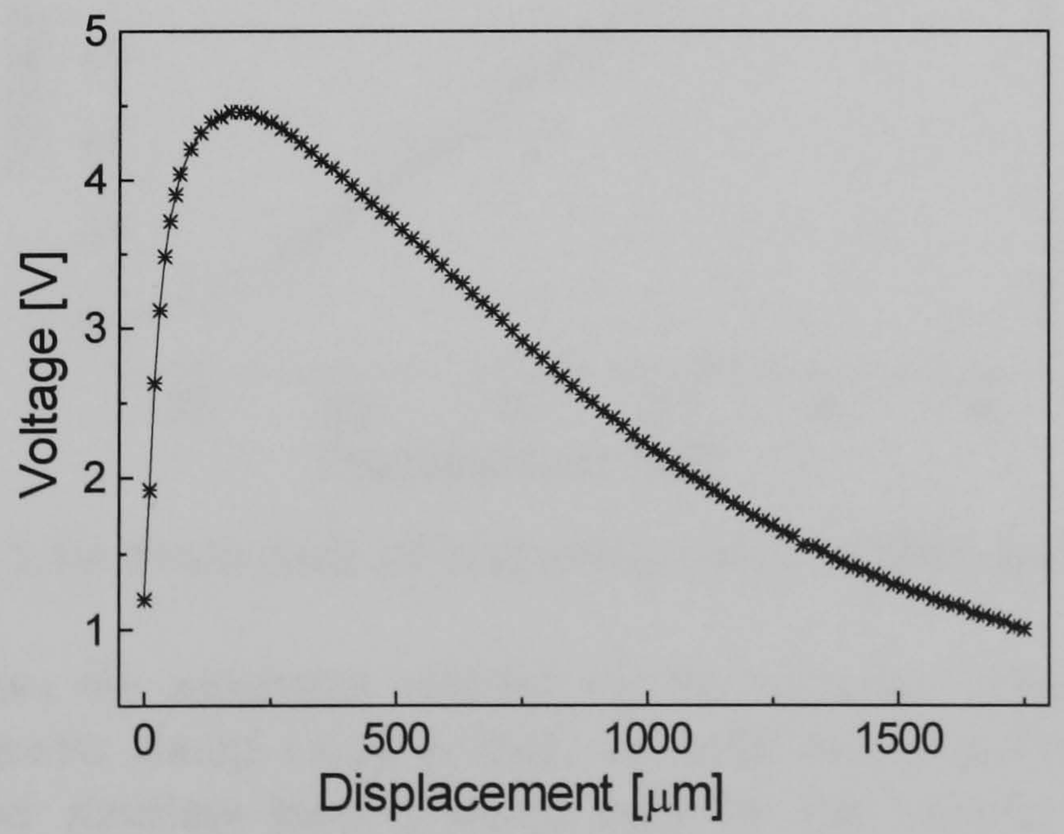

Figure 5.9 Calibration curve of fibre-optic sensor

The fibre-optic sensor was arranged to target a diamond-turned aluminium artefact attached to the vacuum chuck of the spindle. In theory, the target position should be the

centre of the aluminium artefact to measure the axial thermal growth. The artefact, however, has a small flaw at the centre as a result of turning operation, so a slightly higher position was used for the target point of the fibre-optic sensor. In this arrangement, the fibre-optic sensor was calibrated against the aluminium target.

Figure 5.9 shows the calibration curve obtained by reading the dc level of the fibre-optic sensor output while moving the sensor stepwise towards the target using the in feed unit. The displacement was measured by a dial indicator. It is noted that the displacement in Figure 5.9 does not represent absolute distance between the target and sensor.

For the high resolution measurement required in this test, the front flank representing high sensitivity was chosen, so several calibrations were carried out within that range an example of which is shown in Figure 5.10. The sensitivity was evaluated by employing the least-square procedure and found to be 0.241 V/μm.

Two major defects were found in the calibration work. The first was in using a dial indicator as a reference metrology instrument because it is considered to be less accurate than the fibre-optic sensor. The second is the non-linearity of the calibration curve of Figure 5.10. This is likely to be mainly due to the fine in feed unit. The sensitivity obtained, therefore, may have large errors, but the trends of the axial thermal growth can be identified even under the large sensitivity error of the sensor. Also an inductive sensor was used to complement the fibre-optic sensor measurements.

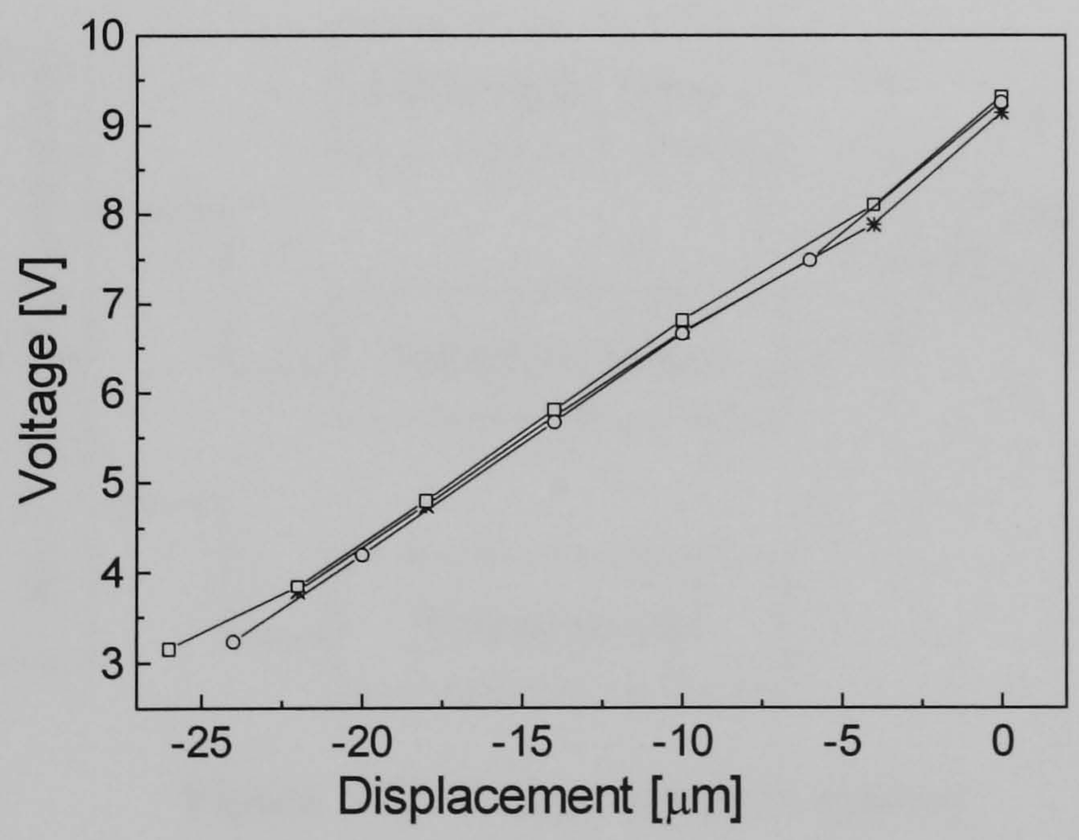

Figure 5.10 Front flank of calibration curve of fibre-optic sensor

Figure 5.8(b) shows the mounting method of the inductive sensor. The sensor was attached to a magnetic clamp using a small extender that positions the sensor at the centre of a ground stainless steel artefact, held by the vacuum chuck. The whole assembly was fixed onto the fine in feed unit. The sensitivity of the inductive sensor was calculated using factory-calibrated data, as shown in Figure 5.11. Using a least-squares procedure, the sensitivity of 0.200 V/μm was obtained.

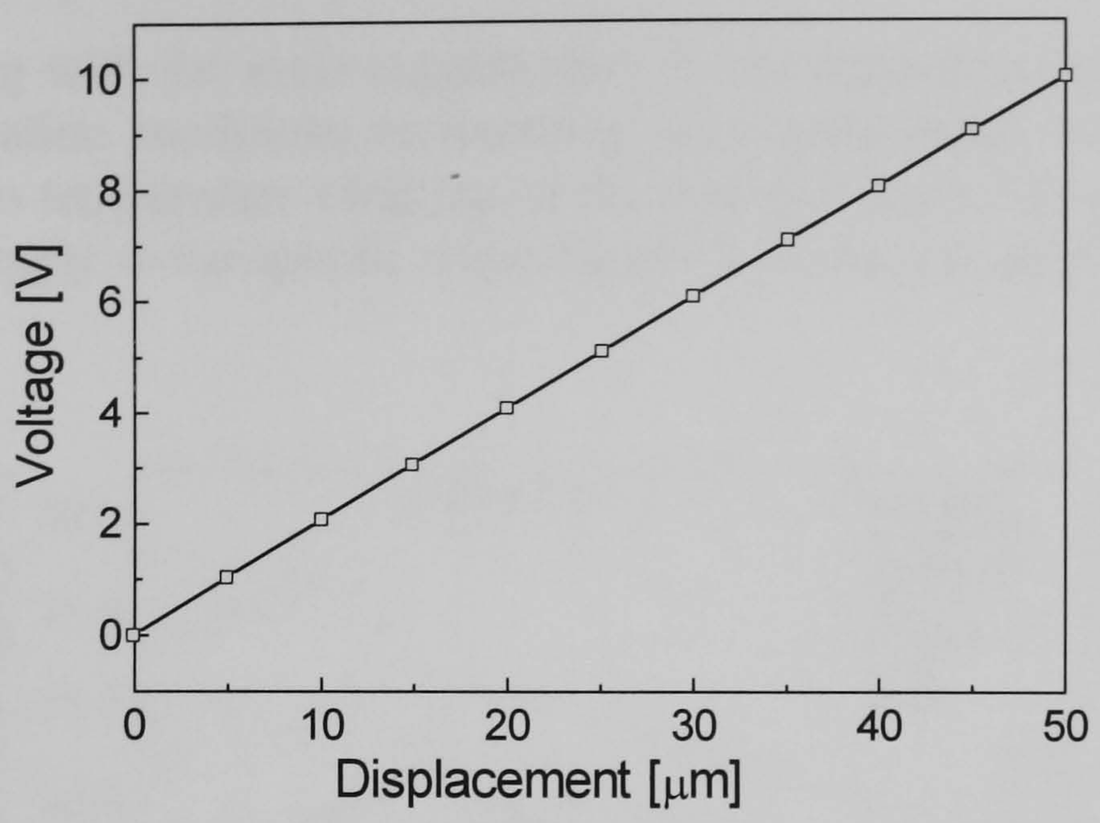

Figure 5.11 Calibration curve of inductive sensor

A data acquisition system was developed to facilitate the test as shown in Figure 5.12. A thermocouple thermometer was connected to a 386SX PC via RS-232C. The voltage signal from the inductive sensor was fed into an AD converter, AT-MIO-16DL-9 from National Instruments*. The fibre-optic sensor used was stand-alone because of its convenient dc level meter. An oscilloscope was used also to monitor the signals from two displacement measuring sensors.

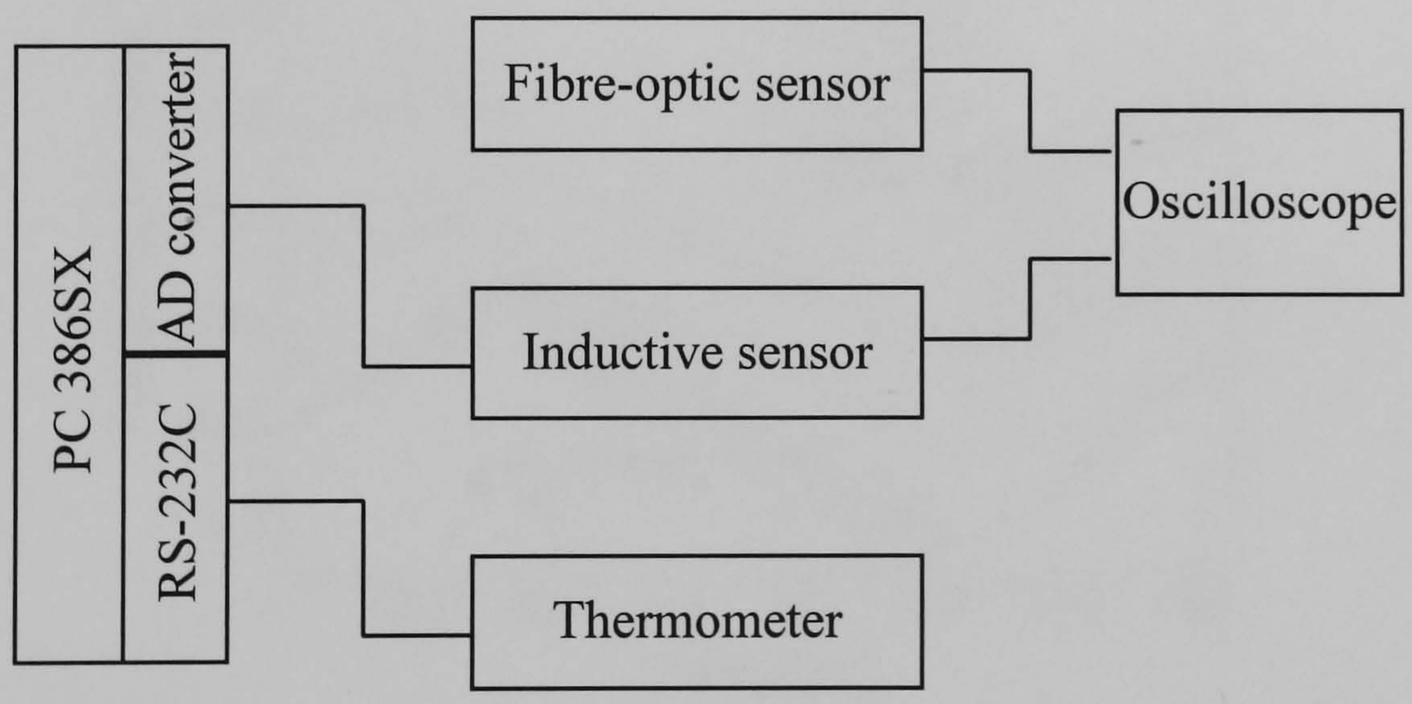

Figure 5.12 Data acquisition system

The sampling time was chosen to be 5 minutes because the measurand will not greatly fluctuate with time. Also, considering the long time-constant of thermal systems, 5 minutes were considered to be appropriate for this test. The signal from the inductive sensor has ac components as well as dc ones. Because we needed the dc components, the value was taken by averaging 500 samples for 5 seconds.

---

* National Instruments, 21 Kingfisher Court, Hambridge Road, Newbury, Berkshire RG14 5SJ

5.4 Results of Test

Before proceeding with the main experiments, it was considered appropriate to record thermal and vibration conditions surrounding the experimental set-up as a first step. Figure 5.13 shows temperature variation of the machine under idling conditions and no pressurised-air supply to the spindle while Figure 5.14 was obtained with the air supply on.

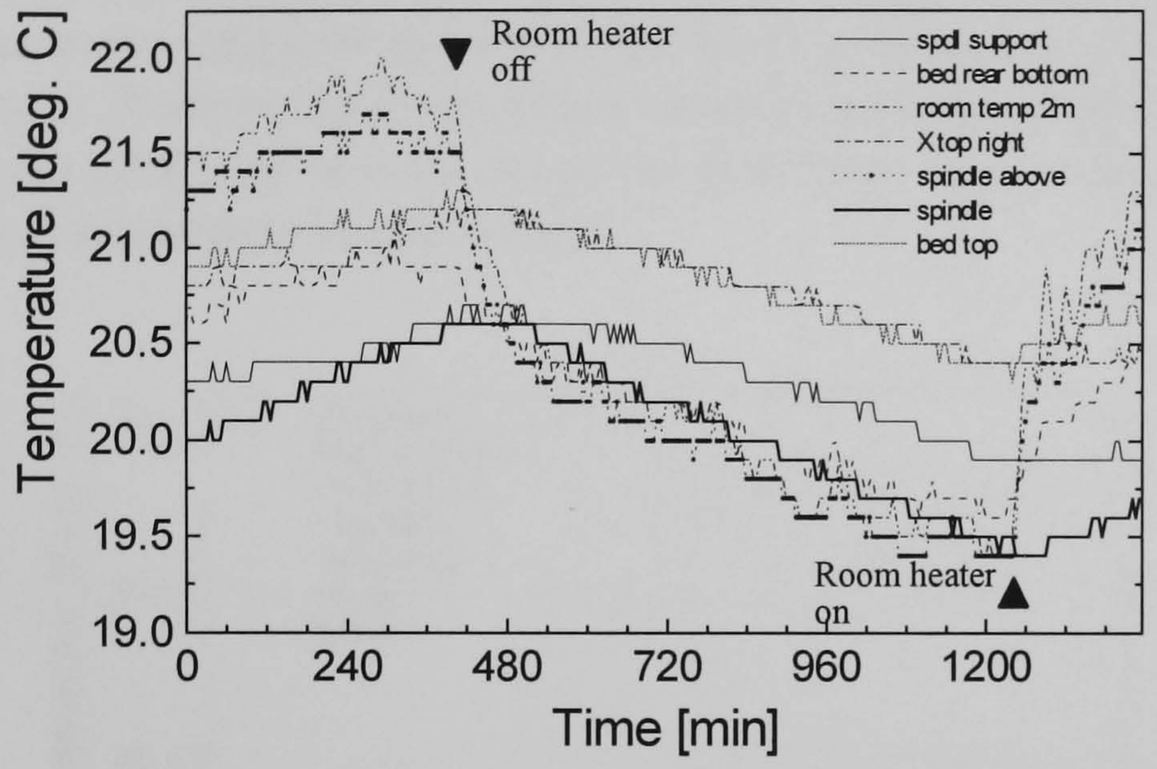

Figure 5.13 Temperature variation of idle machine without air supply to spindle

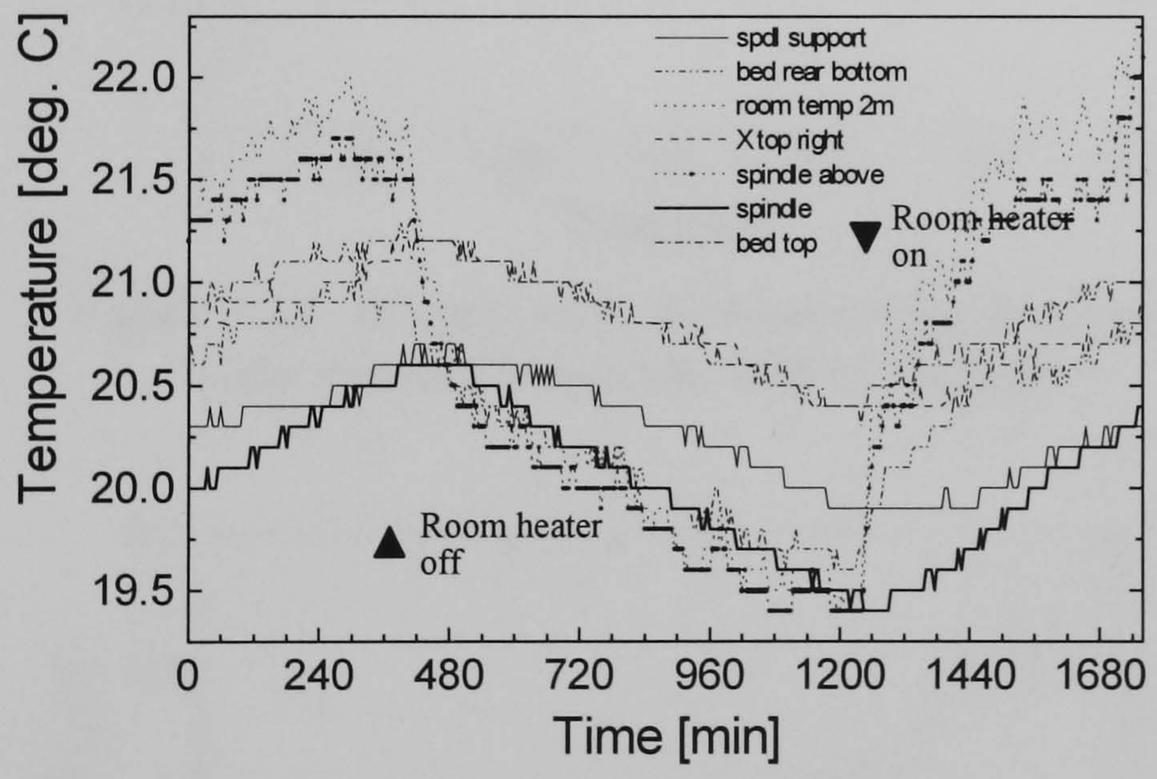

Figure 5.14 Temperature variation of idle machine with air supply to spindle

The data was recorded from noon through the night to the following morning. Firstly, a remarkable resemblance between the two graphs indicates that the repeatability of the thermometer is acceptable. Also, the two figures show that room temperatures varied with time in such a way that the air in the room heated up steadily from morning to evening, cooling down sharply after power-off of the main room heater, and then cooling down steadily during the night, heating up sharply after power-on of the main room heater*. Thus, the temperature of the room varies one cycle per day. Furthermore,

---

* This test was conducted during the winter season.

a stable gradient temperature difference of about 2 °C was observed between the air at the floor of the room and that 2 meters above it during the day time due to the location of hot air outlets of the heater and slow blow speeds of the hot air from the outlets. Also the room temperature in the afternoon was more stable than in the morning. The gradient disappears during the night.

As can be seen in Figures 5.13 and 5.14, the machine components follow the pattern of the room temperature variations. The machine units are directly affected by the room temperature variations. The machine temperature is rising and falling within about 1 °C according to the room temperature in a cyclic form as shown in Figures 5.13 and 5.14. Figures 5.15 and 5.16 show the temperature variation and associated axial growth of the spindle during the afternoon when most of the tests were carried out (with the inductive sensor used for displacement measurement).

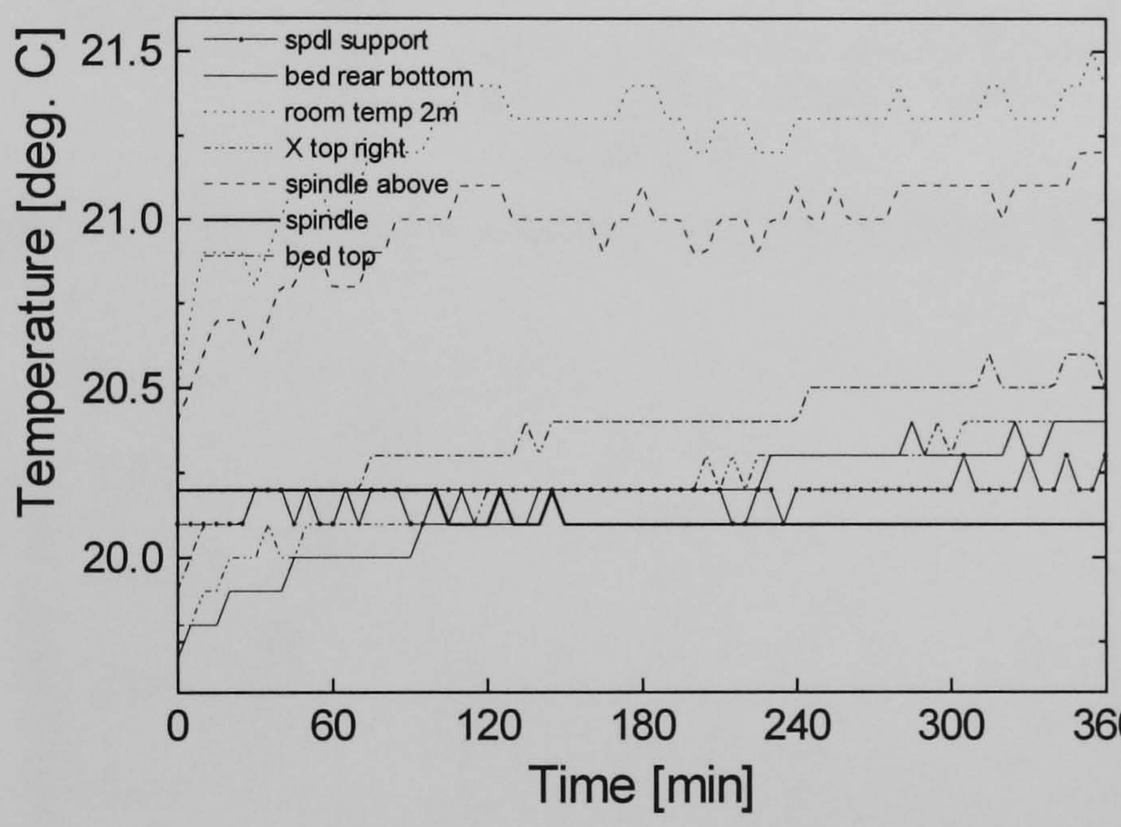

Figure 5.15 Temperature variation during afternoon
(idle machine condition with air supply)

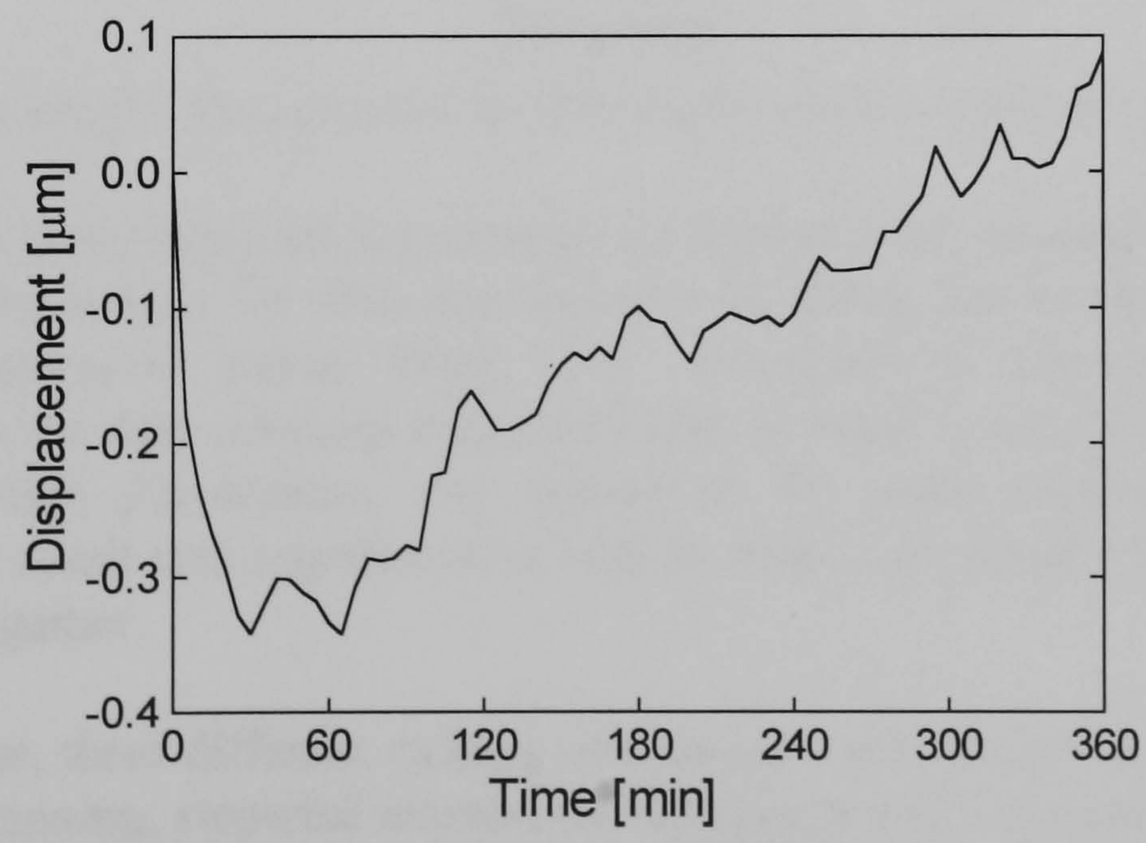

Figure 5.16 Axial growth of spindle measured by inductive sensor
(idle machine condition with air supply)

Figures 5.15 and 5.16 indicate that during the afternoon the room temperature is relatively stable and displacement measurements using the inductive sensor are reliable enough to characterise small thermal axial growth of the spindle. On the other hand, Figures 5.17 and 5.18 show the results using the fibre-optic sensor.

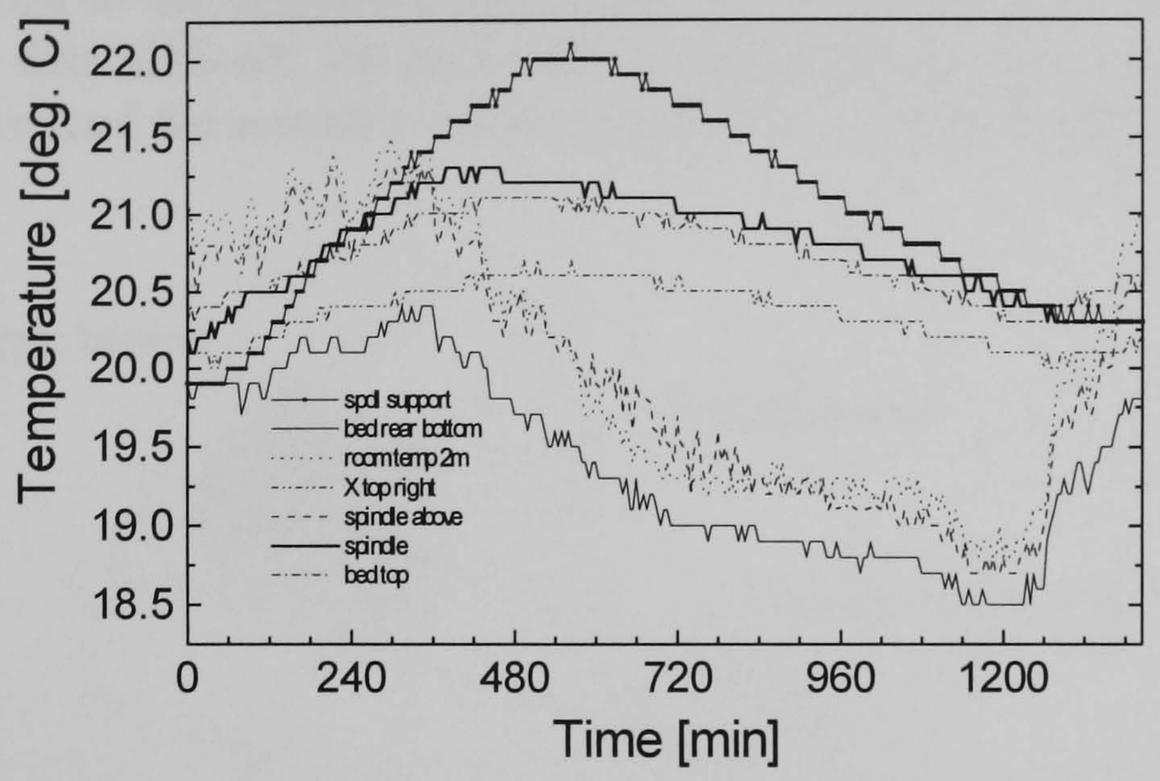

Figure 5.17 Temperature variation at spindle speed of 1000 rpm

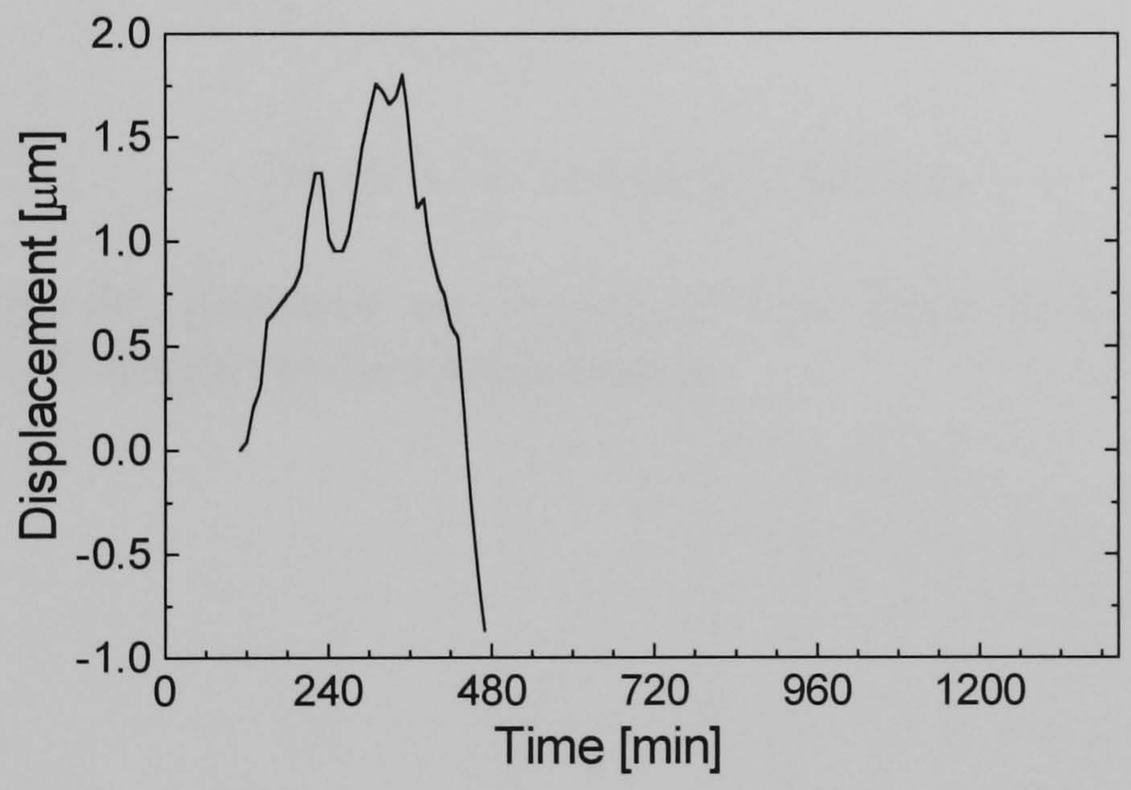

Figure 5.18 Axial growth measured by fibre-optic sensor at spindle speed of 1000 rpm

From these we can see the poor presentation of displacement measurements by the fibre-optic sensor. The reason for this was deduced as being due to the extender used to support the fibre-optic sensor being very susceptible to surrounding temperature variations. Thus the data obtained was unreliable. In order to overcome this problem an insulation material, polystyrene, was applied to the outer surface of the extender. Afterwards, the result was impressive as will be seen in Appendix B where test results are presented together.

For the main test, three different running conditions were devised for the spindle. They were constant running, stepwise increase of the speeds and intermittent running, which are likely to excite the machine in different ways. Also, three different spindle speeds, 500, 1000 and 1500 rpm were selected to provide different heating conditions for the

machine. Although the spindle can run at 2000 rpm, the machine seemed to be noisy at that speed.

Figures B.1 to B.4 of Appendix B are test results using the fibre-optic sensor while Figures B.5 to B.12 are those using the inductive sensor. They seem to be acceptable but some fluctuations in the displacement curves are observed. Such fluctuations make the analysis of the data difficult. An enclosure made of thick polystyrene boards, therefore, was built to surround the sensitive measurement area as illustrated in Figure 5.19.

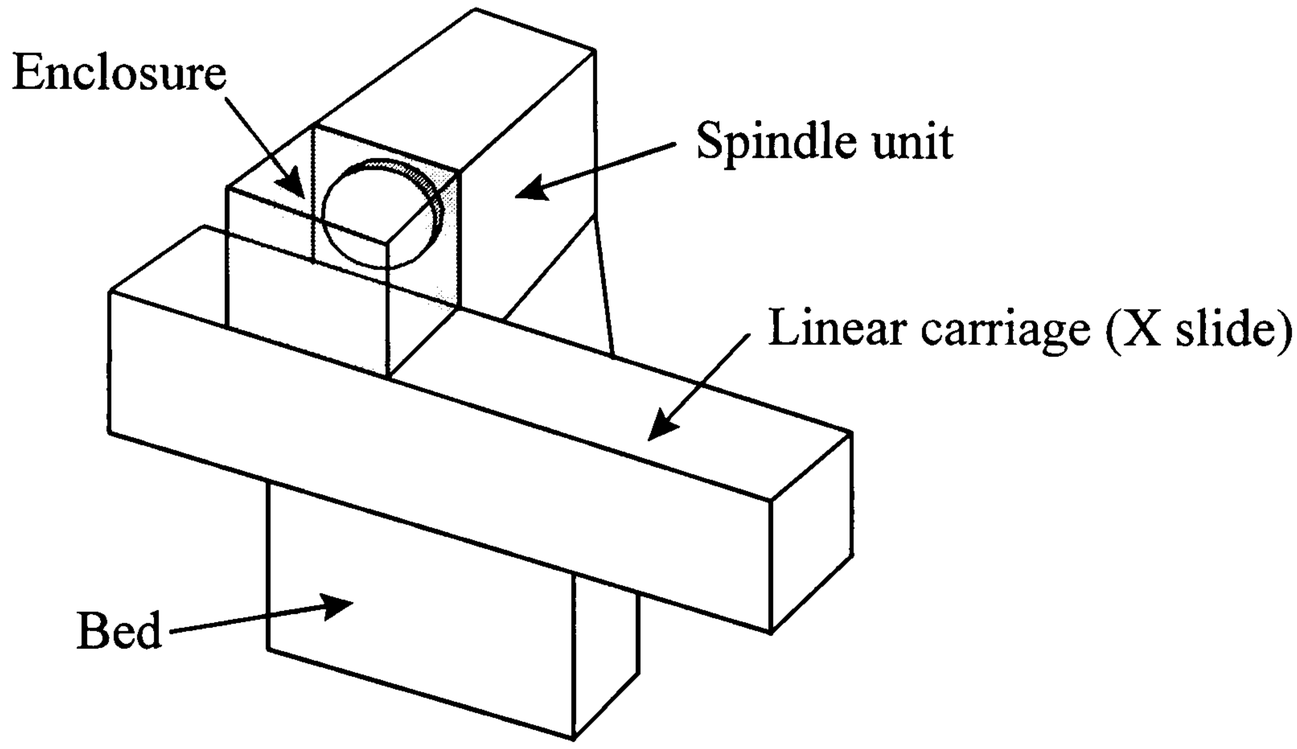

Figure 5.19 Test using enclosure

Test results using the enclosure are Figures B.13 to B.25 of Appendix B, showing improved fidelity in displacement measurements.

Chapter 6
Analysis of Test Data

6.1 Descriptive Interpretation

The results of the axial thermal growth tests (Appendix B) and environment tests (Figures 5.13 and 5.14 in Section 5.4) provide a rich insight into the thermal response of the machine under consideration. From the daily temperature variation environment test results shown in Figures 5.13 and 5.14, we can see that, irrespective of the sharp drop and rise of the room temperature, the pattern of the machine temperature variations shows a near sinusoidal form. That implies the machine units have large time constants, i.e. they act like a low pass filter having very low frequency cut-offs.

From Figures 5.13 and 5.14 in Section 5.4, the unit whose temperature is least affected by the room temperature variations is found to be the spindle support shown in Figure 5.8, which is indirectly exposed due to other machine components. The temperature curves representing the spindle support show the presence of large time-delay, approximately 3 hours, due to the long path of thermal energy transportation. Also, we can see that the air supply to the spindle does not cause any difference in the responses of the machine to the room temperature variations because the air will follow the temperature of the room air anyway.

During the course of the test using the fibre-optic sensor, unexpected external disturbances happened frequently, so only two sets of the data were considered to be minimally affected by measurement noises caused by the room environment variations to the measurement set-up, as shown in Figure B.1 to B.4, although many more tests were carried out. The disturbances were a) abrupt malfunction of the room heating equipment, b) exposure to the freezing outside air and lastly c) movement of a large group of students in the building. For the tests using an inductive sensor and enclosure, more care was taken to avoid such disturbances so that most of test data was reasonable. From the test results shown in Appendix B, we can see these common facts:

- The temperature of the spindle rises during its constant-speed running operation (Figures* B.1, B.3, B.13, B.15, B.17 and B.19). In turn, the axial growth of the spindle increases in accordance with the temperature in a form of exponential growth (Figures B.2, B.4, B.14, B.16, B.18 and B.20). The amount of growth is a few micrometres and the time-constant is more than 1 hour. Comparing Figure B.18 and Figure B.20, it can be seen that the spindle grows more as the rotational speed becomes higher. Also, the time-delay of the spindle growth from the starting point occurs due to delayed heat transmission to the spindle shaft. This is more or less 10 minutes as can be seen in Figures B.2, B.4 and B.8. During the night the spindle contracts due to the drop of the room temperature (Figures B.5, B.7 and B.9). The displacement data measured (Figures B.6, B.8 and B.10) shows an exponentially decreasing pattern for the night followed by an exponentially increasing pattern for the morning.

- The temperature of the spindle support is least affected by the room temperature variations as shown in Figures 5.13 and 5.14, but under running conditions (Figures B.1, B.3, B.7, B.9, B.11, B.13, B.15, B.17, B.19, B.21, B.23 and B.24), the heat from the spindle motor is directly conducted into the spindle support, also from heat generated due to shearing of the air lubricant in the bearing gap. The spindle motor is considered to be the most harmful heat source in machine tools. Eventually, the temperature of the spindle support rises more than that of the spindle as can be seen particularly in Figure B.1, which means that the spindle motor is a serious heat source in this machine too. Moreover, the temperature of the spindle support barely achieves its equilibrium state. This implies the thermal mass of the spindle support is large (the mass is about 120 Kg) and the cooling is poor.

- The temperature of the linear carriage and bed is largely under control of the room temperature variations. A part of the bed near the spindle support is likely to be affected by the heat stored in the spindle support. Nothing interesting was found for those components.

It is hard to say which of the sensors was better for the test. Comparison of the test results using the fibre-optic sensor and inductive sensor reveals no appreciable facts under some defects, as stated in Section 5.3.2, in the calibration of the fibre-optic sensor. The fibre-optic sensor, however, is more susceptible to changes in its set-up environment because it uses a light beam and has small dimension. The test using an enclosure employed the fibre-optic sensor, but it gave highly reliable data as can be seen in Figures B.13 to B.25. The type of sensor, therefore, appears not to be a key element in the measurements, but the physical set-up has more importance.

The test results reveal a serious matter, inconsistency of data sets under the same input condition. For example, Figures B.2 and B.18 were plotted from test results when the

---

* The thick line represents the temperature of the spindle housing. But in the figures as well as main text, the associated notation is just *spindle*.

spindle was running at 500 rpm. Comparing Figures B.18 and B.2, the measured growth is more than doubled and the time-constant more than trebled. Examining the corresponding temperature plots (Figures B.1 and B.17), we can see that, in Figure B.1, there is an ever-increasing trend in environment temperature during the measurement due to effects other than running of the spindle. In contrast, the environment temperature is very stable in Figure B.17. Figure B.18, therefore, represents more precisely the response of the spindle due to its friction losses.

On the other hand, from Section 4.4 we see that parameters governing thermal response of a machine tool vary with time. Irrespective of whether errors in measurement are large or small, the thermal responses are expected to differ at every instance of measurement although apparent conditions, such as spindle speeds, are the same. What is really important is how to diagnose information relevant to a specific kind of heat input from noisy data.

Figures B.4, B.14 and B.20 depict the axial growth at 1000 rpm, which also deviate considerably. Accepting such deviations, i.e. the deviations have their own right in the thermal response of the spindle unit, some may be from the past thermal memory of machine components and others may be due to considerable changes in the room environment. Thermal memory of machine components would seem to be mostly responsible for such deviations. In fact, the heat transfer mechanism is very sensitive to the initial conditions provided because heat flux is directly proportional to temperature difference between a body and its surrounding as can be seen in Equation 4.2.

However, we cannot discard effects due to poor arrangement of measurement set-ups. We can see two types of trends followed by one another in the thermal growth in Figure B.4. The change of trends matches with the decreasing period of the room temperature in Figure B.3. The decrease of the temperature affects sensory equipment also. Thus, the results using an enclosure are likely to have more importance in analysing the test results. Figure 6.1 depicts trends of the axial growth of the spindle with test results using an enclosure. They seem to be reasonably well behaved.

Figures B.8, B.10 and B.25 show the behaviour of the spindle during its running at some duty cycles. They show, when the spindle is idle, the rate of decrease of the spindle temperature is much less than the rate of increase of the temperature when the spindle is running. Sometimes the temperature continues rising although the spindle has stopped. This implies natural convection and conduction are acting as a cooling mechanism when the spindle is not running.

Figures B.12 and B.22 depict the axial growth under stepwise decrease and increase of the spindle speed each other. The graphs indicate that this kind of excitation gives low fidelity in test data. In every step, thermal memory of the past step is still active so interpretation is difficult. We need another means for analysis for this sort of difficulty.

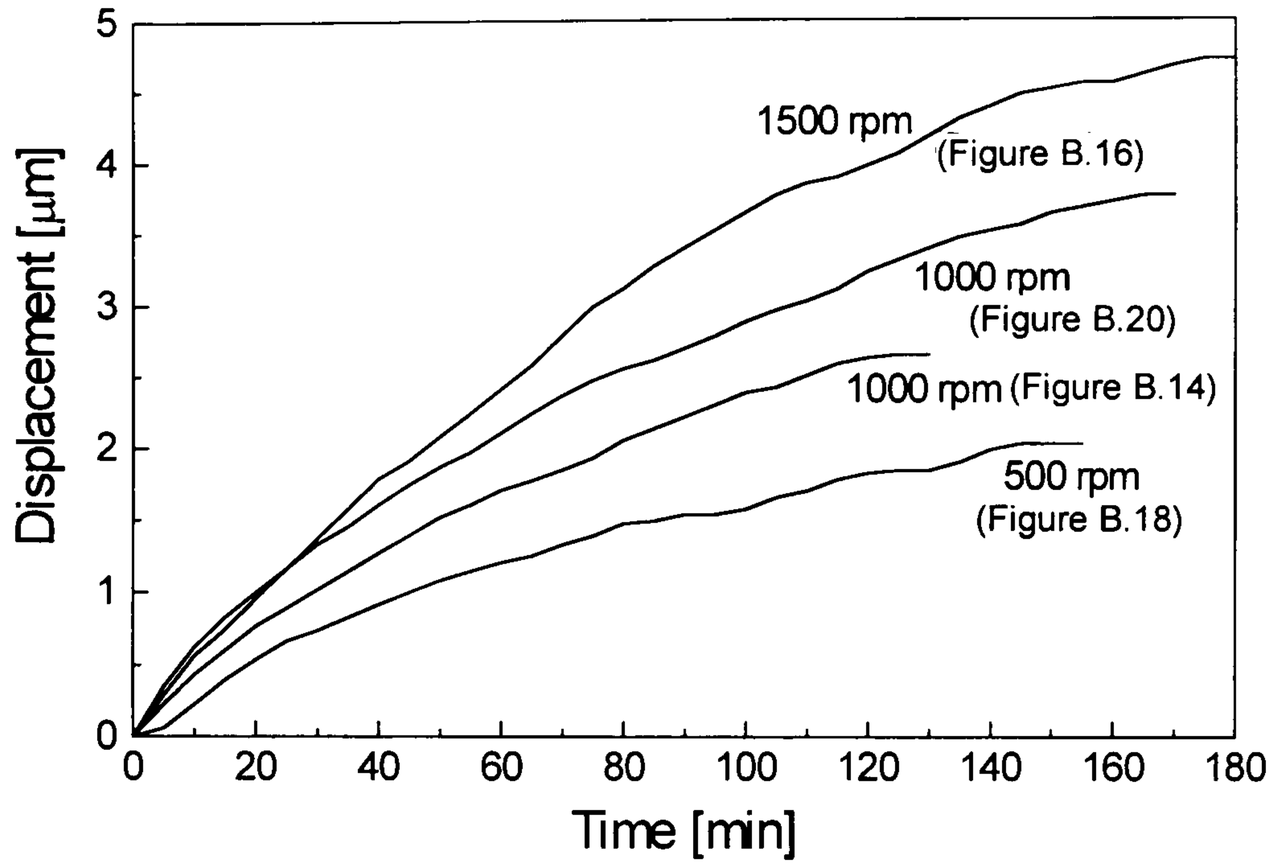

Figure 6.1 Axial thermal growth of spindle

Lastly, the predictions given in Chapter 5, i.e. Table 5.3, compared with Figure 6.1, turn out to have large errors in calculating the axial growth theoretically. In the calculations the reference length was chosen to be the length of the spindle from the thrust plate and nose face. We considered the thrust plate as a thermal reference plane that does not move with respect to the tool. But in reality there are added effects from the spindle support, vacuum chuck, aluminium target, etc. Probably, the heated spindle support evokes the movement of the spindle unit as a whole in the axial direction. Most of the measured axial growth is likely to be due to deformation of the spindle support. The outcome is axial displacement of the spindle due to thermal disturbances.

6.2 Parameter Identification

6.2.1 Problem Definition

An analysis method is required to interpret the test results quantitatively, i.e. we need an analytical tool to calculate three thermal parameters, time-delay, time-constant and gain from the test data. This is a realm of parameter identification by which a finite number of parameters governing a system can be deduced from experimental data and a system function whose form is assumed. The system function we are going to deal with is the solution of Equation 4.6. From Section 4.4, we can write the governing differential equation of thermal deformation of a point of a body under one heat input such that

$$\tau(t)\frac{du}{dt} + u = K(t)F_{th}\left[t - t_D(t)\right]H\left[t - t_D(t)\right] \tag{6.1}$$

This equation forms a basic model structure for parameter identification that makes it possible to obtain time-constant τ, gain K and time-delay t_D using experimental test data.

A machine tool has many thermally affected bodies and heat sources, so in general we have to evaluate sets of thermal parameters. This is conceptually illustrated in Figure 6.2. A machine model of Figure 6.2 is composed of N_M sets of thermal parameters each representing the behaviour of an individual unit. Each set has three thermal parameters that are in general represented by a matrix form because several heat sources or inputs act upon a unit. Each element of a parameter matrix is related with a specific heat input.

A machine model will eventually produce as many deformation elements as the number of heat sources multiplied by the number of machine units. The sum of individual deformations finally represents the total thermal error of a machine tool. In developing such a model, an estimator using methods of parameter identification will constantly monitor the input and output of the thermal response of a machine, and change parameters according to deviations of a machine model from real machine behaviour. In this study we are dealing with basically one heat input to one unit producing one deformation element.

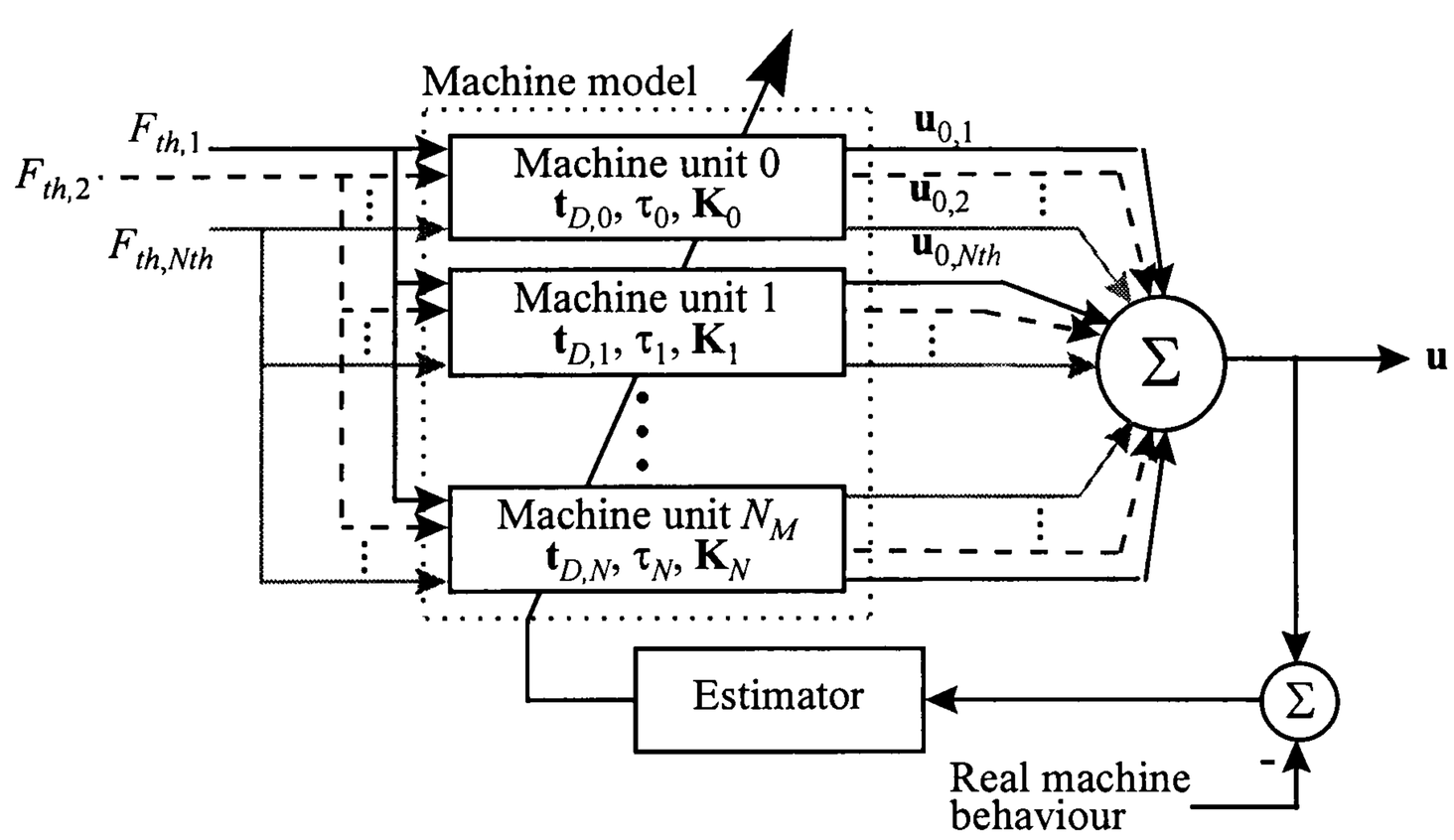

Figure 6.2 Thermal parameter identification of machine tools
($\mathbf{t}_{D,i}$ = time delay of machine unit i;
τ_i = time constant of machine unit i;
$\mathbf{K}_i$ = gain of machine unit i;
$\mathbf{u}_{i,j}$ = deformation of machine unit i associated with heat input $F_{th,i}$;
$\mathbf{u}$ = total thermal deformation)

6.2.2 Review of Identification Algorithms

A general expression for an N_ath-order difference equation of a linear causal system is of the form (Goodwin and Payne, 1977, pp. 62-64):

$$y(t) + \sum_{k=1}^{Na} a_k(t) y(t-k) = \sum_{k=1}^{Nb} b_k(t) x(t-k)$$

where $x(t)$, $y(t)$ are the input and output respectively; $\{a_k\},\{b_k\}$ characterise the appropriate system; N_a and N_b denote the number of possible delays of the output and input respectively. It is noted that t in the above equation is a integer-valued time scale for discrete-time models. Considering that we have obtained input sequence $\{x(t)\}$ and output sequence $\{y(t)\}$ by experiments for such a system with time-invariant parameters, we may think that the sampled values (input and output sequences) can be related through the following linear difference equation:

$$y(t) + \sum_{k=1}^{Na} a_k y(t-k) = \sum_{k=1}^{Nb} b_k x(t-k) + v(t) \tag{6.2}$$

where $v(t)$ is some disturbance of unspecified character, called an equation error. Using a delay operator q^{-1}, i.e. $q^{-1}y(t) = y(t\text{-}1)$, Equation 6.2 can be written as

$$A(q^{-1})y(t) = B(q^{-1})x(t) + v(t)$$

$$A(q^{-1}) = 1 + a_1 q^{-1} + \cdots + a_{Na} q^{-Na} \quad \text{and} \quad B(q^{-1}) = b_1 q^{-1} + \cdots + b_{Nb} q^{-Nb}$$

Also Equation 6.2 can be put into a linear regression form such that (Jerbi *et al.*, 1993)

$$y(t) = \theta^{\mathrm{T}} \varphi(t) + v(t) \tag{6.3}$$

where θ is a parameter vector taken as

$$\theta = \begin{bmatrix} a_1 & \cdots & a_{Na} & b_1 & \cdots & b_{Nb} \end{bmatrix}^{\mathrm{T}}$$

and φ is a vector of lagged input-output data, of which components are called regressors:

$$\varphi(t) = \begin{bmatrix} -y(t-1) & \cdots & -y(t-N_a) & x(t-1) & \cdots & x(t-N_b) \end{bmatrix}^{\mathrm{T}}$$

This model describes the observed variable $y(t)$ as an unknown linear combination of the components of the observed vector $\varphi(t)$ plus noise. Thus the problem leads to how to identify a parameter vector θ.

The most common residual model is to describe $\{v(t)\}$ as a moving average of a white noise sequence $\{e_w(t)\}$ (Candy, 1986, pp. 28-30):

$$A(q^{-1})y(t) = B(q^{-1})x(t) + C(q^{-1})e_w(t)$$
$$A(q^{-1}) = 1 + a_1 q^{-1} + \cdots + a_{Na} q^{-Na};\ B(q^{-1}) = b_1 q^{-1} + \cdots + b_{Nb} q^{-Nb};\ C(q^{-1}) = 1 + c_1 q^{-1} + \cdots + c_{Nc} q^{-Nc}$$

This model structure is known as an ARMAX model (*ibid.*), which is short for an AutoRegressive Moving Average model with an exogenous signal and represents the general form of popular time-series and digital-filter models. Thus we are going to treat unmeasured disturbances and measurement errors as realisation of stochastic processes.

The model also can be put into a pseudo-linear regression form:

$$\begin{aligned} y(t) &= \theta^{\mathrm{T}} \varphi_0(t) + e_w(t) \\ \theta &= [a_1 \quad \cdots \quad a_{Na} \quad b_1 \quad \cdots \quad b_{Nb} \quad c_1 \quad \cdots \quad c_{Nc}]^{\mathrm{T}} \\ \varphi_0(t) &= [-y(t-1) \quad \cdots \quad -y(t-N_a) \quad x(t-1) \quad \cdots \quad x(t-N_b) \quad e_w(t-1) \quad \cdots \quad e_w(t-N_c)]^{\mathrm{T}} \end{aligned} \tag{6.4}$$

A special case of an ARMAX model interesting to this study is

$$\begin{aligned} A(q^{-1})y(t) &= B(q^{-1})x(t) + e_w(t) \\ y(t) &= \theta^{\mathrm{T}} \varphi_0(t) + e_w(t) \\ \theta &= \left[a_1 \quad \cdots \quad a_{Na} \quad b_1 \quad \cdots \quad b_{Nb}\right]^{\mathrm{T}} \\ \varphi_0(t) &= \left[-y(t-1) \quad \cdots \quad -y(t-N_a) \quad x(t-1) \quad \cdots \quad x(t-N_b)\right]^{\mathrm{T}} \end{aligned} \tag{6.5}$$

This is called an ARX (controlled autoregressive) model. It is noted that the regressors are not deterministic functions.

The identification methods have two branches, i.e.

- Off-line or batch identification: A batch of data is collected from the systems and subsequently as a separate procedure this batch of data is used to construct a model.
- Recursive or real-time identification: A model is inferred at the same time as the data is collected and then is updated at each time instant when some new data becomes available.

Recursive identification methods have a small requirement on memory since not all data are stored, and can be easily modified into real-time algorithms, aimed at tracking time-varying parameters. Recursive methods are suited to this study.

Considering a system described by Equation 6.3, we introduce an equation error as

$$\varepsilon(t) = y(t) - \theta^{\mathrm{T}}\varphi(t)$$

The least squares estimate of the parameter vector θ is defined as the vector $\hat{\theta}$ that minimises the following criterion function:

$$V_N(\theta) = \frac{1}{2}\sum_{i=1}^{N}\varepsilon(t)^2$$

where N is the number of data points. Then $V_N(\theta)$ has a unique minimum point given by (Söderström and Stoica, 1989, pp. 60-65)

$$\hat{\theta} = \left(\Phi^{\mathrm{T}}\Phi\right)^{-1}\Phi^{\mathrm{T}}\mathbf{Y} \tag{6.6}$$

where:

$$\Phi = \left[\varphi(1) \quad \cdots \quad \varphi(N)\right]^{\mathrm{T}} \quad \text{and} \quad \mathbf{Y} = \left[y(1) \quad \cdots \quad y(N)\right]^{\mathrm{T}}$$

$$\Phi = \begin{bmatrix} -y(t-1) & \ldots & x(t-N_b) \\ \vdots & & \\ -y(N-1) & & x(N-N_b) \end{bmatrix} \quad (N \times N_\varphi \text{ matrix})$$

This is the least-squares estimation method for off-line identification. Its recursive form is given by (*ibid.*, pp. 321-324)

$$\hat{\theta}(t) = \hat{\theta}(t-1) + \mathbf{K}(t)\varepsilon(t)$$

$$\varepsilon(t) = y(t) - \varphi^{\mathrm{T}}(t)\hat{\theta}(t-1)$$

$$\mathbf{K}(t) = \mathbf{P}(t)\varphi(t) = \frac{\mathbf{P}(t-1)\varphi(t)}{1 + \varphi^{\mathrm{T}}(t)\mathbf{P}(t-1)\varphi(t)}$$

$$\mathbf{P}(t) = \mathbf{P}(t-1) - \frac{\mathbf{P}(t-1)\varphi(t)\varphi^{\mathrm{T}}(t)\mathbf{P}(t-1)}{1 + \varphi^{\mathrm{T}}(t)\mathbf{P}(t-1)\varphi(t)}$$

where $\mathbf{P}(t)$, $N_\varphi \times N_\varphi$ matrix, has the following form used for the derivation:

$$\mathbf{P}(t) = \left[\sum_{s=1}^{t}\varphi(s)\varphi^{\mathrm{T}}(s)\right]^{-1}$$

and $\mathbf{K}(t)$ is an $N_\varphi \times 1$ vector. Here the term $\varepsilon(t)$ should be interpreted as a prediction error. It is the difference between the measured output $y(t)$ and the one-step-ahead prediction

$$\hat{y}(t|t-1;\hat{\theta}(t-1)) = \varphi^{T}(t)\hat{\theta}(t-1)$$

of $y(t)$ made at time t-1 based on the model corresponding to the estimate $\hat{\theta}(t-1)$. The circumflex accent denotes the estimated value of a parameter. If $\varepsilon(t)$ is small, the estimate $\hat{\theta}(t-1)$ is good and should not be modified very much. The vector $\mathbf{K}(t)$ is interpreted as a weighting or gain factor showing how much the value of $\varepsilon(t)$ will modify the different elements of the parameter vector.

Any recursive algorithm requires some initial values to be started up, i.e., we need $\hat{\theta}(0), \mathbf{P}(0)$. Strictly speaking, the proper initial values are obtained if we start the recursion at an elapsed time t_0. It is more common, though, to start the recursion at $t = 0$ with some guesses. The relative importance of the initial values decays with time, as the magnitude of the sums increase. Thus, a common choice of initial values is to take some large constant multiplied by a unity matrix for $\mathbf{P}(0)$ and a null matrix for $\hat{\theta}(0)$.

When the properties of the process change slowly with time, the recursive algorithm should be able to track the time-varying parameters describing such a process. By using a forgetting factor we can modify the recursive least squares algorithm to a real-time method. The modified criterion function is (Söderström and Stoica, 1989, pp. 324-327)

$$V_t(\theta) = \sum_{s=1}^{t} \lambda^{t-s}\varepsilon(s)^2$$

where λ is a forgetting factor that has a numeric value somewhat less than 1 (for example 0.99 or 0.95). This means that with increasing t the measurements obtained previously are discounted. The smaller the value of λ, the quicker the information in previous data will be forgotten. The recursive least squares method with a forgetting factor is thus

$$\begin{aligned}
\hat{\theta}(t) &= \hat{\theta}(t-1) + \mathbf{K}(t)\varepsilon(t) \\
\varepsilon(t) &= y(t) - \varphi^{T}(t)\hat{\theta}(t-1) \\
\mathbf{K}(t) &= \frac{\mathbf{P}(t-1)\varphi(t)}{\lambda + \varphi^{T}(t)\mathbf{P}(t-1)\varphi(t)} \qquad (6.7) \\
\mathbf{P}(t) &= \frac{1}{\lambda}\left[\mathbf{P}(t-1) - \frac{\mathbf{P}(t-1)\varphi(t)\varphi^{T}(t)\mathbf{P}(t-1)}{\lambda + \varphi^{T}(t)\mathbf{P}(t-1)\varphi(t)}\right]
\end{aligned}$$

In the pseudo-linear model for an ARMAX model structure we used the following regressor vector:

$$\varphi_0(t) = [-y(t-1) \quad \cdots \quad -y(t-N_a) \quad x(t-1) \quad \cdots \quad x(t-N_b) \quad e_w(t-1) \quad \cdots \quad e_w(t-N_c)]^{T}$$

Variables $e_w(i)$ entering the φ_0 vector are not measurable. However, they can be replaced by the estimated prediction errors, i.e.

$$\varphi(t) = [-y(t-1) \quad \cdots \quad -y(t-N_a) \quad x(t-1) \quad \cdots \quad x(t-N_b) \quad \varepsilon(t-1) \quad \cdots \quad \varepsilon(t-N_c)]^{\mathrm{T}}$$

This approach gives an extended least squares algorithm (Söderström and Stoica, 1989, pp. 328-334)

$$\hat{\theta}(t) = \hat{\theta}(t-1) + \mathbf{K}(t)\varepsilon(t)$$

$$\varepsilon(t) = y(t) - \varphi^{\mathrm{T}}(t)\hat{\theta}(t-1)$$

$$\mathbf{K}(t) = \mathbf{P}(t)\varphi(t) = \frac{\mathbf{P}(t-1)\varphi(t)}{1+\varphi^{\mathrm{T}}(t)\mathbf{P}(t-1)\varphi(t)} \tag{6.8}$$

$$\mathbf{P}(t) = \mathbf{P}(t-1) - \frac{\mathbf{P}(t-1)\varphi(t)\varphi^{\mathrm{T}}(t)\mathbf{P}(t-1)}{1+\varphi^{\mathrm{T}}(t)\mathbf{P}(t-1)\varphi(t)}$$

An advantage of this algorithm is that it is computationally equivalent to the usual recursive least squares algorithm.

6.2.3 Test of Algorithms

Before applying identification algorithms, a difference equation describing thermal deformation of a body should be obtained, such as a form given by Equation 6.2. This can be done by integrating Equation 6.1 or using a transfer function. In the case of a first-order system with no time-delay, the transfer function is given in Section 4.4.2 such that

$$G(s) = \frac{K}{1 + \tau s} \tag{6.9}$$

One method of the construction of discrete equivalents to continuous transfer function is hold equivalence using the z transform, that is (Franklin and Powell, 1980, pp. 62-66)

$$G'(z) = (1 - z^{-1})\mathbf{Z}\left(\frac{1}{s}G(s)\right)$$

where z represents a z-transformed variable. The hold equivalence of Equation 6.9 becomes

$$G'(z) = \frac{\bar{u}(z)}{\bar{F}_{th}(z)}$$

$$= (1 - z^{-1})\mathbf{Z}\left(K\frac{1/\tau}{s(1/\tau + s)}\right) = K \cdot \frac{z-1}{z} \cdot \frac{z\left(1 - e^{-t_s/\tau}\right)}{(z-1)\left(z - e^{-t_s/\tau}\right)} = K\frac{z^{-1} - e^{-t_s/\tau}z^{-1}}{1 - e^{-t_s/\tau}z^{-1}}$$

and

$$\bar{u}(z)\left(1 - e^{-t_s/\tau}z^{-1}\right) = K\bar{F}_{th}(z)\left(z^{-1} - e^{-t_s/\tau}z^{-1}\right)$$

where the overbar denotes z-transformed quantities; t_s is a sampling period. By employing the shift theorem of the z transform (*ibid.*, pp. 36-40), we have

$$\bar{u}(t) - e^{-t_s/\tau}\bar{u}(t-1) = K\left(1 - e^{-t_s/\tau}\right)\bar{F}_{th}(t-1) \tag{6.10}$$

and in analogy with Equation 6.2

$$a_1 = -e^{-t_s/\tau}$$

$$b_1 = K\left(1 - e^{-t_s/\tau}\right)$$

When a first-order system has a time delay t_D, the corresponding transfer function will be

$$G' = \frac{\overline{u}(z)}{\overline{F}_{th}(z)} = K\frac{z^{-(1+N_D)} - e^{-tS/\tau}z^{-(1+N_D)}}{1 - e^{-tS/\tau}z^{-1}}$$

The discretised governing equation becomes

$$\overline{u}(t) - e^{-t_s/\tau}\overline{u}(t-1) = K\left(1 - e^{-t_s/\tau}\right)\overline{F}_{th}\left[t - \left(1 + N_D\right)\right] \tag{6.11}$$

Generally, a delayed-input system can be modelled as

$$A(q^{-1})y(t) = B(q^{-1})\left\{q^{-(k-1)}x(t)\right\} + C(q^{-1})e_w(t)$$

where k is an integer, $k \geq 1$. For a delayed-input system, firstly, compute the delayed input according to

$$x'(t) = q^{-(k-1)}x(t) = x(t-k+1)$$

where $t = k, k+1, k+2, \ldots, N$. Next, estimate the parameters of the ARMAX model applying a standard method using $x'(t)$ as an input signal instead of $x(t)$ and do another scanning for k, etc.

In order to validate the effectiveness of the algorithms and find an efficient application procedure, an arbitrary machine unit, showing thermal responses governed by Equation 6.10, is considered here. That is, the machine unit may be a spindle or ball screw, and its longitudinal thermal growth is assumed to have two parameters represented by the time-constant and gain. The input is in the form of step functions, assumed to be the rotation of the spindle at 1000 rpm from $t = 0$. The time-constant and gain are arbitrarily chosen to be 1.3 hours and 0.00786 μm/rpm. The exact output response can be calculated using Equation 4.7 and Figure 6.3 shows its curve denoted by *pure response*. The sampling time was chosen to be 5 minutes.

Another output sequence was prepared to take measurement noise into account. Adding a normally distributed random noise to the exact response, a response contaminated with noise can be obtained as shown by *added noise* in Figure 6.3. Lastly, a moving-averaged output sequence of the contaminated response was considered as filtered measurement data. The moving average was taken as

$$y_{avg}(t) = \frac{1}{5}\sum_{k=-2}^{2} y(t-k)$$

because, when a large number of data points are moving-averaged, the averaged response will have a considerable time-delay in comparison with the original response. Taking two

data points in either side is likely to be reasonable in order to achieve rejection of the noise as well as reduction of the associated time-delay. As can be seen in Figure 6.3, the contaminated data becomes much smoother by employing moving averages.

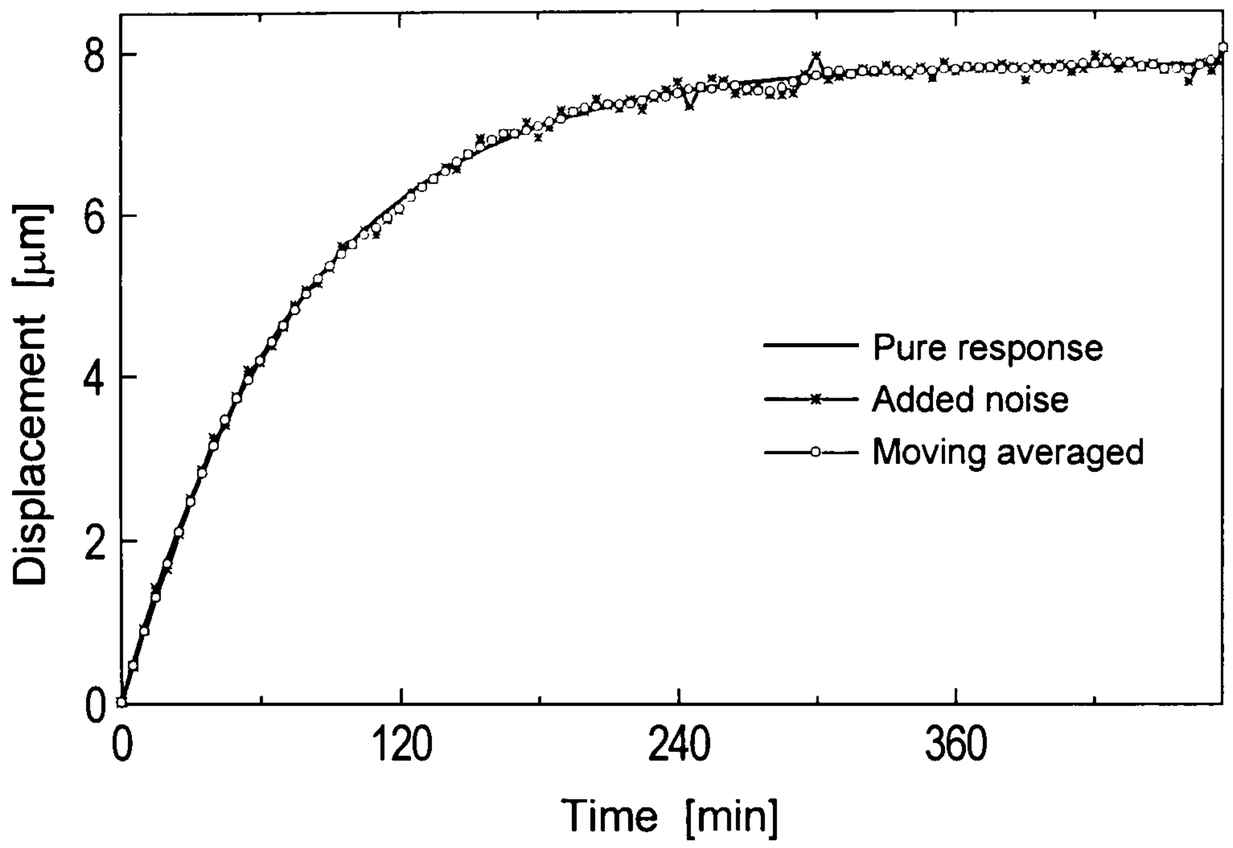

Figure 6.3 Output responses used in testing algorithms

A small program using MATLAB from the MathWorks* was coded to test the extended least squares algorithm of Equation 6.8 with the added forgetting factor under the ARX model structure of Equation 6.5.

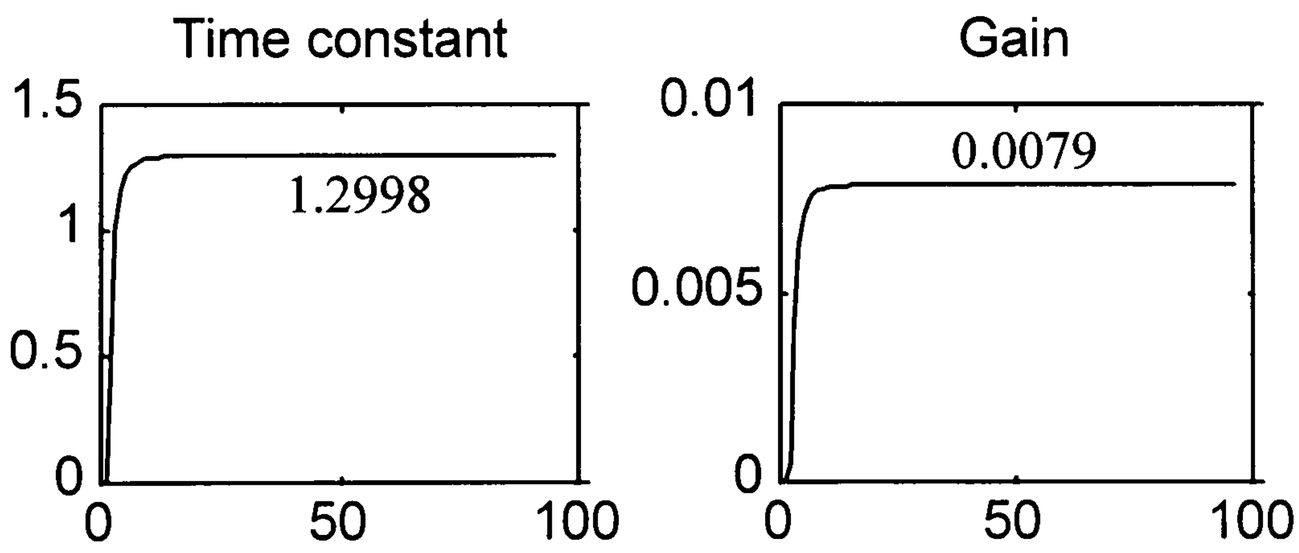

Figure 6.4** Parameter identification test for pure output sequence
(real value: time constant =1.3, gain = 0.00786)

Figure 6.4 shows the result of thermal parameter identification using the program described above. The curve starts with a transient period that is inevitable when using recursive

---

* The MathWorks, Inc., Cochituate Place, 24 Prime Park Way, Natick, MA 01760, USA

** The horizontal axis denotes time. Each unit equals 5 minutes. The meaning of the vertical axis is given at the top, i.e. time-constant in hours and gain in μm/rpm. This convention is used for most of plots for time-constant and gain.

algorithms, but soon stabilises and gives consistent, exact estimated values for time-constant and gain. Because high fidelity data was used, the algorithm produces nearly perfect results. With the same means, the contaminated output was processed and the result is shown in Figure 6.5. A very large fluctuation is observed in the figure.

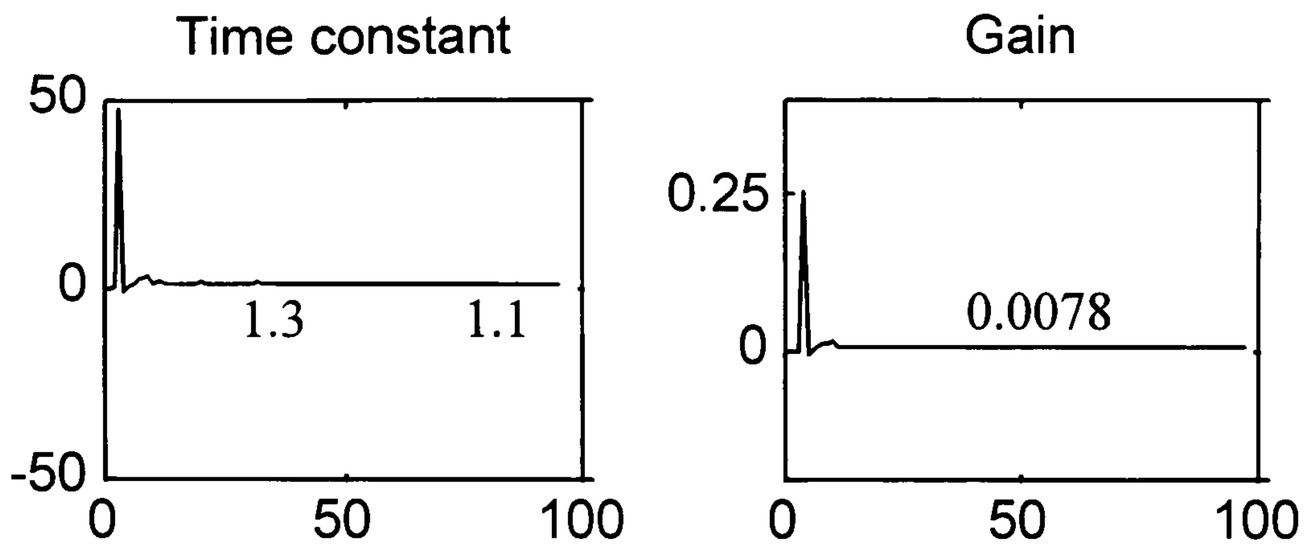

Figure 6.5 Parameter identification test for contaminated output sequence
(real value: time constant =1.3, gain = 0.00786)

To remove such a large transient that seems to be unsatisfactory, an ARMAX model structure of Equation 6.4 setting N_c = 5 was considered to take account of the noise components. The same algorithm with a more complex model structure was programmed. The new methodology removes the large transient as can be seen in Figure 6.6. The consistency of the presentation, however, is unsatisfactory. Under conditions of noisy data, this kind of outcomes might be inevitable. This means that care must be taken in interpreting the results of recursive identification process. Time-constant and gain are fluctuating with time according to the results under noisy conditions, but the true values are constant.

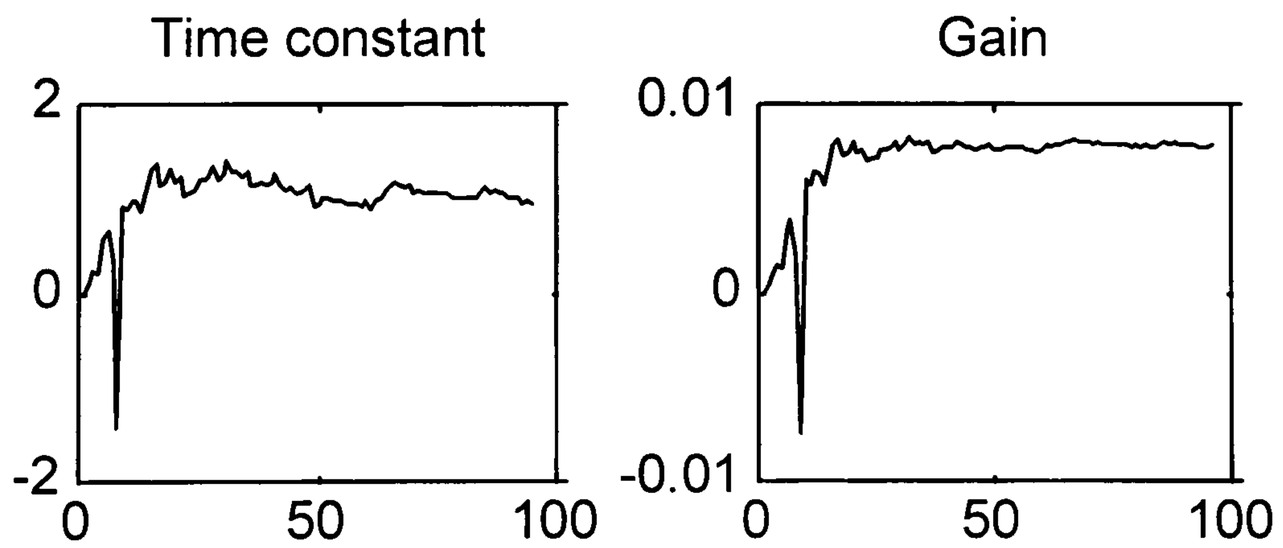

Figure 6.6 Parameter identification test for contaminated output sequence
(real value: time constant =1.3, gain = 0.00786)

Thus, it is clear that problems in interpreting identification results obtained by recursive algorithms arise from the noise added to the measurement data. The best possible way is to use the off-line identification procedure given by Equation 6.6. However, that is restricted to time-invariant parameter systems only. With recursive methods, one way to remove the

harmful contribution of measurement noise is using a highly sophisticated metrology arrangement, but this is costly. Another possibility is to pre-process measurement data prior to main analysis. An example of the latter was given by the moving-averaged output sequence. Figure 6.7 is the result of parameter identification using the moving-averaged data under an ARMAX model structure. The response characteristics seem to be much more improved than those of the prior results, but still long period fluctuations remain.

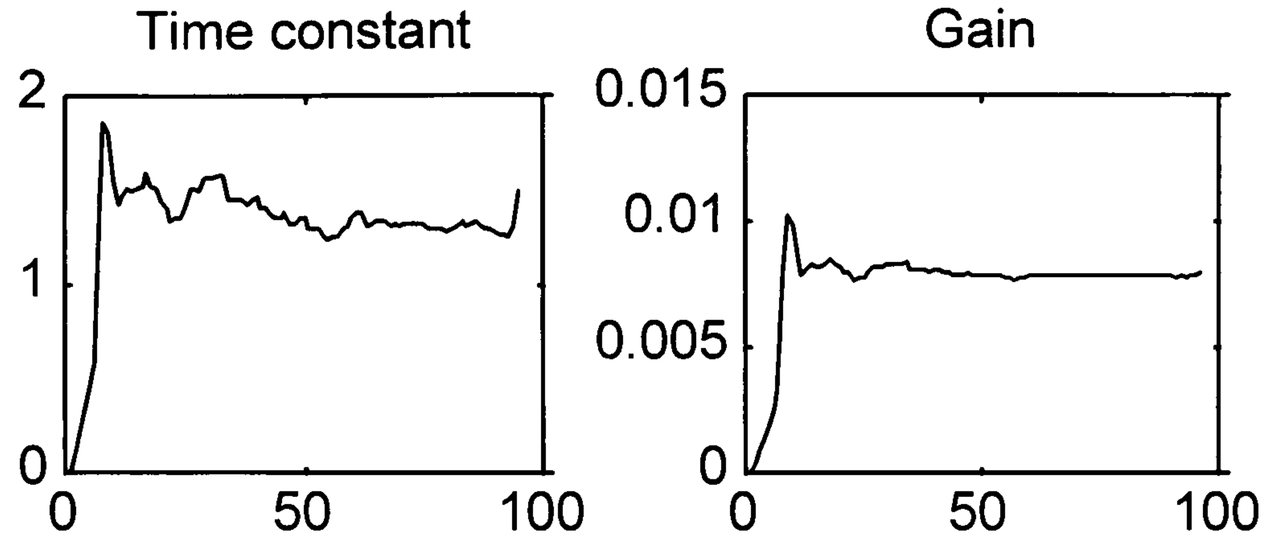

Figure 6.7 Parameter identification test for moving averaged output sequence
(real value: time constant =1.3, gain = 0.00786)

The response characteristics during a transient period were improved by using an ARMAX model but the estimated values fluctuated continuously. This means the ARMAX model structure employed is not useful for this sort of problem. Only the complication in manipulation is added, so that the ARX model used at the beginning will be used hereinafter. Also the test data will be moving-averaged for better prediction. Figure 6.8 represents the identification results using the program based on an ARX model structure with the moving averaged output sequence. Although the transient characteristics are worse, long-term consistency is good under the circumstances.

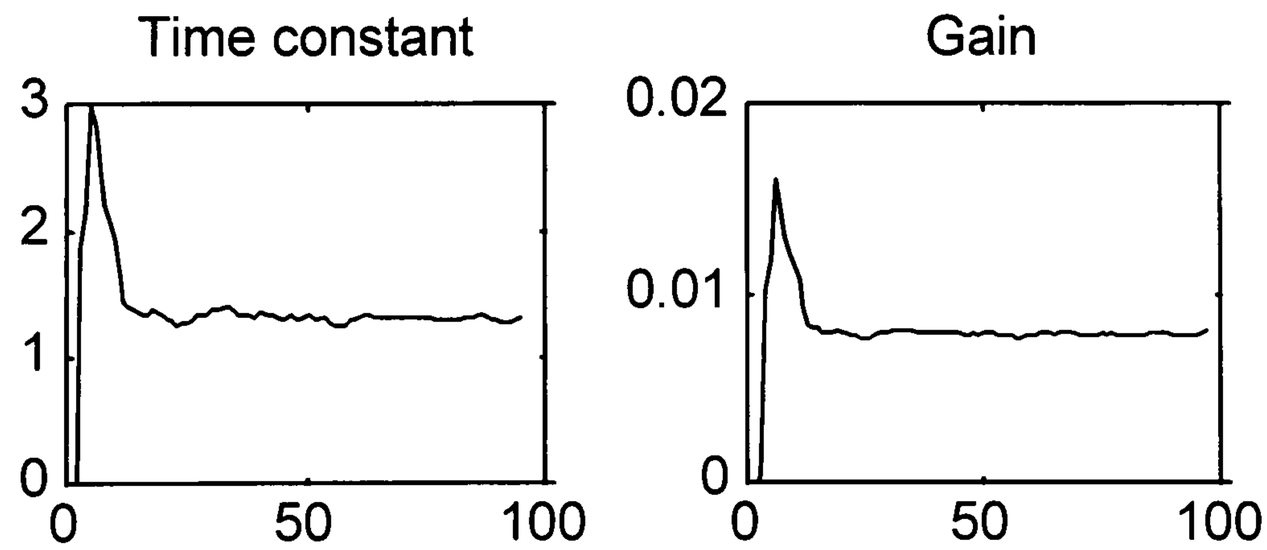

Figure 6.8 Parameter identification test for moving averaged output sequence
(real value: time constant =1.3, gain = 0.00786)

Now consider a parallel system shown in Figure 6.9. This can be seen as a reduced form of Figure 6.2. The situation in Figure 6.9 is that two machine units are under the influence of the same heat source. Due to the heat input F_{th} from the source, two units deform by u_1 and

u_2 respectively, giving total thermal deformation u. By analysing this system, we can obtain a method of how to reduce measurement points when testing the thermal response of a machine tool. The method will dramatically reduce the time and efforts necessary for the calibration of a machine tool under thermal disturbances. It is related with a problem of how to identify three thermal parameters in two units with the knowledge of just one input F_{th} and one total summed output u.

The governing difference equation of the system of Figure 6.9 can be obtained using a z transformed type of Equation 6.10, i.e.

$$G_1(z) = K_1 \frac{z^{-1} - e^{-t_s/\tau_1} z^{-1}}{1 - e^{-t_s/\tau_1} z^{-1}} \quad \text{and} \quad G_2(z) = K_2 \frac{z^{-1} - e^{-t_s/\tau_2} z^{-1}}{1 - e^{-t_s/\tau_2} z^{-1}} \tag{6.12}$$

where $G_1(z)$, $G_2(z)$ are the pulse transfer functions of units 1 and 2 respectively.

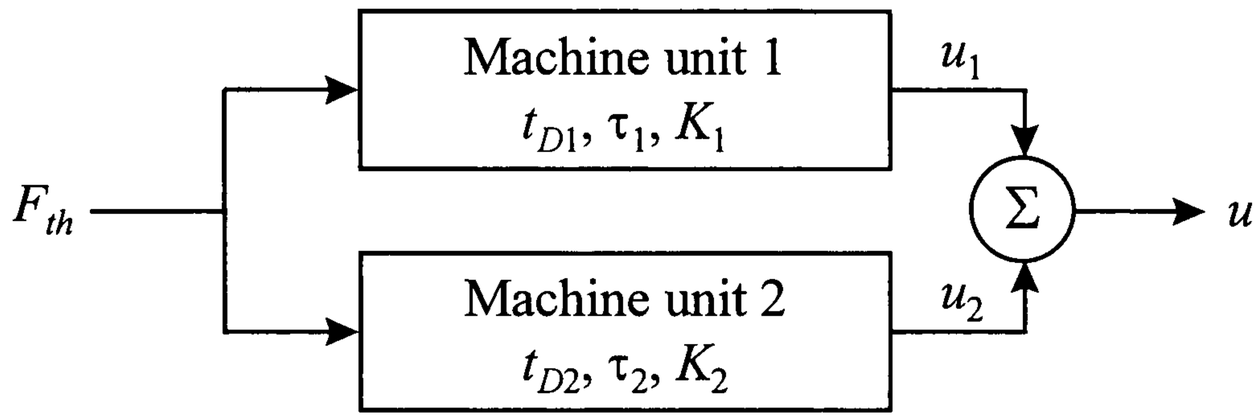

Figure 6.9 Parallel system under same heat input

The total transfer function of parallel systems is the sum of each transfer function, so that

$$G(z) = G_1(z) + G_2(z) = \frac{\overline{u}}{\overline{F}_{th}} \tag{6.13}$$

Substituting Equation 6.12 into Equation 6.13 and using the shift theorem, we have the following difference equation from the total pulse transfer function:

$$u(t) + a_1 u(t-1) + a_2 u(t-2) = b_1 F_{th}(t-1) + b_2 F_{th}(t-2) \tag{6.14}$$

where

$$a_1 = -e^{-t_s/\tau_1} - e^{-t_s/\tau_2}$$

$$a_2 = e^{\frac{-t_s\tau_1 - t_s\tau_2}{\tau_1\tau_2}}$$

$$b_1 = K_1 - K_1 e^{-t_s/\tau_1} + K_2 - K_2 e^{-t_s/\tau_2}$$

$$b_2 = -K_1 e^{-t_s/\tau_2} + K_1 e^{\frac{-t_s\tau_1 - t_s\tau_2}{\tau_1\tau_2}} - K_2 e^{-t_s/\tau_1} + K_2 e^{\frac{-t_s\tau_1 - t_s\tau_2}{\tau_1\tau_2}}$$

Then the problem becomes one of identifying the following parameter vector

$$\theta = \begin{bmatrix} a_1 & a_2 & b_1 & b_2 \end{bmatrix}^T$$

using the following lagged input-output vector

$$\varphi = \begin{bmatrix} -u(t-1) & -u(t-2) & F_{th}(t-1) & F_{th}(t-2) \end{bmatrix}$$

From the identified parameter vector, we can calculate the thermal parameters of the two units.

When the algorithm used so far is exposed to the parameter identification of the parallel system, the initial condition of the parameter vector governs the quality of the identification process. Just filling them with zero gave meaningless results. Thus, some prior knowledge on the range of the parameters are necessary. In order to know the order of magnitudes of the parameters, the elements of the parameter vector were evaluated, as shown in Table 6.1, by using Equation 6.14, the gain and time-constant data in Table 5.3 and the guessed values of the gain and time-constant.

K_1 (μm/rpm)	K_2 (μm/rpm)	τ_1 (s)	τ_2 (s)	a_1	a_2	b_1	b_2
0.00010	0.0008	8244	12000	-1.93957	0.940456	2.33E-05	-2.3E-05
0.00013	0.001	5076	10000	-1.91306	0.914753	3.7E-05	-3.5E-05
0.000147	0.001	3816	8000	-1.88759	0.890372	4.79E-05	-4.5E-05
0.000155	0.0013	3132	3600	-1.8287	0.836007	0.000118	-0.00011

Table 6.1 Order of magnitudes of parameters

Initial values were taken to be the average value of numbers listed in Table 6.1. To test the effectiveness of parameter identification applied to parallel systems, the following arbitrary condition was used:

- *Input*: rotation of spindle at 1000 rpm from $t = 0$
- *Unit 1*: time constant = 7200 s (2 hrs), gain = 0.003 μm/rpm
- *Unit 2*: time constant = 2520 s (0.7 hrs), gain = 0.001 μm/rpm
- *Sampling time*: 300 s

Figure 6.10 shows the result of parameter identification of the parallel system. Unlike the identification processes so far, it takes a long time to settle down at consistent estimated values. Nevertheless this demonstrates it is possible to break down the total response of a machine tool for identifying the contribution of each machine unit.

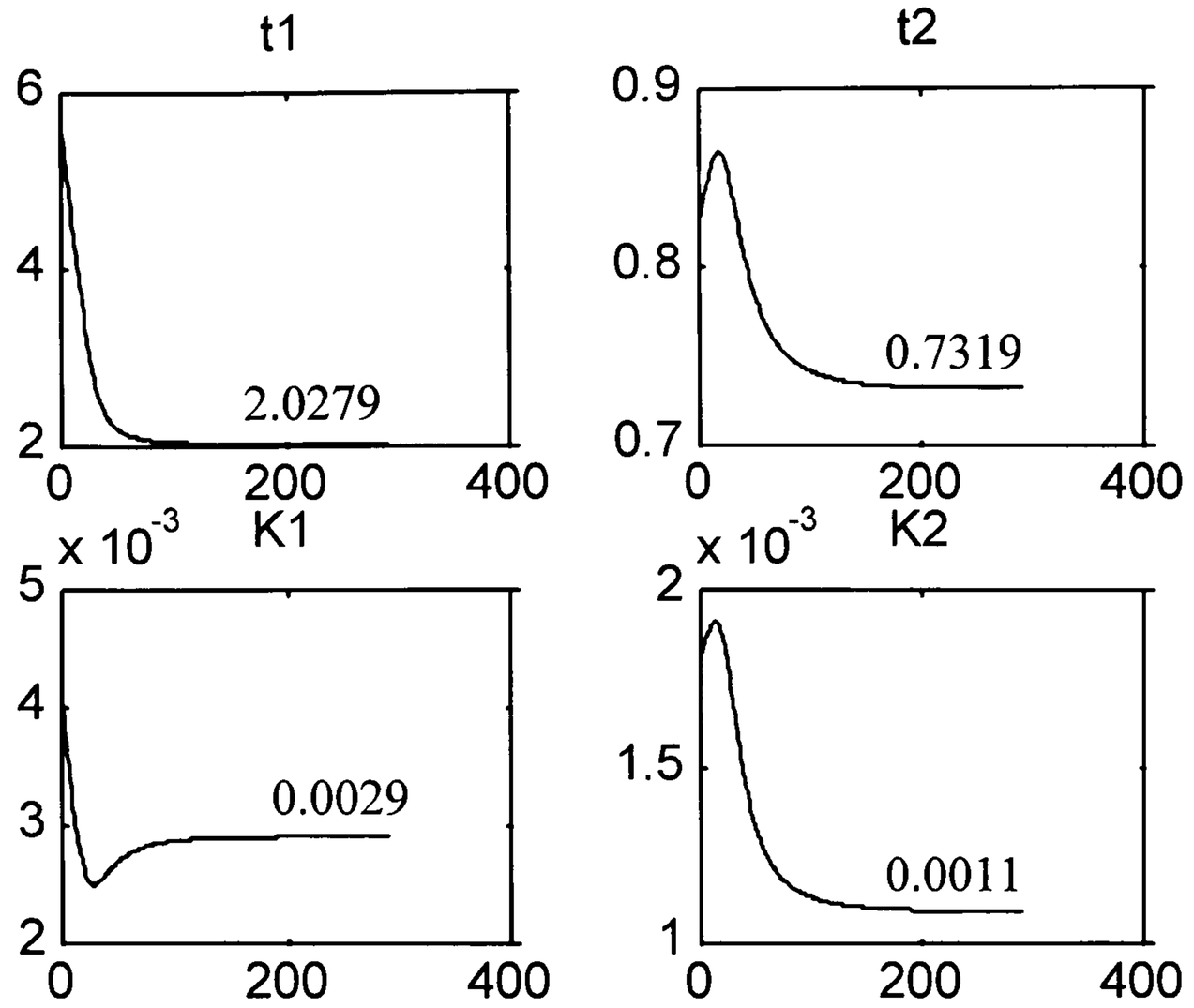

Figure 6.10* Parameter identification test for parallel system
(real value: $\tau_1 = 2$ hrs, $\tau_2 = 0.7$ hrs, $K_1 = 0.003$, $K_2 = 0.001$)

---

* In the figure, t1 and t2 represent the time-constant of units 1 and 2 respectively.

6.3 Thermal Parameters from Test Data

A machine component has a set of thermal parameters, i.e. time-delay, time-constant, and gain, in the presence of a heat input source. Also, the parameters are considered to be time-varying in a general sense. When several heat input sources act upon a machine component, it will have the same number of sets of thermal parameters. In Section 6.1, it was mentioned that heat input to the spindle is provided by the frictional losses in the bearing gap, spindle motor and air temperature variations. The first two sources are due to running of the spindle, so the rotational speed of the spindle and variations of air temperature are two independent heat inputs to the spindle. The measured data for the axial thermal growth in Appendix B can be considered as the differential response of the structural loop (from the spindle through the bed to the tool) under the two heat sources in a broad sense.

Firstly, consider the effect of air temperature variations on the structural loop. Figure 6.11(a) shows the thermal parameters of the spindle during a cooling period, i.e. the night, estimated from the exponentially decreasing part of Figure B.10 in Appendix B. A recursive least-squares method (Equation 6.7) based on the ARX model structure (Equation 6.5) was used.

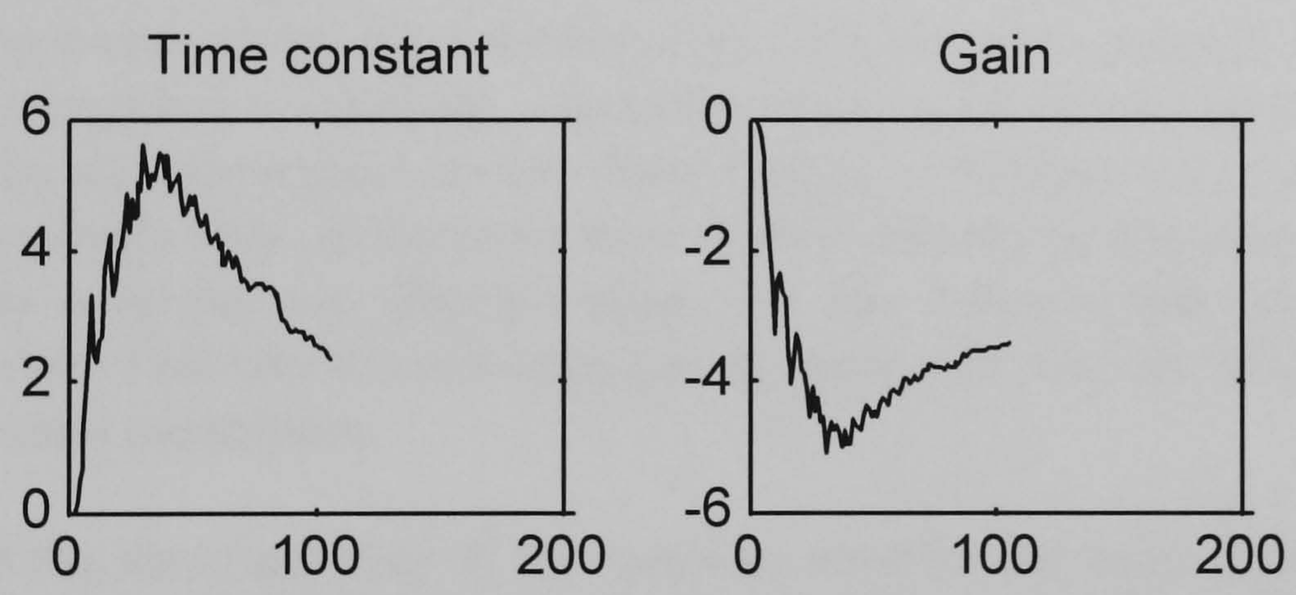

(a) Recursive identification*

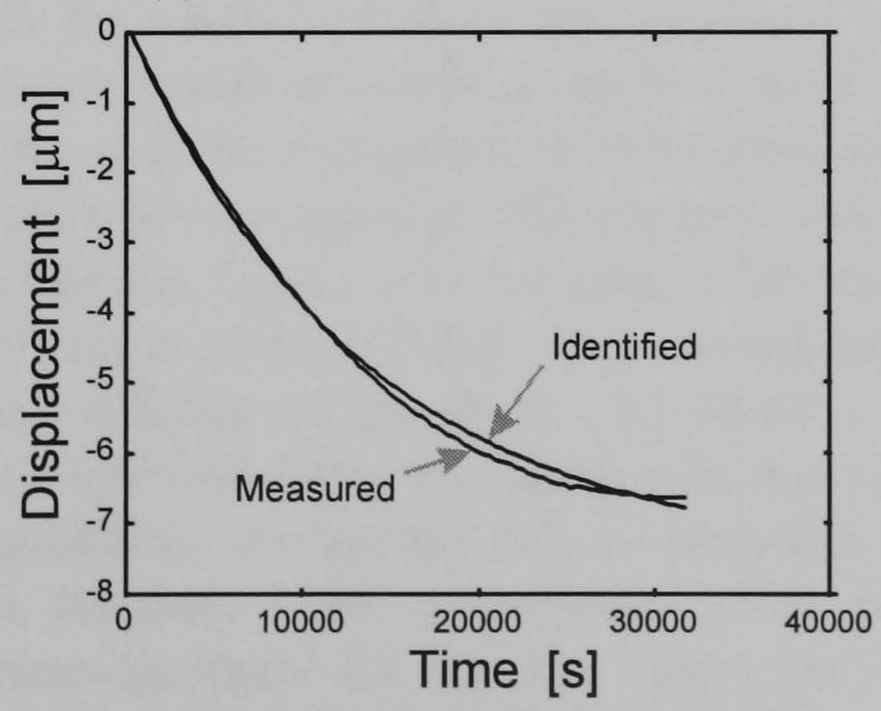

(b) Off-line identification

Figure 6.11 Identification regarding effects of air temperature variations

* The unit of gain is μm/K for this plot only

The input sequence was chosen to be the approximate step form of the variation of air temperature above the spindle, of which magnitude was 2 K, thus the figure represents the response of the structural loop to air temperature variations. The effects of air temperature variations were expected to be very small, but were found to be a serious heat source to the machine according to the identification result. Because it is difficult to express representative values for thermal parameters from Figure 6.11(a), the off-line identification method given by Equation 6.6 was applied to the same data and Figure 6.11(b) shows the results, measured data and the corresponding fitted curve. The gain obtained is -3.72μm/K* and the time-constant 3.66 hours. The large time-constant is due to the low heat transfer coefficient provided by natural convection. This means that a temperature difference of one degree can result in approximately 2 μm axial deformation of the spindle over 3 or 4 hours. It is noted that the gain obtained is large because the data used were measured during a rapid cooling period of the spindle from its highly elevated thermal state.

Many of the tests were conducted for 3 to 4 hours during afternoons. Therefore, in order to determine thermal parameters due to the rotation of the spindle, which should be free from the effect of air temperature variations, the surrounding temperature must be stable. Some tests such as those shown in Figure B.17 and B.19 were conducted in a rather stable environment, but some were not. Using an enclosure or any other means for controlling the surrounding environment ought to be an everyday practice when dealing with thermal problems of precision machines to characterise the thermal response due to other than air temperature variations. Inevitably the test data were contaminated by the variations of the air temperature for the identification of thermal parameters due to the rotation of the spindle only. If the parameters related with the temperature variations are assumed to be constant, i.e. time-invariant, we can remove that portion from the measurement data. This sort of correction can be made with the help of thermal models using three thermal parameters.

Assuming that the structural loop of the machine used for the axial growth test can be modelled as two dominant thermal elements that are affected equally by the effect of the spindle rotation, Figures 6.12 and 6.13 show the results of an identification process employing a parallel system model structure given by Equation 6.14. In this case, the structural loop is considered to be composed of two unknown sub-units 1 and 2, but there is no prior information about each unit. This should be deduced from the physical meaning of the estimated results. Figure 6.12 is a case of 500 rpm input (Figure B.2) and Figure 6.13 of 1000 rpm input (Figure B.20). The corresponding temperature records show the air temperature variation of less than 1 K, which is considered to be stable under the circumstances. Although large fluctuations in the estimation arose, from the test of identification algorithms, we learned that a consistent estimated value appears after time elapses for a duration. Later estimations can be taken as a representative value. The estimated time-constants for the two cases are nearly equal. The time-constant of unit 1 is 1.8 to 2 hrs, and that of unit 2 is about 6 minutes. For 500 rpm input, the gain of unit 1 is about 0.009 μm/rpm, and that of unit 2 about 0.0006 μm/rpm.

---

* The sign is negative because this is related with a cooling period.

For 1000 rpm input, the gain of unit 1 is about 0.005 μm/rpm, and that of unit 2 about 0.00026 μm/rpm.

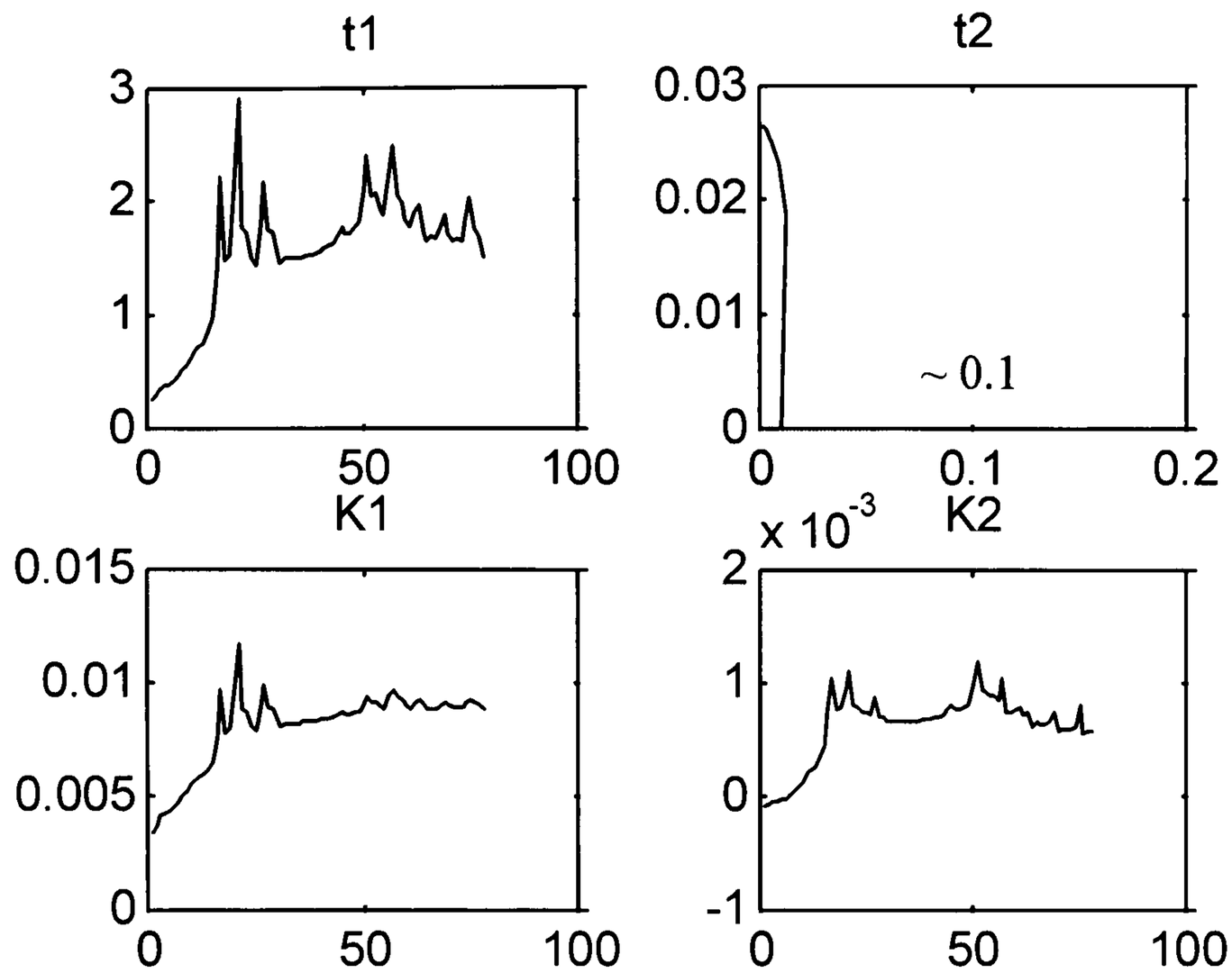

Figure 6.12 Parallel system identification using data of Figure B.2

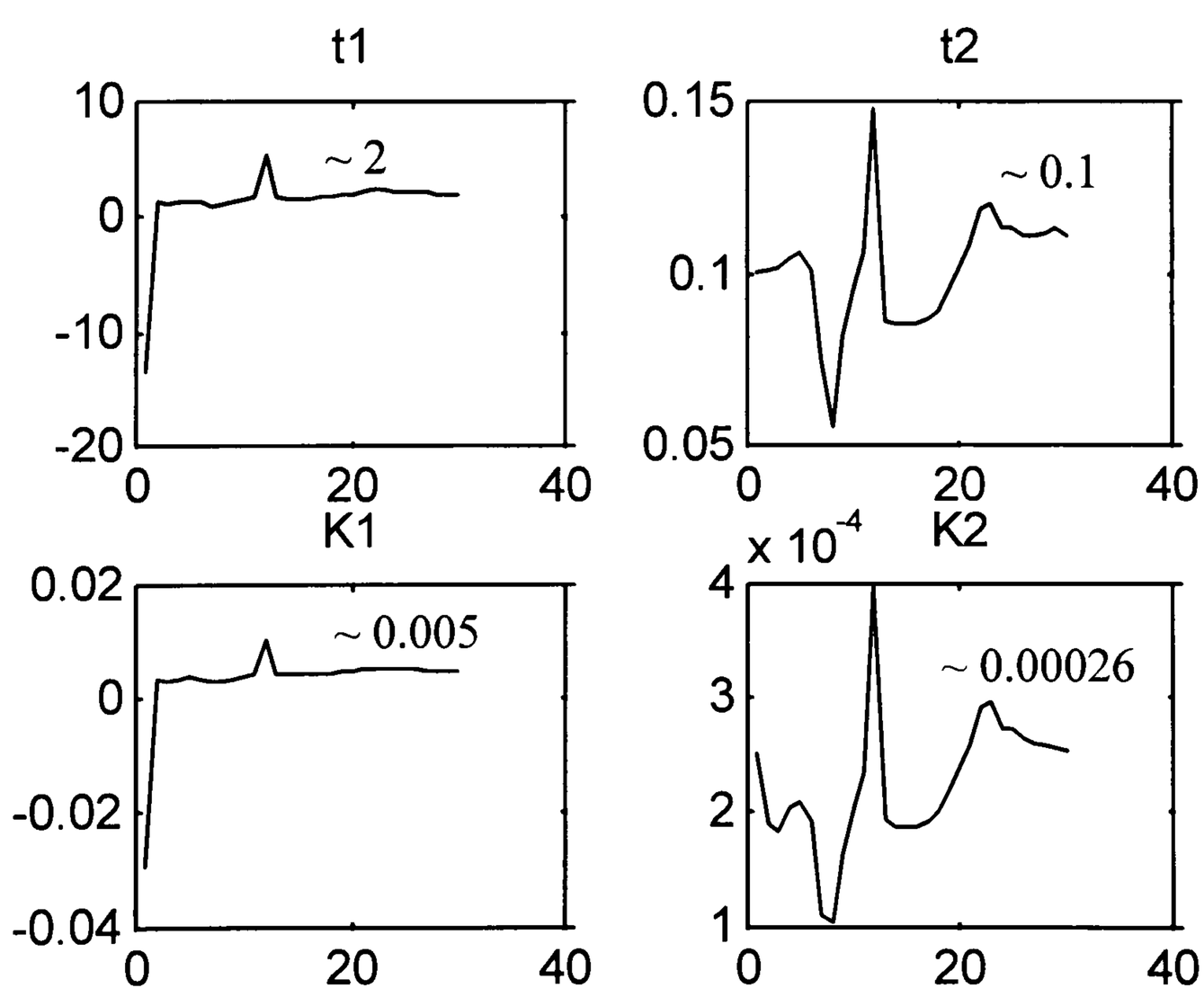

Figure 6.13 Parallel system identification using data of Figure B.20

However we have little information about which part of the structural loop can be considered as unit 1 and unit 2. The small time-constant of unit 2 can be due to measurement noise or the small aluminium target attached on the spindle but this cannot be determined unless their thermal characteristics are known. Considering the small time-constant of unit 2, it is likely to be the aluminium target. The identified

parameters do not agree with the theoretical calculations of Section 5.3.1 in terms of their magnitudes. There the theoretically calculated gain of the invar spindle shaft is shown to be about 0.0001 μm/rpm from Table 5.3 and its time-constant is approximately 1.5 hrs. Unit 2 therefore represents total thermal behaviour of the spindle shaft, housing and spindle support as a whole with respect to the position of the sensor tip regarding the great temperature rise of the spindle support due to heat from the spindle motor.

Because the above parallel system postulate showed one dominant sub-unit with the associated negligible one, just one first-order element is considered to be the model structure of the spindle unit or structural loop. Figures 6.14 to 6.17 show the results of parameter identification based on the total response of the spindle unit. Two 1000 rpm input cases are depicted in Figures 6.15 and 6.16 for comparison, and they seem to have nearly the same characteristics. This means that under constant thermal environments thermal parameters can be considered to be constant.

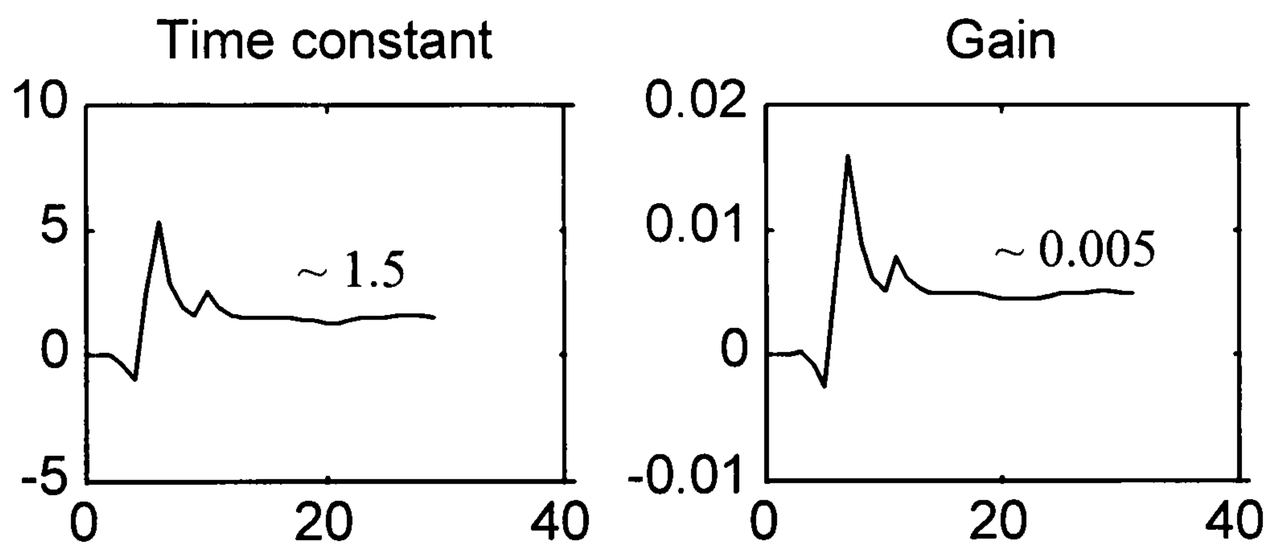

Figure 6.14 Parameters from Figure B.18 (500 rpm)

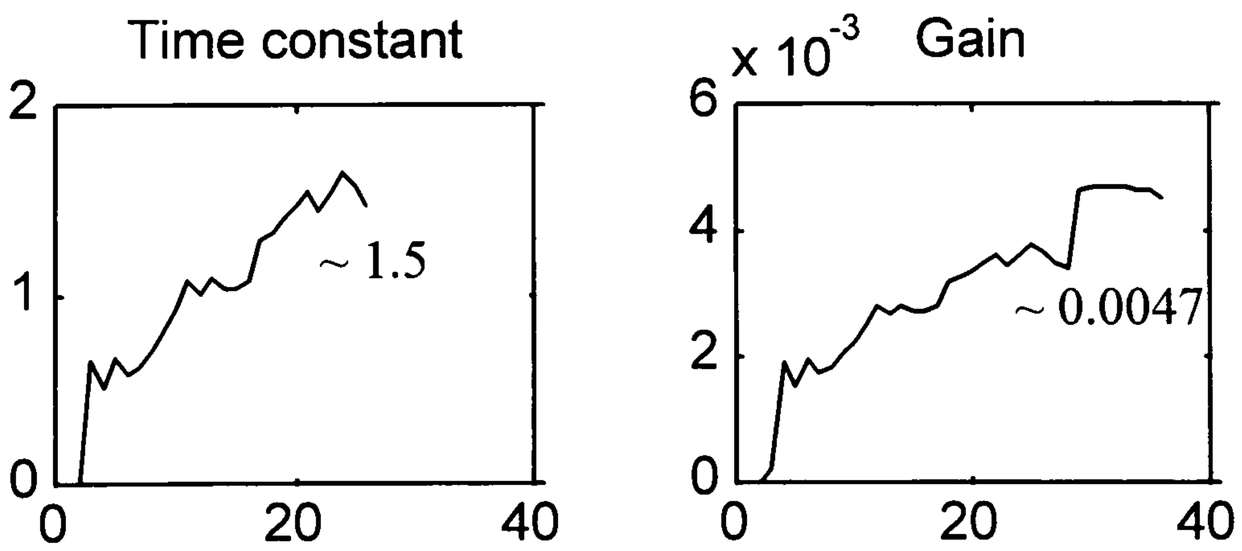

Figure 6.15 Parameters from Figure B.14 (1000 rpm)

Now consider the trends of time-constant and gain with respect to the spindle speeds. Referring to the figures, the gain is slightly decreasing as the spindle speed increases. This is at variance with the theoretical calculations of Chapter 5 (Table 5.3), based on the fact that the generated heat is proportional to the square of the spindle speed. The reason is likely to be that the frictional heat loss of the spindle does not increase as predicted, but just slightly increases as the spindle speed increases. Turbulence within the bearing gap seems to be responsible for such behaviour. Thus, the resulted gain decreases a little as the spindle speed increases.

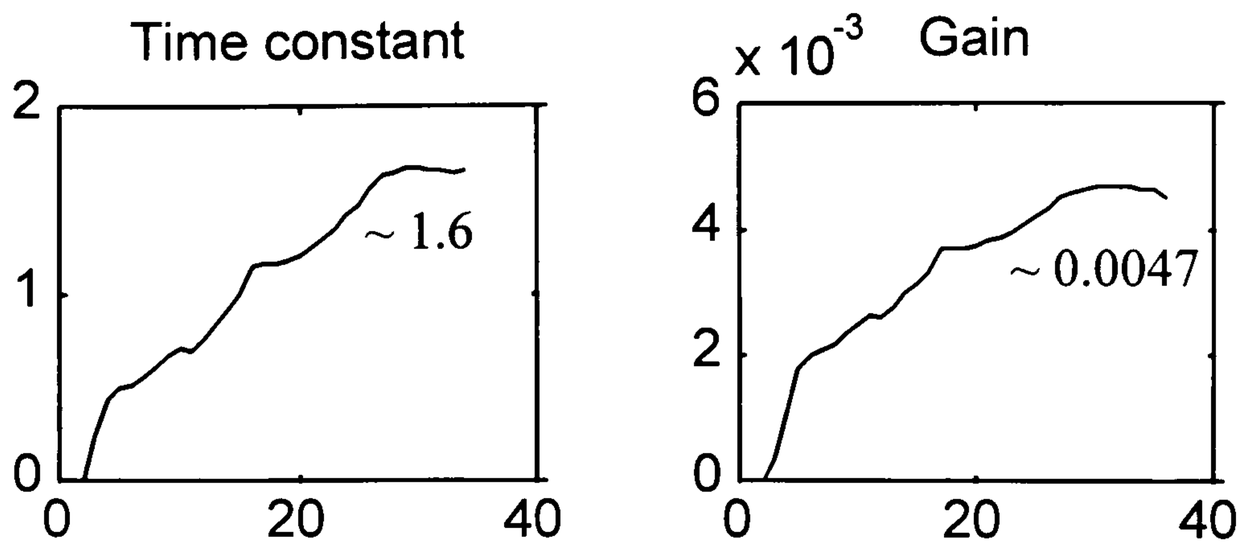

Figure 6.16 Parameters from Figure B.20 (1000 rpm)

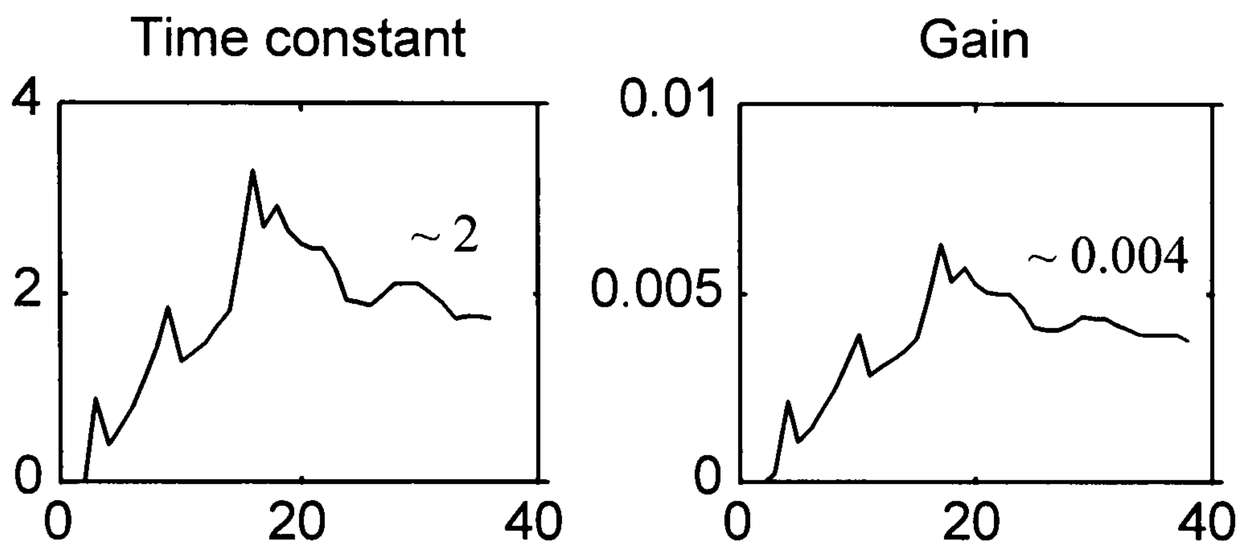

Figure 6.17 Parameters from Figure B.16 (1500 rpm)

As the spindle speed increases, no great changes in time-constant are observed in Figures 6.14 to 6.17, even the time-constant seems to increase as the spindle runs at higher speeds. The controlling factor in time-constant, the heat transfer coefficient, is likely to be the cause of such negligible changes in time-constant because the fluid surrounding the spindle unit becomes turbulent once the spindle rotates and is likely to give nearly equal cooling effects regardless of the spindle speeds.

The system parameters representing thermal behaviour of machine tools are modelled as having time-varying characteristics. A challenge in this study is consideration of the thermal environment that is no longer uniform around a machine. This sort of modelling seems to be general and realistic, but it is difficult to develop suitable strategies to counteract such time-varying effects. According to the tests, the parameters vary with the spindle operating conditions, and indeed machine tools are subject to continuously changing operating conditions. Under constant thermal and operating environment such as those shown in Figures 6.15 and 6.16, however, the time-varying characteristics of the parameters can be neglected because they gave nearly equal thermal parameters under the same heat input conditions.

Thus, the off-line identification method given by Equation 6.6 can be applied for constant thermal and operating conditions. The thermal parameters are considered to change abruptly according to changes in thermal and operating conditions of a machine. The total thermal response of a machine is the linear sum of responses due to the various heat inputs, i.e. room temperature variations, spindle rotation, etc.

Figure 6.18 shows two examples of graphical plots of the off-line identification results and Table 6.2 is the list of thermal parameters with respect to the rotational speed of the spindle.

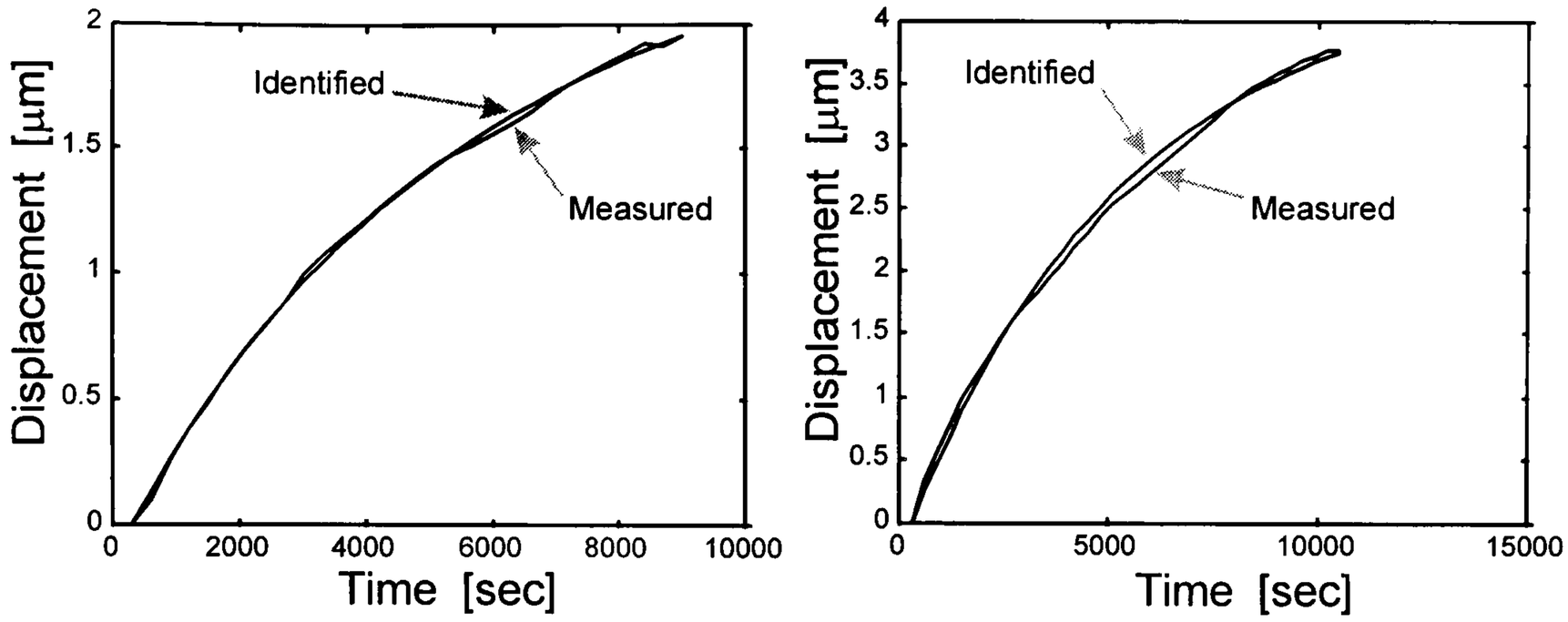

(a) 500 rpm input (Figure B.18) (b) 1000 rpm input (Figure B.20)

Figure 6.18 Results of off-line identification

Heat input condition	Time constant (hours)	Gain (μm/rpm)
500 rpm (Figure B.18)	1.50	0.0049
1000 rpm (Figure B.14)	1.37	0.0034
1000 rpm (Figure B.20)	1.48	0.0044
1500 rpm (Figure B.16)	1.80	0.0039

Table 6.2 Results of off-line identification

Chapter 7
Design of Thermally Insensitive Machines

7.1 Stiffness of Machine Tools

Accuracy is a primary criterion in assessment of the performance of a machine tool. Many attempts have been made to improve the accuracy of machine tools, thereby most modern machine tools provide adequate motion fidelity that is sufficient to produce high quality products in large quantities. During this improvement process, the following factors have been identified as the most bothersome problems to solve: a) deformations occurring throughout the machine structure, b) non-linearities in motion control and the cutting process, and c) poor damping of machine structure (Gim, 1994, pp. 118-162).

Except for non-linearities, the problems can be generally associated with one area, i.e. stiffness, which can be divided into three specific types: static stiffness, dynamic stiffness, and thermal stiffness. The first two are now well recognised and numerical software packages provide a good basis in dealing them nowadays. Thermal stiffness is considered here as insensitivity to thermal disturbances. However, for the purposes of this work a more quantitative definition is necessary.

Fischer (1970) used a term *thermal compliance* c_{th} in his study to assess the thermal behaviour of a machine component such as

$$c_{th} = \frac{\delta_{th}}{T'}$$

where δ_{th} is thermal deformation; T' is excess temperature, which may take a mean value. In other words, thermal stiffness is understood to be the amount of temperature rise resulting in a unit deformation.

From the point of view of this study, it is considered that the above relation neglects the fundamental mechanism of thermal deformation. It only considers the coefficient of

thermal expansion and mechanical constraint conditions, i.e. a part of gain. Because three thermal parameters, i.e. time-delay, time-constant and gain, are dependent on the way that heat is propagated to a machine or dissipated to the surrounding environment, the denominator should be the generated heat from the heat sources such that

$$c_{th} = \frac{\delta_{th}}{q_{\text{Heat}}} \tag{7.1}$$

Consider a machine component subject to the heat from a motor as an example. If the component has an efficient dissipation mechanism such as fins on the surface, the resulting deformation will be smaller than without any means of heat dissipation under the same heat source. In this simple case, the thermal compliance is considered to be lower with an efficient heat dissipation mechanism.

As stated in Chapter 1, few works have been done in the field of design methodology for thermally insensitive machines. What is needed is the development and implementation of techniques for the design of thermally-stiff structures. In investigating the problem of thermal errors, the physical phenomena of thermal deformation are understood by the abstraction of three thermal parameters.

7.2 Design Recommendations in Reducing Thermal Errors

Thermal deformations arising in machine tools are too complex to predict their exact values prior to building and testing a new machine. Although the room environment may remain stable, with a form of stratified air, the operating condition of a machine is continuously changing, causing the behaviour of the heat sources to be changed all the time. In addition, successive movements of machine components re-route the paths of heat transmission and thermal conductivity. Numerical computing packages may be beneficial in obtaining thermal behaviour of a solid component accurately, but it is still difficult to attain that of a whole machine in a precise manner due to the reasons indicated above. Moreover, the construction of a machine tool makes use of many bolted fixed-joints, sliding joints and mating surfaces with clearances, which makes them very difficult to model in numerical computing packages. Thus, it is a logical decision to investigate design methods for thermally insensitive machines in a manner that is pragmatic, and which will provide descriptive recommendations at a glance.

At present, some design methods are available to reduce thermal errors such as:

- *Reduction of the power loss of internal heat sources*. The fundamental reason for thermal deformations is the presence of heat sources in a machine. Reduction of mechanical or electrical power losses is the first step to enhancing the machine's thermal performance. Designers should look into the sizing of motors, lubrication methods, bearing preload, etc. in this regard.

- *Isolation of heat sources*. Heat sources can be thermally isolated by blocking the path of heat transmission or separating them from the machine. Some of machine components can be separated from a machine main structure, such as cutting fluid tanks, chip conveyors, oil coolers, etc. Blocking the transmission of heat to the rest of the machine can be achieved by the use of high thermal-resistance mounting materials and radiation shields to form a thermal break (Slocum, 1992, pp. 101-103), so that most of heat generated from the heat sources are emitted into the surrounding environment. Radiation shields are used in motors to prevent the transmission of radiative thermal energy from the motor housing to a machine body by the use of reflective sheet metals.

- *Machine frame with geometric and thermal symmetry*. Introducing symmetry in machine construction makes the machine more stable against thermal disturbances. While this is commonly understood to be geometric symmetry, this alone is insufficient and symmetry must be maintained in heat transmission characteristics as well as in the material properties, such as the coefficient of thermal expansion (Nakazawa, 1994, pp. 106-116). In Figure 7.1(a), the position of a spindle is unaffected by thermal deformation because the symmetry of thermal property as well as that of geometry is achieved. However, in Figure 7.1(b), if a sheet with low radiation characteristics exists on one side of the column, the spindle centre is likely to shift in the direction indicated by the arrow in the figure, since the right-hand column will heat up more quickly, resulting in greater thermal deformation.

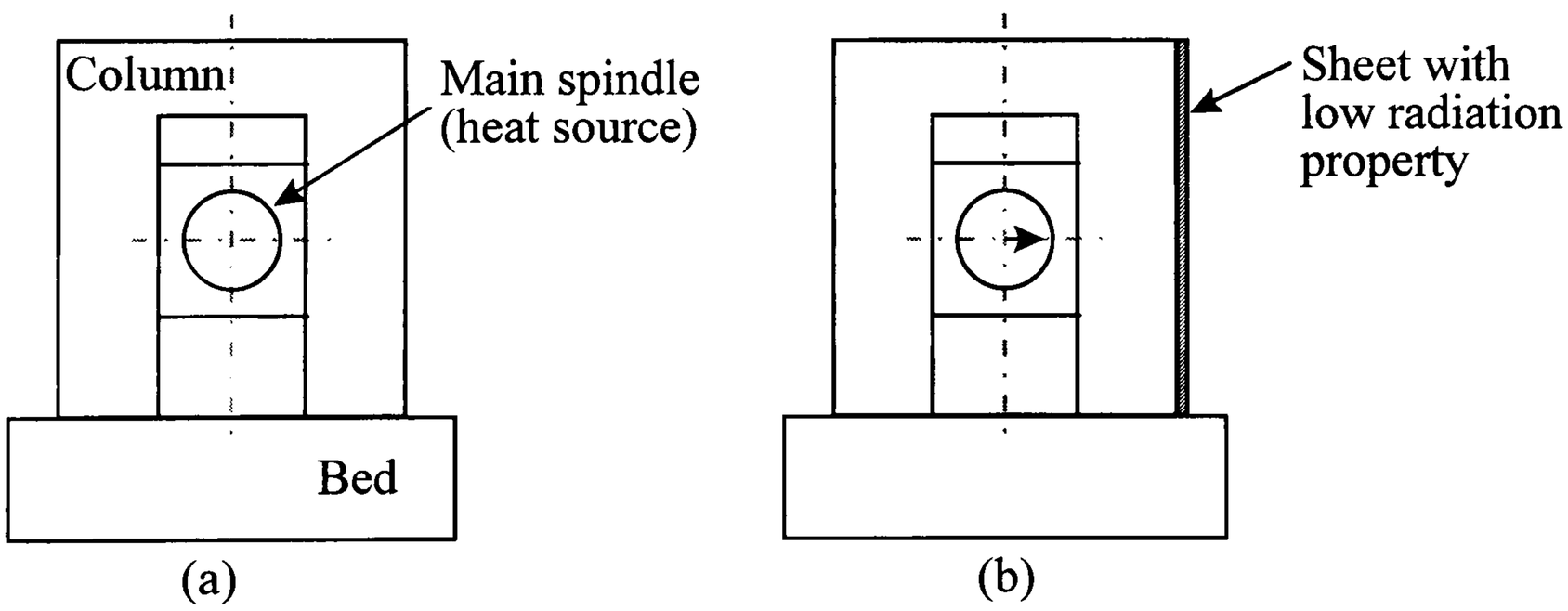

Figure 7.1 Machine with geometric symmetry

- *Constraint surfaces to be in line with the direction of thermal expansion*. While symmetry is one way to achieve thermal insensitivity, the arrangement of constraint surfaces also affects sensitivity to thermal deformation. Figure 7.2 shows a body, e.g. a carriage, with a bore whose axis must not shift due to thermal deformation. The bore may accommodate a feed drive mechanism or even a spindle. The effect of thermal deformation of the body (shown exaggerated by the dotted outline of the enlarged part) causes every point to move radially in proportion to its distance from a given point. If we consider the origin to be the centre of the bore, and if we arrange for all the constraint surfaces to be radial, the position of the bore will not shift as a result of thermal expansion (Blanding, 1992, pp. 15).

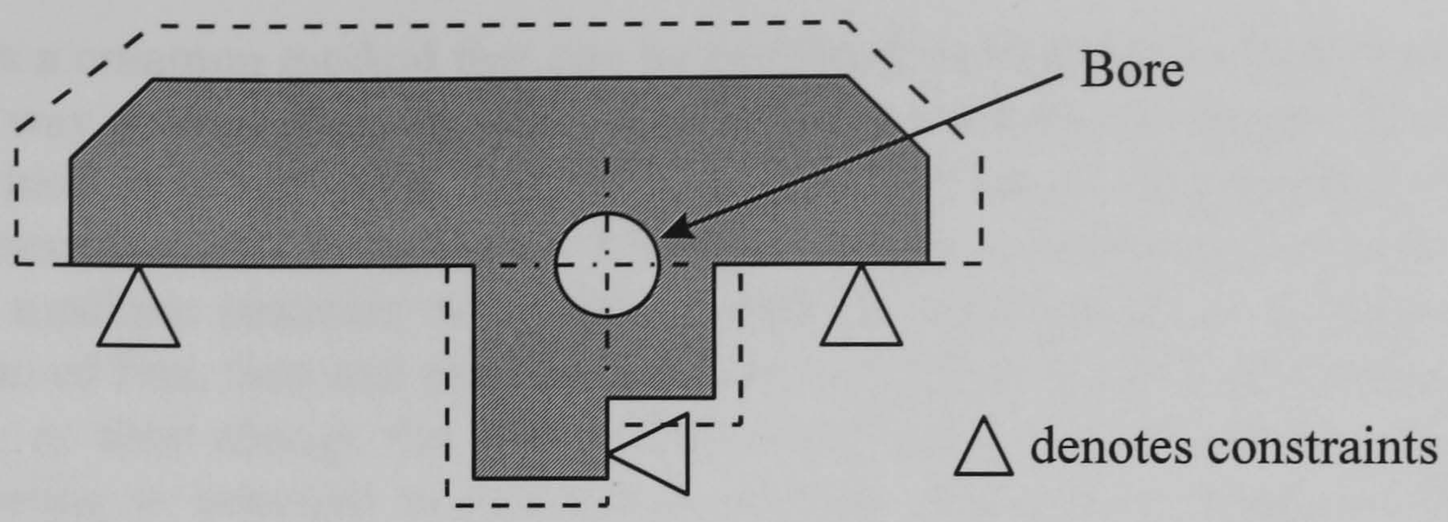

Figure 7.2 Carriage having thermally insensitive bore

- *Temperature control of a machine*. Many cooling methods are used to quickly expel generated heat from main heat sources such as spindles, motors, etc. An air shower and oil circulation are popular examples. Because the heat capacity of liquids is much higher than gases, they respond faster and are thus more effective for the temperature control of a machine. In some cases, a machine itself can be temperature controlled with a liquid flowing through internal passages or over its surface. The NION machine developed by CPE* incorporates a multi-loop temperature control system in the form of a liquid temperature control system (Weck *et al.*, 1995). Each loop controls separate functional components of the machine, including an oil shower over the machine structure.

- *Use of low expansion materials*. Thermal strain is directly proportional to the coefficient of thermal expansion, so the thermal deformation can be minimised by using low expansion materials such as Invar and Zerodur** .

The last two methods seem to be the ultimate solution to thermal error problems, and most of state-of-the-art ultra-precision machines are built with appropriate use of such methods. They are, however, still difficult to apply to ordinary machine tools due to economic constraints. Most ordinary machine tools are designed with cast-iron structures and simple cooling methods. The other methods are generally appropriate and should be in the realm of everyday design practices.

Three parameters discussed so far in this study, i.e. time-delay, time-constant and gain, encompass, in a concise manner, all the necessary information to represent various dynamic states of thermal deformations of a machine. This fact, in turn, can play a key role in designing thermally-insensitive machines. One common feature about these three parameters is that they are all vulnerable to changes in thermal environments as identified in Chapter 4. This means that we can attain a desirable condition for the three parameters by manipulating the thermal environment. That can be achieved by employing efficient cooling mechanisms, by which we can boost heat transfer on the surface of a machine component. Another possibility is heating, which can also change the state of heat transfer, but eventually this results in another heat source.

---

* Cranfield Precision Engineering Ltd., Cranfield, Bedford

** Zerodur is a trademark of Schott Glass Technologies Inc.

Cooling is a common method that can be applied for changing the three parameters in a desirable way because they are dependent on the thermal environment. The temperature of a machine structure rises according to the distribution of generated heat from a spindle, bearings, etc. If cooling is effective enough to reduce some of the generated heat, the machine structure will achieve thermal stabilisation in a shorter time. The application of fins, fans and radiative shields is effective in cooling (Slocum, 1992, pp. 101-103), as they change the heat transfer coefficient of surfaces in a positive way. When cooling is intended to stabilise a machine structure by means of temperature-controlled devices, only transient fluctuations will occur in the early stage of running. In other words, cooling is the most obvious, effective means of reducing thermal deformations.

Now consider the time-delay parameter alone. Time-delays arise from a delayed heat-input to machine components due to long paths of heat transmission. They occur significantly in large machines. The greater the path length of heat transmission, the longer it takes for heat to penetrate into a component. The path can comprise of solid machine frames or passages of fluids such as cutting fluid, lubrication oil, etc. Time-delays result in undesirable effects on the accuracy of a machine because they delay thermal stabilisation of the machine structure. It takes extra time for a machine to achieve a uniform temperature if there is a considerable time-delay.

Time-delays are much dependent on the sizes of a component and thermal diffusivity of the material of the component used. The thermal diffusivity of granite and Zerodur is considerably lower than that of iron or aluminium. That means a component made of granite or Zerodur exhibits a long time-delay in heat transmission, resulting in severe thermal deformation of adjacent components made of conventional materials such as cast iron. It is noted that the paths of heat transmission are changing all the time in a running machine due to the relatively large movement of machine components.

Guidelines obtained from the facts about time-delays include:

- Avoid long heat-transmission paths to minimise or diminish time-delays.
- Consider high diffusivity materials such as aluminium for components with anticipated long time-delays.
- Isolate heat sources.

The time-constant is the most important parameter in dealing with dynamic thermal errors. Because the temperature of individual components can differ considerably due to their own time constants, a relative expansion can be greater than that which is found in the steady, final state. Small time-constants result in rapid development of the temperature field, and thus a machine can achieve a uniform temperature quickly. In this regard, a machine with the small time-constant is desirable.

Large time-constants give considerable attenuating effects to rapidly changing temperature environments as stated in Chapter 4, but they also produce long transient periods where a machine is not completely soaked out in a time-varying temperature

environment. Thus the smaller the time-constant, the better a machine behaves in a time-varying thermal environment.

It is desirable for machine components to have equal time-constants, so that differential responses exhibit thermal errors no greater than that of the final state. Deviations will be minimised with such components during temperature changes. Moreover we can devise a counteracting mechanism in the structural loop of a machine by matching time-constants of two components and opposing their expansion directions. A simple way of achieving equal time-constants is to make use of Equation 3.6, i.e.

$$\tau = \frac{\rho c_p V}{hA} \tag{3.6}$$

If two components have the same material and thermal environment, the ratio of the volume V to the heated surface area A governs their time-constants. Thus two objects having equal volume to area ratio reveals approximately the same time-constants. Referring to Figure 7.3(a), the volume to area ratio (V/A) of a rectangular object heated from the top surface is represented as

$$\frac{V}{A} = \frac{W \times H \times L}{W \times L} = H \tag{7.2}$$

The volume to area ratio of a hollow cylindrical object heated from inside will be

$$\frac{V}{A} = \frac{\pi\left(R_o^2 - R_i^2\right)L}{2\pi R_i L} \tag{7.3}$$

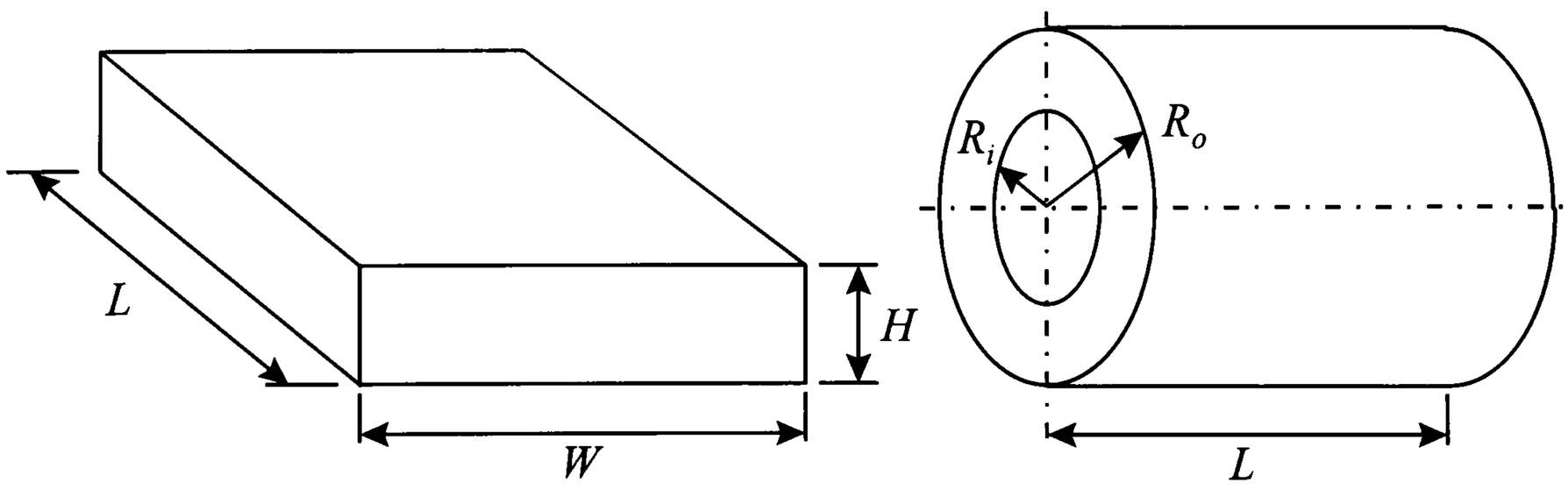

(a) Rectangular body (b) Cylindrical body

Figure 7.3 Volume to area ratio of rectangular and cylindrical bodies

Similarly, the volume to area ratio of a hollow cylinder heated from outside is obtained as

$$\frac{V}{A} = \frac{\pi\left(R_o^2 - R_i^2\right)L}{2\pi R_o L} \tag{7.4}$$

A solid cylinder heated from outside can be obtained by modifying Equation 7.4 such as

$$\frac{V}{A} = \frac{R_o}{2} \tag{7.5}$$

Guidelines determined from the time-constant analysis are:

- Smaller time-constants minimise the time it takes for a machine to attain a uniform temperature state. Smaller time-constants can be realised by designing for low volume to surface ratio and surface heat transfer enhancements.
- Design machine components having equal time-constants in order to minimise large errors resulting from a differential response.
- If possible, devise counteracting mechanisms as in Section 7.3.2.

It follows that low gain is better. Gain is closely related with the thermal expansion coefficient of a material and the intensity of heat sources. It is also affected by mechanical restraints. By the careful arrangement of mechanical restraints, a component can exhibit very small gain, but the component and its mating component may be subject to severe thermal stress.

Interestingly, gain is dependent on the configuration of a machine from the design point of view. Gain can be considerably different depending on where the thermal reference plane is placed. A thermal reference plane is a plane in a machine component, which can be considered as an origin of deformation. The direction of deformation is usually opposite, and either side, of the thermal reference plane. The thrust plate of an aerostatic spindle is an example of such a thermal reference plane. The growth of a spindle shaft occurs with reference to a thrust plate. The length from the thrust plate governs the gain of a spindle. Also, zero gain points are important to fulfil some functional requirements. The spindle centre of Figure 7.1(a) and the bore centre of Figure 7.2 are such points. Zero gain points are achieved by careful design of the machine configuration and location of the mechanical constraints, as described above. It is noted that a zero gain point is on a thermal reference plane. Guidelines from a knowledge of gain are:

- Reduce the intensity of heat sources.
- Devise mechanical restraints to reduce the gain of components as far as the resulting thermal stress will allow.
- Carefully locate thermal reference planes on machine components and minimise the distances between them.
- Zero gain points can be achieved by careful design of the machine configuration and arrangement of mechanical constraints.
- If costs allow, use low expansion materials.

Finally it is recommended to use numerical computing packages to evaluate the three parameters for critical components, as done in Chapter 4.

7.3 Case Studies

7.3.1 Guideways subject to Temperature Gradients

The bending of a simply supported beam subject to vertical temperature gradients is investigated here to simulate guideways under a thermally stratified room condition. As found in Chapter 5, a room usually has a stable thermally-stratified environment. The model is depicted in Figure 7.4.

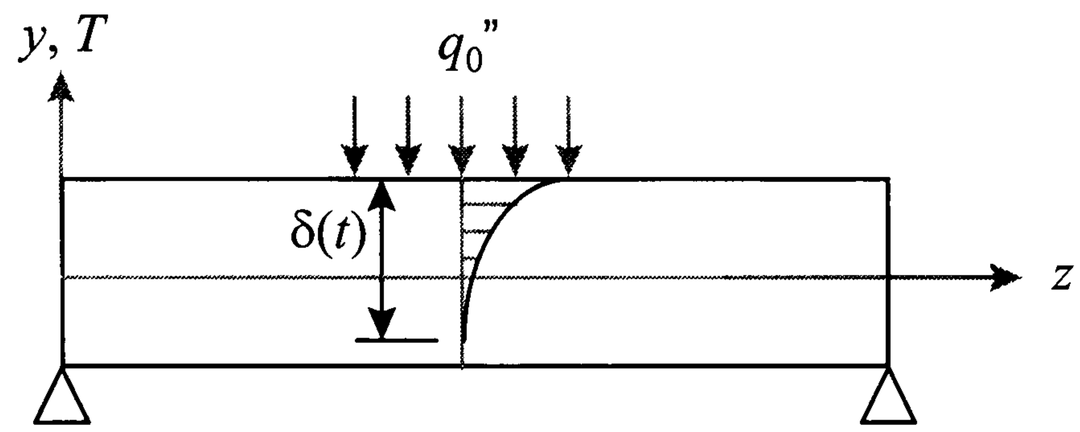

Figure 7.4 Simply supported beam subject to temperature gradient

Deflection of a beam, measuring length L, width B and height H due to a thermal loading was derived as Equation 3.18b

$$v = -\frac{\alpha T}{2I_{xx}}z^2 + \frac{\alpha TL}{2I_{xx}}z \tag{3.18b}$$

where

$$\overline{T} = B\int_{-H/2}^{H/2} yT'dy$$

$$I_{xx} = \frac{BH^3}{12}$$

It is assumed that

- Constant heat flux is applied on the top of the beam.
- Thermal convection is realised at the bottom of the beam.
- All the other vertical surfaces are insulated.

Then the temperature distribution of the beam is obtained using Equation 3.9 and Equation 3.10, such as

$$T' = \frac{q_0''\sqrt{6\beta t}}{2k}\left[1 - \frac{2(y+H/2)}{\sqrt{6\beta t}} + \frac{(y+H/2)^2}{6\beta t}\right]$$

This solution has a limited time range up to $\delta^2/(6\beta)$ where δ is penetration depth. After δ reaches H, the solution is no longer appropriate, but it serves a basis for identifying some aspects. Using the following relation

$$\overline{T} = B\int_{H/2-\sqrt{6\beta t}}^{H/2} yT'dy = \frac{q_0''B}{24k}\left(6H^3 - 24H^2\sqrt{6\beta t} + 204H\beta t - 102\beta t\sqrt{6\beta t}\right)$$

we obtain the deflection v due to temperature gradients:

$$v = -\frac{q_0''\alpha}{4kH^3}\left(6H^3 - 24H^2\sqrt{6\beta t} + 204H\beta t - 102\beta t\sqrt{6\beta t}\right)z(z-L)$$

Deflection at the middle of the beam at time $t = H^2/(6\beta)$, i.e. when the heat penetrates all the way to the bottom, is readily obtained as

$$v = -\frac{1}{16}L^2\frac{q_0''\alpha}{k} \tag{7.6}$$

The above equation represents the gain of the middle point when $t = H^2/(6\beta)$. At this point, the gain is proportional to the coefficient of thermal expansion and inversely proportional to the thermal conductivity. Thus high conductivity materials give a small gain in this particular case.

Breyer and Pressel (1991) have described the development of a thermally insensitive guideway made of aluminium in their paper, arguing that

"A guideway component with a large cross-section (solid material) and good thermal conductivity (e.g. aluminium) builds up only a minor internal gradient and is therefore only subject to minimum bending in the case of one-sided temperature changes."

A small cross-section implies high thermal resistance, which will result in considerable temperature gradients. They also represented a simple relationship such as

$$\text{Maximum deflection} \sim \frac{\text{Constant external heat flux} \times \text{thermal expansion coefficient}}{\text{Thermal conductivity} \times \text{Cross-section ratio}}$$

where the cross-section ratio is the total thickness of the wall to the width in the case of hollow beams. The cross-section ratio for solid beams will be 1. This relationship resembles closely Equation 7.6.

7.3.2 Thermally Insensitive Hydrostatic Spindle

Hydrostatic spindles are widely used in machine tools when high precision and high stiffness/load capacity are necessary. They can rotate at high speeds so that the viscosity

of oil produces a substantial amount of heat in the bearing gap. The generated heat is dissipated into the spindle, bearing and housing, and some is carried away by the oil itself. Due to a requirement for precision in hydrostatic spindles, thermal performance must be analysed and their thermal deformations must be minimised. The following requirements relate to their thermal performance:

- The centre of the spindle unit should lie on the axis of rotation and it should not shift during running. The centre serves as a reference point when machining workpieces. Any shift results in errors in machining.
- The clearance of the bearing is a critical factor in determining its stiffness and load-carrying capacity. It is required to keep the clearance constant irrespective of temperature changes.
- It is necessary to minimise the thermal growth of the spindle. This can be considerable when not using low-expansion materials or temperature controllers, which may be due to economic reasons.

Solutions have been sought to meet the above requirements from the point of view of a general machine layout. The first requirement is to realise a zero-gain point in the direction perpendicular to the spindle rotation axis. One way is to arrange mechanical restraints or constraints in such a way that the direction of the expansion coincides with the surface of the restraints or constraints. This case exactly matches the example shown in Figure 7.2. A solution to the first requirement is illustrated in Figure 7.5, where a spindle body is supported along the centre line of the spindle by four supports. Also this configuration achieves geometric and thermal symmetry. The number of supports can be changed to three if necessary. When the spindle heats up, the body expands freely downwards and upwards in a same manner, so that the position of spindle centre can be kept nearly constant regardless of thermal disturbances.

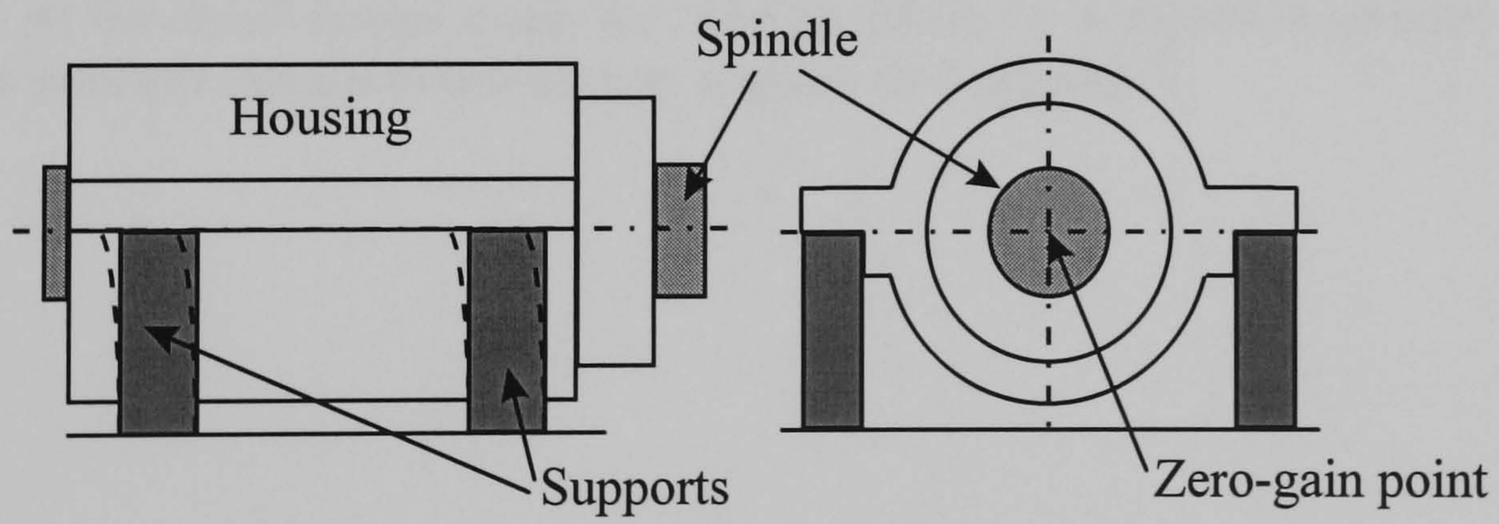

Figure 7.5 Configuration of hydrostatic spindle

When the spindle and bearing sleeves heat up, both of them experience radial thermal expansion in such a way that the clearance could become smaller and smaller due to the rapid development of temperature fields in the spindle shaft. This situation can be avoided by employing an arrangement such as that illustrated in Figure 7.6. The bearing sleeves are fixed axially but can expand freely radially due to the small clearance with the housing. This allows the bearing sleeves to act more quickly upon temperature changes. In addition, in order to keep the changes in the clearance small, the time

constants of two components are designed to be approximately the same. This can be done by assigning the same ratio of volume to heated area to each of the components assuming the materials and thermal environments to be equal, and by using equations 7.2 to 7.5.

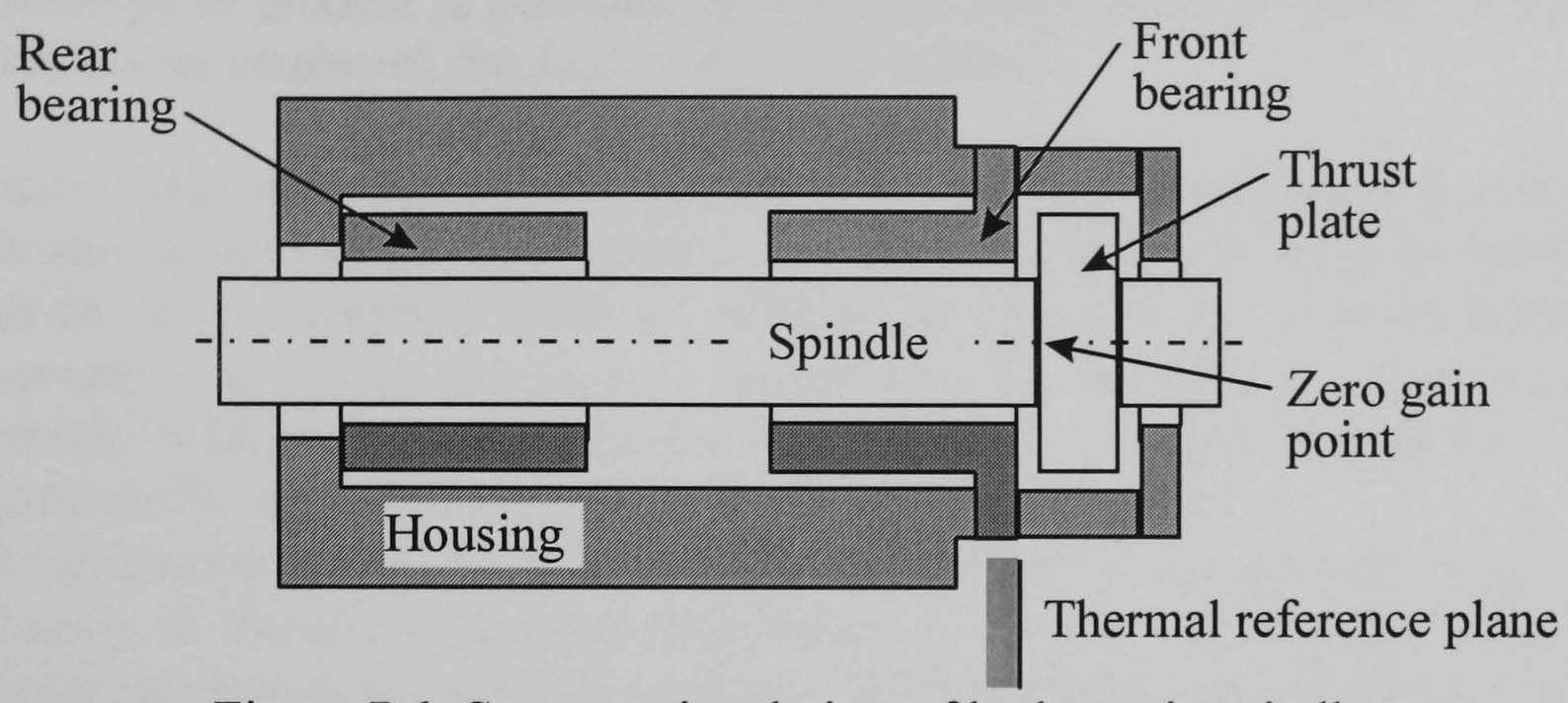

Figure 7.6 Cross-sectional view of hydrostatic spindle

A solution to the last requirement is to minimise the spindle overhang from the thrust plate or thermal reference plane as denoted in Figure 7.6, such that the length subject to thermal expansion is minimised. A further improvement can be achieved by devising a counteracting mechanism which can move the spindle unit backwards in harmony with the spindle growth, such as that illustrated in Figure 7.5 (dotted line). Supports using bimetallic materials, exposed to the leakage oil and having the same time constant with the spindle, will serve such a purpose. Because the leakage oil has the same thermal characteristics with the oil in the bearing gap and carries away a considerable amount of the generated heat, the support can deform to neutralise the axial thermal growth. However, angular displacements and height changes of the support could be a serious concern. At the detail design stage, the bearing should be designed to generate less heat. A design example related to this section is given in Appendix C.

7.4 Model Test

7.4.1 Necessities

Many engineering disciplines make use of model tests, where the performance of a full-scale prototype or product is assessed using a small scale physical model. In this study, model tests were employed due to the following reasons:

- A knowledge of temperature distribution in machine components is essential in determining the thermal performance of a machine tool. The complex geometry of machine tools, however, makes it difficult to calculate the exact distribution of temperature in their components analytically. In addition to that complexity, uncertain boundary conditions add another difficulty. Therefore, only a few simple objects can be analysed successfully as discussed in Chapter 3.
- The monitoring of successive changes in temperature of the machine components is necessary to identify time-dependent behaviour, which can be represented by two parameters, time-delay and time-constant. Still, only a few simple objects, subject to particular kinds of thermal boundary conditions, can be analysed successfully, as seen in Chapter 3.
- Thermal deformation of various points of a machine tool, i.e. gain, should be obtained finally by using the result of the temperature calculations. However, the complexity of machine geometry and mechanical constraints cannot be accommodated in a analytical way.
- Numerical computing packages employing finite-element methods can calculate the thermal deformation of a geometrically-complex object. However, even a simple object, such as that shown in Chapter 4 was analysed via the use of an enormous quantity of calculations because a calculation was needed at every time step of a designated time interval. It takes an enormous time to calculate the time-varying thermo-elastic behaviour of an object unless a dedicated computing package is used.
- When using a numerical computing package, it is necessary to model the machine tool by using a pre-defined set of elements provided in the package. However, bolted joints, which are used a lot in building machine tools and clearances in machine units are difficult to handle by numerical computing packages. They both affect thermal and mechanical conditions significantly. It is necessary to use empirical correlations that show the thermal characteristics of such joints when using a numerical computing package.

For these reasons, an empirical method using a scaled model was adopted in order to overcome the shortcomings of the analytical and numerical techniques discussed above. Moreover, a model test can be a part of the design procedures, validating the concept of an original or modified design. Using a model test, the three thermal parameters of the components can be obtained, so that it is possible to change dimensional, thermal and material properties of machine components to meet the design requirements, or the thermal deformation model of a machine can be obtained. The real benefit of a model test is to facilitate the identification of thermally vulnerable components, which contribute significantly to the total thermal errors of a machine.

7.4.2 Similarity Analysis

The idea of similarity is of fundamental importance when scaled physical models are used to predict the performance or behaviour of a full-scale prototype or product. Similarity is apparent if the relationship of at least one physical quantity in the basic series is constant. When two physical systems are similar and behave similarly, any knowledge about one system also provides knowledge of the other system. The technique which enables the results of the model test to be applicable to the full-scale arrangement is called similarity analysis (Welty *et al.*, 1984, pp. 150-162). Similarity analysis is widely used in engineering disciplines, particularly in fluid mechanics and heat transfer.

For two bodies to be geometrically similar, every length must be in a fixed ratio to the corresponding length on the other (Pahl and Beitz, 1988, pp. 315-361). The physical similarity of two bodies however signifies more than the geometric similarity of their forms. In this study, similarity in temperature has to be realised also. For two bodies to be similar in temperature, differences of temperature between particular points in one system bear a fixed ratio to the differences of temperature between the corresponding points of the other system (*ibid.*). Thus we have to achieve simultaneous invariance of length and temperature or thermal similarity.

Dimensional analysis facilitates similarity analysis, as it is based on the fact that an equation between the measures of physical quantities is dimensionally homogeneous. The result of dimensional analysis can always be put into the form so that certain N non-dimensional quantities are functionally related such that

$$\Pi_1 = f\left(\Pi_2, \Pi_3, \ldots, \Pi_N\right) \tag{7.7}$$

where Π_i is a dimensionless variable. This follows mathematically from the above equation. If each dependent dimensionless variable in Equation 7.7 is the same for the model and prototype, i.e.

$$\Pi_{2,\,\text{Model}} = \Pi_{2,\,\text{Prototype}}\,,\ \Pi_{3,\,\text{Model}} = \Pi_{3,\,\text{Prototype}}\,,\ \text{etc.} \tag{7.8}$$

equation 7.7 guarantees that the desired output $\Pi_{1,\,\text{Model}}$ will be equal to $\Pi_{1,\,\text{Prototype}}$ (White, 1986, pp. 245-286). A model test is completely similar if all relevant dimensionless parameters have the same corresponding values for the model and prototype. Dimensional analysis also establishes scaling laws which relate the results of experiments on models with those obtained with their full-scale arrangement using Equation 7.8.

One way to find dimensionless variables is to non-dimensionalise governing equations of a physical phenomenon, thus dimensionless variables related to thermal similarity can be found by non-dimensionalising the heat conduction equation, initial condition and boundary conditions of Section 3.3.1. The following dimensionless variables are used to non-dimensionalise those equations:

$$x^* = x / L, \quad y^* = y / L, \quad z^* = z / L, \quad n^* = n/L, \quad t^* = \beta t / L^2, \quad T^* = T / T_0$$

where x^*, y^*, z^* and n^* are dimensionless coordinates (n is an outward normal coordinate at boundaries); L is a characteristic length that is the most significant or representative dimension of a physical object; t^* is dimensionless time or Fourier number, Fo (White, 1988, pp. 191-193); T^* is dimensionless temperature. Environment temperature T_∞ and initial temperature T_0 are taken to be constant, i.e. the initial condition is $T = T_0$. Substituting the above relations into Equations of Section 3.3.1 yields:

Dimensionless heat conduction equation: $$\frac{\partial^2 T^*}{\partial x^{*2}} + \frac{\partial^2 T^*}{\partial y^{*2}} + \frac{\partial^2 T^*}{\partial z^{*2}} = \frac{\partial T^*}{\partial t^*}$$

Dimensionless initial condition: $$T_0^* = 1$$

Dimensionless boundary condition:

$$T^*\big|_b = T_b^* \qquad \text{for known temperature boundary}$$

$$\left.\frac{\partial T^*}{\partial n^*}\right|_b = 0 \qquad \text{for insulated boundary}$$

$$\left.\frac{\partial T^*}{\partial n^*}\right|_b = -\frac{hL}{k_b}\left(T_b^* - T_\infty^*\right) = -\mathrm{Bi}\left(T_b^* - T_\infty^*\right) \qquad \text{for convection boundary}$$

$$\left.\frac{\partial T^*}{\partial n^*}\right|_b = -\frac{q_b'' L}{k_b T_0} \qquad \text{for prescribed heat flux}$$

where the subscript b represents quantities at a boundary.

From the derived dimensionless equations, we can find all the necessary dimensionless variables that constitute Equation 7.7 such as

$$T^* = f\left[x^*, y^*, z^*, \mathrm{Bi}, \mathrm{Fo}, \frac{q_b'' L}{k_b T_0}\right] \tag{7.9}$$

It is noted that the last dimensionless parameter of Equation 7.9, i.e.

$$\frac{q_b'' L}{k_b T_0} \tag{7.10}$$

represents a type of Biot number due to prescribed heat flux boundary conditions. Thus we can see that solutions for the temperature at any point in systems of like geometry depend only on the dimensionless time (Fourier number) and Biot number. If the two dimensionless parameters, Fo and Bi, are equal for the model and prototype, it is possible to have thermal similarity between them.

Equating dimensionless groups of the model and prototype, as represented by Equation 7.8, ways of how to design a model test and scaling laws can be obtained. Equating the Biot numbers yields

$$\left(\frac{L_M}{L_P}\right) = \left(\frac{k_M}{k_P}\right)\left(\frac{h_P}{h_M}\right) \tag{7.11}$$

where the subscript M represents model and P prototype. It is noted that the length ratio, or scale factor L_M/L_P, is applicable to any length of model and the corresponding length of a full-scale arrangement in accordance with geometric similarity. Here some drawbacks of applying similarity to the thermal process can be seen. As the length of a model decreases, either the thermal conductivity of a model should decrease or the heat transfer coefficient of a model should increase correspondingly in a linear fashion. However the exact match with the scale factor is difficult in either case. In cases of heat transfer coefficient, differently sized geometrically similar objects will be subject to different convection conditions, and moreover the exact calculation and realisation of a convection condition will involve a lot of work. Some deviations from similarity is inevitable in model tests involving thermal processes.

The physical meaning of Equation 7.11 is interesting, explaining the nature of scaling in thermal processes. That is, a decrease in size will decrease the importance of conductivity and increase the importance of the surface resistance to heat transfer. So for larger bodies the conductivity is of paramount importance, while for small bodies surface heat transfer controls time-dependent behaviour.

The equal requirement of the Fourier number gives the following relationship:

$$\left(\frac{L_M}{L_P}\right)^2 = \left(\frac{\beta_M}{\beta_P}\right)\left(\frac{t_M}{t_P}\right) \tag{7.12}$$

This indicates that the time related with a model is proportional to the square of the scale factor, i.e. a smaller model develops thermal behaviour faster, by as much as the square of a decrease in length when the materials of a model and prototype are the same.

The last dimensionless group proposes the following requirement:

$$\left(\frac{L_M}{L_P}\right) = \left(\frac{T_{0,M}}{T_{0,P}}\right)\left(\frac{k_M}{k_P}\right)\left(\frac{q''_P}{q''_M}\right) \tag{7.13}$$

When the initial temperature of a model and prototype is the same, the heat flux to a model should be increased or the thermal conductivity of a model should be decreased in line with a linear decrease of model dimensions.

If all the requirements of thermal similarity are fulfilled, the temperature of a prototype can be evaluated using the following relationship from the definition of dimensionless temperature:

$$T_P = \left(\frac{T_{0,P}}{T_{0,M}} \right) T_M \tag{7.14}$$

Considering the deformation phenomena, the governing equation of a uniaxial bar, subject to thermal loadings only, can be represented using Equation 3.15, such as

$$\frac{dw_o}{dz} = \alpha T'$$

by setting $p(z) = 0$. Selecting the following dimensionless variables:

$$z^* = z / L, \quad w_o^* = w_o / L$$

we obtain a non-dimensional equation:

$$\frac{dw_o^*}{dz^*} = \alpha T'$$

In this case, the functional relationship can be described as

$$w_o^* = f\left(z^*, \alpha T'\right)$$

For example, whenever the dimensionless group $\alpha T'$ of a model and prototype is equal, thermal deformation of a prototype can be evaluated, using the following relationship:

$$w_P = \left(\frac{L_P}{L_M} \right) w_M \tag{7.15}$$

The meaning of the above equation is straightforward, i.e. total thermal deformation is the integration of thermal strain along the total length of a body.

7.4.3 Simulation Model for Spindle

In the model test of this study, the test model built was not intended to simulate exactly the aerostatic spindle of the machine used for the thermal error test described in Chapter 5. The real intention was to demonstrate how to use a model test under some encountered difficulties. However, the aerostatic spindle of the machine used in Chapter 5 served as a reference model.

A test model simulating the aerostatic spindle of the facing machine depicted in Figure 5.2 is illustrated in Figure 7.7. For the convenience of making displacement measurements, the model was placed in an upright position on a cast iron plate supported by three small ceramic insulators. The scale of the model was chosen to be 1/3 because a model of that size was easy to build and handle. There were basically two components in the model, i.e. shaft and housing. All the components were made of mild steel. The thrust bearing of the spindle was simulated by the 3 set screws that held the shaft to the housing. As the temperature of the shaft increased, the shaft expanded both ends with respect to the plane fixed by the set screws.

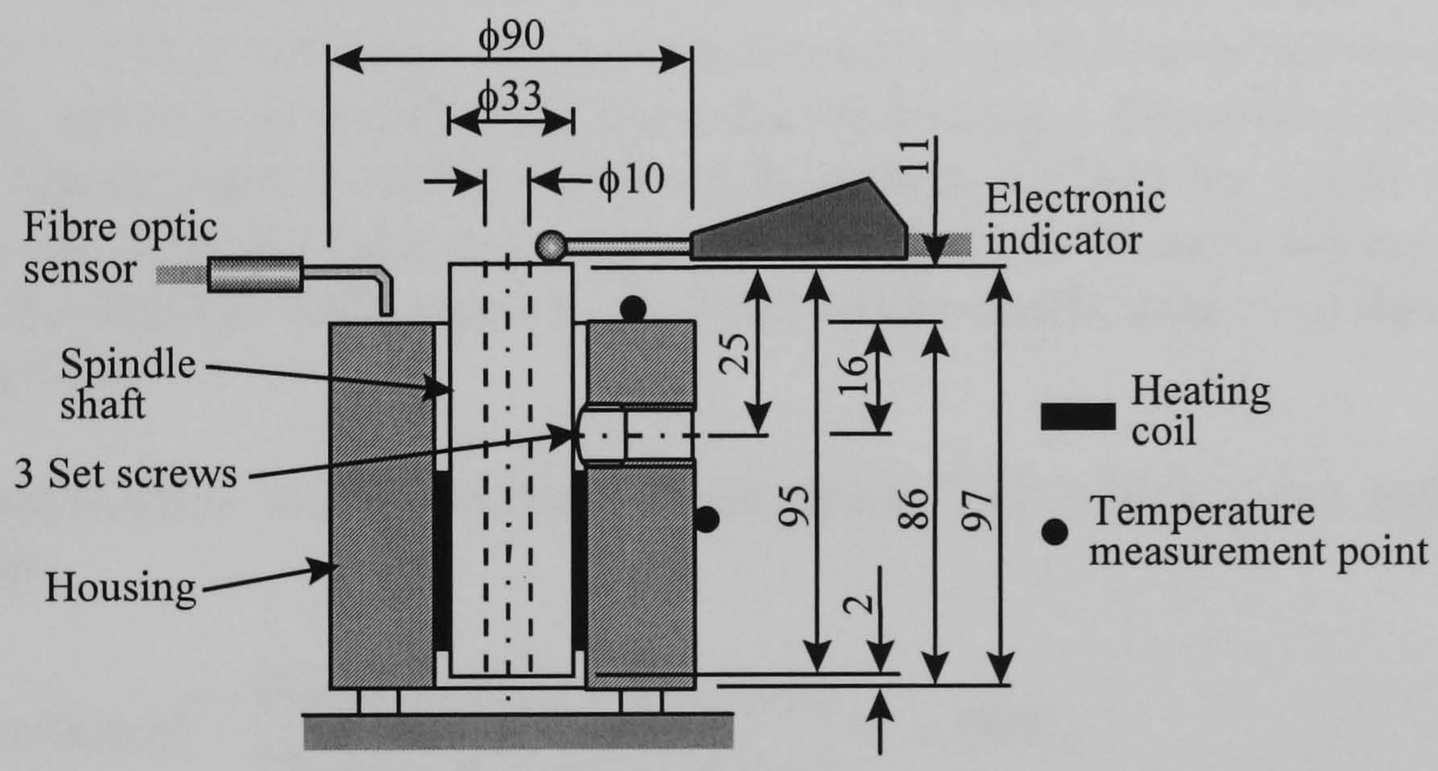

Figure 7.7 Test model for spindle unit

The heat was generated in three independent bearings in the aerostatic bearing, but in the model the heat was generated in the area shaded in black in Figure 7.7. Thus, the heat generating area was simulated in the model in an average sense. Heat was generated by the heating coil wound around the shaft. The coil was bonded to the shaft with a high electric resistance and high thermal conductivity epoxy purchased from RS Components*, and the gap between the shaft and housing where the coil was placed was filled with a high thermal-conductivity silicone paste to ensure sufficient heat transmission. The power consumed by the coil was assumed to represent the total frictional loss of the aerostatic spindle.

---

* RS Components Ltd., PO Box 99, Corby, Northants NN17 9RS

The linear thermal deformation of the shaft was measured by an electronic indicator, model type GN22EM from TESA* and that of the housing by the fibre-optic sensor discussed in Chapter 5. The temperature of the housing was measured by the thermometer used in the test described in Chapter 5. Two points on the top and side of the housing, were chosen to represent the history of the housing temperature, as denoted by the small black circles in Figure 7.7. The temperature of the shaft was not recorded, but if necessary, this could be calculated by using the test data of linear deformation, because the shaft is considered to be a uniaxial, uniform temperature element as explained in Chapter 3.

Considering the requirements of the test conditions from Equation 7.11, the heat transfer coefficient of the model h_M is related with that of the aerostatic spindle h_P such that

$$h_M = \frac{1}{\text{Scale factor}} \cdot \frac{\text{Thermal conductivity of steel}}{\text{Thermal conductivity of Invar}} h_P = 16.4 h_P \tag{7.16}$$

Serious problems arise from the above relationship. Firstly the exact value of the heat transfer coefficient representing the cooling mechanism of the aerostatic spindle is not known. As a reference, the result of Section 5.3.1 using Equation 5.10 and 5.11 could be used, i.e. $h_P = 172$ at 1000 rpm. Then the heat transfer coefficient of the model is found to be 2821, which is extremely high but achievable using a forced convection process involving liquids such as water. Secondly it is more difficult to realise the cooling process having a certain value of heat transfer coefficients. These problems impose the necessity of a database with regard to the heat transfer coefficients of cooling processes in machine tools.

Time characteristics are represented by Equation 7.12 which gives the following relationship:

$$t_M = (\text{Scale factor})^2 \cdot \frac{\text{Thermal diffusivity of Invar}}{\text{Thermal diffusivity of steel}} t_P = 0.02 t_P \tag{7.17}$$

Also, this relation implies some difficulties in model tests. Because the scale factor for the time constant was too small, the fast response of the instruments used and a very small sampling time were necessary for a reliable test.

In order to overcome the difficulties presented by the above two requirements, the following, modified relation for time characteristics can be used:

$$t_M = (\text{Scale factor})^2 \cdot \frac{\text{Thermal diffusivity of Invar}}{\text{Thermal diffusivity of steel}} \cdot \frac{h_M}{h'_M} t_P = 0.02 \frac{h_M}{h'_M} t_P \tag{7.18}$$

where h_M is the result of Equation 7.16; h'_M is the heat transfer coefficient actually used in a model test. From Equation 3.6, it can be seen that the time constant of a body is

---

* TESA SA, Bugnon 38, CH-1020 Renens, Switzerland

inversely proportional to the heat transfer coefficient involved. The ratio of the required heat transfer coefficient to the actual value used, therefore, can be employed as a correction factor. By using the relationship given by Equation 7.18, an easier achievable cooling processes can be realised and the time lengthened in order that the requirements of the instruments and sampling time can be relaxed.

However, there is a pitfall when using the relationship given by Equation 7.18. Because the heat transfer coefficient is to be reduced intentionally, the temperature gradient of the inside of the full scale spindle will not be exactly simulated by the model. The spindle shaft is likely to be uniform in its temperature distribution, so that this can be neglected. For larger structures vulnerable to temperature gradients, this kind of modification can induce a considerable error in the model test.

Finally, from Equation 7.13, the relationship for the heat flux is stated as

$$q''_M = \frac{1}{\text{Scale factor}} \cdot \frac{\text{Thermal conductivity of steel}}{\text{Thermal conductivity of Invar}} q''_P = 16.4 q''_P$$

At 1000 rpm, the heat flux generated by the aerostatic spindle is 264 W/m^2. Therefore the heat flux of the model should be 4330 W/m^2. In terms of heat generation rate, i.e. the heat flux multiplied by heated area, corresponds to 27 W on the model. The magnitude of the heat flux, which is related to the steady-state thermal deformation, is not seriously important in the model test; Because the main interest was in relative deformations among machine components, the identification of the sensitive components to thermal disturbances is considered to be sufficient for the model test of a machine tool for the design stage.

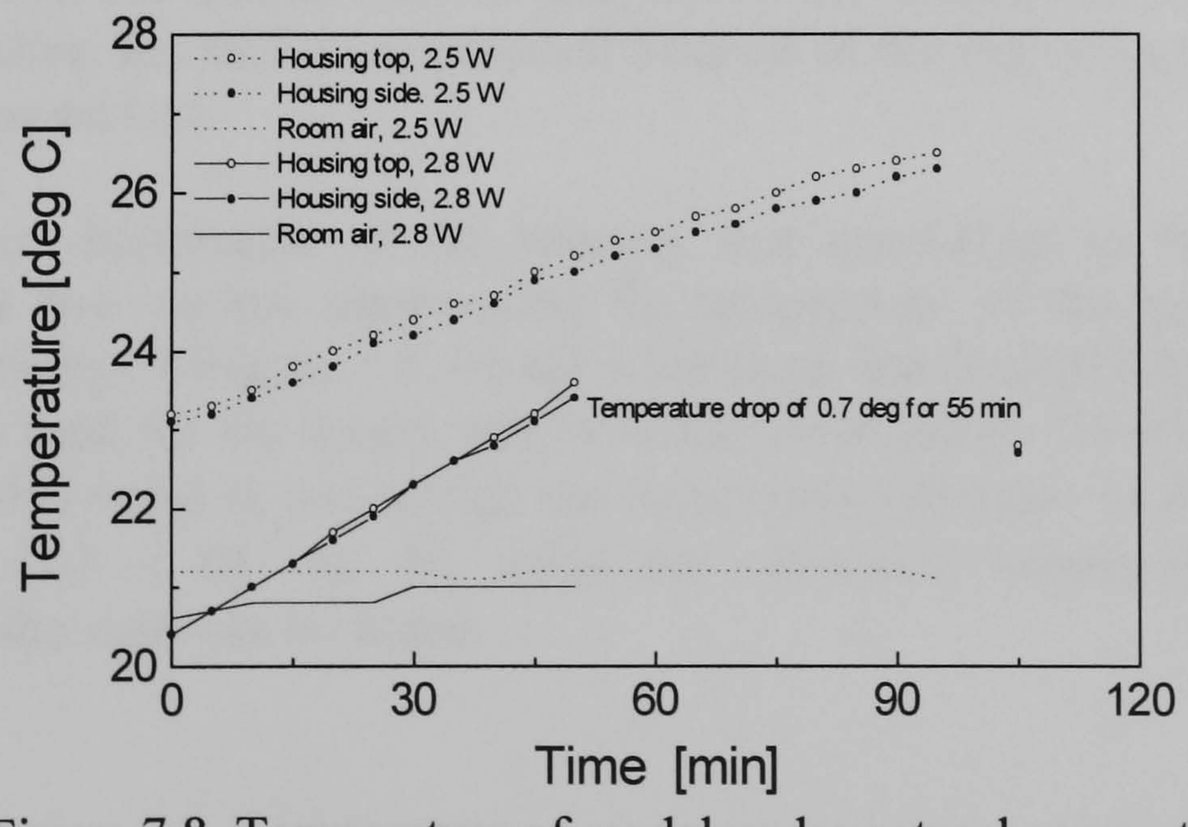

Figure 7.8 Temperature of model under natural convection

During the course of the test, it was found that the bond used for fixing the heating coil was melting when high power was applied to the coil. Due to this problem, the power input was restricted to under 10W, but for safety reasons, less than 5W was used. Figure 7.8 and 7.9 shows the results of trial tests. In the displacement graph of Figure 7.9, the notation *differential* denotes the differential response of the shaft and housing, i.e. the

difference between the measurement signals of the fibre-optic sensor and electronic indicator shown in Figure 7.7. The displacement of the shaft measured by the indicator has two components: one is the expansion of the housing from its bottom to the set screws; the other is the expansion of the shaft from the set screw to its top. Thus, the curve representing the shaft is actually meaningless, and is only applicable to decide the differential response.

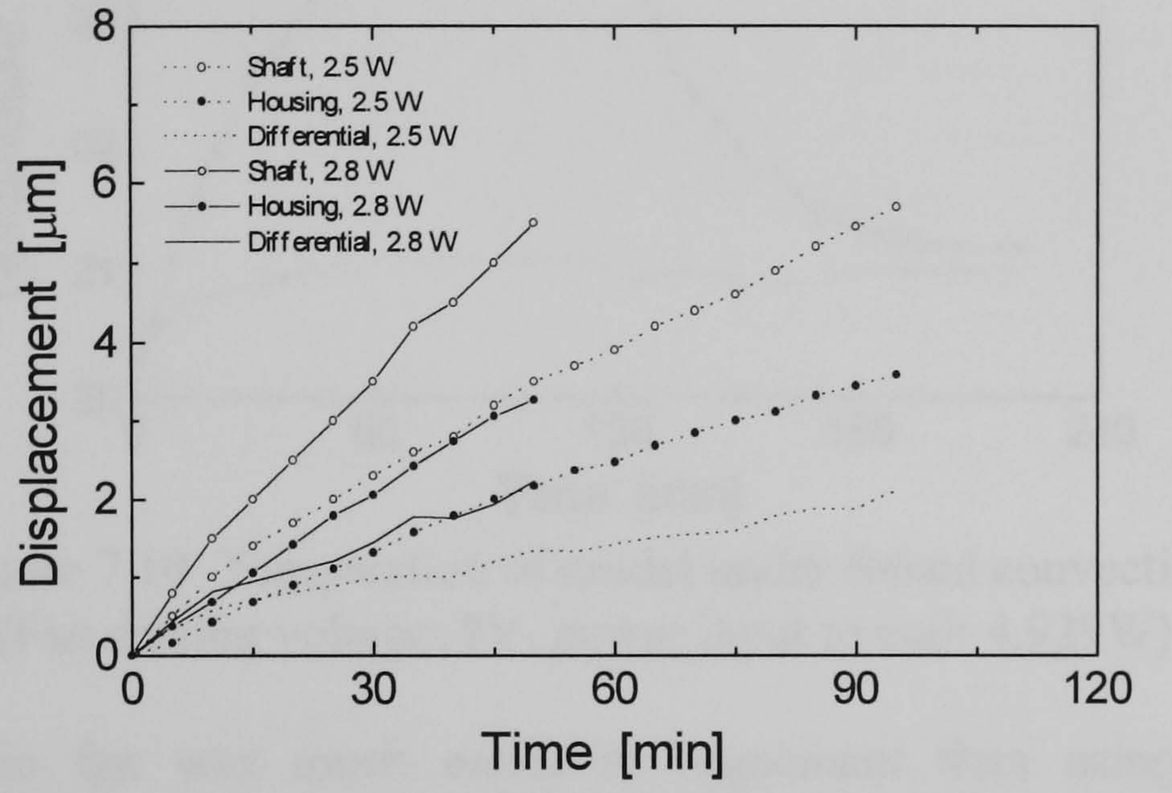

Figure 7.9 Displacement of model under natural convection

In the trial tests, no means of external cooling was employed due to an attempt to find the feasibility of model test without using any external cooling means. However, as can be seen in Figure 7.8, the temperature was not stabilised within a time of around 1 hour. After several tens of minutes, the temperature was still increasing even though less than 3W was applied to the coil. This was due to the very small heat transfer coefficient involved in natural convection. After a long period, the temperature of the model would eventually stabilise, but this is not practical because of the very long time it would take to complete a model test.

The temperature distribution of the housing was considered to be nearly uniform referring to the two curves, representing the temperature of the top and side of the housing respectively, in Figure 7.8. On the other hand, the thermal expansion coefficient of the material used for the model can be found from Figure 7.8 and 7.9 to be about 10.7×10^{-6} /K. This value is well within the uncertainty boundary of the tabulated value for steel, i.e. 11.7×10^{-6} /K. By using the calculated expansion coefficient, the temperature of the shaft can be found.

In order to enhance the cooling process of the model, a DC brushless axial flow fan purchased from RS components was used, and Figure 7.10 and 7.11 show the results.

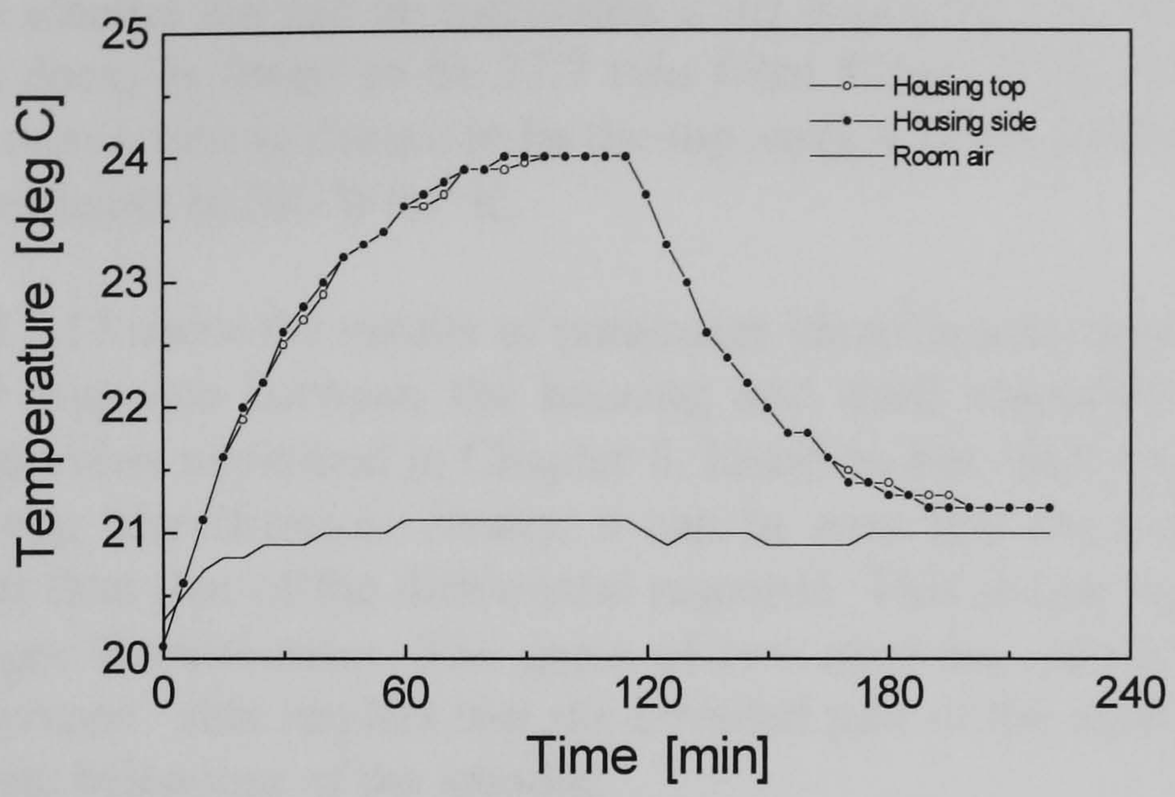

Figure 7.10 Temperature of model under forced convection
(Fan driving voltage: 8V, power input to coil: 4.929W)

Using an electric fan was much easier to implement than using liquid cooling equipment. The fan was placed just over the model and its driving voltage was first chosen to be 8V, which seemed to be the lower driving limit for the fan. The power input to the coil was about 5W, allowable limit for safety. This increased the amount of the growth of the model to obtain a high signal to noise ratio for the displacement measurements.

In Figure 7.10 and 7.11, the enhanced cooling process of the model can be seen. The temperature stabilised in the form of an exponential growth in an acceptable time, when heat was generated in the coil. This decreased when the power cut off. The fan was always running during the test. Although the data were taken at 5 minute intervals, the figures show acceptable results.

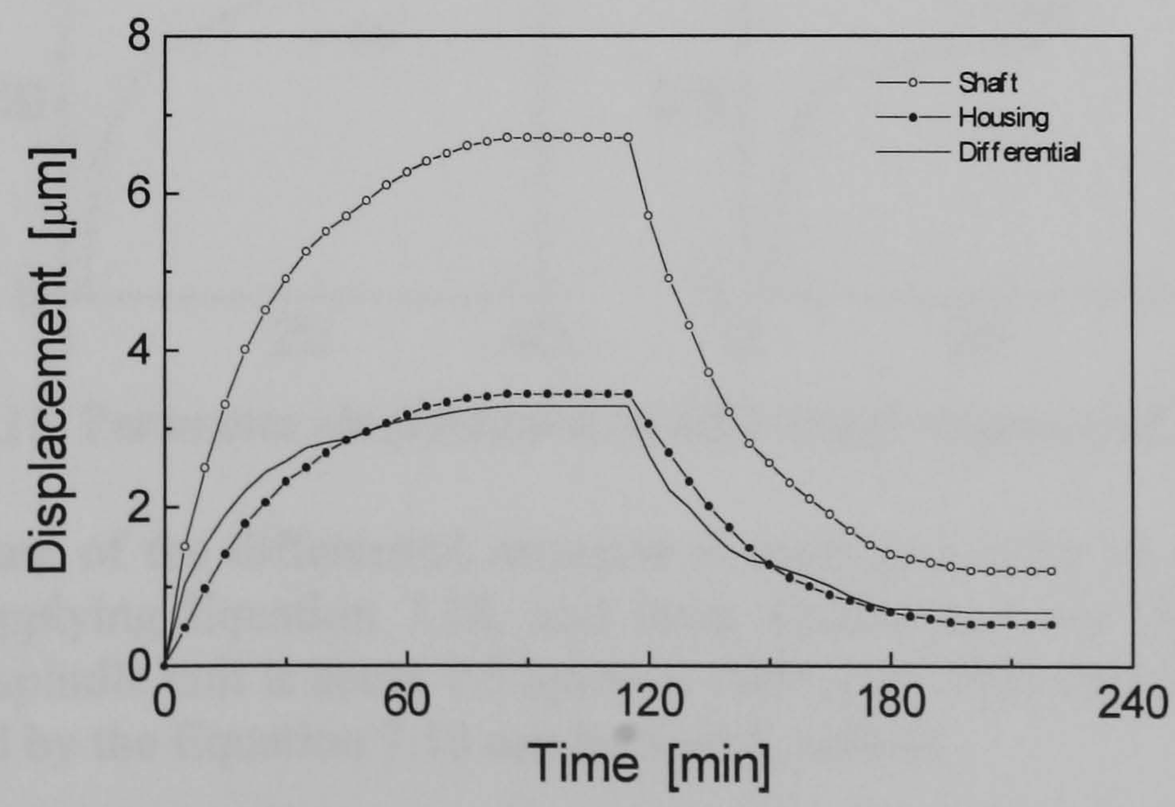

Figure 7.11 Displacement of model under forced convection
(Fan driving voltage: 8V, power input to coil: 4.929W)

From the temperature curve of the housing when heating power was cut off (exponential decay part of Figure 7.10), the heat transfer coefficient of the forced convection provided by the electric fan can be calculated using Equation 3.6. The time constant of the exponential decay is found to be 27.7 min from Figure 7.10, and the surface area involved in the convection is chosen to be the top surface of the housing. The calculated heat transfer coefficient is 200 $W/m^2 \cdot K$.

Figure 7.12 and 7.13 show the results of parameter identification applied to the housing and differential response between the housing and shaft respectively. The modified least-squares algorithm explained in Chapter 6, based on the ARX model structure, was used for parameter identification. Firstly, it can be seen that the time constant of the housing is larger than that of the differential response. This is true because the housing has a much larger thermal mass. The gains of two response curves do not, however, have much difference. This implies that the intruded part of the shaft from the housing governs the whole behaviour of the spindle.

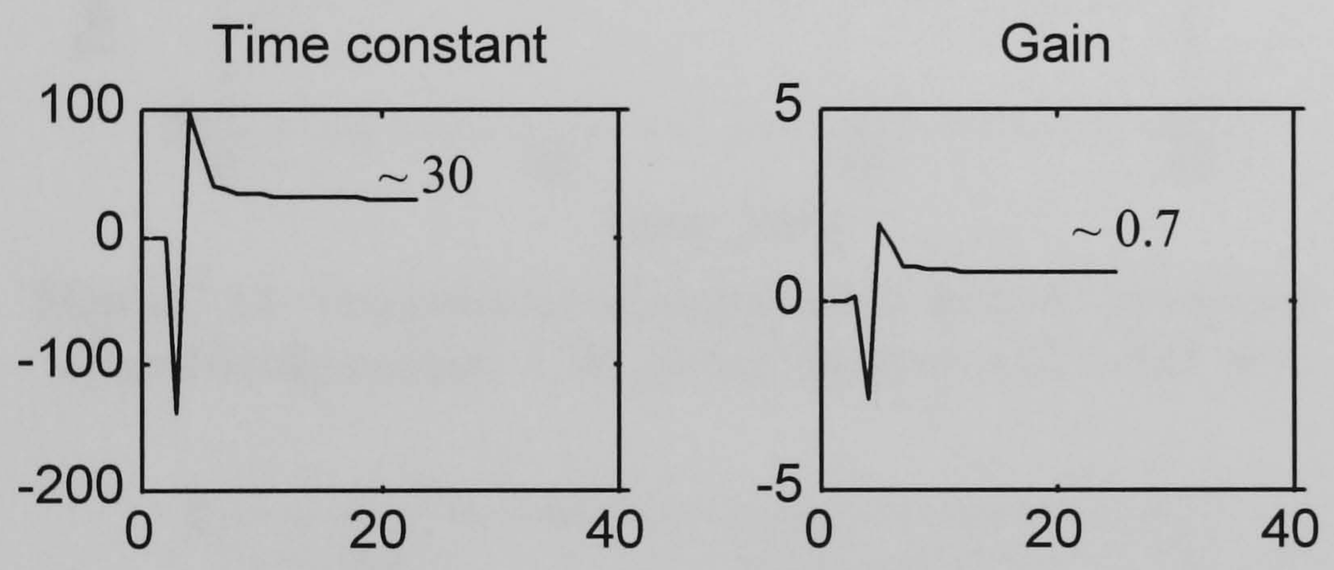

Figure 7.12* Parameter identification of housing of Figure 7.11

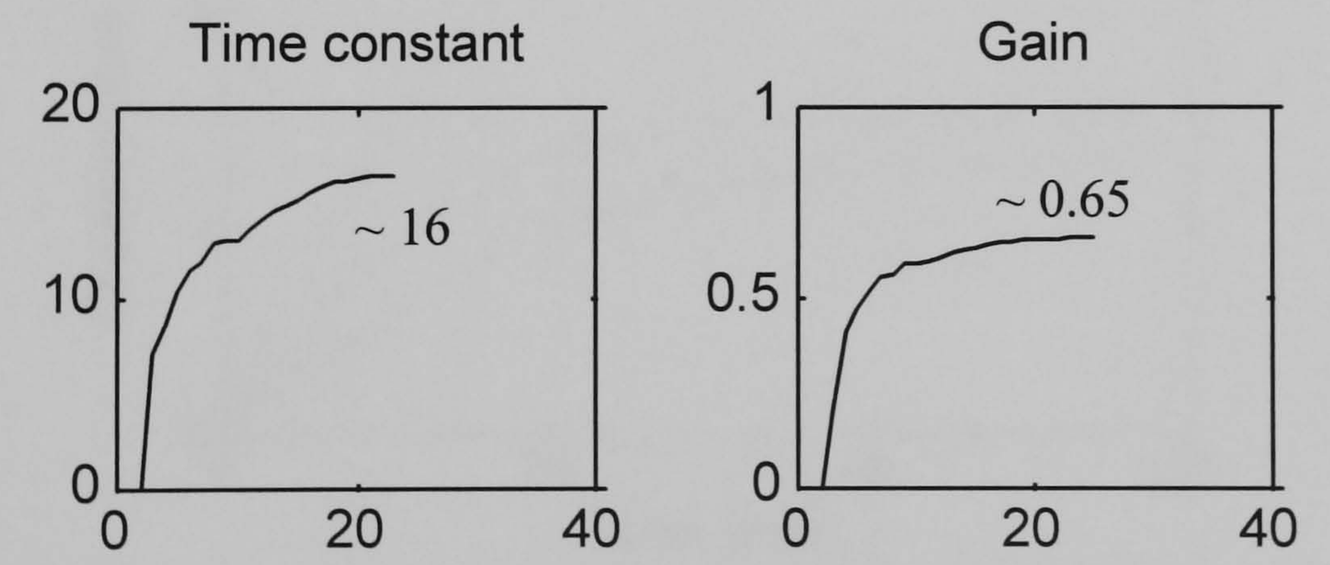

Figure 7.13 Parameter identification of differential response of Figure 7.11

The time constant of the differential response is estimated to be 16 minutes using the test data. By applying Equation 7.18, and from Section 6.3, we know that the time constant of the spindle unit is about 1.5 hours at 1000 rpm. Thus the time constant of the model predicted by the Equation 7.18 can be found, such as

---

* The unit of time constant is minutes and that of gain is μm/W. The followed figures will have the same units.

$$\tau_M = 0.02 \frac{h_M}{h'_M} \tau_P = 0.02 \times \frac{2821}{200} \times (1.5 \times 60) = 25 \text{ min}$$

The difference between the actual time constant and predicted value given by Equation 7.18 is not great considering the simple methods applied to the model test. Most of the errors are likely to arise from predicting the heat transfer coefficient and selecting the corresponding surface area.

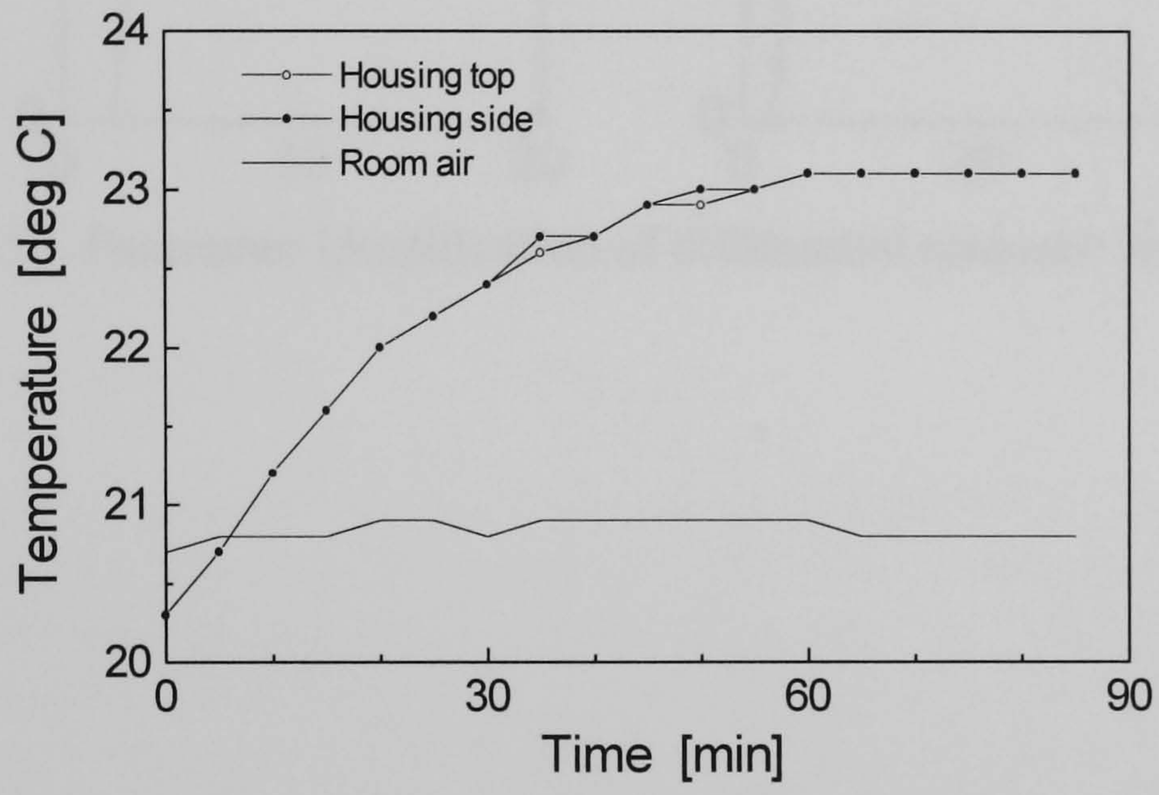

Figure 7.14 Temperature of model under forced convection
(Fan driving voltage: 12V, power input to coil: 5.022 W)

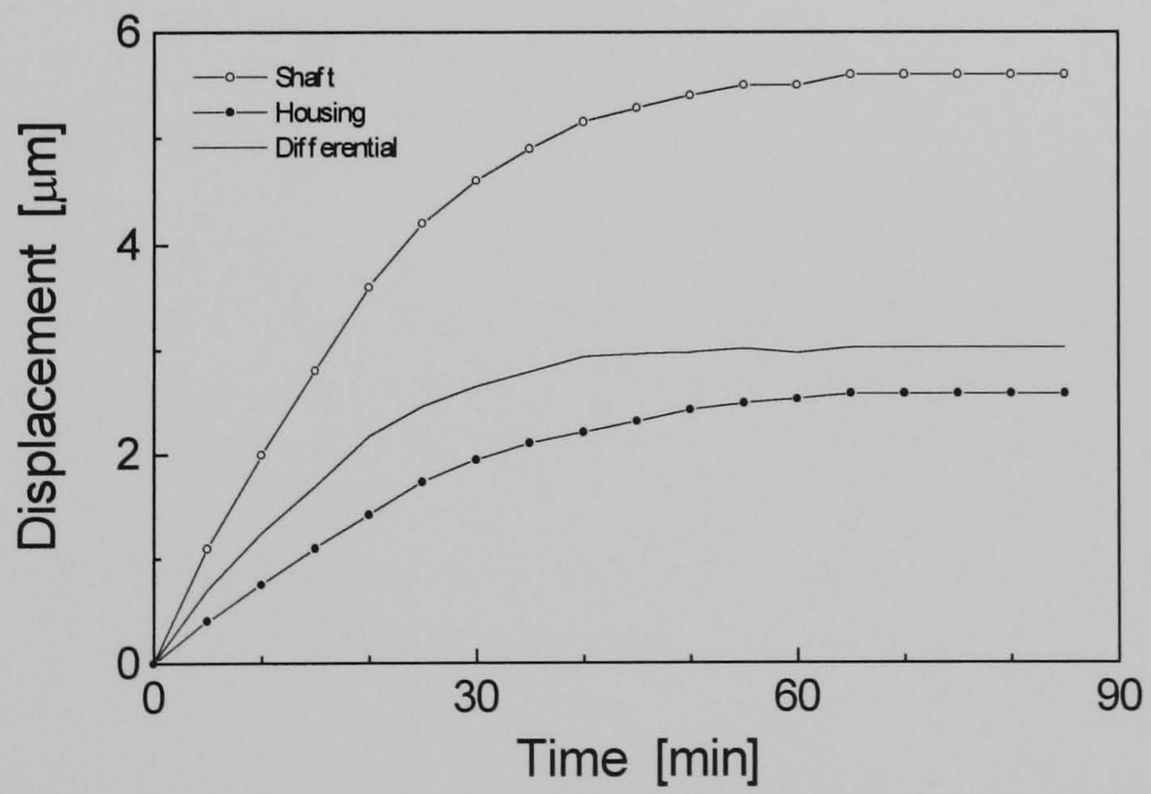

Figure 7.15 Displacement of model under forced convection
(Fan driving voltage: 12V, power input to coil: 5.022 W)

Figure 7.14 and 7.15 were obtained using a different fan speed. Because the driving voltage to the fan was 12 V, which is larger than the prior case, greater convection cooling effects were expected. According to Figure 7.16, however, which shows the estimated time constant and gain of the differential response, not much difference in cooling effects can be identified by increasing the driving voltage, while in turn increases the rotational speed of the fan. Also in Chapter 6, the time constant of the

spindle was not changed very much by varying its rotational speed. Perhaps a bigger fan would produce greater convection cooling.

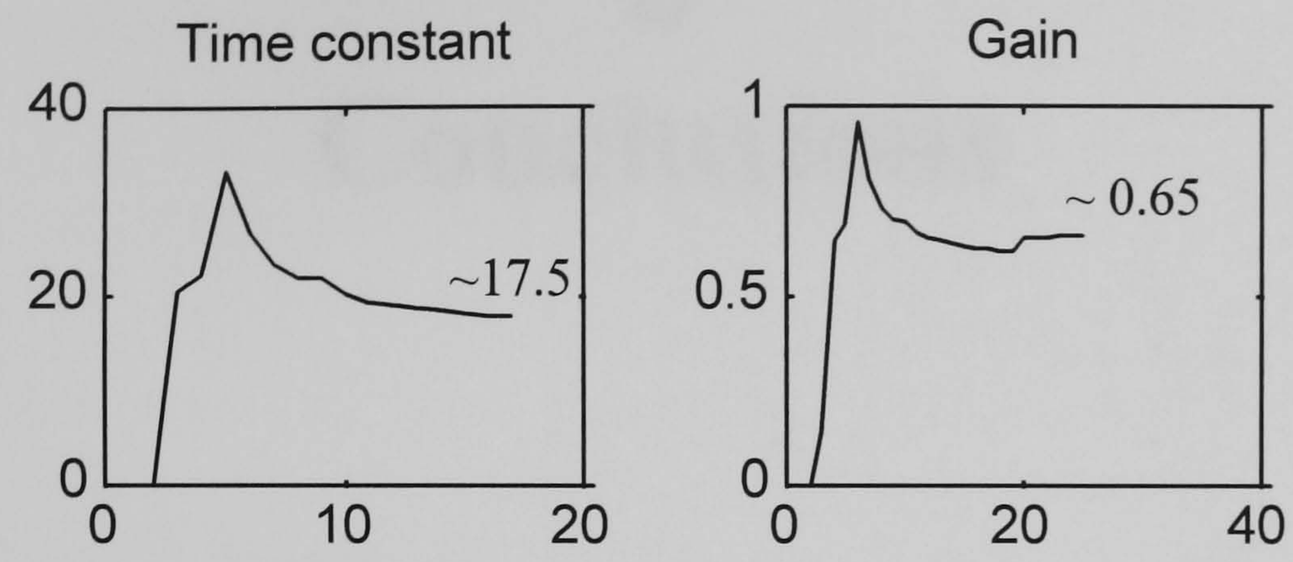

Figure 7.16 Parameter identification of differential response in Figure 7.15

Chapter 8 Conclusions

8.1 Review of the Work

A method of analysing time-varying (or dynamic) thermal errors in machine tools was investigated in this study, using three thermal parameters, i.e. time-delay, time-constant and gain. Chapter 1 introduced the importance of thermal errors in machine tools, which account for as much as 70 % of workpiece inaccuracy according to Bryan (1990). As the literature review (Section 1.2) showed, time-varying thermal errors in machine tools, as the result of the effects of temperature variations, had not been investigated satisfactorily, but compensation techniques using empirical correlations had been a main research subject. Under consideration of design applications, developing a simple yet systematic, physically meaningful modelling method of time-varying thermal errors using some physically-meaningful thermal-parameters was decided to be the prime objective of this study as stated in Section 1.3.

Before the main research work, the fundamentals of machine tool metrology and errors were studied in Chapter 2. Particular attention should be paid to Section 2.3, where machine tool errors were classified by their time dependency. That is, time-invariant errors are dependent only on the position of machine carriages while time-varying ones have dependency on the position and time. Also a brief description of the kinematic modelling technique using homogeneous transformation matrices was given in Section 2.4. The technique was expanded to take account of the thermal deformation of machine components (Section 2.4.1.).

The process of finding the three thermal parameters was based on theoretical analyses (Chapters 3 and 4) supported by experiment (Chapters 5 and 6). Analytical tools were deployed in Chapter 3 to calculate the thermal deformation of simple machine elements. It was shown in Section 3.3 that the calculation of transient temperature fields using analytical methods was not easily achievable even for simple problems, so a numerical technique was introduced in Section 3.3.5. Under the theory of uncoupled thermoelasticity, described in Section 3.1, the development of temperature fields governed the time-dependent behaviour of the thermal deformation, e.g. as Equations 3.6, 3.9, 3.13 and Figure 3.4 indicate. The elastic deformation of simple machine

elements, such as bars, beams and cylinders, was investigated in Section 3.4. It is noted that there is the extension deformation, independent of transverse bending, of beams due to temperature gradients as shown in Section 3.4.2.

Because the modelling parameters of thermal deformation were not identified at the stage of Chapter 3, more investigations employing a scientific approach (Section 4.2.1) and numerical simulation (Section 4.3) were carried out in Chapter 4. The results of the numerical simulation (Section 4.3.4) based on a straightedge subject to room temperature variations implied a close relationship with the response of first-order systems with time-delay. Also, the heat-balance equation under forced convection was found to be governed by linear first-order differential equations (Section 4.2.2). The implications of these led to the proposal of the three thermal parameters, i.e. time-delay, time-constant and gain, as described in Section 4.4. The three thermal parameters were assigned to points of interest on a machine body so that the spatially distributed characteristics of its temperature were taken into account. Such a technique is named *the point-wise description method* in this study (Section 4.4.1). Regarding the dependence of thermal parameters on heat transfer mechanisms as explained in Section 4.4.1, a more refined description requires a time-varying linear first-order differential equation (Section 4.4.3).

Because there are many drawbacks to theoretical approaches, as explained in Section 5.1, experimental techniques are considered essential to reinforce them. In Chapters 5 and 6, direct experimental evaluation of the thermal parameters using a full-scale model was investigated with a single-point, diamond turning, research machine (Section 5.2, Figure 5.1) at Cranfield University. The experimental test of thermal errors (Chapter 5) and parameter evaluation (Chapter 6) using the test data was performed on the aerostatic spindle unit (Figure 5.2) because the main function of the machine is the facing of thin disks. Before the test, the expected thermal deformation of the spindle unit was calculated as described in Section 5.3.1. The results of the thermal error test showed that the three thermal parameters could describe the thermal deformation of machine tools (Section 6.1). In order to identify time-varying system parameters quantitatively, some modified recursive least-squares methods were employed (Section 6.2.2). They were, however, found to be sensitive to noise in the measurement data as stated in Section 6.2.3. Some facts complementary to theoretical analysis were identified such as the compromising premise concerning time-varying quantities as described in Section 6.3.

In Chapter 7, some design guidelines (Section 7.2) were proposed in relation to the three thermal parameters in order to minimise thermal deformation. Also, a scaled physical test model method was investigated, regarding its use as a design test method in Section 7.4. Also, it can be regarded as an indirect evaluation method of the three thermal parameters employing smaller scaled models as a feasible solution when dealing with large machine tool structures. It was found that there were some problems in directly applying similarity rules in thermal processes (Section 7.4.3). These are due to the very large increases in the heat transfer coefficient and much smaller time scale for test models. This was overcome by using the inversely proportional relationship between the time-constant and heat transfer coefficient.

8.2 Conclusions

Errors in machine tools, in general, are dependent on the position of machine carriages and time as stated in Section 2.3. Thermal errors are strongly dependent on the continuously changing operating conditions of a machine and its surrounding environment because heat sources are directly related to them as shown in Section 3.2. As a consequence, the three thermal parameters, i.e. time-delay, time-constant and gain, were treated as being time-varying (Sections 4.4 and 6.3). Uniform temperature rises or stable temperature gradients, which produce time-invariant thermal errors, are considered to be rare in ordinary shop floor environments.

The analytical and numerical methods employed for the derivation of the three thermal parameters in Chapters 3 and 4 can be deployed in order to evaluate thermal parameters of components of a machine. Also, two other evaluation methods based on experimental techniques were investigated in Chapters 5, 6 and 7. They are a direct method using a full-scale machine and an indirect method utilising a scaled model of a machine. Thus this work encompasses most approach methods of engineering, resulting in a comprehensive approach to time-varying thermal errors.

This is a summary of the mechanism of the thermal deformation. The difference between heat generated by the heat sources around a machine and heat removed by cooling mechanisms brings forth the changes in internal energy of a machine unit, i.e. for solids changes in temperature such as that represented by Equation 3.6 in Section 3.3.2. During the course of heat transmission, a delay may occur due to those reasons as outlined in Section 4.4.1. When the rate of heat generation is greater than that of removal by cooling, the temperature of a machine unit increases so that it expands in an exponential fashion represented by the time-constant such as that described by Equation 4.4 in Section 4.4.2. The intensity of heat removal by cooling determines the time-constant as Equation 3.6 in Section 3.3.2 suggests. Eventually the temperature of a unit stabilises and so does its expansion. The final expansion is a product of gain and the corresponding heat input. When the rate of heat generation is smaller than that of removal by cooling, the temperature of a machine unit decreases and the foregoing theory can be adaptable to that case.

The above theory was assigned to points of interest on a machine body discretely as described in Section 4.4.3. Many engineering practices make use of the benefits from such discretisation either in space or time. They include, for example, finite-element techniques, metrological calibration of instruments, etc., and moreover most of the experimental work is considered to be carried out along a discretised time sequence. Although the state-space equation in Section 4.4.3 was not directly applied to a real machine tool in this study, the application is believed to be straightforward in the sense that it is a collection of first-order equations.

Benefits of using the three thermal parameters are that, first of all, complex thermo-elastic behaviour of a machine unit are represented by three simple parameter-numbers as shown particularly in Chapter 6 and they provide good compatibility between theoretical and experimental analyses (Direct comparison of theoretical results in

Chapter 5 was made with the experimental ones given in Chapter 6). Moreover, many sets of the parameters, of which each represents a particular machine component, can be brought together to attain total thermal behaviour for a machine tool as explained in Section 6.2.1. Another benefit of using the parameters comes from the fact that with some knowledge of the thermal behaviours of a machine system, the parameters of each machine component are obtainable using the total response of the system as stated in Section 6.2.3. This will, of course, dramatically reduce time consuming calibration work on machine tools. In this study, that feasibility was investigated in Sections 6.2.3 and 6.3, but the potential could be large. Also some design recommendations could be drawn directly from the meaning of the three thermal parameters in Section 7.2.

An interesting fact found from the experimental work is that small changes in thermal parameters were observed in some different operating conditions (Section 6.3). This was probably because of the effect of turbulence around the spindle unit and in the bearing gap that caused moderate changes in the surrounding thermal environment as explained in Section 6.3. The experimentally identified parameters in Section 6.3 deviated from the theoretical counterparts (Section 5.3.1). The most obvious cause was due to neglecting an important component (i.e. the spindle support) in the theoretical calculations as explained in Section 6.3. The test data shows large temperature rises in the spindle support, a thick steel plate used as a base for the spindle unit and spindle motor (Section 6.1). The generated heat from the spindle motor is directly dissipated into the spindle support. Other errors may arise from deciding the heat transfer coefficient and area of the heat-affecting region.

Using a test model, we can obtain three thermal parameters of components as demonstrated in Section 7.4, so that we can change dimensional, thermal and material properties of machine components to meet specific design requirements or obtain the thermal deformation model of a machine. The real benefit of a test model is to facilitate the identification of thermally vulnerable components, which contribute significantly to total thermal errors of a machine because in the end the relative thermal deformations among machine components will result.

The introduction of time-varying thermal parameters provided more versatility in this study such as that shown in Section 4.4, although it also gave some difficulties in handling time-varying thermal parameters as stated in Section 6.3. A compromise that can be made is that under uniform operating and surrounding conditions, the three thermal parameters can be regarded as constant, i.e. they changed abruptly according to the conditions of a machine as explained in Section 6.3.

All the methods investigated in this study will eventually produce thermal parameters of a machine unit or several units as a whole, dependent upon various kinds of heat sources. It is believed that the application of one method only cannot give satisfactory results. The determination of thermal parameters of a machine tool should be a continuously updated process along with the development of machine tools. At some stage, it is theoretically possible that just one method will be sufficient in determining the parameters if sufficient knowledge of the real physical behaviour of the thermal deformation in machine tools can be accumulated. Although this work was concentrated

on machine tools, the developed methodology is believed to be applicable to other mechanical systems subject to thermal disturbances because it is based upon the theory of uncoupled thermoelasticity.

8.3 Suggestions for Future Work

The following subjects are recommended for the further study of time-varying thermal errors:

- The heat transfer coefficient associated with cooling mechanisms is necessary to calculate thermal parameters. The evaluation of the heat transfer coefficient of the cooling mechanisms in machine tools is likely to be a serious hurdle in analysing their thermal deformation for the time being.

- In this study, most investigations were devoted to machine members. However, machine tools have a large number of fixed and sliding joints that provide mechanical and thermal discontinuity. It is necessary to consider the effect of machine joints in the development of time-varying thermal errors.

- A systematic methodology by which a set of independent heat inputs to a machine can be chosen was not considered in this study. Considering it is the starting point of every modelling, the methodology should be developed.

- Experimental techniques that extract nearly pure responses only for one heat input condition are necessary to evaluate the exact thermal parameters of a machine component. Also they should be designed carefully because highly sophisticated temperature controlling equipment tends to be expensive.

- In cases of professional application, it is recommended to use a pre-processor by which the data analysed in the identification algorithms are smoothed or averaged for an interval around the sampling points.

- The improvement of the thermal insensitivity of a machine can be prohibited by the requirement of its mechanical stiffness as can be seen in Appendix C. An optimisation technique that yields the best compromise between thermal and mechanical requirements is worth investigating.

- An introduction of the three thermal parameters to the kinematic modelling method is necessary to establish the full spectrum of the mathematical modelling of a machine tool. This seems to require some support from the theory of deformable multibody dynamics.

References

Adams, J.A. and Rogers, D.F. (1973), *Computer-aided heat transfer analysis*, McGraw-Hill, New York, NY

Allen, D.H. and Haisler, W.E. (1985), *Introduction to aerospace structural analysis*, John Wiley, New York, NY

Allen, J.P., Postlethwaite, S.R. and Ford, D.G. (1996), "Practical thermal error correction for CNC machine tools", *ASPE 1996 Annual Meeting Proceedings*, Nov. 9-14, Vol. 14, pp. 648-653

Anderson, J.T. and Saunders, O.A. (1953), "Convection from an isolated heated horizontal cylinder rotating about its axis", *Proc. Roy. Soc., A.*, Vol. 217, pp. 555-562

ANSI Standard B5.54 (1992), *Methods for performance evaluation of computer numerically controlled machining centers*, ASME, 345 E. 47th St. New York, NY

ANSI Standard B89.3.4M (1985), *Axis of rotation: Methods for specifying and testing*, ASME, 345 E. 47th St. New York, NY

ANSI Standard B89.6.2 (1973), *Temperature and humidity environment for dimensional measurement*, ASME, 345 E. 47th St. New York, NY

Arpaci, V.S. (1966), *Conduction heat transfer*, Addison-Wesley, Reading, MA

Attia, M.H. and Kops, L. (1978), "On the role of fixed joints in thermal deformation of machine-tool structures", *Ann. CIRP*, Vol. 27, No. 1, pp. 305-310

Attia, M.H. and Kops, L. (1979a), "Nonlinear thermoelastic behavior of structural joints - solution to a missing link for prediction of thermal deformation of machine tools", *Trans. ASME: J. Engineering for Industry*, Vol. 101, pp. 348-354

Attia, M.H. and Kops, L. (1979b), "Computer simulation of nonlinear thermoelastic behavior of a joint in machine tool structure and its effect on thermal deformation", *Trans. ASME: J. Engineering for Industry*, Vol. 101, pp. 355-361

Baker, R.E. and Hornung, K.G. (1970), "Effects of heat generation in an air hydrostatic journal bearing", *Trans. ASME: J. Lubrication Technology*, pp. 607-616

Balkrishna, C.R., Robert, X.G. and Craig, R.F. (1995). "Temperature modelling for orthogonal diamond machining", *Proc. American Soc. for Prec. Engg*, Vol. 12, pp. 223-226

Balsamo, A., Marques, D. and Sartori, S. (1990), "A method for thermal-deformation corrections of CMMs", *Ann. CIRP*, Vol. 39, No. 1, pp. 557-560

Barrett, C.R., Nix, W.D. and Tetelman, A.S. (1973), *The principles of engineering materials*, Prentice-Hall, Englewood Cliffs, NJ

Bejan, A. (1993), *Heat transfer*, John Wiley, New York, NY

Berthold III, J.W. and Jacobs, S.F. (1976), "Ultraprecise thermal expansion measurements of seven low expansion materials", *App. Opt.*, Vol. 15, No. 10, pp. 2344-2347

Blanding, D.L. (1992), *Principles of exact constraint mechanical design*, Eastman Kodak Co., Rochester, NY

Breyer, K.H. and Pressel, H.G. (1991), "Paving the way to thermally stable coordinate measuring machines", In: Seyfried, P., Kunzmann, H., McKeown, P. and Weck, M. (eds.), *Progress in Prec. Engg*, Springer-Verlag, Berlin, pp. 56-75

Bryan, J.B. (1979a), "Design and construction of an 84 inch diamond turning machine", *Prec. Engg*, Vol. 1, pp. 13-17

Bryan, J.B. (1979b), "The Abbe principle revisited: An updated interpretation", *Prec. Engg*, Vol. 1, pp. 129-132

Bryan, J.B. (1990), "International status of thermal error research", *Ann. CIRP*, Vol. 39, No. 2, pp. 645-656

Candy, J.V. (1986), *Signal processing*, McGraw-Hill, New York, NY

Carslaw, H.S. and Jaeger, J.C. (1959), *Conduction of heat in solids*, 2nd ed., Oxford Univ. Press, London

Cebon, D. and Ashby, M.F. (1994), "Materials selection for precision instruments", *Meas. Sci. Technol.*, Vol. 5, pp. 296-306

Chen, J.S., Yuan, J.X., Ni, J. and Wu, S.M. (1993), "Real-time compensation for time-variant volumetric errors on a machining center", *Trans. ASME: J. Engineering for Industry*, Vol. 115, pp. 472-479

Chen, J.S. (1995), "Computer-aided accuracy enhancement for multi-axis CNC machine tool", *Int. J. Machine Tools and Manufacture*, Vol. 35, No. 4, pp. 593-605

Chou, C. and DeBra, D. (1990), "Liquid temperature control for precision tools", *Ann. CIRP*, Vol. 39, No. 1, pp. 535-543

Churchill, S.W. and Chu, H.H.S. (1975), "Correlating equations for laminar and turbulent free convection from a vertical plate", *Int. J. Heat Mass Transfer*, Vol. 18, pp. 1323-1329

CIRP STC <<Me>> Working Party on 3DU (1978), "A Proposal for Defining and Specifying the Dimensional Uncertainty of Multi-axis Measuring Machines", *Ann. CIRP,* Vol. 27, No. 2, pp. 623-630

Cobb, E.C. and Saunders, O.A. (1956), "Heat transfer from a rotating disk", *Proc. Roy. Soc., A.*, Vol. 220, pp. 343-351

Donaldson, B.K. (1993), *Analysis of aircraft structures: An introduction*, McGraw-Hill, New York, NY

Donmez, M.A., Liu, C.R. and Barash, M.A. (1988), "A generalized Mathematical Model for Machine Tool Errors", In: Srinivasan, K. *et al.* (eds.), *Modelling, Sensing, and Control of Manufacturing Processes*, ASME Press, New York, NY, pp.231-243

Dusinberre, G.M. (1961), *Heat-transfer calculations by finite differences*, International Textbook, Scranton, PA

Ehmann, K.F. and Hong, M.S. (1994), "A generalized model of the surface generation process in metal cutting", *Ann. CIRP*, Vol. 43, No. 1, pp. 483-486

Eskin, S.G. and Fritze, J.R. (1940), "Thermostatic bimetals", *Trans. ASME*, pp. 433-442

El-Zafrany, A. (1993), *Techniques of the boundary element method*, Ellis Horwood, Chichester

Fung, Y.C. (1965), *Foundations of solid mechanics*, Prentice-Hall, Englewood Cliffs, NJ

Fischer, H. (1970), "Beitrag zur untersuchung des thermischen verhaltens von bohr- und fräsmaschinen ", *Dr. -Ing. Dissertation, TU Berlin*

Franklin, G.F. and Powell, J.D. (1980), *Digital control of dynamic systems*, Addison-Wesley, Reading, MA

Gasvik, K.J. (1987), *Optical metrology*, John Wiley, Chichester

Gim, T. (1994), *Structural and motion capabilities of an aspheric surface generator*, MSc Thesis, Cranfield University

Gim, T. and Gee, A.E. (1995), "A critical assessment method applied to a precision aspheric generator", In: Hope, A.D., Smith, G.T. and Blackshaw, D.M.S. (eds.), *Laser Metrology and Machine Performance II*, Computational Mechanics, Southampton, pp. 309-318

Goldstein, R.J., Sparrow, E.M. and Jones, D.C. (1973), "Natural convection mass transfer adjacent to horizontal plates", *Int. J. Heat Mass Transfer*, Vol. 16, pp. 1025-1035

Goodman, T.R. (1964), "Application of integral methods to transient nonlinear heat transfer", In: Irvine Jr., T.F. and Hartnett, J.P. (eds.), *Advances in heat transfer*, Volume 1, Academic Press, New York, NY

Goodwin, G.C. and Payne, R.L. (1977), *Dynamic system identification*, Academic Press, New York, NY

Grand, P. (1952), "Contribution a la metropole industrielle des longueurs", *Rev. Gen Mec. 36*, Nos. 41,42,45

Grand, P. (1955), "Influence de la temperauture sur l'etalonnage des jauges", *Rev. Gen Mec*. 39, Nos. 74,79,83,84

Hatamura, Y., Nagao, T., Mitsuishi, M., Kato, K., Taguchi, S., Okumura, T., Nakagawa, G. and Sugishita, H. (1993), "Development of an intelligent machining center incorporating active compensation for thermal distortion", *Ann. CIRP*, Vol. 42, No. 1, pp. 549-552

Hildebrand, F.B. (1976), *Advanced calculus for applications*, 2nd ed., Prentice-Hall, Englewood Cliffs, NJ

Hocken, R.J. (Working group chairman) (1980), *Technology of machine tools Vol. 5: Machine tool accuracy*, Lawrence Livermore National Laboratory, Livermore, CA

Ish-Shalom, J. and Wasfy, T. (1994), "A finite element model for real-time compensation of the thermal deformation of the platen of a planar step motor", *Proc. 1994 IEEE Int. Conf. Robotics and Automation*, Pt 2, IEEE, San Diego, CA, pp. 1490-1495

ISO (1993), *Guide to the expression of uncertainty in measurements*, Geneva, Switzerland

Jedrzejewski, J. and Modrzycki, W. (1992), "A new approach to modelling thermal behaviour of a machine tool under service conditions", *Ann. CIRP*, Vol. 41, No. 1, pp. 455-458

Jerbi, A., Kamen, E.W. and Dorsey, J.F. (1993), "Construction of a robust adaptive regulator for time-varying discrete time systems", *Int. J. Adaptive Control and Signal Processing*, Vol. 7, pp. 1-12

Kays, W.M. and Bjorklund, I.S. (1958), "Heat transfer from a rotating cylinder with and without cross flow", *Trans. ASME, Series C*, Vol. 80, pp. 70-78

Kimura, H., Akatsu, T. and Mori, S. (1991), "Measurement of thermal deformation by interferometer utilizing optical fiber", *J. Japan Soc. Prec. Engg*, Vol. 57, No. 11, pp. 140-144

Kunzmann, H., Pfeifer, T. and Flugge, J. (1993), "Scales vs. laser interferometers: performance and comparison of two measuring systems", *Ann. CIRP*, Vol. 42, No. 2, pp. 753-767

Lardner, T.J. (ed.) (1983), *An introduction to the mechanics of solids*, 2nd ed., McGraw-Hill, New York, NY

Marshall, P. and Hardwick, B. (1989), "The heat is off", *Manuf. Engineer*, June, pp. 22-25

Mishima, N., Mizuhara, K. and Okazaki, Y. (1993), "Thermal properties of a hydrostatic air spindle (1st report)", *J. Japan Soc. Prec. Engg*, Vol. 59, No. 3, pp. 129-134

Moriwaki, T. (1988), "Thermal deformation and its on-line compensation of hydrostatically supported precision spindle", *Ann. CIRP*, Vol. 37, No. 1, pp. 393-396

Moriwaki, T., Horiuchi, A. and Okuda, K. (1990), "Effect of cutting heat on machining accuracy in ultra-precision diamond turning", *Ann. CIRP*, Vol. 39, No. 1, pp. 81-84

Moriwaki, T., Zhao, C. and Nishiuchi, M. (1991), "Thermal deformation of machining center due to temperature change in the environment", *Trans. Japan Soc. Mech. Engineers*, Pt C, Vol. 57, No. 539, pp. 281-286

Mou, J. and Liu, C.R. (1993), "A methodology for machine tool error correction - An adaptive approach", *PED-Vol. 64: Manufacturing Science and Engineering*, ASME, pp. 69-81

Nakazawa, H. (1994), *Principles of precision engineering*, Oxford Univ. Press, London

Nasar, S.A. (ed.) (1987), *Handbook of electric machines*, McGraw-Hill, New York, NY

NMTBA (1972), *Definition and Evaluation of Accuracy and Repeatability for Numerically Controlled Machine Tools*, 2nd ed., National Machine Tool Builders' Association, Mclean, Virginia

Ogata, K. (1970), *Modern control engineering*, Prentice-Hall, Englewood Cliffs, NJ

PAFEC (1984), *PAFEC theory*, PAFEC Ltd., Strelley Hall, Strelley, Nottingham NG8 6PE

PAFEC (1991), *PAFEC data preparation user manual level 7.1*, PAFEC Ltd., Strelley Hall, Strelley, Nottingham NG8 6PE

Pahl, G. and Beitz, W. (1988), *Engineering design: a systematic approach*, Rev. ed., The Design Council, London

Peters, C. and Boyd, H. (1920), "The calibration and dimensional changes of precision gage blocks", *American Machinist*, Oct. 7

Phillips, S.D. (1995), "Performance evaluations", In: Bosch, J.A. (ed.), *Coordinate measuring machines & systems*, Marcel Dekker, New York, NY, pp. 137-226

Polak, P. (1979), *Systematic errors in engineering experiments*, Macmillan, London

Reshetov, D.N. and Portman, V.T. (1988), *Accuracy of machine tools*, ASME Press, New York, NY

Rolt, F.H. (1929), *Gauges and fine measurements*, Macmillan, London

Samarskii, A.A. and Vabishchevich, P.N. (1995), *Computational heat transfer: Volume 1 Mathematical modelling*, John Wiley, Chichester

Sartori, S. and Zhang, G.X. (1995), "Geometric error measurement and compensation of machines", *Ann. CIRP*, Vol. 44, No. 2, pp. 599-609

Sata, T., Takeuchi, Y., Sato, N. and Okubo, N (1973), "Analysis of thermal deformations of machine tool structure and its application", *Proc. 14th Int. MTDR-Conference*, Macmillan, London, pp. 275-280

Schneider, P.J. (1955), *Conduction heat transfer*, Addison-Wesley, Reading, MA

Schulz, H. and Schmitt, T. (1994), "Model-based determination of heat generation in the mechanical structure of high speed feed drive systems", *Prod. Engg*, Vol. 1/2, pp. 89-92

Shabana, A.A. (1989), *Dynamics of multibody systems*, John Wiley, New York, NY

Shen, Y.-L., Duffie, N.A. (1993), "Comparison of combinatorial rules for machine error budgets", *Ann. CIRP*, Vol. 42, No. 1, pp. 619-622

Slocum, A.H. (1992), *Precision machine design*, Prentice-Hall, Englewood Cliffs, NJ

Smith, G.D. (1985), *Numerical solution of PDEs*, 3rd ed., Oxford Univ. Press, London

Smith, S.T. and Chetwynd D.G. (1992), *Foundations of ultraprecision mechanism design*, Gordon and Breach, Switzerland

Soderstrom, T. and Stoica, P. (1989), *System identification*, Prentice-Hall(UK), Hemel Hempstead

Spur, G. and De Haas, P. (1973), "Thermal behavior of NC machine tools", *Proc. 14th Int. MTDR-Conference*, Macmillan, London, pp. 267-273

Spur, G., Hoffmann, E., Paluncic, Z., Benzinger, K. and Nymoen, H. (1988), "Thermal behavior optimization of machine tools", *Ann. CIRP*, Vol. 37, No. 1, pp. 401-405

Srinivasa, N. and Ziegert, J.C. (1993), "Real-time learning of thermal errors in machine tools using a fuzzy logic based neural network", *PED-Vol. 64: Manufacturing Science and Engineering*, ASME, pp. 235-240

Srinivasa, N., Ziegert, J.C. and Mize, C.D. (1996), "Spindle thermal drift measurement using laser ball bar", *Prec. Engg*, Vol. 18, pp. 118-128

Stein, J.L. and Tu, J.F. (1991), "A state-space model for monitoring thermally-induced preload in anti-friction spindle bearings of high-speed machine tools", *DSC-Vol. 28/ PED-Vol. 52: Control of Manufacturing Processes*, ASME, pp. 31-44

Sugano, T., Takeuchi, K. and Yoshida, Y. (1993), "Diamond turning of oxygen-free copper for mirrors", *JSME Int. J. Series C*, Vol. 36, No. 4, pp. 549-555

Swyt, D.A. (1991), *New concepts of precision dimensional measurement for modern manufacturing*, NISTIR 4644, NIST, Gaithersburg, MD

Swyt, D.A. (1992), *Challenge to NIST in dimensional metrology: The impact of tightening tolerances in the US discrete-part manufacturing industry*, NISTIR 4757, NIST, Gaithersburg, MD

Tanabe, I. and Takada, K. (1991), "Thermal behaviour of concrete bed of machine tool in fluctuating ambient temperature", *Int. J. Japan Soc. Prec. Engg,* Vol. 25, No. 4, pp. 323-324

Tanabe, I. and Takada, K. (1994), "Thermal deformation of machine tool structures using resin concrete", *JSME Int. J. Series C*, Vol. 37, No. 2, pp. 384-389

Teeuwsen, J.W.M.C., Soons, J.A. and Schellekens, P.H.J. (1989), "A general method for error description of CMMs using polynomial fitting procedures", *Ann. CIRP*, Vol. 38, No. 1, pp. 505-510

Timoshenko, S. and Goodier, J.N. (1951), *Theory of elasticity*, 2nd ed., McGraw-Hill, New York, NY

Tlusty, J. and Mutch, G.F. (1973), "Testing and evaluating thermal deformations of machine tools", *Proc. 14th Int. MTDR-Conference*, Macmillan, London, pp. 285-297

Touloukian, Y.S. *et al.* (1970-1977), *Thermophysical properties of matter*, 13 vols. plus index, IFI/Plenum, New York, NY

Trapet, E. and Waldele, F. (1989) "Coordinate measuring machines in the production line: Influence of temperature and measuring uncertainties", In: *IV Congress Intl. Metrologia Industrial*, Zaragosa, Spain, Nov.

Trylinski, W. (1971), *Fine mechanisms and precision instruments*, Pergamon, New York, NY

Venugopal, R. and Barash, M. (1986), "Thermal effects on the accuracy of numerically controlled machine tools", *Ann. CIRP*, Vol. 35, No. 1, pp. 255-258

Wagner, C. (1948), "Heat transfer from a rotating disk to ambient air", *J. Appl. Phys.*, Vol. 19, pp. 837-842

Waldram, J.R. (1985), *The theory of thermodynamics*, Cambridge Univ. Press, Cambridge, England

Wasson, K.L., Slocum, A.H. and Lienhard V, J.H. (1993a), *Straightness errors of rectangular beams caused by ambient air temperature gradients*, MIT Industrial Liaison Program Report No. 10-40-93, Dept. of Mechanical Engineering, MIT, Cambridge, MA

Wasson, K.L., Lienhard V, J.H. and Slocum, A.H. (1993b), "Thermal performance of hydrostatic radial bearings for precision machine tool applications", *HTD-Vol. 259: Transport Phenomena in Nonconventional Manufacturing and Materials Processing*, ASME, pp. 101-111

Weck, M. and Zangs, L. (1975), "Computing the thermal behavior of machine tools using the finite element method - possibilities and limitations", *Proc. 16th Int. MTDR-Conference*, Macmillan, London, pp. 185-194

Weck, M. and Schroeder, H.B. (1994), "Influences of thermal expansion of tool and workpiece on form accuracy in high-precision turning", *Proc. 3rd Int. Con. on Ultraprecision in Manufacturing Engineering*, May, Aachen, Germany, pp. 265-269

Weck, M., McKeown, P., Bonse, R. and Herbst, U. (1995), "Reduction and compensation of thermal errors in machine tools", *Ann. CIRP*, Vol. 44, No. 2, pp. 589-598

Welty, J.R., Wicks, C.E. and Wilson, R.E. (1984), *Fundamentals of momentum, heat, and mass transfer*, 3rd ed., John Wiley, New York, NY

White, F.M. (1986), *Fluid Mechanics*, 2nd ed., McGraw-Hill, New York, NY

White, F.M. (1988), *Heat and mass transfer*, Addison-Wesley, Reading, MA

Wills-Moren, W.J. (1993), "Error budgeting: The mechanical design of high precision machines", *Precision Engineering Course Notes*, Cranfield University

Wylen, G.J.V. and Sonntag, R.E. (1976), *Fundamentals of classical thermodynamics*, 2nd ed., John Wiley, New York, NY

Youden, D.H. (1990), "Diamond turning achieves nanometer smoothness", *Laser Focus World*, Feb., pp. 105-116

Yurin, V.N. (1990), "Computerized selection of a method for controlling thermal deformations of machine tools", *Soviet Engg Res.*, Vol. 10, No. 11, pp. 73-77

Ziegert, J.C., Olson, D.G. and Datseris, P. (1992), "Description of Machine Tool Errors Using Screw Coordinates", *J. Mech. Design*, Vol. 114, pp. 531-535

Appendix
A
Results of FEM Simulation*

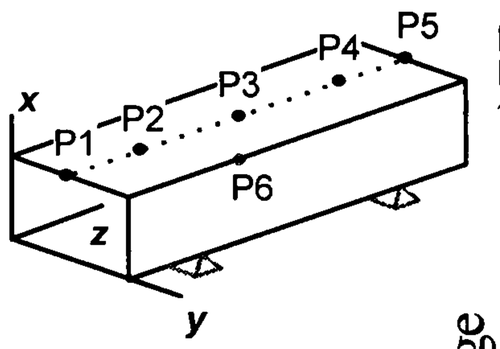

Figure A.1
5 deg step temp. rise

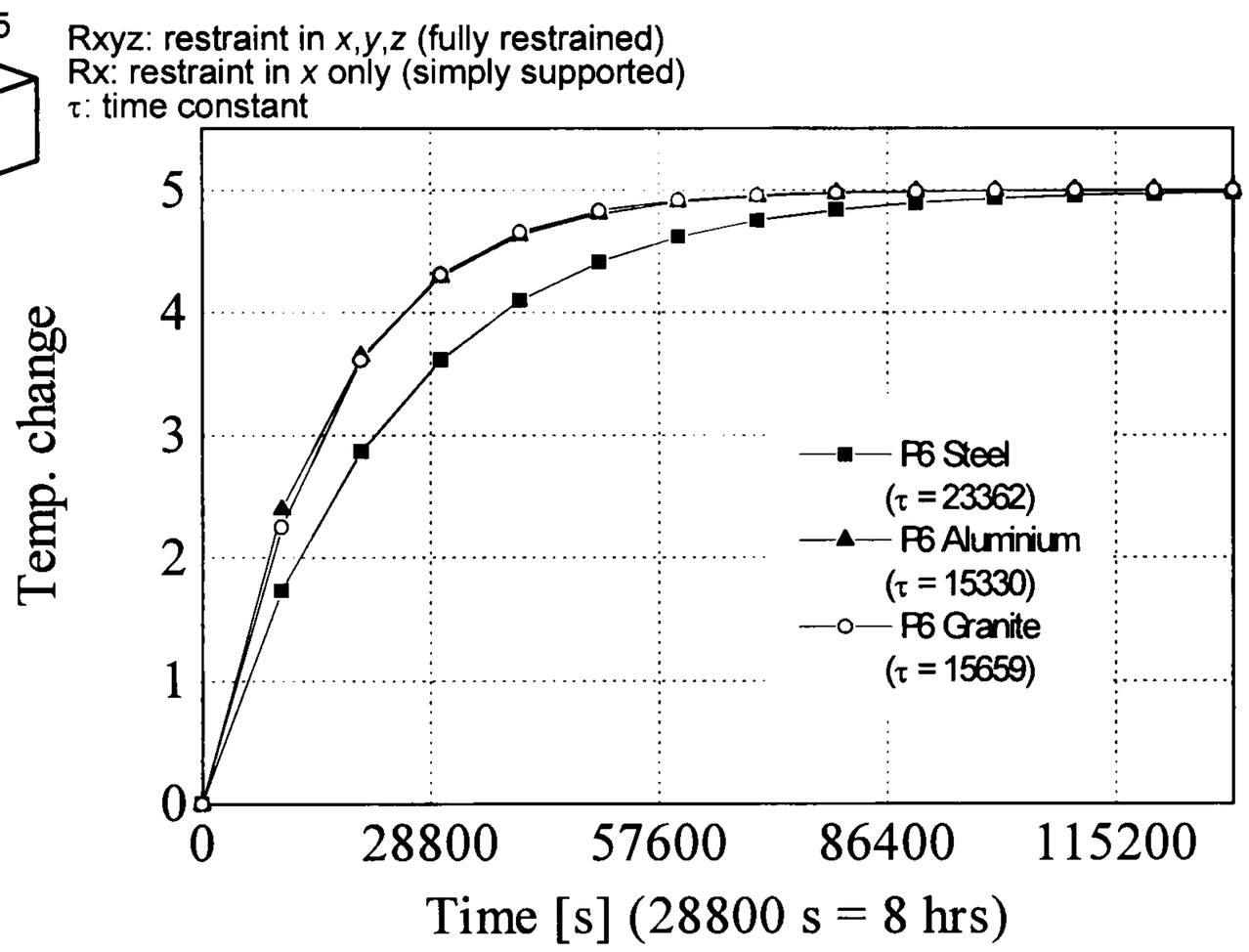

Figure A.2
5 deg step temp. rise

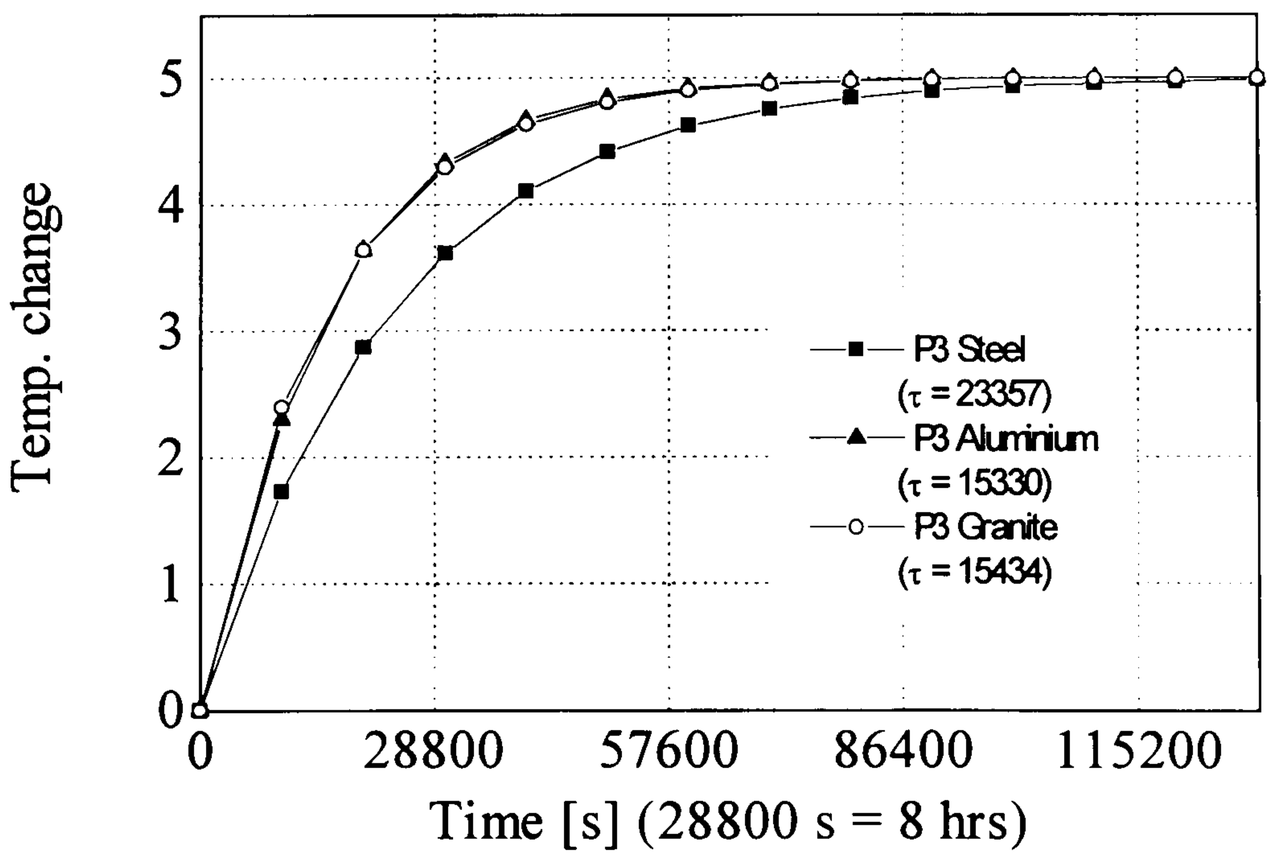

* The unit of temperature is °C.

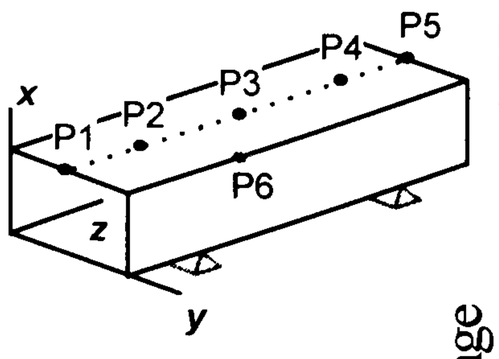

Figure A.3
5 deg step temp. rise

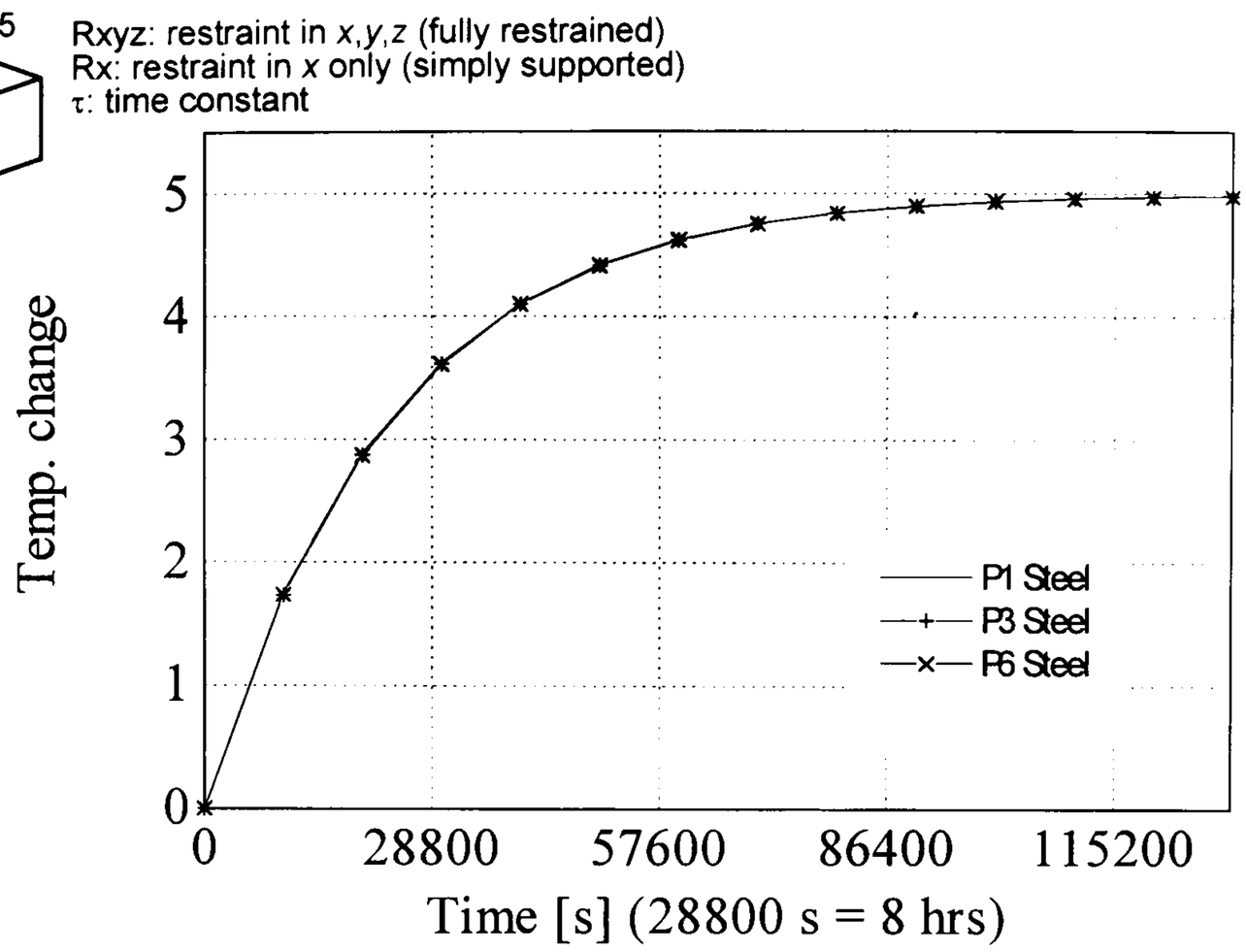

Figure A.4
5 deg step temp. rise

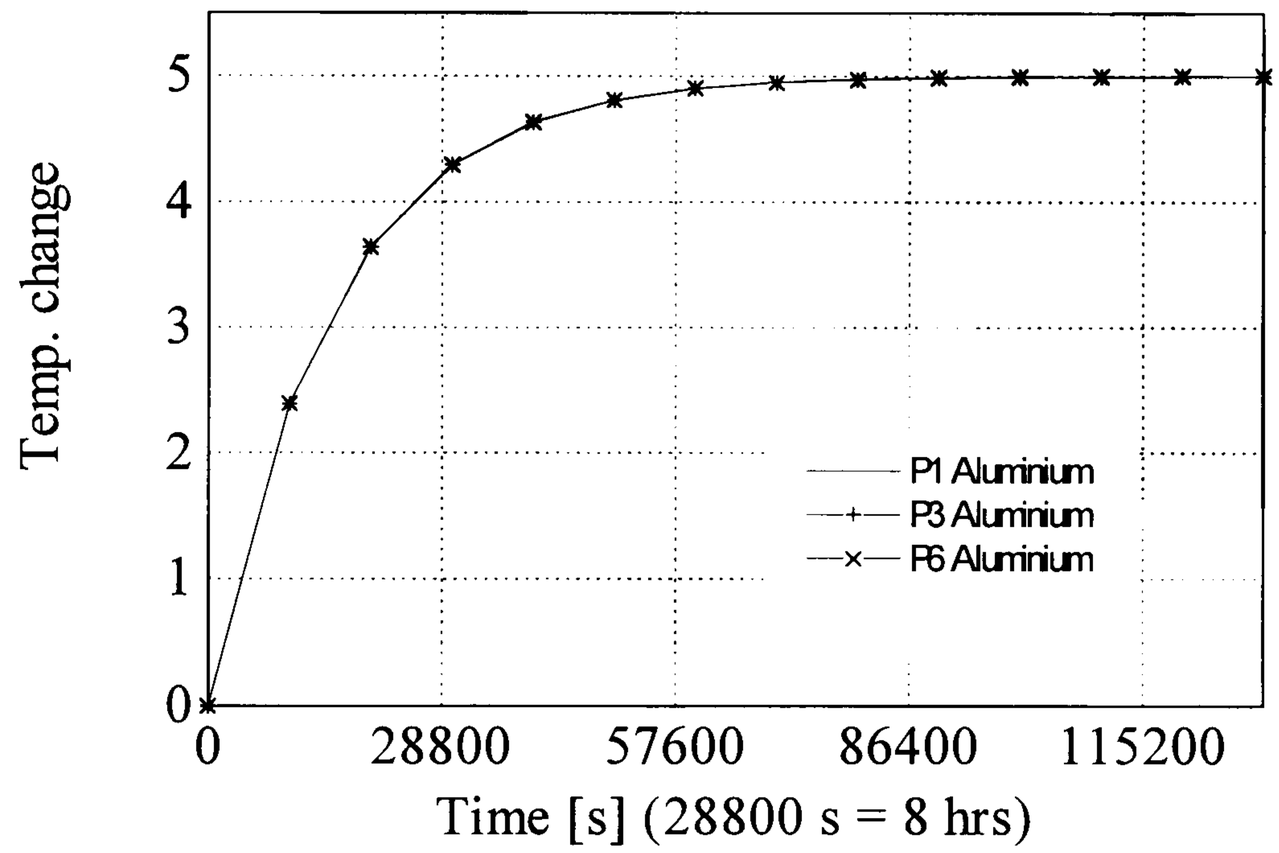

Figure A.5
5 deg step temp. rise

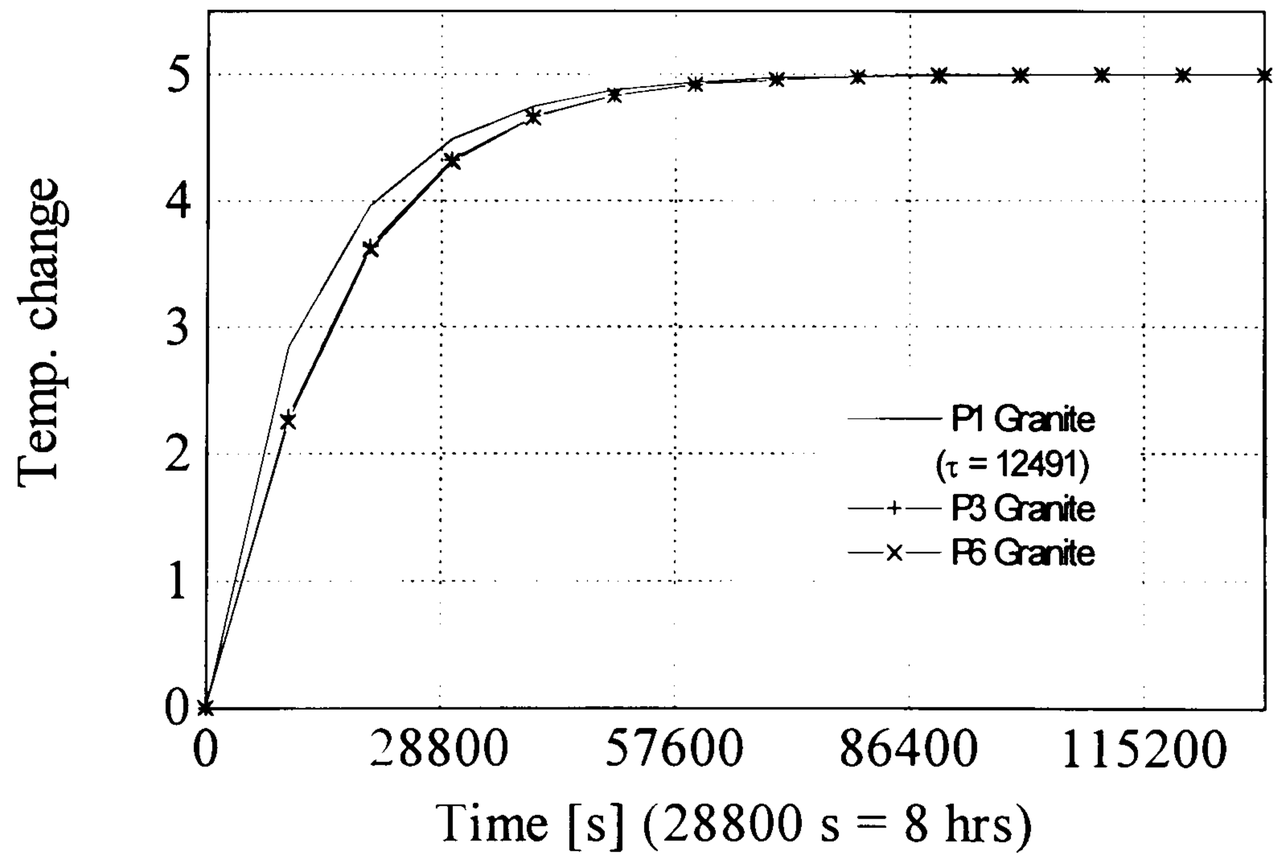

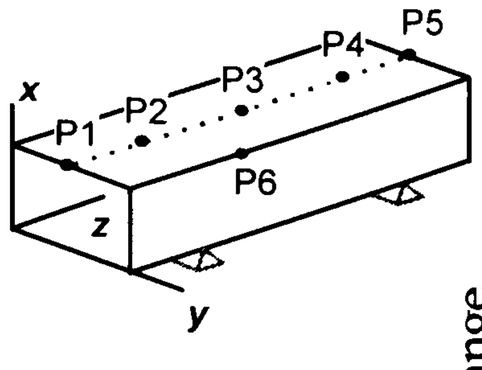

Figure A.6
2.5 deg
step temp. rise

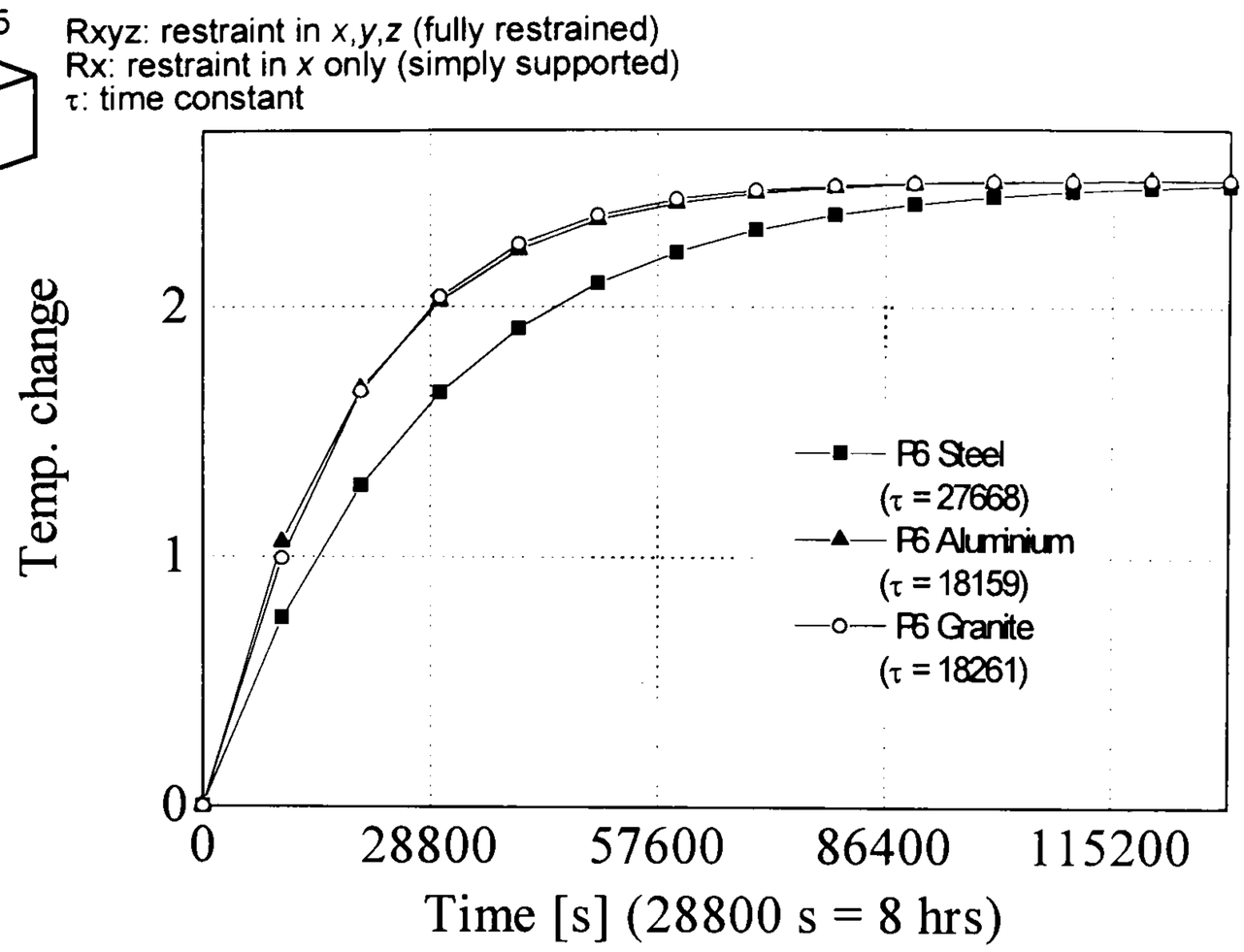

Figure A.7
2.5 deg
step temp. rise

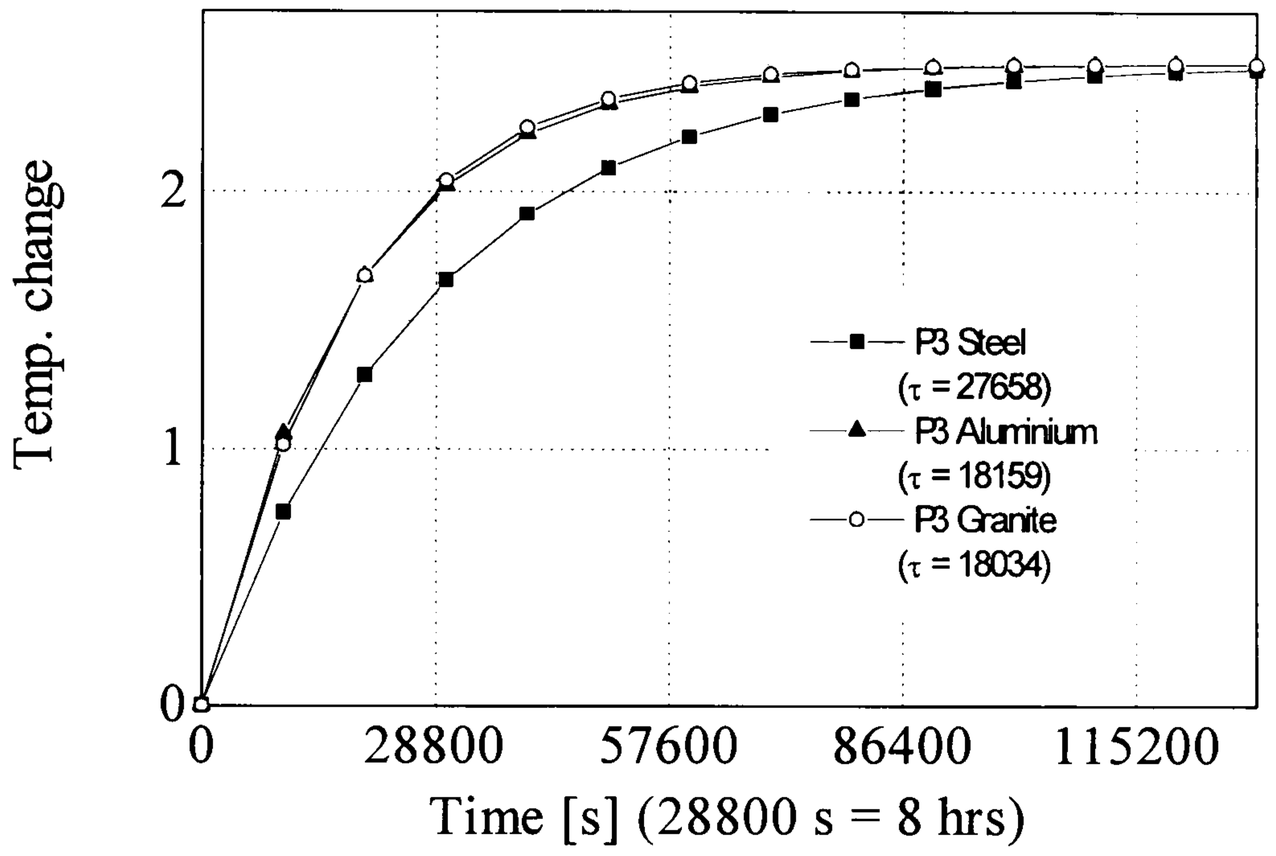

Figure A.8
2.5 deg
step temp. rise

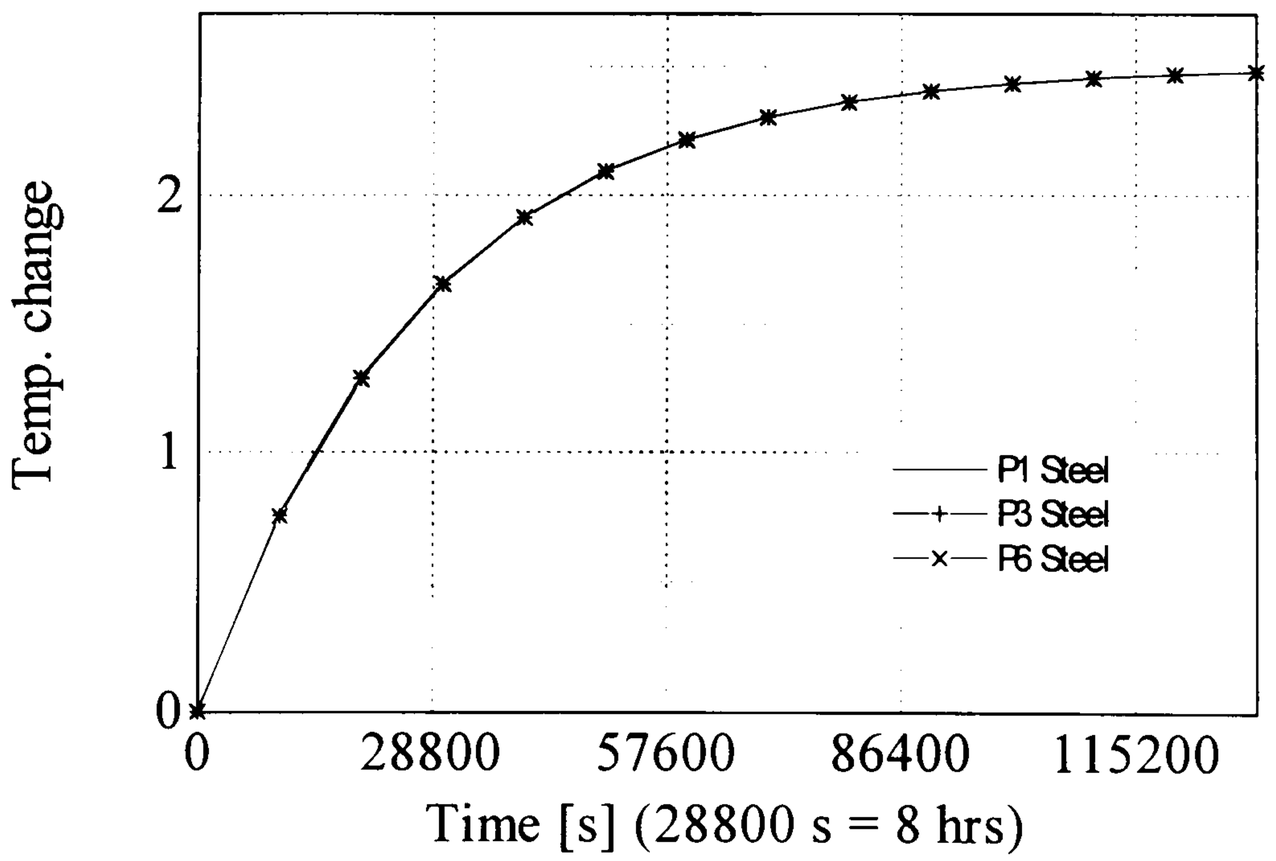

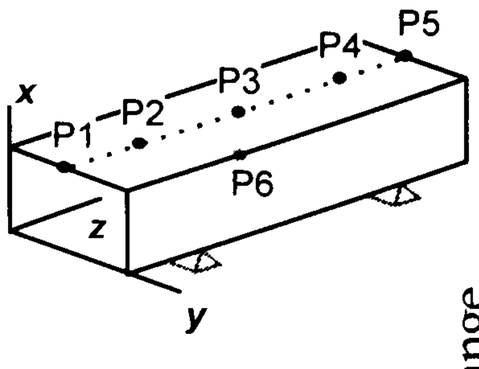

Figure A.9
2.5 deg
step temp. rise

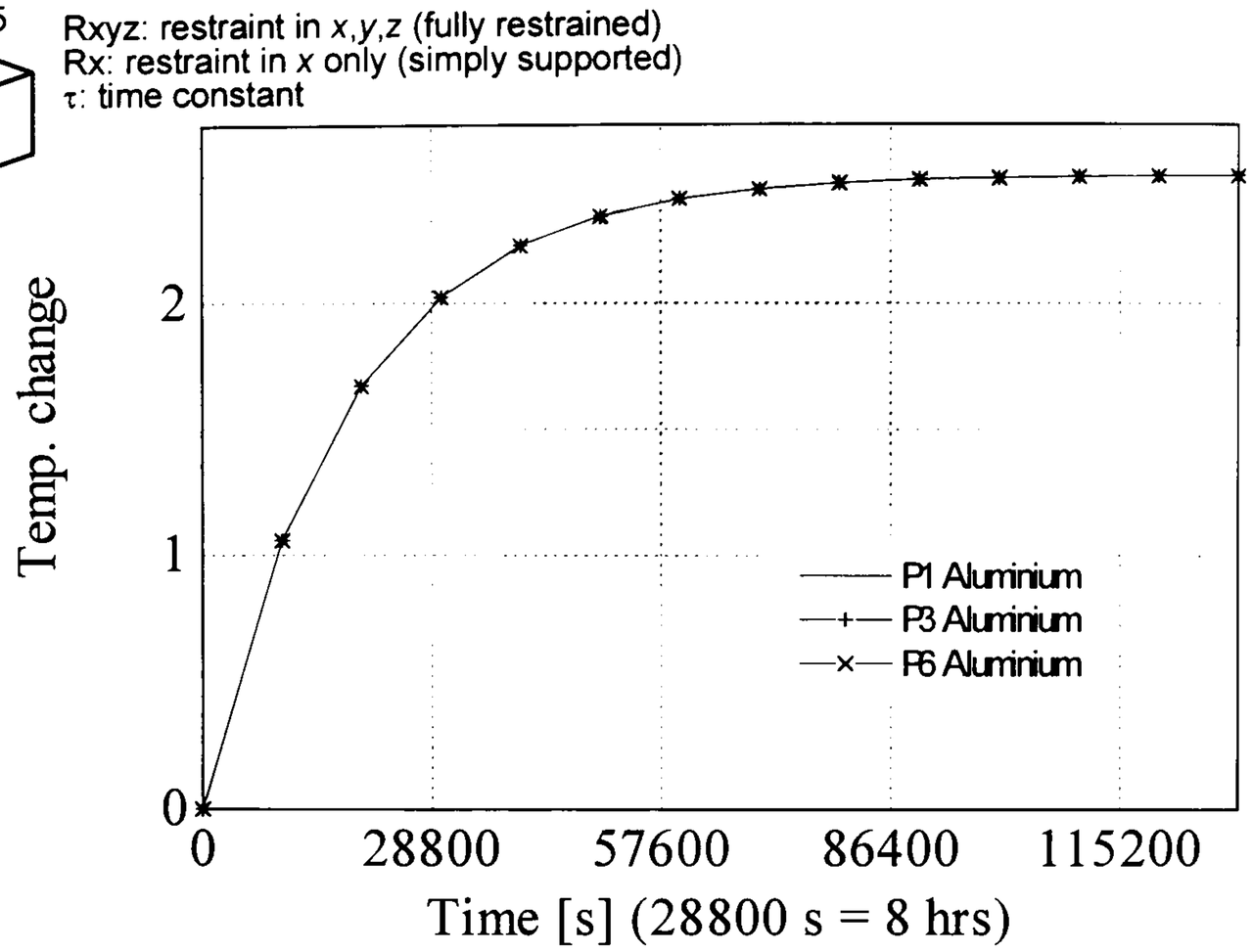

Figure A.10
2.5 deg
step temp. rise

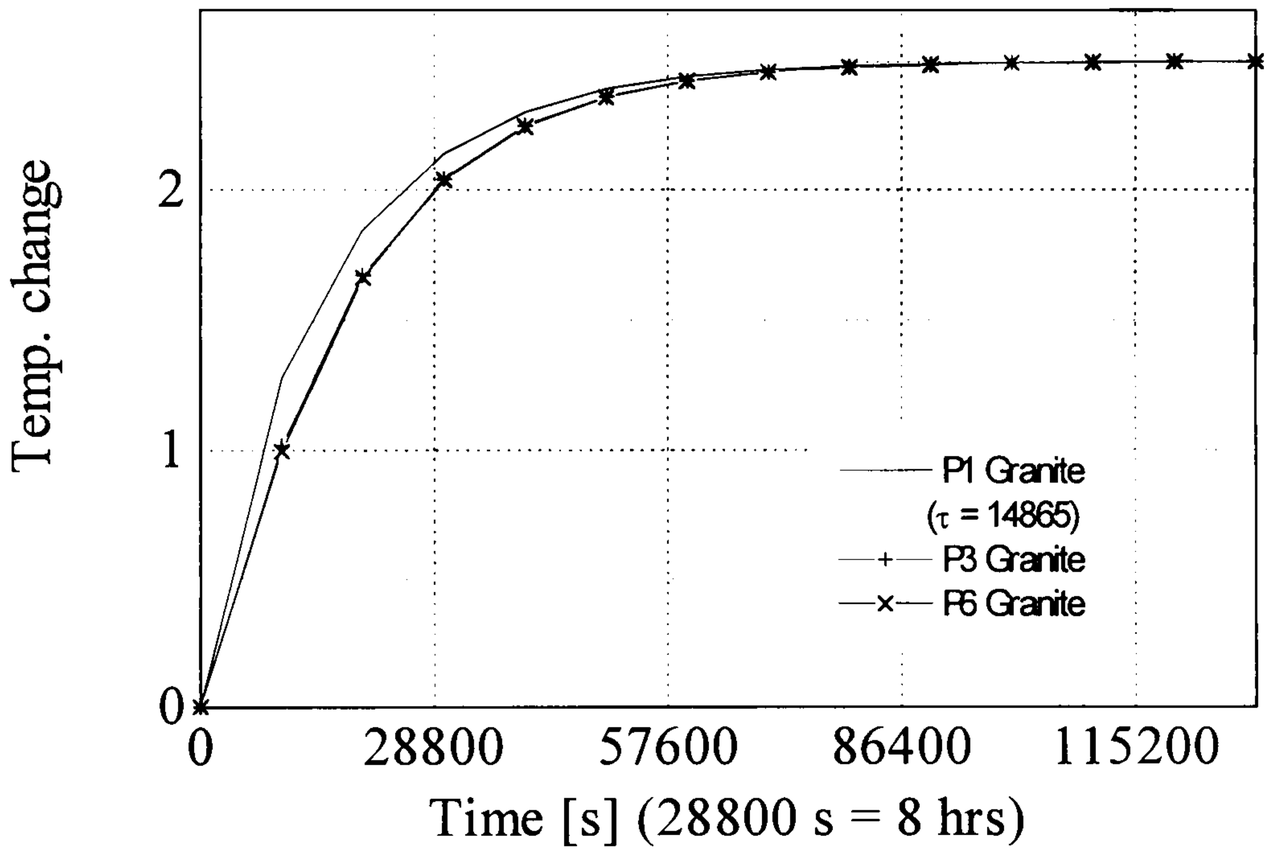

Figure A.11
1 deg step temp. rise

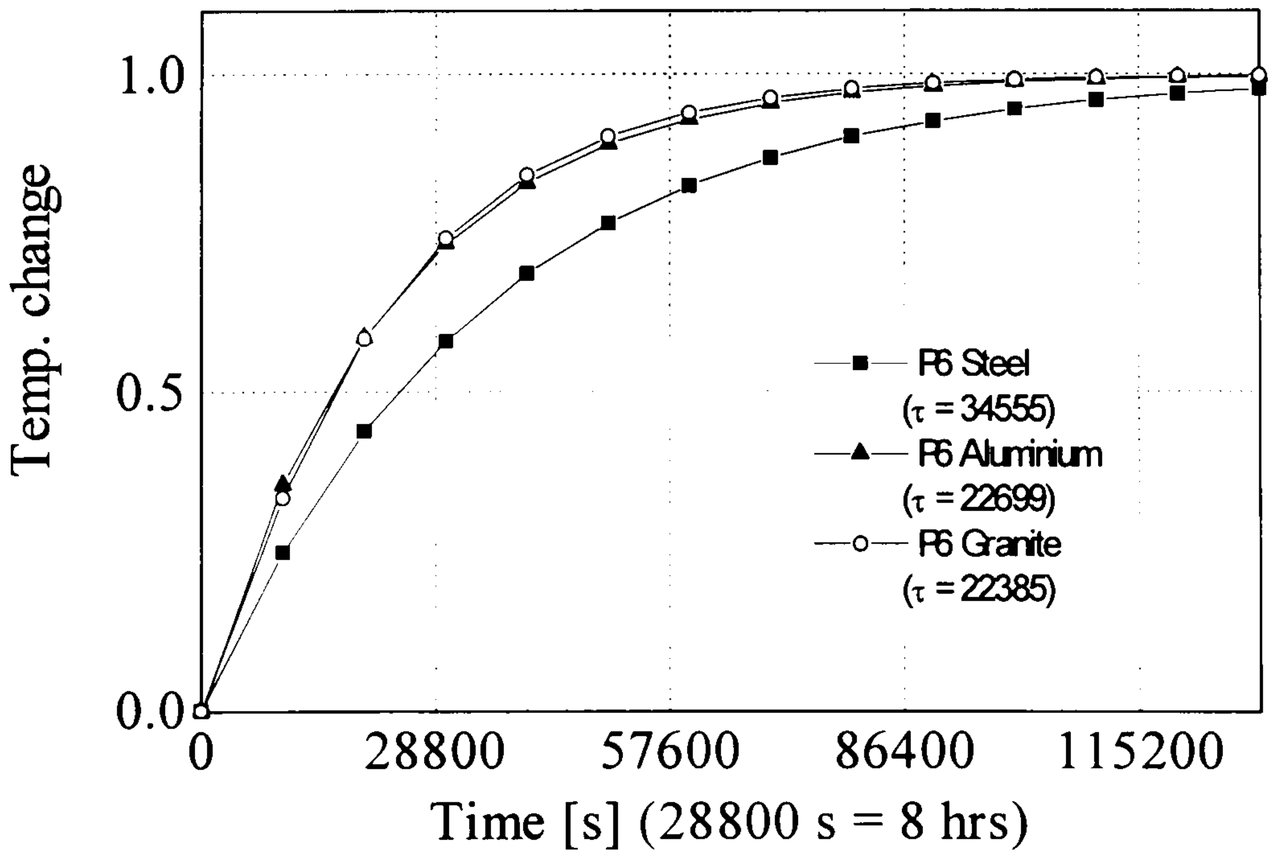

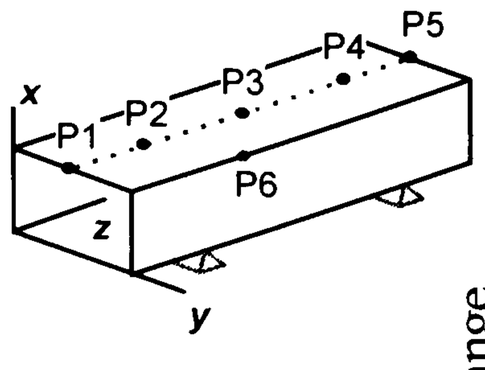

Figure A.12
1 deg step temp. rise

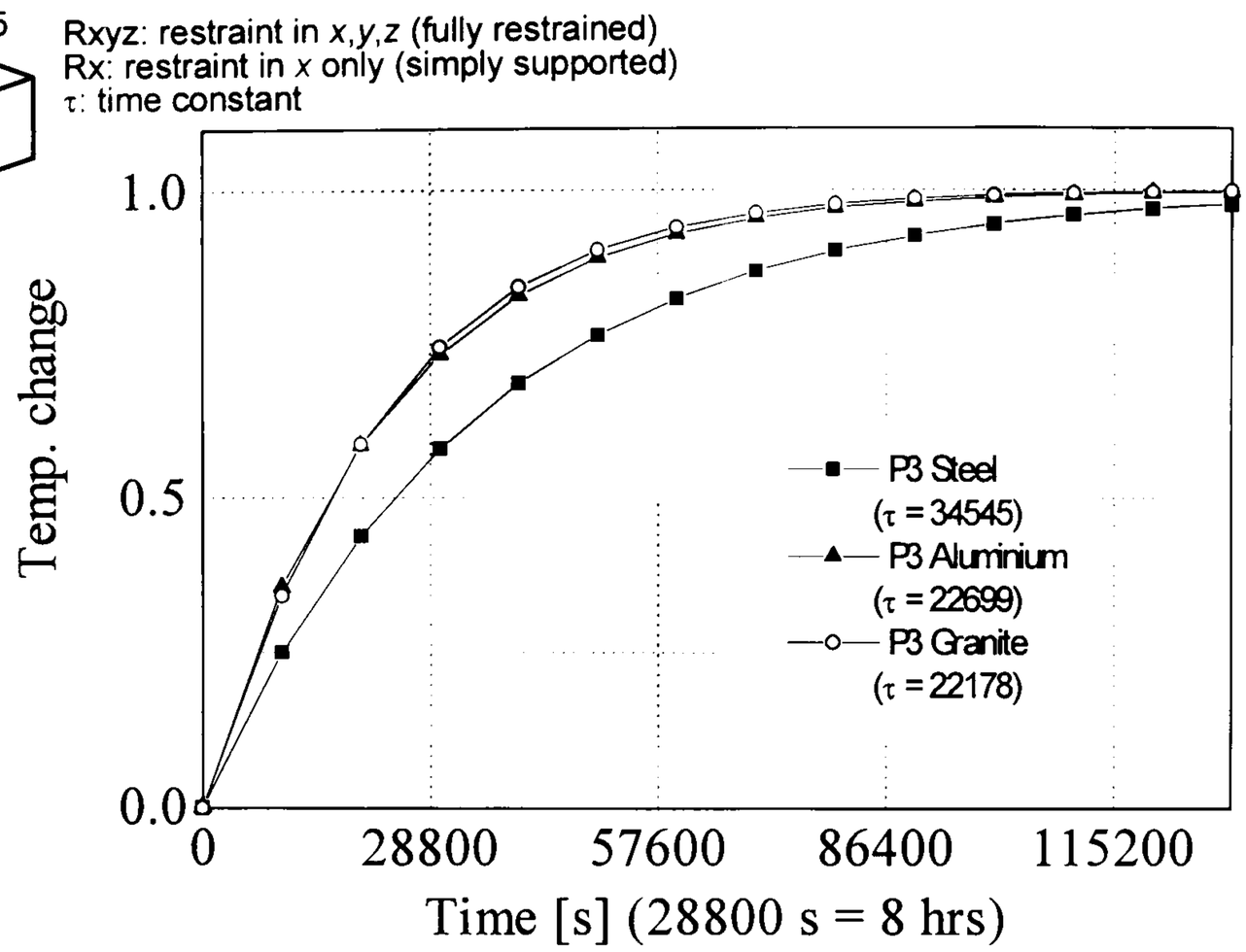

Figure A.13
1 deg step temp. rise

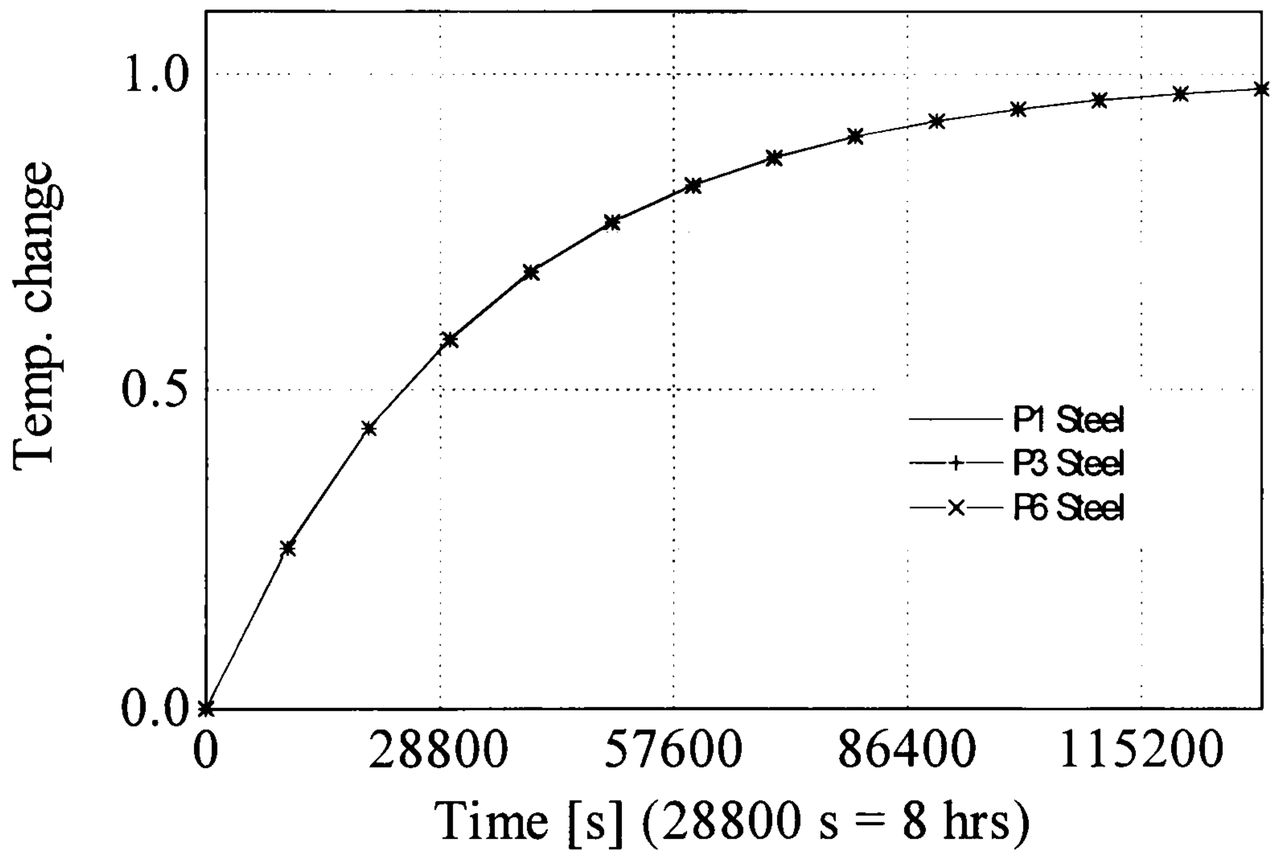

Figure A.14
1 deg step temp. rise

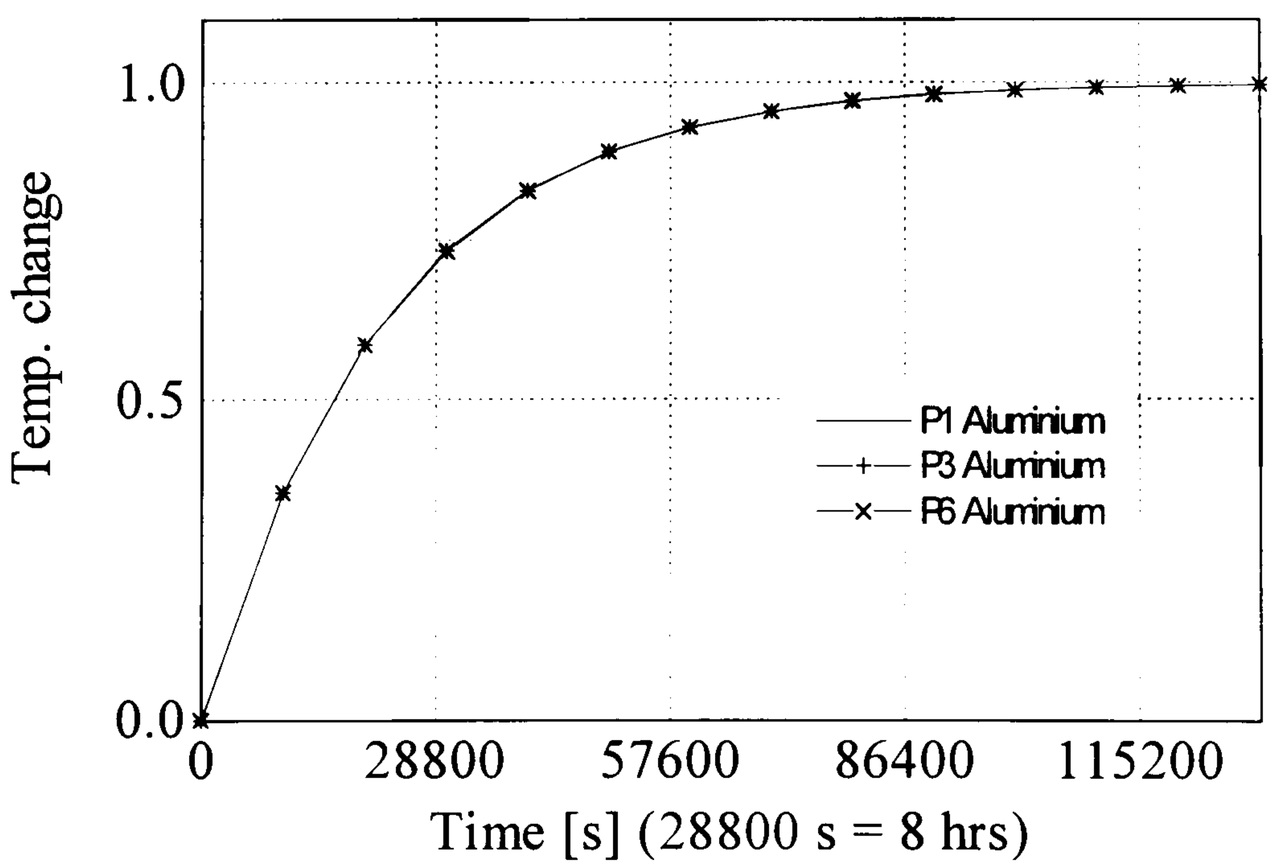

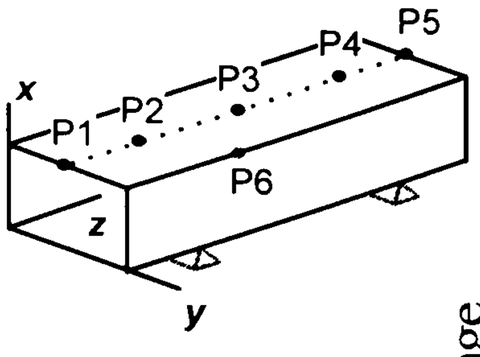

Figure A.15
1 deg step temp. rise

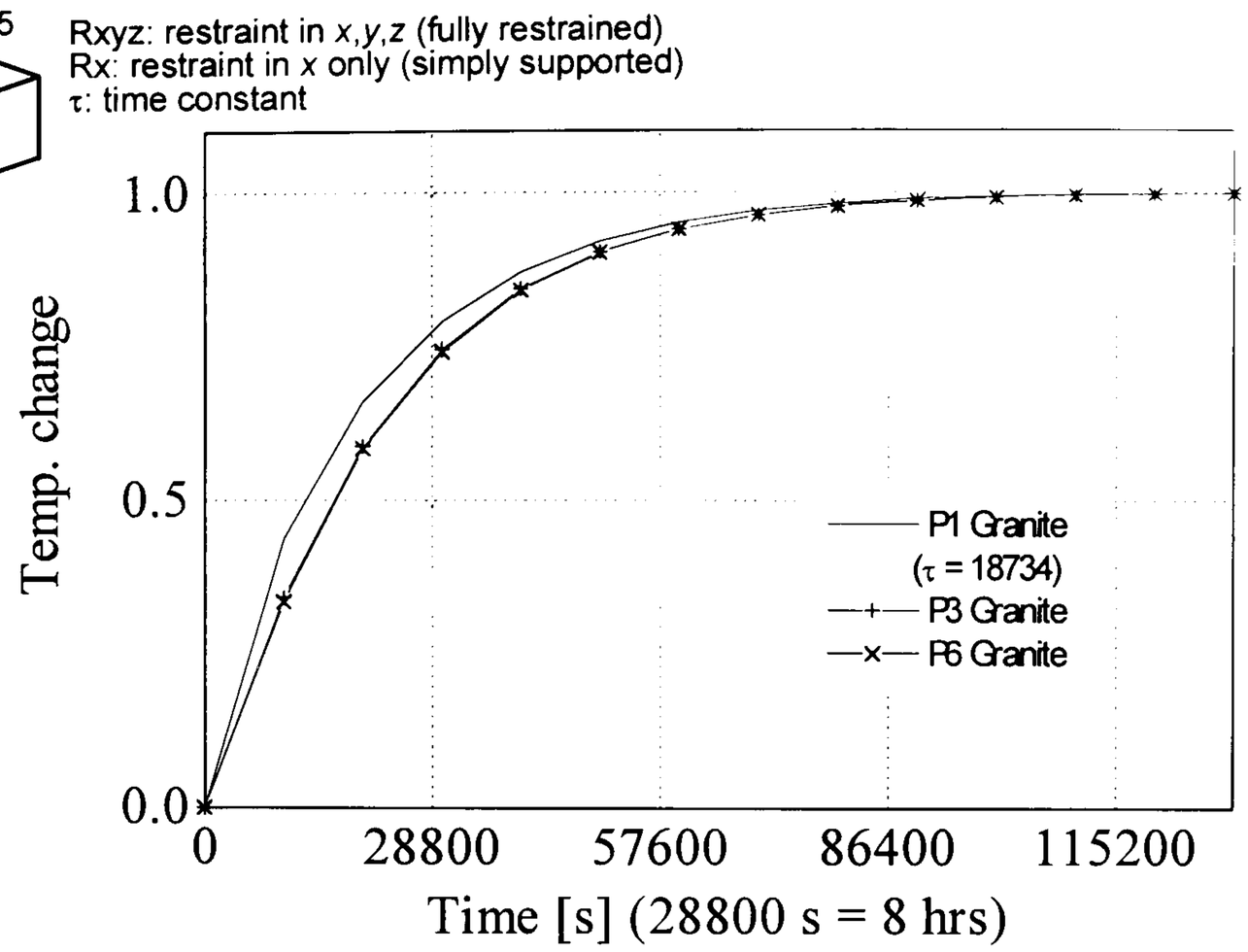

Figure A.16
5 deg step temp. rise

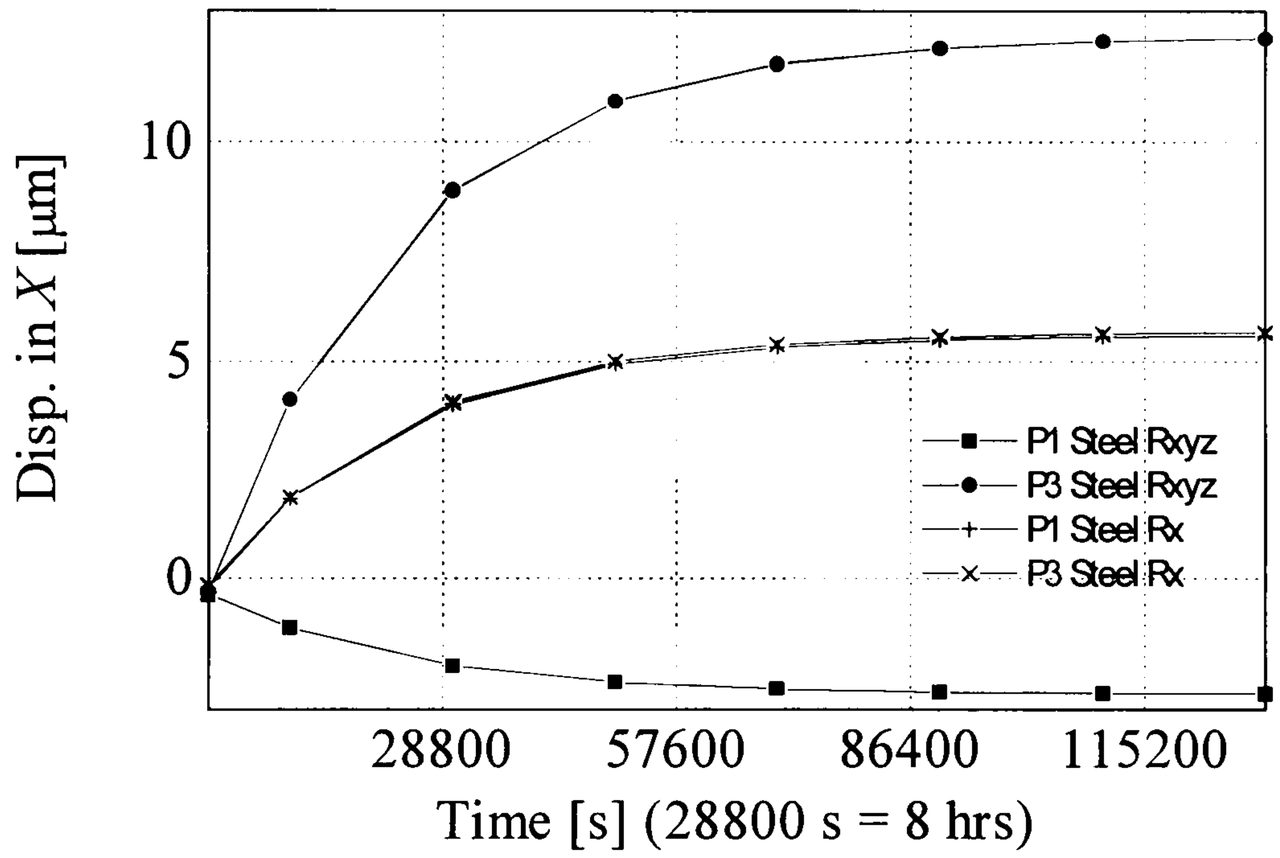

Figure A.17
2.5 deg step temp. rise

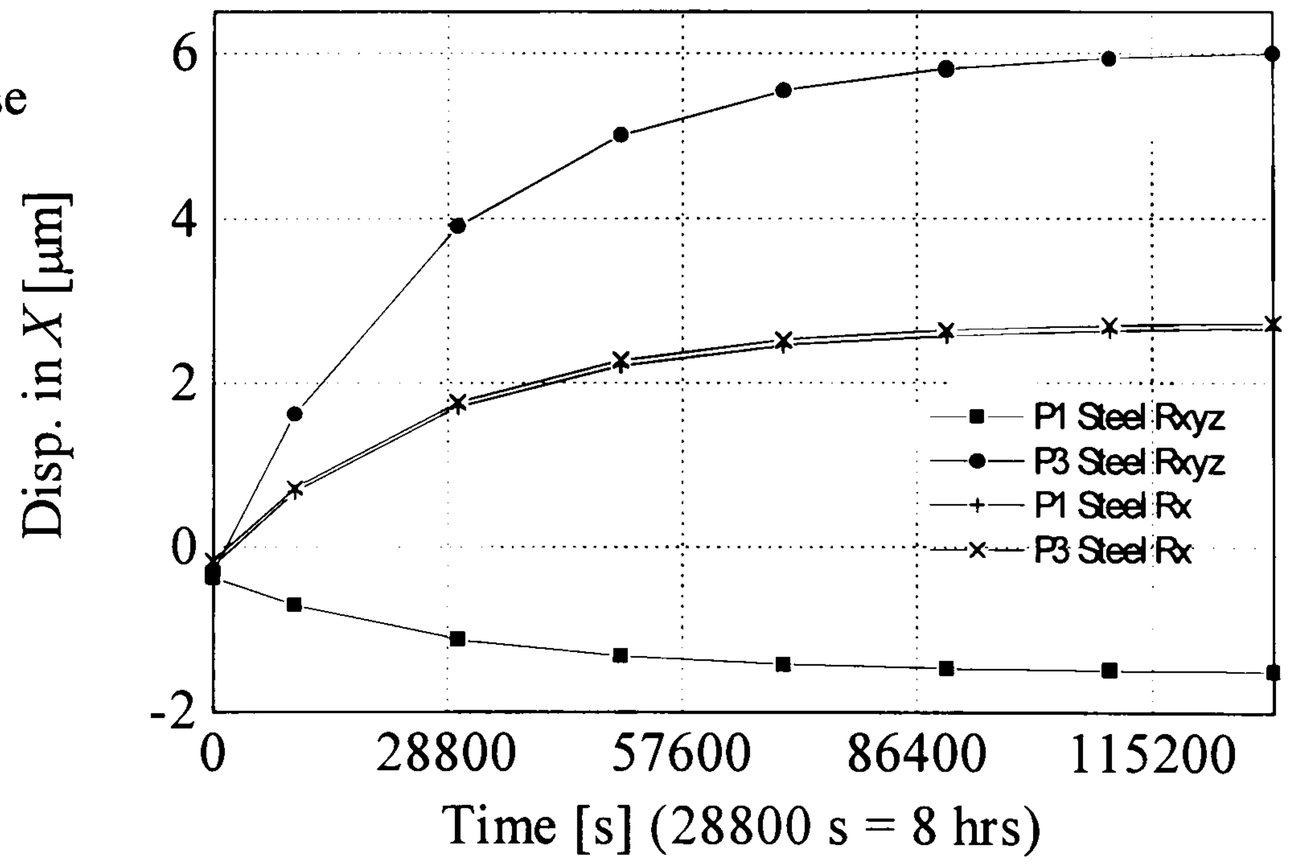

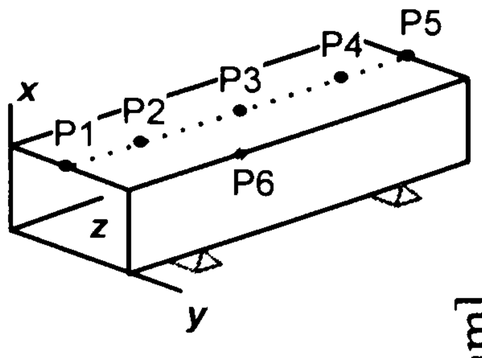

Figure A.18
1 deg step temp. rise

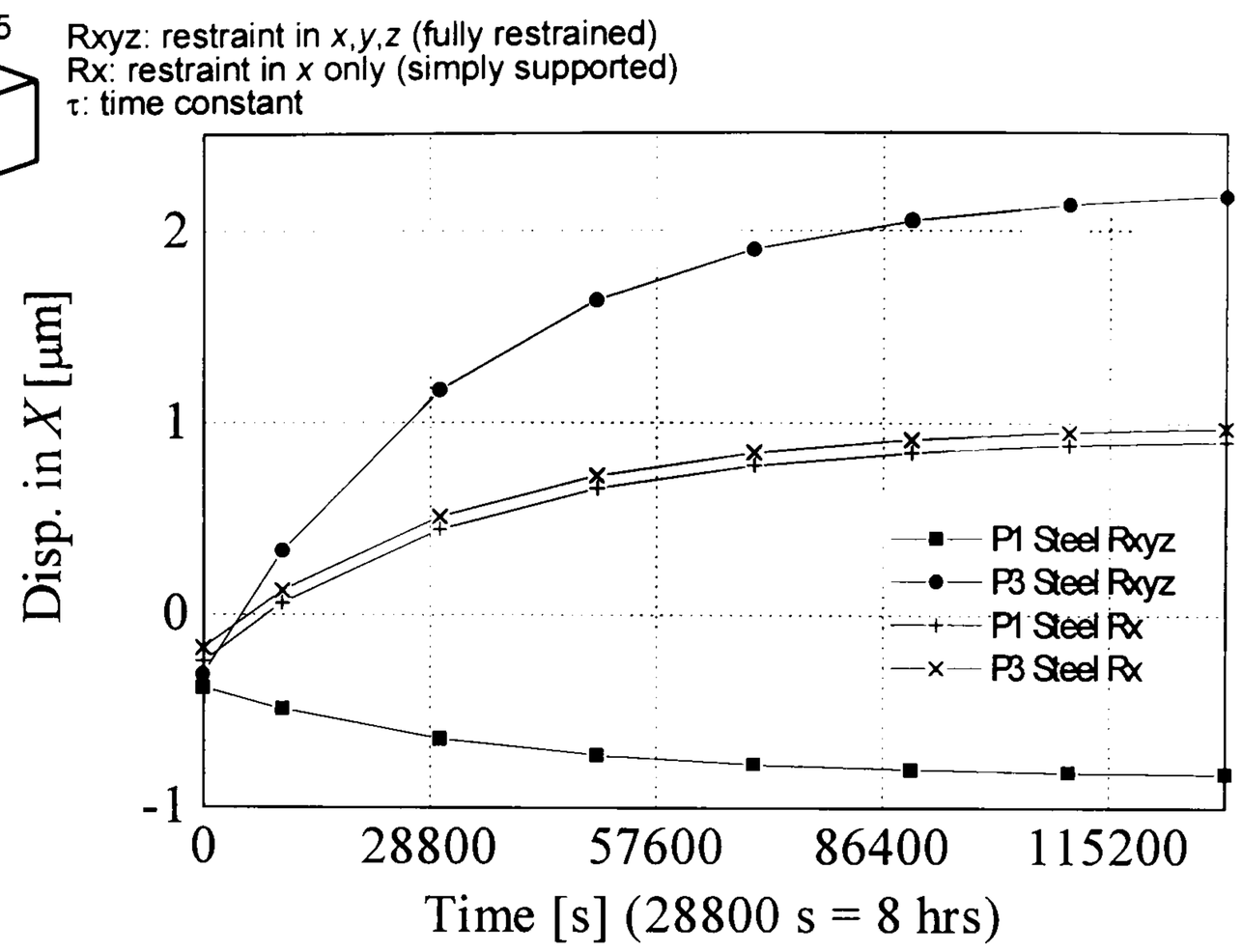

Figure A.19
5 deg step temp. rise

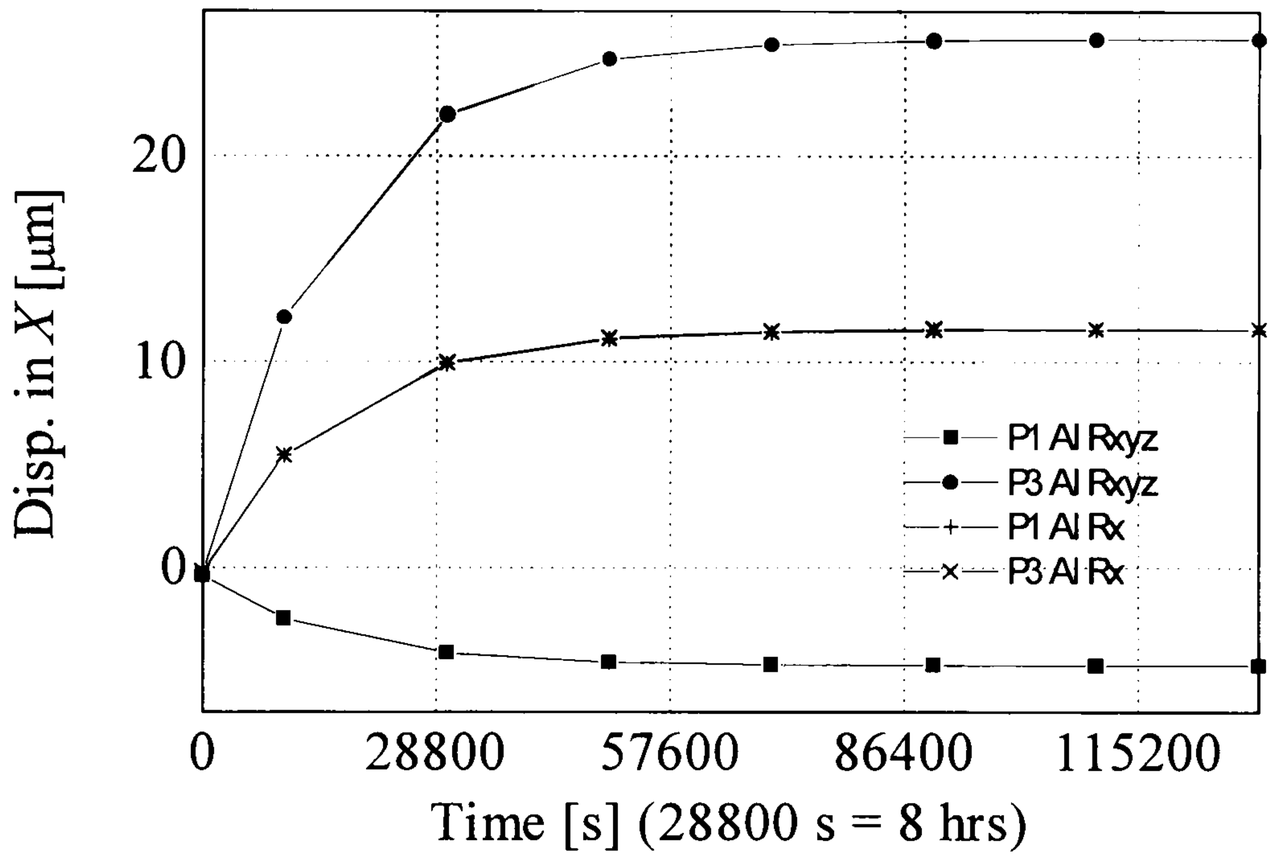

Figure A.20
2.5 deg step temp. rise

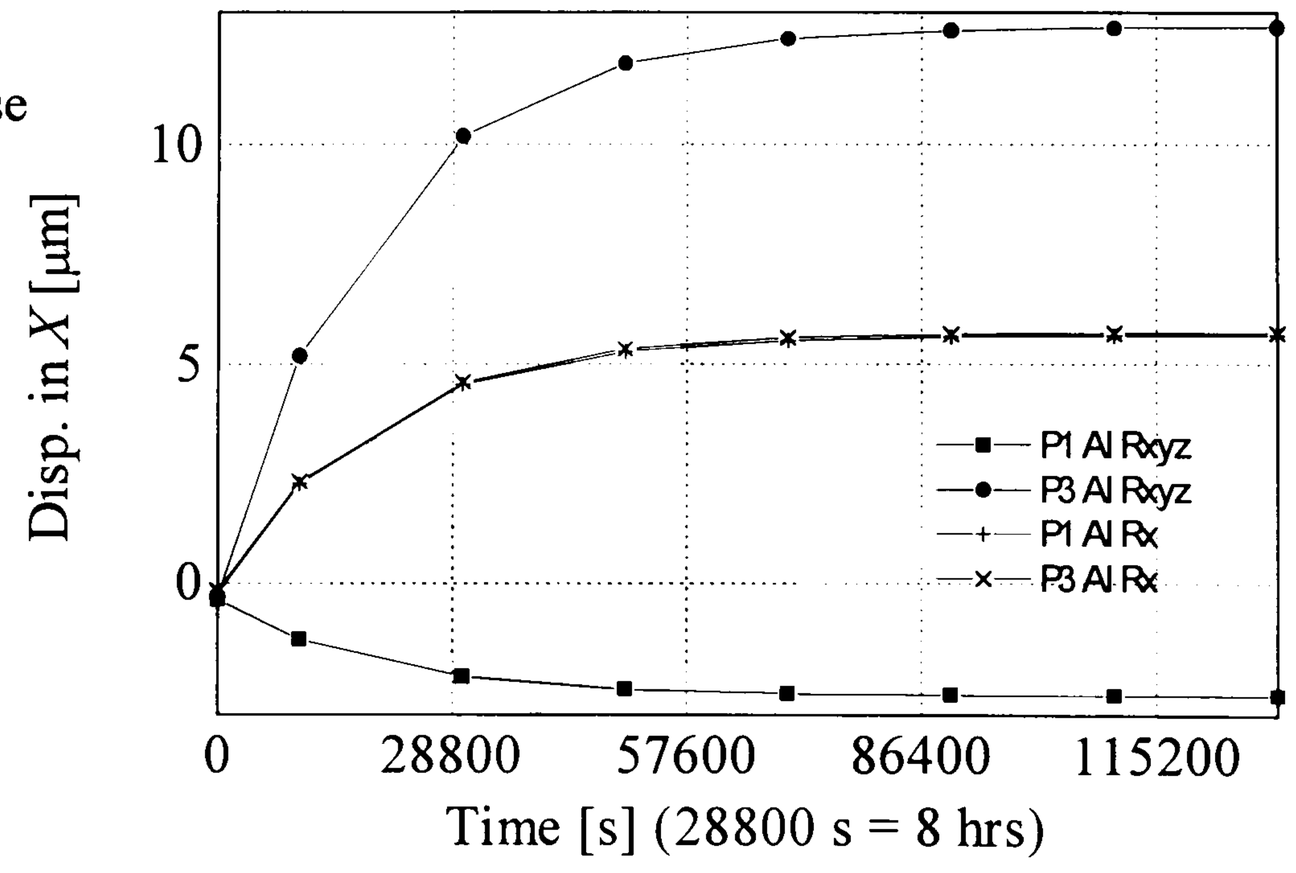

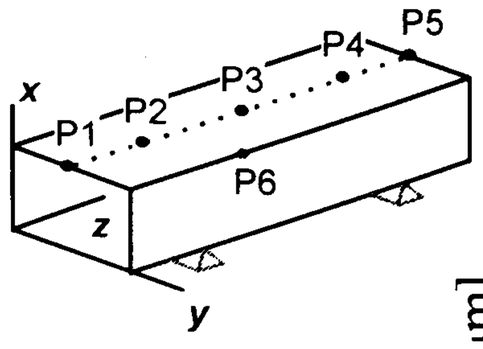

Figure A.21
1 deg step temp. rise

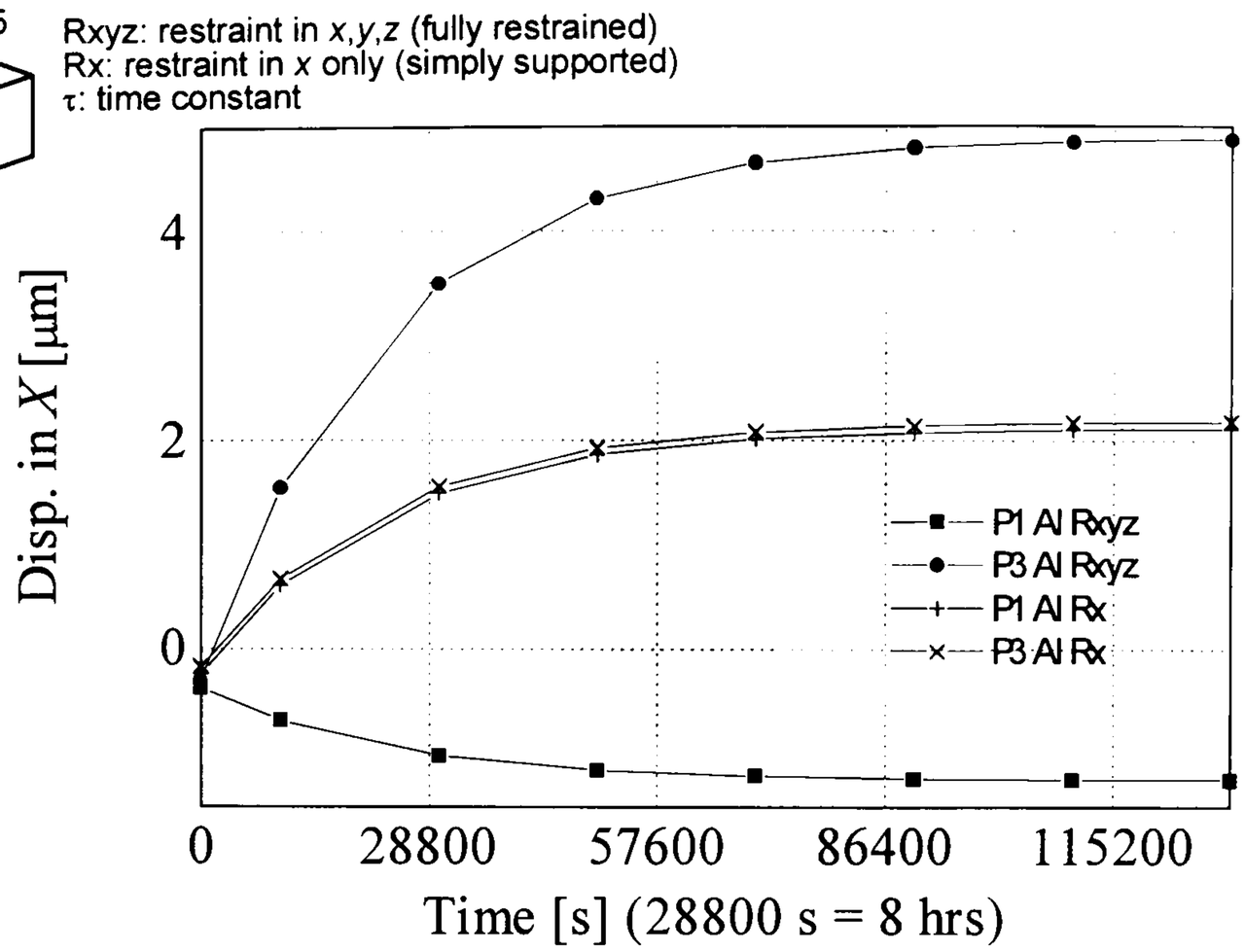

Figure A.22
5 deg step temp. rise

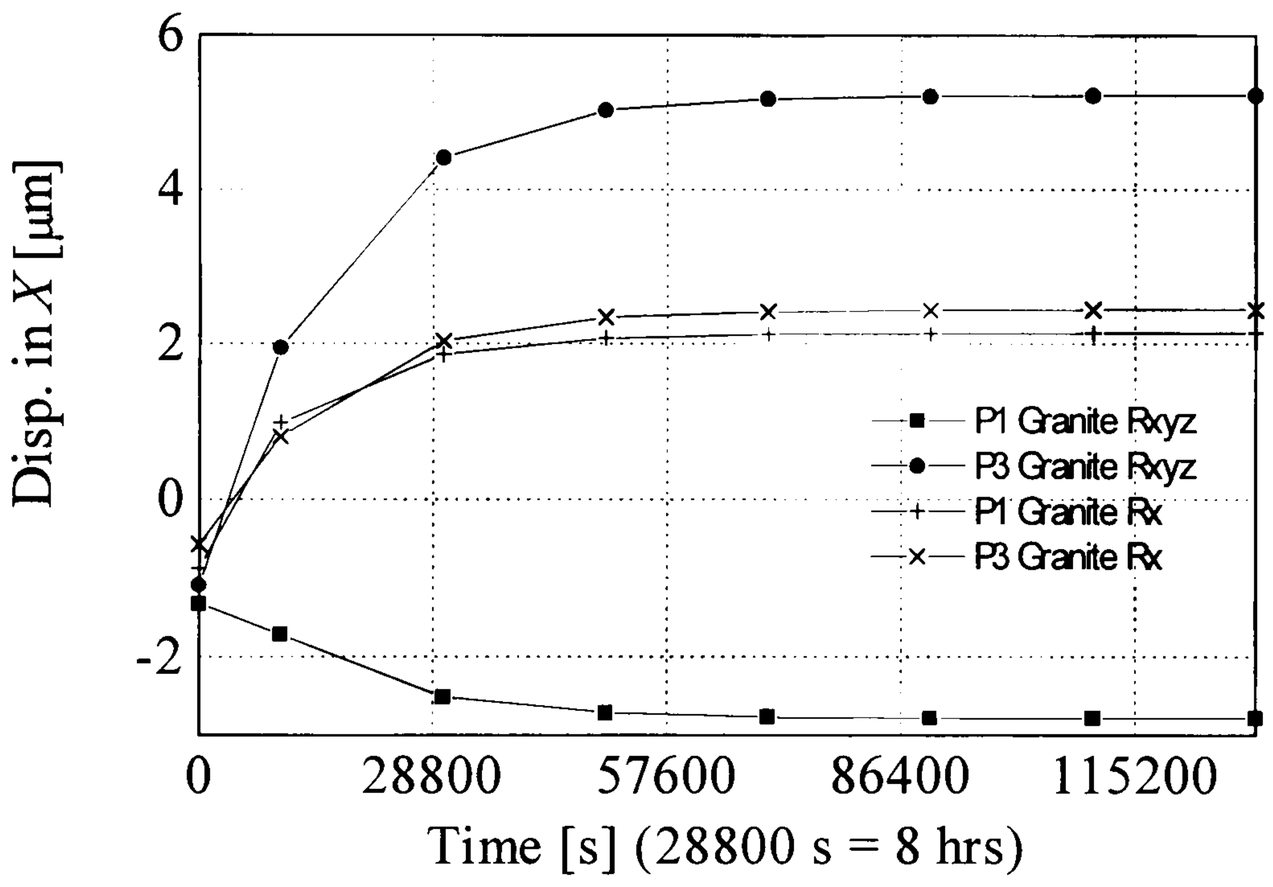

Figure A.23
2.5 deg step temp. rise

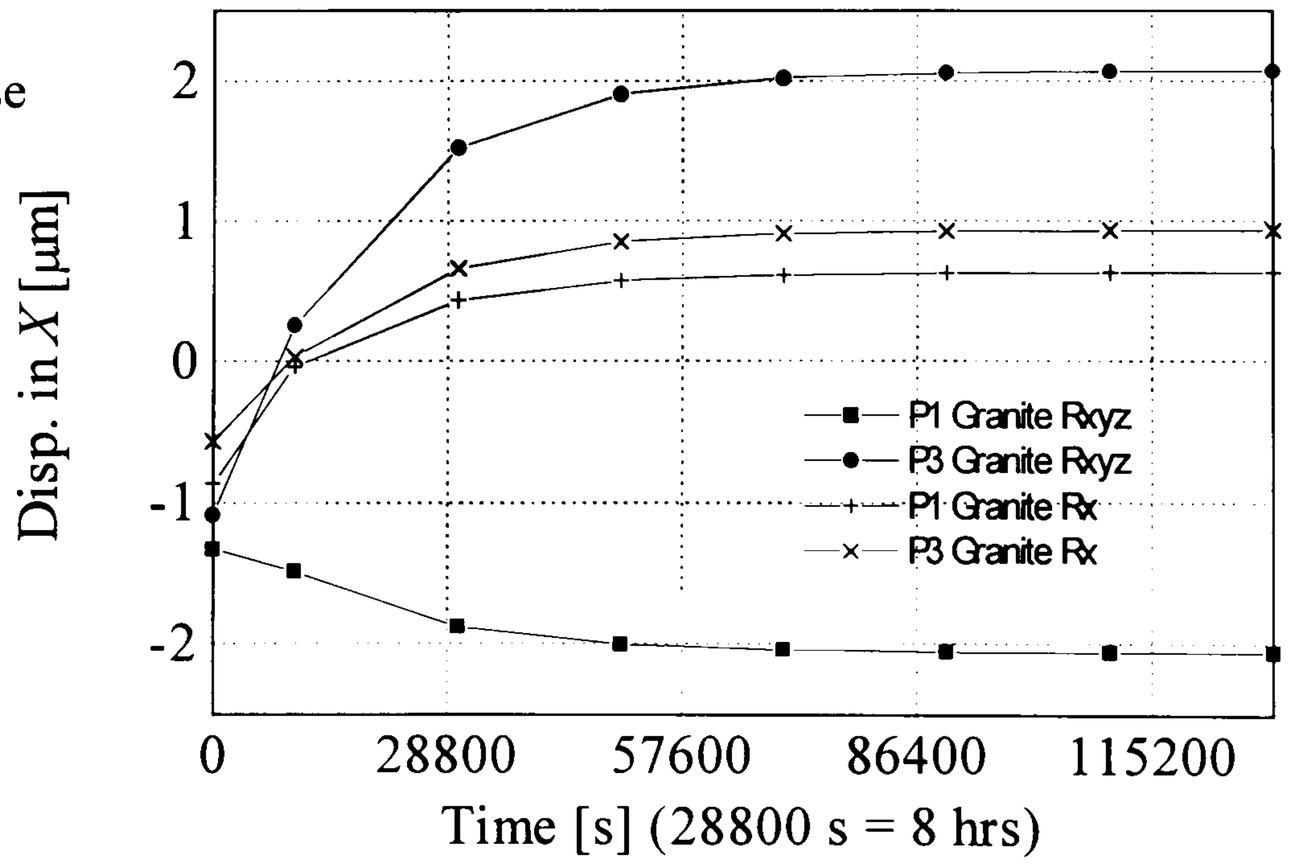

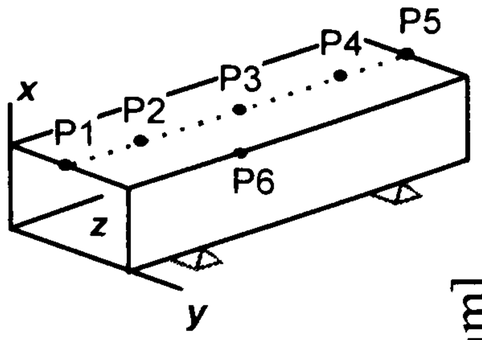

Figure A.24
1 deg step temp. rise

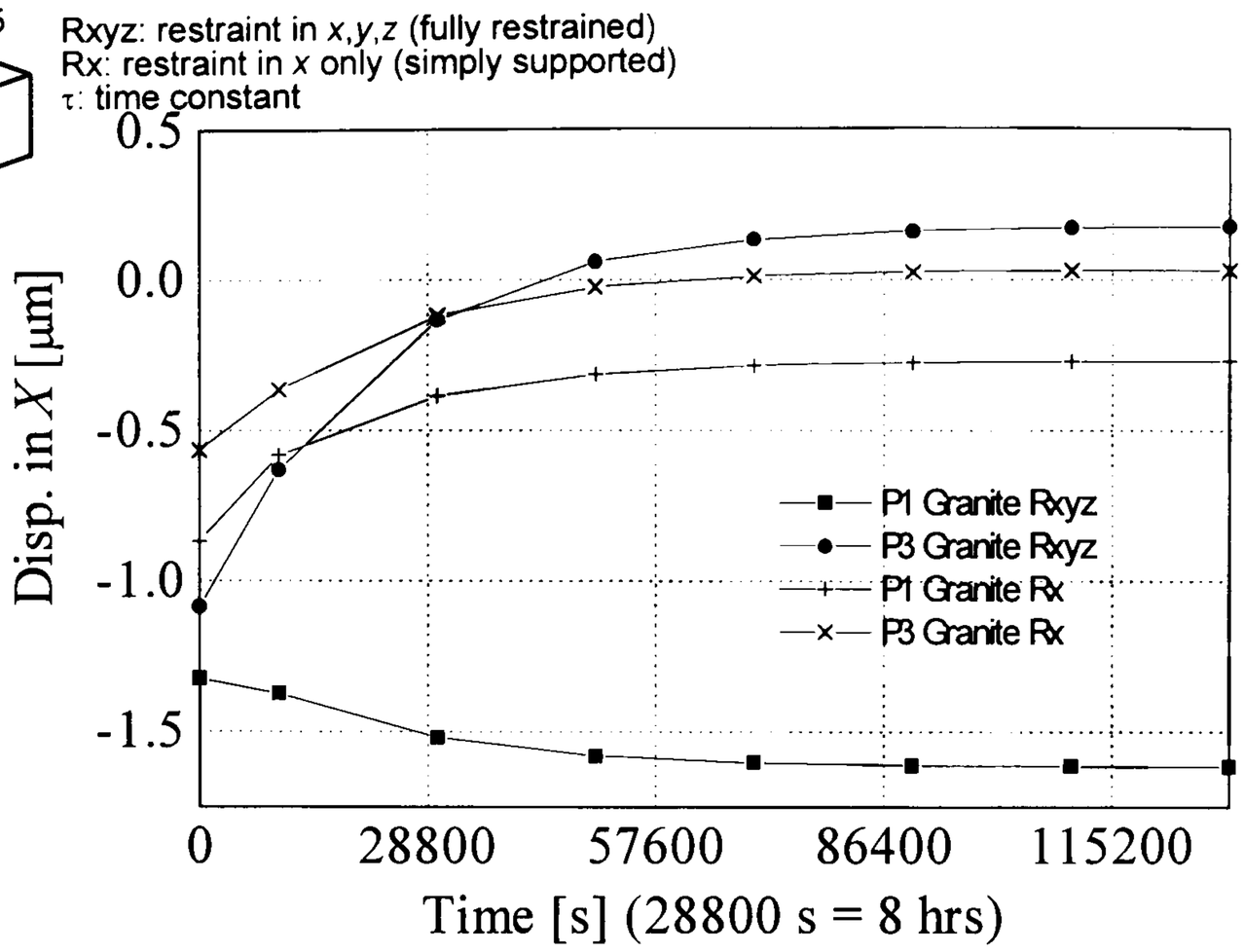

Figure A.25
Magnitudes of
step temp. rise
and corresponding
maximum
displacement

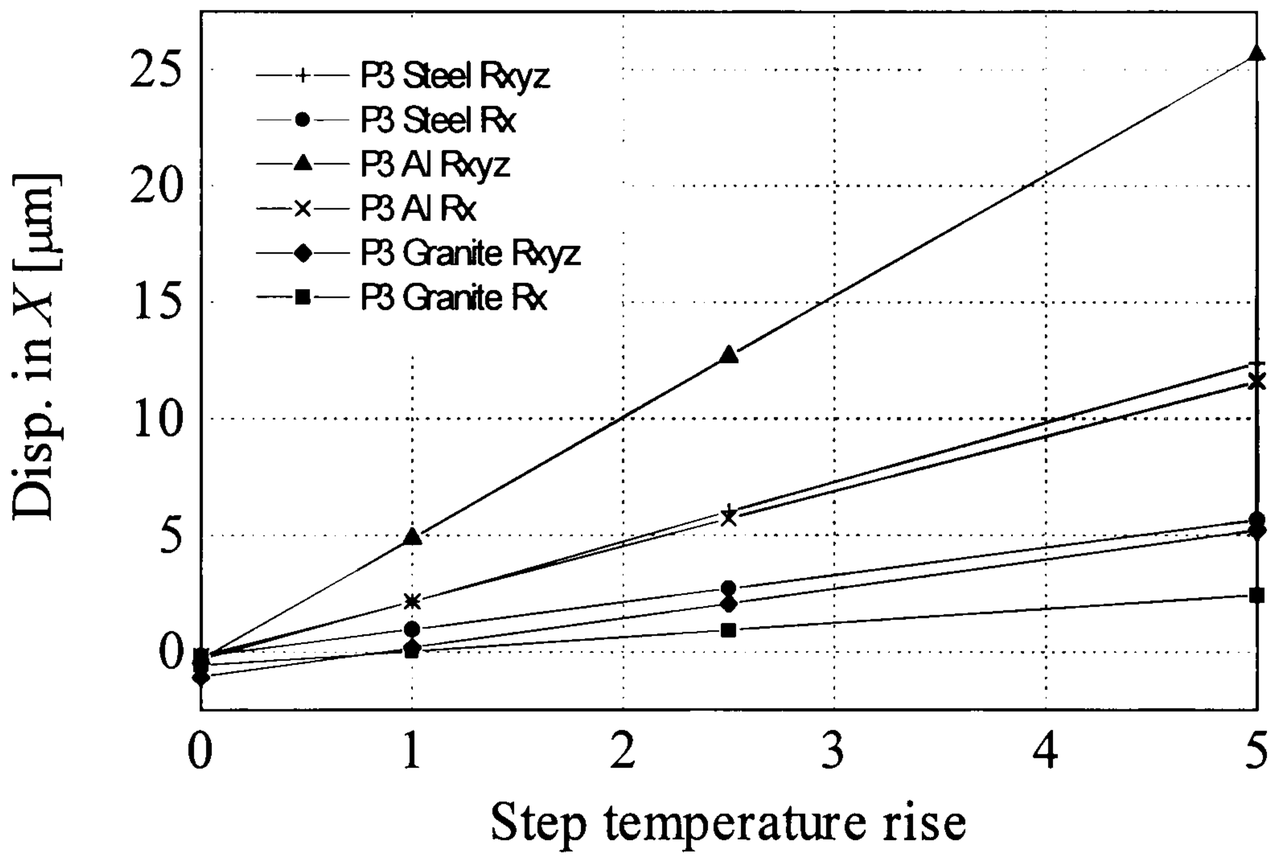

Figure A.26
Steel
1 deg step temp. rise
Rxyz

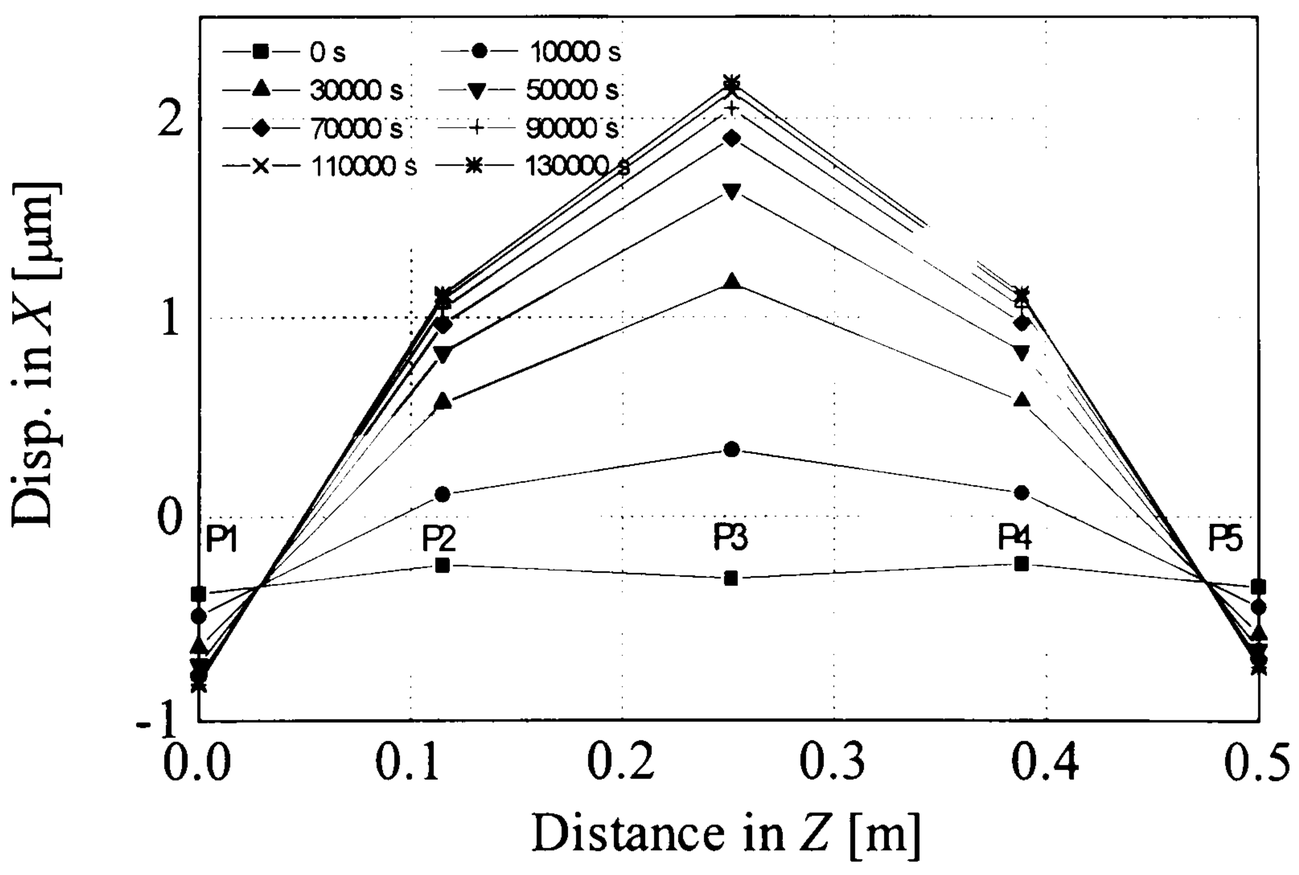

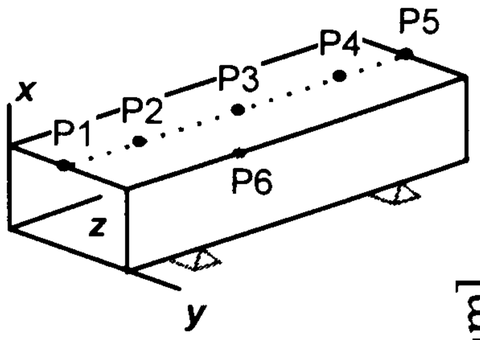

Figure A.27
Steel
1 deg step temp. rise
Rxyz

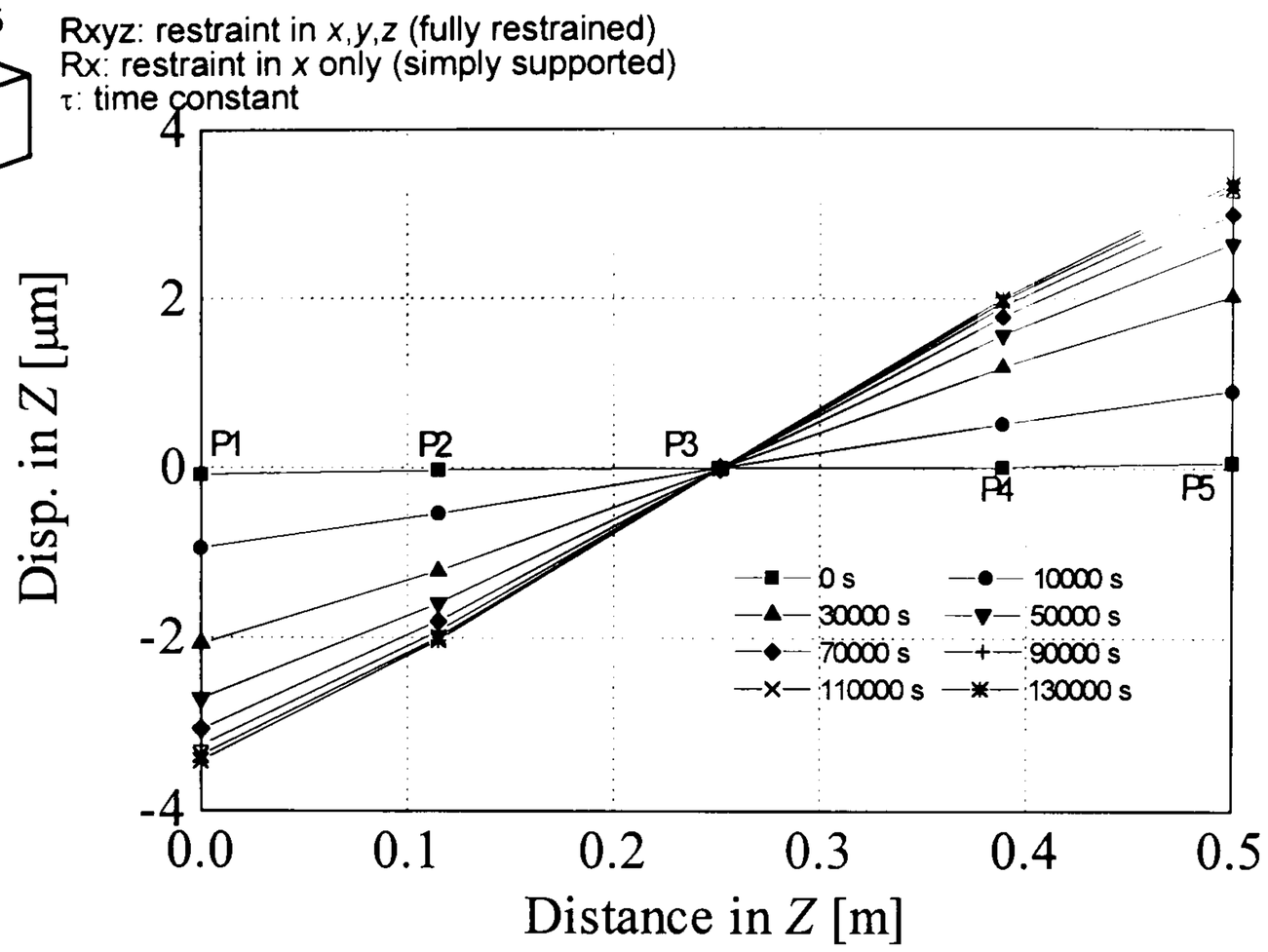

Figure A.28
Steel
1 deg step temp. rise
Rx

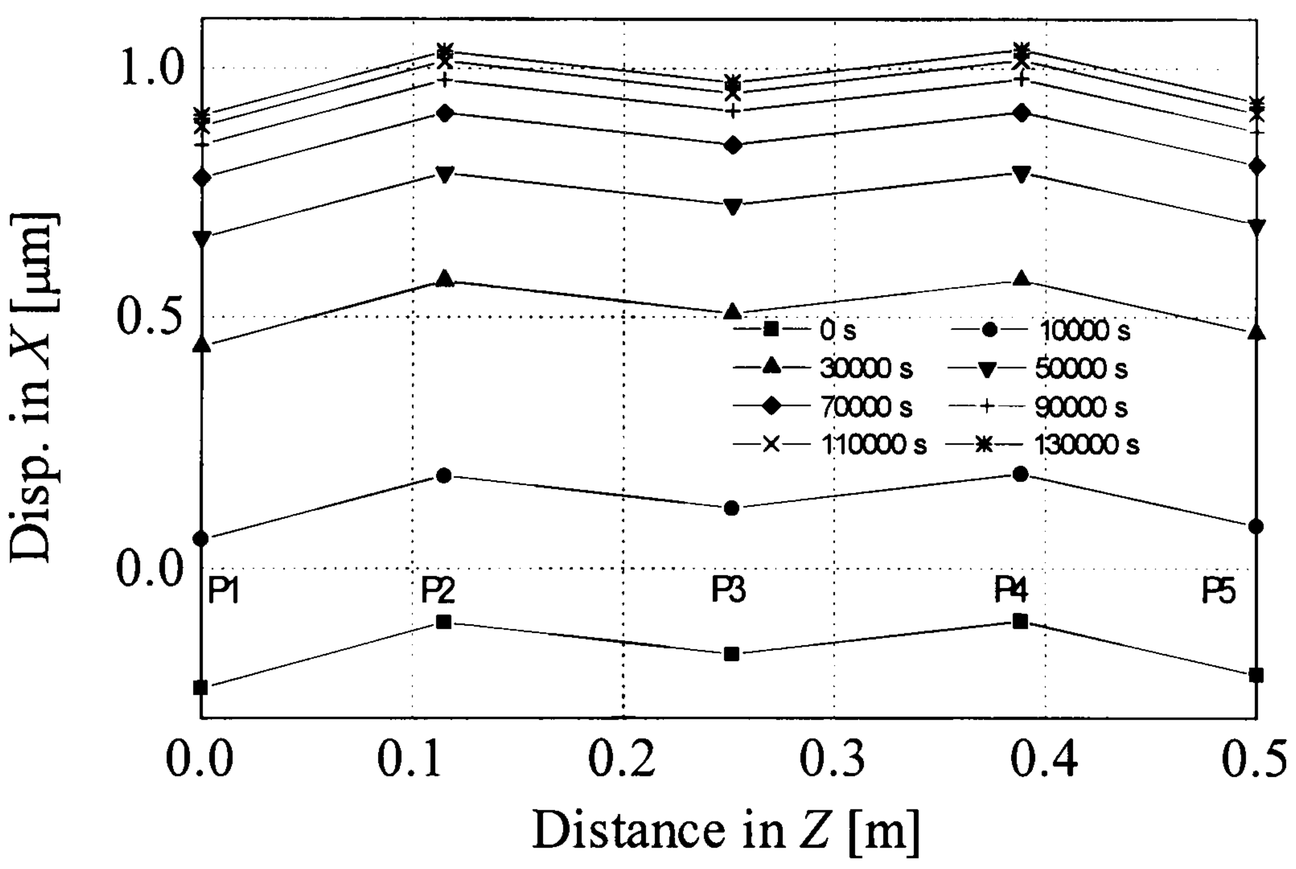

Figure A.29
Steel
1 deg step temp. rise
Rx

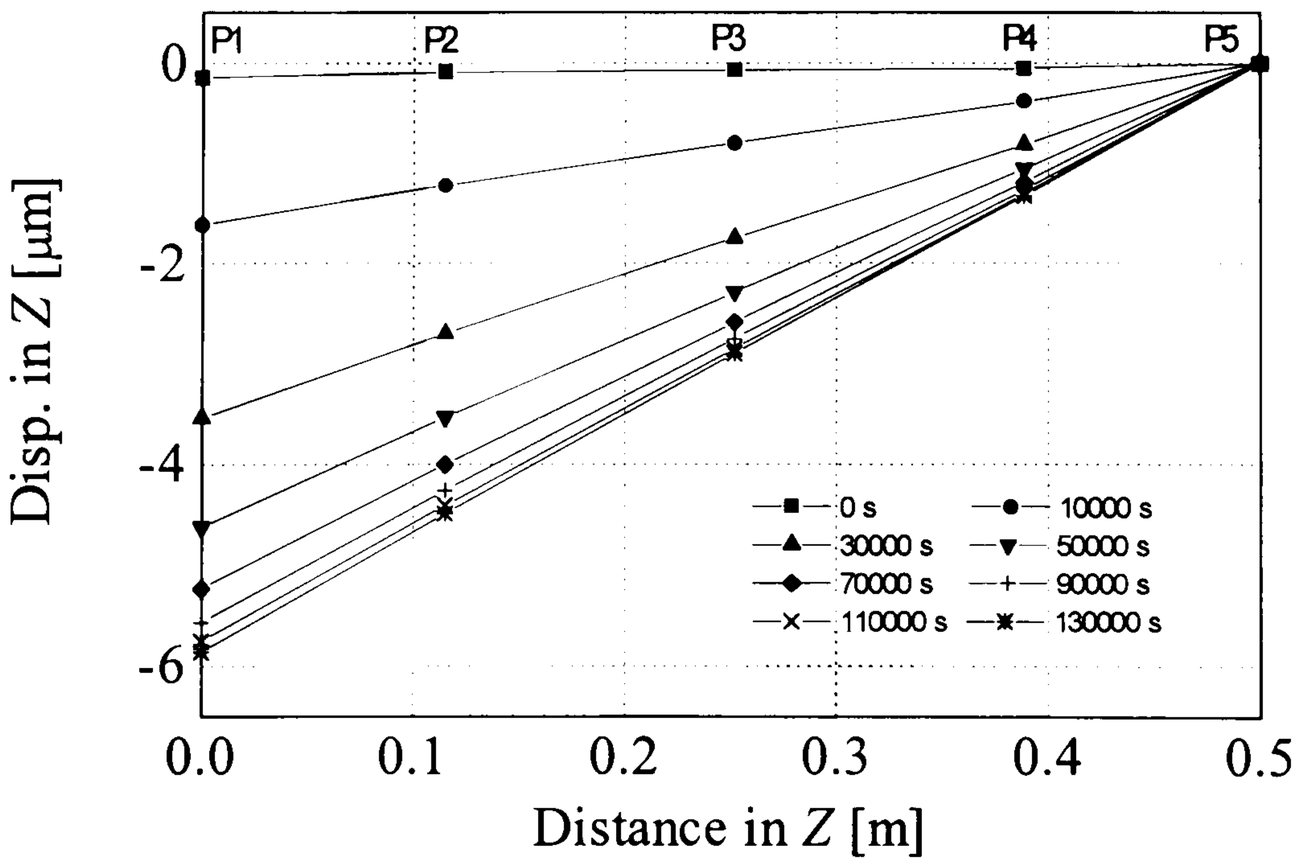

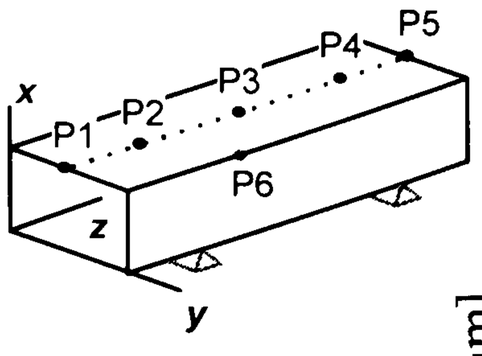

Figure A.30
Aluminium
1 deg step temp. rise
Rxyz

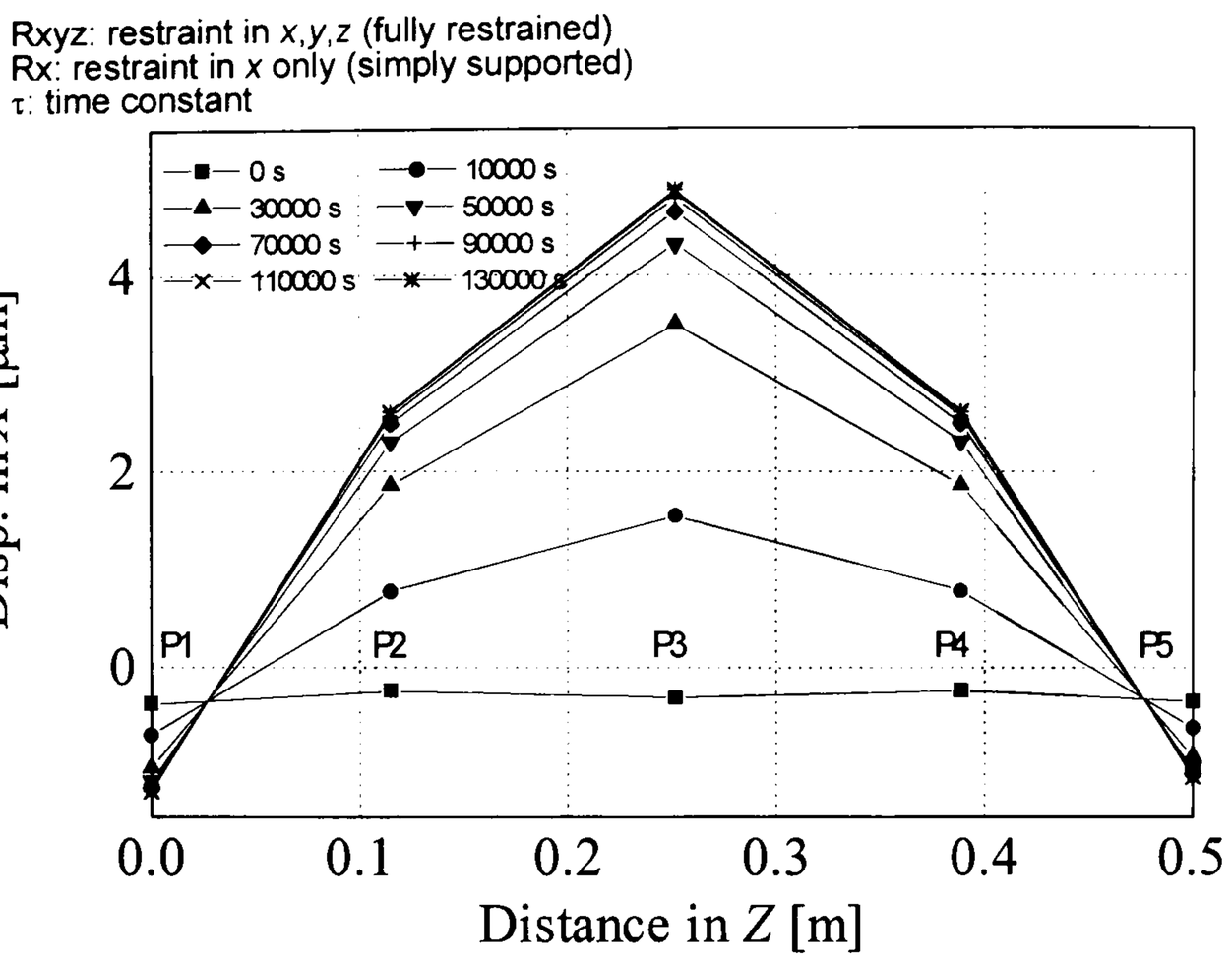

Figure A.31
Aluminium
1 deg step temp. rise
Rxyz

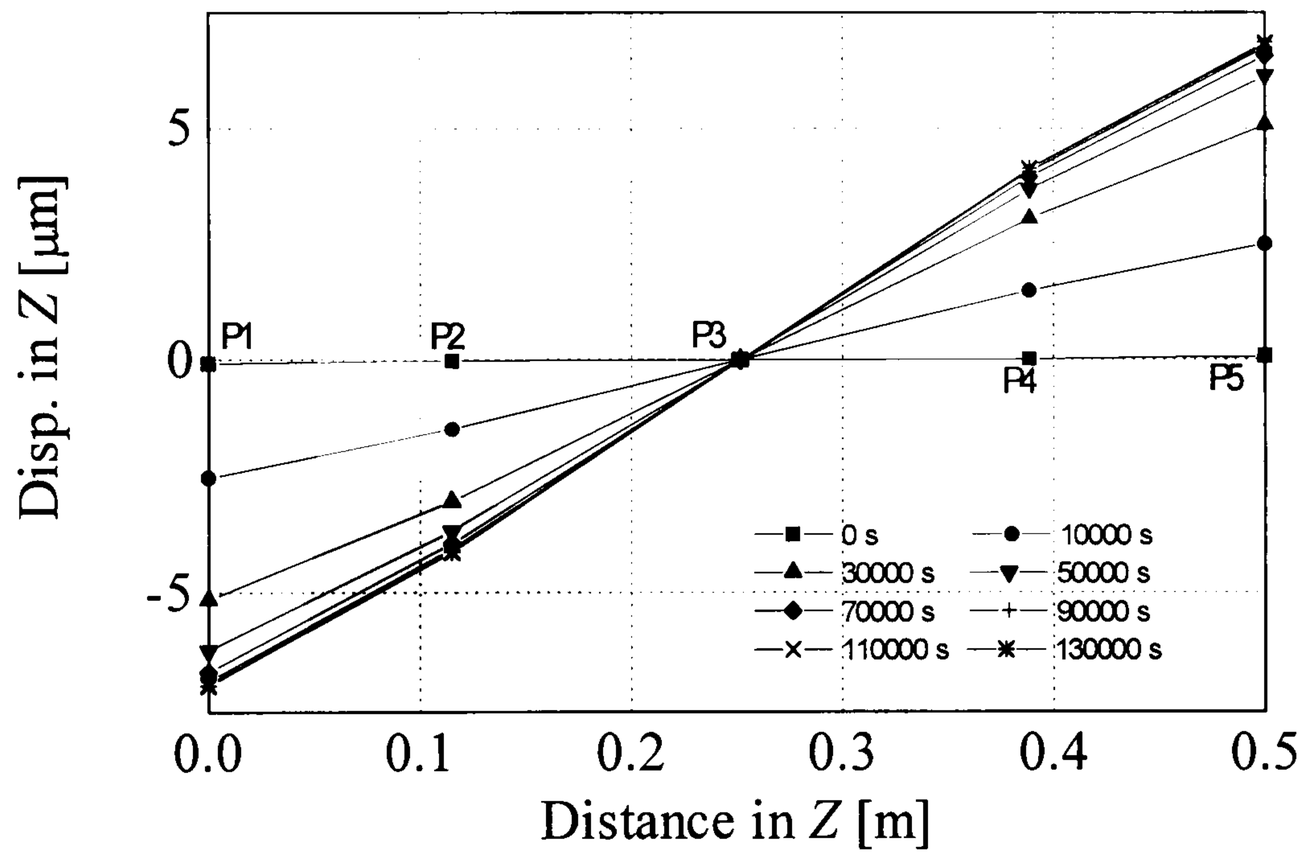

Figure A.32
Aluminium
1 deg step temp. rise
Rx

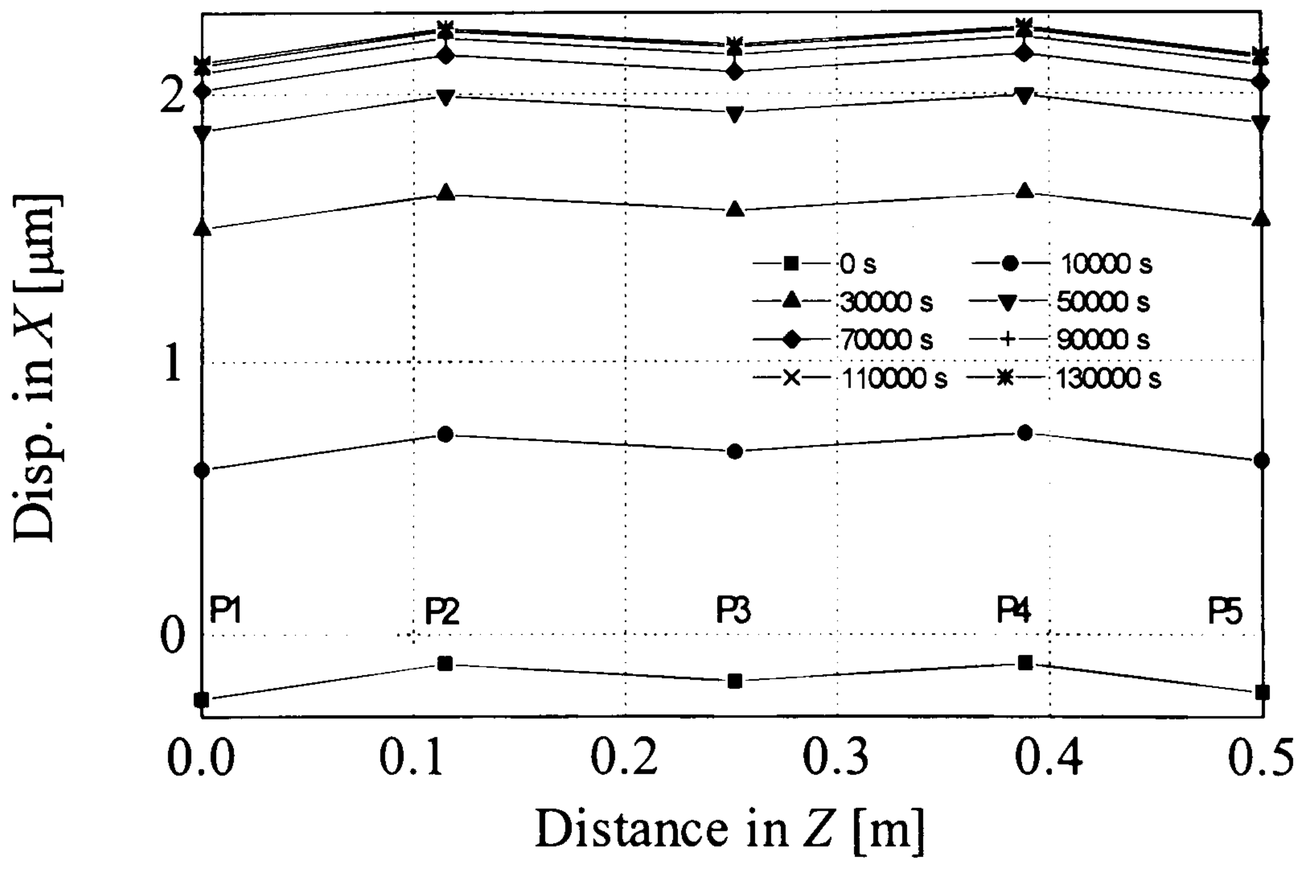

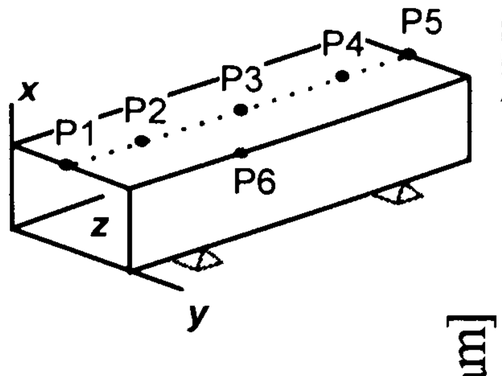

Figure A.33
Aluminium
1 deg step temp. rise
Rx

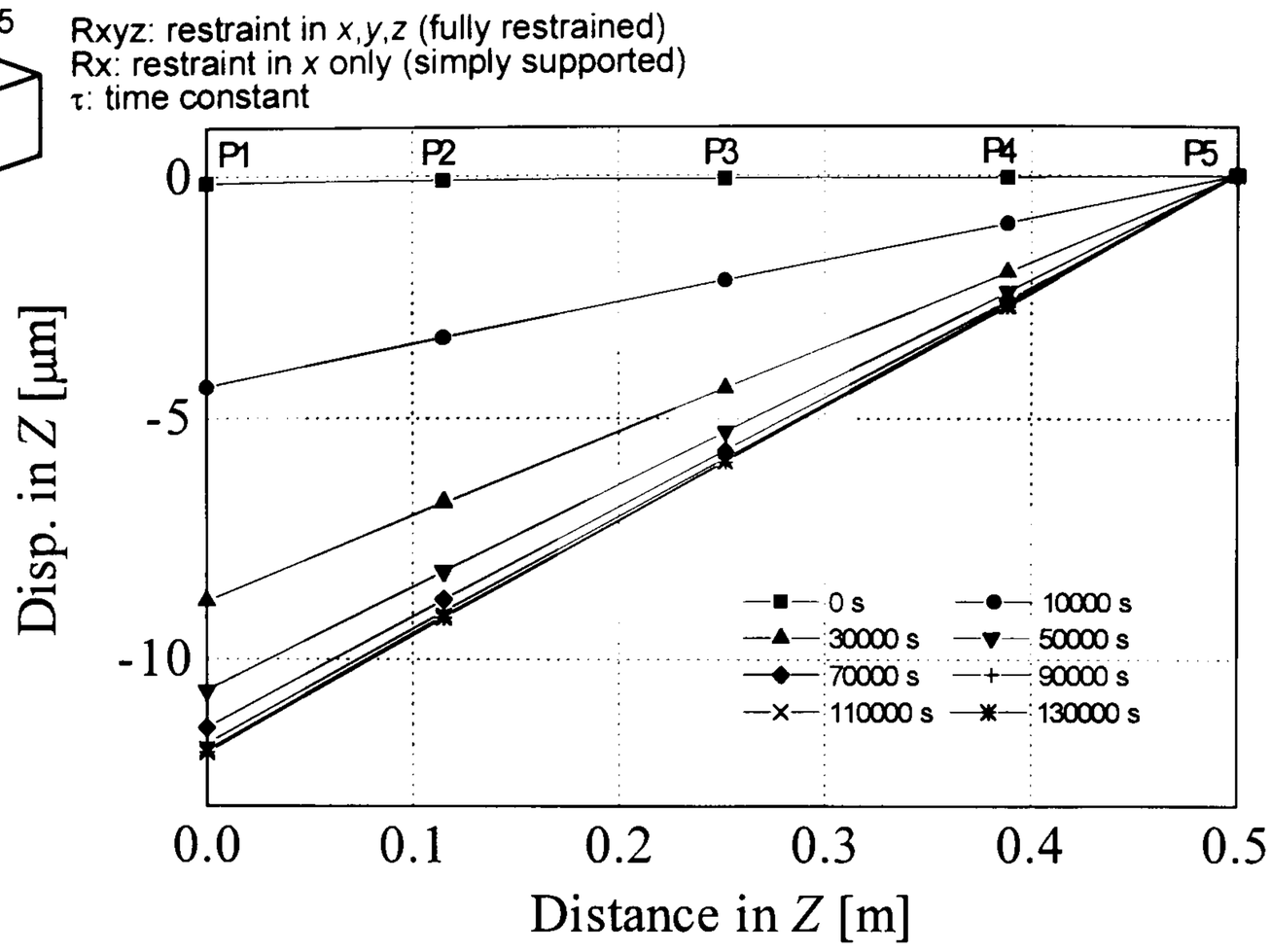

Figure A.34
Granite
1 deg step temp. rise
Rxyz

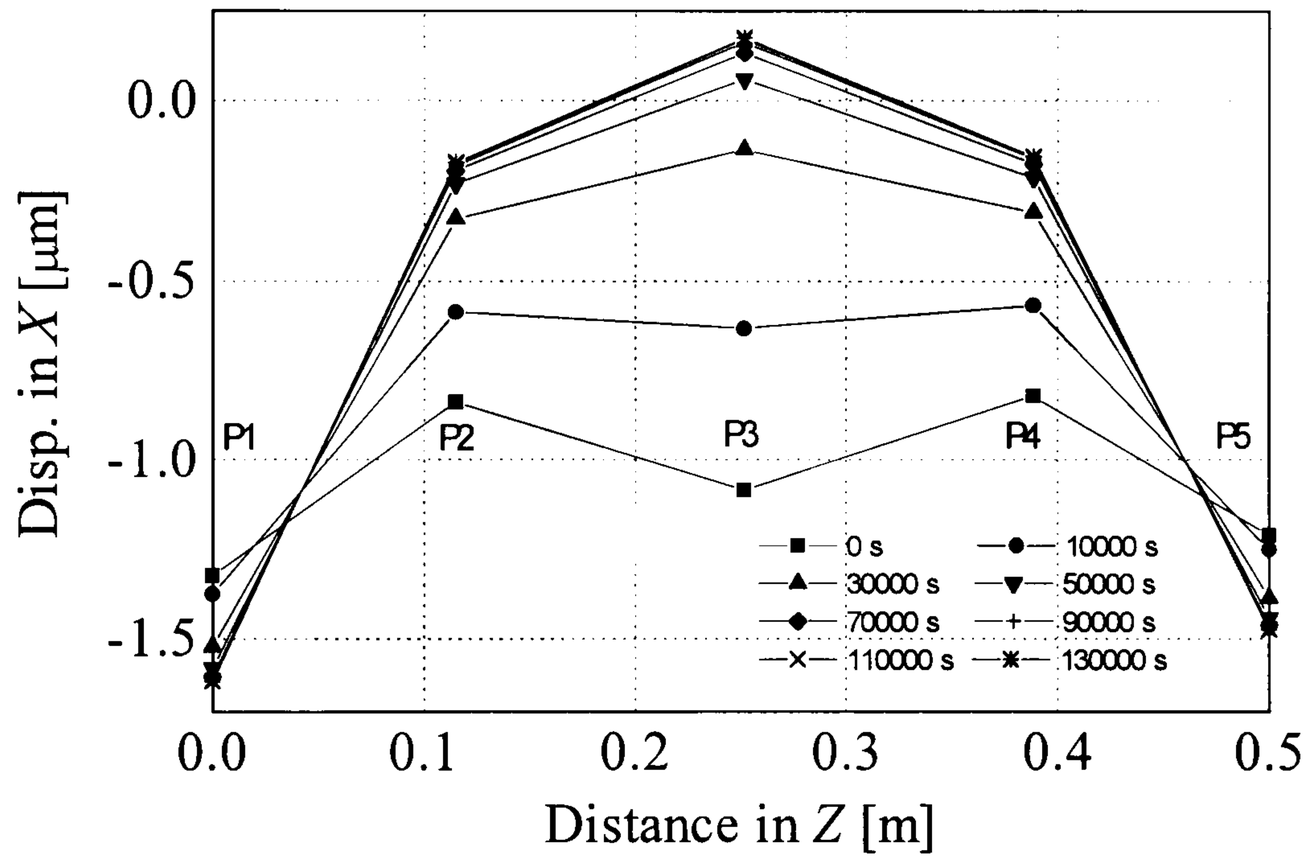

Figure A.35
Granite
1 deg step temp. rise
Rxyz

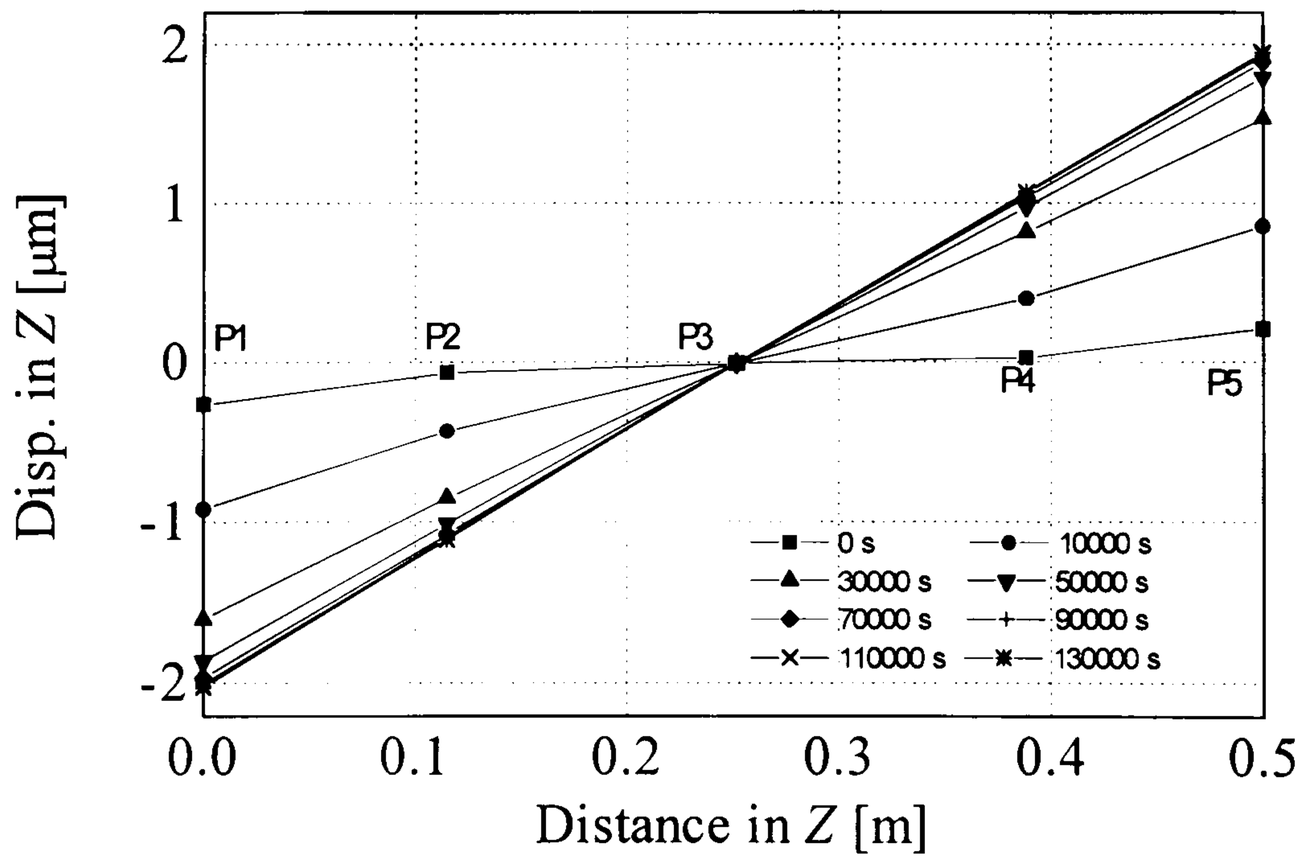

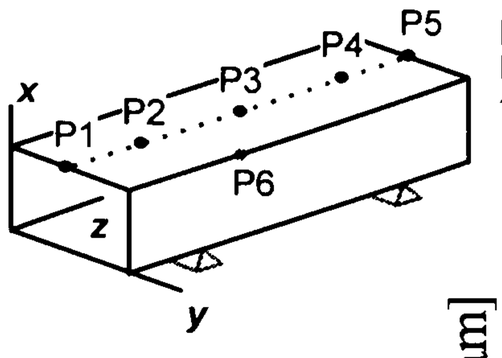

Figure A.36
Granite
1 deg step temp. rise
Rx

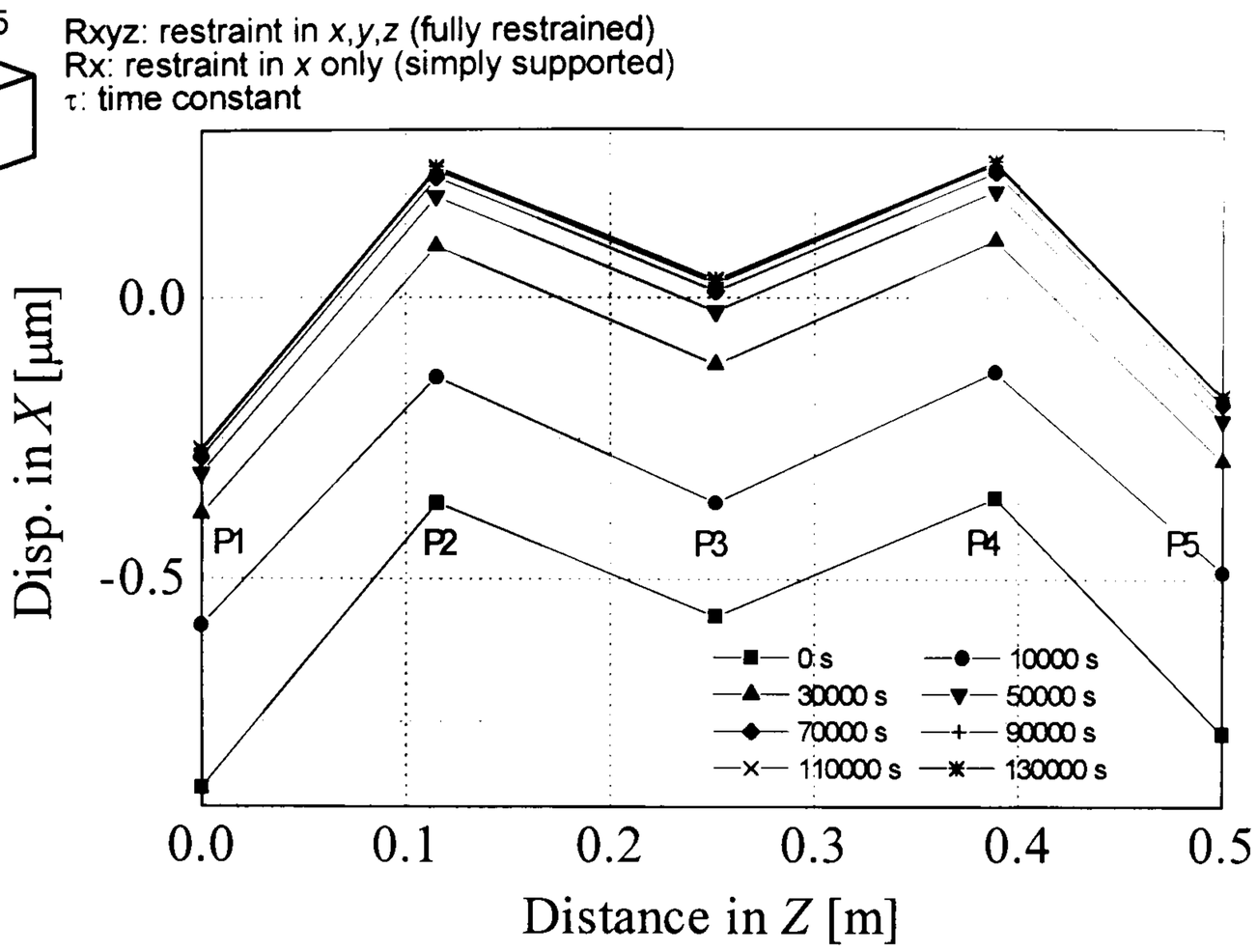

Figure A.37
Granite
1 deg step temp. rise
Rx

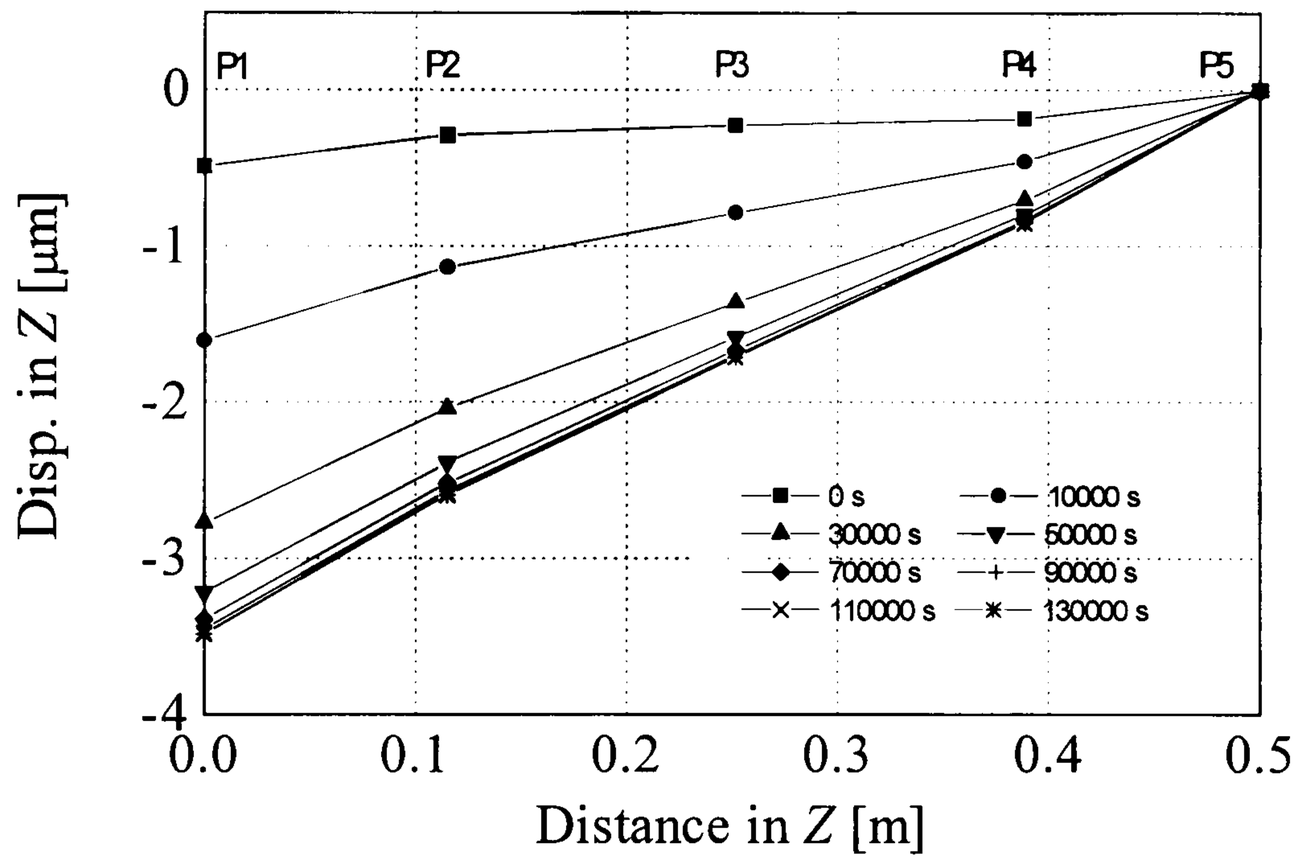

Figure A.38
Steel
Amp.=2.5
Period=7200
Phase = 0

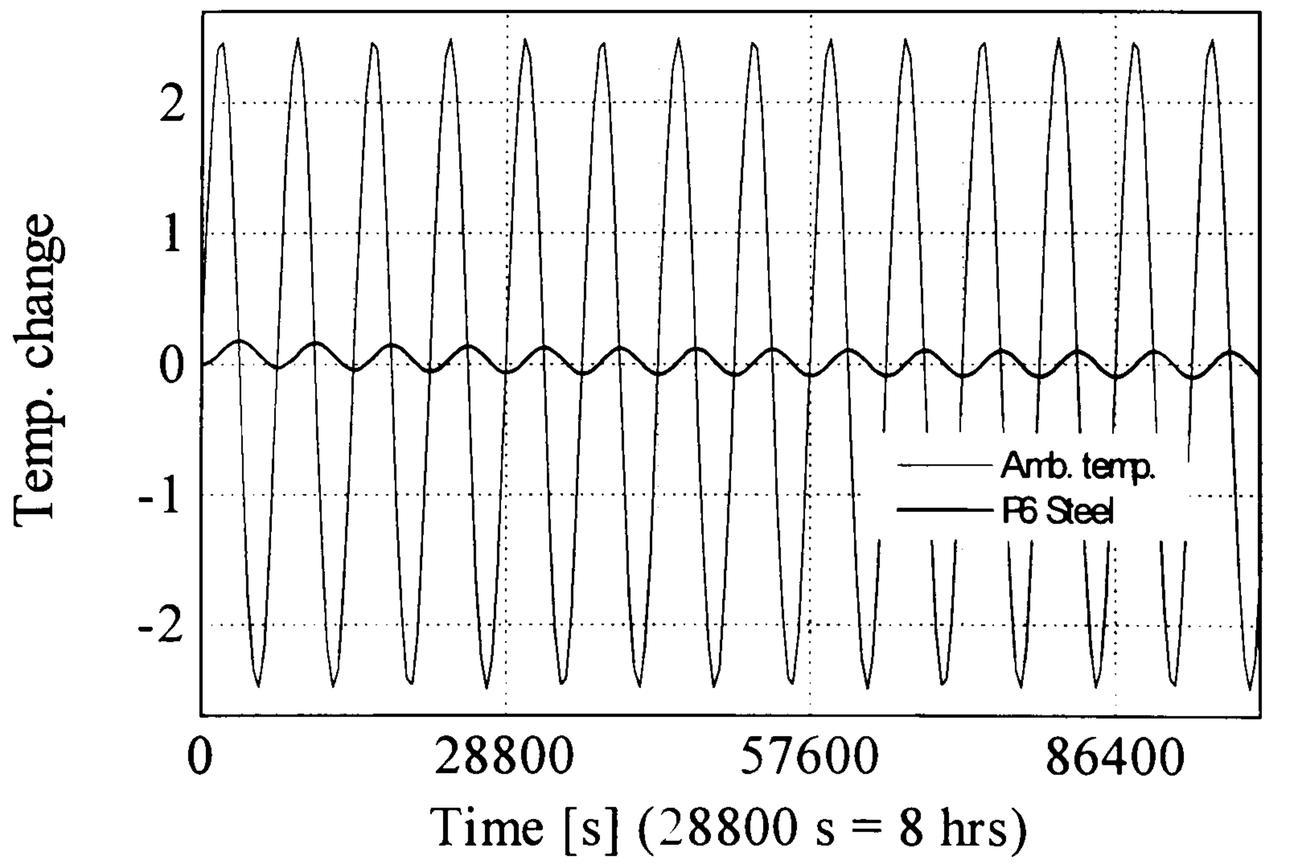

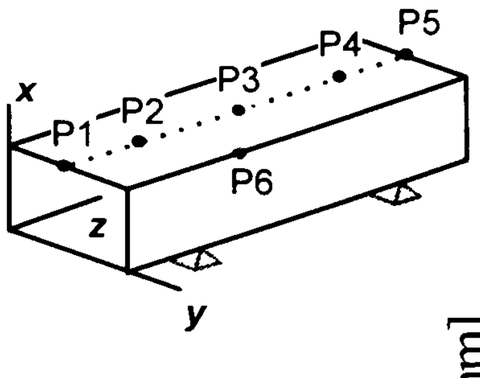

Rxyz: restraint in *x*,*y*,*z* (fully restrained)
Rx: restraint in *x* only (simply supported)
τ: time constant

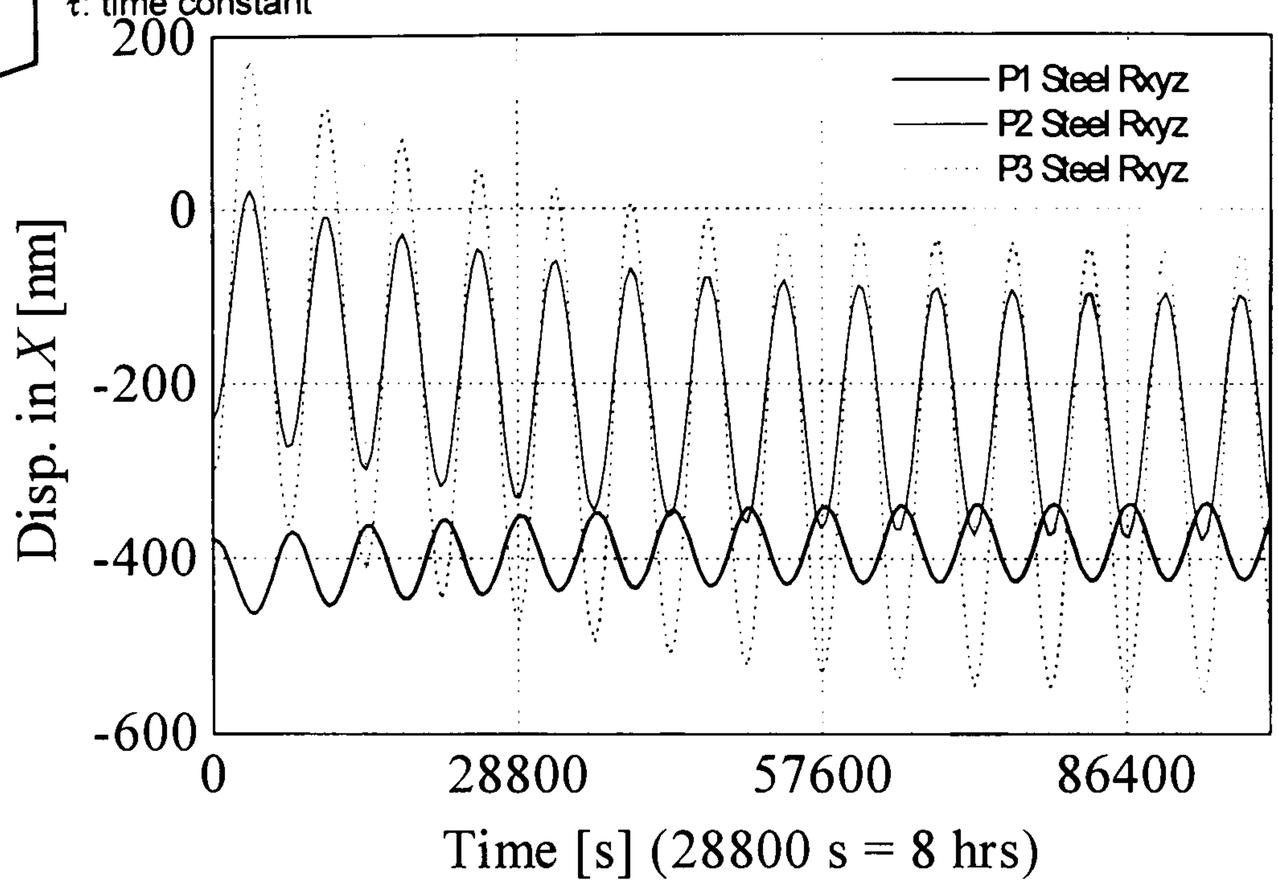

Figure A.39
Steel
Amp.=2.5
Period=7200
Phase = 0
Rxyz

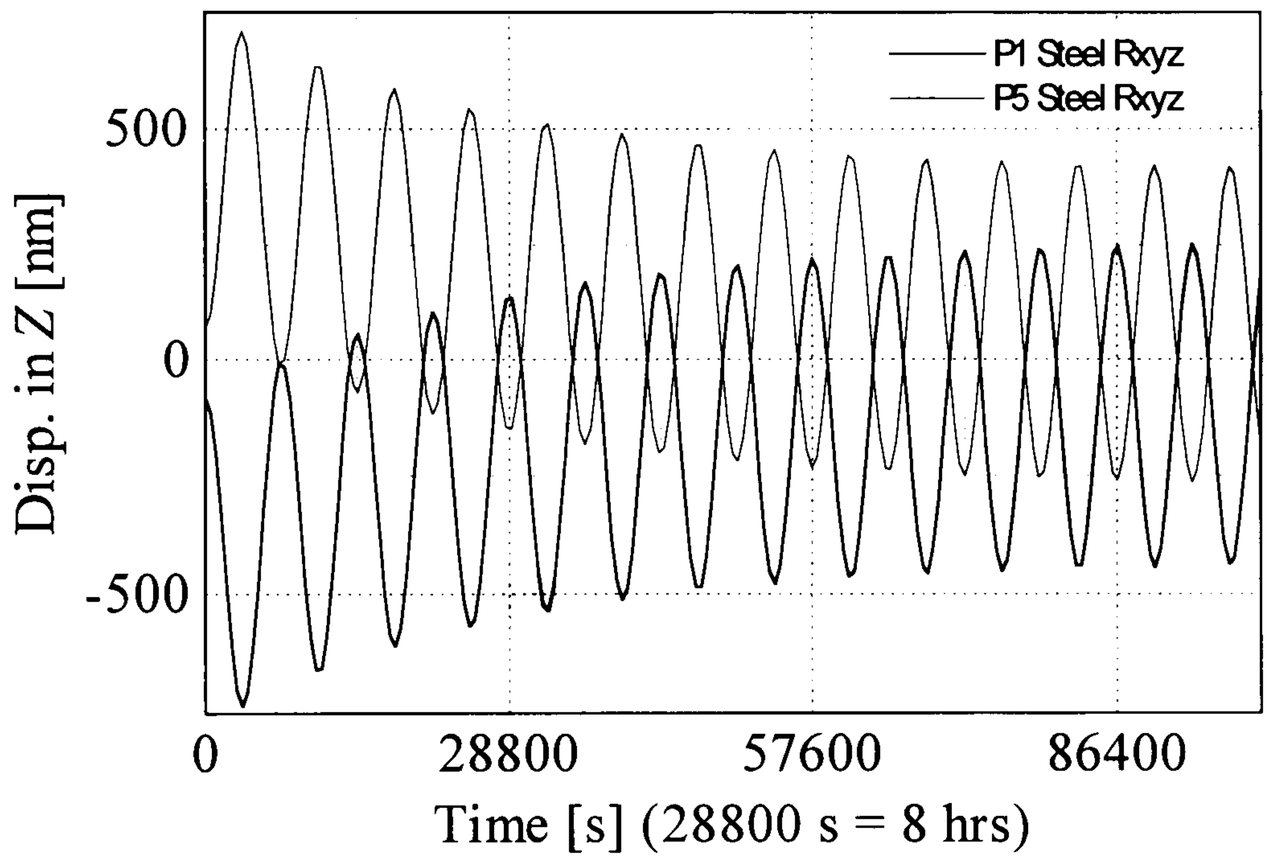

Figure A.40
Steel
Amp.=2.5
Period=7200
Phase = 0
Rxyz

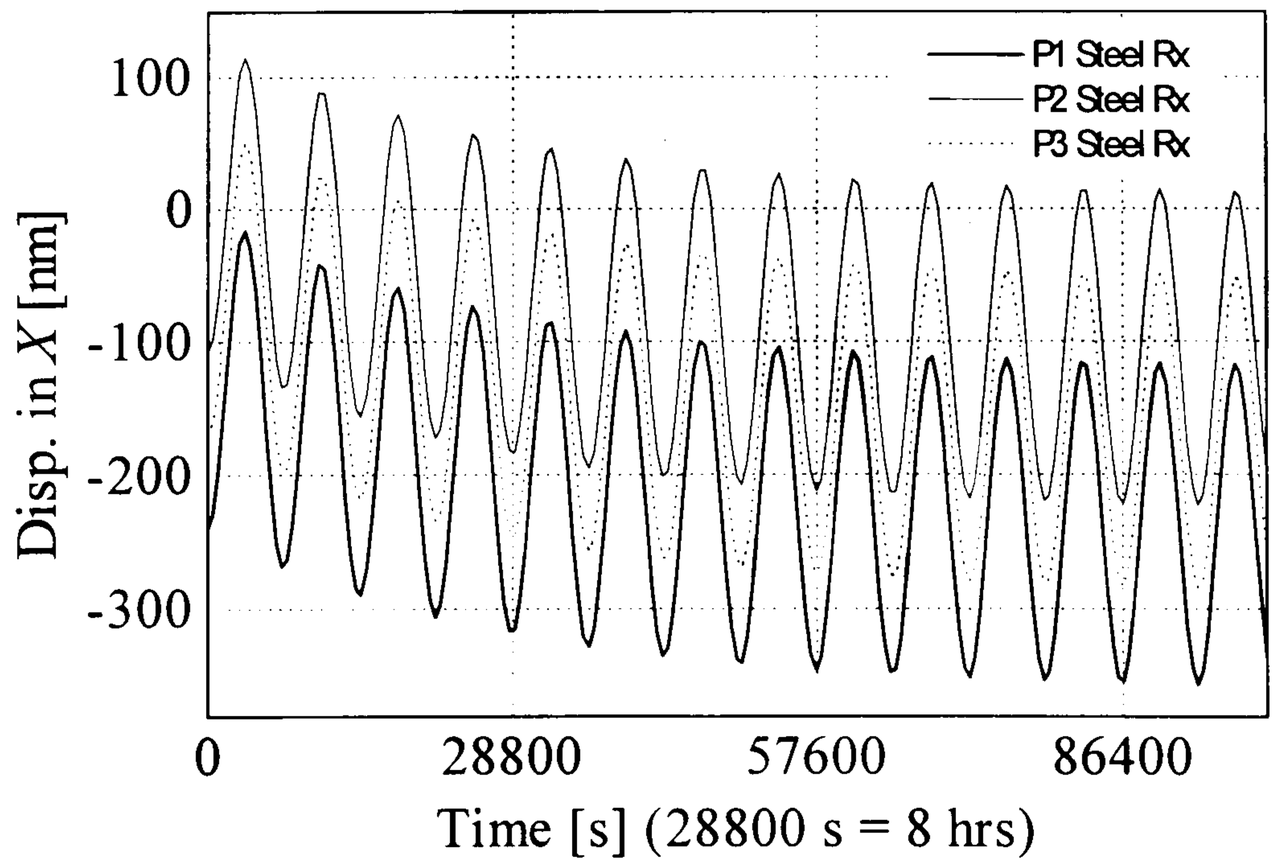

Figure A.41
Steel
Amp.=2.5
Period=7200
Phase = 0
Rx

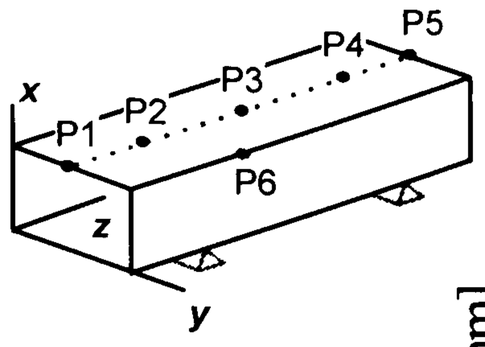

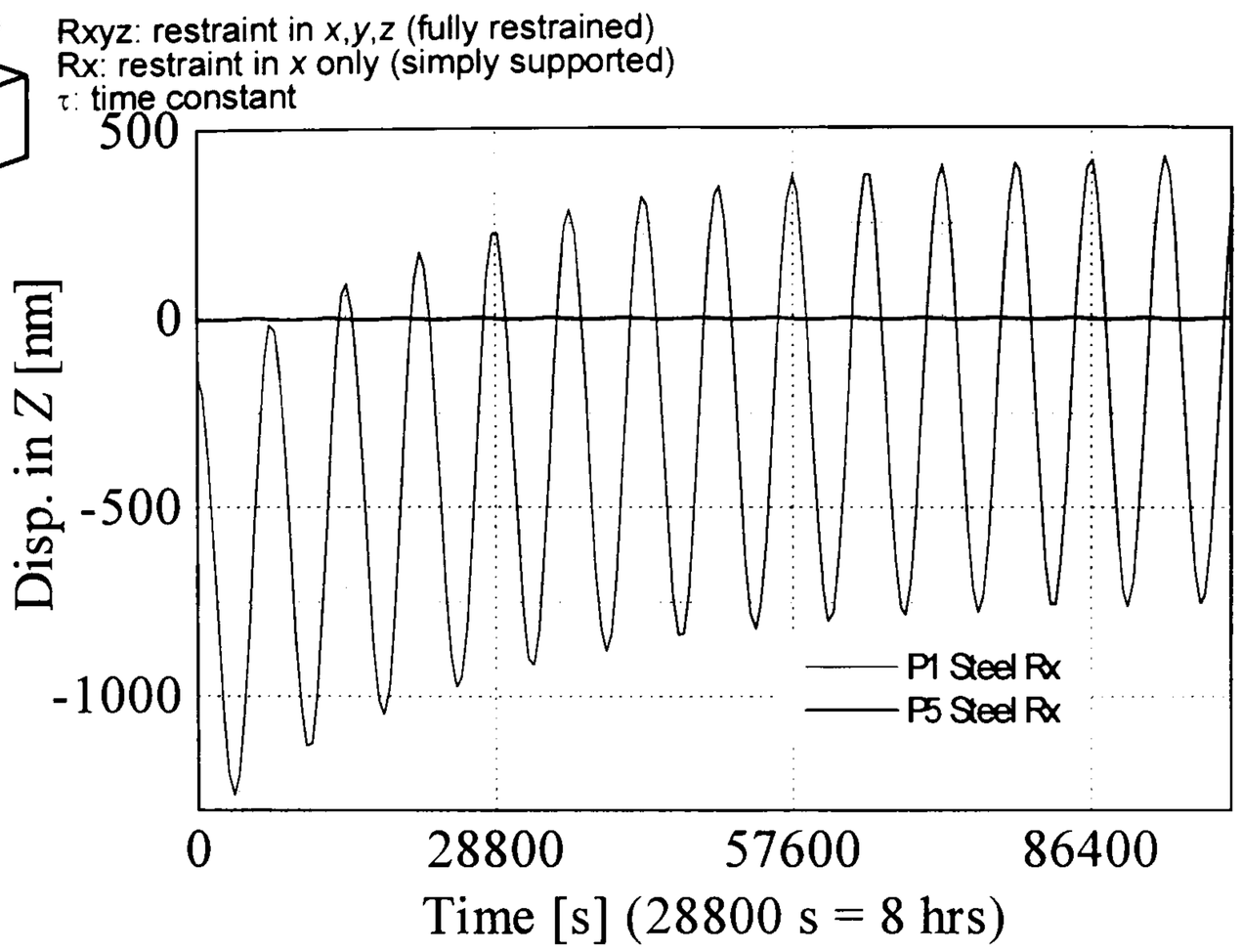

Figure A.42
Steel
Amp.=2.5
Period=7200
Phase = 0
Rx

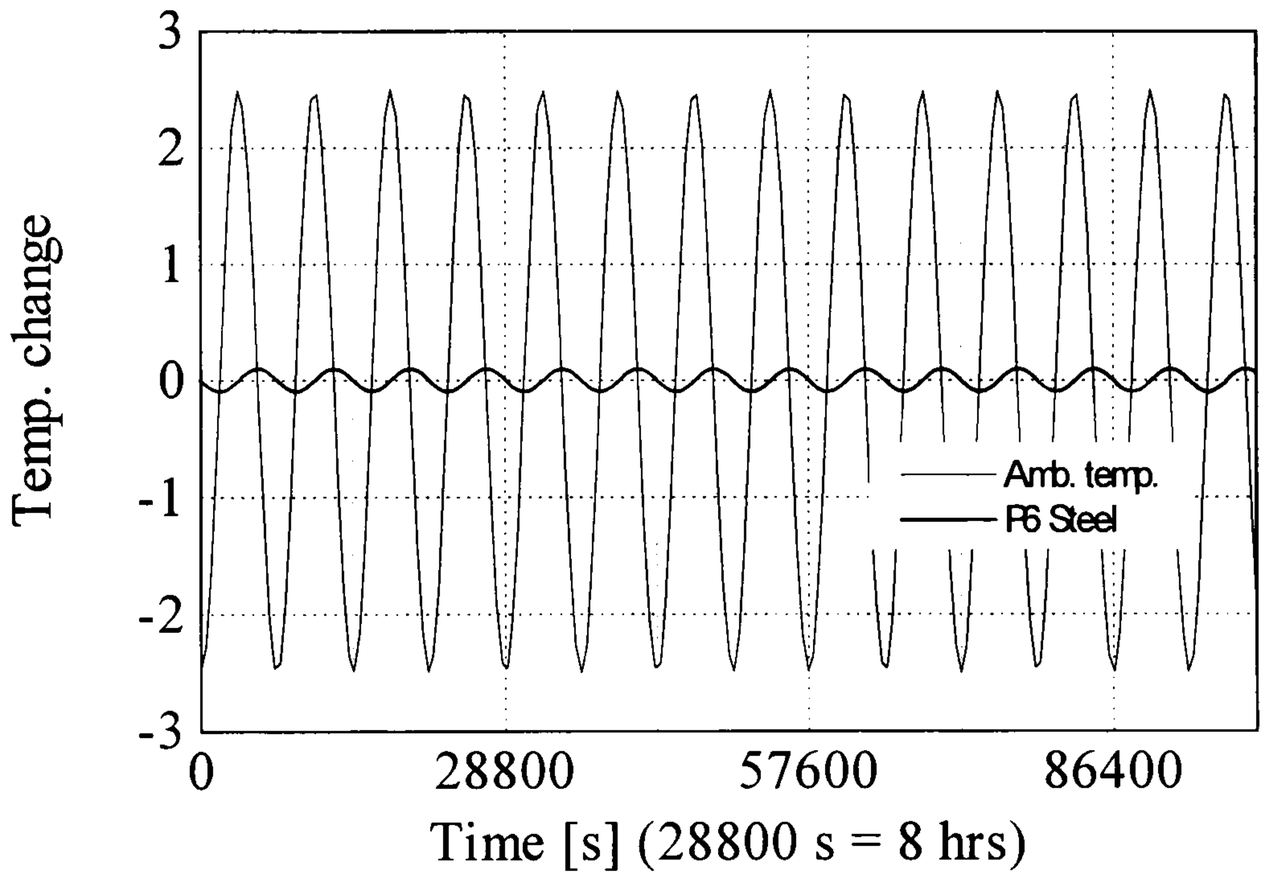

Figure A.43
Steel
Amp.=2.5
Period=7200
Phase = -90

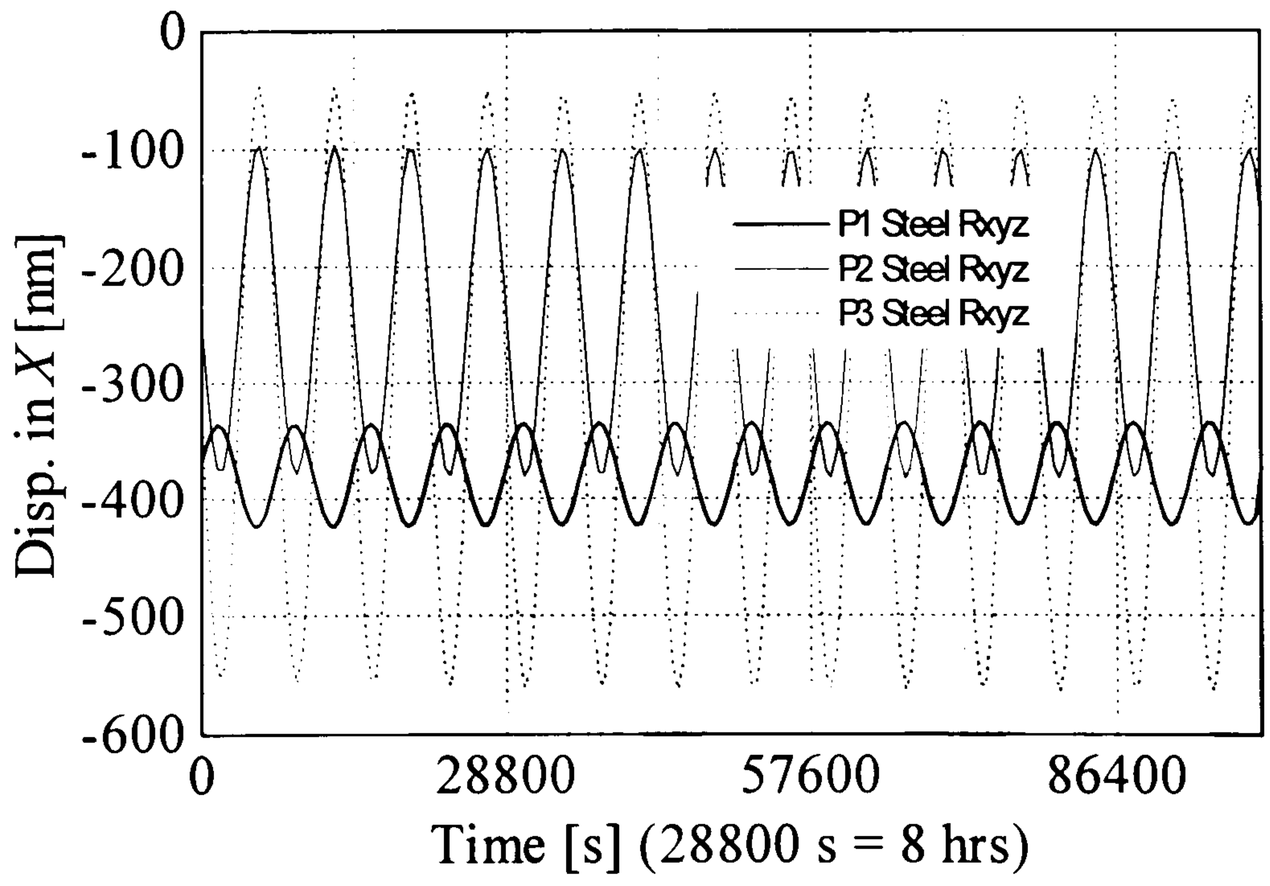

Figure A.44
Steel
Amp.=2.5
Period=7200
Phase = -90
Rxyz

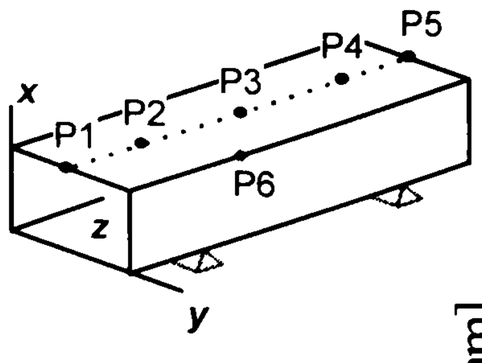

Figure A.45
Steel
Amp.=2.5
Period=7200
Phase = -90
Rxyz

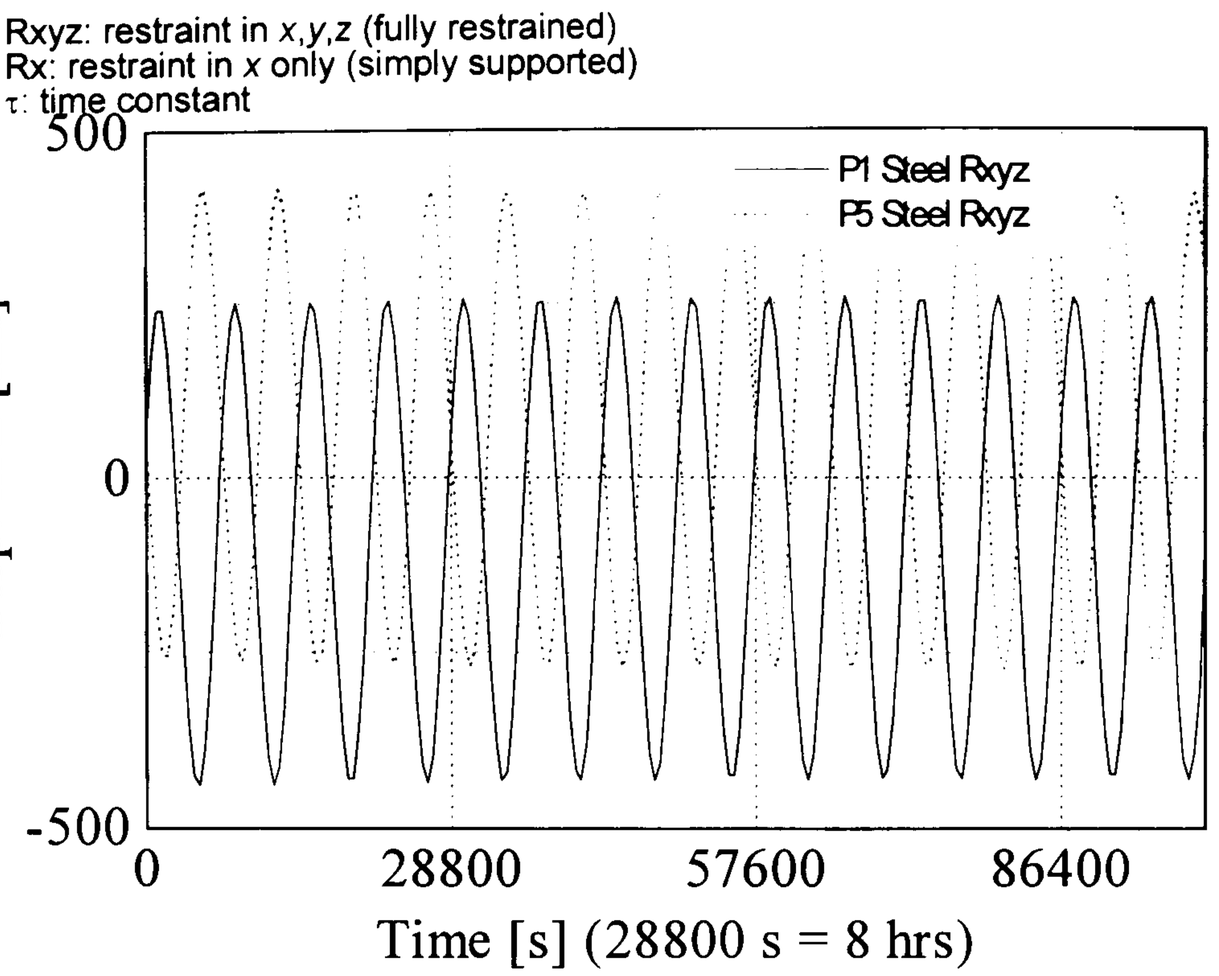

Figure A.46
Steel
Amp.=2.5
Period=7200
Phase = -90
Rx

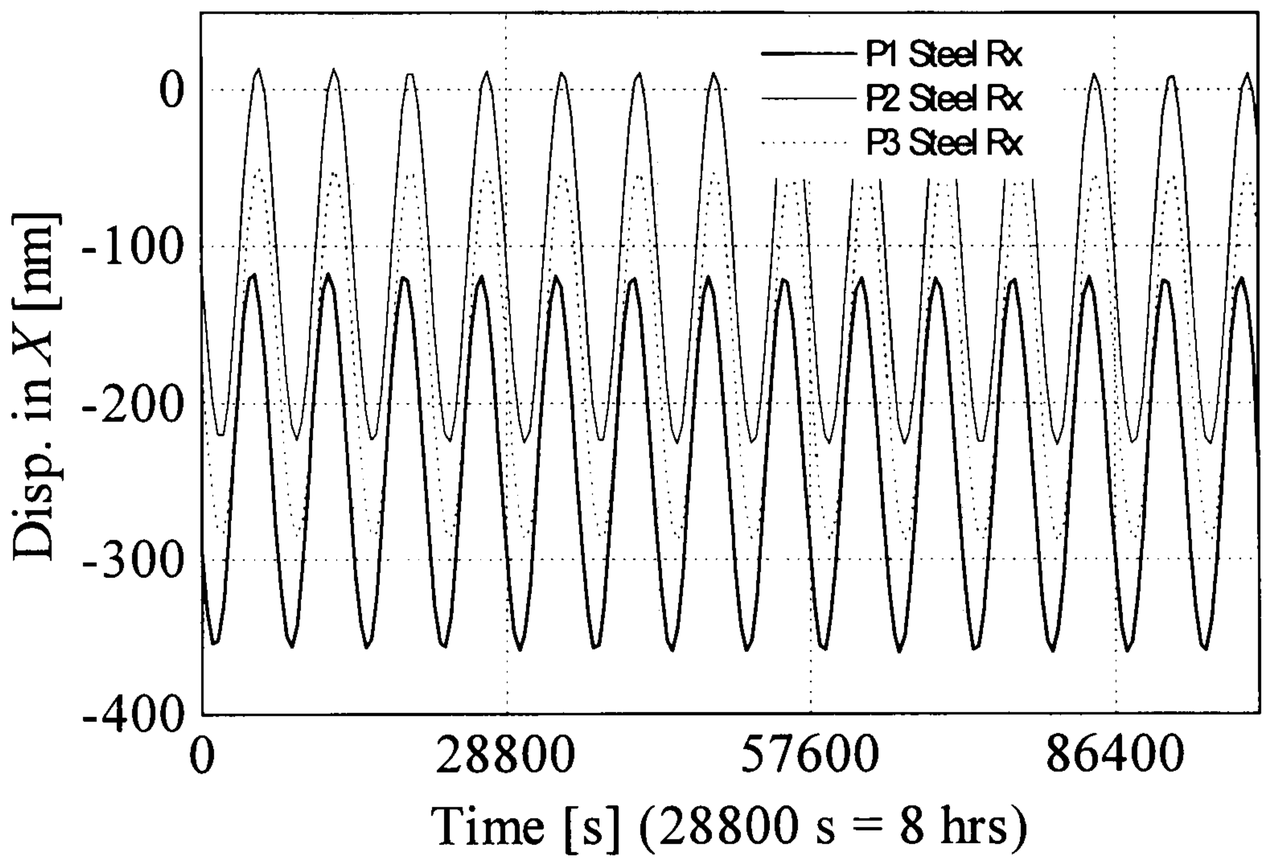

Figure A.47
Steel
Amp.=2.5
Period=7200
Phase = -90
Rx

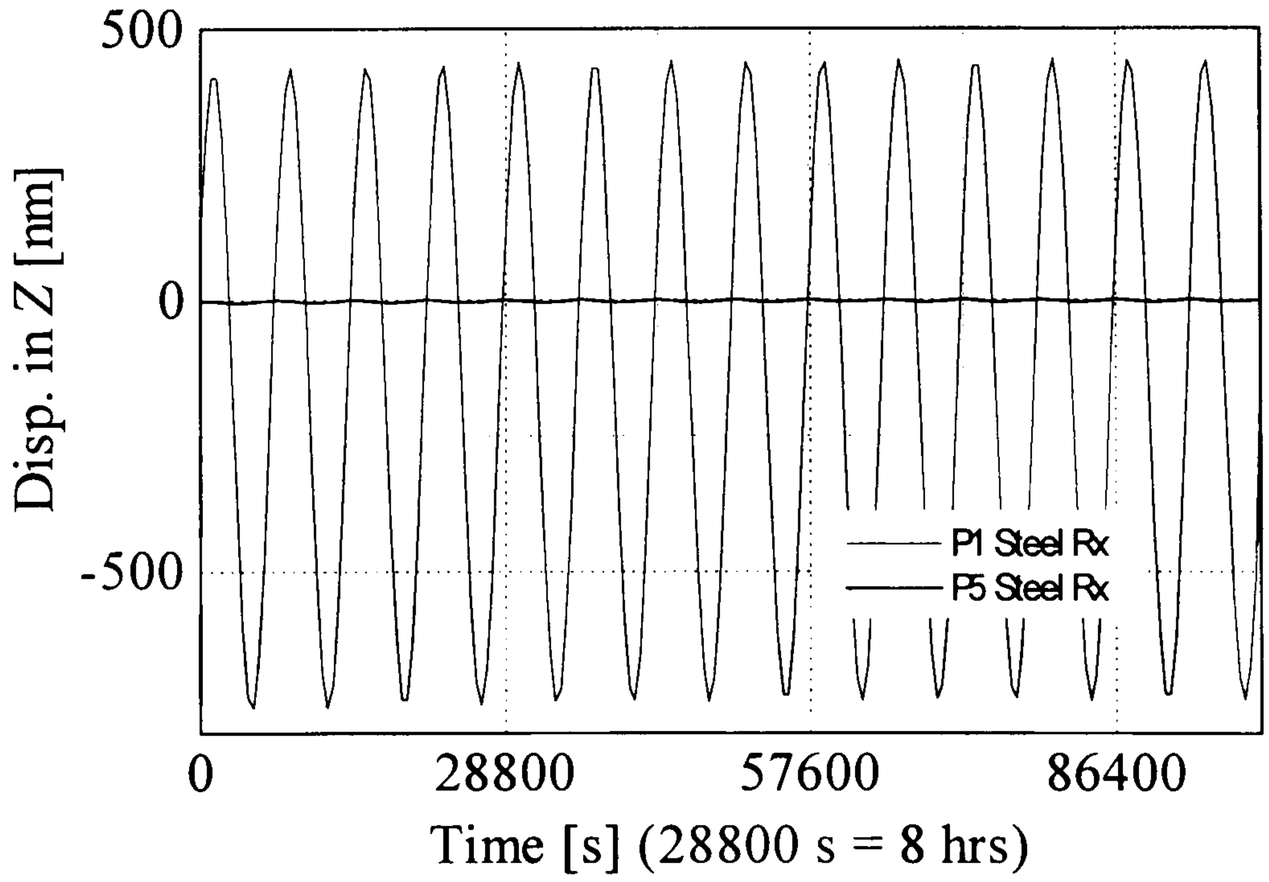

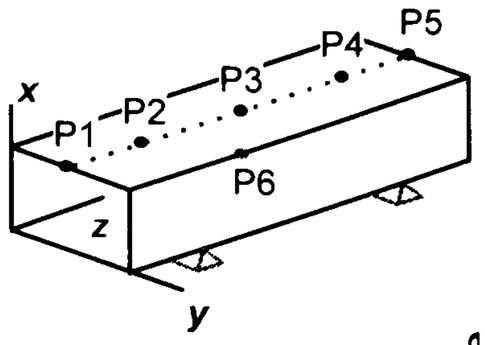

Figure A.48
Al
Amp.=2.5
Period=7200
Phase = 0

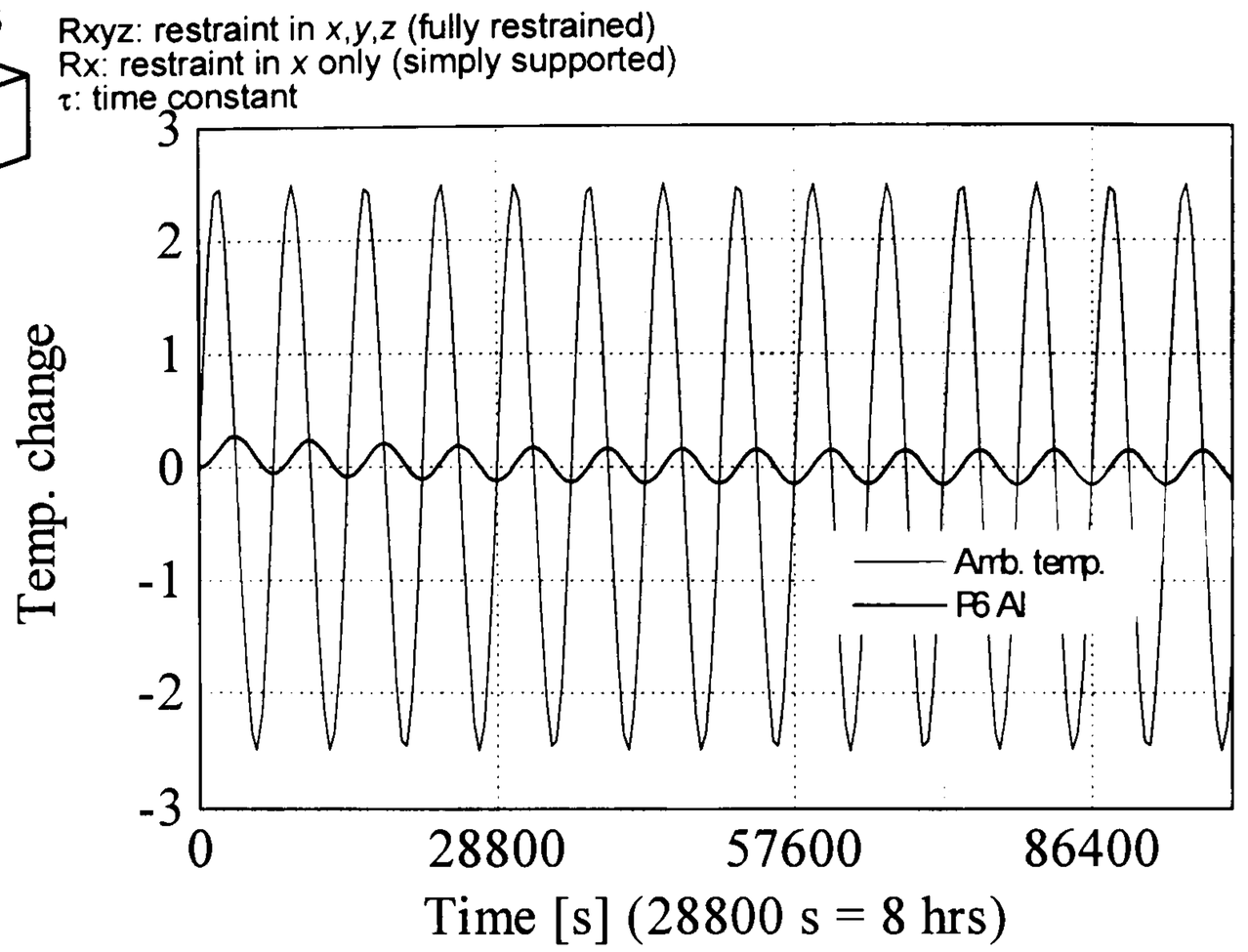

Figure A.49
Al
Amp.=2.5
Period=7200
Phase = 0
Rxyz

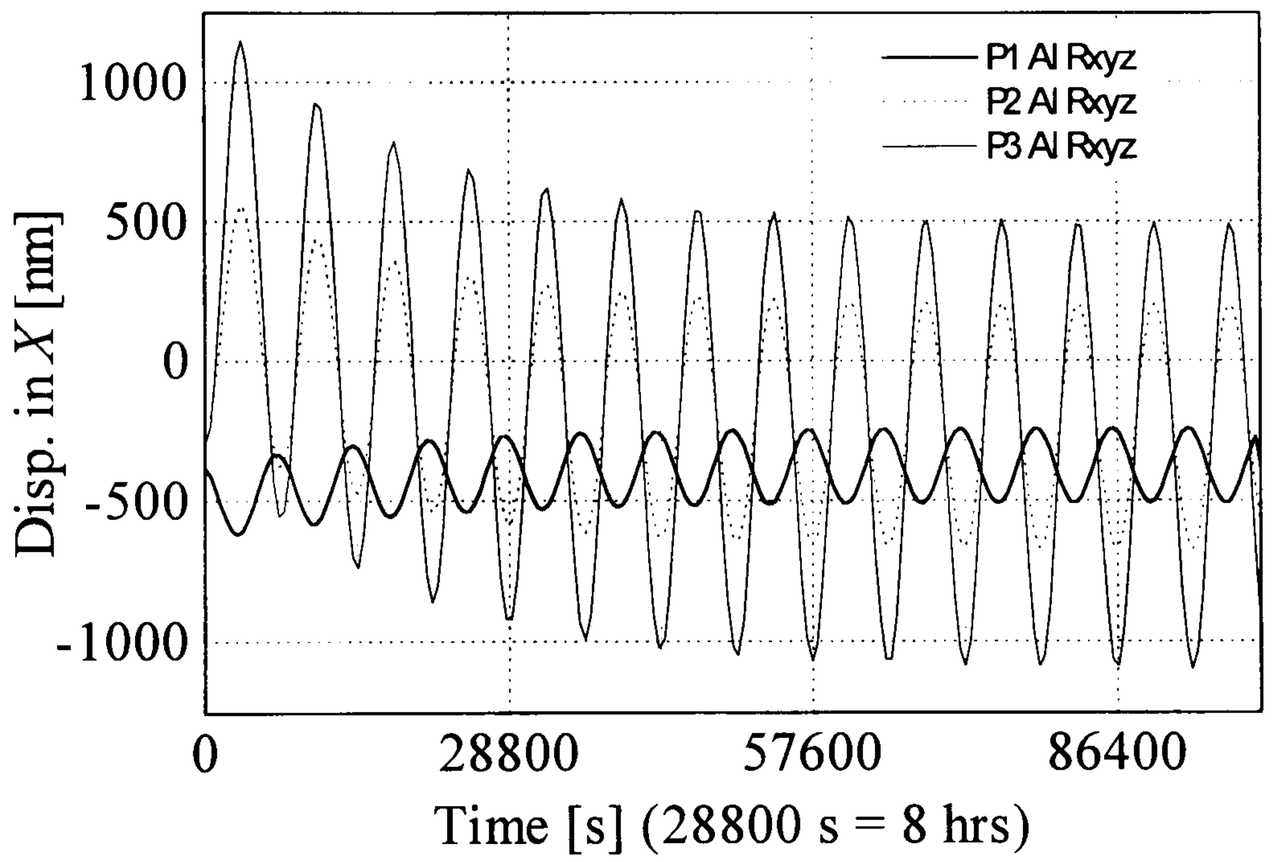

Figure A.50
Al
Amp.=2.5
Period=7200
Phase = 0
Rxyz

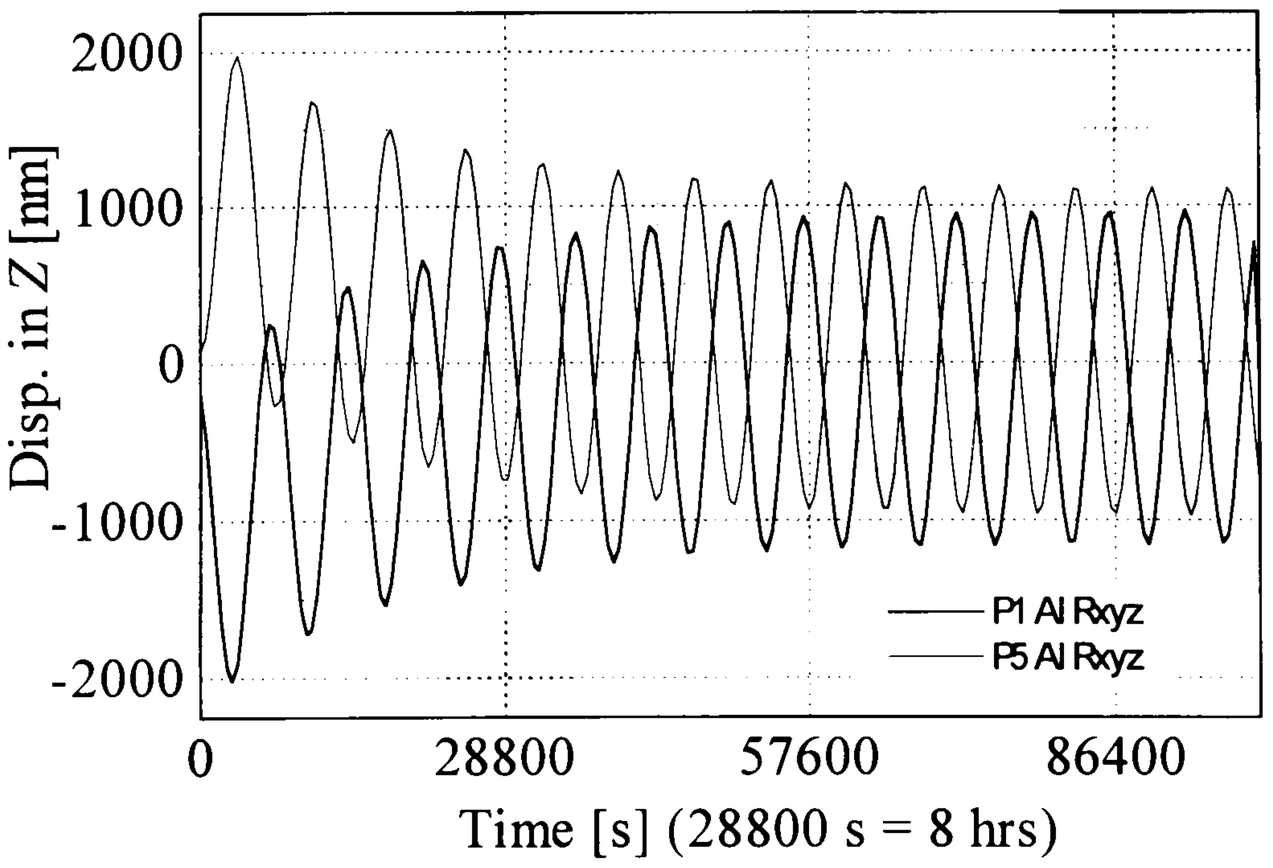

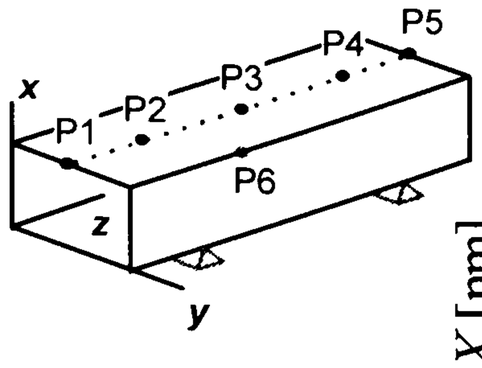

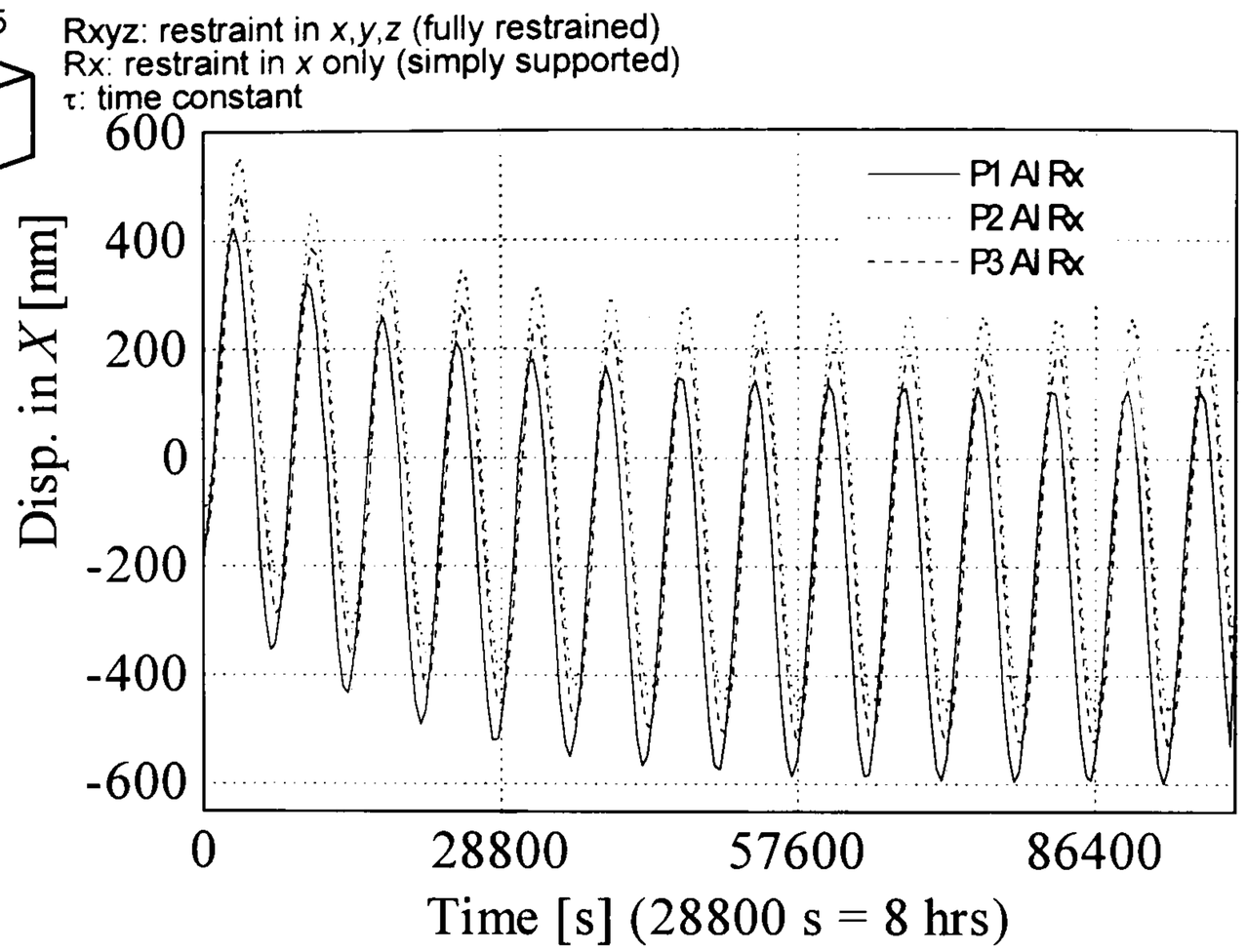

Figure A.51
Al
Amp.=2.5
Period=7200
Phase = 0
Rx

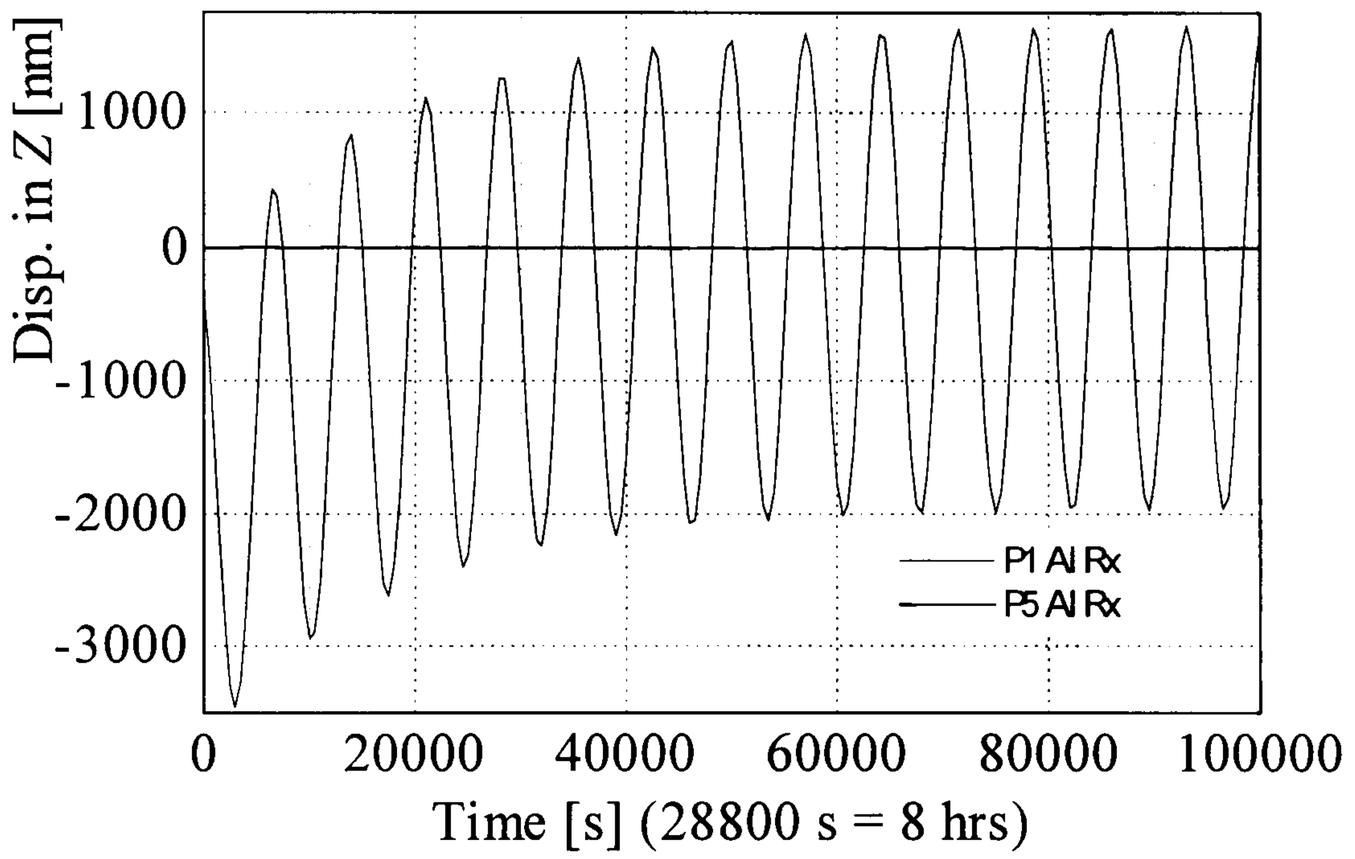

Figure A.52
Al
Amp.=2.5
Period=7200
Phase = 0
Rx

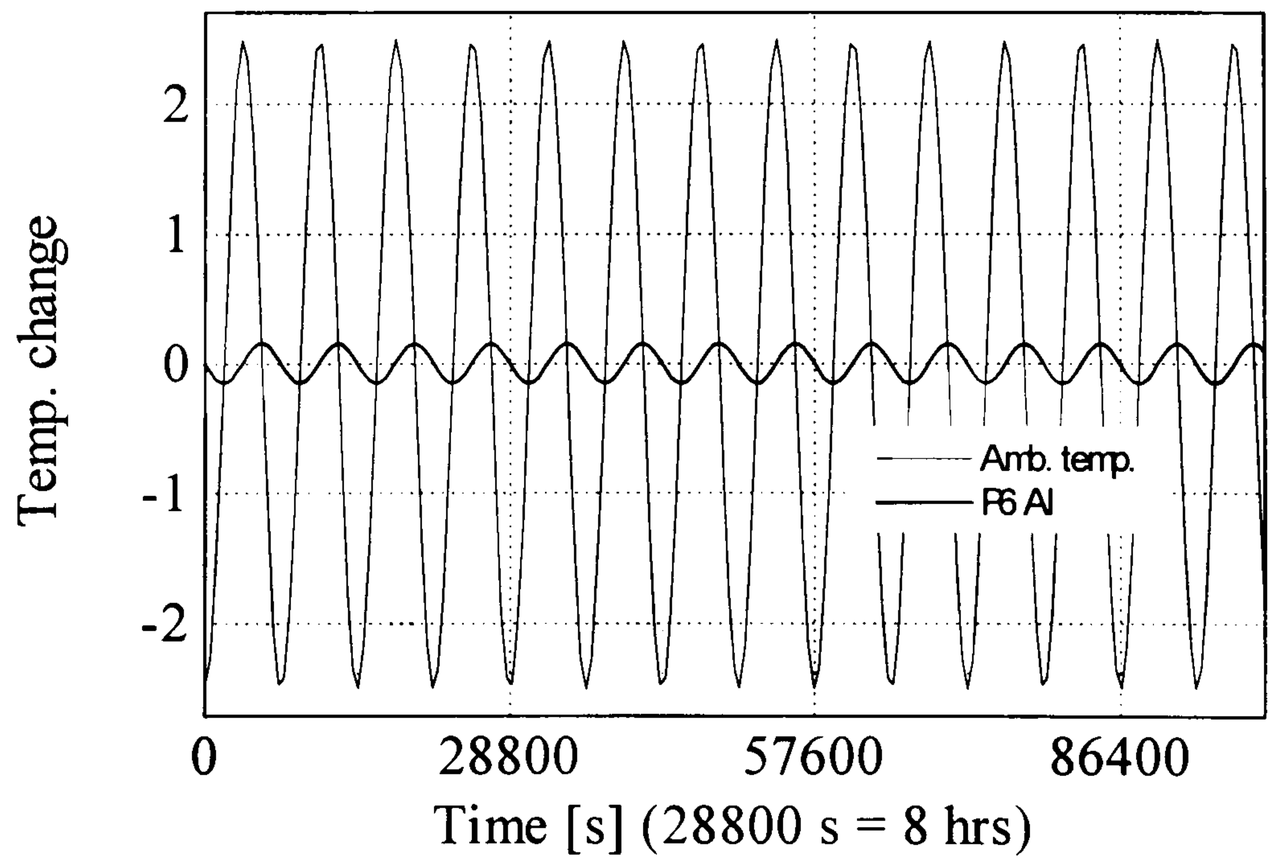

Figure A.53
Al
Amp.=2.5
Period=7200
Phase = -90

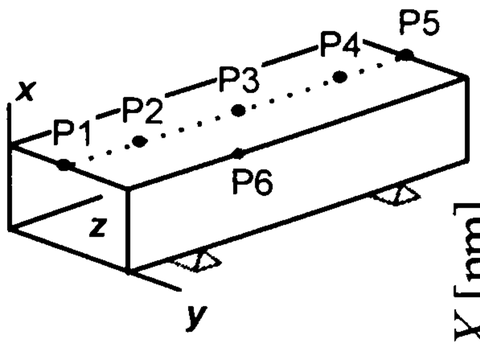

Figure A.54
Al
Amp.=2.5
Period=7200
Phase = -90
Rxyz

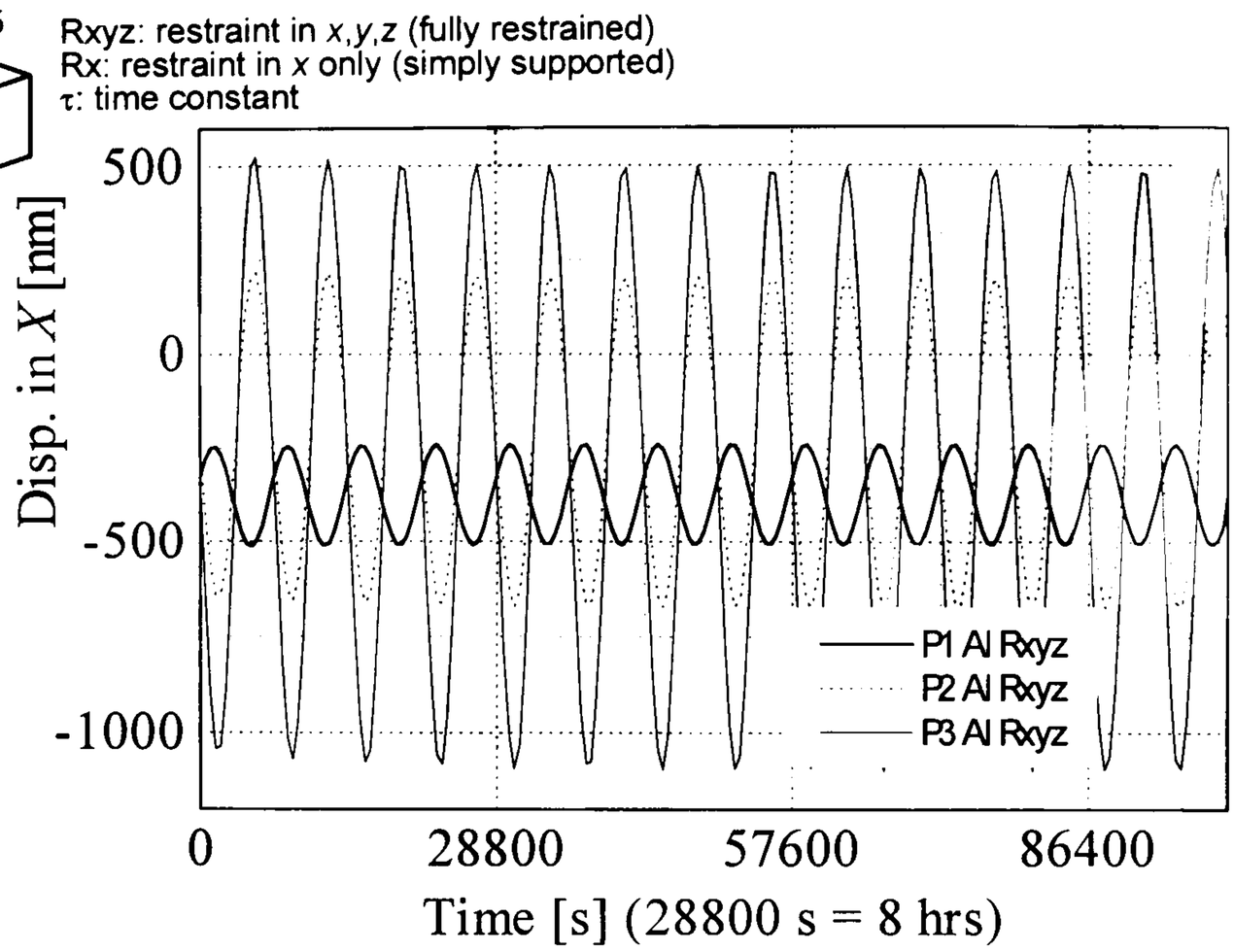

Figure A.55
Al
Amp.=2.5
Period=7200
Phase = -90
Rxyz

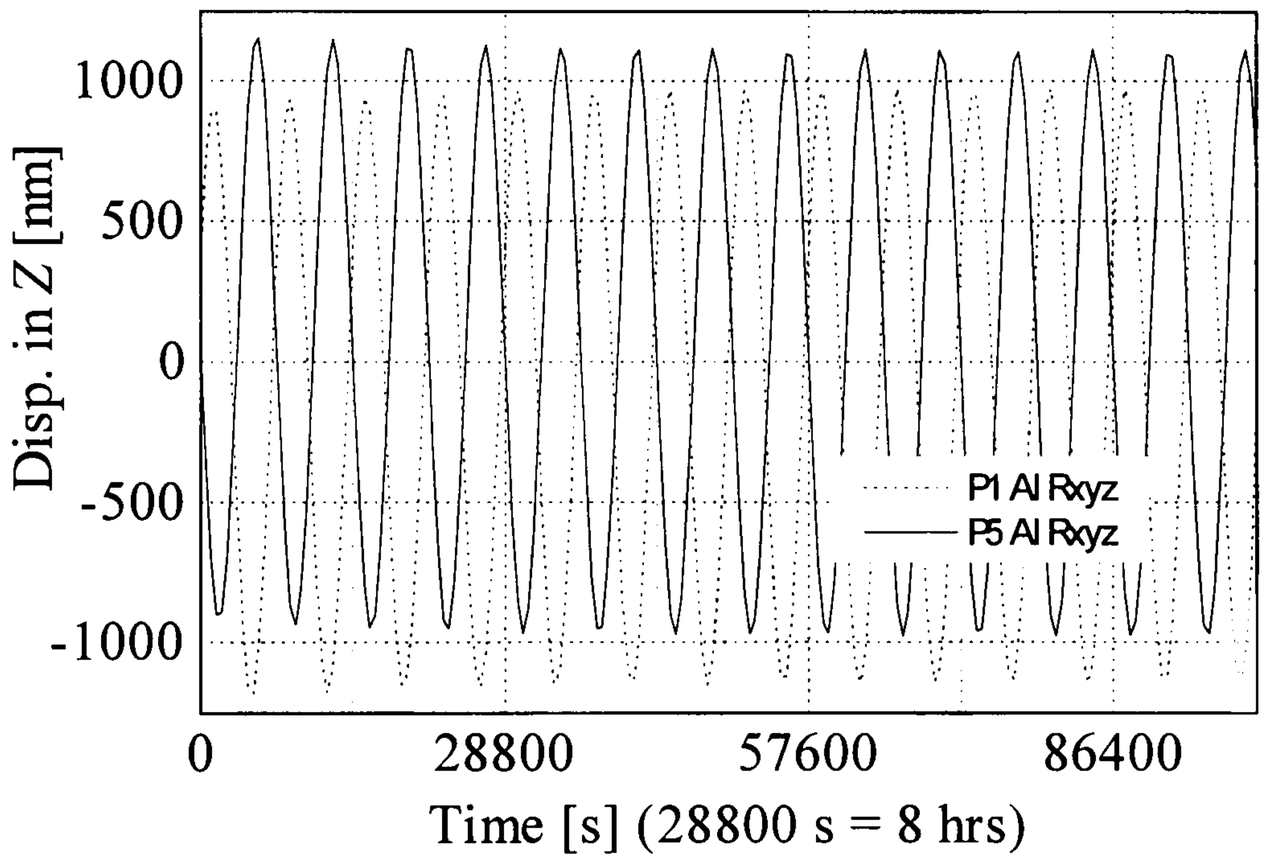

Figure A.56
Al
Amp.=2.5
Period=7200
Phase = -90
Rx

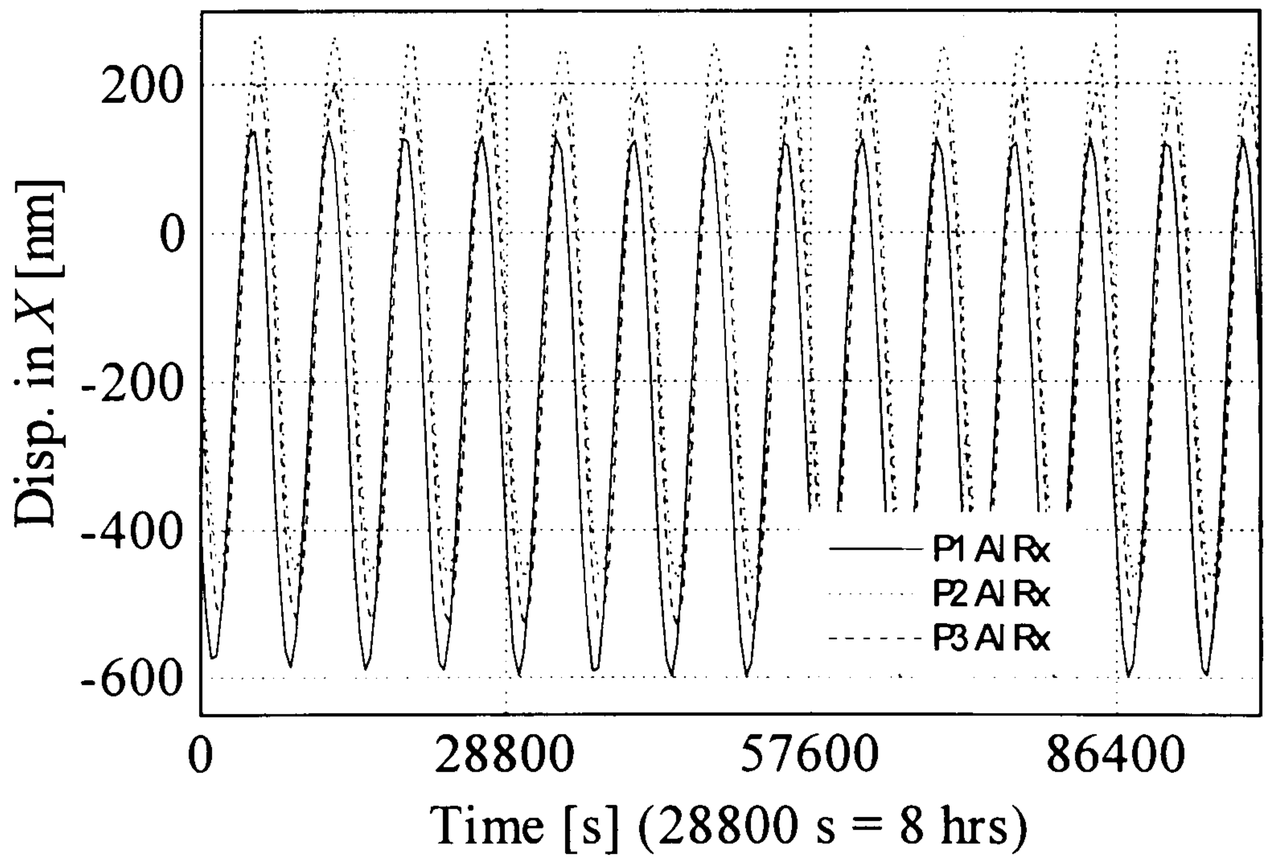

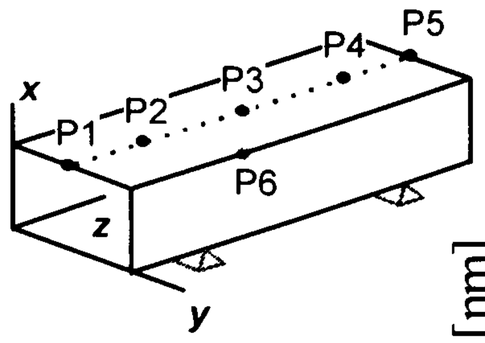

Figure A.57
Al
Amp.=2.5
Period=7200
Phase = -90
Rx

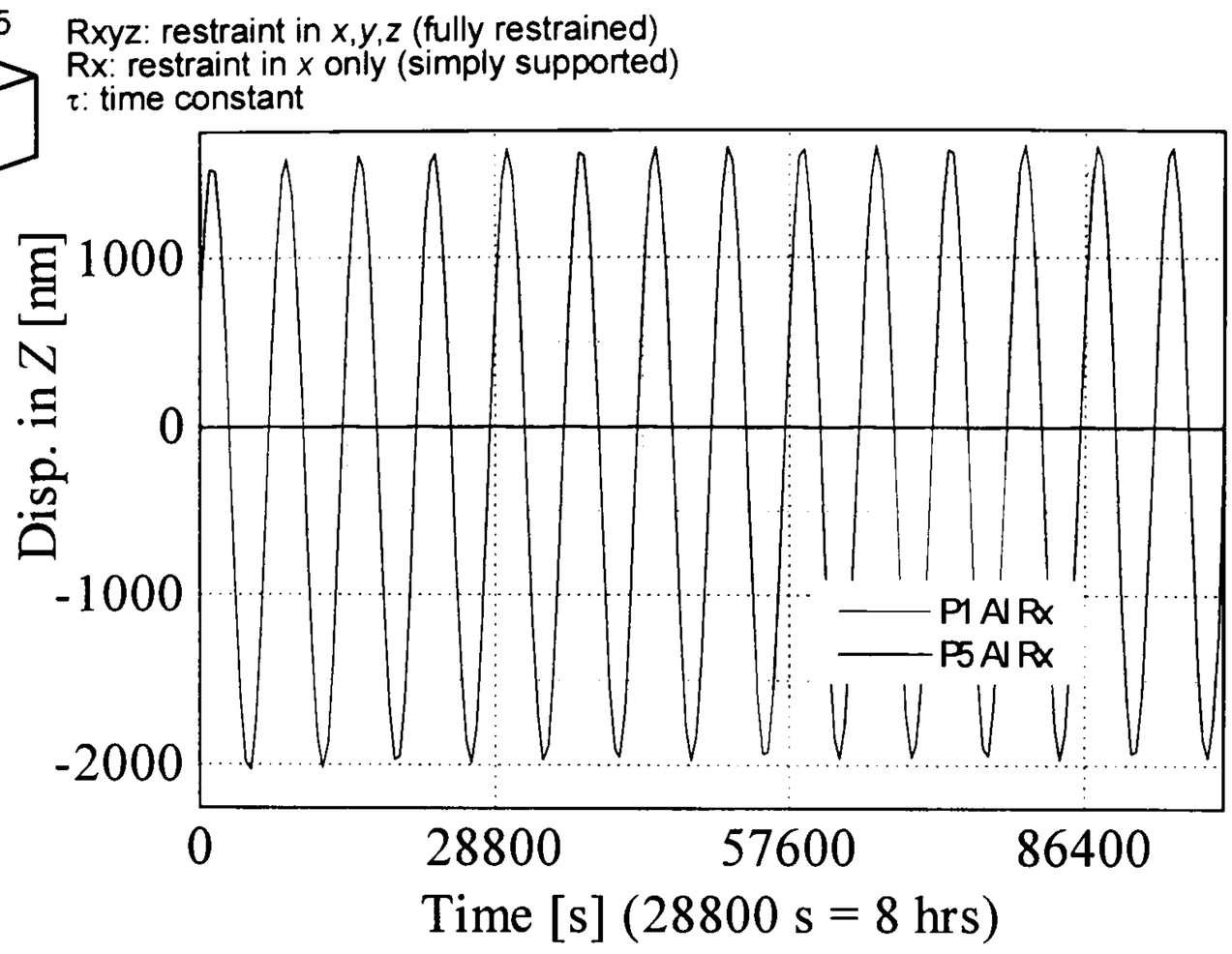

Figure A.58
Granite
Amp.=2.5
Period=7200
Phase = 0

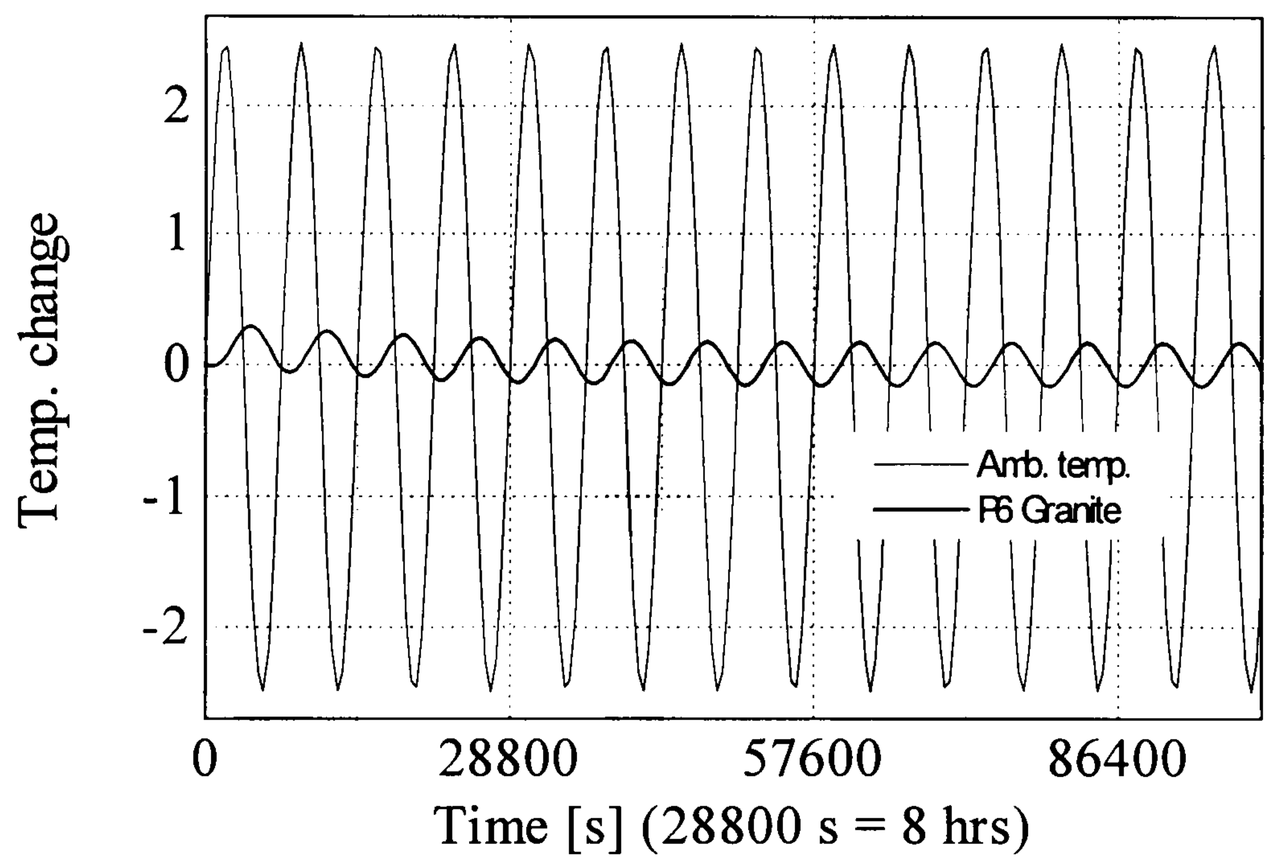

Figure A.59
Granite
Amp.=2.5
Period=7200
Phase = 0
Rxyz

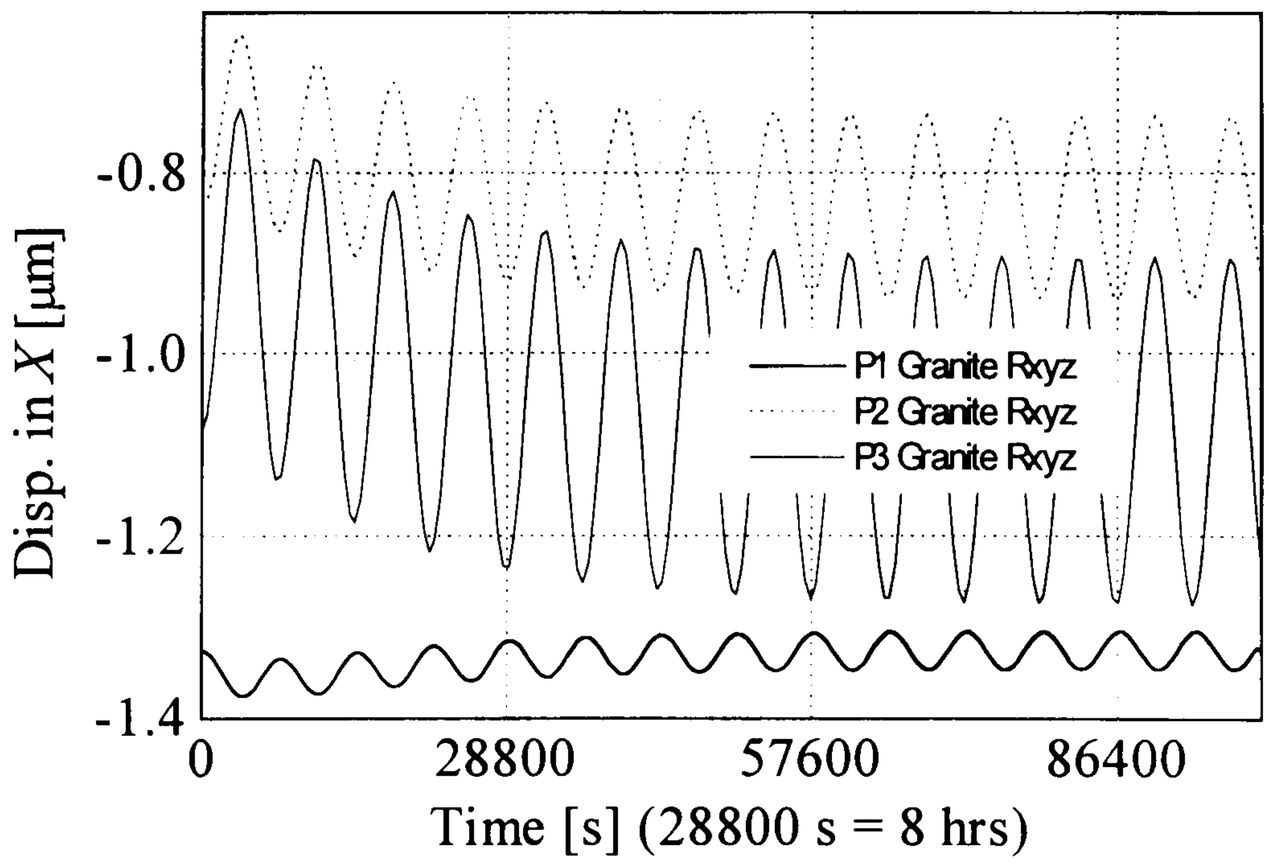

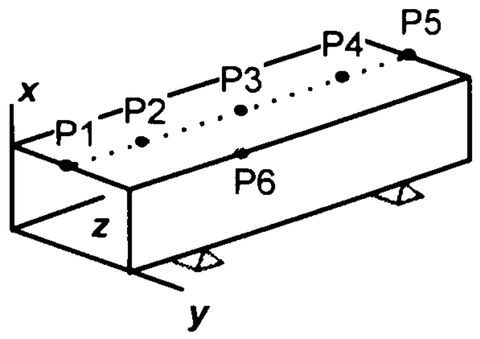

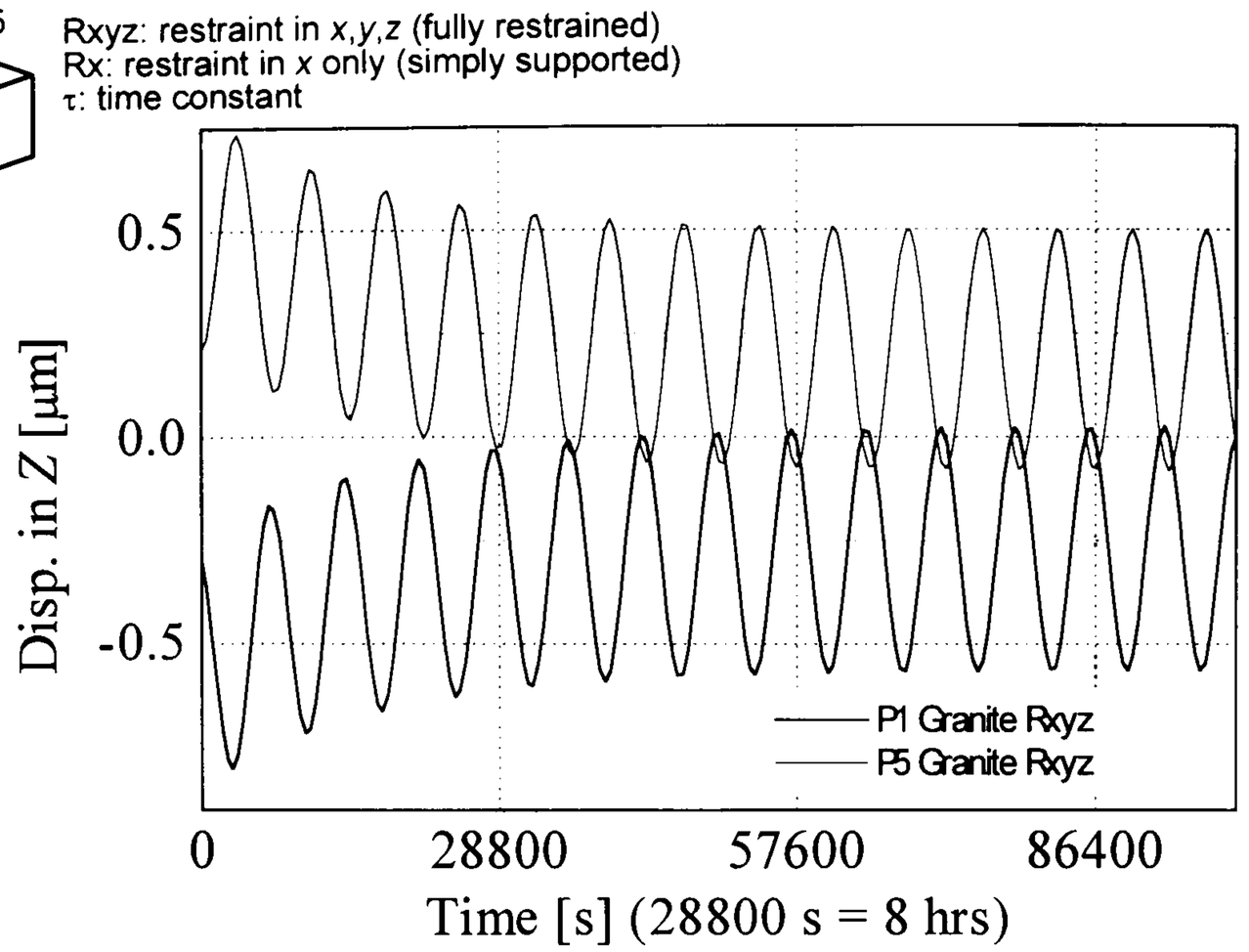

Figure A.60
Granite
Amp.=2.5
Period=7200
Phase = 0
Rxyz

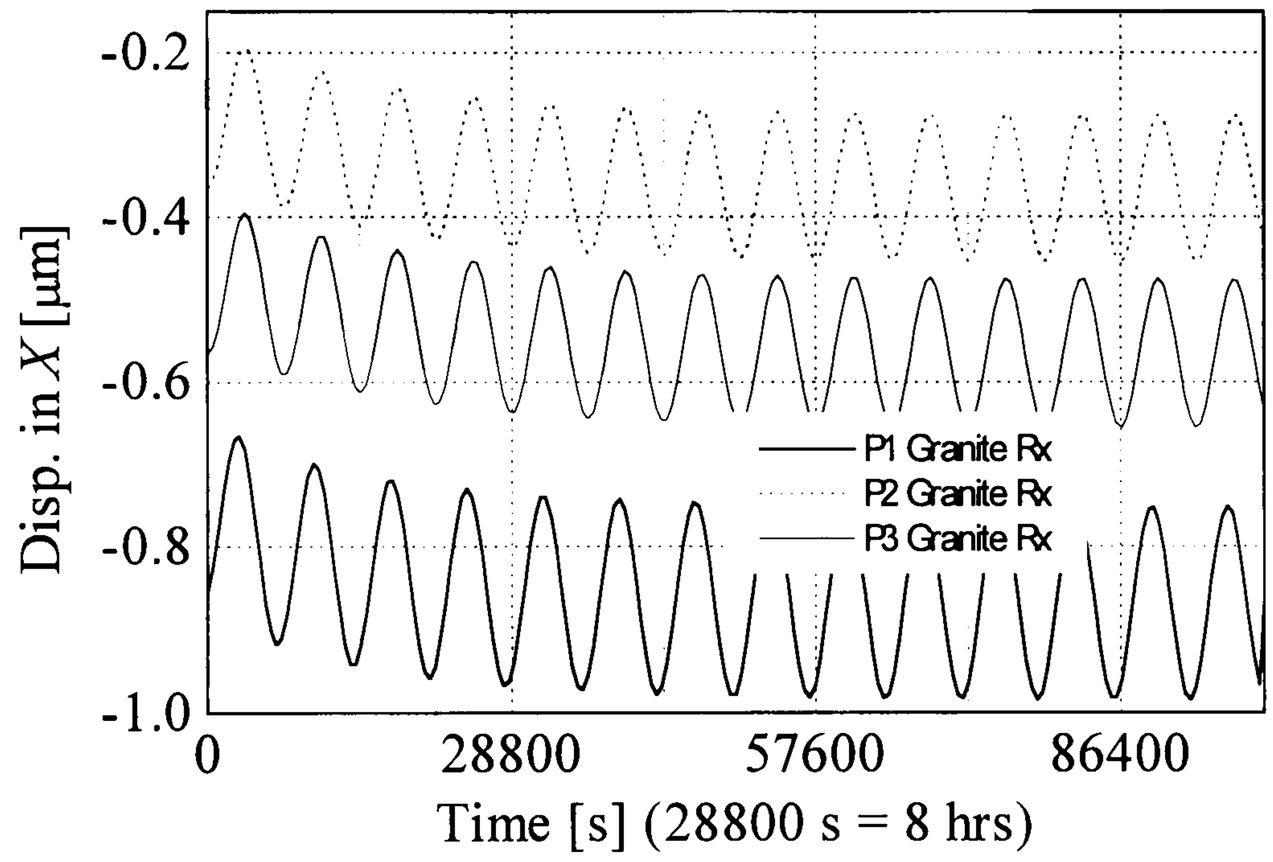

Figure A.61
Granite
Amp.=2.5
Period=7200
Phase = 0
Rx

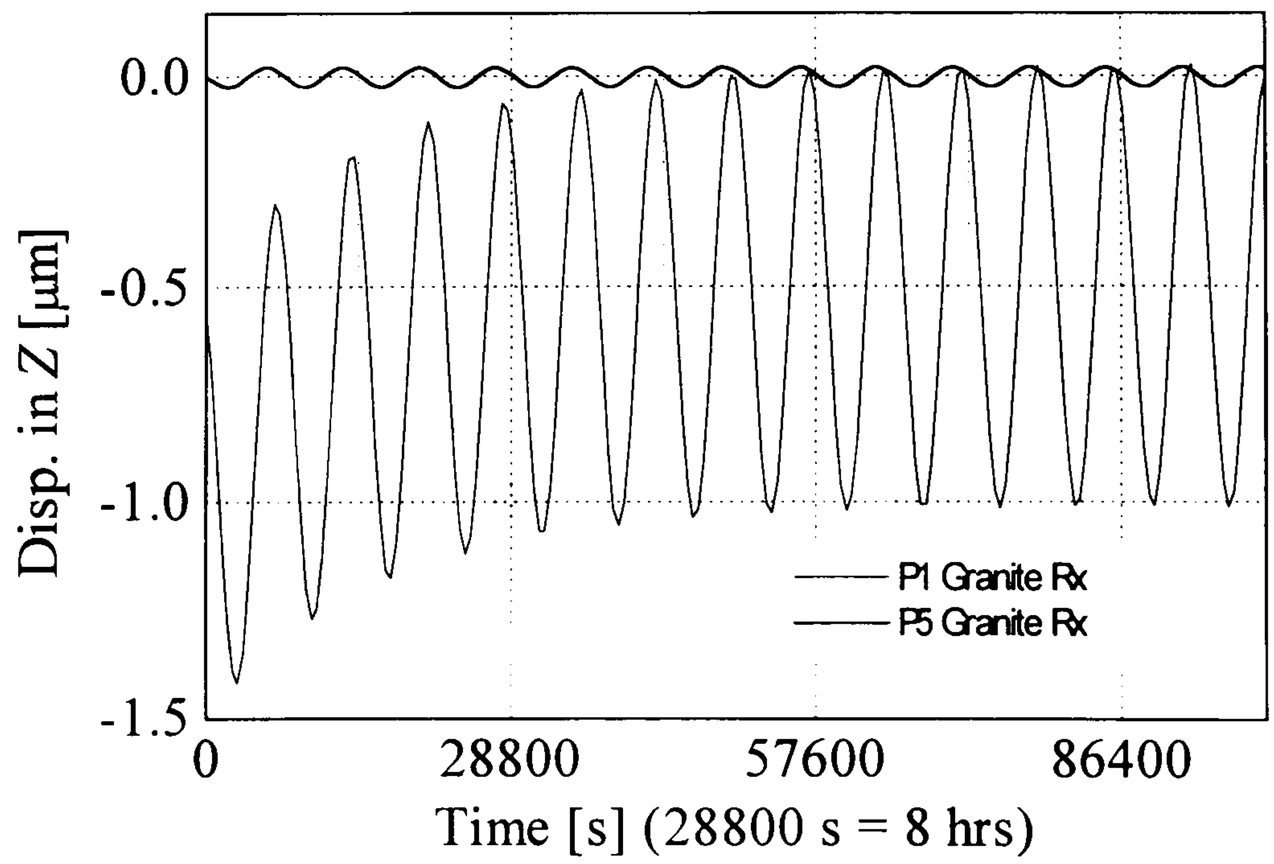

Figure A.62
Granite
Amp.=2.5
Period=7200
Phase = 0
Rx

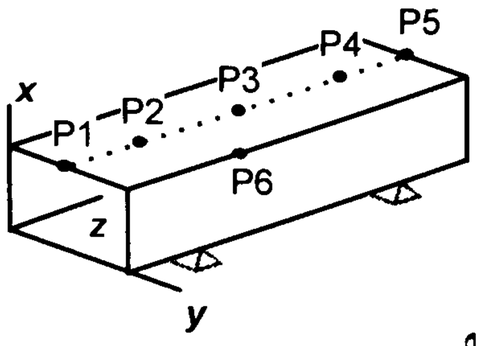

Figure A.63
Granite
Amp.=2.5
Period=7200
Phase = -90

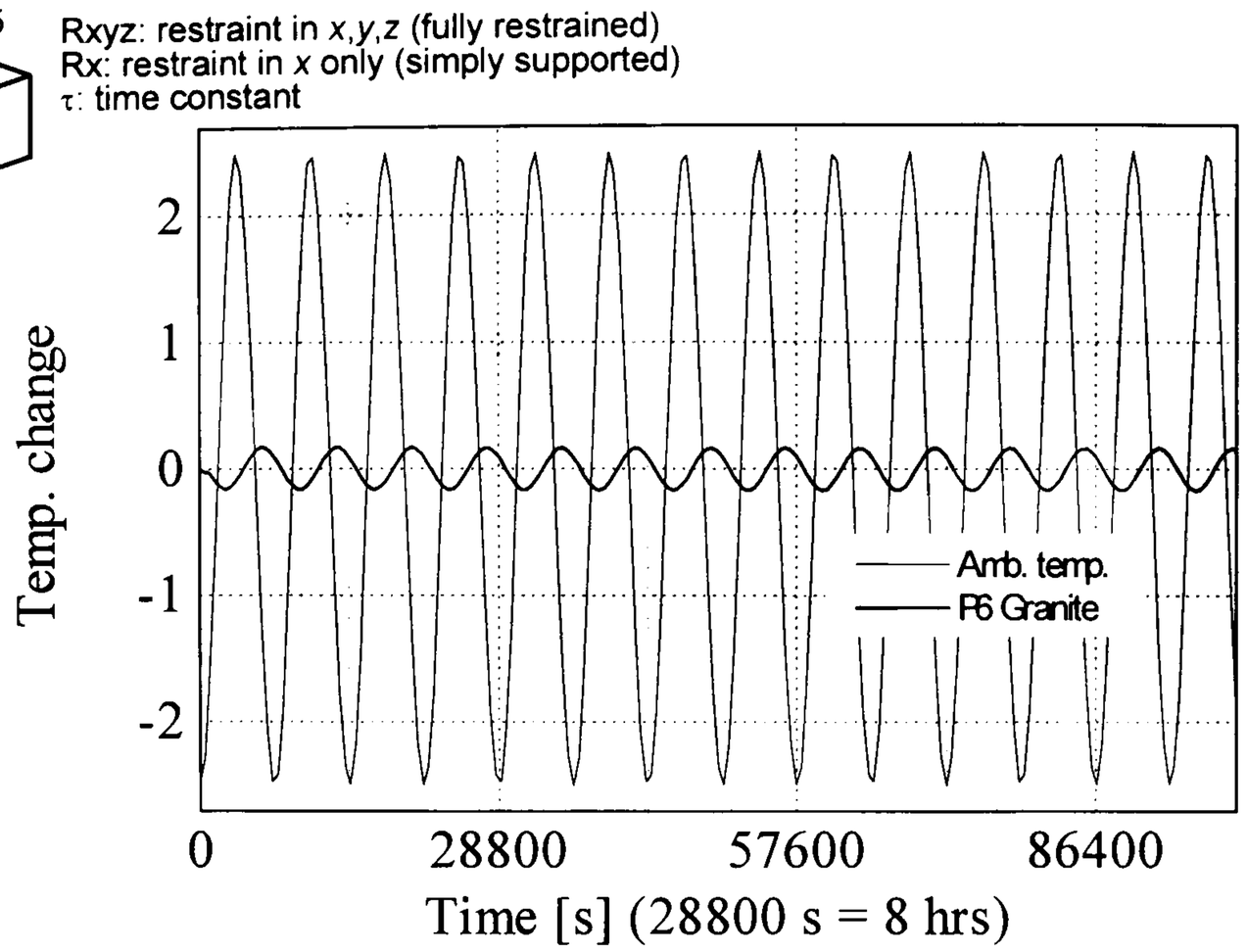

Figure A.64
Granite
Amp.=2.5
Period=7200
Phase = -90
Rxyz

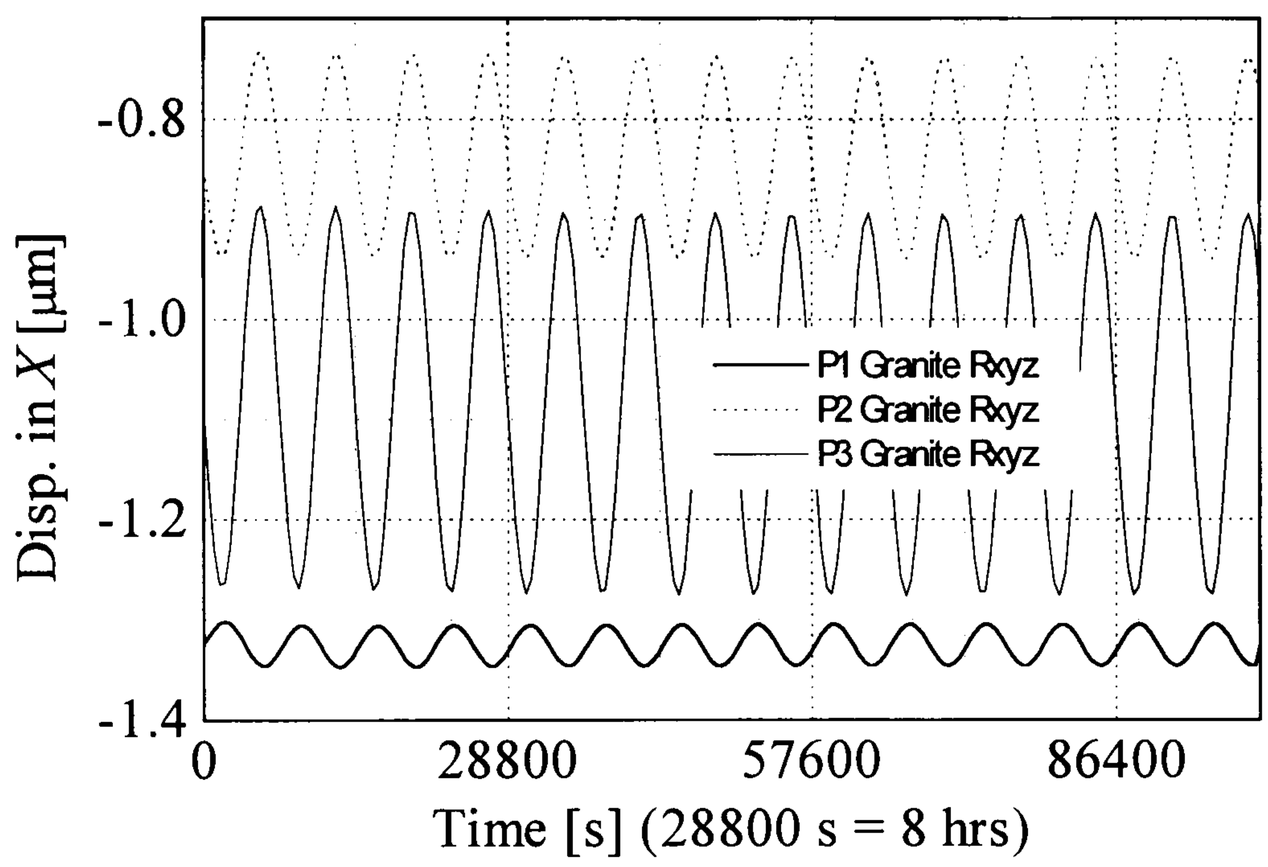

Figure A.65
Granite
Amp.=2.5
Period=7200
Phase = -90
Rxyz

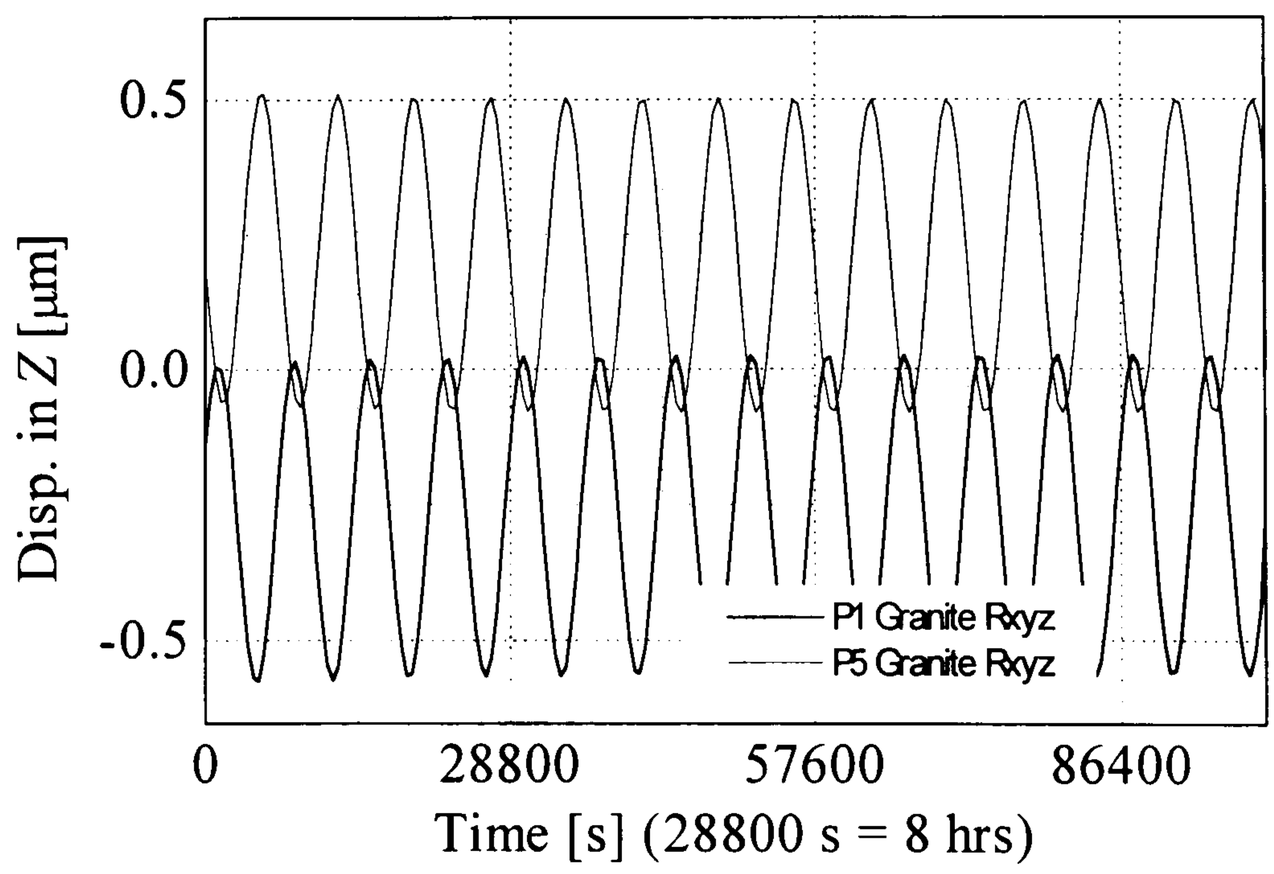

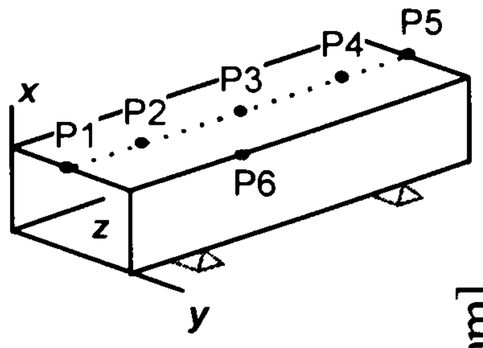

Figure A.66
Granite
Amp.=2.5
Period=7200
Phase = -90
Rx

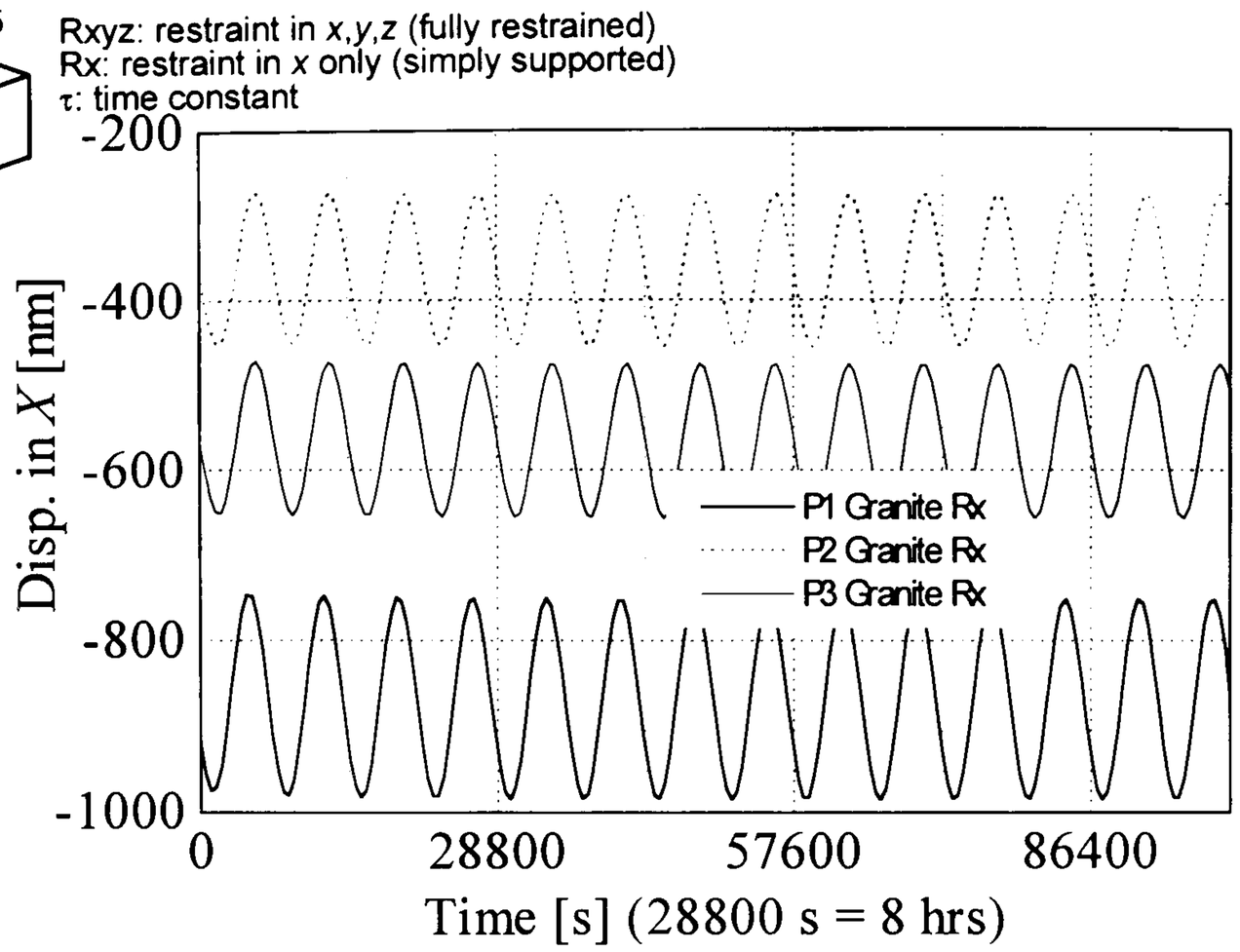

Figure A.67
Granite
Amp.=2.5
Period=7200
Phase = -90
Rx

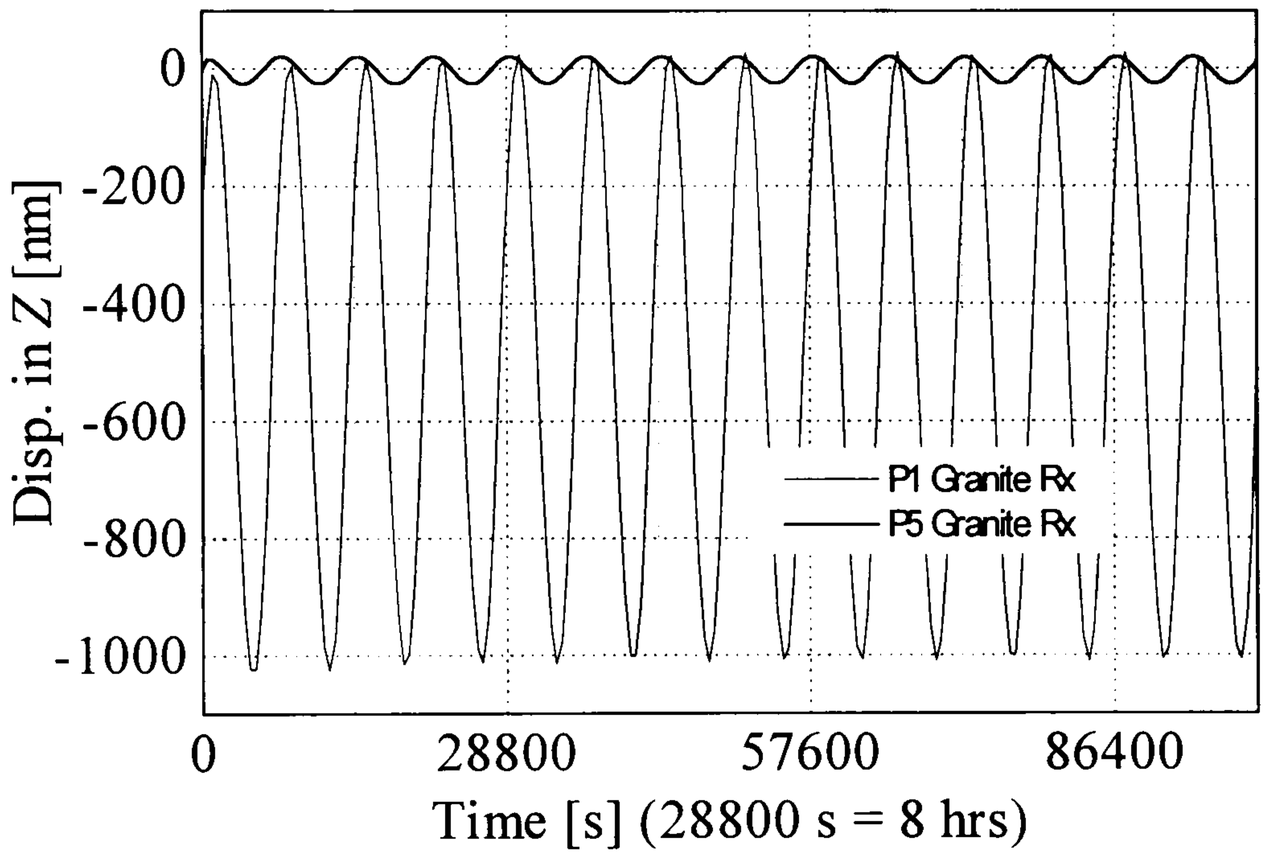

Appendix
B
Results of
Axial Thermal Growth Test*

Figure B.1
Temperature measurement:
Spindle 500 rpm
from 0 to 420 min

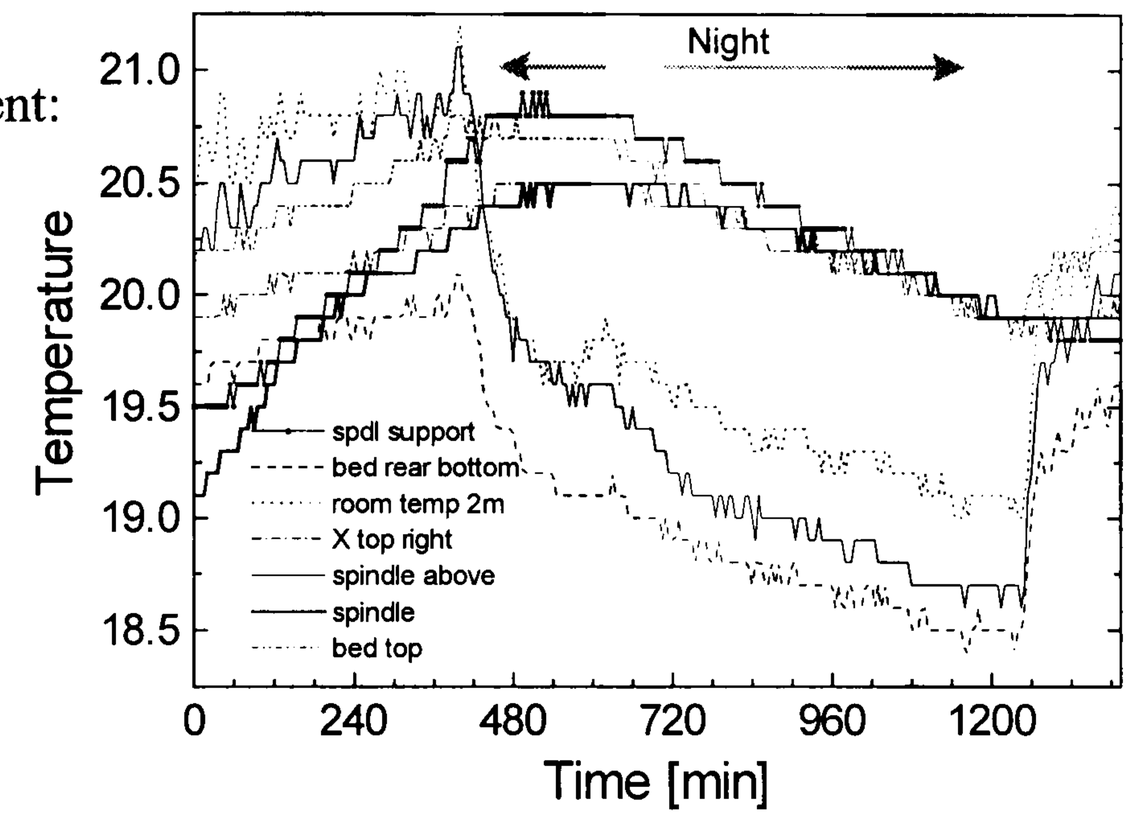

Figure B.2
Displacement measurement
under condition of
Figure B.1
using fibre-optic sensor

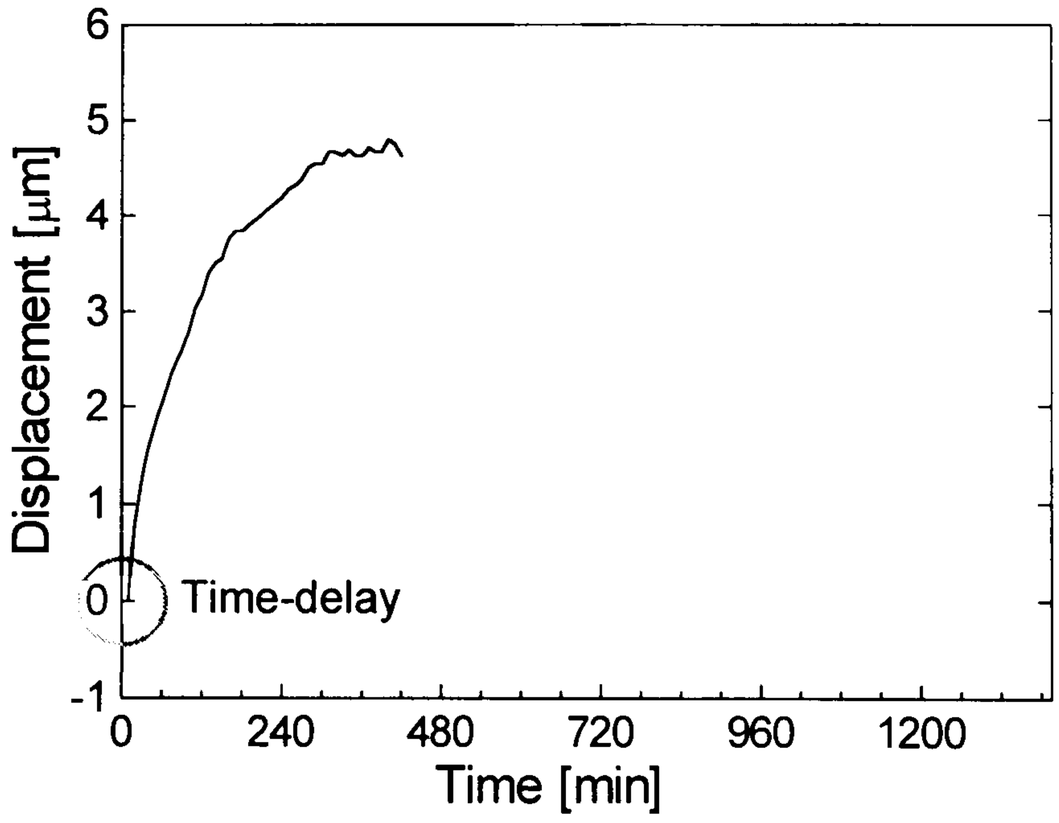

---

* The unit of temperature is °C.

Figure B.3
Temperature measurement:
Spindle 1000 rpm
from 10 min

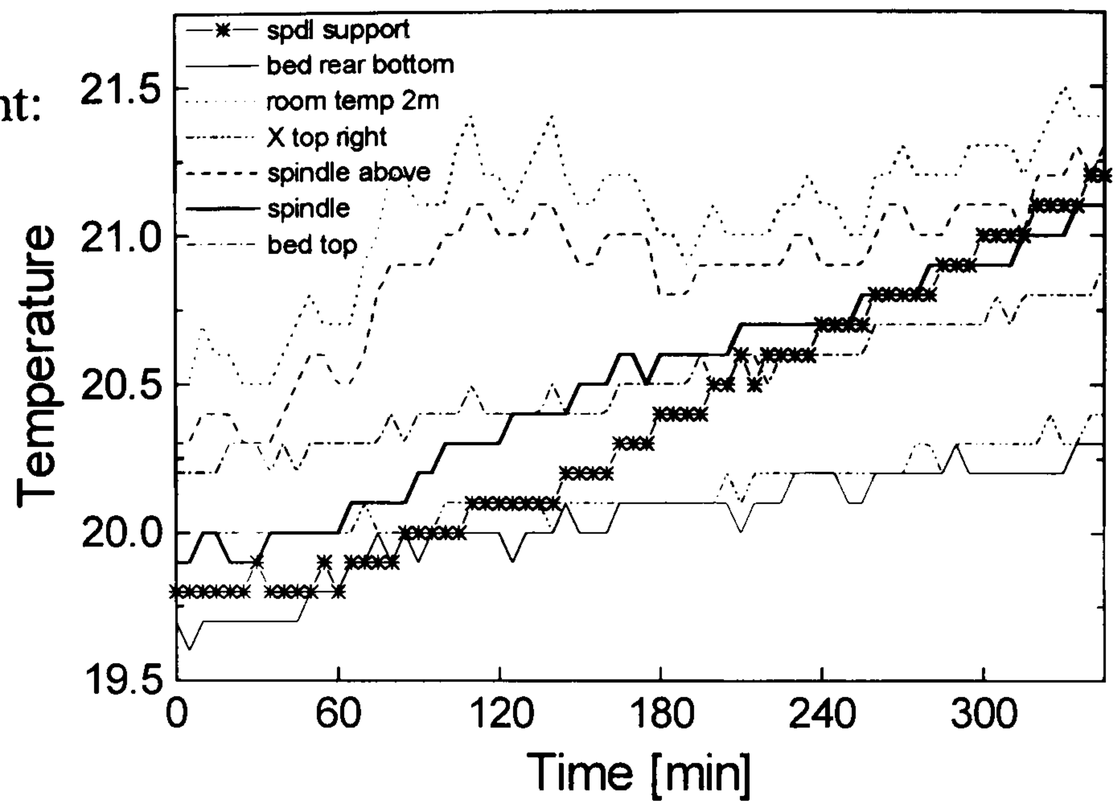

Figure B.4
Displacement measurement
under condition of
Figure B.3
using fibre-optic sensor

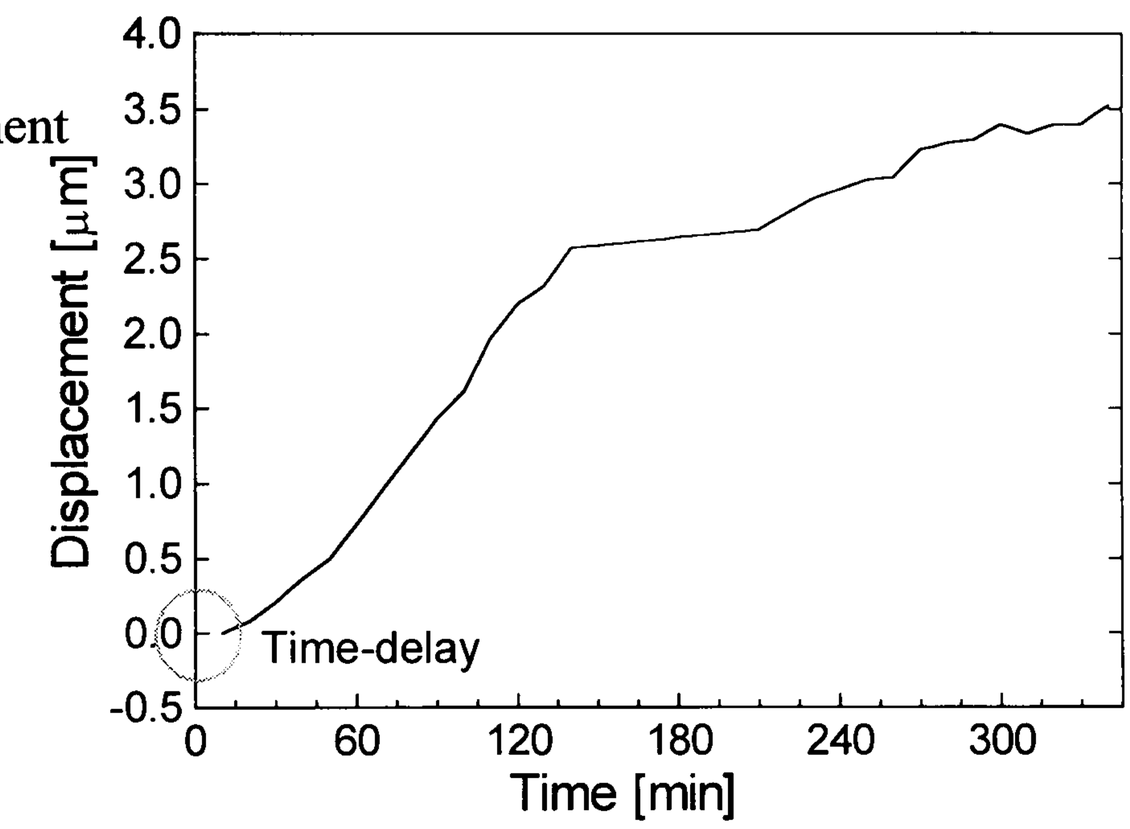

Figure B.5
Temperature measurement:
Idle spindle, no air supply
from evening
to following morning

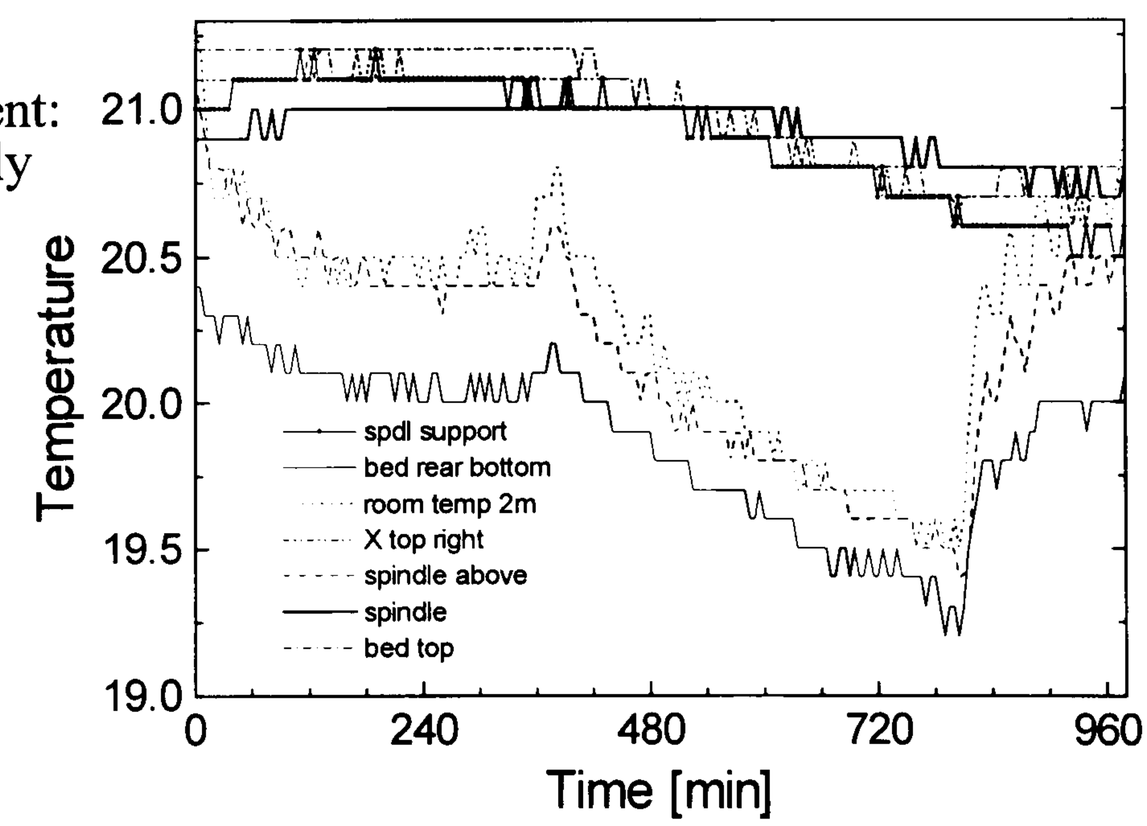

Figure B.6
Displacement measurement
under condition of
Figure B.5
using inductive sensor

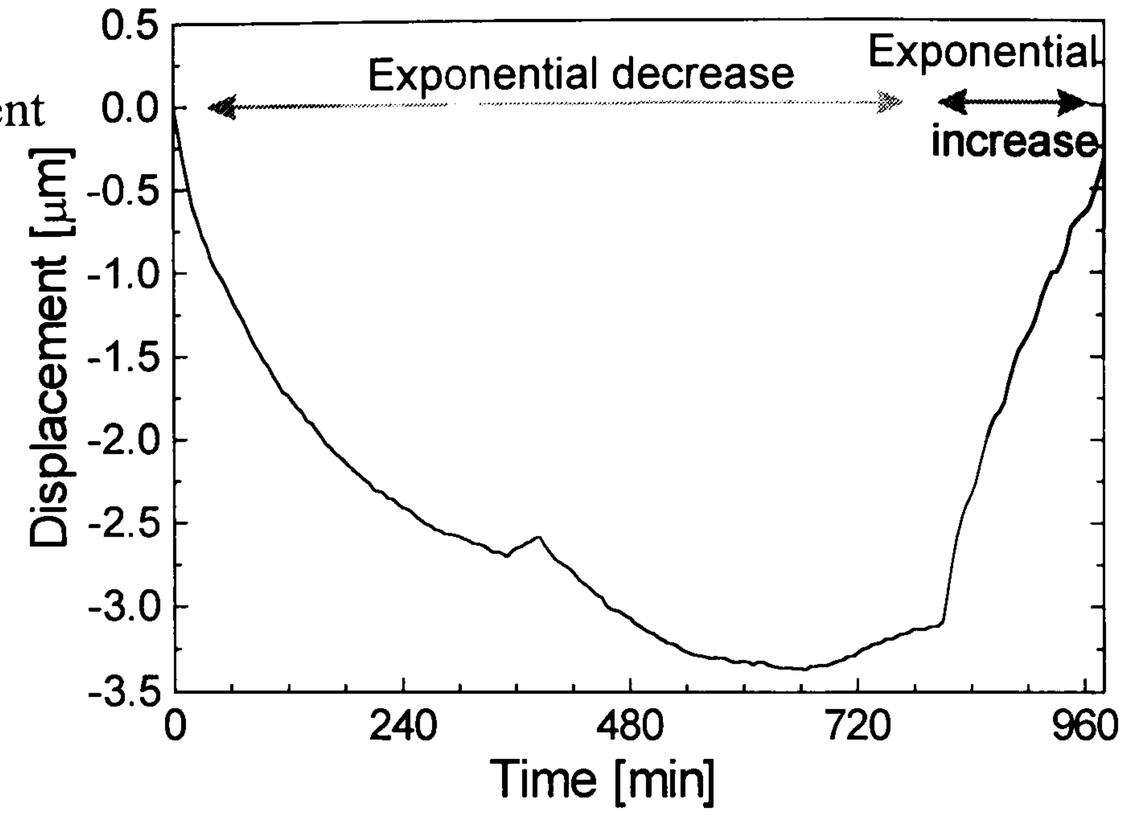

Figure B.7
Temperature measurement:
Spindle running at
1000 rpm from 20 to 200 min
idle from 200 to 1220 min
1000 rpm from 1220 to
1280 min
idle from 1280 to 1340 min
1000 rpm from 1340 to
1400 min

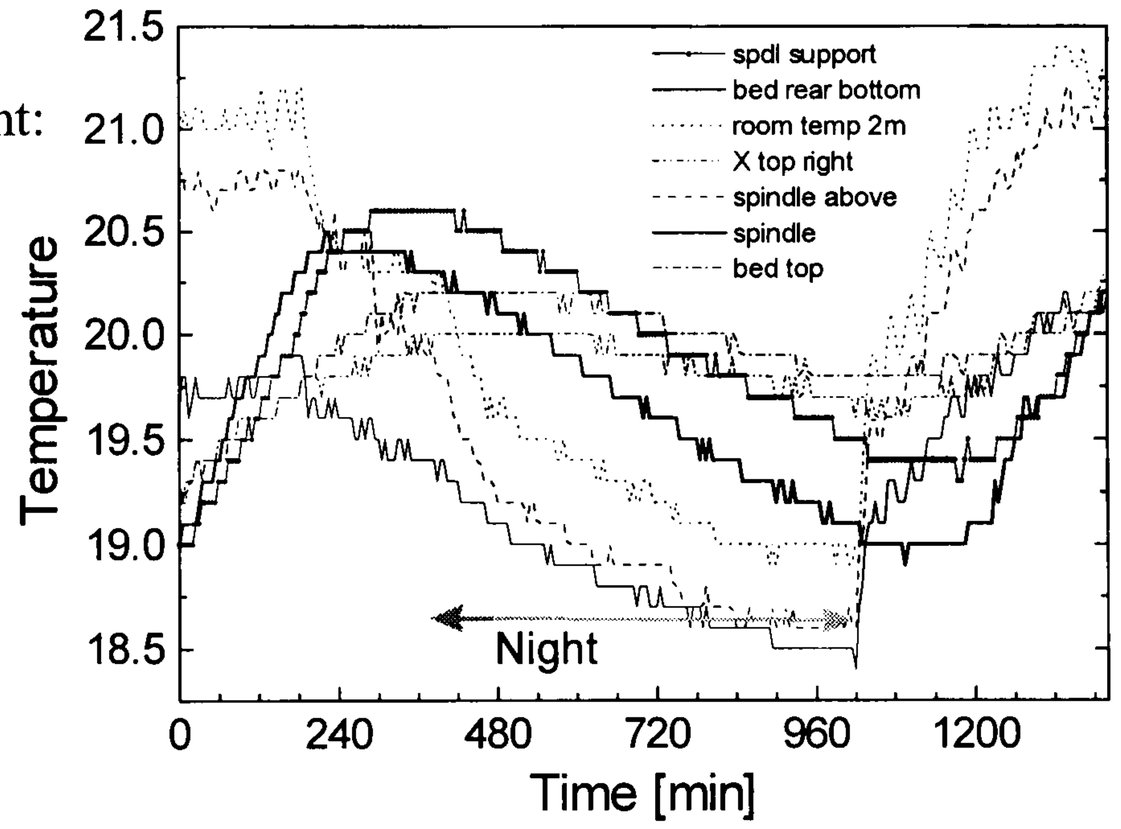

Figure B.8
Displacement measurement
under condition of
Figure B.7
using inductive sensor

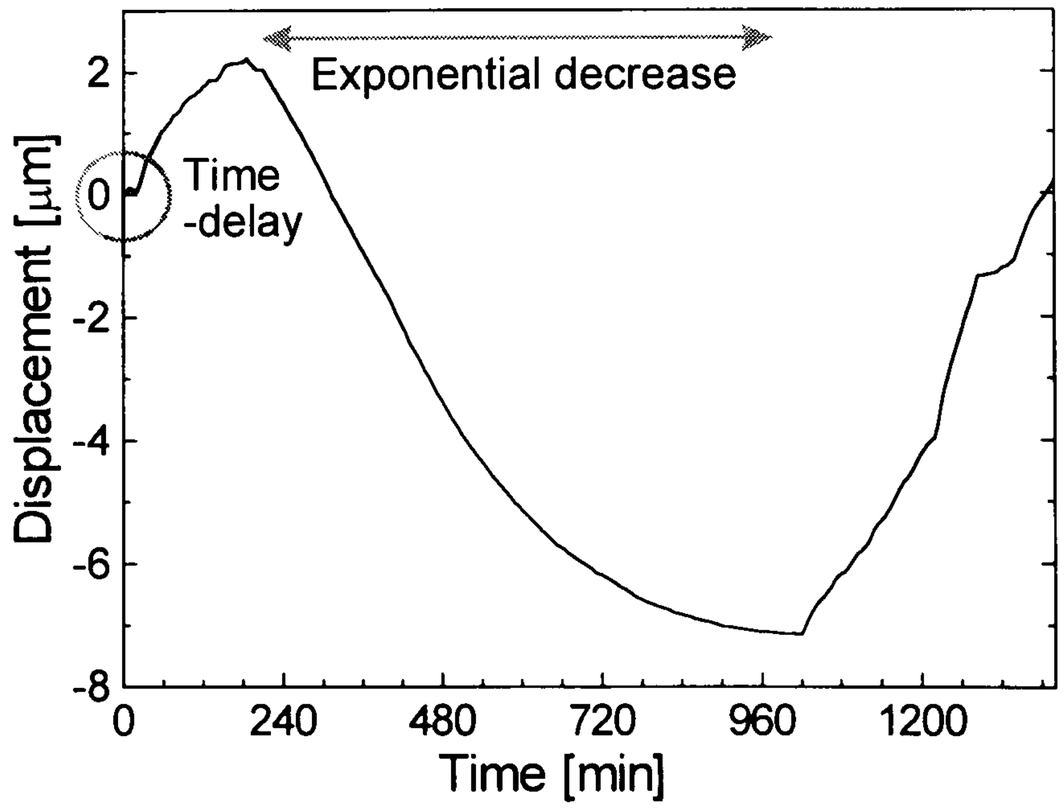

Figure B.9
Temperature measurement:
Spindle running at
1000 rpm from 0 to 120 min
idle from 120 to 240 min
1000 rpm from 240 to 360 min

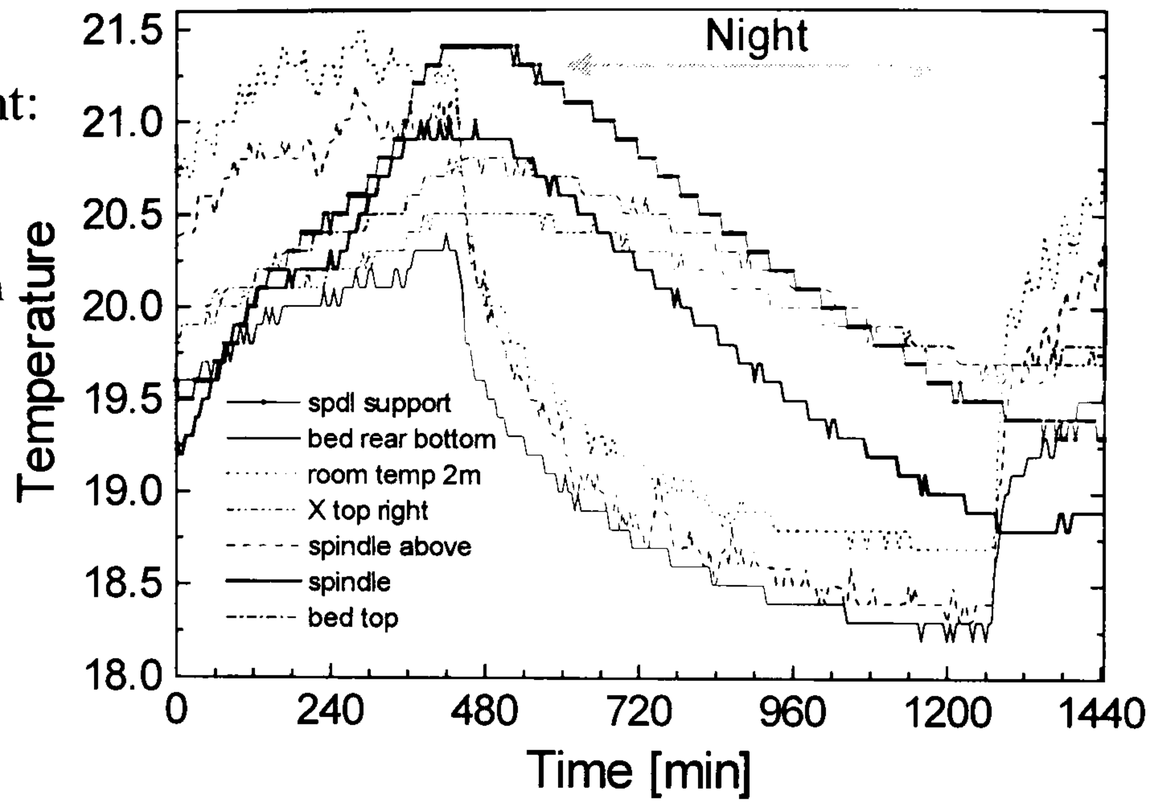

Figure B.10
Displacement measurement
under condition of
Figure B.9
using inductive sensor

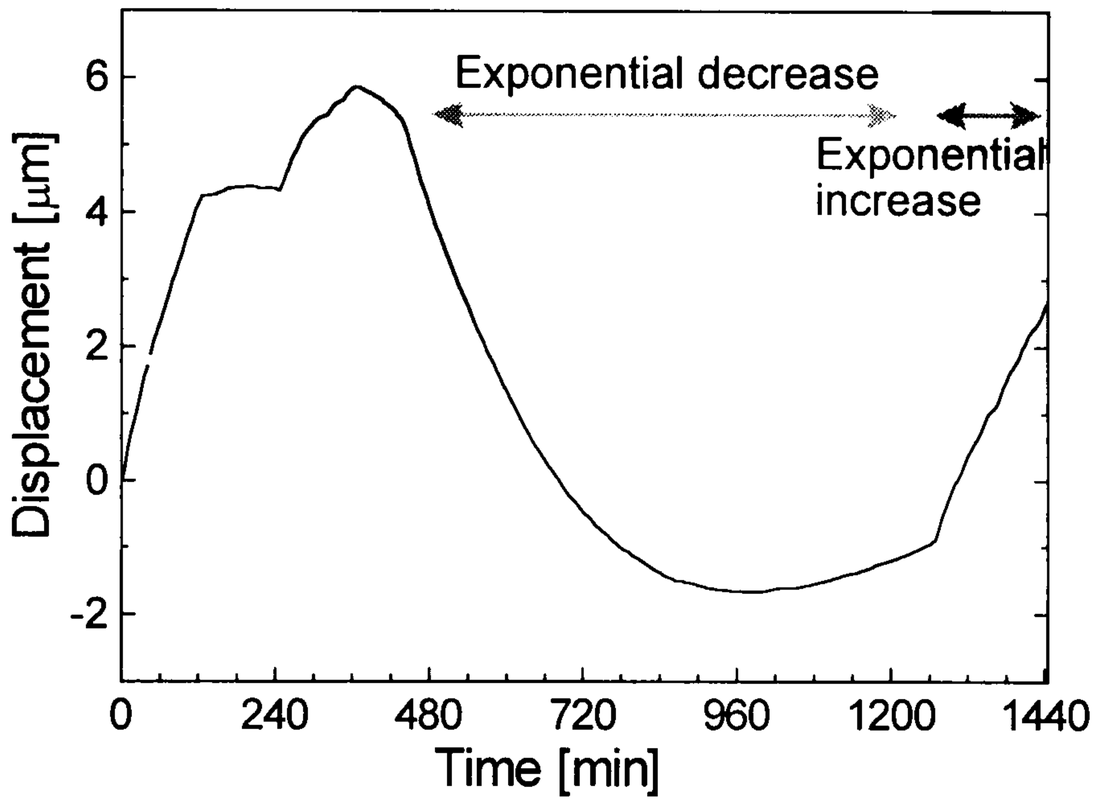

Figure B.11
Temperature measurement:
Spindle running at
1500 rpm form 165 to 255 min
1000 rpm from 255 to 345 min
500 rpm from 345 to end

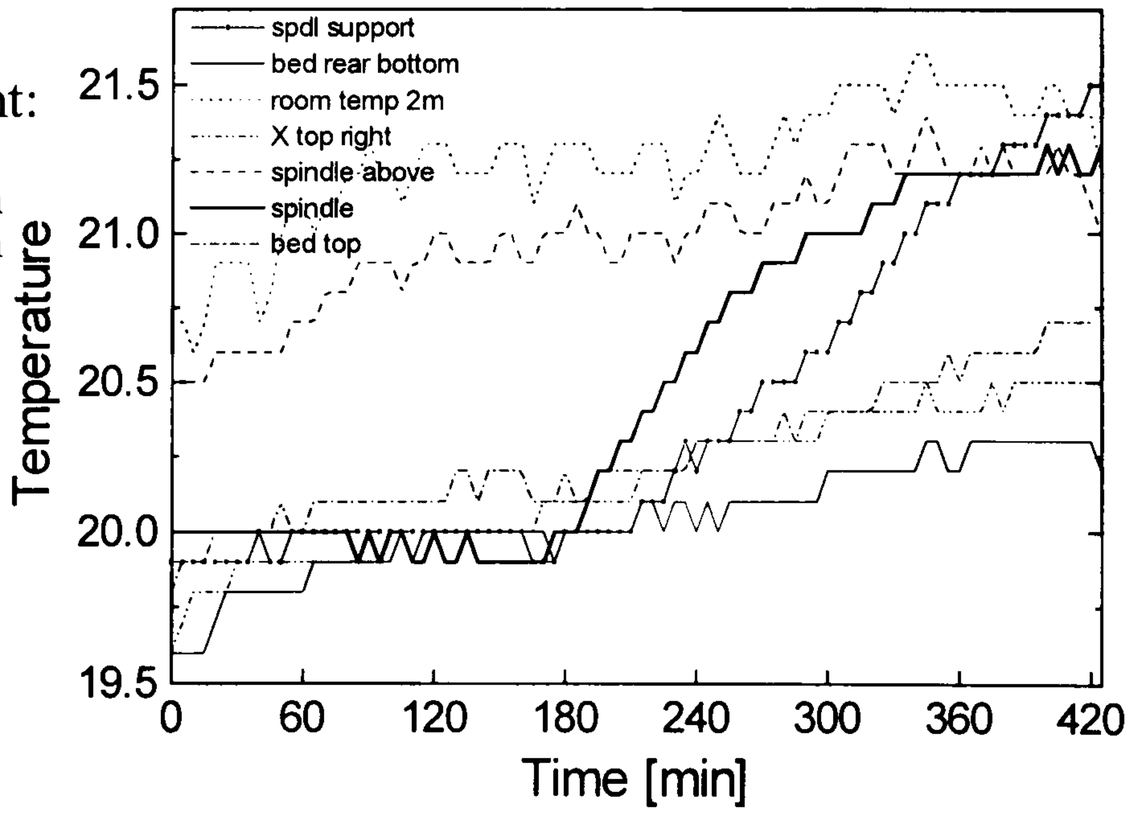

Figure B.12
Displacement measurement under condition of Figure B.11 using inductive sensor

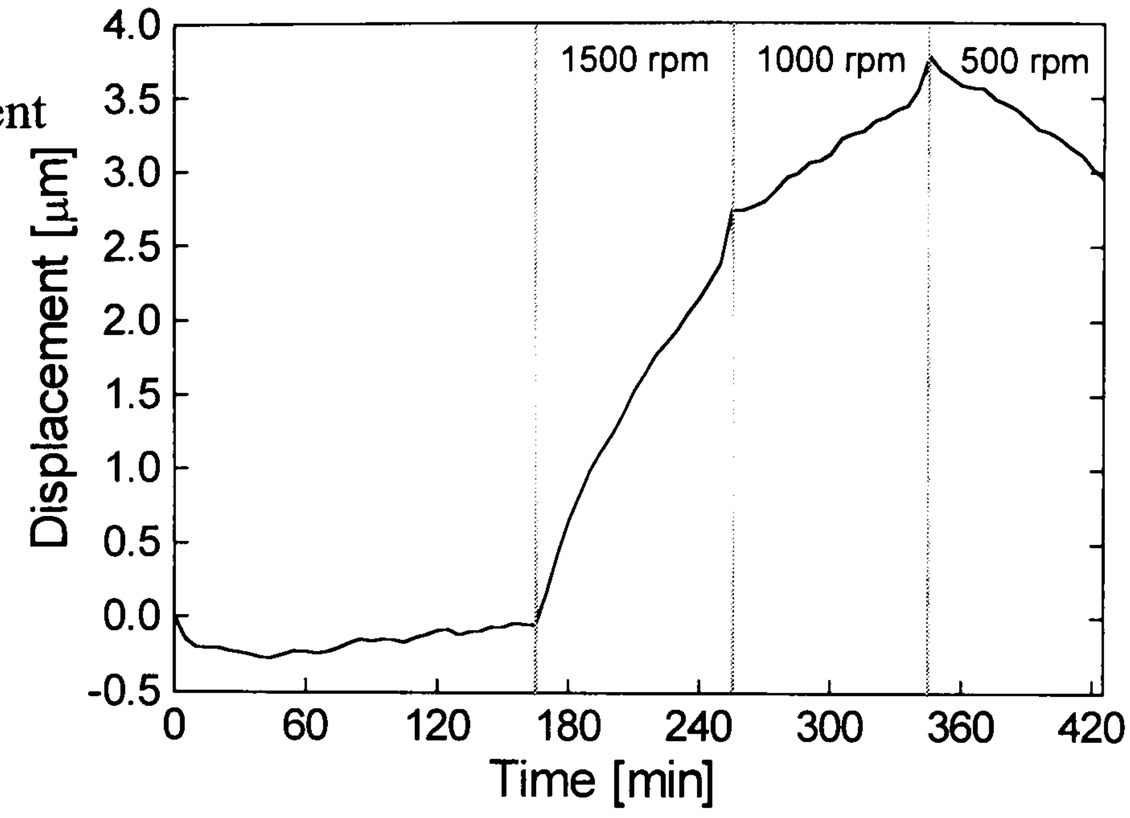

Figure B.13
Temperature measurement: Spindle running at 1000 rpm

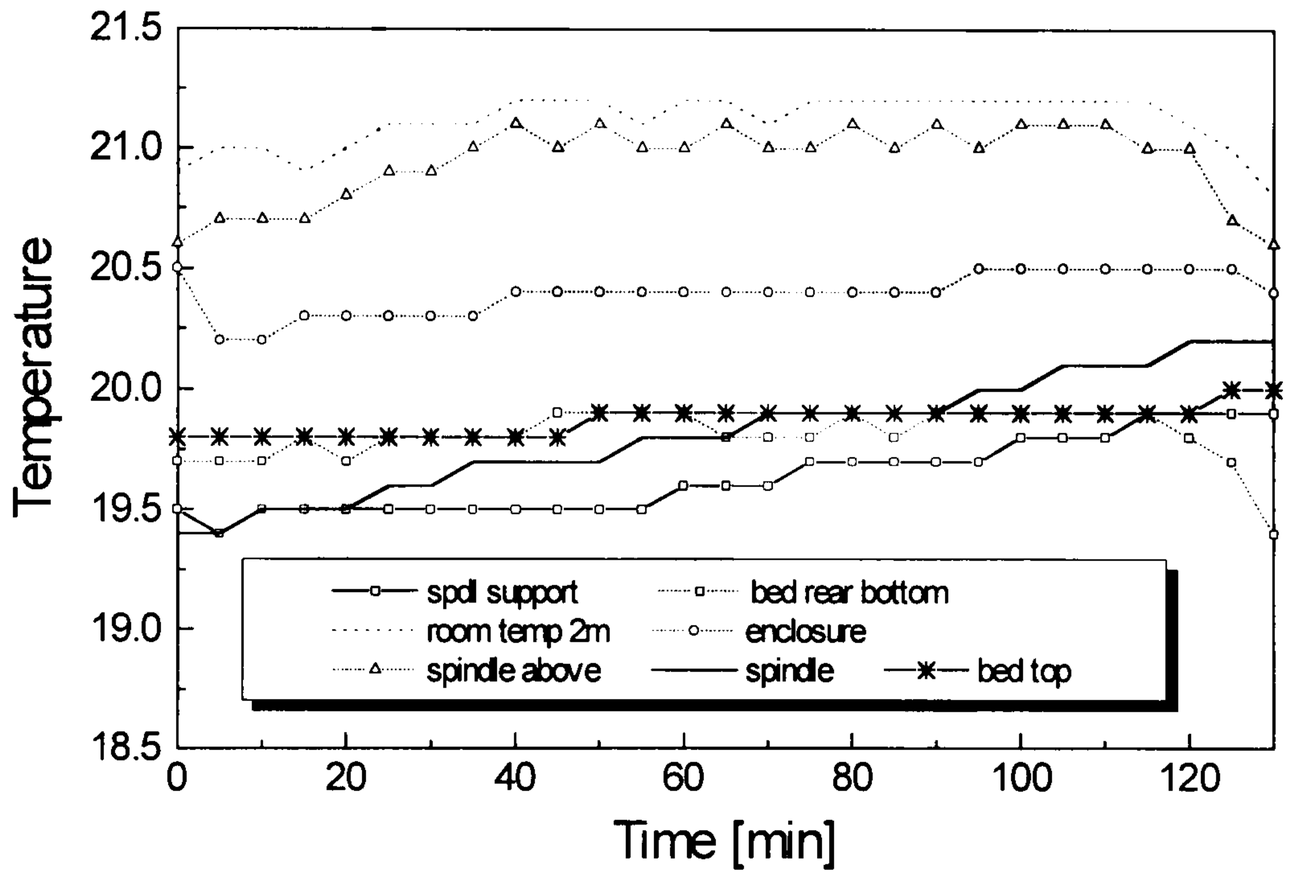

Figure B.14
Displacement measurement under condition of Figure B.13 using enclosure and fibre-optic sensor

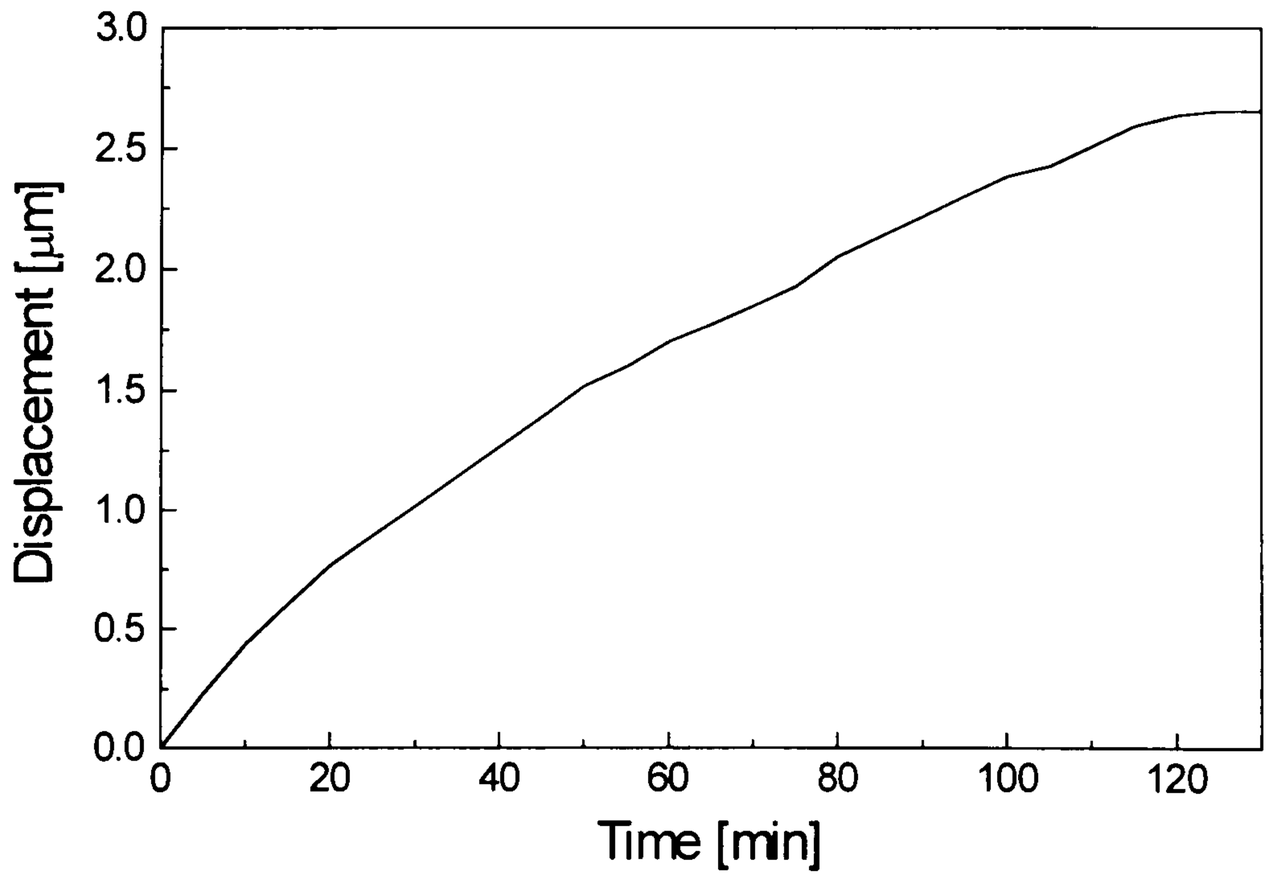

Figure B.15 Temperature measurement: Spindle running at 1500 rpm

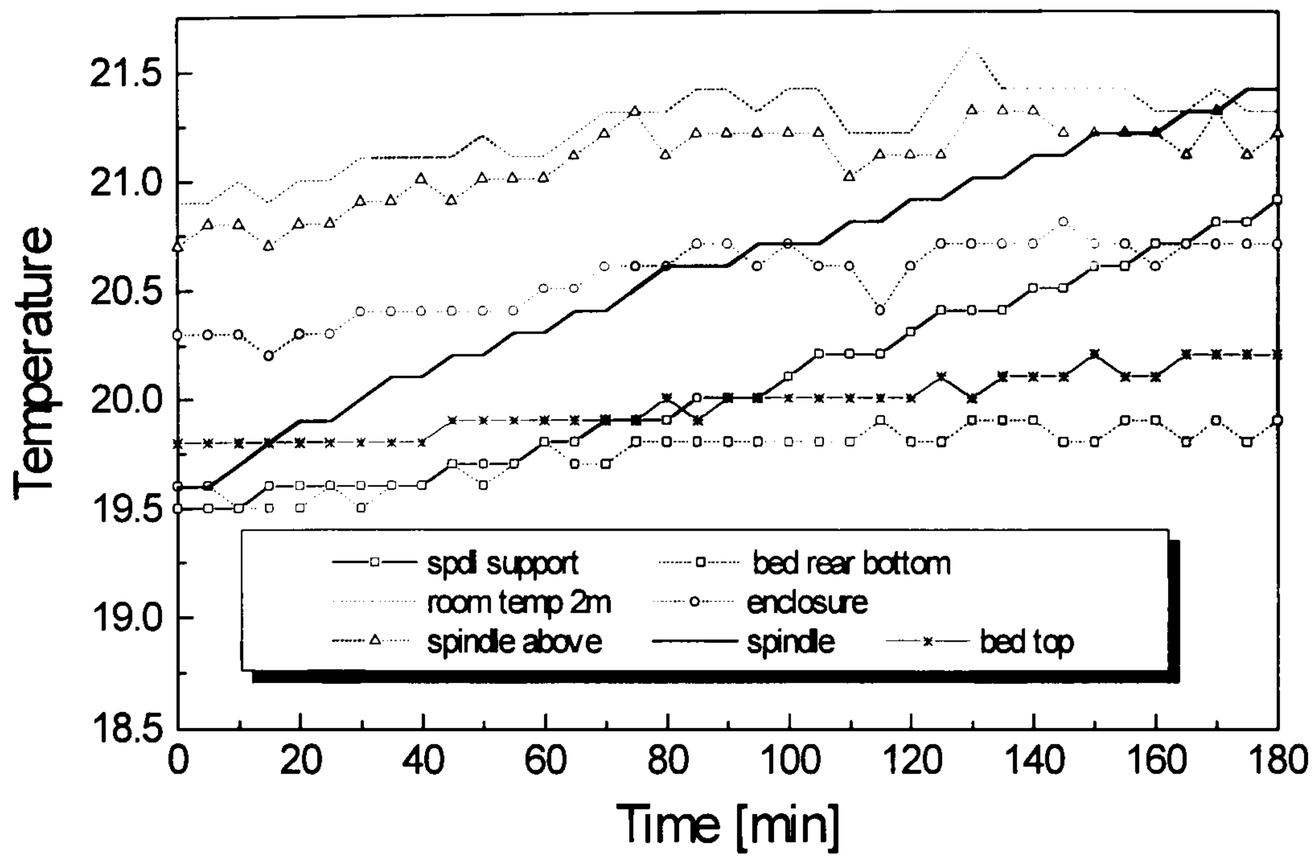

Figure B.16 Displacement measurement under condition of Figure B.15 using enclosure and fibre-optic sensor

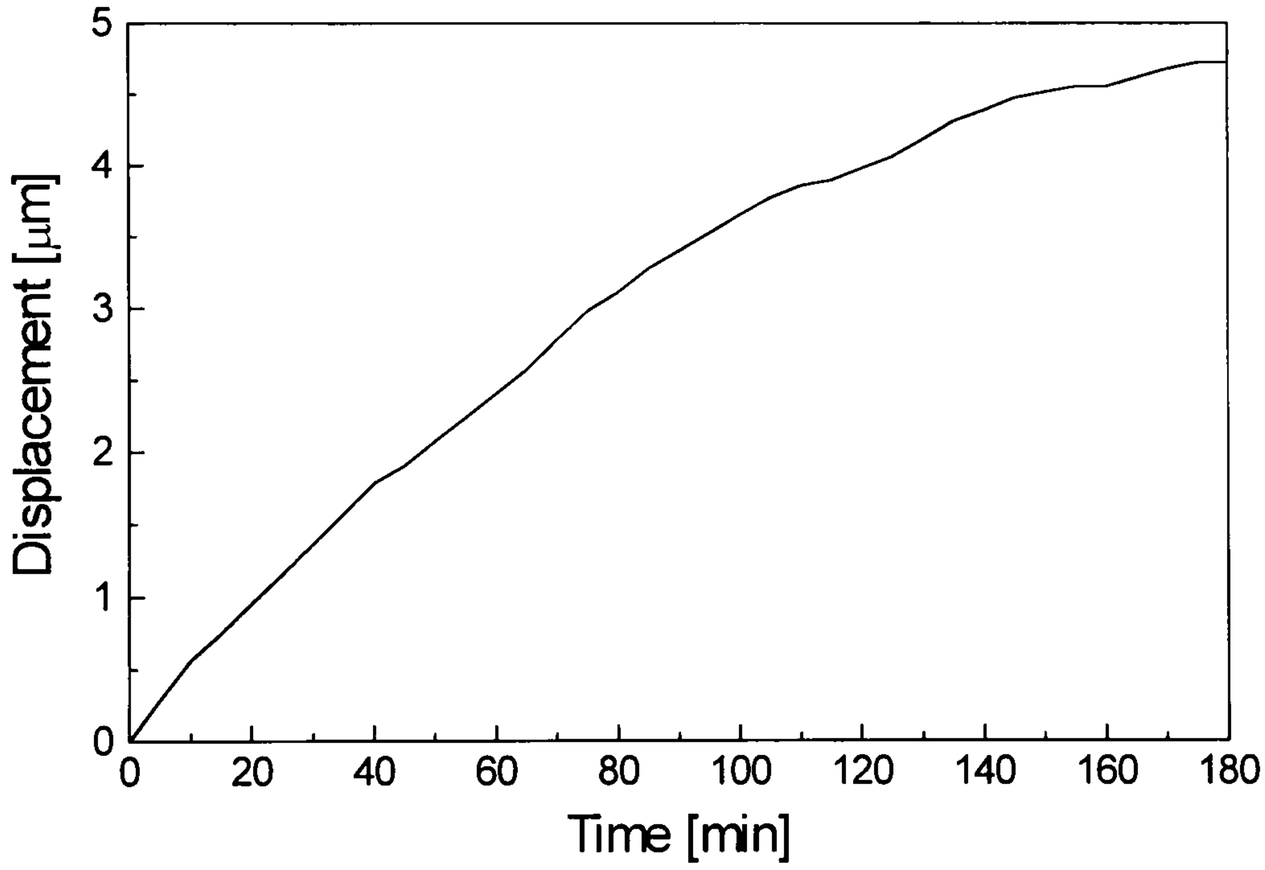

Figure B.17 Temperature measurement: Spindle running at 500 rpm

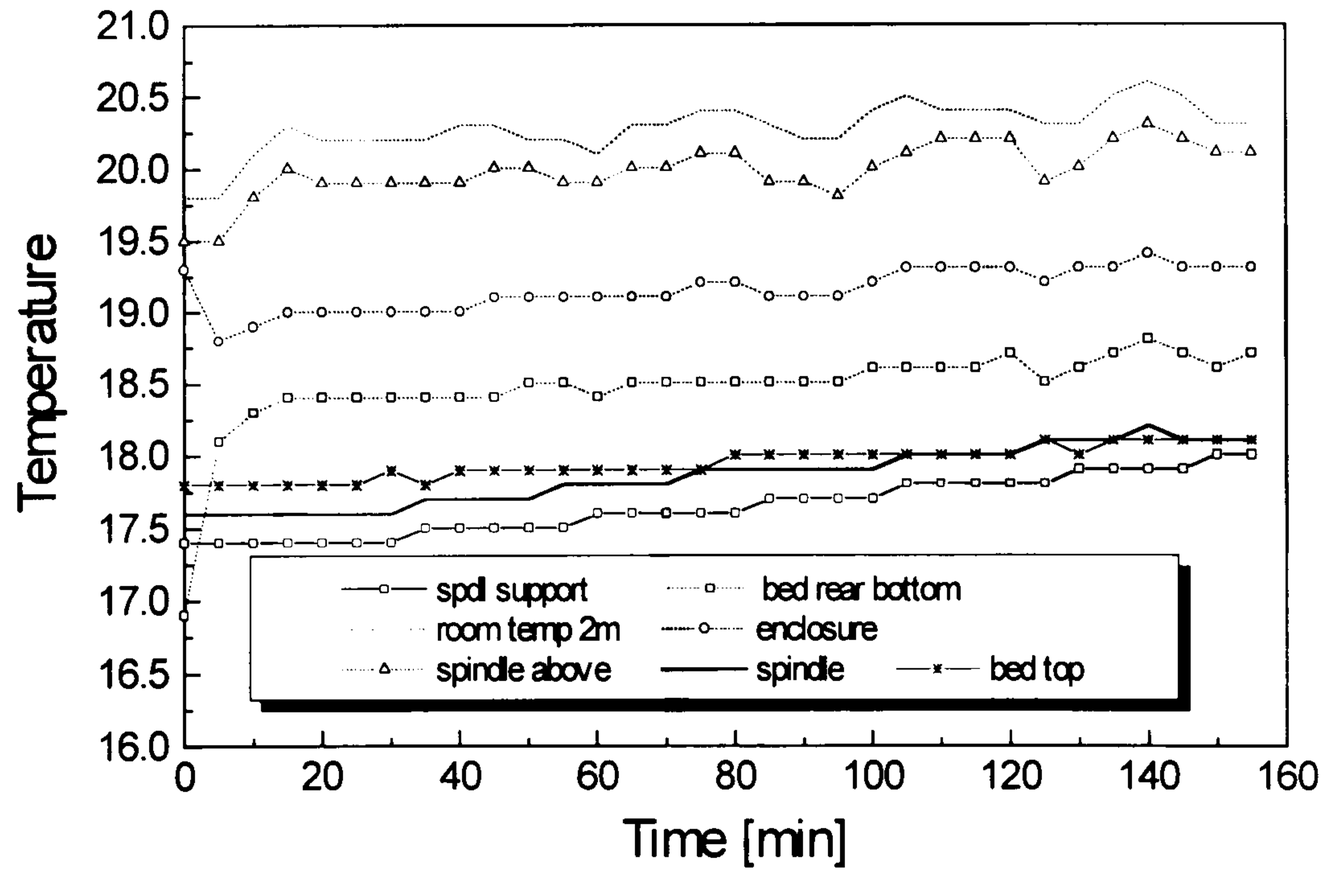

Figure B.18 Displacement measurement under condition of Figure B.17 using enclosure and fibre-optic sensor

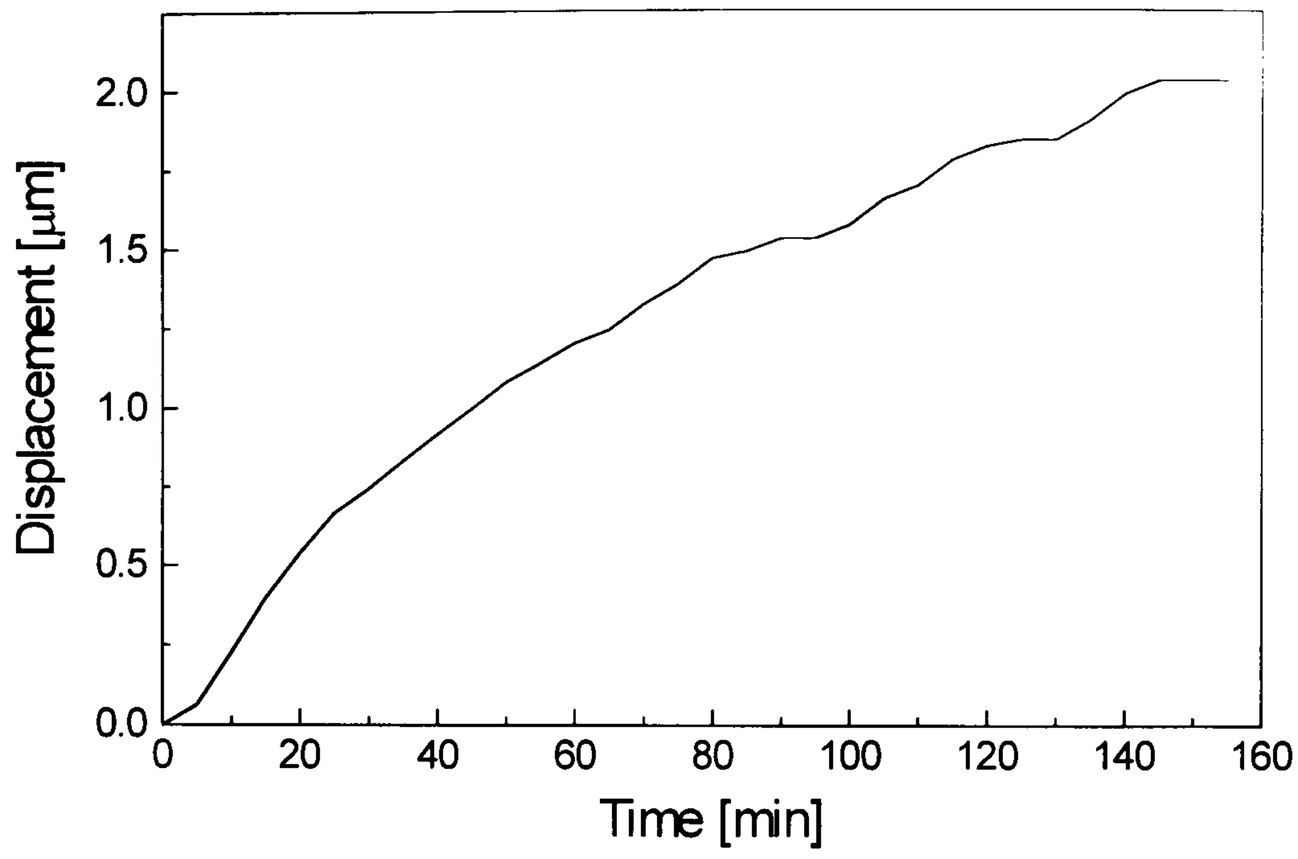

Figure B.19 Temperature measurement: Spindle running at 1000 rpm

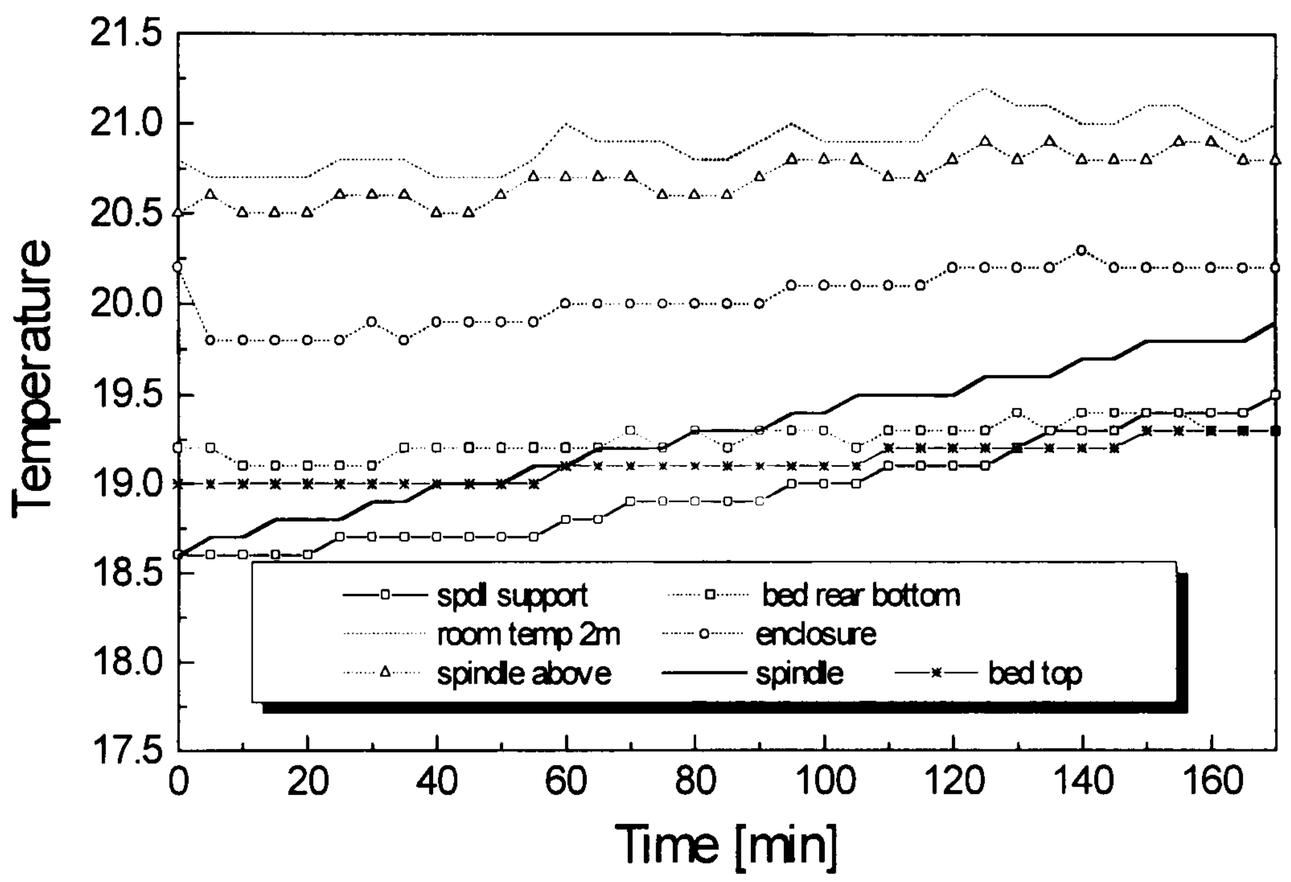

Figure B.20 Displacement measurement under condition of Figure B.19 using enclosure and fibre-optic sensor

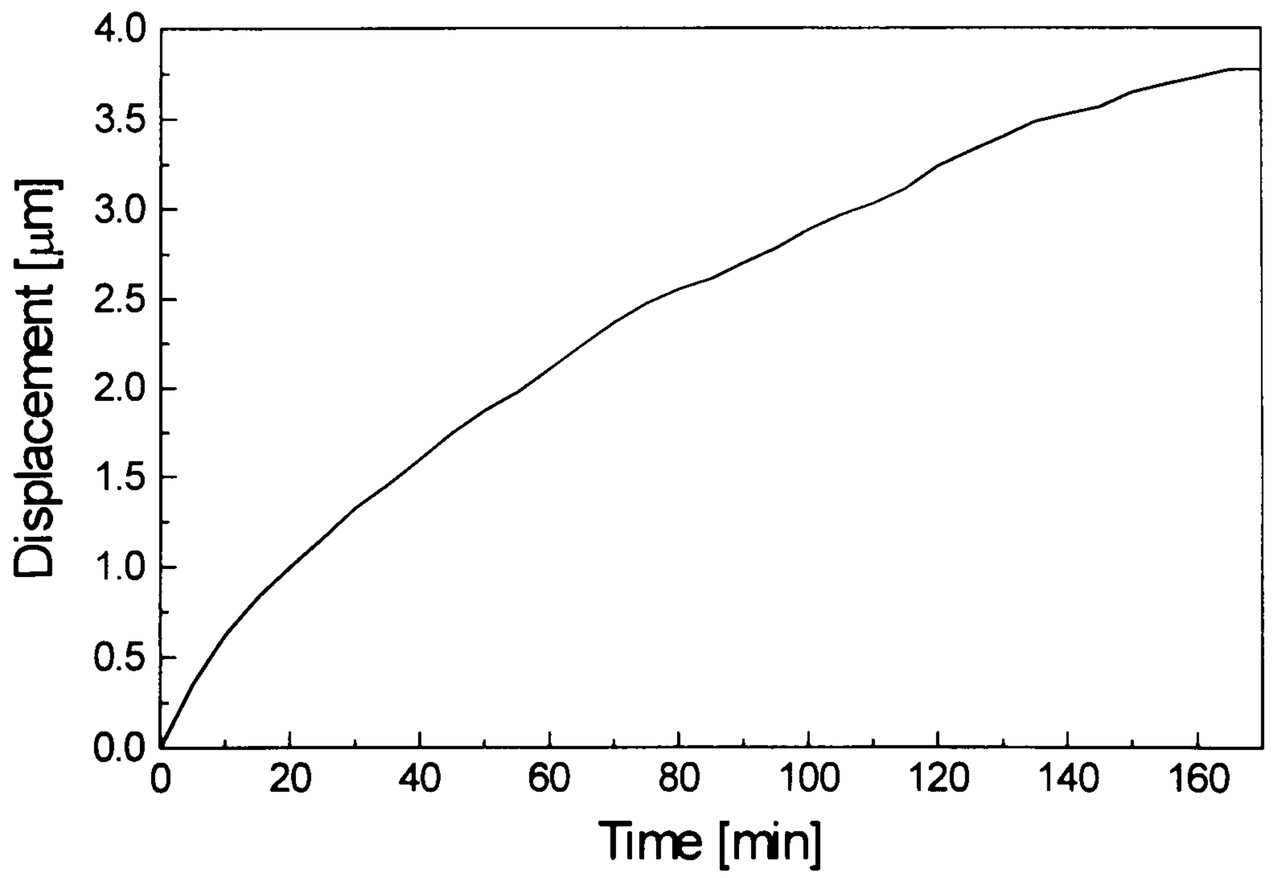

Figure B.21
Temperature measurement: Spindle running at Stepwise increase as shown in B.22

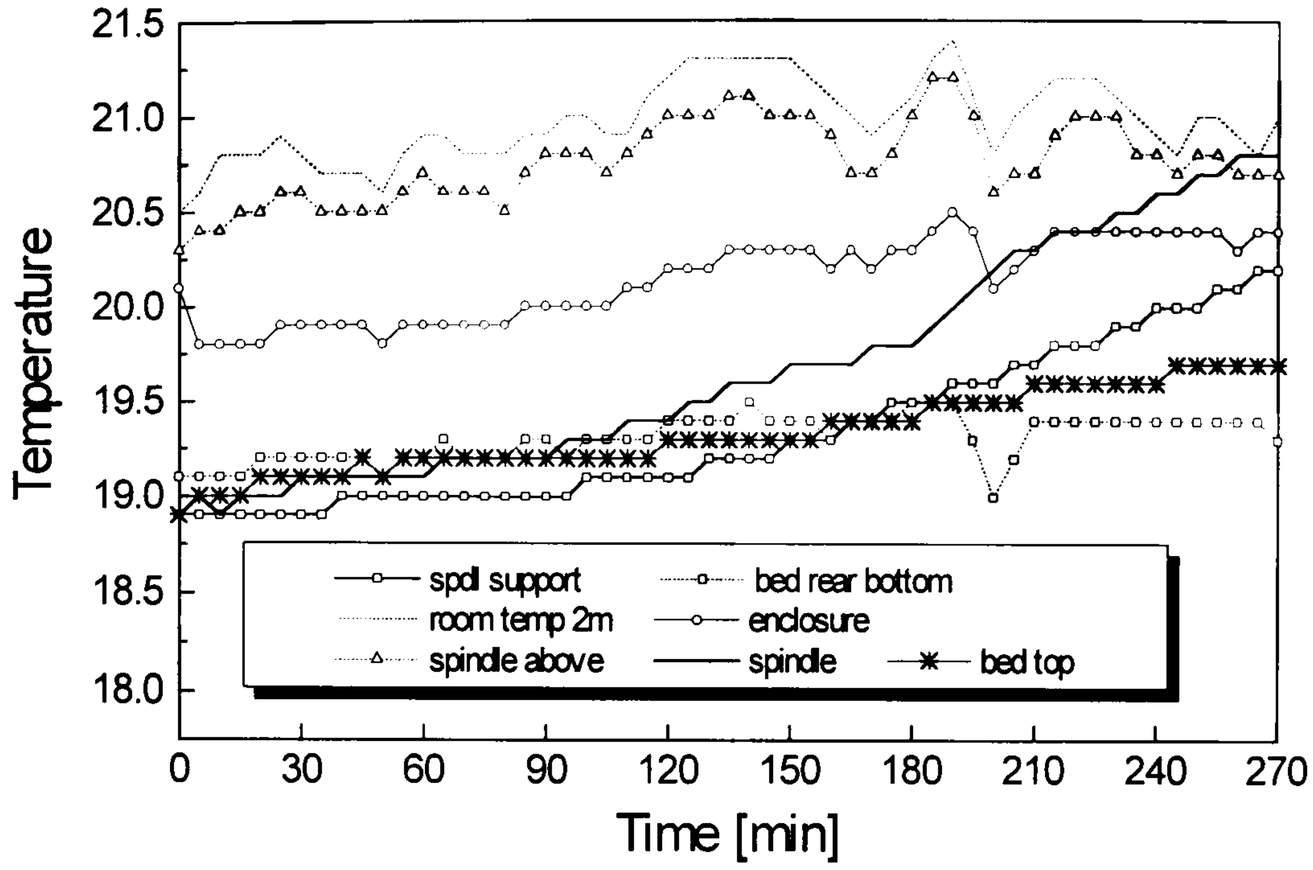

Figure B.22
Displacement measurement under condition of Figure B.21 using enclosure and fibre-optic sensor

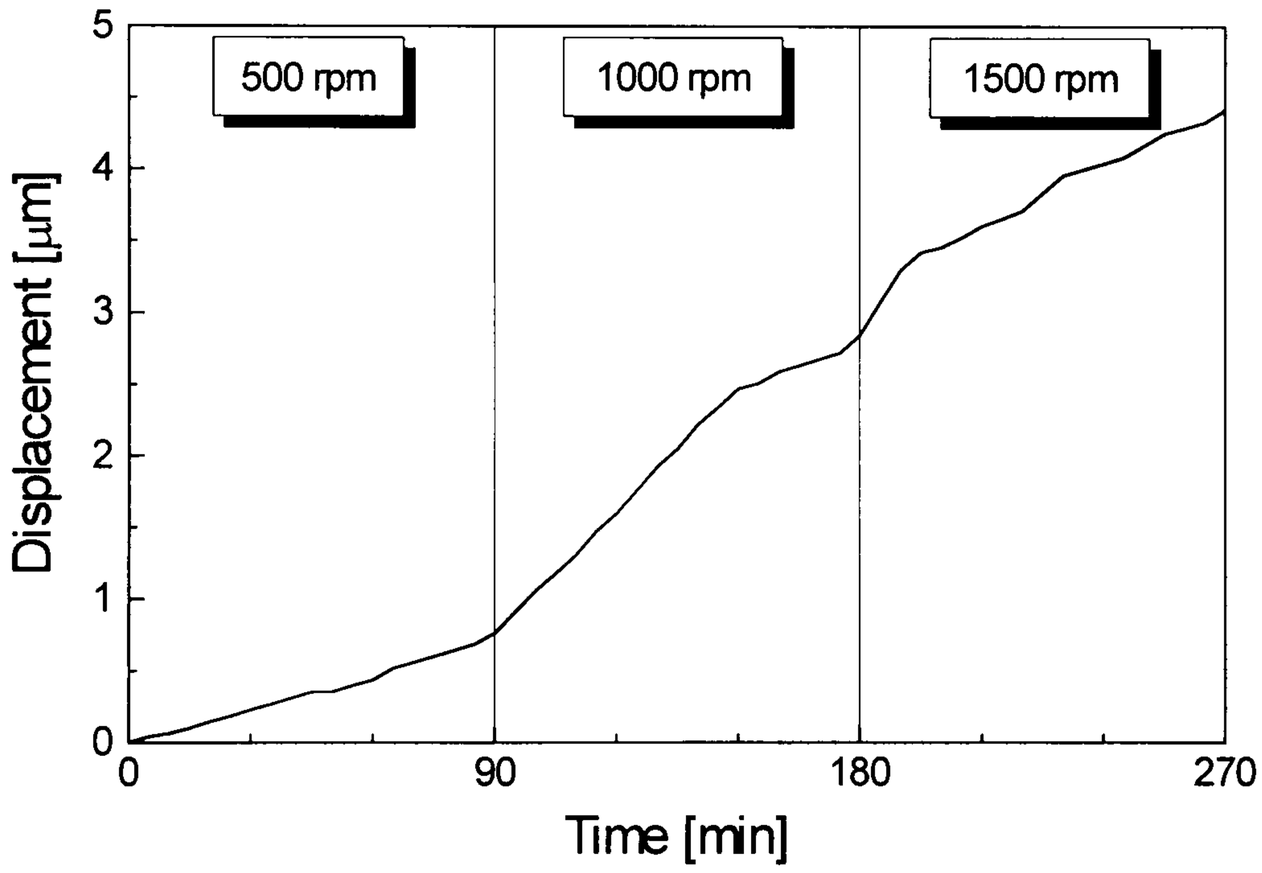

Figure B.23
Temperature measurement: Spindle running at 1000 rpm from 0 to 60 min idle from 60 to 95 1000 rpm afterwards

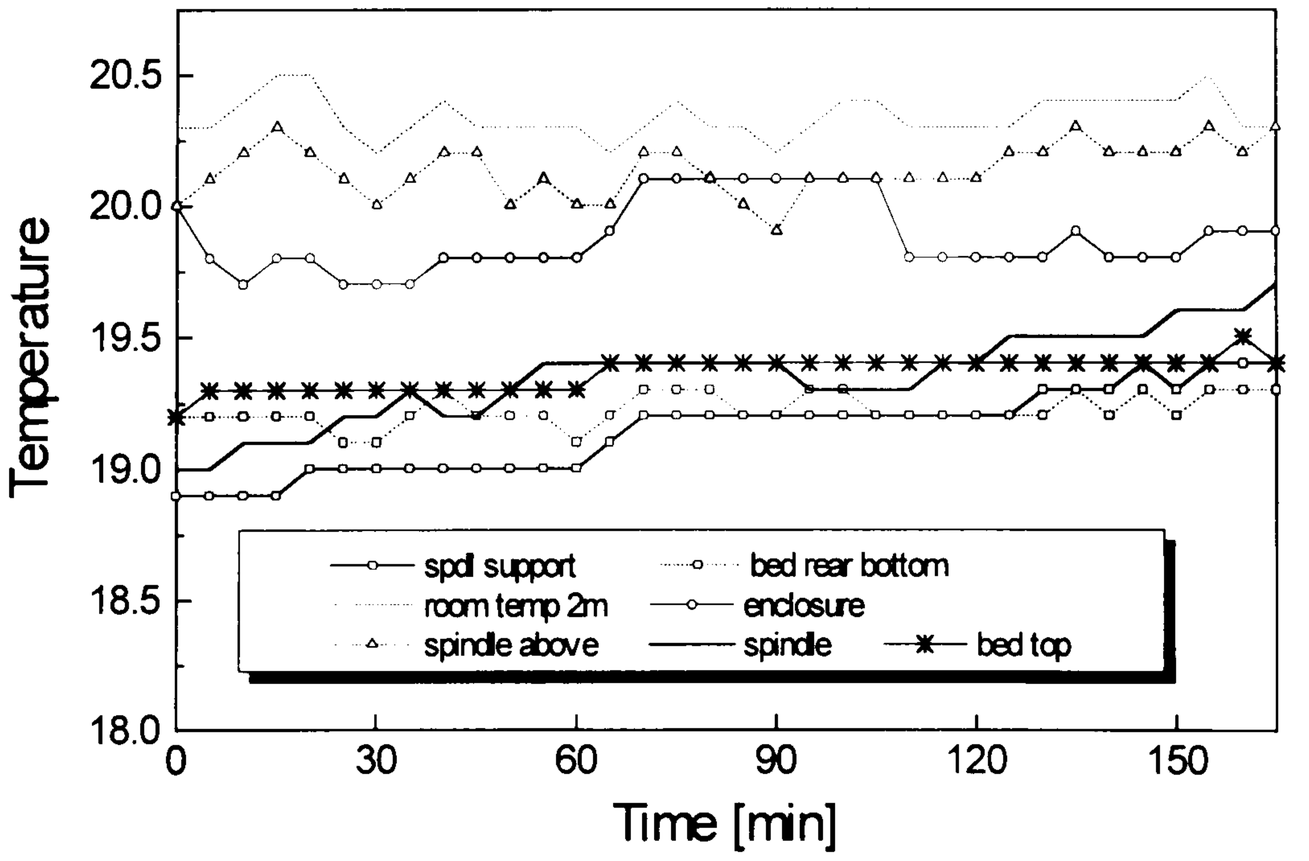

Figure B.24
Temperature measurement:
Spindle running at 1000 rpm from 0 to 60 min idle
from 60 to 105 1000 rpm afterwards

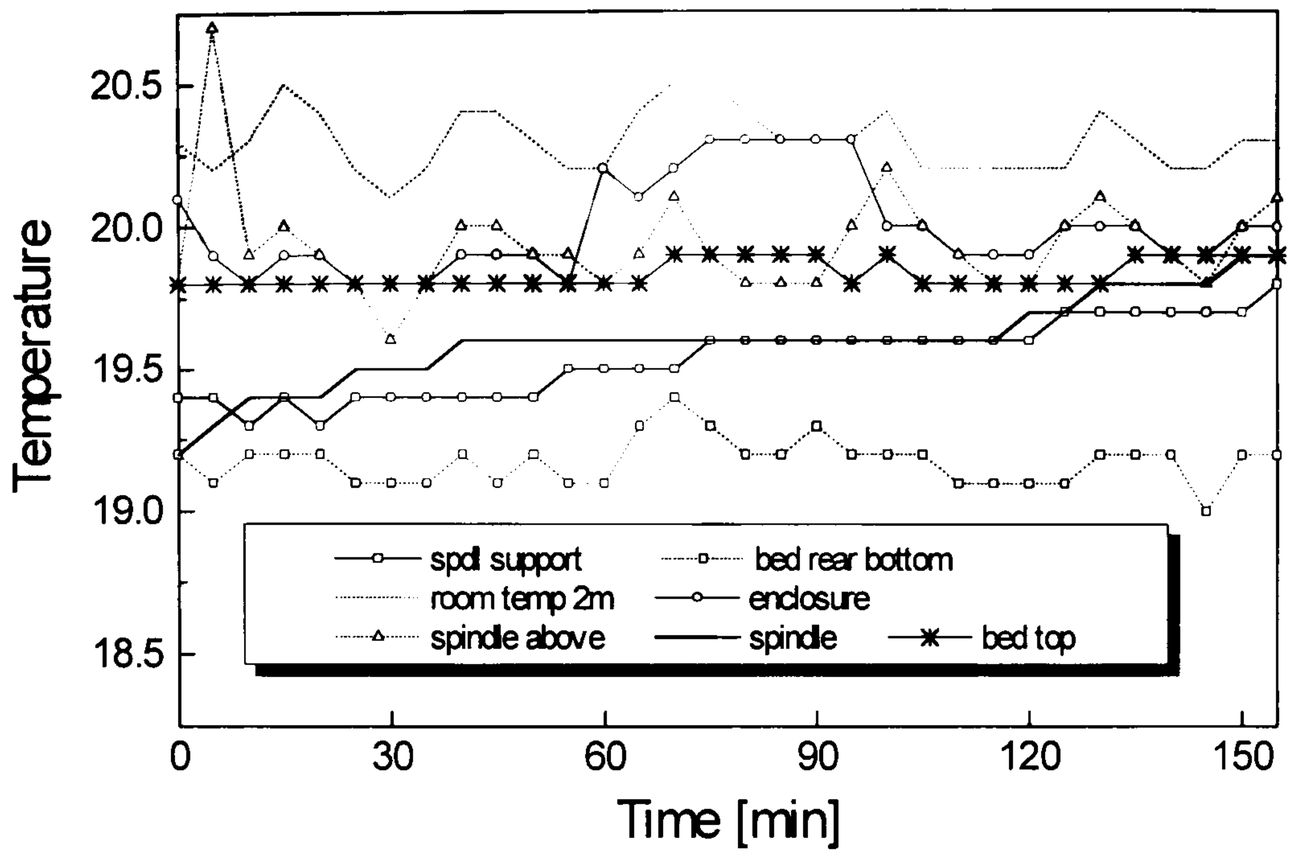

Figure B.25
Displacement measurement under condition of Figure B.23,24 using enclosure and fibre-optic sensor

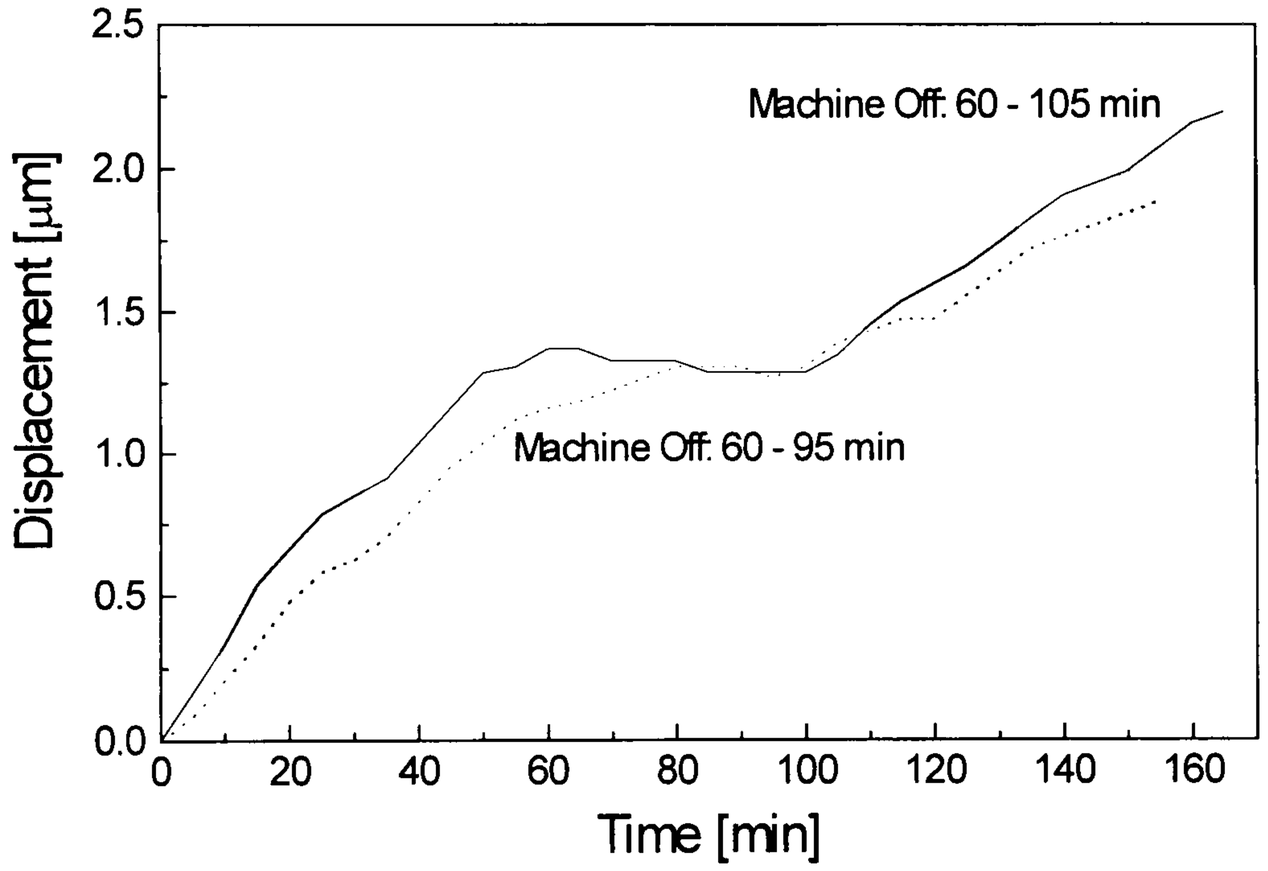

Appendix
C
Design of Thermally Insensitive Hydrostatic Spindle*

C.1 Introduction

Externally-pressurised hydrostatic-bearings are often applied to machine tool spindles, since they have a high degree of stiffness and damping, and a rugged structure. One of the most unique characteristics of fluid-film bearings is their built-in error correcting capability**. Hydrostatic bearings have a large projected area of load-carrying surface at a corresponding low level of pressure. The film pressure over the area is also constant in spite of local variations in surface roughness or minute deviations from local geometry that may exist. As a result, hydrostatic bearings provide an averaging effect, so that motion of hydrostatically supported elements has less deviation than that found in the bearing elements themselves. Another advantage of hydrostatic bearings is that the shaft or slide may be positioned with extreme accuracy after assembly by adjusting flow-control valves. However, oil-lubricated spindles can be thermally deflected by up to a tens of micrometres due to the viscous friction at high speeds***. This is not acceptable in precision machine tools.

There might be a situation where the development of a thermally insensitive hydrostatic spindle for a precision lathe is required under a tight budget. The radial stiffness measured at the spindle nose should be over 100 N/μm, and the axial stiffness 250 N/μm. The author thinks that lathes are the most price sensitive machine-tool variety in the market. That is, sophisticated temperature controlling equipment and low-expansion material cannot be allowed to be a part of the spindle and a large temperature rise of the spindle should be catered for. In this case the following can be considered to achieve the objective:

---

* This appendix was intended to be independent of the main text.
** Levesque, G.N. (1965). "Error-correcting action of hydrostatic bearings", *ASME Paper 65-Lubs-12*
*** Wasson, K.L., Lienhard V, J.H. and Slocum, A.H. (1993b), "Thermal performance of hydrostatic radial bearings for precision machine tool applications", *HTD-Vol. 259: Transport Phenomena in Nonconventional Manufacturing and Materials Processing*, ASME, pp. 101-111

- ❑ Reduction of frictional heat generation in the bearings.
- ❑ More heat removal by lubricant leakage (less heat conduction to the bearing).
- ❑ Reduction of the spindle growth with respect to the tool position (i.e. small gain).
- ❑ Fast stabilisation of the temperature of the spindle (i.e. small time constant).
- ❑ Compensation of the spindle growth by a mechanical means.
- ❑ Cooling of the lubricant and spindle unit.

The last method is to use a simple heat exchanger either in the lubricant supply line or drain line for the lubricant cooling. It is more convenient and gives better results to employ a heat exchanger in the supply line. The cooling of the spindle unit can be achieved by simple arrangements such as fins or a forced draft of air blowing over the bearing housing. Other methods will be discussed in the subsequent sections.

Among many kinds of bearing configurations for machine-tool spindles, an arrangement such as depicted in Figure C.1 is considered here because of its simplicity. The nose part of the spindle from the thrust bearing, which is considered to be directly proportional to the axial thermal growth, can be minimised with this configuration, so that small gain can be achieved. A Yates or tapered-bearing configuration can be considered as an alternative.

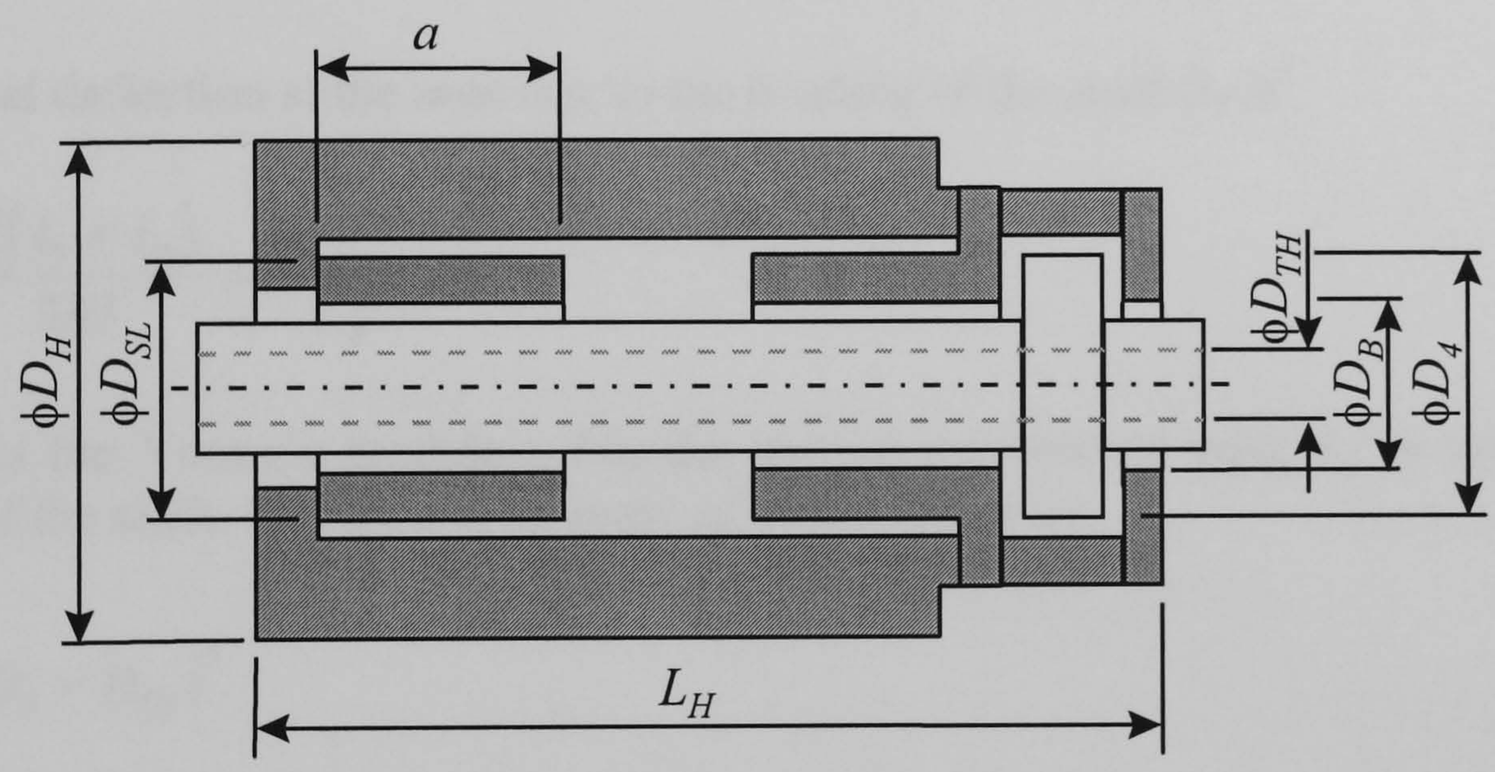

Figure C.1 Hydrostatic spindle under consideration

C.2 Stiffness Budget

In order to reduce heat generation in the bearings, the diameter of the spindle and stiffness of the bearings should be minimised while the total stiffness meets the design requirement. It is necessary to decide the stiffness budget for each component of the spindle. Because the stiffness of the thrust bearing is the axial stiffness of the spindle in this case*, factors affecting the radial stiffness can only be manipulated.

The total radial stiffness of the spindle can be evaluated by considering the bending stiffness of the spindle shaft itself and radial stiffness of the journal bearings. The loading

* The axial stiffness of the spindle shaft itself is very high.

diagram for the spindle shaft is depicted schematically in Figure C.2. Under the application of force F at the spindle nose, reactions at the bearings, F_1 and F_2 are shown in the figure where L_1 is the distance between the front bearing and the nose, and L_2 is the span of the bearing support. The reaction forces are

$$F_1 = F\frac{L_1 + L_2}{L_2} = F\left(1 + \frac{L_1}{L_2}\right)$$

$$F_2 = F\frac{L_1}{L_2}$$

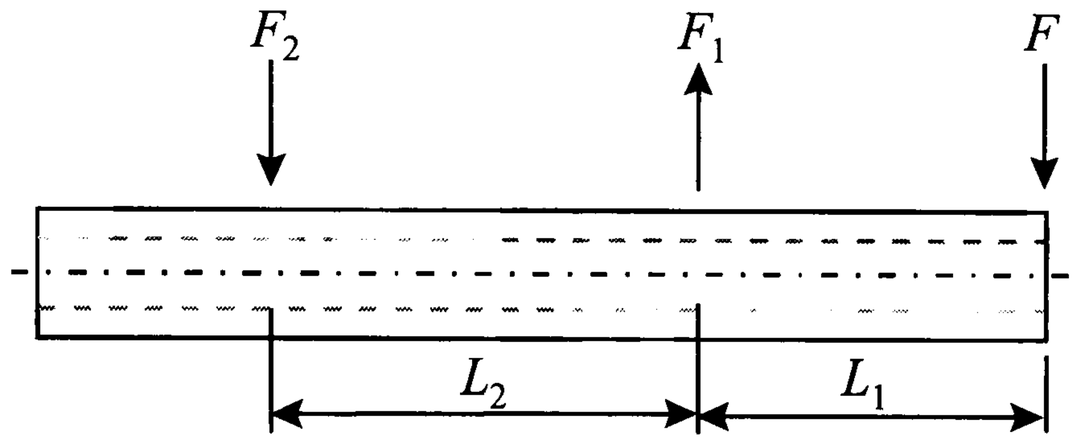

Figure C.2 Loading schematic of spindle shaft

The vertical deflection at the nose due to the bending of the shaft δ_A is*

$$\delta_A = F\frac{L_1^2\left(L_1 + L_2\right)}{3EI} = F\frac{1}{S_A} \tag{C.1}$$

where E is the Young's modulus; I is the second moment of area; S_A is the bending stiffness of the shaft. The second moment of area is given by

$$I = \frac{\pi}{64}\left(D_B - D_{TH}\right)^4$$

where D_B is the diameter of the shaft (or bearing) as can be seen in Figure C.1; D_{TH} is the diameter of the through-hole at the centre of the shaft also as can be seen in Figure C.1.

When the shaft is considered to be rigid, it will be tilted by an angle due to the flexibility of the bearings, and the angle φ can be represented by

$$\varphi \approx \frac{(\delta_1 + \delta_2)}{L_2} = \frac{F_1/S_1 + F_2/S_2}{L_2}$$

where δ_1 and δ_2 are the radial deflections at the front and rear bearing, respectively; S_1 and S_2 are the stiffness of the front and rear bearing, respectively. Therefore, the vertical deflection at the nose due to the flexibility of the bearings δ_B can be expressed such as

---

* Lardner, T.J. (ed.) (1983), *An introduction to the mechanics of solids*, 2nd ed., McGraw-Hill, pp. 531

$$\delta_B \approx (L_1 + L_2)\varphi - \delta_2 = F\frac{L_1^2 S_1 + (L_1 + L_2)^2 S_2}{L_2^2 S_1 S_2} = F\frac{1}{S_B} \tag{C.2}$$

where S_B is the stiffness of the bearings shown at the nose.

Finally, the total radial stiffness is given by

$$S = \frac{S_A S_B}{S_A + S_B} \tag{C.3}$$

The diameter of the spindle and length L_1 cannot be chosen arbitrarily, but they play a great role in the total radial stiffness. Referring to Equation C.1, the diameter of the spindle should be large, but this results in higher circumferential speeds. The length L_1 should be decided in conjunction with the bearing design. Assuming that the front journal bearing is 100mm wide at its maximum, the minimum figure of L_1 is likely to be 100mm. After many trial calculations of Equation C.1 to C.3 for selecting a smaller shaft diameter and less stiff bearings, the following was decided to be the basic dimensions of the shaft:

$L_1 = 100\text{mm}$; $L_2 = 200\text{mm}$; $D_B = 80\text{mm}$; $D_{TH} = 15\text{mm}$

The corresponding stiffnesses are as follows:

$S_A = 175\text{N/}\mu\text{m}$; $S_B = 233\text{N/}\mu\text{m}$; $S_1 = S_2 = 582\text{N/}\mu\text{m}$

The material used was steel. It is noted that the bending stiffness of the spindle shaft greatly affects the stiffness budget of the bearings. In this regard, a Yates configuration is more suitable for the effective distribution of the total stiffness to each component because it has a shorter overhang of which diameter can be easily enlarged.

In Figure C.1, the sleeves are attached to the housing as the form of a cantilever for the easy matching of thermal parameters with the shaft. The deflection of the centre of the sleeves can be calculated by using this equation*:

$$\delta = \frac{F_1 a^3}{22.6EI}$$

where a is the width of the bearing as can be seen in Figure C.1. When the compliance of the sleeve is chosen to be less than 5% of the target radial stiffness, the minimum outer diameter D_{SL} (see Figure C.1) becomes ϕ140mm for steel sleeves. When the flexibility of the sleeves are taken into account, the total resulted radial stiffness is decreased slightly.

---

* *ibid.*

C.3 Hydrostatic Bearings

The lubricant for the spindle can be either oil or water. Table C.1 shows properties of an oil and water. The viscosity of water is an order of magnitude less than that of the oil, and does not change too much with temperature. In this regard, water becomes a strong candidate for the lubricant for hydrostatic bearings. However, a water hydrostatic bearing runs with a high Reynolds number at high rotational speeds, so that turbulence should be taken into account in the thermal performance analysis. Also, because the thermal diffusivity of water is higher than that of oil, more heat is propagated into the bearing and shaft of the spindle. Nevertheless, the heat generated in a water hydrostatic bearing is substantially lower than that of an oil hydrostatic bearing due to its low viscosity.

	Density (kg/m^3)	Viscosity (10^{-3} Pa·s)			Pressure-viscosity coeff. (10^{-9} m^2/N)			Specific heat (J/kg·K)			Thermal conductivity (W/m·K)		
Temp. (°C)	25	30	60	100	30	60	100	30	60	100	30	60	100
Oil	862	18.6	6.3	2.4	21	16	13	1880	1990	2120	0.132	0.131	0.127
Water	995.7	0.80	0.47	0.28	0	0	0	4184	4178	4212	0.617	0.657	0.682

Table C.1 Physical properties of lubricants*

The author believes that engineers should keep a conservative perspective in developing a product, because a newly-developed technology may have low reliability, long-term uncertainty and cost penalties. In this respect, the lubricant is chosen to be oil. Moreover, a water hydrostatic bearing requires expensive auxiliary equipment.

Approximate estimates of the bearing parameters can be calculated by using the following equations**: a) for journals composed of four pads and axial drainage grooves between them

Flow resistance $R = \dfrac{6l\mu}{h^3\sqrt{(a+b)^2 - 4l(a+b-2l)}}$

Flow rate $\dot{V} = 2P_s/R$

Effective area $A_e = \left[(a-l)D_B + \dfrac{4l^2}{3} + (a-2l)l\right]\sin\dfrac{\phi}{2}$

Stiffness $S = \dfrac{3P_sA_e}{2h}$

Load-carrying capacity $W = \dfrac{3P_s\zeta A_e}{2}$

---

* Typical properties of medium viscosity-index naphthenic spindle-oils were taken from Neale, M.J. (1973), *Tribology Handbook*, Butterworths, London, Section B.2. For water, from Welty, J.R., Wicks, C.E. and Wilson, R.E. (1984), *Fundamentals of momentum, heat, and mass transfer*, 3rd ed., John Wiley, N.Y., pp. 772

** Slocum, A.H. (1992), *Precision machine design*, Prentice-Hall, Englewood Cliffs, N.J., pp. 551-580

b) for thrusts

Flow resistance $R = \dfrac{6\mu \ln(D_4/D_3)\ln(D_2/D_1)}{\pi h^3\left[\ln(D_4/D_3)+\ln(D_2/D_1)\right]}$

Flow rate $\dot{V} = P_s/R$

Effective area $A_e = \dfrac{\pi}{4}\left[\dfrac{D_4^2 - D_3^2}{2\ln(D_4/D_3)} + \dfrac{D_2^2 - D_1^2}{2\ln(D_2/D_1)} - D_1^2 - D_2^2\right]$

where b is the pad length, equal to $D_B\phi/2+2l$; ϕ is the arc angle of the pad recess; l is the land width; D_1 is the inside pad diameter; D_2 is the inside recess diameter; D_3 is the outside recess diameter; D_4 is the outside pad diameter; h is the bearing clearance; ζ is the ratio of the displacement of the supported element to the bearing clearance; μ is the viscosity; P_s is the supply pressure. It is noted that these equations assume that the inlet restrictor resistance equals the pad resistance.

Assuming laminar flow and a constant viscosity throughout the bearing (an isothermal bearing), the friction torque τ_f due to the viscosity for journals is obtained as

$$\tau_f = \frac{\mu D_B^2(A_l + f_r A_r)\omega}{h}$$

and the friction torque for thrusts

$$\tau_f = \int_{D_1/2}^{D_2/2} \mu\frac{r\omega}{h} r(2\pi r)dr + \int_{D_2/2}^{D_3/2} 4\mu\frac{r\omega}{h_r} r(2\pi r)dr + \int_{D_3/2}^{D_4/2} \mu\frac{r\omega}{h} r(2\pi r)dr$$
$$= \frac{\pi\mu\left[4h(D_3^4 - D_2^4) + h_r(D_4^4 - D_3^4 + D_2^4 - D_1^4)\right]\omega}{32hh_r}$$

where A_l is the land area; A_r is the recess area; h_r is the recess depth; ω is the angular speed; f_r is a factor given by $f_r = 4h/h_r$. The above equations are based on Equation D.6 and D.7 of Appendix D. The friction power loss or heat generation due to bearing friction in watts becomes

$$q_f = \frac{\mu D_B^2(A_l + f_r A_r)\omega^2}{h} \qquad \text{for journal}$$
$$= \frac{\pi\mu\left[4h(D_3^4 - D_2^4) + h_r(D_4^4 - D_3^4 + D_2^4 - D_1^4)\right]\omega^2}{32hh_r} \qquad \text{for thrust}$$

Looking into the above equations, the supply pressure and land width should be reduced to minimise heat generation in hydrostatic bearings and the following should be increased: the bearing gap, bearing width and recess depth. However, these parameters are directly related with the stiffness so that finding their optimal values is a difficult

task. Also, this signifies the importance of the stiffness budget. After many trial calculations, the bearings were designed such as Table C.2 and C.3.

a mm	b mm	l mm	h μm	h_r mm	P_s MPa	ζ	dV/dt l/min	S N/μm	Re	q_p W	q_f W	q_t W	$q_p/2+q_f$ (W)
100	59	10	30	2.5	3.1	0.1	1.26	588	970	65.2	509	574	541

Table C.2 Journal bearing design details

The viscosity of oil was assumed to be constant in a 30 °C isothermal condition (18.6×10^{-3} Pa·s from Table C.1), and the rotating speed was chosen to be 2000 rpm. In the tables, Re is the Reynolds number in the recess explained in Section D.2 of Appendix D, q_p denotes the pumping power given by Equation D.11 of Appendix D, q_t denotes the total heat dissipated, i.e. $q_t = q_p+q_f$ and $q_p/2+q_f$ is the heat generated in the bearing pad*.

D_1,D_2 mm	D_3,D_4 mm	l mm	h μm	h_r mm	P_s MPa	ζ	dV/dt l/min	S N/μm	Re	q_p W	q_f W	q_t W	$q_p/2+q_f$ (W)
86, 94	112, 120	4	30	2.5	1.25	0.1	1.47	261	970	30.5	206	236	221

Table C.3 Thrust bearing design details

The ratio at which the generated heat is conducted to the shaft and bearing can be estimated by using Equation D.16 to D.18 of Appendix D. In order to increase heat removal by the lubricant leakage and decrease heat transfer to the shaft, the shaft material is changed to 440C stainless steel, which has a smaller thermal conductivity than that of steel but the same Young's modulus. The percentage of heat conducted to the shaft is 19 per cent, that conducted to the bearing sleeve is 10 per cent, and the rest is removed by the lubricant leakage. This assumes that the inner bore temperature of the shaft is the same with the outer surface temperature of the sleeve and outlet temperature of the lubricant.

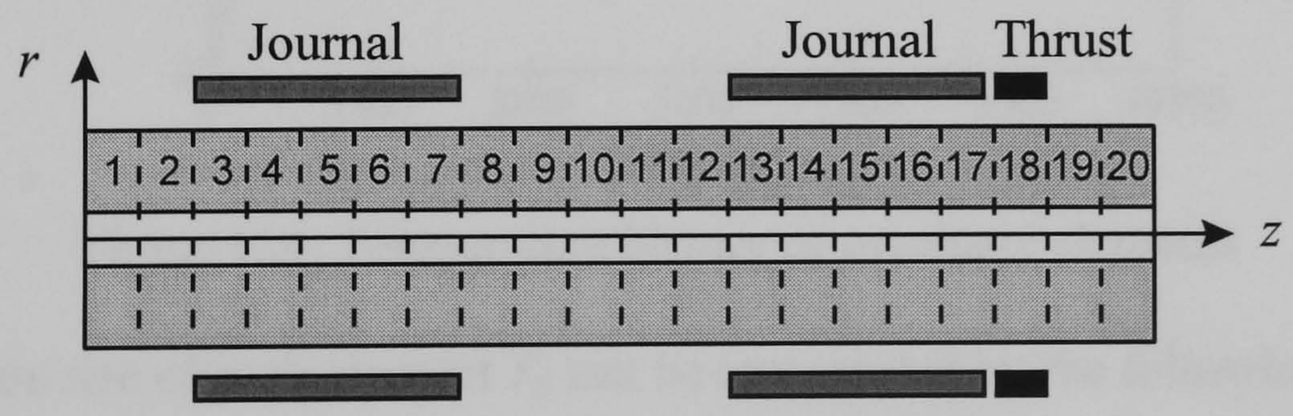

Figure C.3 Discretised model

The temperature of the shaft is likely to be nonuniform due to the high intensity heat sources that located apart along the shaft. For the temperature calculation, it is assumed that the distribution of the temperature is dependent only on the axial coordinate. By discretising the shaft to lumped elements, as shown in Figure C.3, the temperature can be easily evaluated with Equation E.3 of Appendix E. It is considered that cooling air is supplied to the through-hole of the shaft. In this case, the heat transfer coefficient related

* See Appendix D for details

with the cooling mechanism is assumed to be 100 W/m^2·K. The cooling mechanism due to the rotation of the shaft is modelled by employing the following equations:

$$\frac{\bar{h}D}{k} = 0.11\left[\left(0.5\,\mathrm{Re}_{\omega}{}^{2} + \mathrm{Gr}_{D}\right)\mathrm{Pr}\right]^{0.35} \quad * \qquad \text{for the outer surface of the shaft}$$

$$\frac{\bar{h}D}{k} = 0.35\left(\frac{\omega R^2}{\nu}\right)^{1/2} \quad ** \qquad \text{for the end faces of the shaft}$$

where $\bar{h}$ is the average heat transfer coefficient; D is the diameter of a rotating body; R is the radius; k is the thermal conductivity; Gr_D is the Grashof number; Pr is the Prandtl number; ν is the kinematic viscosity; ω is the angular speed; Re_ω is the Reynolds number given by

$$\mathrm{Re}_{\omega} = \frac{\omega \pi D^2}{\nu}$$

The calculated temperature history of the shaft overhang is shown in Figure C.4. Element 18 has thrust pads, Element 19 and 20 is the overhang from the thrust bearing.

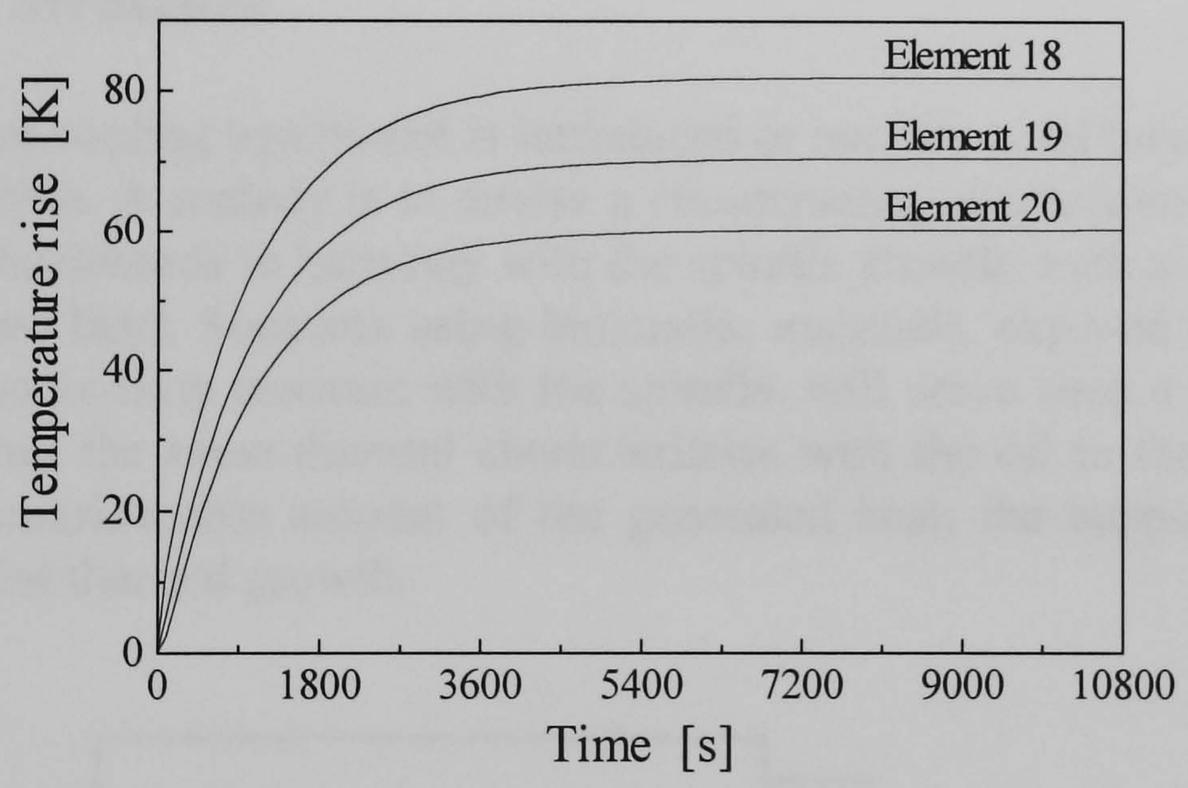

Figure C.4 Temperature history of overhang elements

The temperature rise of each element T_n can be represented by the following equation:

$$T_n = T_{n,\max}(1 - e^{-t/\tau})$$

where $T_{n,max}$ is the maximum temperature rise of an element; τ is the time constant. The time constant of each element can be found by employing a curve-fitting method. Table C.4 shows details of the thermal deformation of some elements of interest.

---

* Kays, W.M. and Bjorklund, I.S. (1958), "Heat transfer from a rotating cylinder with and without cross flow", *Trans. ASME, Series C*, Vol. 80, pp. 70-78

** Cobb, E.C. and Saunders, O.A. (1956), "Heat transfer from a rotating disk", *Proc. Roy. Soc., A.*, Vol. 220, pp. 343-351

Element number	$T_{n,max}$ (K)	Radius increase (μm)	Length increase (μm)	τ (min)
5 (centre of rear bearing)	45	18	9.2	17
10 (centre between rear and front bearing)	25	10	5.1	22
15 (centre of front bearing)	70	29	14	18
18 (thrust bearing)	82	33	17	16
19 (overhang adjacent to thrust)	70	29	14	18
20 (overhang)	60	24	12	19

Table C.4 Thermal deformation of some elements of interest

The maximum temperature rise and time constant of the bearing sleeves can be calculated by using Equation E.2 of Appendix E. When the heat transfer coefficient on the outer surface of the sleeves is chosen to be 82 $W/m^2 \cdot K$, the time constant of the sleeves can be equal to that of the shaft. However, the maximum temperature rise of the sleeves is substantially lower than that of the shaft (about 16°C), so that it is inevitable to introduce some deviations in the bearing gap. This is true for the trust bearing. It is likely to be reasonable to choose the same time constant between the shaft and bearing sleeves and to assign a larger bearing gap.

C.4 Support Structure

Whether lubricant cooling equipment is introduced or not, the axial thermal growth of the spindle is inevitable. A remedy is to devise a counteracting mechanism which can move the spindle unit backwards in harmony with the spindle growth, such as that illustrated in Figure C.5 (dotted line). Supports using bimetallic materials, exposed to the leakage oil and having the same time constant with the spindle, will serve such a purpose. Because the leakage oil has the same thermal characteristics with the oil in the bearing gap and carries away a considerable amount of the generated heat, the support can deform to neutralise the axial thermal growth.

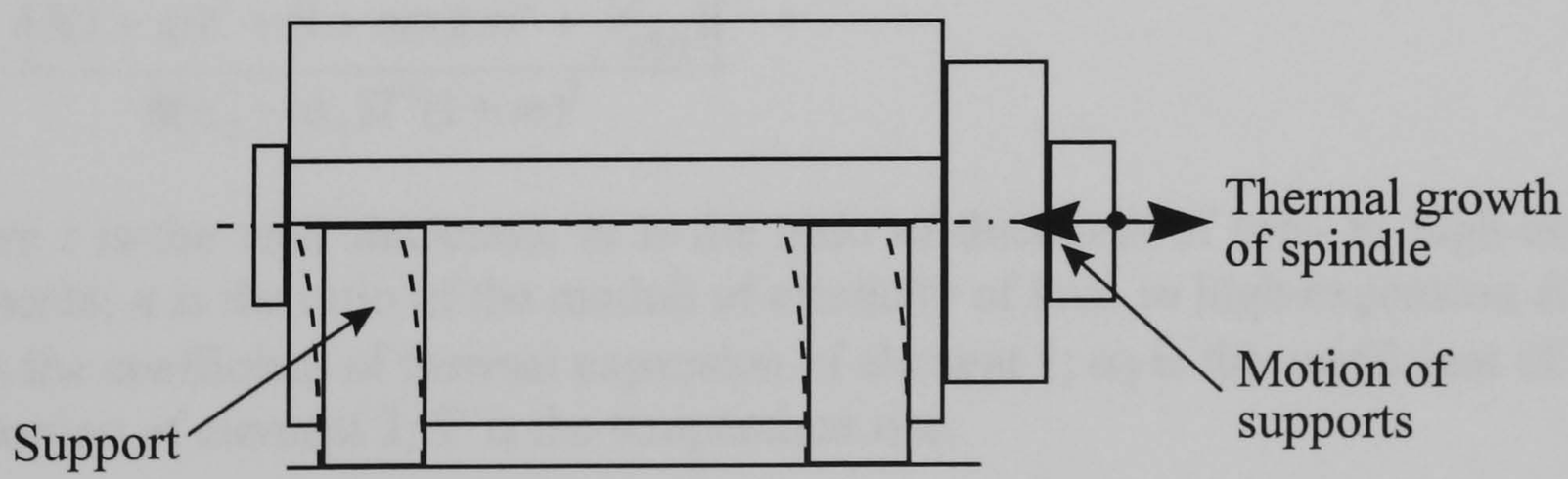

Figure C.5 Support structure

However, the angular displacement and height change of the support could be a serious concern. Supporting the spindle unit at the neutral axis of the support, they can be minimised. The design of this kind of supports is a complex task, which should satisfy the following requirements:

- The time constant of the support should be the same with that of the shaft, i.e.

$$\tau_{shaft} = \tau_1 = \tau_2$$

where subscripts 1,2 denote one of the two beams bonded together, respectively (See Figure C.6). Each time constant can be estimated by using Equation E.2 of Appendix E.

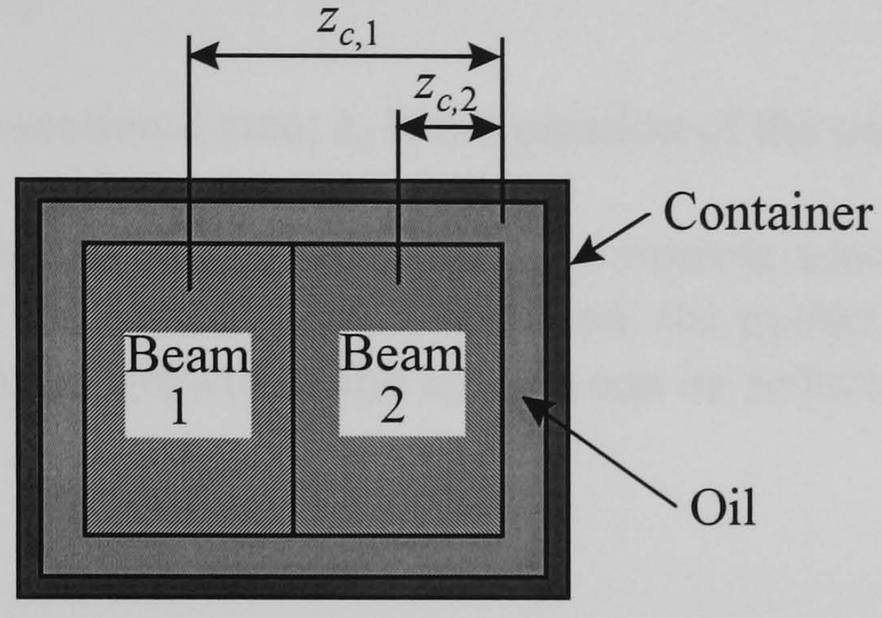

Figure C.6 Cross-section of support

- The maximum deflection of the support should be equal to the maximum axial growth of the spindle. When bimetallic elements are mounted as a cantilever, the maximum deflection at the end $w_{\max}$ can be expressed such as

$$w_{max} = \frac{L^2}{2\rho}$$

where L is the length; ρ is the radius of curvature of the deflection of bimetallic strips given as*

$$\rho = \frac{t\left[3(1+m)^2 + (1+mn)(m^2 + 1/mn)\right]}{6(\alpha_2 - \alpha_1)T'(1+m)^2}$$

where t is the total thickness; m is the ratio of thickness of low- to high-expansion elements; n is the ratio of the moduli of elasticity of low- to high-expansion elements; α_1 is the coefficient of thermal expansion of element 1; α_2 is the coefficient of thermal expansion of element 2; T' is the temperature rise.

- The support fulfils a stiffness requirement if any. The stiffness can be calculated by using the following governing equation about a bimetallic beam** :

---

* Eskin, S.G. and Fritze, J.R. (1940), "Thermostatic bimetals", *Trans. ASME*, pp. 433-442

** Lardner, T.J. (ed.) (1983), *An introduction to the mechanics of solids*, 2nd ed., McGraw-Hill, pp. 495

$$\frac{d^2w}{dy^2} = \frac{M_b}{(EI)_1 + (EI)_2}$$

where M_b is the bending moment; E is the Young's modulus; I is the second moment of area about the neutral surface. The location of the neutral axis is given by

$$z_N = \frac{(EAz_c)_1 + (EAz_c)_2}{(EA)_1 + (EA)_2}$$

where A is the cross-sectional area; z_c is the position of the centroid.

Simultaneous satisfaction of the above three requirements seems to be very difficult. If the contact stiffness of the bolted joints is included, the matter becomes more complex. However, the axial thermal growth of the spindle can be reduced by using the bimetallic support.

Appendix D
Heat Flow in Hydrostatic Bearings

D.1 Governing Equations of Fluid Film Lubrication

In the thin fluid film depicted in Figure D.1, the speed components of the fluid can be derived from the Navier-Stokes equations* such as

$$\frac{\partial p}{\partial x} = \mu \frac{\partial^2 u}{\partial z^2}$$
$$\frac{\partial p}{\partial y} = \mu \frac{\partial^2 v}{\partial z^2} \qquad \text{(D.1)}$$

where p is the pressure; μ is the viscosity; u is the fluid velocity in the x direction; v is the fluid velocity in the y direction. By integrating twice, the two speed components are obtained as

$$u = \frac{1}{2\mu}\frac{\partial p}{\partial x} z(z-h) + \left(1 - \frac{z}{h}\right) U_2 + \frac{z}{h} U_1$$
$$v = \frac{1}{2\mu}\frac{\partial p}{\partial y} z(z-h) + \left(1 - \frac{z}{h}\right) V_2 + \frac{z}{h} V_1 \qquad \text{(D.2)}$$

where h is the film thickness; U_1 and U_2 are the translational velocities of the two bounding surfaces in the x direction as depicted in Figure D.1; V_1 and V_2 are the translational velocities of the two bounding surfaces in the y direction as depicted in Figure D.1.

---

* Welty, J.R., Wicks, C.E. and Wilson, R.E. (1984), *Fundamentals of momentum, heat, and mass transfer*, 3rd ed., John Wiley, N.Y., pp. 123-132

The fluid flow through a thin film can be analysed by the Reynolds equation, which can be derived from Equation D.2 and the continuity equation. The Reynolds equation in two dimensions for compressible or incompressible flow of a Newtonian fluid is represented by*

$$\frac{\partial}{\partial x}\left[\frac{\rho h^3}{\mu}\frac{\partial p}{\partial x}\right]+\frac{\partial}{\partial y}\left[\frac{\rho h^3}{\mu}\frac{\partial p}{\partial y}\right]=6\left[\frac{\partial}{\partial x}(\rho hU)+\frac{\partial}{\partial y}(\rho hV)+2\frac{\partial}{\partial t}(\rho h)\right] \tag{D.3}$$

where ρ is the density; $U = U_1 + U_2$; $V = V_1 + V_2$.

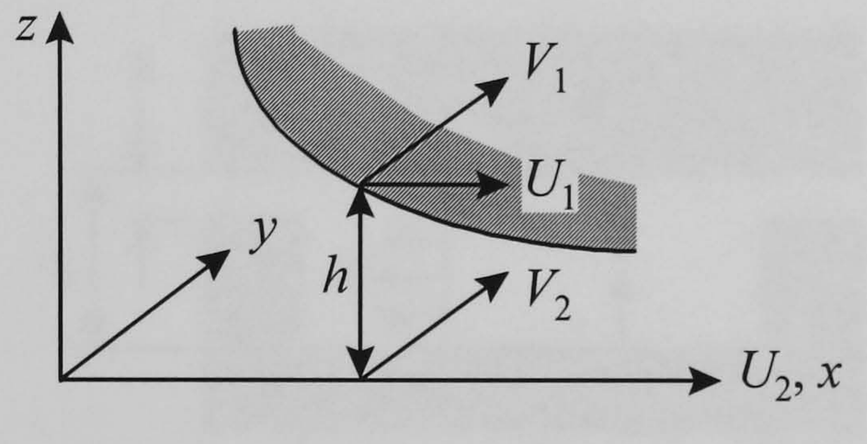

Figure D.1 Thin Fluid Film

Assuming that the specific heat c_v and thermal conductivity k are constant and the heat conduction in the x and y direction is small in comparison with the convection, the steady-state energy equation for the incompressible fluid film can be derived such that**

$$\rho c_v\left(u\frac{\partial T}{\partial x}+v\frac{\partial T}{\partial y}\right)=k\frac{\partial^2 T}{\partial z^2}+\Phi \tag{D.4}$$

where u and v are the velocities of the fluid in the x and y direction, respectively; the dissipation function Φ is

$$\Phi=\mu\left[\left(\frac{\partial u}{\partial z}\right)^2+\left(\frac{\partial v}{\partial z}\right)^2\right]$$

The load capacity **W** of the fluid film is the resultant of the pressure field defined by Equation D.3:

$$\mathbf{W}=\iint p\mathbf{n}dA$$

where **n** is the unit normal vector to dA. The flow rate per unit length can be calculated by integrating Equation D.2 from $z = 0$ to $z = h$.

---

* Gohar, R. (1988), *Elastohydrodynamics*, Ellis Horwood, Chichester, pp. 58-59

** Freund, N.O. and Tieu, A.K. (1993), "A thermo-elasto-hydrodynamic study of journal bearing with controlled deflection", *Trans. ASME: J. Tribology*, Vol. 115, pp. 550-556

D.2 Friction

The friction of hydrostatic bearings has two components. The first is due to the fully-developed Couette flow in the lands. When a bounding surface moves at a speed U with respect to the other as depicted in Figure D.2, then the friction force F_f is

$$F_f = \mu \frac{U}{h} A_l \tag{D.5}$$

where A_l is the area of the land, i.e. $A_l = (B\text{-}b)L$; B is the width of the bearing; b is the width of the recess; L is the length of the bearing.

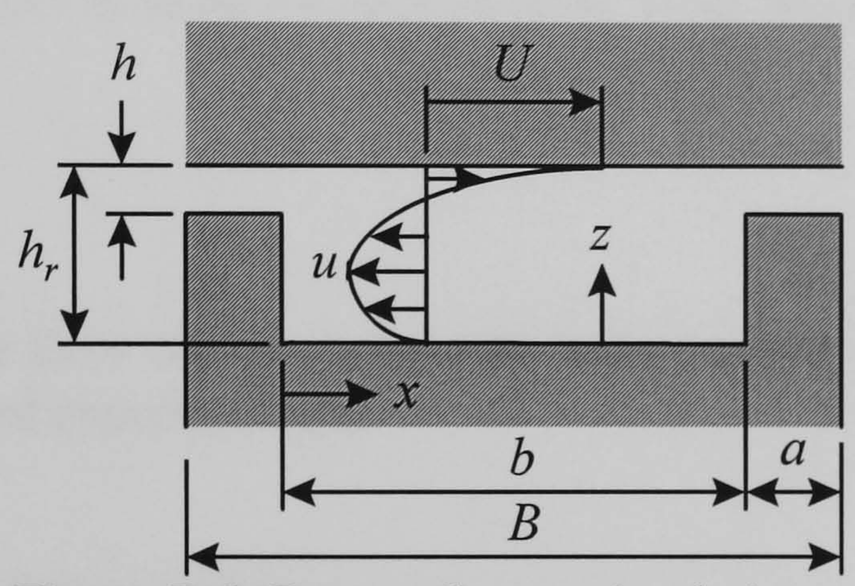

Figure D.2 Recess flow recirculation

The second is due to the continuous recirculation of the fluid in the recess as depicted in Figure D.2*. Neglecting end effects, the velocity profile is given by Equation D.2:

$$u = \frac{1}{2\mu}\frac{\partial p}{\partial x} z(z - h_r) + \frac{z}{h_r} U$$

Because the net flow rate is zero at any given section such as $\int_0^{h_r} u dz = 0$, the following equation can be obtained:

$$\frac{dp}{dx} = 6U \frac{\mu}{h_r^2}$$

Therefore, the friction force in the recess area can be stated such as

$$F_f = \tau_w A_r = \mu \left.\frac{\partial u}{\partial z}\right|_{z=h_r} A_r = 4U \frac{\mu}{h_r} A_r \tag{D.6}$$

where τ_w is the shear stress on the moving component; A_r is the area of the recess.

---

* Shinkle, J.N. and Hornung, K.G. (1965), "Frictional characteristics of liquid hydrostatic journal bearings", *Trans. ASME: J. Basic Engineering*, Vol. 87, pp. 163-169

The total frictional force of a sliding hydrostatic pad is the sum of the two friction components given by Equation D.5 and D.6:

$$F_f = U\frac{\mu}{h}\left(A_l + f_r A_r\right) \tag{D.7}$$

where f_r is

$$f_r = 4\frac{h}{h_r}$$

It is noted that Equation D.7 is valid for laminar flow. If the Reynolds number

$$\mathrm{Re} = \frac{\rho U h_r}{\mu}$$

is smaller than 1000, the flow can be considered to be laminar. For turbulent flow, the factor f_r must be evaluated experimentally.

D.3 Temperature of Fluid Film

In an adiabatic flow condition, the heat generated in the fluid film is assumed to remain in the lubricant itself. However, heat exchanges among various parts, i.e. bearings, shafts, supply pumps, compensating elements, etc., should be taken into account in journal bearings where high heat generation is expected. Figure D.3 shows a quarter of a journal bearing pad in a rolled-out form. The bearing is considered to have axial drainage grooves.

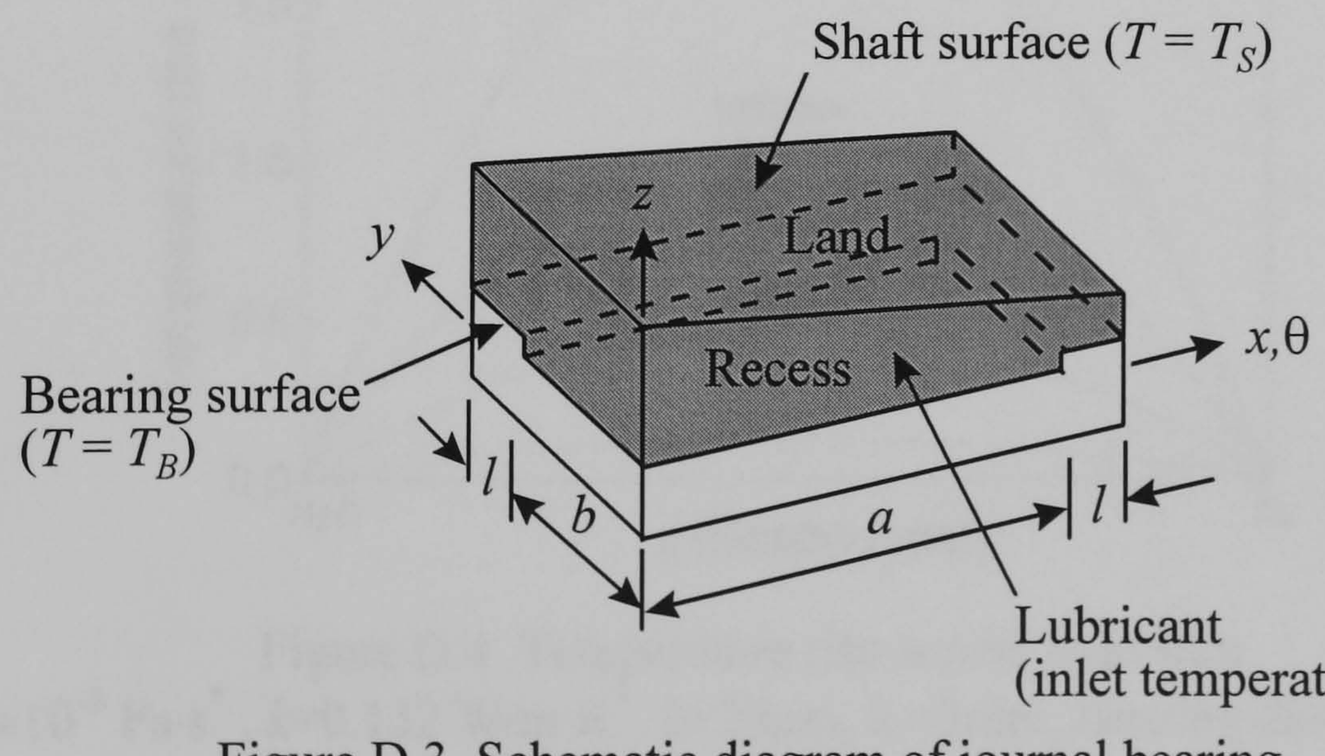

Figure D.3 Schematic diagram of journal bearing

Assuming that heat in the lubricant is transferred only by conduction and the friction due to the velocity component in line with the shaft v is small, Equation D.4 is reduced to

$$\frac{\partial^2 T}{\partial z^2} = -\frac{\mu}{k}\left(\frac{\partial u}{\partial z}\right)^2$$

From Section D.2, the following is obtained for the recess area, i.e. $y = 0$ to b and $x = -a$ to a:

$$u = 3\frac{U}{h_r^2}z^2 - 2\frac{U}{h_r}z, \qquad \frac{\partial u}{\partial z} = 6\frac{U}{h_r^2}z - 2\frac{U}{h_r}$$

For the land area, the velocity component u is obtained as the following: a) for $x = a$ to $(a+l)$ and $y = 0$ to b

$$u = \frac{1}{2\mu}\frac{P_r}{l}z(z - h_r + h) + \frac{(z - h_r + h)}{h}U, \qquad \frac{\partial u}{\partial z} = \frac{1}{2\mu}\frac{P_r}{l}(2z - h_r + h) + \frac{U}{h}$$

b) for $x = -a$ to $-(a+l)$ and $y = 0$ to b

$$u = -\frac{1}{2\mu}\frac{P_r}{l}z(z - h_r + h) + \frac{(z - h_r + h)}{h}U, \qquad \frac{\partial u}{\partial z} = -\frac{1}{2\mu}\frac{P_r}{l}(2z - h_r + h) + \frac{U}{h}$$

c) for $x = -(a+l)$ to $(a+l)$ and $y = b$ to $(b+l)$

$$u = \frac{U}{h}\left(z - h_r + h\right), \qquad \frac{\partial u}{\partial z} = \frac{U}{h}$$

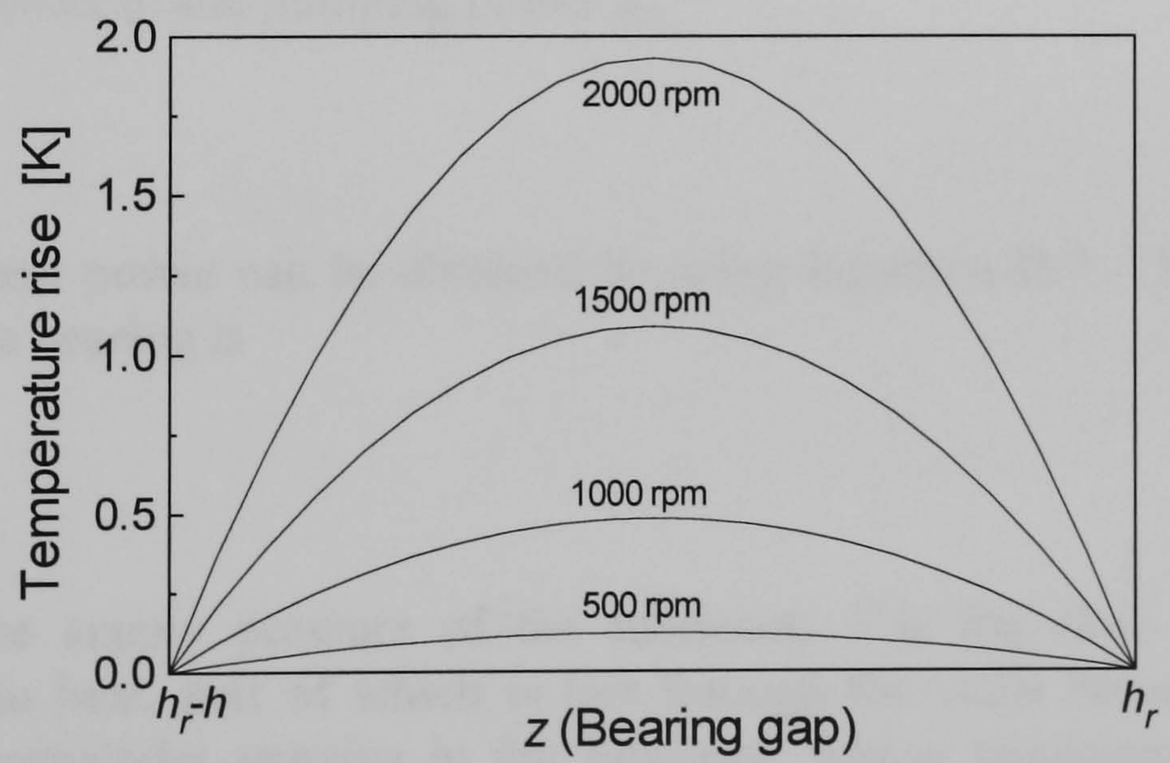

Figure D.4 Temperature rise across fluid film
(μ=18.6×10^{-3} Pa·s* , k=0.132 W/m·K*, h=20μm, h_r=3mm, Bearing diameter=ϕ100mm)

* Typical properties of medium viscosity-index naphthenic spindle-oils at 30°C (Neale, M.J. (1973), *Tribology handbook*, Butterworths, London, Section B.2)

When the temperatures of the bearing and shaft surfaces are considered to be the same at the initial stage, i.e. $T_B = T_S = T_i$, the temperature of the film over the land bounded by $x = -(a+l)$ to $(a+l)$ and $y = b$ to $(b+l)$ is obtained as

$$T(z) = -\frac{1}{2kh^2}\left[\mu U^2 z^2 + \mu U^2 (h - 2h_r)z + \mu U^2 (h_r^2 - h_r h) - 2T_i kh^2\right] \qquad \text{(D.8)}$$

An example of temperature profiles across the film is depicted in Figure D.4. As the spindle speed increases, the temperature difference across the film is greater. Because the velocity component u varies with y, the average temperature of the film may be assumed to increase with y.

The fluid film may be assumed to be isothermal for the ease of calculation. In this case the effective or average temperature T_{eff} of the isothermal film can be represented by*

$$T_{eff} = T_{inlet} + 0.8\Delta T \qquad \text{(D.9)}$$

where T_{inlet} is the inlet temperature of the lubricant; ΔT is the increase of the lubricant temperature. The viscosity of lubricants decreases exponentially as the temperature rises. The effective viscosity, which is constant across the film, can be taken at the effective temperature.

D.4 Heat Balance

The total heat generation rate q_t in a hydrostatic bearing system is a function of the viscous shear power q_f and pumping power q_p:

$$q_t = q_p + q_f \qquad \text{(D.10)}$$

The viscous shear power can be obtained by using Equation D.7. The pumping power dissipated in the bearing is

$$q_p = P_s \dot{V} \qquad \text{(D.11)}$$

where P_s is the supply pressure of the lubricant; $\dot{V}$ is the flow rate. Power q_t is transformed into heat, part of which is lost through the walls bounding the lubricant path, and the remainder remains in the lubricant, whose temperature increases as it passes through the compensating devices and bearing clearance. The pumping power dissipated in the bearing is

$$q_r = P_r \dot{V} \qquad \text{(D.12)}$$

where P_r is the recess pressure.

---

* Cameron. A. (1983), *Basic lubrication theory*, 3rd ed., Ellis Horwood, Chichester, pp. 128-133

If all the dissipated power q_t remains in the lubricant in an adiabatic condition, the temperature increase of the lubricant ΔT is

$$\Delta T = \frac{q_t}{\rho c_p \dot{V}} = \frac{P_s}{\rho c_p}\left(1 + \frac{q_f}{q_p}\right) \tag{D.13}$$

Similarly, the rise of temperature in the compensating elements can be stated such as

$$\Delta T_c = \frac{\Delta P_c}{\rho c_p} \tag{D.14}$$

The heat balance in the journal bearing depicted in Figure D.3 can be stated such that

$$q_r + q_f = q_S + q_B + q_L \tag{D.15}$$

where q_S is the heat transfer rate to the shaft; q_B is the heat transfer rate to the bearing; q_L is the rate of heat removal by lubricant leakage. q_L can be expressed by the volume flow rate $\dot{V}$, effective temperature and inlet temperature:

$$q_L = \rho c_p \dot{V}(T_{eff} - T_{inlet}) = C_L(T_{eff} - T_{inlet}) \tag{D.16}$$

where C_L is the thermal conductance. q_S and q_B can be expressed in the form of Equation D.16 such as

$$\begin{aligned} q_S &= C_S(T_{eff} - T_{inlet}) \\ q_B &= C_B(T_{eff} - T_{inlet}) \end{aligned} \tag{D.17}$$

where C_S and C_B are the thermal conductance of the shaft and housing, respectively. The expression given by Equation D.17 is based on the assumption that the inner surface of the shaft and outer surface of the bearing have the same temperature with the supply lubricant at the steady state. The thermal conductance of a hollow cylinder (length L, outer radius R_o, inner radius R_i) can be found in many textbooks*:

$$C_{cylinder} = \frac{2\pi kL}{\ln\left(R_o / R_i\right)} \tag{D.18}$$

*e.g. Welty, J.R., Wicks, C.E. and Wilson, R.E. (1984), *Fundamentals of momentum, heat, and mass transfer*, 3rd ed., John Wiley, N.Y. pp. 256-259

Appendix E
Temperature Distribution in Hollow Cylinder

E.1 Lumped Model

From the first law of thermodynamics*, the following governing equation is derived for a lumped hollow cylinder (length L, inner diameter R_i, outer diameter R_o) subject to boundary heat flux input q and convection cooling:

$$\rho c_p V \frac{dT}{dt} = q - hA(T - T_\infty) \tag{E.1}$$

where ρ is the density; c_p is the specific heat; V is the volume of the cylinder; T is the temperature of the body; h is the heat transfer coefficient; A is the area of the cooling surface; T_∞ is the temperature of the cooling fluid. When the initial temperature is T_∞, the solution of Equation E.1 can be readily obtained such as

$$T = \frac{q}{hA}(1 - e^{-t/\tau}) + T_\infty \tag{E.2}$$

where τ is the time constant given by

$$\tau = \frac{\rho c_p V}{hA}$$

and the volume is

$$V = \pi(R_o^2 - R_i^2)L$$

---

* Wylen, G.J.V. and Sonntag, R.E. (1976), *Fundamentals of classical thermodynamics*, 2nd ed., John Wiley, N.Y., pp. 85-165

E.2 Temperature Changes in Axial Direction

When the axial temperature distribution is expected, the solution given by Equation E.2 is no longer valid. The approximate solution can be obtained by dividing the cylinder into N lumped elements, having an equal length, such as depicted in Figure E.1.

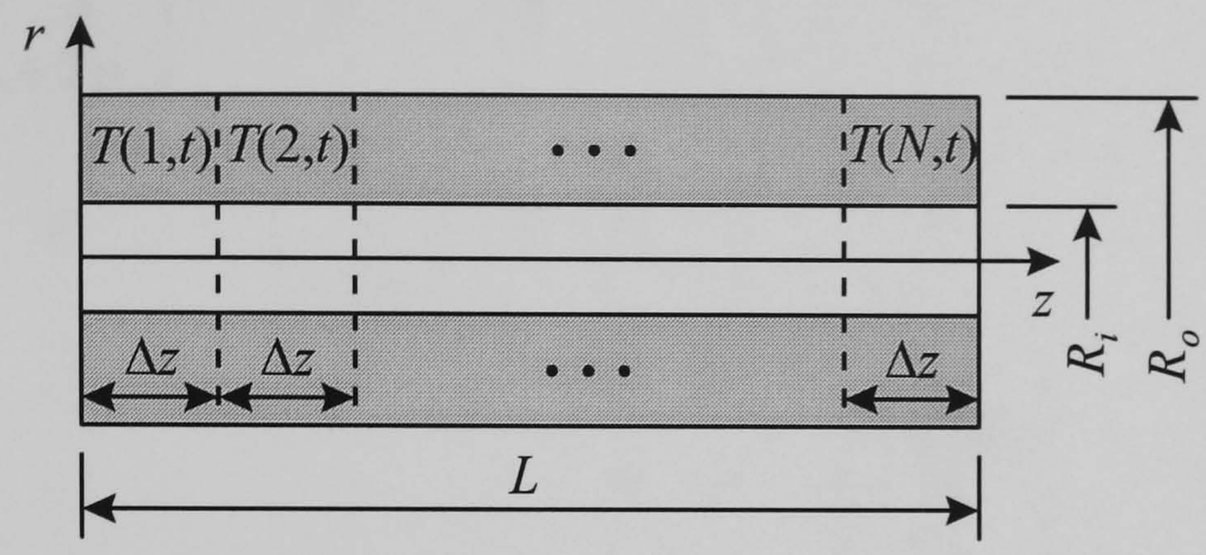

Figure E.1 Cylinder divided into N lumped elements in the axial direction

For the inside elements subject to boundary heat flux input q_n and convection cooling, the following equation describes their temperature behaviour:

$$\rho c_p V \frac{dT_n}{dt} = q_n - (hA)_n\left(T_n - T_\infty\right) + kA_s \frac{T_{n-1} - T_n}{\Delta z} - kA_s \frac{T_n - T_{n+1}}{\Delta z}$$

$$V = \pi(R_o^2 - R_i^2)\Delta z$$

where the subscript n denotes a quantity related to the nth body; k is the thermal conductivity; A_s is the cross-sectional area of the cylinder; Δz is the length of each element, i.e. $\Delta z = L/N$; $z = n\Delta z$, $n = 1,2,\ldots,N$.

For the boundary elements, the temperature is described by

$$\rho c_p V \frac{dT_1}{dt} = q_1 - (hA)_1\left(T_1 - T_\infty\right) - kA_s \frac{T_1 - T_2}{\Delta z}$$

$$\rho c_p V \frac{dT_N}{dt} = q_N - (hA)_N\left(T_N - T_\infty\right) + kA_s \frac{T_{N-1} - T_N}{\Delta z}$$

The governing equations of all the elements can be put into a state-space form such that:

$$\dot{\mathbf{v}} = \mathbf{A}(t)\mathbf{v} + \mathbf{B}(t)\mathbf{x} \tag{E.3}$$

where:

$$\mathbf{v} = \begin{bmatrix} T_1 & T_2 & \cdots & T_N \end{bmatrix}^{\mathrm{T}} \quad \text{(state vector)}$$

$$\mathbf{x} = \frac{1}{S}\begin{bmatrix} q_1 + (hA)_1 T_\infty) & q_2 + (hA)_2 T_\infty & \cdots & q_N + (hA)_N T_\infty \end{bmatrix}^{\mathrm{T}} \quad \text{(input vector)}$$

$$\mathbf{A}(t) = \begin{bmatrix}
-\left(\dfrac{(hA)_1}{S}+p\right) & p & 0 & \cdots & \cdots & \cdots & \cdots & 0 \\
p & -\left(\dfrac{(hA)_2}{S}+2p\right) & p & 0 & \cdots & \cdots & \cdots & \vdots \\
0 & p & -\left(\dfrac{(hA)_3}{S}+2p\right) & p & 0 & \cdots & \cdots & \vdots \\
\vdots & \vdots & \vdots & \ddots & \ddots & \ddots & \ddots & 0 \\
0 & \cdots & \cdots & \cdots & 0 & p & -\left(\dfrac{(hA)_{N-1}}{S}+2p\right) & p \\
0 & \cdots & \cdots & \cdots & \cdots & 0 & p & -\left(\dfrac{(hA)_N}{S}+p\right)
\end{bmatrix}$$

$$\mathbf{B}(t) = \begin{bmatrix} 1 & 0 & \cdots & 0 \\ 0 & 1 & \cdots & \vdots \\ \vdots & \vdots & \ddots & \vdots \\ 0 & \cdots & \cdots & 1 \end{bmatrix}$$

It is noted that:

$$S = \rho c_p V\,, \qquad p = \frac{kA_s}{S\Delta z}$$

In order to obtain the solution, all the eigenvalues of the matrix **A** should be less than unity so that the model is convergent or stable. Once the matrices **A**, **B** are known, the temperature rise of each element can be calculated.

E.3 Temperature Changes in Radial Direction

If the temperature of a hollow cylinder is considered to be dependent on the radial coordinate, the governing equation is obtained from the heat conduction equation*:

$$\frac{\partial T}{\partial t} = \beta\left(\frac{\partial^2 T}{\partial r^2} + \frac{1}{r}\frac{\partial T}{\partial r}\right)$$

---

* Samarskii, A.A. and Vabishchevich, P.N. (1995), *Computational heat transfer: Volume 1 Mathematical modelling*, John Wiley, Chichester, pp. 16-21

where β is the thermal diffusivity, i.e. $\beta = k/\rho c_p$. Assuming that the cylinder is divided into N concentric elements in the radial direction, as depicted in Figure E.2 and the temperature is uniform within each element, the finite-difference method** can be applied.

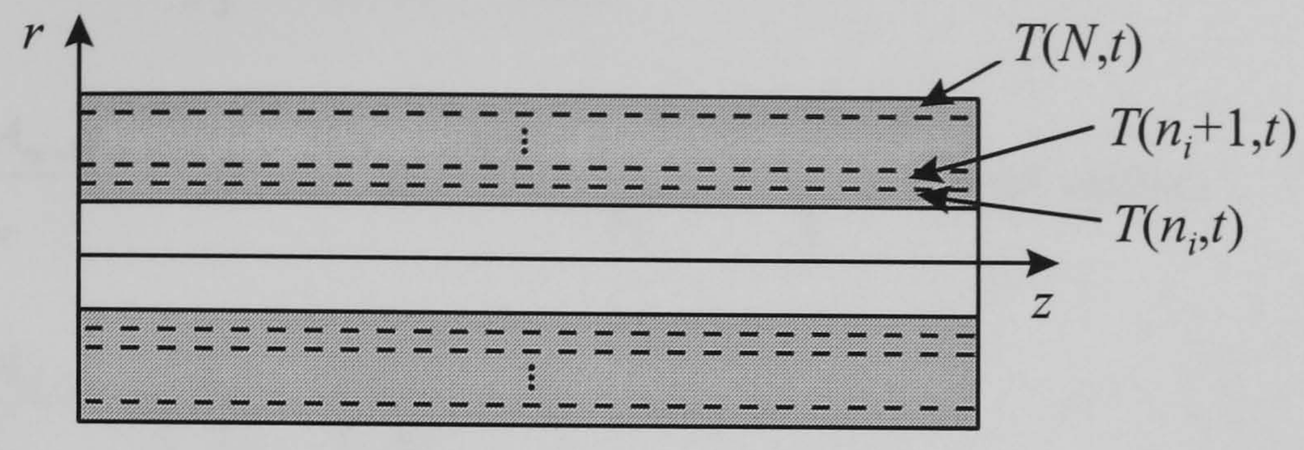

Figure E.2 Finite-difference mesh for hollow cylinder

The first and second order partial differential terms may be written in the approximate difference form as follows:

$$\frac{\partial T(r,t)}{\partial t} \approx \frac{dT(n\Delta r,t)}{dt}$$

$$\frac{\partial T(r,t)}{\partial r} \approx \frac{T(n\Delta r,t) - T((n-1)\Delta r,t)}{\Delta r}$$

$$\frac{\partial^2 T(r,t)}{\partial r^2} \approx \frac{T((n+1)\Delta r,t) - 2T(n\Delta r,t) + T((n-1)\Delta r,t)}{(\Delta r)^2}$$

where Δr is the thickness of each element, i.e. $\Delta r = R_o/N$; $r = n\Delta r$, $n = n_i, n_i+1,\ldots,N$; n_i is the index number of the inner hole element. The one-dimensional unsteady heat-conduction equation becomes

$$\frac{dT(n,t)}{dt} = \frac{\beta}{n(\Delta r)^2}\left[(n-1)T(n-1,t) + (1-2n)T(n,t) + nT(n+1,t)\right]$$

This equation applies to the inside elements. For the boundary cells subject to heat flux input q and convection cooling, the following equations are applicable:

$$\frac{dT(n_i,t)}{dt} = \frac{q_{ni}}{\rho c_p V_{ni}} - \frac{h_{ni} A_{ni-1}}{\rho c_p V_{ni}}\left(T(n_i,t) - T_{\infty,i}\right) - \frac{kA_{ni}}{\rho c_p V_{ni}\Delta r}\left(T(n_i,t) - T(n_i+1,t)\right)$$

$$\frac{dT(N,t)}{dt} = \frac{q_N}{\rho c_p V_N} - \frac{h_N A_N}{\rho c_p V_N}\left(T(N,t) - T_{\infty,o}\right) + \frac{kA_{N-1}}{\rho c_p V_N \Delta r}\left(T(N-1,t) - T(N,t)\right)$$

where A_n is the outer surface area of the nth element.

The governing equations of all the elements can be put into a state-space form such that:

** Smith, G.D. (1985), *Numerical solution of PDEs*, 3rd ed., Oxford Univ. Press, London

$$\dot{\mathbf{v}} = \mathbf{A}(t)\mathbf{v} + \mathbf{B}(t)\mathbf{x} \tag{E.4}$$

where:

$$\mathbf{v} = \begin{bmatrix} T_{ni} & T_{ni+1} & \cdots & T_N \end{bmatrix}^{\mathrm{T}} \quad \text{(state vector)}$$

$$\mathbf{x} = \begin{bmatrix} \dfrac{q_{ni} + h_{ni} A_{ni-1} T_{\infty,i}}{S_{ni}} & 0 & \cdots & 0 & \dfrac{q_N + h_N A_N T_{\infty,o}}{S_N} \end{bmatrix}^{\mathrm{T}} \quad \text{(input vector)}$$

$$\mathbf{A}(t) = \begin{bmatrix} -\dfrac{h_{ni} A_{ni-1}}{S_{ni}} - \dfrac{kA_{ni}}{S_{ni}\Delta r} & \dfrac{kA_{ni}}{S_{ni}\Delta r} & 0 & \cdots & \cdots & \cdots & \cdots & 0 \\ \Phi_{ni+1} & \Theta_{ni+1} & \Gamma & 0 & \cdots & \cdots & \cdots & \vdots \\ 0 & \Phi_{ni+2} & \Theta_{ni+2} & \Gamma & 0 & \cdots & \cdots & \vdots \\ \vdots & \vdots & \vdots & \vdots & \vdots & \vdots & \vdots & 0 \\ 0 & \cdots & \cdots & \cdots & 0 & \Phi_{N-1} & \Theta_{N-1} & \Gamma \\ 0 & \cdots & \cdots & \cdots & \cdots & 0 & \dfrac{kA_{N-1}}{S_N \Delta r} & -\dfrac{h_N A_N}{S_N} - \dfrac{kA_{N-1}}{S_N \Delta r} \end{bmatrix}$$

$$\mathbf{B}(t) = \begin{bmatrix} 1 & 0 & \cdots & 0 \\ 0 & 1 & \cdots & \vdots \\ \vdots & \vdots & \ddots & \vdots \\ 0 & \cdots & \cdots & 1 \end{bmatrix}$$

where:

$$S_n = \rho c_p V_n, \qquad \Gamma = \frac{\beta}{(\Delta r)^2}, \qquad \Phi_n = \left(\frac{n-1}{n}\right)\Gamma, \qquad \Theta_n = \left(\frac{1-2n}{n}\right)\Gamma$$

In this finite-difference equation, the lumped-parameter technique was applied to each element.